# Alaska Department of Environmental Conservation

**Amendments to:**
**State Air Quality Control Plan**

**Vol. III: Appendix III.D.7.08**

**{Appendix to Volume II. Analysis of Problems, Control Actions; Section III. Area-wide Pollutant Control Program; D. Particulate Matter; 7. Fairbanks North Star Borough PM2.5 Control Plan, Serious Requirements}**

**Draft**

May 10, 2019

**Michael J. Dunleavy**
**Governor**

**Jason W. Brune**
**Commissioner**

**(This page serves as a placeholder for two-sided copying)**

# Appendix III.D.7.08

Contents

EPA Model Guidance on the Use of Models and Other Analyses for Demonstrating Attainment of Air Quality Goals for Ozone, PM2.5 , and Regional Haze" (USEPA, 2007), recommends the Species Modeled Attainment Test (SMAT) to estimate future concentrations of daily PM2.5 concentration

Gaudet, B.J., & Stauffer, D.R. (2010). Stable boundary layer representation in meteorological models in extremely cold wintertime conditions. Final Report to Environmental Protection Agency. Purchase Order EP08D000663, Reporting Period: 1 September 2008 – 31 January 2010.

Molders, N., Tran, H.N.Q., & Leelasakultum, K. (2011). Investigations of means for $PM_{2.5}$ mitigation through atmospheric modeling. Final Report Phase 1 (1 December 2008 – 31 December 2010) Prepared for the Fairbanks North Star Borough

Gaudet, B.J., & Stauffer, D.R. (2011). Final Report to Alaska Department of Environmental Conservation. Grant Number 127617. Reporting Period; 8 March 2011 – 31 January 2012)

Ward, T.J., Palmer, C.P., Hooper, K., Bergauff, M., & Noonan, C.W. (2013). The impact of a community-wide woodstove changeout intervention on air quality within two schools. *Atmospheric Pollution Research, 4*, 238-244

Joyce, P.L., von Glasow, R., & Simpson, W.R. (2014). The fate of $NO_X$ emissions due to nocturnal oxidation at high latitudes: 1-D simulations and sensitivity experiments. *Atmospheric Chemistry and Physics, 14*, 7601-7616. doi: 10.5194/acp-14-7601-2014

Nattinger, K., Huff, D., & Simpson, W.R. (2014). Spatial and temporal analysis of the composition of fine particulates in Fairbanks, Alaska. Final Results Presentation.

Kotchenruther, R.A. (2016). Source apportionment of $PM_{2.5}$ at multiple Northwest U.S sites: Assessing regional winter wood smoke impacts from residential wood combustion. *Atmospheric Environment, 142*, 210-219. http://dx.doi.org/10.1016/j.atmosenv.2016.07.048

Excel Spreadsheets available as electronic files separately:

Precursor_Analysis_Serious_SIP_SMAT_2019

Preliminary_Precursor_20170306

Serious_SIP_SMAT_v0.5_042519

**SMAT (Speciated Modeled Attainment Test)**

EPA model guidance, "Guidance on the Use of Models and Other Analyses for Demonstrating Attainment of Air Quality Goals for Ozone, $PM_{2.5}$, and Regional Haze" (USEPA, 2007), recommends the Species Modeled Attainment Test (SMAT) to estimate future concentrations of daily $PM_{2.5}$ concentration. The method combines monitoring data with outputs from simulation models to estimate future $PM_{2.5}$ concentrations. It can be used to determine whether emission reductions will bring ambient concentrations to or below the National Ambient Air Quality Standard (NAAQS) (<=35 $\mu g/m^3$ for 24-hr $PM_{2.5}$). The SMAT is combined with other modeling techniques and relevant supplemental evidence to develop a technically-sound, weight-of-evidence recommendation on whether the proposed control strategies will meet the goal of pollution levels below the NAAQS.

SMAT recommends a nine-step process to take historically-measured $PM_{2.5}$ concentrations, apply factors to represent changes from the historical period to a future year, and estimate the future $PM_{2.5}$ design value (DV). The historically-measured $PM_{2.5}$ concentrations are sampled from the top 25% of polluted wintertime days within a five-year period. For each major chemical component of $PM_{2.5}$ (sulfates, nitrates, ammonium, organic carbon, elemental carbon; particle bound water, other primary particulate matter (Figure 1)), an air pollution model projects the change in concentration from the historical period to the future year. For instance, if the organic carbon concentration is projected to be in 2014 half of what it was in 2008, then the organic carbon concentration from the polluted days in the historical period is divided by two. The process is done for each chemical species and then summed across species to the get the projected future $PM_{2.5}$ after implementation of control strategies.

One important aspect of SMAT is how speciated $PM_{2.5}$ measurements from the Speciated Trends Network (STN) monitor are melded with the standard federal reference method (FRM) measurement of total $PM_{2.5}$ concentration. Care must be taken in this step because the STN monitor and FRM monitor use different measurement techniques. As the NAAQS are based on FRM monitored values, the speciated data from the STN monitor must be transformed into the values that would have been recorded by the FRM monitor. EPA modeling guidance in Section 5.1.4 describes this transformation technique, called Sulfate, Adjusted Nitrate, Derived Water, Inferred Carbonaceous material balance approach (SANDWICH), which follows the peer-reviewed, scientific methodology of Frank (2006) and references therein.

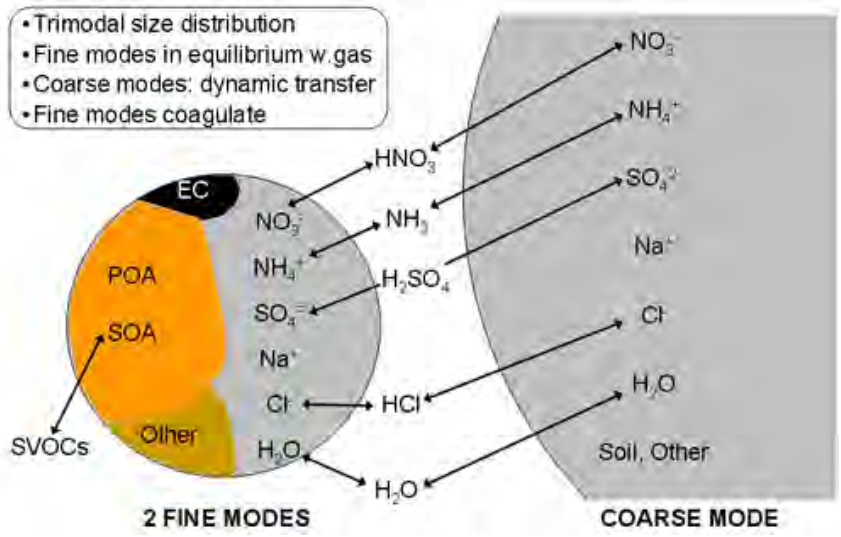


Figure 1: Major Components of $PM_{2.5}$
http://www.epa.gov/AMD/ModelDevelopment/aerosolModule.html

## STEP 1:

The first step in the SMAT analysis is to identify the high observed $PM_{2.5}$ days at each monitoring site for each year used for the baseline design value (DV). The baseline design value represents the pollution levels at the time the area violated the NAAQS and was designated nonattainment. In Fairbanks, the State Office Building is the only monitoring station that was used to determine a non-attainment area (NAA). Following the EPA emission inventory guidance (USEPA, 2005), 2008 was chosen as the base year, and following Section 3.1 of the EPA modeling guidance the baseline design value was calculated as an average of the 2006-2008, 2007-2009, and 2008-2010 three-year design values. The three-year design value is the same one as in the calculation of compliance with the PM2.5 NAAQS: an average of three consecutive years' worth of 98$^{th}$ percentiles. The baseline design value for the Fairbanks non-attainment area the design value is 44.7μg/m$^3$ (Table 1).

The baseline design value is not directly used in the calculation of the future year design value. Rather, the species-specific changes from the base (historical) year to the future year are applied to all the individual 24-hour averages in the 2006-2010 period and then the same procedure as used to calculate the baseline design value (98$^{th}$ percentiles for each year, three year design values, average of three year design values) is used to calculate the future design value (USEPA Update to the 24 hour PM2.5 NAAQS model attainment test, 2011). The baseline design value is not useless, however. The difference between the baseline design value and the NAAQS determines the overall reductions needed to reach attainment. After the amount of pollution reduction needed to reach attainment (9.2 μg/m$^3$) is divided by the number of years between designation of nonattainment and the Moderate Area attainment date (5), we arrive at the one year's worth of progress value relevant for Reasonable Further Progress and Contingency Measures (1.84 μg/m$^3$).

Table 1: The 98%-tile $PM_{2.5}$ (μg/m$^3$) concentration days and resulting 5-year rolling average DV for Fairbanks, excluding Exceptional Events[1].

| Year | High Concentrations | 98th Percentile | 3- year design value |
|---|---|---|---|
| 2006 | 51.9 | 42.2 | |
| | 42.2 | | |
| 2007 | 51.6 | 33.1 | |
| | 34.1 | | |
| | 33.1 | | |
| 2008 | 114.5 | 46.7 | 40.7 |
| | 50.7 | | |
| | 46.7 | | |
| 2009 | 59.0 | 51.0 | 43.6 |
| | 52.7 | | |
| | 51 | | |
| 2010 | 83.2 | 51.8 | 49.8 |
| | 57.1 | | |
| | 51.8 | | |
| 5-yr Baseline Design Value | | | 44.70 |

[1]Exceptional Events for the 2009 data have been flagged by DEC and concurred by EPA. 2010 Exceptional Events have been flagged by DEC and are in the EPA concurrence process. If the 2010 data is not concurred on by EPA, the baseline design value will be 51.8 $\mu g/m^3$. These Exceptional Events become official when EPA acts on them in the Federal Register, which will come when the EPA acts upon this SIP revision.

## STEP 2:

The intent of Step 2 to is to develop the average $PM_{2.5}$ chemical speciation for representative polluted days. For Fairbanks we designated the top 25% of winter days during Quarter 1 and 4 of 2006-2010—as indicated by the $PM_{2.5}$ concentration from the FRM filter -- for this task as a balance of choosing the relevant polluted days and having a statistically strong dataset to use (Table 2). We develop a post-SANDWICH average speciation for Quarter 1 (January, February, and March) and Quarter 4 (October, November, and December) separately, according to EPA modeling guidance. We then use the average of the Quarter 1 and Quarter 4 speciated concentration because Fairbanks experiences polluted days across all winter months.

We developed the species concentration fractions from the STN monitor located at the same State Office Building location as the violating FRM monitor. As mentioned previously, the speciated concentration from the STN measurement cannot be directly used as the speciated concentration from the FRM. The speciated concentration must be converted into the concentration that would have been measured by the FRM monitor after accounting for the differences between the instruments. For example, the FRM measurements do not capture all ambient particles, loss of ammonium nitrate, and addition of particle bound water (PBW) from the STN speciation measurement. The SANDWICH method (Frank, 2006) carries out this conversion process and is described briefly below. We followed the SANDWICH method described from Frank and by EPA modeling guidance exactly in most cases, but made a couple changes specific to woodsmoke-dominated areas in consultation with the EPA Regional Office and in collaboration with other states with woodsmoke issues.

Table 2: The top 25% of high $PM_{2.5}$ ($\mu g/m^3$) days at the State Office Monitor for the years 2006-2010 for Quarter 4 (Q4) and Quarter 1 (Q1).

| Q4 Date | Q4 FRM Concentration ($\mu g/m^3$) | Q1 Date | Q1 FRM Concentration ($\mu g/m^3$) |
|---|---|---|---|
| 20081229 | 114.5 | 20100126 | 83.2 |
| 20071220 | 51.6 | 20090107 | 59 |
| 20091209 | 51 | 20090110 | 52.7 |
| 20081114 | 50.7 | 20060117 | 51.9 |
| 20081202 | 46.7 | 20100102 | 51.8 |
| 20091230 | 43.1 | 20100105 | 51.8 |
| 20091221 | 41.5 | 20100108 | 44.4 |
| 20101201 | 41.2 | 20060111 | 42.2 |
| 20091212 | 40.8 | 20080209 | 40.4 |
| 20081214 | 38.3 | 20090104 | 39 |
| 20081108 | 37 | 20100120 | 38.1 |
| 20101207 | 36.9 | 20060105 | 38 |
| 20091124 | 35.3 | 20100111 | 36.9 |
| 20081217 | 34 | 20070205 | 34.1 |
| 20071223 | 33 | 20070223 | 33.1 |
| 20061219 | 32.1 | 20060129 | 32.7 |
| 20061125 | 31.1 | 20100204 | 31.5 |
| 20071129 | 29.6 | 20100213 | 30.9 |
| 20081223 | 29.1 | 20070220 | 29.7 |
| 20081111 | 27.4 | 20070127 | 29.6 |
| 20081205 | 27.1 | 20090113 | 29.1 |
| 20071217 | 26.7 | 20100201 | 28.8 |
| 20091121 | 26.2 | 20100123 | 28.5 |
| 20081220 | 25.7 | 20070301 | 28.2 |
| 20091227 | 25.2 | 20090215 | 28 |
| 20101210 | 25.2 | 20090101 | 27.7 |
| 20091206 | 25.1 | 20060123 | 27.6 |
| 20061119 | 23.7 | 20100129 | 27.4 |
| 20081123 | 23.6 | 20070112 | 26.7 |
| 20061207 | 22.8 | 20090125 | 26.2 |
| 20071111 | 22.7 | 20100216 | 26 |

SANDWICH addresses the 7 major measured components of $PM_{2.5}$:

- Measured sulfate [$SO_{4STN}$]
- Adjusted nitrate [$NO_{3FRM}$] (retained on the FRM filter)
- Adjusted ammonium [$NH_4FRM$] (retained on the FRM filter)
- Measured elemental carbon [$EC_{STN}$] (corrected IMPROVE to NIOSH analysis)
- Organic carbonaceous mass estimated from a mass balance [OCMmb]
- Estimated particle bound water [PBW]
- Estimated other primary $PM_{2.5}$ components [OPP]

Measured sulfate

There are no major differences in how the STN and FRM instruments measure sulfate. It is assumed that the sulfate measured by the STN is equal to what was captured by the FRM.

Retained Nitrate Mass

Nitrate volatilizes from the FRM filter but not the STN measurement. SANDWICH calculates the amount that would have volatilized if the amount of nitrate measured by STN had been deposited on the FRM filter. The volatilized nitrate mass concentration, delta $NO_3$, in units of μg/m$^3$ is

$$\Delta NO_3 = \frac{745.7}{T_R(K)} x \frac{1}{24} \sum_{i=1}^{24} K_i^{1/2}$$ Eq. 5.2 (USEPA, 2007) ;( Eq. 5, (Frank, 2006)).

The dissociation constant for ammonium nitrate ($K_i$) is evaluated for every hour of every day of nitrate measurements we are using for the analysis. The hourly temperature and relative humidity data used for the associated equations (Frank, 2006) in determining $K_i$ are from the Fairbanks Airport (PAFA). The reference temperature $T_R$ in Eq. 5.2 is the daily average ambient temperature and then $\Delta NO_3$ averaged to 24-hour. The retained nitrate [$NO_{3FRM}$] is estimated by

$NO_{3FRM} = NO_{3STN} - \Delta NO_3$.

A limit was applied to $NO_{3FRM}$ as follows,

If $NO_{3FRM} < 0$, then $NO_{3FRM} = 0$.

The potential nitrate loss using local Fairbanks meteorology is shown in Figure 2. The graph is labeled as potential nitrate loss, because the loss of nitrate is bound by the nitrate on the filter ($NO_{3FRM}$). The amount of nitrate volatilization during the winter in Fairbanks is low. The maximum nitrate loss of all the days analyzed from 2006-2010 was 1.2 μg/m$^3$ and was during the summer on exceptional event day.

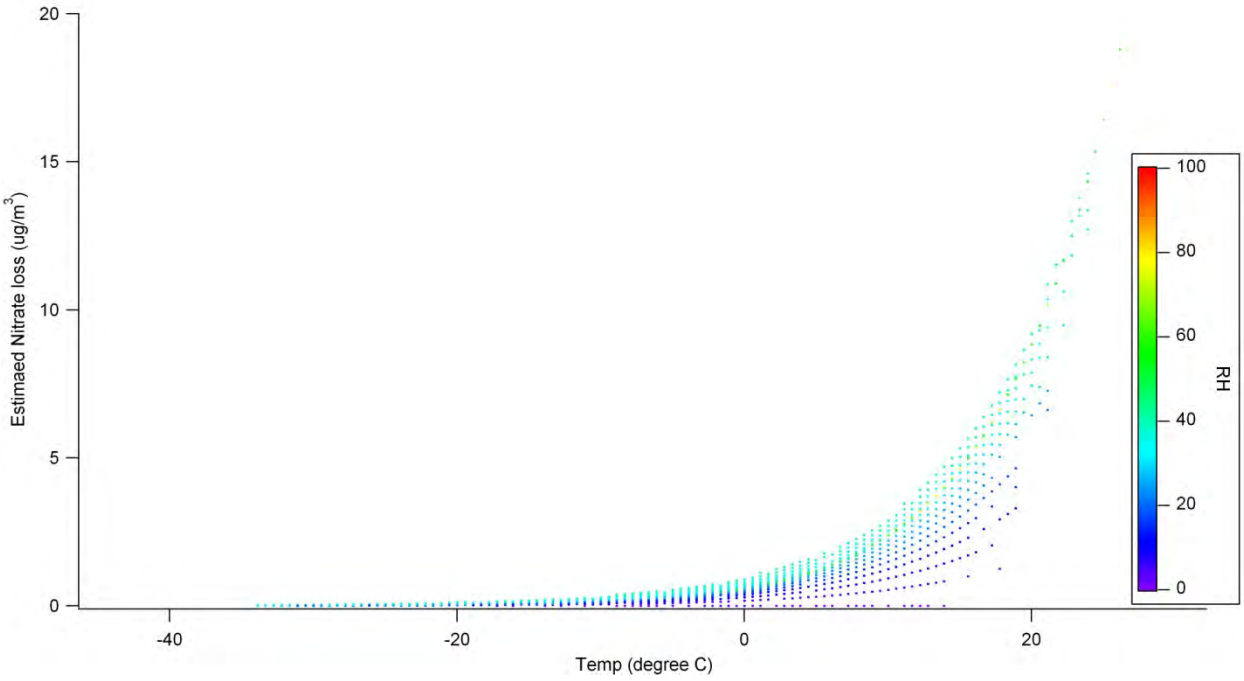


Figure 2: Fairbanks Potential 1-hr $NO_3$ loss as a function of temperature and relative humidity.

Adjusted Ammonium Mass

EPA modeling guidance recommends using the measured STN ammonia ($NH_4$) as the measured FRM ammonia. Many of the questions raised in the guidance about the validity of such a recommendation are not problems in Fairbanks because Fairbanks winters are very cold and the amount of ammonium nitrate volatilization is very small. Thus,

$[NH_{4FRM}] \cong [NH_{4STN}]$.

In cases where the ammonia concentration exceeds the amount necessary to neutralize the FRM sulfate and nitrate, the ammonia concentration was adjusted to ensure charge balance. This is a deviation from the USEPA recommended adjustment, but has been noted in other adjusted ammonium concentration calculations (Turner, 2010). The adjustment used was:

$NH_{4FRM} = 2 \times SO_4^{2-} + NO_{3FRM} - H^+$ when $H^+ > 0$ or else $H^+ = 0$

The hydrogen ion concentration results from the calculation of particle bound water, as described below.

Elemental Carbon Mass

Elemental carbon (EC) concentrations as measured by the STN instrument are used directly as the concentrations for the FRM measurement. In October 2009, the STN instrument at the Fairbanks State Office Building changed its technique for measuring elemental and organic carbon; the MetOne SASS using the NIOSH analysis method was replaced with the URG 3000N using the IMPROVE analysis method. Since most of the measurements were made on the SASS sampler and NIOSH method and evidence of high wood smoke $PM_{2.5}$ areas are more accurately measured by the NIOSH method, the EC

measurements from October 2009 on were corrected to reflect the NIOSH method (Hixson, 2011). Traditionally in the Lower 48 the NIOSH data is corrected to reflect the IMPROVE method, but the opposite makes sense for the particular case of a wood smoke dominated area with primarily NIOSH data in the 2006-2010 analysis timeframe.

$EC_{FRM} = EC_{SASS/NIOSH}$ (Before October 2009)
$EC_{FRM} = (EC_{URG/IMPROVE} * 0.5722) + 0.2509$ (After October 2009)

Other primary $PM_{2.5}$ components

We calculate the other primary $PM_{2.5}$ (OPP) directly as recommended by EPA modeling guidance:

OPP= 3.73 x [*Si*] + 1.63 x [*Ca*] + 2.42 [*Fe*] + 1.94 x [*Ti*].

Particle Bound Water Mass

Because the STN speciation does not measure the particle bound water (PBW) that would be present in the $PM_{2.5}$ if it were being measured by a FRM monitor, we calculate the PBW with the Aerosol Inorganic Model II (http://www.aim.env.uea.ac.uk/aim/model2/model2a.php). Inputs to the model are using the ammonia, nitrate, and sulfate concentrations as calculated above. As suggested by Frank (2006), the model is evaluated at 295K and 35% RH because these are the equilibrium atmospheric conditions under which the FRM filter is weighed in the laboratory. In the model we assume there is no ammoniated compound solid formation and us the following ion mass balance equation:

$H^+ = [2 \times SO_4^{2-}] + NO_3^- - NH_4^+$.

The measured sulfate, retained nitrate mass and adjusted ammonium mass allowed an estimated hydronium ion proton molar concentration and a PBW water mass was directly calculated from the AIM model.

Organic Carbonaceous Mass

SANDWICH estimates organic carbonaceous mass, [OCMmb], as the amount that is not explained by other chemical species:

$OCMmb = [PM2.5_{FRM}] - \{[SO_{4STN}] + [NO_{3FRM}] + [NH_{4FRM}] + [EC_{FRM}] + [OPP] + [PBW] + 0.5$

The STN instrument measures organic carbon directly, but the techniques to quantify the organic mass have considerable uncertainties. The mass balance technique is reasonable since all other species can be well-quantified and it is likely the remaining mass is organic carbon. As a benefit mass closure is assured. To guard against spurious results, the organic carbon mass is bound on the lower end by 70% of the measured organic carbon and on the upper end by 80% of the total mass. As with the elemental carbon concentration, organic carbon concentrations obtained with the URG/IMPROVE method were converted using the correlation in Hixon (2011) to the SASS/NIOSH method. When a bound is applied, the speciated concentration no longer adds up to the total concentration. When this happens all species are adjusted proportionally such that they add up to the total measured concentration by the FRM instrument. The upper bound was never invoked by the Fairbanks data set, while the lower bound was used on three

occasions (5% of the total dataset). The concentration closure adjustment in these three cases modified the sum of the species' concentration by less than 10%.

Quarterly average FRM-derived species concentration fractions

The SANDWICH process is done separately for every 24-hour measurement in the dataset. The top 25% polluted days in 2006-2010 for Quarter 1 and Quarter 4 represent 31 and 27 samples, respectively. The average speciation for Quarter 1 and Quarter 4 is presented in Table 3 and Figures 4-5. These values represent the chemical composition of $PM_{2.5}$ on polluted wintertime days in Fairbanks for the baseline 2006-2010 period.

Table 3: Quarterly average percentage of SANDWICH'ed $PM_{2.5}$, calculated from the top 25% of $PM_{2.5\ days}$ for years 2006-2010

| | $SO_{4STN}$ | $NO_{3FRM}$ | $NH_{4FRM}$ | PBW | $EC_{URG/IM>SASS/NI}$ | OPP | $OCMmb_{URG/IM>SASS/NI}$ |
|---|---|---|---|---|---|---|---|
| Q4 | 17.40% | 3.64% | 7.57% | 5.82% | 6.89% | 1.25% | 57.43% |
| Q1 | 19.15% | 5.0% | 8.54% | 6.27% | 6.19% | 1.01% | 53.82% |

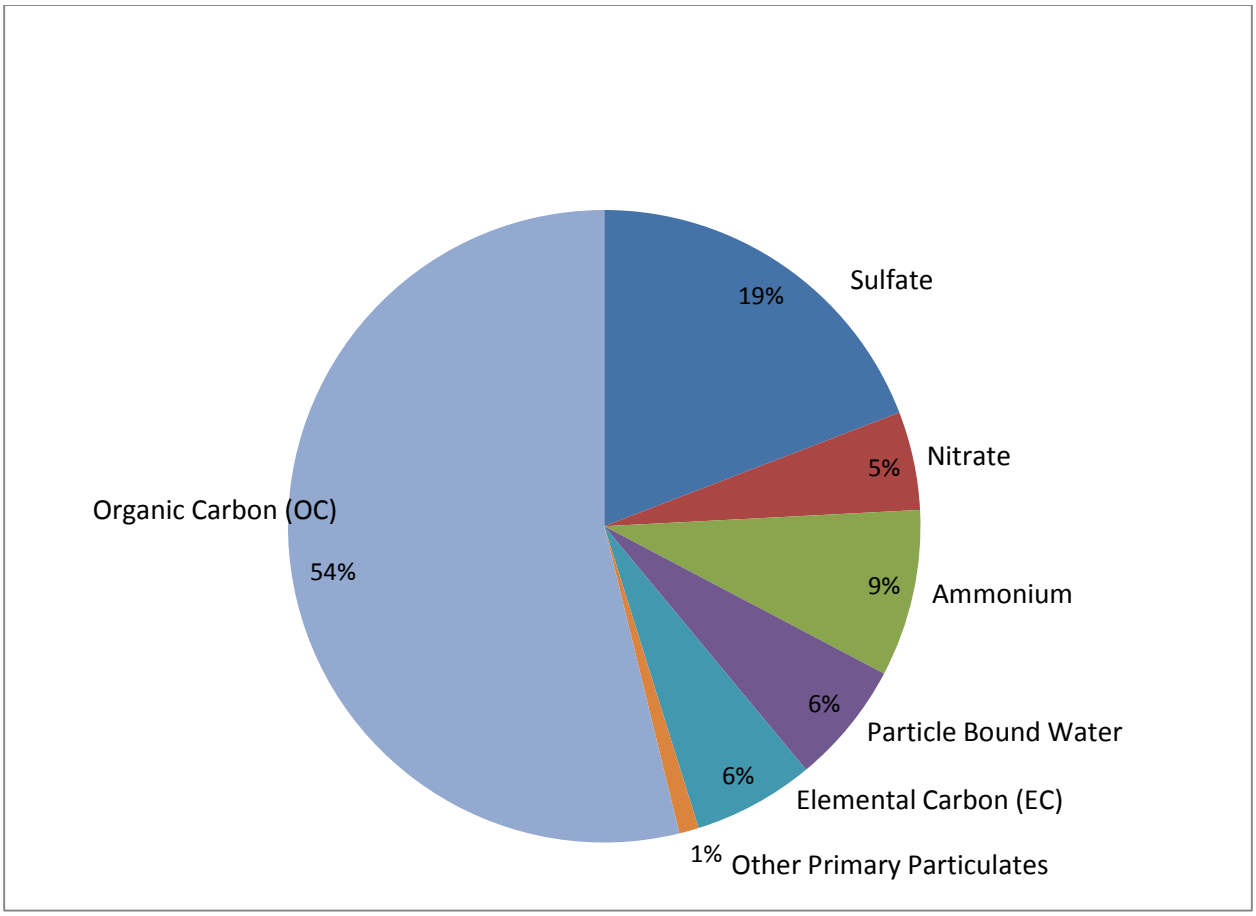


Figure 4: Quarter 1, FRM-derived species percentage of high 24-hr average $PM_{2.5}$ days from the Fairbanks State Office Building for years 2006-2010.

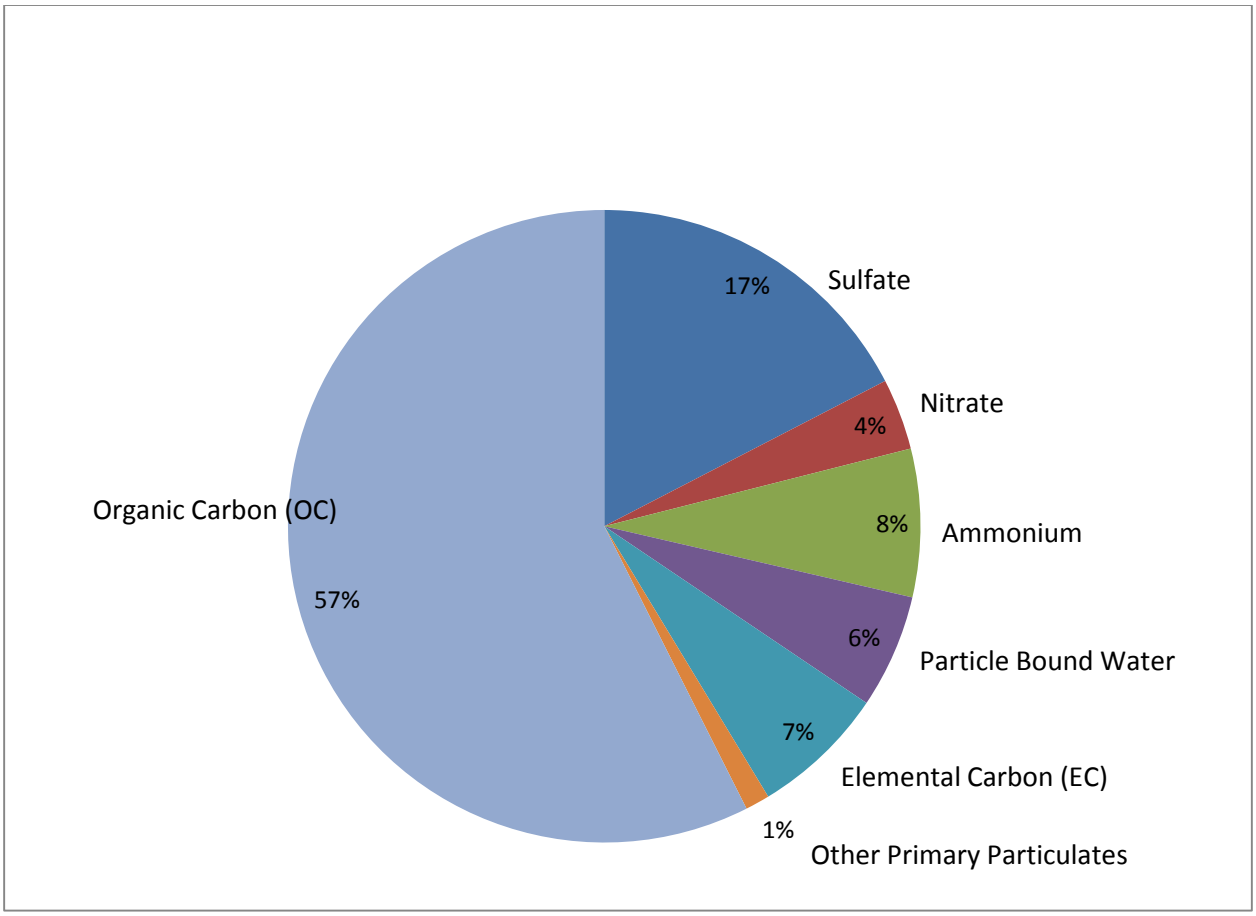


Figure 5: Quarter 4, FRM-derived species percentage of high 24-hr average $PM_{2.5}$ days from the Fairbanks State Office Building for years 2006-2010.

After SANDWICH was complete and the Q1 and Q4 average species concentrations and percentages were calculated (Table 4), the average species percentage was multiplied by the baseline design value of 44.7 $\mu g/m^3$ from Step 1. While not necessary for the model attainment test, this information has been helpful in guiding other parts of the attainment plan.

Table 4: Averaged Quarter 1 and 4, FRM-derived species percentage of high $PM_{2.5}$ days and average concentration based on the baseline design value (DV) of 44.7$\mu g/m^3$.

| Species | Sulfate | Nitrate | Ammonium | Water | elemental carbon | OPP | Organic carbon |
|---|---|---|---|---|---|---|---|
| Q4 % | 17.40 | 3.64 | 7.57 | 5.82 | 6.89 | 1.25 | 57.43 |
| Q1 % | 19.15 | 5.03 | 8.54 | 6.27 | 6.19 | 1.01 | 53.82 |
| Average of Q1 and Q4 % | 18.28 | 4.34 | 8.05 | 6.05 | 6.54 | 1.13 | 55.62 |
| Average DV($\mu g/m^3$) | 8.17 | 1.94 | 3.60 | 2.70 | 2.92 | 0.50 | 24.86 |

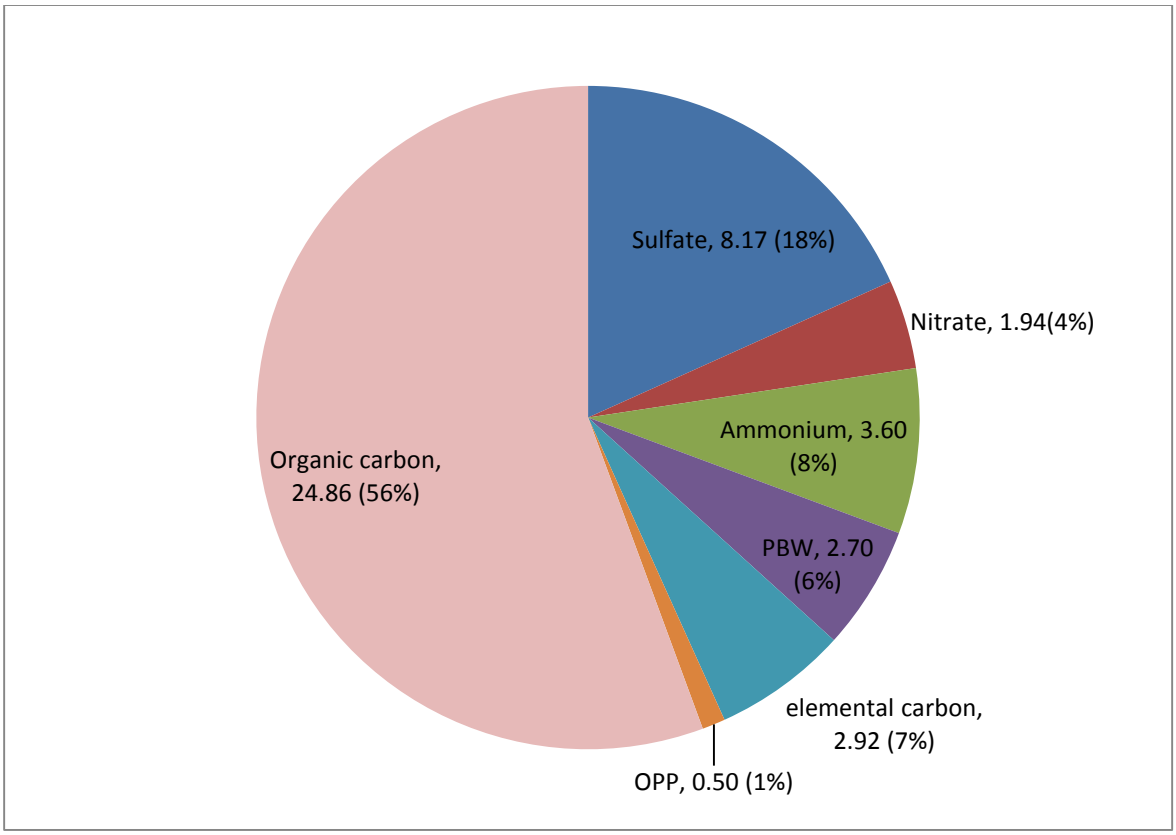


Figure 6: Averaged Quarter 1 and 4, FRM-derived species percentage of high PM2.5 days from years 2006-2010 and average concentration based on the baseline design value (DV) of 44.7 µg/m$^3$.

## Step 3: Calculate species concentration for each of the high ambient days

Step 3 calculates the concentration of chemical species on each of the high ambient days in 2006-2010. For example, the highest $PM_{2.5}$ from 2006 was 51.9 µg/m$^3$ on January 17$^{th}$ (see Table 1,STEP1), Using the Quarter 1 average speciation percentages (Table 4), we calculate the species concentrations in µg/m$^3$on that day at the Fairbanks State Office Building in Table 5:

Example for sulfate:

51.9 µg/m$^3$ - 0.5 µg/m$^3$ (blank filter) = 51.4 µg/m$^3$ x 0.1915 (SO4, Q1 % from Table 3) = 9.84 µg/m$^3$

Table 5: $PM_{2.5}$ Species concentrations in µg/m$^3$ for the highest day in the year 2006

| Date | FRM PM2.5 | Blank | Non blank FRM | Sulfate | Nitrate | Ammonium | Water | Elemental Carbon | OPP | Organic Carbon |
|---|---|---|---|---|---|---|---|---|---|---|
| 1/17/06 | 51.9 | 0.50 | 51.40 | 9.84 | 2.58 | 4.39 | 3.22 | 3.18 | 0.52 | 27.66 |

The same process is done for the top 25% of high days during the winter (Quarter 1 and 4) and all of these high days are listed in Table 2, STEP 2.

## STEP 4: Calculate the component specific RRFs (Relative Response Factor)

The relative response factor is a ratio between the modeled projected concentrations divided by the present baseline modeled concentration for each species. Two episodes from 2008 are modeled using emissions from 2008 (present baseline) and then using emissions from 2015 (future baseline) plus emission reductions from emission reduction strategies (future control). The modeled concentrations from the 2015 future control case are divided by the modeled concentrations from the 2008 present baseline. This is done for each chemical species and for every grid cell of the modeling domain. The result is a table of RRFs similar to Table 5, which is just an illustration for explanatory purposes. The RRFs for the emission reductions proposed in this attainment plan are presented in Chapter 5.9. Concentrations in the both the present and future model runs are calculated as 24-hour average values for each component of PM for the baseline and each component of the future. Then the future components were divided by the baseline for the episode-long 24-hour PM species averages for all episode days except for the two model spin up days at the start of each episode. The resulting RRFs for the modeled State Office Building grid cell are in Table 6. Table 7 shows an example of data from the high days of 2008 with the species-specific RRFs applied in order to calculate the concentration of each $PM_{2.5}$ chemical species in 2015 given a scenario of emission controls.

Example calculation:

Sulfate RRF = 2015 future modeled concentration x 2008 baseline modeled concentration = 0.89 RRF

Sulfate RRF = 8.78/9.82 = 0.89 RRF

Table 6: Relative Response Factor (RRF) example averaged over days in episode 1 and 2 derived from a present baseline 2008 simulation and future year control strategies.

| Species | Sulfate | Nitrate | Ammonium | Water | Element Carbon | OPP | Organic Carbon |
|---|---|---|---|---|---|---|---|
| RRF | 0.89 | 0.95 | 0.94 | 1.00 | 0.88 | 0.99 | 0.77 |

There are no RRFs for particle bound water or the blank, they do not change as control strategies changes. For example, in Table 6, the OCMmb (organic carbon mass balance) RRF is 0.77 and a large decrease in OC is observed from controls that largely only affect organic carbon.

## STEP 5-6: Apply the component specific RRFs to the observed air quality by quarter

Step 5-7 are represented as an example in Table 7 for the year 2008, high $PM_{2.5}$ days and the species are added together to calculate the future year $PM_{2.5}$ species (step6). The left side of the Table 7 follows the exact same method as shown in Table 5 for January 17$^{th}$, 2006. The FRM derived species concentrations based on the Sandwich method on the left and the right side is the future species concentrations based on the example RRFs in Table 6.

Example calculation for future sulfate:

Future Sulfate = 2008 FRM-derived species concentration x 2015 sulfate RRF = 17.66 μg/m$^3$

Future Sulfate = 19.84 x 0.89 = 17.66 μg/m$^3$

Table 7: Example RRF future year concentrations based on the RRFs in Table 5 and the top high days in year 2008.

| Observed FRM PM 2.5 | Blank | Non blk FRM | Observed Sulfate | Observed Nitrate | Observed Ammonium | Water | Observed Elemental Carbon | OPP | Observed Organic Carbon | | Future Sulfate | Future Nitrate | Future Ammonium | Water | Future Elemental Carbon | Future OPP | Future Organic Carbon | Blank | Future FRM |
|---|---|---|---|---|---|---|---|---|---|---|---|---|---|---|---|---|---|---|---|
| 114.5 | 0.50 | 114.00 | 19.84 | 4.16 | 8.62 | 6.64 | 7.85 | 1.42 | 65.47 | | 17.66 | 3.95 | 8.11 | 6.64 | 6.91 | 1.41 | 50.41 | 0.50 | 95.58 |
| 50.7 | 0.50 | 50.20 | 8.74 | 1.83 | 3.80 | 2.92 | 3.46 | 0.63 | 28.83 | | 7.78 | 1.74 | 3.57 | 2.92 | 3.04 | 0.62 | 22.20 | 0.50 | 42.37 |
| 46.7 | 0.50 | 46.20 | 8.04 | 1.68 | 3.50 | 2.69 | 3.18 | 0.58 | 26.53 | | 7.16 | 1.60 | 3.29 | 2.69 | 2.80 | 0.57 | 20.43 | 0.50 | 39.03 |
| 40.4 | 0.50 | 39.90 | 7.64 | 2.01 | 3.41 | 2.50 | 2.47 | 0.40 | 21.47 | | 6.80 | 1.91 | 3.20 | 2.50 | 2.17 | 0.40 | 16.54 | 0.50 | 34.02 |
| 40.4 | 0.50 | 39.90 | 6.94 | 1.45 | 3.02 | 2.32 | 2.75 | 0.50 | 22.91 | | 6.18 | 1.38 | 2.84 | 2.32 | 2.42 | 0.49 | 17.64 | 0.50 | 33.78 |
| 38.3 | 0.50 | 37.80 | 6.58 | 1.38 | 2.86 | 2.20 | 2.60 | 0.47 | 21.71 | | 5.86 | 1.31 | 2.69 | 2.20 | 2.29 | 0.47 | 16.72 | 0.50 | 32.03 |
| 37 | 0.50 | 36.50 | 6.35 | 1.33 | 2.76 | 2.13 | 2.51 | 0.46 | 20.96 | | 5.65 | 1.26 | 2.60 | 2.13 | 2.21 | 0.45 | 16.14 | 0.50 | 30.94 |
| 34 | 0.50 | 33.50 | 5.83 | 1.22 | 2.53 | 1.95 | 2.31 | 0.42 | 19.24 | | 5.19 | 1.16 | 2.38 | 1.95 | 2.03 | 0.41 | 14.81 | 0.50 | 28.44 |
| 32.6 | 0.50 | 32.10 | 5.59 | 1.17 | 2.43 | 1.87 | 2.21 | 0.40 | 18.43 | | 4.97 | 1.11 | 2.28 | 1.87 | 1.95 | 0.40 | 14.19 | 0.50 | 27.27 |
| 25.9 | 0.50 | 25.40 | 4.86 | 1.28 | 2.17 | 1.59 | 1.57 | 0.26 | 13.67 | | 4.33 | 1.21 | 2.04 | 1.59 | 1.38 | 0.25 | 10.53 | 0.50 | 21.84 |
| 23.7 | 0.50 | 23.20 | 4.44 | 1.17 | 1.98 | 1.45 | 1.44 | 0.23 | 12.49 | | 3.95 | 1.11 | 1.86 | 1.45 | 1.26 | 0.23 | 9.61 | 0.50 | 19.99 |
| 23.5 | 0.50 | 23.00 | 4.40 | 1.16 | 1.96 | 1.44 | 1.42 | 0.23 | 12.38 | | 3.92 | 1.10 | 1.85 | 1.44 | 1.25 | 0.23 | 9.53 | 0.50 | 19.82 |
| 23.4 | 0.50 | 22.90 | 4.39 | 1.15 | 1.96 | 1.44 | 1.42 | 0.23 | 12.32 | | 3.90 | 1.09 | 1.84 | 1.44 | 1.25 | 0.23 | 9.49 | 0.50 | 19.74 |
| 21.5 | 0.50 | 21.00 | 4.02 | 1.06 | 1.79 | 1.32 | 1.30 | 0.21 | 11.30 | | 3.58 | 1.00 | 1.69 | 1.32 | 1.14 | 0.21 | 8.70 | 0.50 | 18.14 |
| 19.8 | 0.50 | 19.30 | 3.70 | 0.97 | 1.65 | 1.21 | 1.19 | 0.19 | 10.39 | | 3.29 | 0.92 | 1.55 | 1.21 | 1.05 | 0.19 | 8.00 | 0.50 | 16.71 |
| 19.5 | 0.50 | 19.00 | 3.64 | 0.96 | 1.62 | 1.19 | 1.18 | 0.19 | 10.23 | | 3.24 | 0.91 | 1.53 | 1.19 | 1.03 | 0.19 | 7.87 | 0.50 | 16.46 |
| 14.4 | 0.50 | 13.90 | 2.22 | 0.00 | 0.80 | 0.77 | 0.76 | 2.07 | 7.28 | | 2.22 | 0.00 | 0.80 | 0.77 | 0.76 | 2.07 | 7.28 | 0.50 | 14.40 |

## Step 7: Sum the species components to get total $PM_{2.5}$ concentrations for each day

The species concentrations from the future year are added together to arrive at the modeled projected concentrations given changes in emissions between 2015 and 2008 plus changes from emission controls. Table 7 is the result of this process for when or example RRFs (from Step5) are applied to our high ambient days (from Step1). It is an estimate of the $PM_{2.5}$ concentration that would have been observed in 2006-2010 if the area had the pollutant emissions from 2015 and from the proposed emission control strategy. The result of this process for the emission controls proposed in this attainment plan is in Section Chapter 5.6 and Appendix 5.6.

## Step 8: Determine future year 98th percentile concentrations for each site year.

The 98th percentile concentration is usually the 3rd highest concentration from a year for the sampling schedule followed in 2006-2010 but it depends on how many valid samples were obtained from the year [Appendix N reference]. For the 2006 $PM_{2.5}$ data, the 2nd highest concentration is the 98th percentile and is the 3rd highest for 2007 through 2010. Table 8 identifies the 98th percentile for the future year control case.

## Step 9: Calculate future 5 year 24-hr DV.

The future year control design value is calculated as an average of the 3-year design values from 2006-2008, 2007-2009, and 2008-2010. For our example case:

Table 8: Baseline and Future 5-year Design Values based example RRFs (Table 5)

| Year | **98%-tile** | **98%-tile** |
|---|---|---|
| 2006 | 42.2 | 36.6 |
| 2007 | 33.1 | 28.7 |
| 2008 | 46.7 | 39.0 |
| 2009 | 51.0 | 45.6 |
| 2010 | 51.8 | 44.9 |
| **Design Values** | **44.70** | **38.6** |

References

Frank, N.H. (2006): Retained Nitrate, Hydrated Sulfates, and Carbonaceous Mass in Federal Reference Method Fine Particulate Matter for Six Eastern U.S. Cities.

Hixson, M. (2011): Reconciling Trends in Carbon Measurements for Fairbanks 2006-2010.

Turner, J. (2010): $PM_{2.5}$ Species Mass Fractions for the Species Modeled Attainment Test.

USEPA (2007): Guidance on the Use of Models and Other Analyses for Demonstrating Attainment of Air Quality Goals for Ozone, $PM_{2.5}$ , and Regional Haze, EPA-454/B-07-002,United States Environmental Protection Agency, Office of Air Quality Planning and Standards, April 2007.

USEPA (2011): Attachment A and B. http://www.epa.gov/ttn/scram/guidance/guide/Update_to_the_24-hour_PM25_Modeled_Attainment_Test.pdf

USEPA(1993): Appendix N.

Final Report

To

Environmental Protection Agency (EPA)

Purchase order EP08D000663

Reporting Period: 1 September 2008 – 31 January 2010

# 'Stable Boundary Layers Representation in Meteorological Models in Extremely Cold Wintertime Conditions'

Dr. Brian J. Gaudet, co-PI

Dr. David R. Stauffer, co-PI

The Pennsylvania State University

Dept. of Meteorology

University Park, PA 16802

bjg20@met.psu.edu

12 May 2010

## EXECUTIVE SUMMARY

This final report describes work performed by Penn State for the EPA-funded Purchase Order EP08D000663 titled 'Stable Boundary Layers Representation in Meteorological Models in Extremely Cold Wintertime Conditions'. The purpose of the project was to develop, adapt, and test a methodology for stable boundary layer representation (initial onset, space/time evolution, dissipation) in three-dimensional numerical models, with a specific focus on the dark, extremely cold environments such as those in the winter in the Fairbanks, AK region. A particular concern is the frequent occurrence of very high fine particular matter (PM2.5) concentrations within the stable boundary layers that form in these conditions.

Ten tasks were defined in the Statement of Work (SOW) for this project. A summary of these tasks and a brief overview of the work completed can be found in the Appendix to this report. Two twenty-day episodes were selected from the 2007-2008 winter season to study periods of extremely cold temperatures and high PM2.5 concentrations and to evaluate model performance: one in near total darkness (14 Dec 2007 – 03 Jan 2008), and the other in partial sunlight (23 Jan 2008 – 12 Feb 2008). One baseline physics configuration and three physics sensitivity experiments were performed for each episode. The physics sensitivity experiments were used to assess the impact of different planetary boundary layer (PBL) parameterizations, land surface models, and atmospheric radiation schemes on the simulations. Each simulation used three nested grids: Grid 1 (12-km horizontal grid spacing) and Grid 2 (4-km) utilized the multiscale multigrid data assimilation strategy of Stauffer and Seaman (1994) in order to ensure the model and observations remain close over the extended duration of the simulations, and Grid 3 (1.3-km) did not use any direct data assimilation, and so was best-suited for quantifying the physics sensitivity. Grid 3, which is centered over the Fairbanks region, also possesses sufficient horizontal resolution to be used by the EPA as meteorological input to chemical and air transport and dispersion models. From the different physics packages one was to be recommended to the EPA for further mesoscale modeling of the region.

The major findings and impacts of this project are as follows:

- The use of the three-grid configuration with a multiscale, multigrid four-dimensional data assimilation (FDDA) strategy on the outer two grids and no direct FDDA on Grid 3 consistently produced qualitatively plausible atmospheric fields throughout the variety of meteorological conditions found in the episodes, despite the relatively sparse data density. Quantitatively, the multiscale, multigrid FDDA strategy led to improved root-mean-square-error (RMSE) scores for both wind and temperature on all grids. The FDDA on the outer domains had the desired effect of improving the simulations of Grid 3 without FDDA and used for physics sensitivity tests, by providing improved lateral boundary conditions.

- The best RMSE scores for the combination of both surface and sounding data required modification of the default FDDA procedure. These modifications included applying surface wind observational data to the third model vertical level instead of the lowest model level because wind observations are normally taken at a height of 10 m which is the height of the third level in the high vertical resolution configuration used here. The influence of surface observations was also restricted to approximately the lowest 100 m, instead of the top of the PBL, because the model-predicted PBL height in these simulations, based on the turbulent kinetic energy profile, was often found to be 1 km or higher. This correction applied the surface innovation (observation minus model value) in these predominantly stable boundary layers over a much shallower layer and produced improved statistical results in the lower troposphere.

- All model physics combinations tended to have a positive temperature bias on Grid 3, especially during the most extremely cold periods. All of the physics sensitivity tests tended to reduce the warm bias in comparison with the selected baseline physics package.

- Switching from the RRTM longwave / Dudhia shortwave radiation package to the RRTMG longwave and shortwave radiation package led to significantly reduced warm biases and better RMSE statistics. RRTMG was then used in all future physics sensitivity tests. The reduced warm bias seemed to be due to the longwave component, both because of direct examination of surface fluxes in the partial sunlight case, and due to the fact that the difference was more pronounced in the near total darkness episode.

- The simulation with the Rapid Update Cycle (RUC) land surface model, the Mellor-Yamada-Janjić (MYJ) PBL model, and the RRTMG radiation package was the coldest of the four physics suites tested, and had the lowest positive temperature bias and best statistics during those periods when the temperature was coldest. It was thus selected as the physics configuration of choice, since the coldest temperature conditions are those with the potential for the highest PM2.5 concentrations. However, there were periods in each episode, generally when the temperature was steadily decreasing in advance of an extremely cold period, during which the models had a cold bias. During these periods the RUC/MYJ/RRTMG configuration would usually be even colder and thus have worse magnitude temperature biases and RMSE scores. Thus, while this configuration was recommended, we also strongly recommended that the final fine-scale atmospheric data (i.e., from Grid 3) to be provided to EPA should come from an additional simulation in which FDDA is performed directly on Grid 3, in order to reduce some of this error.

- Wind component and wind speed statistics generally showed much less variability among the model physics sensitivity experiments than that seen for temperature. The MYJ/RUC/RRTMG (MRR) configuration usually produced slightly better wind statistics than the other configurations.

- Use of obs nudging for temperature and humidity (and not surface wind) on Grid 3 produced large improvements in the mass fields as expected, and also improvements in the wind fields

above the surface. Results were very encouraging and suggested that a smaller (larger) time window should be used for the surface (above-surface) data assimilation. This capability present in the Penn State MM5 FDDA system has been added to the new-release version of WRF.

- In addition to this final report, deliverables to the EPA will include the full three-dimensional output at relatively fine temporal resolution (every 1 hour for Grid 1; every 12 minutes for Grids 2 and 3) for the final Grid 3 nudging simulation as well as all the baseline and physics sensitivity simulations. Model namelists, initialization files, and modifications to the model source code will also be provided.

- The development and refinement of WRF FDDA capabilities and supporting software, including the surface analysis nudging, observation nudging and the OBSGRID objective analysis and obs-nudging pre-processing code, occurred concurrently with this project. This separate development effort led by PI Dave Stauffer and funded by the Defense Threat Reduction Agency (DTRA) allowed us rapid access to the most recent and robust versions of the WRF FDDA code, and this greatly benefited this project.

- The results of the default FDDA procedures not performing well in this high vertical resolution modeling study of stable boundary layer environments motivated an additional FDDA code development effort to make the vertical influence functions of surface observations within the FDDA be a function of stability regime type, as well as to provide the user with greater flexibility in specifying the vertical influence functions. These modifications were not finalized in time to be used for this project but are scheduled to appear in the next official release of the WRF model.

- An extended abstract and oral presentation were made at the 13$^{th}$ Conference on Mesoscale Processes (Gaudet et al. 2009), and a manuscript based on the project is in preparation.

- Since the first draft of the final report, the Grid 3 FDDA design and simulations have been completed for both twenty-day episodes. The results showed that the use of obs nudging for temperature and humidity (but not surface wind) on Grid 3 produced large improvements in the mass fields (as expected), and also improvements in the wind fields above the surface. Results were very encouraging and suggested that a smaller (larger) time window should be used for the surface (above-surface) data assimilation. This capability present in the Penn State MM5 FDDA system has been added to the new-release version of WRF.

## 1. INTRODUCTION

Fine particulate matter (PM2.5, referring to particles with aerodynamic diameters equal or less than 2.5 microns) has been implicated in a variety of health problems, including respiratory disease. With the recent decrease in the allowable 24-hour PM2.5 concentration to 35 micrograms per cubic meter, there is now an even greater need to be able to determine the sources primarily responsible for exceedance events when they occur, as well as to predict the potential impact of source emission changes. Modeling the behavior of fine particulate matter typically involves coupling between an inventory of emissions sources, chemical and air transport and dispersion models, and synoptic and mesoscale atmospheric models. (Synoptic atmospheric models are designed to represent features with characteristic horizontal scales greater than about 2000 km; mesoscale atmospheric models represent features with scales of approximately 2 – 2000 km.) The purpose of the meteorological models is to use physical predictive equations and assimilation of available meteorological data to capture the evolution of the local atmospheric state over sufficiently long periods for use by the other models.

During the winter season the part of interior Alaska consisting of Fairbanks and the surrounding Fairbanks North Star Borough often have extremely cold temperatures due to the strong longwave radiative cooling, the absence of moderating marine influences, and the generally weak winds. Although this region often has a clean, relatively pristine atmosphere, the periods of coldest temperatures are often accompanied by some of the strongest low-level temperature inversions that have been observed, with temperature increases up to 20°C as one ascends from the surface (Benson 1970). The inversions cap stable boundary layers (SBLs) that can be as shallow as tens of meters in clear nocturnal conditions (Sereze et al. 1992; Vickers and Mahrt 2004). Emissions from vehicular traffic, power plants, and home heating (mostly diesel and wood fuels) remain trapped within the SBL, leading to high concentrations of particulates and other pollutants. In the extremely cold conditions of interior Alaska an additional problem that arises is ice fog that can be triggered by combustion-generated water vapor at temperatures below approximately -25°C (Benson 1970; Girard and Blanchet 2001). The dispersal of pollutants is further hindered by the fact that winds and turbulence are quite weak in these conditions. The winds and turbulence that do exist in the SBL are strongly modulated by drainage flows, gravity waves, and other less understood phenomena (Hanna 1983; Mahrt 2009). Thus predicting the behavior of SBLs becomes a complex problem involving synoptic weather patterns, topography, turbulence, surface energy budgets, and precipitation.

The tool used for the meteorological modeling component of this project is the Weather Research and Forecasting (WRF) model (Skamarock et al. 2008), more specifically, the Advanced Research WRF dynamic core (WRF-ARW, henceforth simply called WRF). WRF contains separate modules to compute different physical processes such as surface energy budgets and soil interactions, turbulence, cloud microphysics, and atmospheric radiation. Since turbulent eddies in the SBL are typically much smaller than mesoscale model horizontal grid spacing (e.g., ten meters vs. a thousand or more meters), they cannot be modeled directly (e.g., Wyngaard 2004), but typically their effect is parameterized by a Planetary Boundary Layer (PBL) scheme that predicts turbulent kinetic energy (TKE). Within WRF the user has many options for selecting the different schemes for each type of physical process. There is

also a WRF Preprocessing System (WPS) that generates the initial and boundary conditions used by WRF, based on topographic datasets, land use information, and larger-scale atmospheric and oceanic models. New software associated with objective analysis and data assimilation will be discussed later.

The goal of this project was to select and perform two twenty-day simulations down to 1-km horizontal grid spacing for two episodes from the 2007-2008 winter season characterized by high PM2.5 exceedance events in the Fairbanks region. One episode was to be characterized by near total darkness, while the second was to contain partial sunlight. From a set of modeling experiments including a baseline physics configuration and a series of physics sensitivity tests, modified as appropriate to be suitable to the unique Alaskan atmospheric conditions, a best performing physics suite was to be selected and delivered to the EPA, along with source code and the model output. The project had two main components: (1) creating the best possible representation of the atmosphere through the use of a mesoscale model with continuous data assimilation, and (2) determining the best set of physics parameterizations by performing a series of sensitivity tests without the direct effects of data assimilation. Both components are included in a multiscale, multigrid data assimilation procedure, which will be described in more detail below.

## 2. METHODOLOGY AND BASELINE EXPERIMENTAL DESIGN

### 2.1 Grid Configuration

The simulations presented in this report involve three one-way nested horizontal grids with horizontal grid spacing of 12 km, 4 km and 1.3 km, respectively (Table 1 and Fig. 1). Grid 1 covers the entirety of Alaska and extends from Siberia to the northwestern continental United States. Grid 2 closely coincides with the extent of the Alaskan landmass south of the Brooks range; it includes the Anchorage region and the Gulf of Alaska in the south. Grid 3, centered around Fairbanks and extending south to the Alaska Range and north past the White Mountains and other uplands just north of Fairbanks, includes all of the proposed non-attainment area within the Fairbanks North Star Borough (Fig. 2). It can be seen in the figure that Fairbanks is located next to a semicircle of low mountains that are generally a few hundred meters above the city; this tends to restrict airflow near the city and further reduce the dispersion of pollutants in stable conditions.

| Grid | Dimensions | Horizontal Grid Spacing |
|---|---|---|
| 1 | 401 x 301 | 12 km |
| 2 | 202 x 202 | 4 km |
| 3 | 202 x 202 | 1.3 km |

*Table 1: Specifications of model grids.*

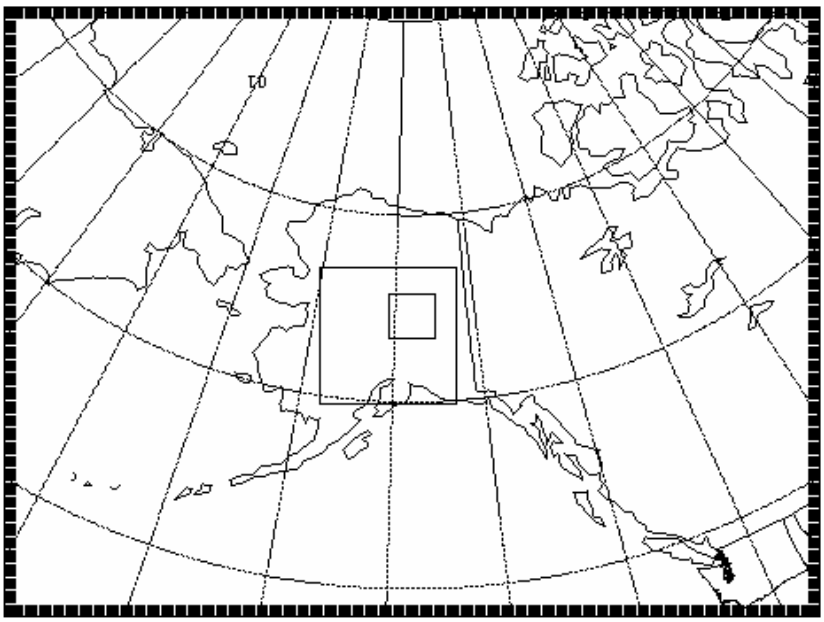

*Fig. 1: Nested grid configuration of WRF, showing the 12-km Grid 1, the 4-km Grid 2, and the 1.3-km Grid 3 described in the text.*

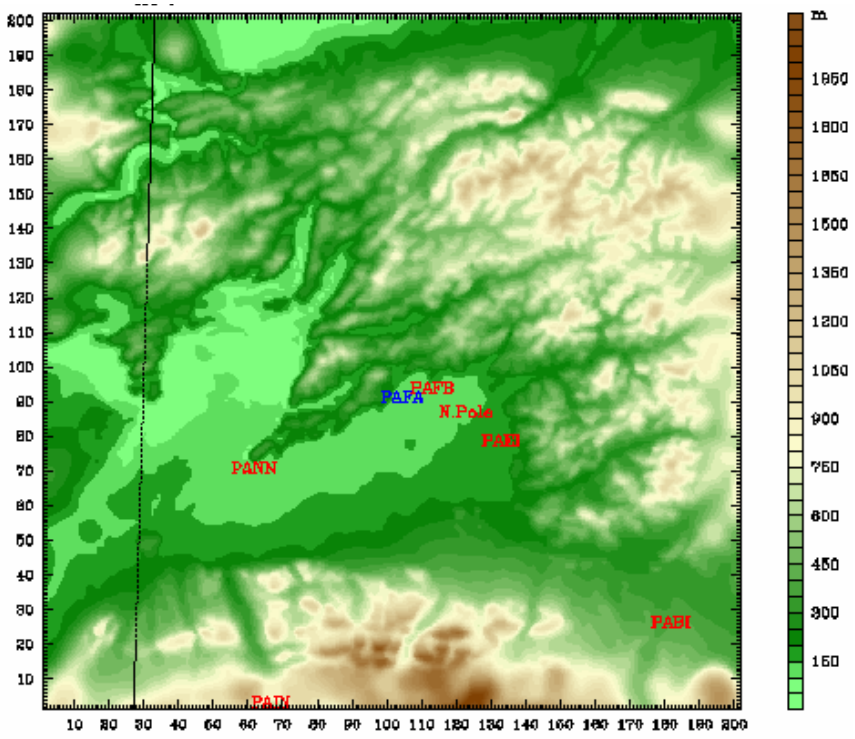


*Fig. 2: Elevation on Grid 3 used in study. The location of the Fairbanks sounding is labeled in blue; other local METAR stations are shown in red.*

The vertical grid spacing needed to be fine enough to resolve the structure of SBLs that can be only tens of meters deep, but not so fine that numerical instabilities arise in regions of steep topography (in particular the Alaska Range). After a series of initial tests a vertical grid configuration with 38 half layers (39 full levels) was defined, with a minimum vertical grid spacing of 4 m near the surface (see Fig. 3). Numerical stability was achieved through the use of time steps of 24 s, 8 s, and 4 s on the 12-km, 4-km and 1.3-km grids, respectively. These parameters are comparable to those used over central PA in the Seaman et al. (2008) SBL study. but with 4-m rather than 2-m vertical resolution near the surface, and slightly shorter timesteps.

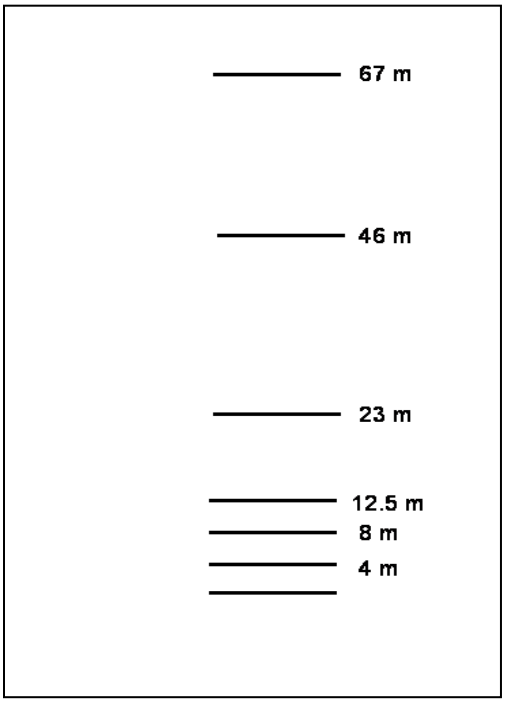


*Fig. 3: Lowest few vertical full levels (i.e., locations where vertical velocity is calculated) in WRF model configuration, roughly to scale.*

Two twenty-day episodes from the 2007-2008 winter season were selected for study. One episode was from 14 Dec 2007 to 03 Jan 2008, a time of year when there is little solar radiation in the Fairbanks area (approximately three hours of daylight per day near the solstice). During this episode the temperature rapidly decreased to near -40°C by 21 Dec, accompanied by rapid increases in PM2.5 concentrations, and then temperatures generally increased and PM2.5 decreased for the remainder of the episode (Fig. 4). The second episode was from 23 Jan 2008 to 14 Feb 2008, when solar insolation was more significant (between five and eight hours of sunlight per day), and provides an example of 'partial

sunlight' conditions. During this episode temperatures were initially relatively warm (near 0°C), decreased briefly to near -35°C by 27 Jan, rebounded slightly, and then decreased during the most extensive period of sub -35°C weather of the season. Consistent with the prolonged period of cold temperatures were recurring violations of the PM2.5 standard in the Fairbanks area.

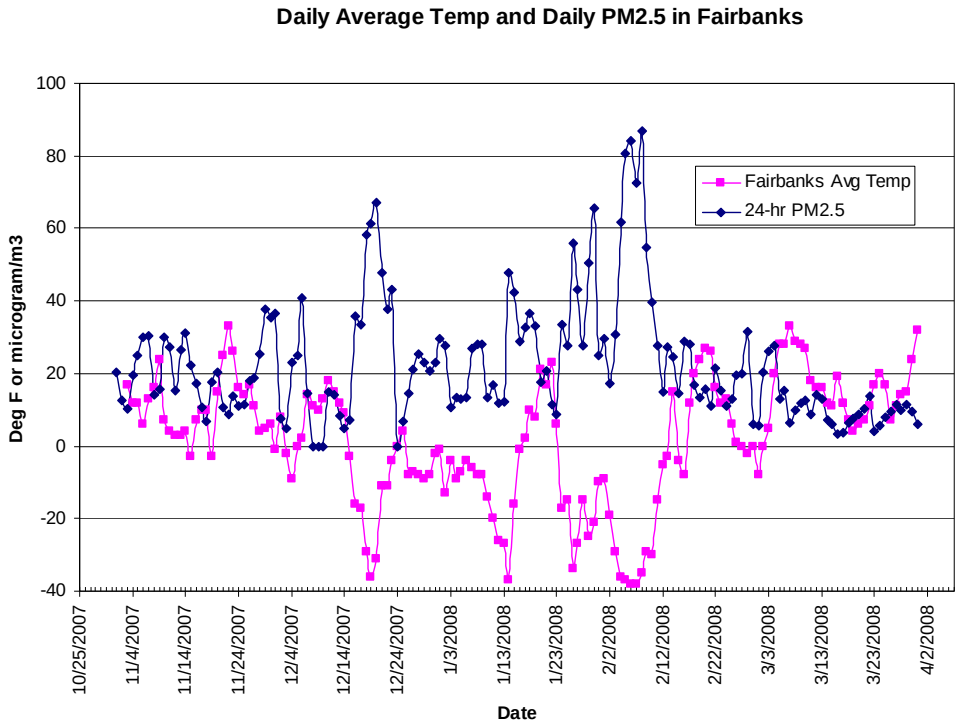


*Fig. 4: Observations of daily average temperature and 24-hr PM2.5 concentrations taken in Fairbanks during 2007-2008 winter season. Courtesy Robert Dulla, Sierra Research, Inc.*

In the initial period of a regional model simulation there is generally a period of several hours when the atmospheric state, whose initial conditions are usually provided by a global or coarser regional model, is still dynamically adjusting to the finer scale resolution and topography of the regional model. Therefore the model output from this initial 'spin-up' period is not completely reliable as an indicator of the true atmospheric state. However, if a regional model simulation is allowed to progress for too long without re-initialization (normally several days), it tends to drift away from the actual observed atmospheric state. Therefore, our method of obtaining realistic regional atmospheric analyses over an entire twenty-day episode was to divide each episode into four overlapping simulation segments. Each segment is around five days long with a twelve-hour overlap between each segment to avoid spin-up effects. (Specifically, the near total darkness episode was divided into successive segments of 6 days, 5.5 days,

5.5 days, and 4.5 days; the partial sunlight episode was divided into successive segments of 5 days, 5.5 days, 5.5 days, and 5.5 days).

Initial conditions and most of the Grid 1 lateral boundary conditions were obtained from the half-degree Global Forecast System (GFS) zero-hour analyses that were obtained from the NOAA National Operational Model Archive and Distribution System (NOMADS) website maintained by the National Climatic Data Center. The exceptions were some analysis times during the near total darkness episode when the half-degree GFS product was unavailable; in these instances the one-degree GFS analysis was used. All simulation segments for the near total darkness episode were selected such that all initial conditions could be obtained from half-degree global analyses.

The simulations were performed on one of two Linux clusters: one local cluster with 128 available processor cores, and the other cluster with 512 processor cores maintained by the Research Computing and Cyberinfrastructure High Performance Computing Group (RCC HPCG) at Penn State. Each 5.5 day simulation segment took 1-2 days to complete. The full 3D model output from each simulation was saved at a frequency of one hour for the 12-km Grid 1, and at a frequency of 12 minutes for the 4-km Grid 2 and 1.3-km Grid 3. For our configuration as shown in Table 1, the file size at each model output time is 500 MB for Grid 1 and 170 MB for each of Grids 2 and 3 (although this size can be approximately halved through file compression).

**2.2 Four-Dimensional Data Assimilation (FDDA)**

Even with the overlapping simulation segment strategy, it is difficult to ensure that the interior of a regional model simulation remains close to observations for simulations of more than a day or so. Therefore, dynamic analyses of historical cases are often performed, in which a Four-Dimensional Data Assimilation (FDDA) strategy is applied throughout the model integration. Relaxation terms based on the differences between actual observations and the corresponding model fields at the observation sites (also known as the 'innovations') are added to the model's predictive equations. In this way the model error is constrained based on available observations while the model still provides dynamic consistency and finer mesoscale structure not present in the observations. The version of FDDA used in these simulations is the multiscale, multigrid nudging FDDA strategy developed by Stauffer and Seaman (1994) for the MM5 mesoscale model. Nudging is also known as Newtonian relaxation, where the nudging relaxation terms are proportional to the innovation divided by a characteristic e-folding time inversely proportional to a nudging coefficient G. Nudging does not perform a direct insertion of observational information at a single point in space and time, but rather it applies the correction or innovation gradually in time and space based on the model terrain influences and prescribed / assumed weighting functions. For example, when a well-mixed PBL is present, one would generally want the influence of surface observations to be extended throughout the PBL, because in these conditions there is high correlation between errors in atmospheric fields at the surface and those anywhere within the PBL.

The multiscale multigrid FDDA method uses a combination of two forms of nudging: analysis nudging and observation ('obs') nudging. Analysis nudging is performed in model grid space where an objective

analysis of observations (e.g., with a modified Cressman scheme (Benjamin and Seaman 1985)) is performed using the interpolated global analyses (e.g., from the GFS) as a background field. The resultant 'enhanced analysis' can then be used as the basis for analysis nudging. Analysis nudging is generally applied on coarser model domains where synoptic data can be used to produce a reasonable gridded analysis. Obs nudging is more attractive for finer-scale domains and asynoptic data. It is particularly effective where observational data density is sparse and corrections are applied only in the neighborhood of the observations, allowing the model to still add value in regions without any data by propagating observation information into the data-sparse regions and creating mesoscale structure not in the observations. In this case the nudging is performed in observation space, and the model field is interpolated to the observation site to compute the innovation that is then analyzed back to the model grid over some three-dimensional neighborhood in space, and over some time window. Quality control (QC) of observations is critically important for the success of both analysis nudging and observation nudging.

In the multiscale multigrid FDDA method applied in this study, 3D-analysis nudging, as well as surface analysis nudging using higher temporal frequency surface data within the PBL (e.g., Stauffer et al. 1991), are performed on the outermost 12-km domain. Obs nudging is applied on at least the 12-km and 4-km domains. (Obs nudging is not applied on the finest 1.3-km model nest for the physics sensitivity studies described further below.) The finer domains thus have the benefit of improved lateral boundary conditions from the coarsest 12-km domain using both types of nudging, as well as the obs nudging performed directly on the 4-km nested domain.

This project was one of the first applications of the multiscale FDDA strategy of Stauffer and Seaman (1994) in WRF. It is important to note that many of the WRF FDDA capabilities were not available and still under development via a contract from the Defense Threat Reduction Agency (DTRA) to Penn State at the time that this project was proposed. In fact, the WRF 3D / surface analysis nudging and obs nudging capabilities were still being developed during this contract period. The WRF end-to-end FDDA system is shown in Fig. 5 and described in more detail in Deng et al. (2009). This contract was able to take advantage of the fact that the WRF FDDA developers at Penn State were also working on this contract.

The new OBSGRID module in the WRF end-to-end FDDA system produces gridded objective analyses and observation files similar to those produced by Rawins / Little_r in the MM5 system. These files can be used for 3D/surface analysis nudging and obs nudging within WRF. OBSGRID takes as input raw WMO observations (both surface and upper air) and the output of WPS, which consists of atmospheric initial and boundary gridded data (e.g., GFS output) horizontally interpolated to the model grid to be used in WRF. The outputs of OBSGRID relevant to this study include 1) pressure-level and surface objective analyses of the WMO observations (passing internal QC checks) using the WPS GFS output as background fields; the resultant analyses are then vertically interpolated to the WRF terrain-following "sigma" layers to be used for 3D analysis nudging; 2) surface analysis nudging files that can be directly used by WRF; 3) observation nudging files usable by WRF, and 4) files of the WMO observations including those passing the QC tests for use in the statistical verification software.

As mentioned above, for the physics sensitivity part of this study, 3D analysis nudging, surface analysis nudging, and obs nudging are performed on the 12-km Grid 1; obs nudging is performed on the 4-km Grid 2; and no nudging is performed on the 1.3 km Grid 3. Thus Grid 3 has no direct FDDA tendencies and can be used to determine physics sensitivities, while still benefitting from improved lateral boundary conditions derived from the coarser grids that do have FDDA.

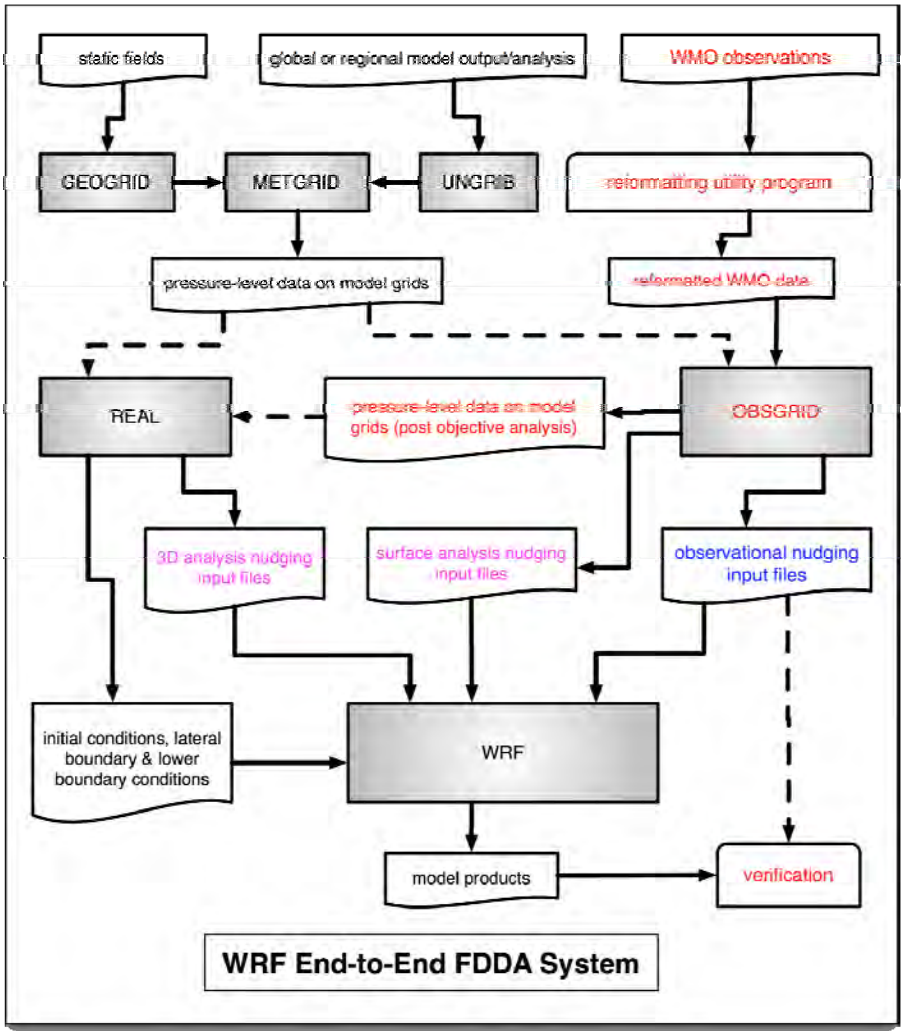


*Fig. 5: Diagram of the WRF End-to-End FDDA system used for this study (from Deng et al. 2009). Items in magenta apply to analysis nudging; items in blue apply to obs nudging; items in red apply to both.*

For the generation of the final dynamic analysis, obs nudging was performed on Grid 3, but with a reduced horizontal radius of influence (from 100 to 75 km), a reduced vertical pressure difference within the terrain-modified radius of influence function used for surface obs nudging (from 75 hPa to 37.5 hPa),

and obs nudging of surface data was performed on mass fields only (i.e., not winds). The values of FDDA-related WRF namelist parameters for these simulations can be found in Table 2.

| | 3D/Sfc Analysis Nudging | | | OBS Nudging | | |
|---|---|---|---|---|---|---|
| Parameter | Grid 1<br>12-km | Grid 2<br>4-km | Grid 3<br>1.3-km | Grid 1<br>12-km | Grid 2<br>4-km | Grid 3<br>1.3-km |
| G (1/sec) | $3*10^{-4}$ | **Not Used** | **Not Used** | $4*10^{-4}$ | $4*10^{-4}$ | $(4*10^{-4})$ |
| Wind field | Yes | **Not Used** | **Not Used** | Yes | Yes | No |
| Mass field | Yes | **Not Used** | **Not Used** | Yes | Yes | (Yes) |
| RINXY (km) | N/A | N/A | N/A | 100 | 100 | (75) |
| TWINDO (hours) | N/A | N/A | N/A | 2 | 2 | (2 – but see Section 5) |
| Time Frequency of Data (hours) | 6 / 3 (Sfc) | **Not Used** | **Not Used** | 1 | 1 | (1) |

*Table 2: List of WRF FDDA namelist parameter values used in this study. Analysis nudging parameters apply to both surface and 3D versions unless otherwise specified. Values in parentheses for Grid 3 do not apply to the physics sensitivity studies, which have no FDDA on Grid 3, but do apply to the final dynamic analysis performed in this study.*

**2.3 Baseline Physics Suite**

Two of the most important controls on the evolution of SBLs in mesoscale models are the PBL scheme and the Land Surface Model (LSM). The former is critical for determining the effects of vertical mixing both within and outside of the PBL, and thus helps regulate how rapidly pollutants can disperse. The LSM helps to determine the details of the surface energy balance and thus the thermal tendency and stability of air near the surface. In addition to these, other physical processes that are important in these conditions are the atmospheric radiation scheme (because of the impact on the thermal cooling and temperature structure of the lower atmosphere) and the microphysics scheme (because of the interactions between radiation, latent heat, and quantities of water vapor and condensate, as well as the value of predicting such features as ice fog).

The baseline physics suite used for these simulations was originally derived from that of Seaman et al. (2008) for central Pennsylvania, but with some modifications. To determine the longwave component of radiation, the RRTM scheme of Mlawer et al. (1997) was used, whereas the Dudhia (1989) scheme was used to determine the shortwave component. The PBL scheme used was a version of the Level 2.5 Mellor Yamada scheme as modified by Janjić (2002); henceforth this will be referred to as the Mellor-Yamada-Janjić (MYJ) scheme. A Level 2.5 scheme explicitly predicts the evolution of turbulent kinetic energy (TKE) at each grid point, and uses the predicted TKE to compute the magnitude and vertical extent of mixing. The MYJ scheme used is that available in version 3.1 of WRF; however, based on subsequent work from the central Pennsylvania study, the threshold of minimum TKE within the MYJ scheme was reduced to 0.01 $m^2 s^{-2}$, due to the extremely weak winds and turbulence expected in these stable conditions.

The LSM for the baseline was originally the 5-layer thermal diffusion model used in Seaman et al. (2008). However, we performed a series of preliminary tests with the Alaska grid configuration using the Noah LSM, originating from NCEP, Oregon State University and AFWA (Chen and Dudhia 2001). This was done because the Noah LSM includes a number of features that are potentially important in the central Alaska environment, including time-dependent snow cover, time-dependent snow density, and snow-dependent emissivities and ground conduction. Some properties of the Noah LSM that had just been incorporated into standard WRF (e.g., a more rigorous treatment of latent heat release in the presence of ice) were based on the 'Polar-WRF' and 'Polar-MM5' versions of Noah used for high latitude simulations (Bromwich et al. 2001; Hines and Bromwich 2008). A number of other features of the polar-modified Noah were not in the standard WRF at the time, but not directly relevant to central Alaska (e.g., modification of sea ice properties). Preliminary tests in the relatively mild conditions immediately prior to the partial sunlight episode revealed that the use of the Noah LSM initialized directly from the soil levels of the half-degree GFS resulted in smaller surface temperature biases. Thus, based on our preliminary favorable results, we used the version of Noah in WRF v3.1 as the LSM for the baseline simulation.

The microphysics model selected for the baseline was the Morrison et al. (2005) scheme, also new to WRF v3.1. This scheme was developed specifically for high-latitude cold temperature microphysics, and includes the prediction of two moments (mixing ratio and number concentration) for rain, snow, graupel, and cloud ice, in addition to single moment prediction of cloud water. We thus felt it was worth using this scheme in the baseline even though file sizes and computational costs were significantly increased (by 50% in time) from the simple ice scheme used previously.

**3. Initial Baseline Testing and FDDA Modifications**

Initial testing of the baseline WRF configuration for the two episodes began in January 2009. The purpose of the 'pre-baseline' testing was to confirm that the proposed WRF grid configuration would remain numerically stable and physically realistic for simulation segments of several days, to determine the resource and timing requirements of the simulations, and to confirm that the WRF FDDA features were working as expected. Furthermore, a number of key WRF system features to be used in this study

were still under development at the beginning of 2009; in particular, surface analysis nudging, OBSGRID, and the official WRF v3.1 release itself, which included the QNSE PBL scheme and a modified version of the Noah LSM. Thus all of these new features had to be tested and evaluated when they became available.

At the beginning many of these tests were performed on the first segment of the partial sunlight episode (23 – 28 Jan 2008). Not only was this a convenient place to begin, but it began as a time of relatively warm temperatures in central Alaska, allowing the model configurations to be evaluated in relatively mild conditions before being used in the extreme cold conditions of the high exceedance episodes. Nonetheless, a brief period of colder temperatures occurred toward the end of the 23-28 Jan 2008 period, so some evaluation of model performance in different temperature regimes could be determined.

A preliminary assessment of the skill of the FDDA components of the WRF end-to-end system for the baseline simulation of the 23-28 Jan 2008 period, made in April 2009, is shown in Table 3 for the 12-km (Grid 1) and 4-km (Grid 2) domains. Raw WMO observations from both surface METAR and rawinsonde stations were given QC codes within OBSGRID, and only those observations of sufficient quality to be used in the objective analysis were retained for verification. The table compares a simulation without FDDA, a simulation using only analysis nudging on Grid 1; a simulation using only obs nudging on Grids 1 and 2; and a simulation combining the analysis nudging and obs nudging features, corresponding to the proposed multiscale multigrid FDDA procedure. Furthermore, since the surface analysis nudging feature of WRF had only just become available from Penn State, two versions of each simulation including analysis nudging were performed: one with and one without surface analysis nudging.

The table confirms that, for virtually every grid, observation station type, and variable, the best root-mean-square error (RMSE) scores occur for multiscale multigrid FDDA, and the worse RMSE scores occur for the simulation without any FDDA. However, a more careful analysis of the table revealed a few puzzling results. While surface analysis nudging led to expected improvements in temperature on Grid 1 (vs. analysis nudging without surface analysis nudging) when verified against surface METAR stations, the RMSE scores of METAR winds and relative humidity actually became slightly worse. Furthermore, when the verification was performed against rawinsondes on Grid 1, surface analysis nudging made temperature RMSEs considerably worse, and wind RMSEs far worse, than the corresponding runs without surface analysis nudging.

For Grid 2 verified against rawinsonde data, we see the expected result that a simulation with only obs nudging improves the RMSE scores more than either version of the analysis nudging only simulation. (Since analysis nudging is always applied to Grid 1 only, the analysis-nudging-only simulations have only indirect FDDA improvements on Grid 2, through the lateral boundary conditions from Grid 1; the obs nudging simulations do have direct FDDA on Grid 2.) However, when surface METARs are used for Grid 2 verification, we have the puzzling result that obs nudging only is outperformed by analysis nudging only (except for temperature).

| Verification Domain | Verification Field and Station Type | Simulation FDDA Method ( O – Obs Nudging; 3DA – 3D Analysis Nudging; SA – Surface Analysis Nudging; No – No Nudging ) | | | |
|---|---|---|---|---|---|
| Grid 1 (12 km) | | Grid 1: No Grid 2: No | Grid 1: O Grid 2: O | Grid 1: 3DA / 3DA + SA Grid 2: No / No | Grid 1: 3DA + O / 3DA + SA + O Grid 2: O / O |
| | Surface U-Component | 3.2 | 2.6 | 2.3 / 2.4 | **2.1** / 2.2 |
| | Surface V-Component | 3.2 | 2.7 | 2.1 / 2.3 | **2.0** / 2.1 |
| | Surface Temperature | 5.6 | 2.9 | 2.9 / 2.4 | 2.5 / **2.1** |
| | Surface Rel. Humidity | 21.0 | 18.7 | 17.7 / 18.2 | **17.0** / 17.5 |
| | Sounding U-Component | 4.6 | 2.2 | 1.5 / 3.3 | **1.1** / 2.0 |
| | Sounding V-Component | 4.2 | 2.3 | 1.5 / 2.9 | **1.1** / 1.9 |
| | Sounding Temperature | 3.5 | 1.4 | 1.4 / 2.0 | **1.0** / 1.3 |
| | Sounding Rel. Humidity | 21.2 | 10.2 | 11.2 / 16.0 | **8.3** / 10.5 |
| Grid 2 (4 km) | Surface U-Component | 3.8 | 3.3 | **2.2** / 2.3 | 2.5 / 2.7 |
| | Surface V-Component | **2.5** | 3.1 | 2.7 / 2.8 | 2.9 / **2.5** |
| | Surface Temperature | 5.0 | 2.5 | 3.1 / 3.0 | 1.9 / **1.8** |
| | Surface Rel. Humidity | 23.8 | 22.0 | 20.7 / 20.7 | 19.6 / **19.3** |
| | Sounding U-Component | 4.5 | 2.2 | 2.6 / 2.8 | **1.7** / 1.8 |
| | Sounding V-Component | 4.5 | 3.2 | 3.4 / 3.8 | **2.8** / 3.4 |
| | Sounding Temperature | 3.1 | 1.3 | 2.2 / 2.2 | **0.9** / 1.4 |
| | Sounding Rel. Humidity | 27.0 | 14.1 | 21.7 / 24.5 | **12.5** / 13.1 |

*Table 3: Root-mean-square error (RMSE) values of u-component wind (m $s^{-1}$), v-component wind (m $s^{-1}$), temperature (°C) and relative humidity (%) as verified within Grids 1 and 2 during test FDDA simulation of 23-28 Jan 2008 for various FDDA combinations. Verification was performed against METAR stations for the surface and rawinsonde stations for the sounding data. The best value for each row is in bold.*

Investigations into the cause of these puzzling results led to the realization that a number of the components of the WRF end-to-end FDDA system probably needed to be modified to adapt the system to the special conditions of the Alaska configuration. First, in most mesoscale model simulations it can be assumed that surface wind observations, normally made at a height of 10 m above ground level (AGL), and surface temperature and moisture observations, normally made at 2 m AGL, are located within the lowest model layer. In fact, normally the problem is that the midpoint of the lowest model layer (or first half-layer height above the surface) is often tens of meters in height and still well above the height of the surface observations. A proper interpolation of model values to the height of the surface observations usually requires using similarity theory or some similar procedure. For the Alaska configuration, however, a 10-m wind would actually be located within the *third* model layer from the surface, while 2-m temperature essentially corresponds to the height of the lowest model half layer (midway between the surface and the lowest model full level). There are at least two consequences of this. The first is that, for the default procedure of verifying surface wind observations with model output from the lowest model half layer, observed 10-m winds are actually being compared to modeled 2-m winds whereas they should be verified against the modeled 10-m winds of the third model half layer. The second consequence is that the surface wind innovations used in the WRF FDDA code are by default based on the difference between 10-m observed winds and 2-m modeled winds in this case, which is wrong and may introduce erroneous biases into the FDDA simulation.

An additional issue was revealed by examining fields of PBL height produced by the PBL turbulence parameterization in various test simulations. Though, as expected, PBL heights are very low over many large areas within the model domains, especially during the colder periods, some patches of unexpectedly high PBL height values can be seen at times (Fig. 6). PBL heights of 1500 m or greater are more typical of convective boundary layers than of the nocturnal SBL conditions found in interior Alaska. Model soundings taken in the proximity of these patches (Fig. 7) confirm that the atmosphere is certainly rather stable and not well mixed in potential temperature (although some layers above show potential temperatures close to a saturated adiabat). The high PBL height zones appear to be associated with regions of elevated shear-generated TKE and cloudiness, since it is the TKE profile in the MYJ scheme that determines the PBL height. The issue is that the default WRF surface analysis and obs nudging schemes spread the influence of surface innovations throughout the depth of the PBL, but in these stable conditions this may overestimate the vertical error correlation length scale for surface innovations. This helped explain why the use of surface analysis nudging on Grid 1 made the rawinsonde-verified statistics worse.

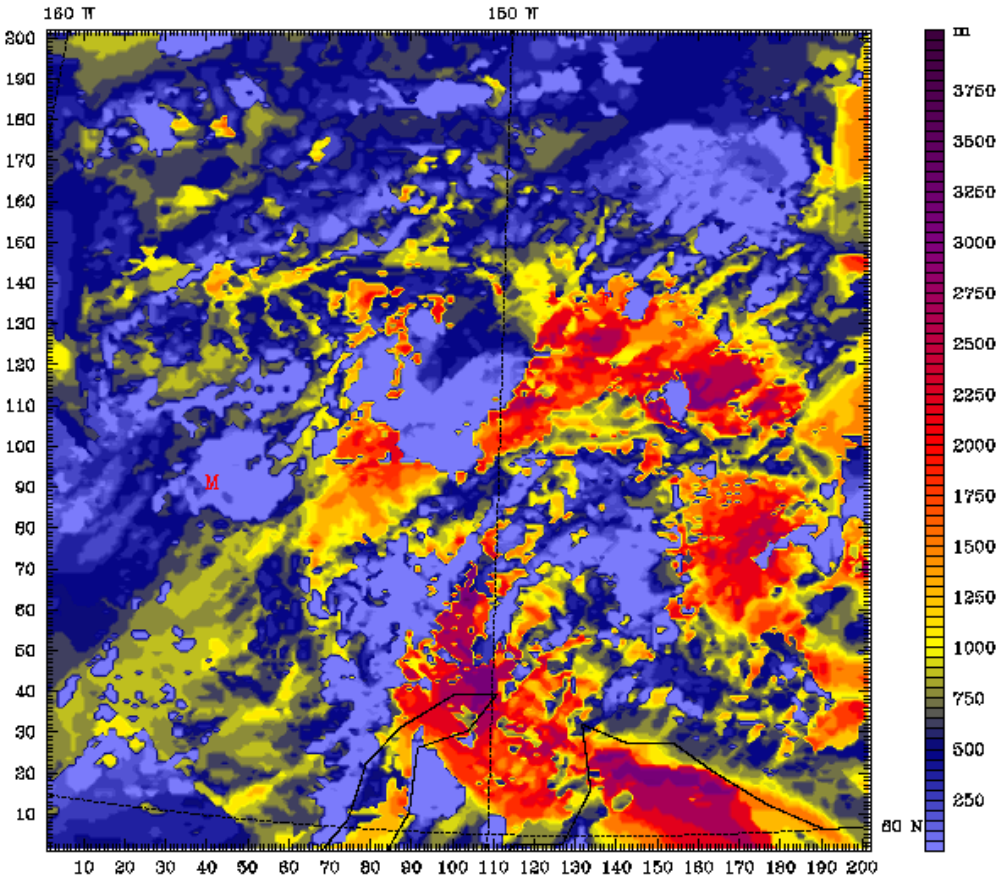


*Fig. 6: WRF-predicted PBL height at 1200 UTC 25 Jan 2008 (60-hour simulation time) within the 4-km Grid 2. Simulation does not include FDDA.*

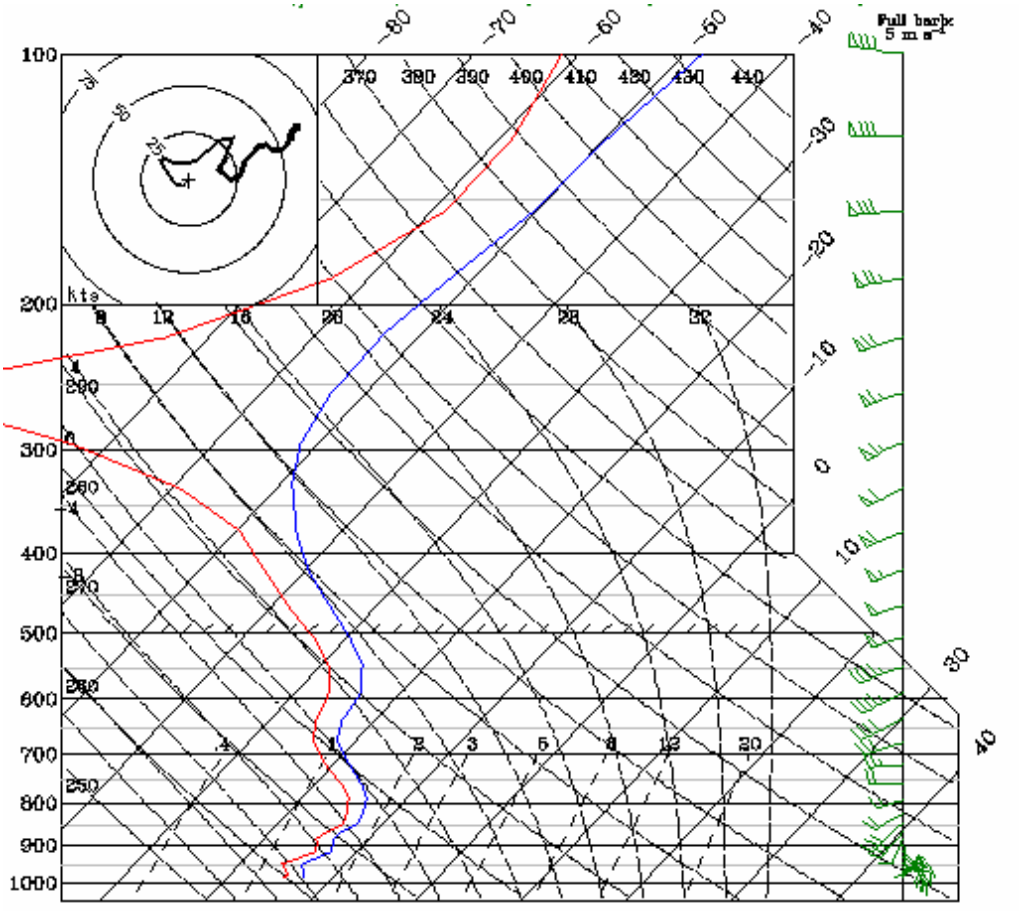


*Fig. 7: WRF-predicted model sounding at Fairbanks for same time and simulation as Fig. 6.*

Based on a series of similar tests, the following modifications were made to the WRF FDDA schemes for use in the baseline Alaska simulations. 1) The verification software was rewritten so that surface wind observations are verified against the third model half-layer from the ground, while surface moisture and temperature observations are verified against the lowest model half-layer. 2) A portion of the verification software that uses an assumed lapse rate to adjust model temperatures based on the difference between modeled and actual elevation was disabled, because this can lead to large errors in very stable conditions. 3) The surface analysis nudging and obs nudging codes were modified so that surface innovations for wind are computed and applied directly at the third model level. 4) Because surface wind observations directly relate to the third model layer and surface temperature and moisture observations directly relate to the lowest model layer, the similarity-based adjustments normally performed on model output for surface innovation computation was also disabled. 5) Hardwired vertical weighting functions for surface innovations were implemented into the surface analysis nudging and obs nudging codes, replacing the default functions that extend surface corrections to the model-predicted PBL height. Trial and error established that the functions shown in Fig. 8 for surface obs

nudging and analysis nudging extend the surface innovations in the vertical enough to improve surface statistics but without degrading rawinsonde-verified RMSE scores; furthermore, the vertical extent of

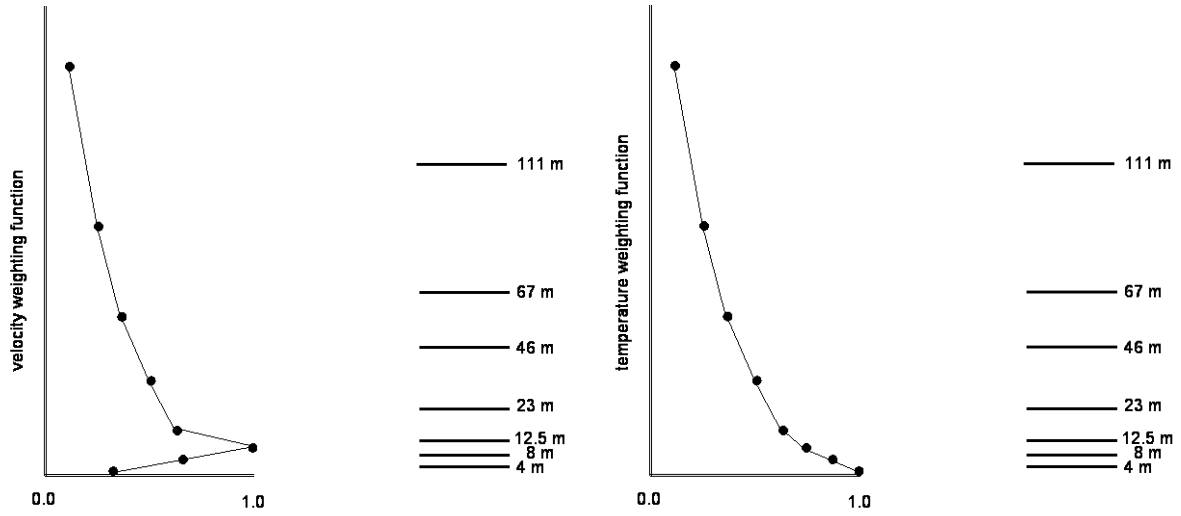


*Fig. 8: Vertical weighting functions at model half-layers for wind components (left) and temperature and moisture (right), as used by modified surface analysis nudging and obs nudging FDDA procedures for Alaska simulations. Heights of model full layers are shown to the right, roughly to scale.*

these functions (about 150 m) is a reasonable order of magnitude estimate for the maximum depth of nocturnal radiatively-driven SBLs.

Results from this phase of the project were presented at an oral presentation at the 13th AMS Conference on Mesoscale Processes in Salt Lake City, UT, from 17-20 Aug 2009. (Gaudet et al. 2009).

## 4. PHYSICS SENSITIVITY EXPERIMENTS

### 4.1 Experimental Design

Three modifications of the baseline physical parameterizations were evaluated in the physics sensitivity component of this project. The first involved modifying the atmospheric radiation schemes so that both the longwave and shortwave components used the new RRTMG radiation package, which uses the RRTM methodology but in a more efficient form adaptable to global climate models. This particular radiation package first became available in WRF v3.1. Though the RRTM and RRTMG longwave radiation schemes should produce very similar clear-sky fluxes, when mult-layered condensate is present the RRTMG makes use of the Monte Carlo Independent Column Approximation (McICA) to take into account 3D scattering effects.

The second involved changing the PBL parameterization from MYJ to the Quasi-Normal Scale Elimination (QNSE) scheme (Sukoriansky et al. 2005; Galperin et al. 2007). The theory behind the scheme is quite

advanced, but it is specifically designed for stable conditions, and allows both turbulent mixing and gravity wave motions to be represented in a unified framework. Dr. Boris Galperin was invited to Penn State University to give a seminar on the theory of the QNSE scheme in October 2008 before it was officially made public in WRF v3.1. The implementation of the QNSE scheme in WRF is actually similar to that of the MYJ, but with the values of vertical mixing parameters derived from the theory as a function of Richardson number (i.e., essentially the ratio of atmospheric stability to the square of the wind shear).

The third modification involved changing the LSM model from Noah to the Rapid Update Cycle (RUC) LSM. Among the features of the RUC LSM that suggest its use for this study is the presence of a snow model that potentially can have multiple layers depending on the snow depth (Smirnova et al. 2000). Other users have reported favorable results from using the RUC LSM in simulations of the Arctic (Mölders and Kramm 2010). The RUC LSM can also be initialized using soil information from the half-degree GFS after minor modification of the WRF source code. By default WRF can use either 6 or 9 soil levels, but we chose 6 because it is closer to the 4 levels of Noah and because it is the typical number of soil levels used in the RUC (e.g, Hines and Bromwich 2008).

**4.2 Model Initialization and Setup**

The objective analyses used for model initialization and analysis nudging were performed using the multi-quadric method within the OBSGRID software designed for WRF. The background analysis files were derived from the half-degree GFS and topographic and land use dataset through the WPS. The background fields also served as the basis for performing QC on the WMO rawinsonde and surface METAR data used for verification and obs nudging, through 'buddy-check' (excluding obs too different from their neighbors) and 'err-max' (excluding obs too different from the background) procedures. A consequence of the current QC methodology is that all observations were located at the surface or at the standard pressure levels of the GFS model.

For the baseline and sensitivity experiments the model setup was the same except for the choice of physics options. Both the near total darkness and the partial sunlight episodes were simulated in their entirety using the four overlapping simulation segments referred to above. The FDDA procedure (using the modified vertical weighting functions) was defined to use surface and 3D analysis nudging on the 12-km Grid 1, obs nudging on both the 12-km Grid 1 and the 4-km Grid 2, and no FDDA on the 1.3-km Grid 3. Physics sensitivities on Grid 3 would thus be given greater weight than sensitivities on the other grids (which would not be expected to be as large due to the influence of FDDA). (However, we left open the possibility of performing a final dynamic-analysis simulation with obs nudging also performed on Grid 3 once a best-choice physics suite was selected; this final simulation would then have our best available model analysis of the atmospheric state during the episodes, and would be appropriate for use in atmospheric chemistry or transport and dispersion models. These results have been added to the report in Section 5 below.)

For each sensitivity experiment verification was performed using model output every 3 hours (excluding the initial time). For the periods of overlapping simulation segments, the model output from the segment at the larger forecast time was used, so all of the verification model output was at least 12 hours after a model initialization (except of course for the first 12 hours of an episode). All three grids were verified against only those stations located within the boundaries of Grid 3, to ensure that statistical differences between grids are not due to the different set of stations available on each domain. As previously discussed, verification of surface METAR data is performed directly with the third model level from the surface for winds, and the lowest model level for temperature and moisture.

The first physics sensitivity test involved changing the radiation to the RRTMG scheme for both longwave and shortwave components. We all agreed that if this produced favorable results we could simply retain the RRTMG radiation scheme rather than the Dudhia shortwave / RRTM longwave radiation suite of the baseline simulation in future sensitivity experiments. An initial three-day test (23-26 Jan) was performed without FDDA on any grid so as to maximize physics sensitivity. It was indeed found that the surface METAR temperature RMSE scores were consistently improved by the use of RRTMG (Fig. 9), although winds and relative humidity were little affected (not shown). The improvement seemed to be related to reduced downward longwave fluxes beneath patches of ice condensate. Thus, the decision was made that all future physics sensitivity tests, this time with FDDA on Grids 1 and 2 as described above, would make use of the RRTMG scheme.

The combinations of physics parameterizations used in the physics sensitivity tests are summarized in Table 4. To facilitate the comparison of different physics sensitivity experiments, the baseline simulation, with the combination of MYJ PBL scheme, Noah LSM, and Dudhia shortwave / RRTM longwave radiation, will henceforth be denoted as experiment MND. Another experiment, with MYJ PBL / Noah LSM / RRTMG radiation, will be noted as MNR, and another with QNSE PBL / Noah LSM / RRTMG radiation will be denoted as QNR. Finally, the experiment with MYJ PBL / RUC LSM / RRTMG radiation will be denoted as MRR.

| Experiment Name | Planetary Boundary Layer (PBL) | Land Surface Model (LSM) | Radiation |
|---|---|---|---|
| MND (Baseline) | Mellor-Yamada-Janjić (MYJ) | Noah | Dudhia Shortwave / RRTM Longwave |
| MNR | Mellor-Yamada-Janjić (MYJ) | Noah | RRTMG Shortwave / RRTMG Longwave |
| QNR | Quasi-Normal Scale Elimination (QNSE) | Noah | RRTMG Shortwave / RRTMG Longwave |
| MRR | Mellor-Yamada-Janjić (MYJ) | Rapid Update Cycle (RUC) | RRTMG Shortwave / RRTMG Longwave |

*Table 4: Names and physical parameterizations used for physics sensitivity studies.*

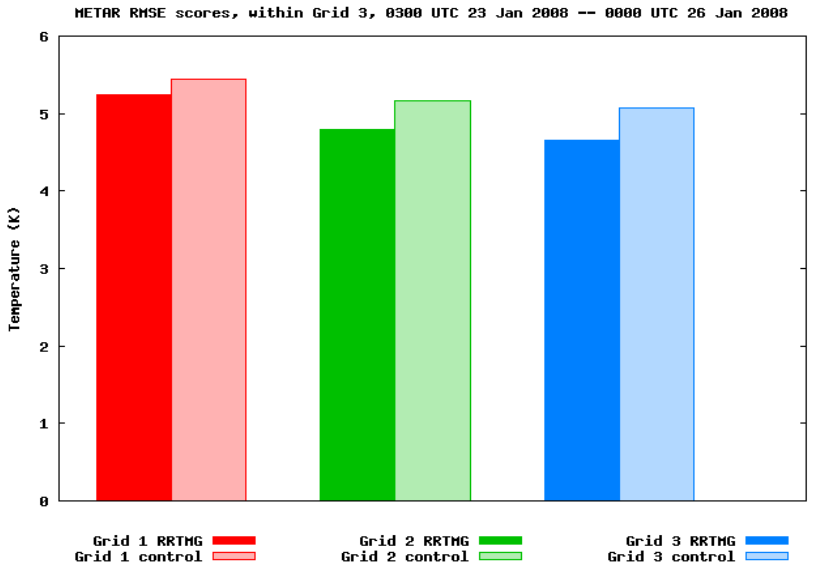


*Fig. 9: Surface METAR RMSE scores for temperature compiled for those stations located within Grid 3 for simulations from 00 UTC 23 Jan 2008 – 00 UTC 26 Jan 2008. Verification statistics are computed every three hours during the period. 'Control' denotes baseline physics configuration; 'RRTMG' denotes baseline physics configuration but with the RRTMG longwave and shortwave radiation schemes. All simulations shown were performed without FDDA.*

### 4.3 Results of Physics Sensitivity Experiments

Figures 10 and 11 present the temperature RMSE and bias scores, respectively, for Grid 3 surface METAR stations for both the partial sunlight and near total darkness episodes. First, it can be seen that the RMSE score increases from Grid 1 to Grid 2 to Grid 3, which can be explained by the fact that less FDDA forcing is being applied from Grid 1 (both analysis and obs nudging) to Grid 2 (obs nudging) to Grid 3 (no nudging). These RMSE scores are large compared to typically reported surface meteorological values (e.g., Seaman and Michelson 2000), but of course the large temperature range through the period (about 40°C for both episodes) and extreme conditions make these challenging forecasts for a numerical model. Second, we see the previously discussed result that switching the radiation to RRTMG (compare MND and MNR) leads to improved temperature RMSE scores and lower positive temperature biases; the improvement is most noticeable on the no-FDDA Grid 3. The fact that the RMSE improvement through the use of the RRTMG is greater for the near total darkness episode than for the

partial sunlight episode was not unexpected, because previous examination of the partial sunlight episode revealed that the reduced positive temperature bias with RRTMG was due to the longwave component while the shortwave component of RRTMG partially counteracted this effect (not shown).

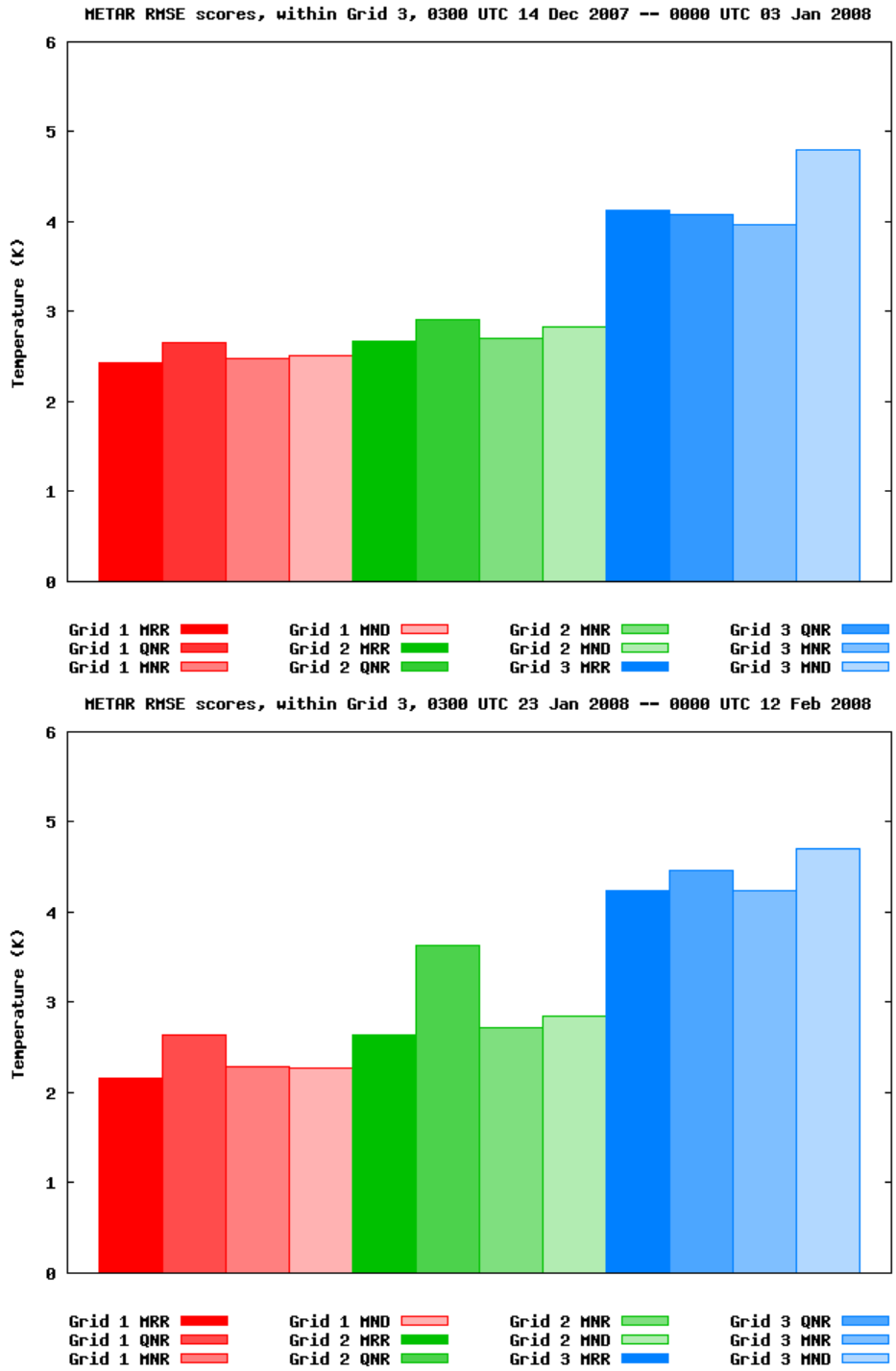


*Fig. 10: Surface METAR RMSE scores for temperature for entire near total darkness episode (top) and partial sunlight episode (bottom). Labels for degree of shading refer to experiment names in Table 3. Verification statistics were computed every 3 hours during each episode as described in text.*

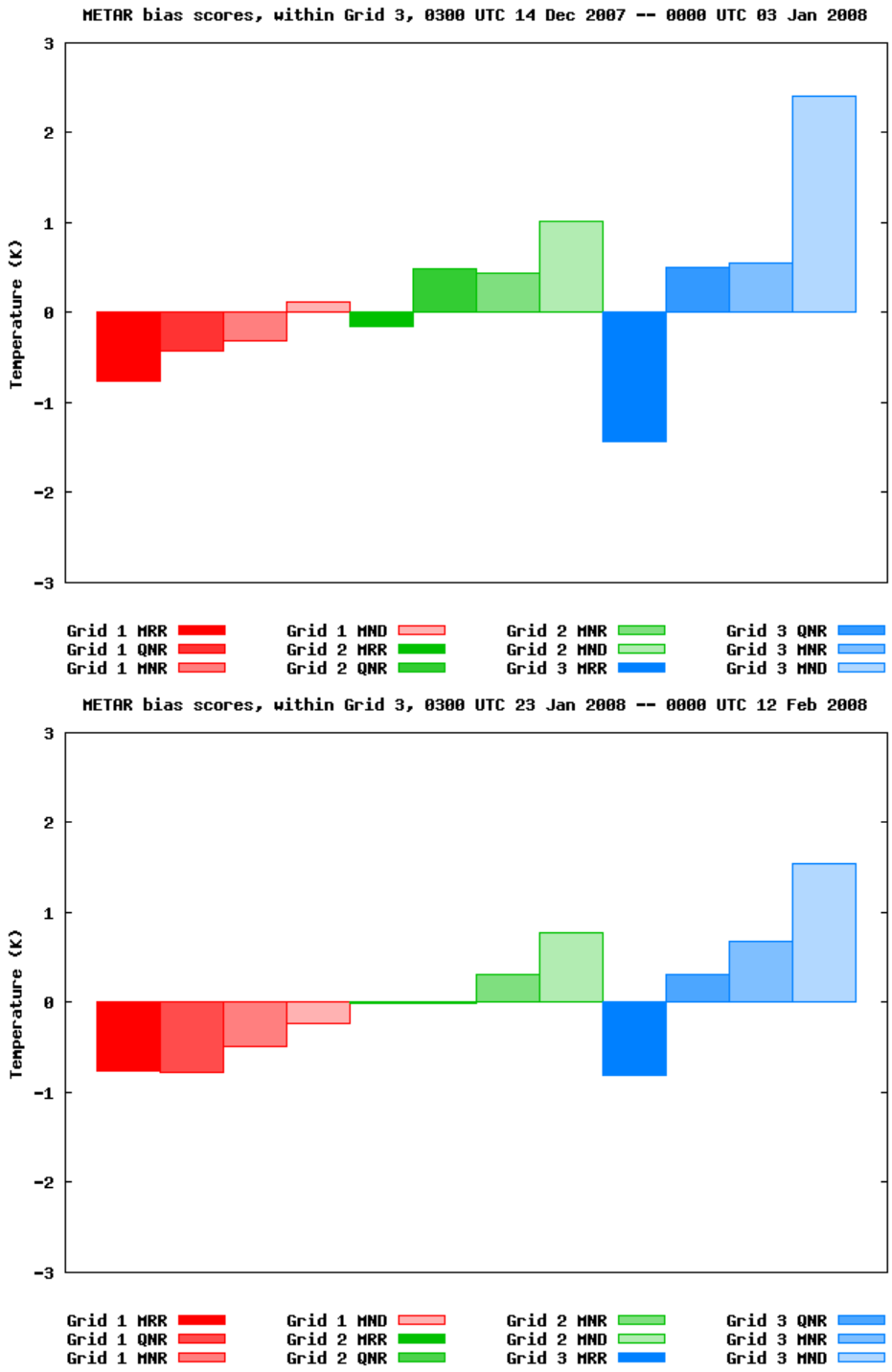


*Fig. 11: Same as Fig. 10, but for surface METAR bias scores for temperature.*

Switching from the MYJ to the QNSE PBL scheme (compare MNR to QNR) further reduced and improved the magnitude of positive METAR temperature bias (for Grid 3 and the Grid 2 partial sunlight episode). However, the temperature RMSE scores for QNR are consistently greater than those for MNR; so this improved bias is not reflected in more skillful forecasts. The results of the QNSE PBL scheme are encouraging and should be analyzed in greater depth in a future project. We decided that the sensitivity test introducing the RUC LSM should use the MYJ scheme due to our greater experience with MYJ in WRF.

The effect of switching from Noah to RUC (compare MNR to MRR) produces the coldest surface temperatures of any of the experiments. While this leads to the best magnitude METAR temperature biases for Grid 2, the MRR Grid 3 temperature bias is considerably more negative, especially for the near total darkness episode. The MRR temperature RMSE scores for the METARs are the best, or tied for the best, of the four physics experiments for Grid 2 and the Grid 3 partial sunlight episode, but slightly worse than MNR and QNR for the Grid 3 near total darkness episode.

In terms of surface METAR wind speed RMSE and bias errors (Figs. 12 and 13) we see that there is less variability among the different physics schemes. For virtually all variables, grids, and episodes, however, the scores for experiment MNR are slightly better than the others. The wind speed RMSE scores tend to be slightly worse on Grid 3 without FDDA than on Grid 2 with obs nudging, but better than those on Grid 1 that uses analysis nudging but with a much coarser horizontal resolution.

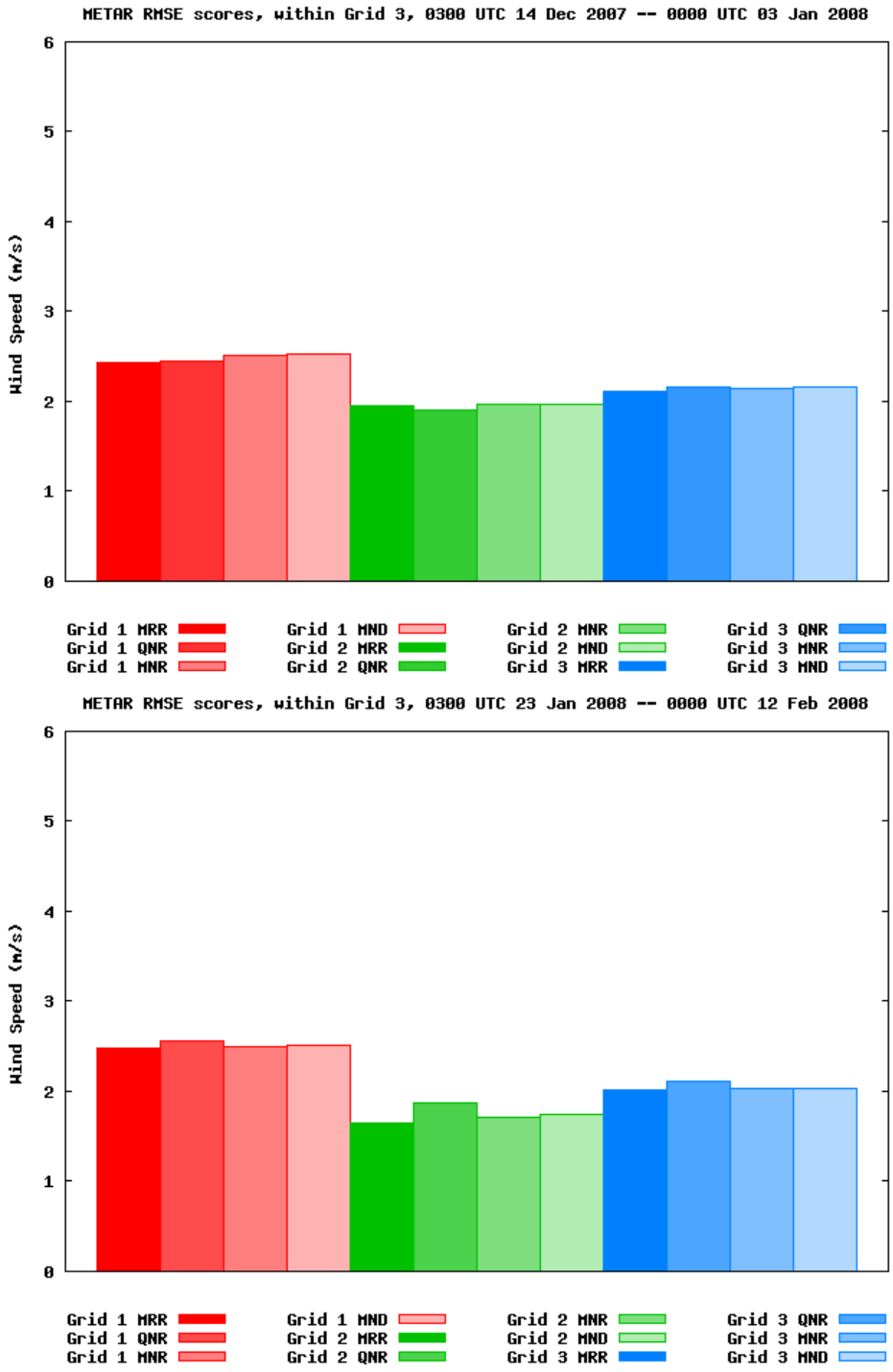


*Fig. 12: Same as Fig. 10, but for surface METAR RMSE scores for wind speed.*

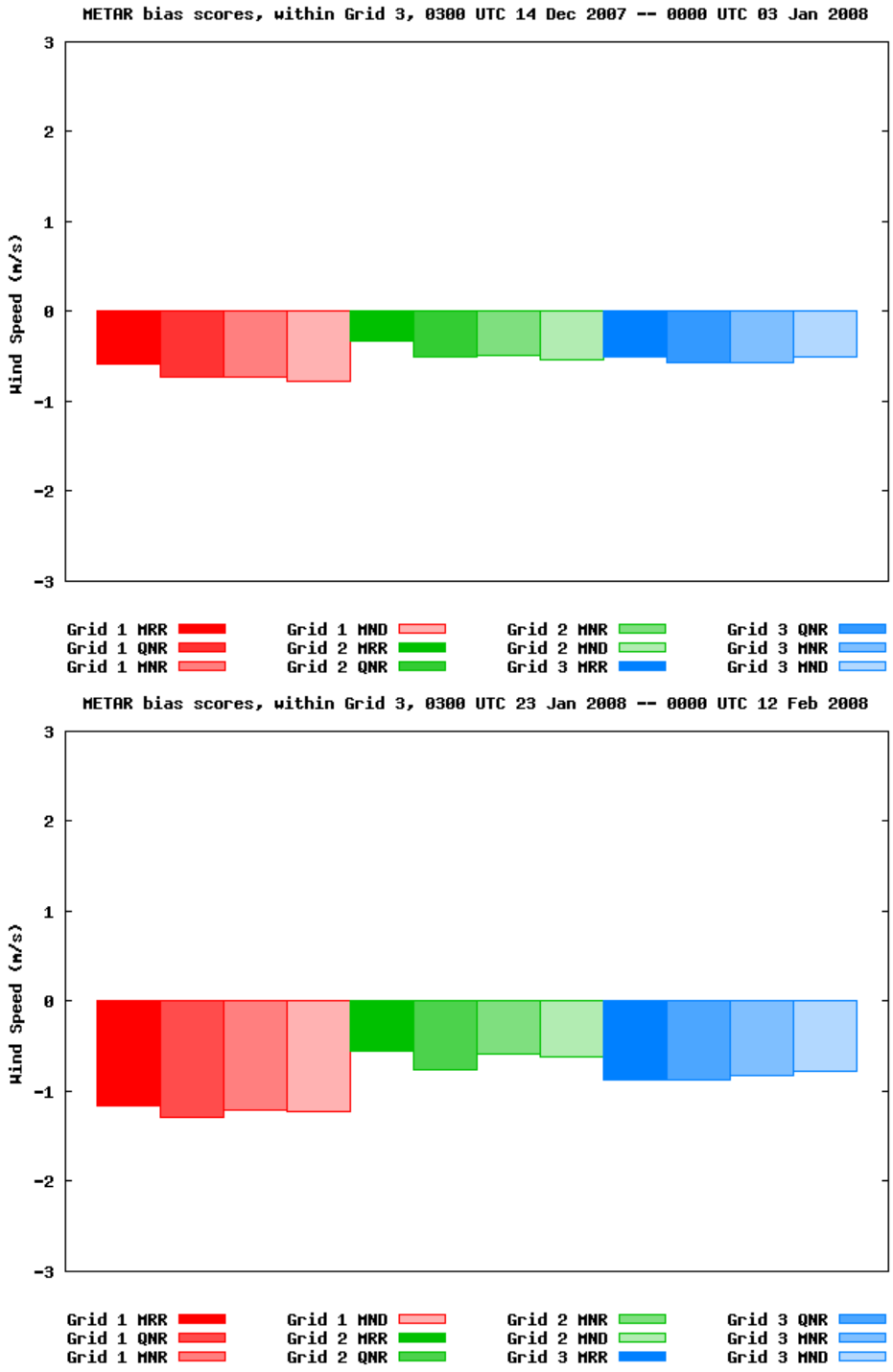


*Fig. 13: Same as Fig. 10, but for surface METAR bias scores for wind speed.*

In order to learn more about the nature of these biases, statistics for each episode can be compiled for each of the four 5-day (or 5.5-day or 6-day) simulation segments. One instructive comparison is between 14-20 Dec 2007 and 20-25 Dec 2007 (Fig. 14). The temperature difference between different physics configurations remains quite consistent between the two periods, but in the 14-20 Dec period the model temperature bias tends to be more negative than for the 20-25 Dec period. It can be shown that the large negative temperature biases of MRR are predominantly from the 14-20 Dec period. It should be noted that the highest exceedances / lowest temperatures for the near total darkness episode occur around 21 Dec. In general, Grid 3 tends to magnify the temperature biases of Grid 2, except for the MRR model for 20-25 Dec, where the Grid 3 temperature bias is reduced to almost zero.

A time series of the averaged observed, MNR, and MRR temperatures at the locations of the Grid 3 METARs is shown in Fig. 15. Note that the strongest MRR negative temperature biases in each episode tend to occur during times when the temperature is decreasing toward the coldest temperatures near 21 Dec in the near total darkness episode and about 05-09 Feb 2008 for the partial sunlight episode. At these times the MNR temperature bias also tends to be negative, but not by as much. However, immediately after the coldest temperatures are reached, the model biases become positive, and then the MRR configuration is preferred because temperature biases are smaller in magnitude. In particular, during the cold 5-9 Feb period MRR lacks the strong positive spikes in temperature bias that occur in the MNR simulation during the afternoons.

Verifying model features above the surface was made difficult by the scarcity of such observations in the region; the only rawinsonde sounding stations within Grid 2 are at Anchorage, McGrath, and Fairbanks, and of these only Fairbanks is located within Grid 3. No other reliable set of above-surface observations within Grid 3 was available for the episodes. A time-averaged composite of the vertical temperature structure of the Fairbanks sounding, compared to that from the different model physics configurations, is shown in Fig. 16. Since the quality-controlled observations used in the verification are located at the background GFS pressure levels, which have 25 hPa spacing near the ground, this is the effective maximum vertical resolution of the figure. The figure shows the zone from 700 hPa down to 975 hPa, which is the lowest pressure bin located entirely above the surface at Fairbanks. Note that the chosen variations in physics packages have virtually no effect above approximately 850 hPa, and all the modeled temperature profiles are extremely close to the observed profile, presumably due to the impact of Grid 2 obs nudging along the boundaries of Grid 3. From about 850 hPa to 925 hPa, the models begin to diverge from the observations for the near total darkness episode; the MND configuration is about one degree C too warm, but the models with the RRTMG radiation package reduce the positive temperature bias by about a factor of two. For the partial sunlight episode all models track the observations closely down to about 900 hPa. Below 950 hPa the MRR configuration becomes the coldest of the models, and the closest to the observed profile, especially for the near total darkness episode. At these lowest levels the RRTMG sensitivity remains much greater for the near total darkness episode than for the partial sunlight episode. The MNR and QNR configurations are always virtually indistinguishable, suggesting that choice of PBL scheme has little impact on the vertical temperature structure at 975 hPa and higher elevations.

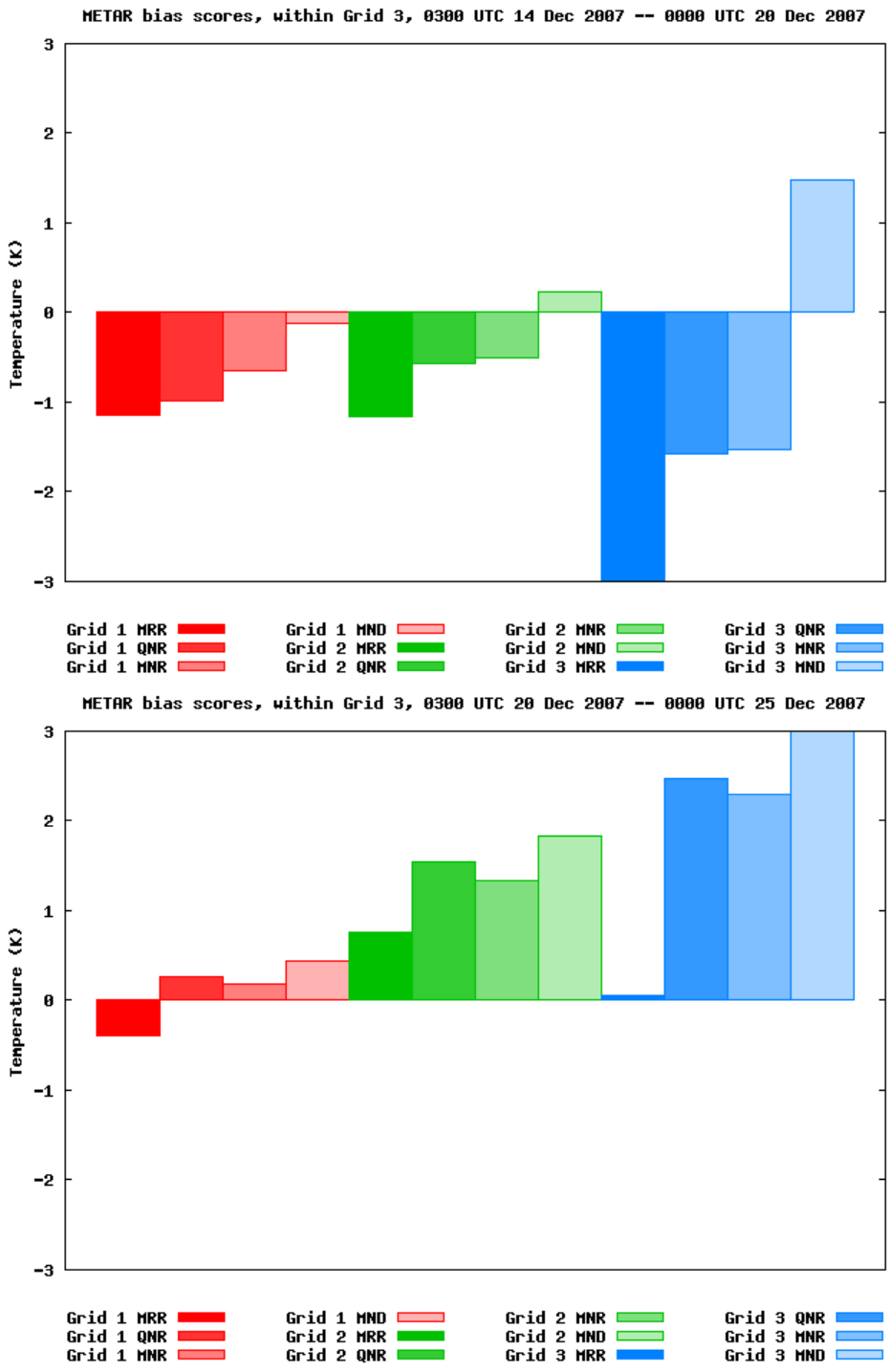


*Fig. 14: Surface METAR bias scores for temperature during the near total darkness episode within the 14-20 Dec period (top) and 20-25 Dec period (bottom). Otherwise, same as Fig. 11.*

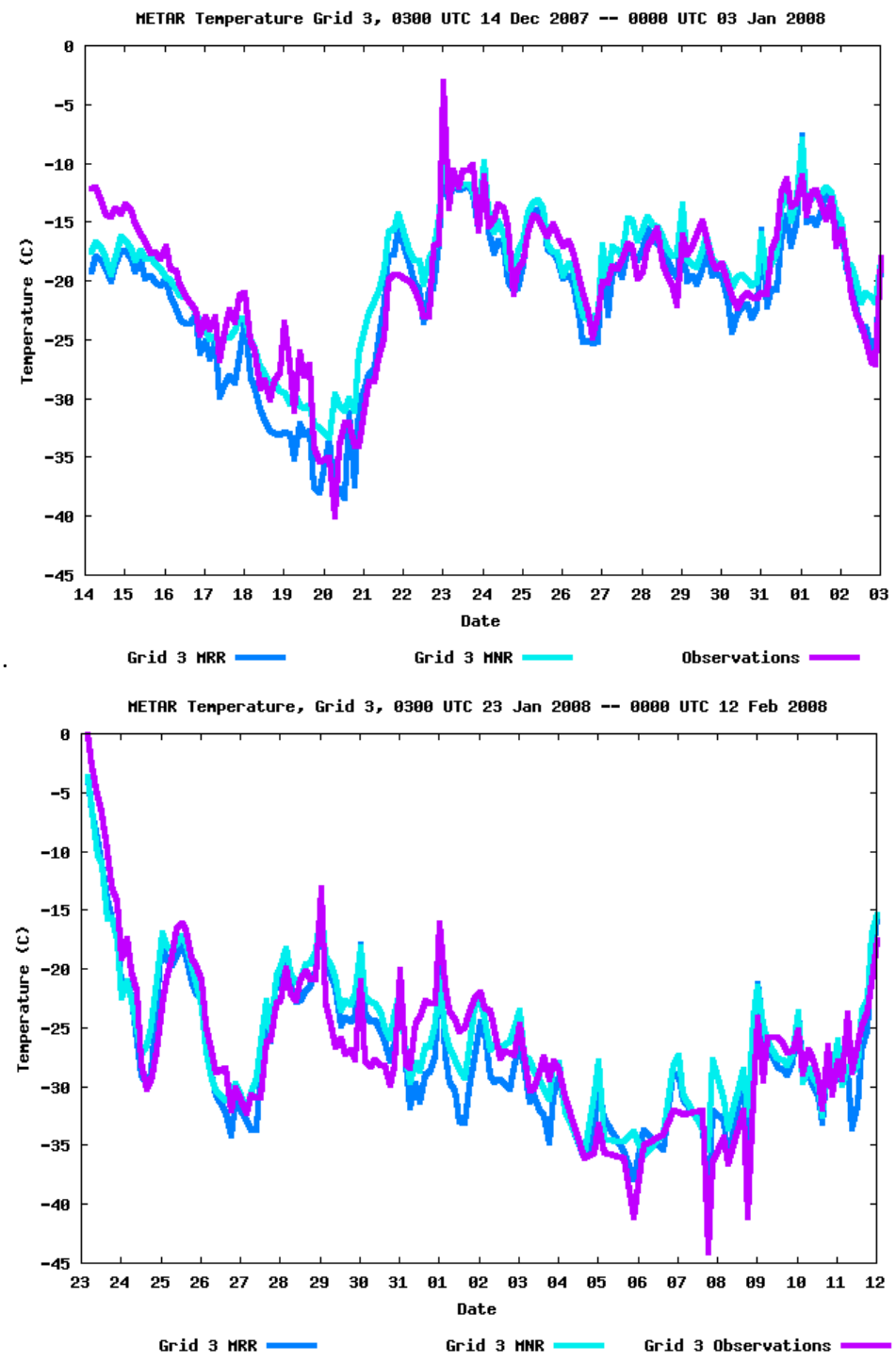


*Fig. 15: Time series of temperature for near total darkness episode (top) and partial sunlight episode (bottom), averaged over the sites of all the surface METAR stations within Grid 3. Dark blue indicates value within Grid 3 from experiment MRR; light blue indicates value within Grid 3 from experiment MNR; purple indicates observed METAR value.*

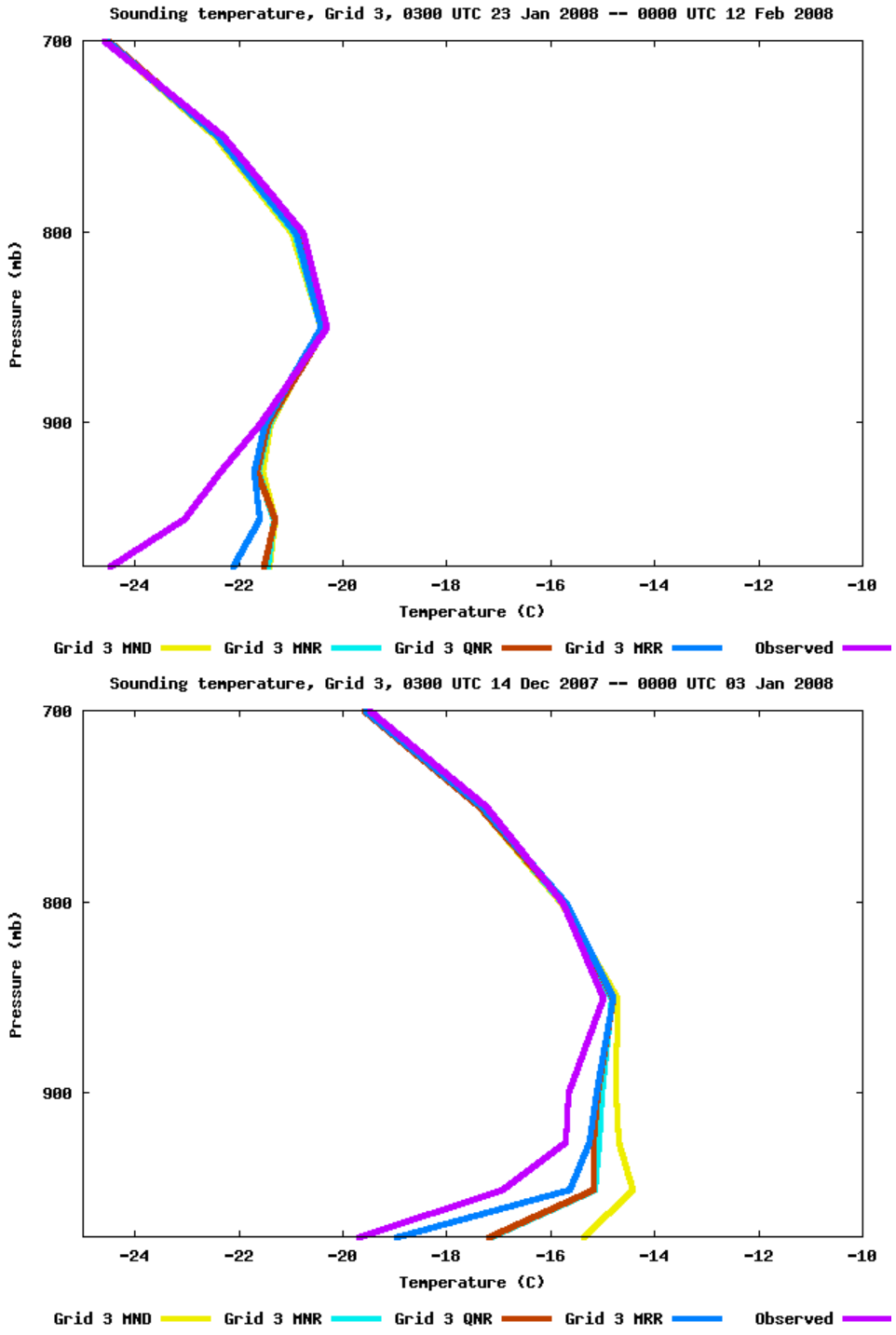


*Fig. 16: Time-averaged vertical profile of Fairbanks sounding (PAFA) temperatures for near total darkness episode (top) and partial sunlight episode (bottom). Dark blue indicates value from experiment MRR; brown indicates value from experiment QNR; light blue indicates value from experiment MNR; yellow indicates value from experiment MND; purple indicates observed sounding value.*

In order to learn more about the behavior of the different models, we examined the time series of the reported surface-level temperature of the raw Fairbanks sounding in comparison to the lowest-level model values at that location. When we compare the time series for the period surrounding the coldest temperatures of each episode (Fig. 17), an obvious diurnal trend appears in the partial sunlight episode observations during the coldest period from about Day 12 to Day 19 (4 – 11 Feb 2008). Little diurnal trend appears in the observations earlier in the episode; by contrast, the models all have a significant diurnal trend in surface temperature throughout the partial sunlight episode. The model diurnal amplitude during the 4-11 Feb 2008 period for the experiments other than MRR is approximately consistent with the observed amplitude, but the temperature values are consistently about 7°C too warm during this period. The MRR diurnal amplitude is somewhat larger than the others, such that it is similar to the other models for the warmer 0000 UTC times, but is much closer to the observations for the colder 1200 UTC times. For the period of rapidly falling temperatures immediately prior to 4-11 Feb the MRR experiment remains colder than the other models at the 1200 UTC times. In this case, the model 0000 UTC soundings are close to the observations, so the presence of a diurnal tendency in the model but not the observations during this time causes the 1200 UTC model soundings to be too cold, and the MRR sounding to be very cold.

During the near total darkness episode there is little diurnal variation in either the model or the observations. However, we again see the feature that when the temperatures are rapidly decreasing below -30°C, the MRR configuration has a substantial cold bias; once the coldest temperatures are achieved, however, the MRR configuration is better able to capture the low temperatures than the other models.

Finally, in order to gain as much insight as possible into the model-predicted PBL structure near the surface during the coldest episodes, we performed an alternate verification procedure using the raw Fairbanks sounding for the last ten days of the partial sunlight episode (2 – 12 Feb 2008). Instead of interpolating the model sounding to 25 hPa increments of the observed sounding, we interpolated the raw sounding to each WRF model level using some basic assumptions. (The WRF model levels are specified in terms of $(p - p_T)/(p_s - p_T)$ where $p_T$ is the specified model top pressure, $p_s$ is the surface pressure, and all pressures are the dry hydrostatic components; here we converted each WRF level to a pressure in the Fairbanks sounding using the observed surface pressure and the assumption that the actual pressure is approximately the dry hydrostatic pressure; the temperature at the resultant pressure was found by log-pressure interpolation. Finally, the physical height for each WRF level in the base state over ocean was used to determine the abscissa coordinate in Fig. 18.) This procedure gives us increased vertical resolution near the surface, where the model levels are much closer than 25 hPa (i.e., roughly 250 m in physical distance) apart. A plot of the temperature structure (Fig. 18) shows the same general trends as in the 25-hPa plot of Fig. 16. The two simulations using the Noah scheme (QNR and MNR) are similar, while the simulation using the RUC LSM (MRR) is consistently colder in the lowest 500 m. However, all simulations have a warm bias in the lowest 700 m. Though in the lowest 100 m the models have average vertical temperature gradients as large as, or even larger than, those in the observations, the vertical temperature gradients comprising the inversions in the observations extend to a much

greater altitude, consistent with the significantly greater temperature differences between the surface and the 1-km level found in the observations.

In summary, it appears that during periods of near total darkness and the cold, dry, calm conditions characteristic of high fine particulate concentrations, all models possess a low-level warm bias, but the bias is minimized and the statistics are generally the best in the MRR (MYJ PBL / RUC LSM / RRTMG radiation) experiment. The reason for the improved statistics in MRR for the extremely cold episodes is not precisely known at present, but it is probably related to some combination of its potentially multi-level snow model (which can serve to reduce the heat flux from the ground to the atmosphere) and the presence of a ground surface 'skin' layer in the RUC LSM (which has no thermal inertia itself and could decrease the time needed for the ground and the adjacent atmosphere to respond to a negative heat budget). A few caveats are in order, however. During the period of decreasing temperatures immediately preceding temperatures below approximately -35°C, the MRR configuration is still colder than the other models, but for these periods MRR tends to exacerbate an already cold model bias instead of improve a warm model bias. Since the observations for these falling temperature periods tend to show fairly continuous frozen precipitation (in contrast to the coldest temperature periods which tend to have ice fog and no precipitation), it is possible that all the model configurations have difficulties with modeling the microphysics/radiation interaction. For example, if the radiation scheme is not taking into account the presence of ice crystals when they exist in the actual atmosphere, the absence of their radiative heating effect on the surface during these extremely cold conditions could be significant. Another caveat is that when partial sunlight is present, MRR tends to warm more rapidly than the other models, and all models tend to have substantial warm biases in these conditions.

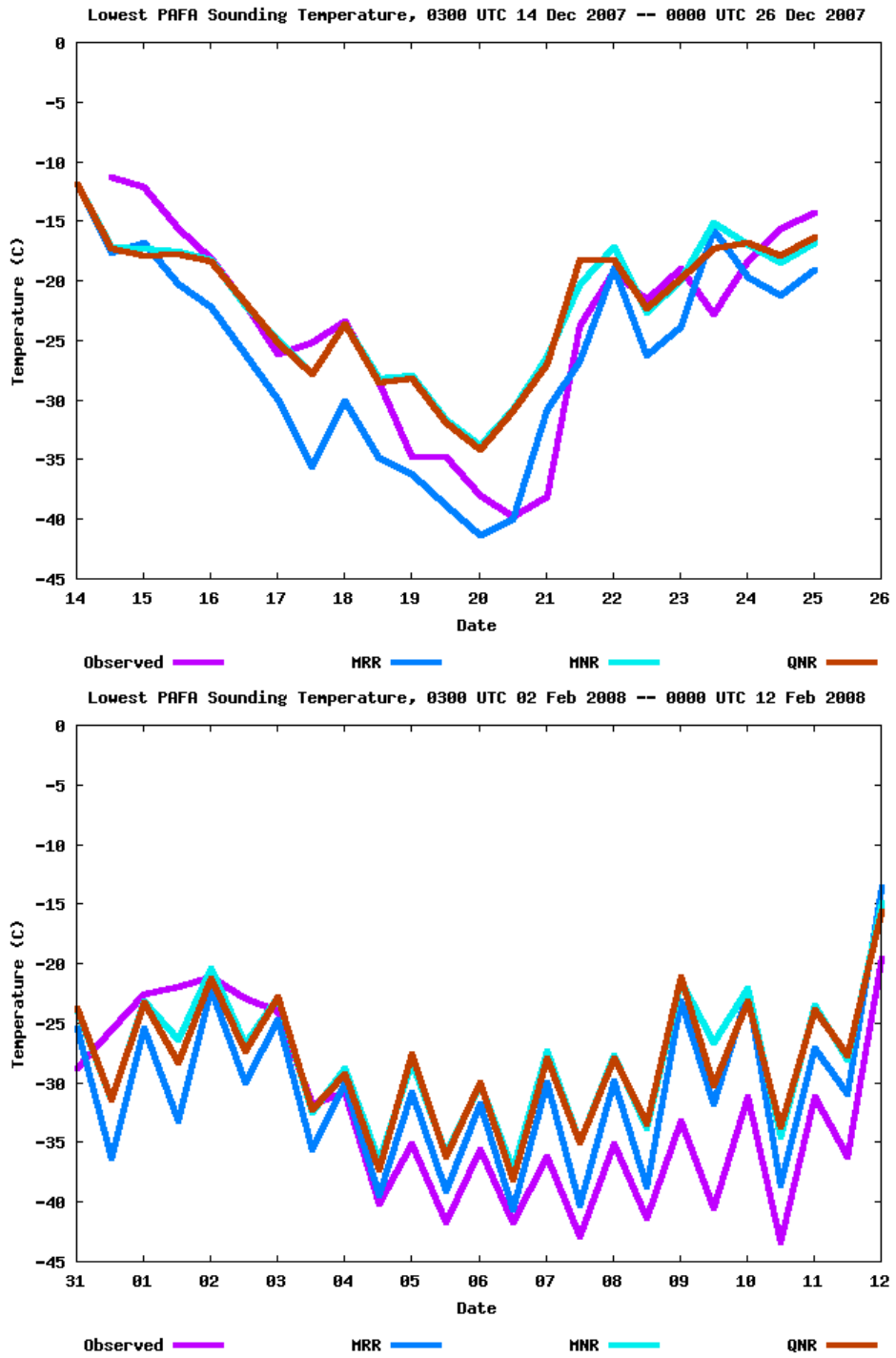


*Fig. 17: Time series of raw Fairbanks surface-level reported sounding temperatures (PAFA) for 14-26 Dec 2007 period of near total darkness episode (top), and 02-12 Feb 2008 period of partial sunlight episode (bottom). Colors are same as in Fig. 16.*

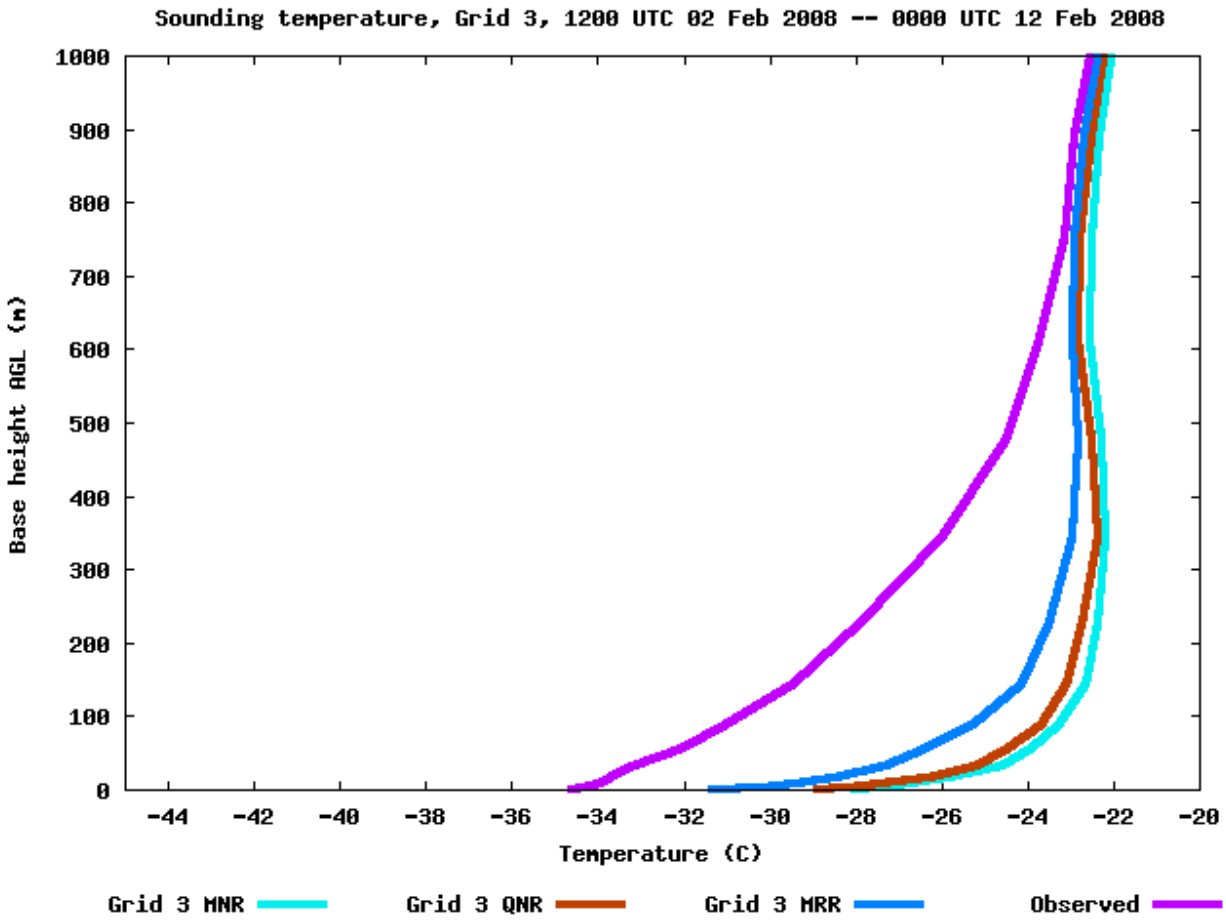


*Fig. 18: Time-averaged vertical profile of Fairbanks sounding (PAFA) temperatures for 02-12 Feb 2008 period during partial sunlight episode, where observations are interpolated to WRF vertical levels as described in text. Dark blue indicates value from experiment MRR; brown indicates value from experiment QNR; light blue indicates value from experiment MNR; purple indicates observed sounding value.*

## 5. SELECTION OF PREFERRED PHYSICS CONFIGURATION AND FINAL DYNAMIC-ANALYSIS SIMULATION

Based on the results of the physics sensitivity test, we concluded that the physics suite contained in experiment MRR (MYJ PBL, RUC LSM, and RRTMG radiation) was the best one to be used to simulate the two episodes. The high exceedance events that are of importance occur during the coldest temperature periods when the RUC LSM appeared to perform the best. However, the tendency of the MRR suite to produce significant negative temperature biases during the falling temperature periods must be noted.

We thus concluded that we should perform an additional dynamic-analysis simulation with the MRR physics package but with Grid 3 obs nudging in order to reduce the noted temperature biases and generate the best atmospheric analysis. Because the MRR Grid 2 statistics, in the presence of obs

nudging, were almost always quite good, we were optimistic that any systematic biases present in the MRR simulation on Grid 3 would be greatly alleviated through obs nudging. As noted above, however, we did not nudge the wind fields from surface data on Grid 3, whose influence is below ~150 m (see Fig. 8), because of concerns that the local topographic drainage flows generated by the model in the topography around Fairbanks may be smoothed out by the FDDA procedure. However, we did retain nudging of wind fields on Grid 3 for observations above the surface (i.e., from the Fairbanks sounding).

The initial specifications of the parameters used for the Grid 3 obs nudging simulation are listed within the parentheses of Table 2. They closely correspond to values on the other grids. However, the value of RINXY (a horizontal radius of influence) was decreased on Grid 3 from a value of 100 km to 75 km. This value was determined by performing a temporal correlation of the Grid 3 temperature innovations within the MRR no-FDDA simulation at the location of the METAR stations, and estimating the characteristic horizontal distance at which the Grid 3 METAR observational-based surface innovations were correlated for (see Fig. 19). The surface pressure difference parameter used in the horizontal weighting function in complex terrain (henceforth $\Delta p_d$) was also reduced from 75 hPa to 37.5 hPa based on the results of the correlation analysis (e.g., note the relationship between correlation value and the elevation difference labels in Fig. 19). This parameter controls how far the influence of a surface observation may spread along topography as the surface pressure varies from that at the obs site; our results suggested that some station pairs close in horizontal distance but with different vertical elevations were much less correlated than similar stations with little terrain difference.

An additional complication derives from the fact that the WRF method of reducing the weight of surface observations based on $\Delta p_d$ is different from the MM5 method defined in Stauffer and Seaman (1994). In default WRF, if there is a difference between the model surface pressure at the location of a surface observation, $p_b$, and the model surface pressure at a grid point in question, $p$, the weight of the surface observation is reduced by a factor $w$ given by:

$$w = \max\left[0.0,\ 1.0 - \frac{|p - p_b|}{\Delta p_d}\right]\left[\frac{r_0^2 - r^2}{r_0^2 + r^2}\right], \tag{1}$$

where $r$ is the horizontal distance between the grid point and the observation, and $r_0$ is the surface radius of influence parameter (RINXY in Table 2). In MM5, on the other hand, the surface pressure difference is used to artificially increase the horizontal radius of influence parameter, according to:

$$w = \frac{r_0^2 - \left[ r + r_0 \frac{|p - p_b|}{\Delta p_d} \right]^2}{r_0^2 + \left[ r + r_0 \frac{|p - p_b|}{\Delta p_d} \right]^2}. \qquad (2)$$

Though the two functions are often similar, the WRF function tends to be more horizontally isotropic and less sensitive to terrain features, as well as generally nonzero over greater horizontal differences. (The WRF method will give nonzero weights to surface observations unless either $|p\text{-}p_b|$ exceeds $\Delta p_d$ or $r$ exceeds $r_0$, whereas the MM5 method can give a zero weight even if neither criterion is met because the terrain difference increases the effective distance from observation to grid point.) In the final Grid 3 FDDA simulations used here, the MM5 method for surface pressure difference weighting was used.

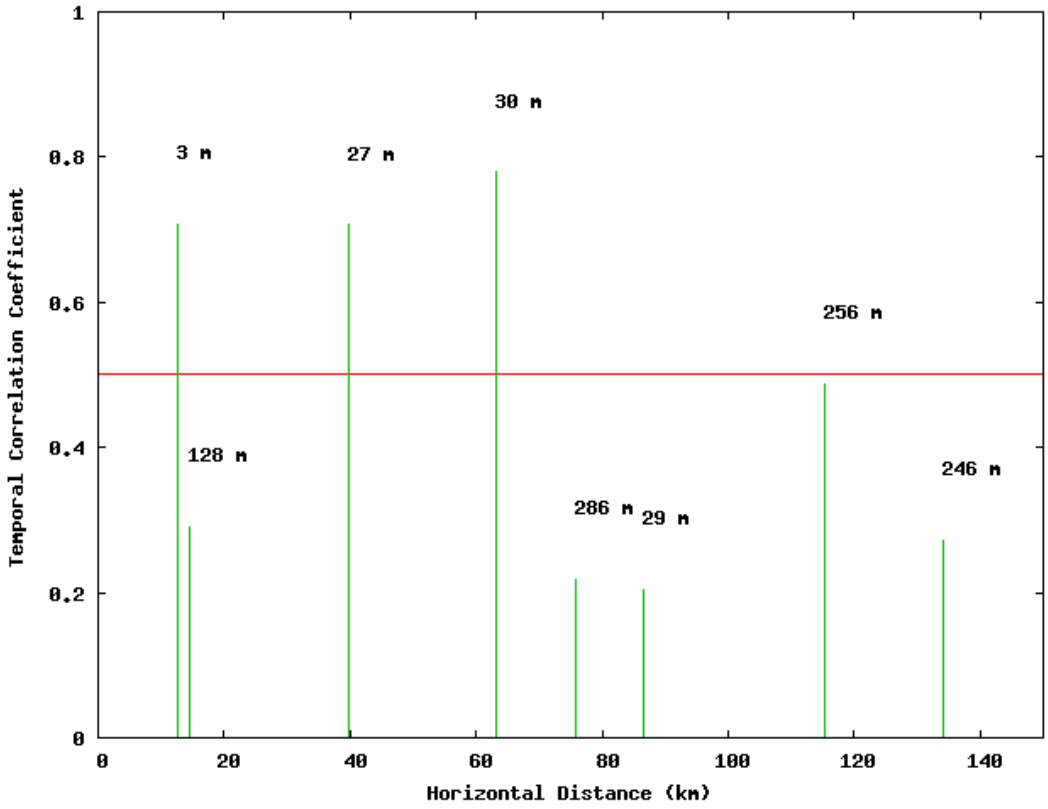


*Fig. 19: Temporal correlation coefficients vs. horizontal separation distance between various pairs of surface METAR stations located within Grid 3 (green). Red line indicates a temporal correlation coefficient of 0.5. Numerical labels indicate elevation distance between stations in meters.*

The value of TWINDO (Table 2), the obs nudging time window half-period defining the temporal influence of an innovation (Stauffer and Seaman 1994), should also be considered. Ideally this parameter would be a function of height and decrease in value towards the surface, to take into account the shorter temporal correlation time scales for surface data reflecting surface processes. Although this capability will be present in WRF version 3.2, in the version 3.1 that we used for this study, it is simply a constant (though it may vary with grid). Our experience suggests that the value chosen, 2.0 hours, is generally best for the assimilation of sounding data, but may be somewhat too large for the surface (Schroeder et al. 2006). For the final version of the Grid 3 FDDA simulations, we manually encoded the Penn State MM5 method used in WRF version 3.2 so that the effective value of TWINDO was 2.0 hours above the surface, but 1.0 hours at the surface.

Finally, two additional modifications were made to the default WRF version 3.1 FDDA procedure. In the default procedure the surface level observation of a sounding is treated differently than a surface observation. Specifically, a surface observation is assumed to be applicable to the lowest model level at the horizontal location of the observation, whereas all sounding observations including one at the surface level are assumed to be applicable at the vertical model location with the same pressure as the pressure of the observation. So a sounding surface level observation will not necessarily be placed at the lowest model level if the model surface pressure is not the same as the observed surface pressure. Also, the surface pressure difference is used to reduce the weight of a surface observation at remote horizontal grid points , but not the weight of a surface-level sounding observation. This inconsistent treatment becomes more of an issue in station-poor regions such as that of the Grid 3 used in this study, where the relative influence of the Fairbanks sounding to all Grid 3 METAR stations may be quite significant. In the final Grid 3 FDDA simulations, the code was modified to remove the surface-level observation from the rest of the sounding and treat it as a separate surface observation. Furthermore, to reflect the Penn State MM5 method, the $\Delta p_d$ weighting function was applied to soundings as a unit, in addition to surface observations.

Figures 20-22 show the vertical profiles of RMSEs verified against the Fairbanks sounding for a series of trial simulations of the first six days of the near total darkness episode (14-20 Dec. 2007) using the MRR physics suite but different variations of the Grid 3 obs nudging procedure. First, the benefit of Grid 3 obs nudging is immediately apparent, and Fig. 21 shows in particular that the simulations with retained Grid 3 wind obs nudging above the near-surface layer have substantially reduced wind speed RMSE scores in comparison with the two simulations that don't. This helps justify our proposed procedure of retaining Grid 3 wind obs nudging above the near-surface layer but turning it off within the near-surface layer to allow the model to generate its own topographic flows. Second, for the non-wind fields shown in Fig. 20 and Fig. 22 we see that the TWINDO = 2.0 hours statistics tend to be somewhat better than the TWINDO = 0.45 hours statistics, in agreement with our past experience. The proposed Grid 3 obs nudging procedure, including, among other modifications, using TWINDO = 2.0 hours above the surface but TWINDO = 1.0 hours at the surface, produces results quite similar to the TWINDO = 2.0 hours simulation.

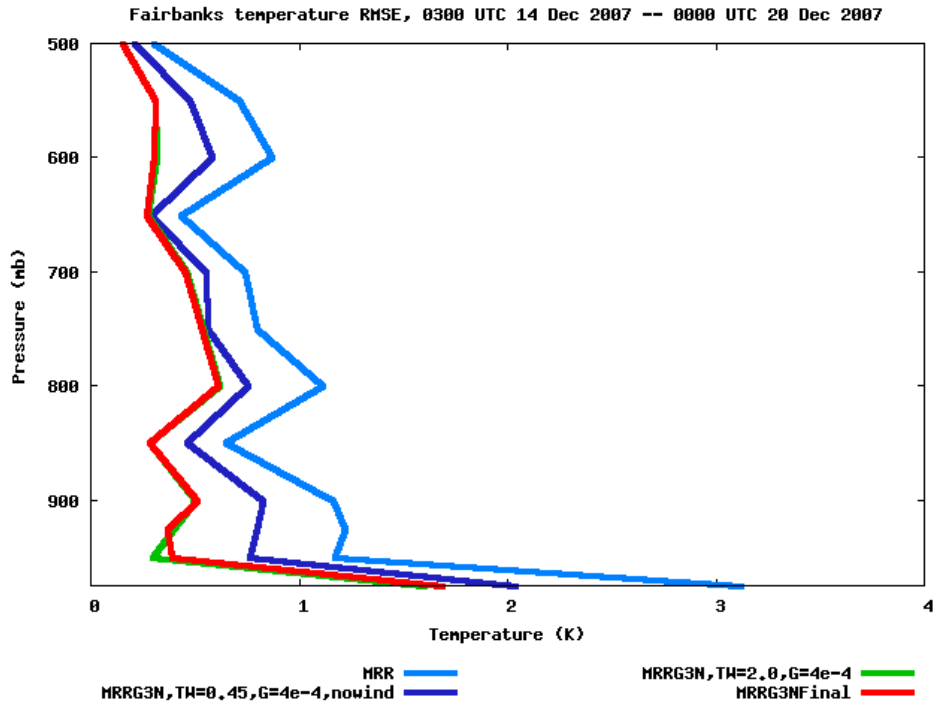


*Fig. 20: Time-averaged vertical profile of Fairbanks sounding (PAFA) temperature RMSE scores for 14-20 Dec 2007 period of near total darkness episode. Blue indicates the value from experiment MRR; violet indicates the value from MRR experiment using default Grid 3 obs nudging with TWINDO = 0.45 hours and no wind nudging; green indicates the value from MRR experiment using default Grid 3 obs nudging with TWINDO = 2.0 hours and nudging of wind above the near-surface layer only; red indicates the value from MRR experiment using the final version of Grid 3 obs nudging with the modifications as described in the text.*

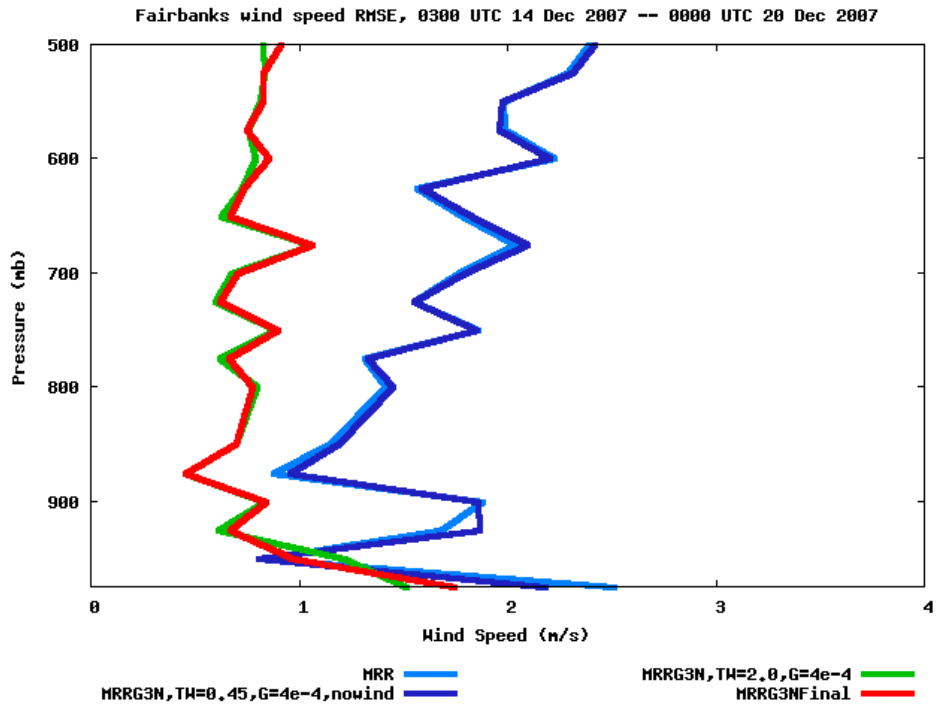


*Fig. 21: Same as Fig.20, but for wind speed RMSEs.*

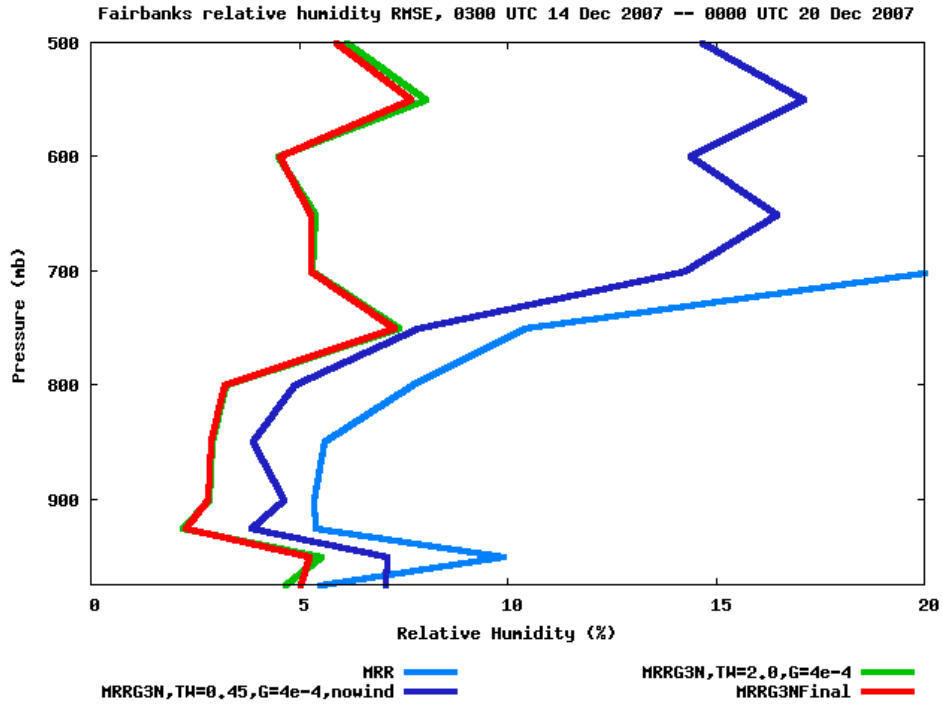


*Fig. 22: Same as Fig. 20, but for relative humidity RMSEs.*

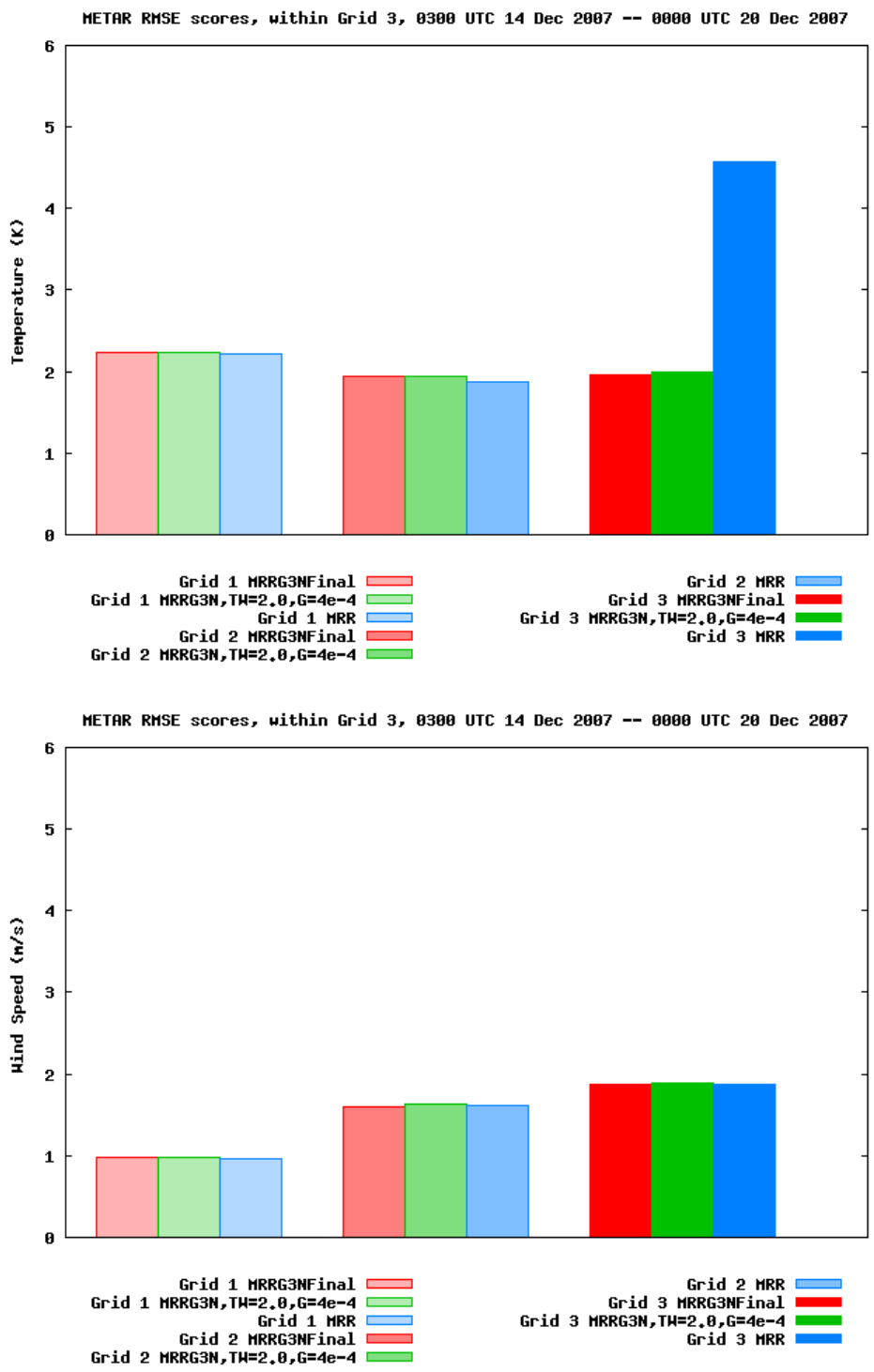


*Fig. 23: Surface METAR RMSE scores for during 14-20 Dec 2007 period of near total darkness for temperature (top) and wind speed (bottom). Blue indicates value from experiment MRR; green indicates value from experiment MRR using default Grid 3 obs nudging with TWINDO = 2.0 hours and nudging of wind above the near-surface layer only (i.e., MRRG3N,TW=2.0,G=4e-4); red indicates the value from MRR experiment using the final version of Grid 3 obs nudging with the modifications as described in the text (i.e., MRRG3NFinal).*

Fig. 23 shows RMSE statistics for the sample period for the surface METAR stations within Grid 3. The lightest, medium, and darkest shades in the histogram plot correspond to the dark blue, brown, and yellow curves in the vertical profile plots. In all cases the improvement of the MRR temperature RMSE scores from the Grid 3 obs nudging is quite dramatic, and shows the utility of our dynamic analysis approach. The fact that some of our modified obs nudging procedures carried over to all grids caused the Grid 1 and Grid 2 results to change from those of the MRR experiment, but the magnitudes of the changes are small. Wind speed statistics for the surface METARs show little sensitivity to the presence of either Grid 3 obs nudging of temperature and humidity, or Grid 3 obs nudging of winds above the near-surface layer. The proposed Grid 3 obs nudging procedure produces only slight differences from those of the more standardized Grid 3 obs nudging procedure shown, but to the extent there are differences they are generally slight improvements.

In summary, the use of our proposed modified Grid 3 obs nudging procedure, at least for this six-day test period, produces the desired effect of greatly improving the surface temperature statistics without significantly degrading the other statistics, and is also consistent with our past experience as to the preferred specification of obs nudging parameters. Therefore, we proceded to perform the final dynamic-analysis simulations in their entirety using the proposed Grid 3 obs nudging procedure.

Figures 24-26 show the overall statistics for the final dynamic-analysis Grid 3 obs nudging simulation for the entire near-total darkness episode in comparison to those of the non-Grid 3 obs nudging simulation MRR. The final temperature biases in comparison to the surface METARs are below 0.5°C in magnitude, with RMSE errors 2-3°C. The temperature RMSE errors decrease below 1°C above 900 hPa. Wind speed biases are under 1 m $s^{-1}$ at the surface, while RMSE errors are on the order of 2 m $s^{-1}$ throughout the lower troposphere. Qualitatively, the statistics for the final partial sunlight episode (Figs. 27-29) show very similar tendencies.

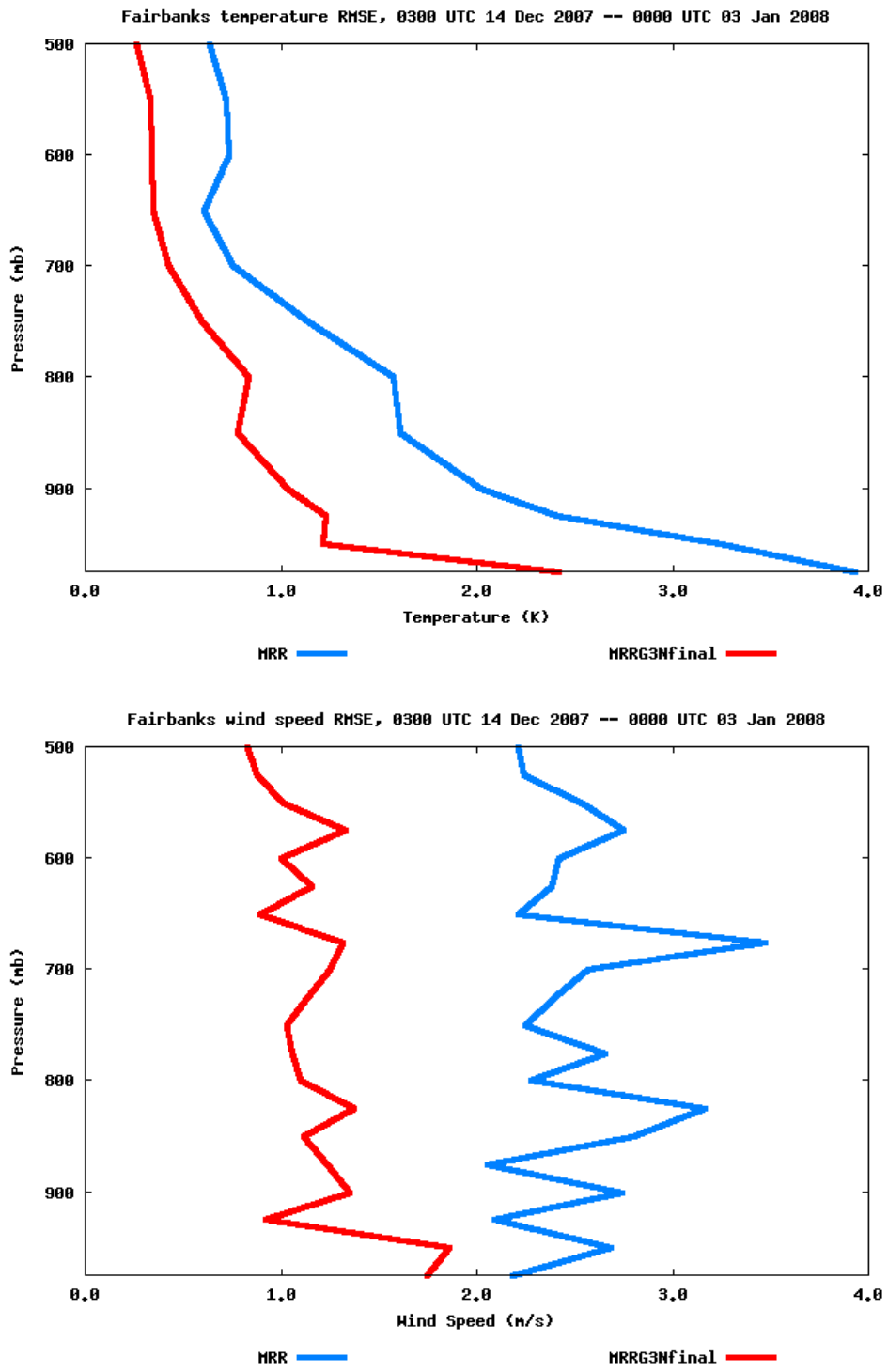


*Fig. 24: Time-averaged vertical profile of Fairbanks sounding (PAFA) on Grid 3 for temperature (top) and wind speed (bottom) for 14 Dec 2007—03 Jan 2008 near total darkness episode. Blue indicates value from experiment MRR; red indicates value from final dynamic-analysis MRR simulation using Grid 3 obs nudging.*

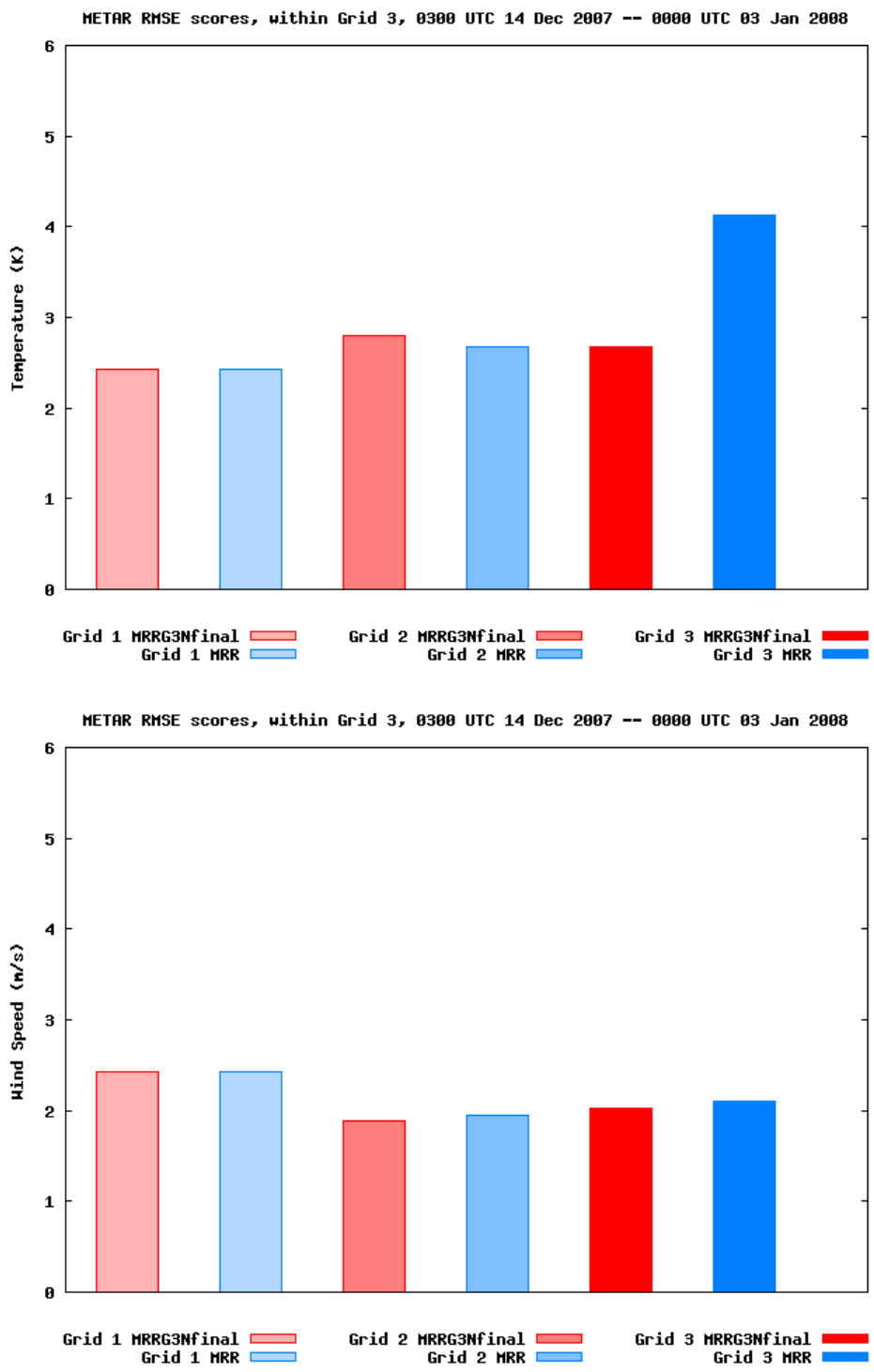


*Fig. 25: Surface METAR RMSE scores during 14 Dec 2007—03 Jan 2008 near total darkness episode for temperature (top) and wind speed (bottom). Blue indicates value from experiment MRR; red indicates value from final dynamic-analysis MRR simulation using Grid 3 obs nudging.*

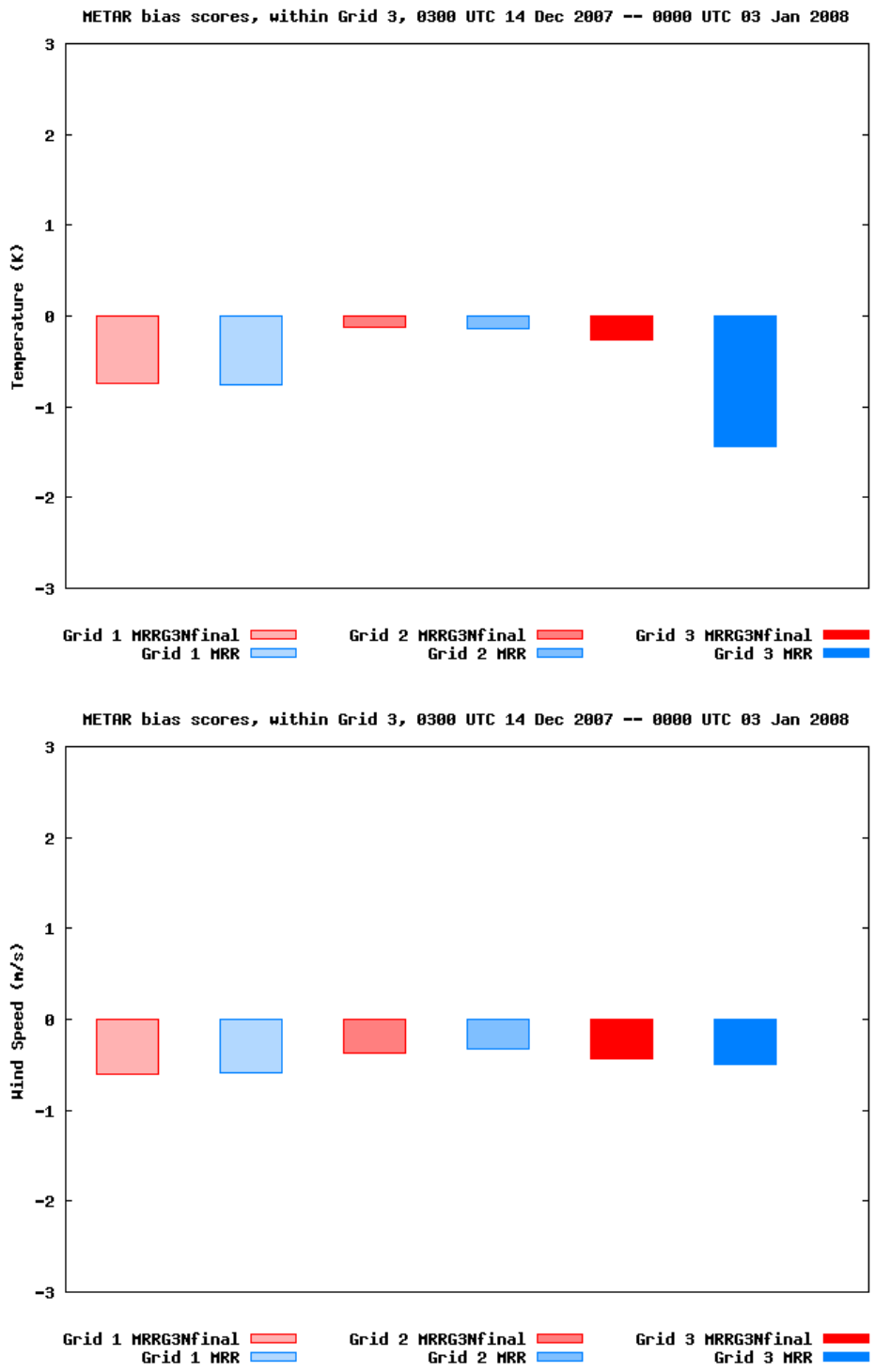


*Fig. 26: Same as Fig. 25, but for bias errors.*

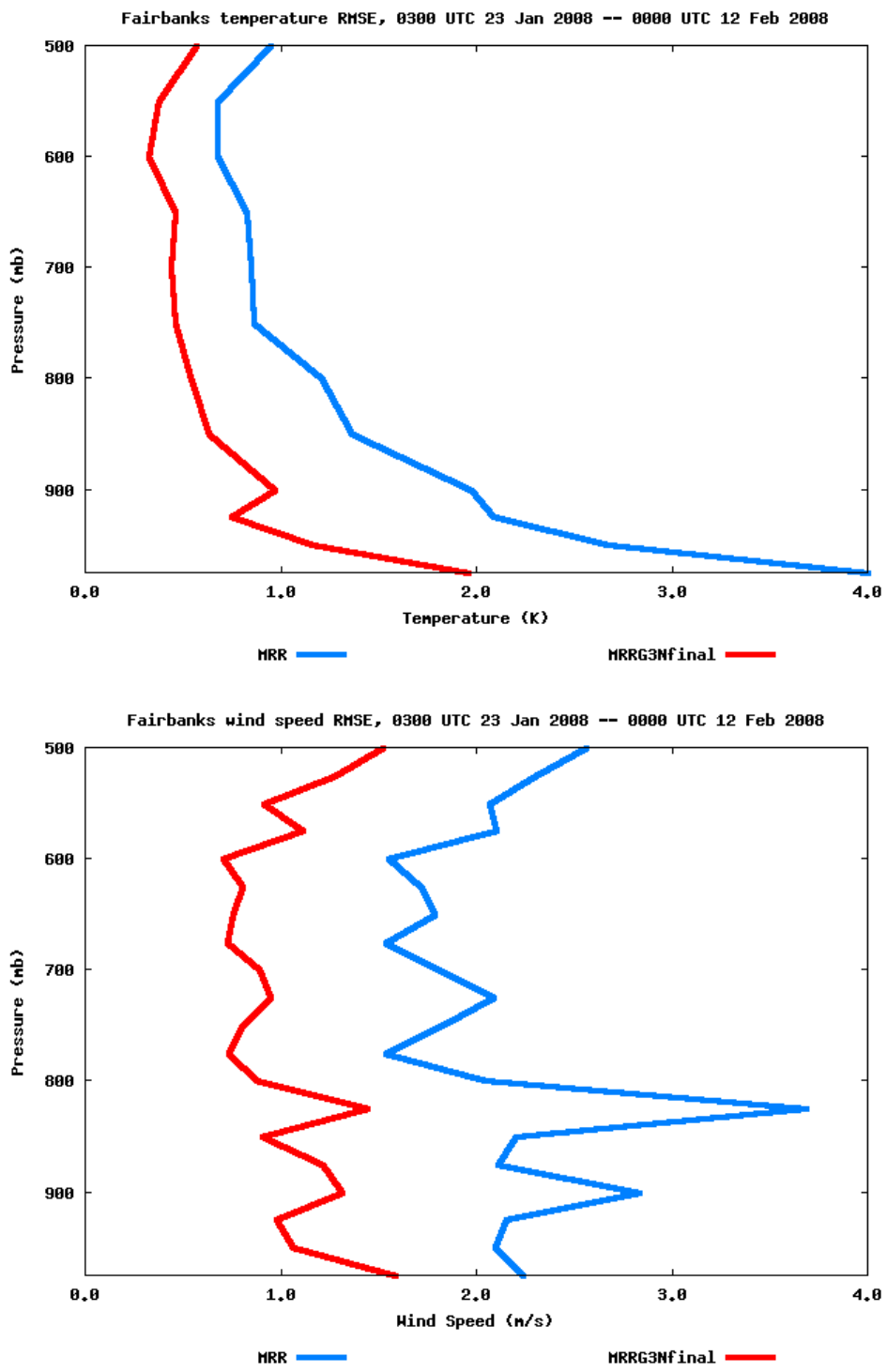


*Fig. 27: Time-averaged vertical profile of Fairbanks sounding (PAFA) on Grid 3 for temperature (top) and wind speed (bottom) for 23 Jan 2008—12 Feb 2008 partial sunlight episode. Blue indicates value from experiment MRR; red indicates value from final dynamic-analysis MRR simulation using Grid 3 obs nudging.*

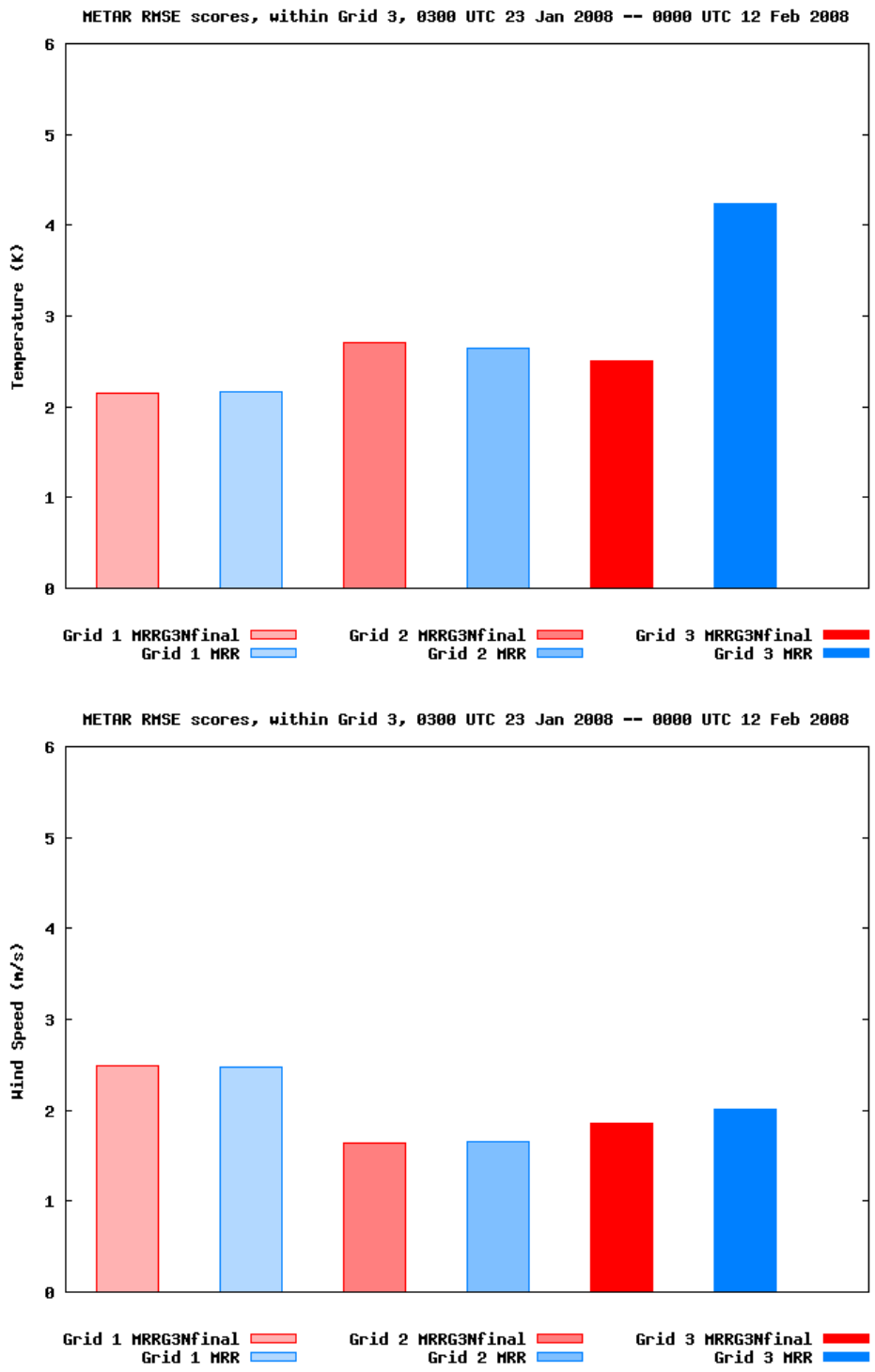


*Fig. 28: Surface METAR RMSE scores during 23 Jan 2008—12 Feb 2008 partial sunlight episode for temperature (top) and wind speed (bottom). Blue indicates value from experiment MRR; red indicates value from final dynamic-analysis MRR simulation using Grid 3 obs nudging.*

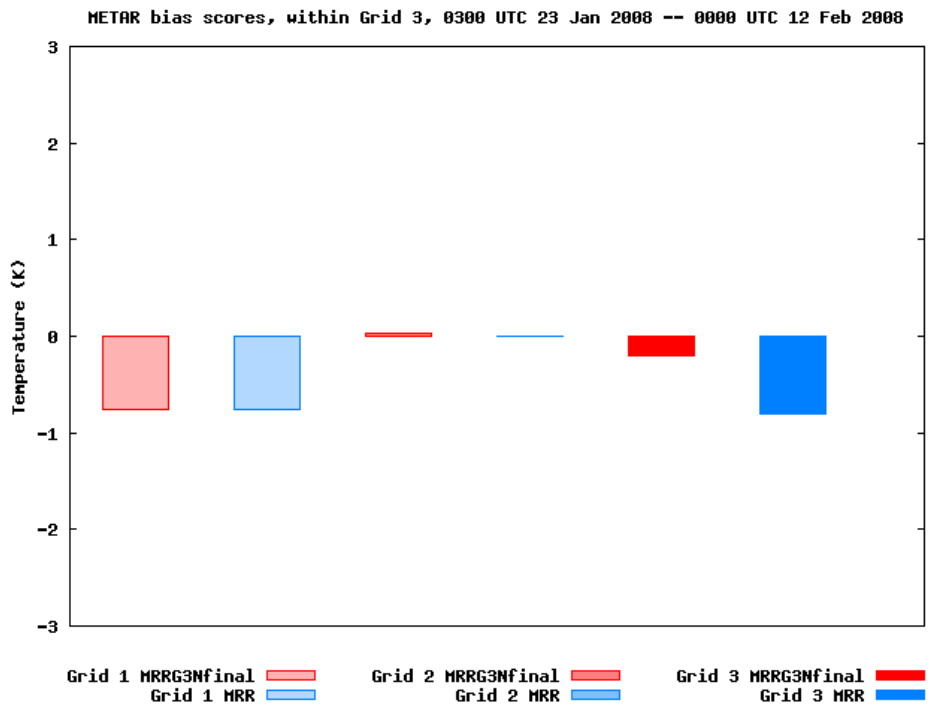


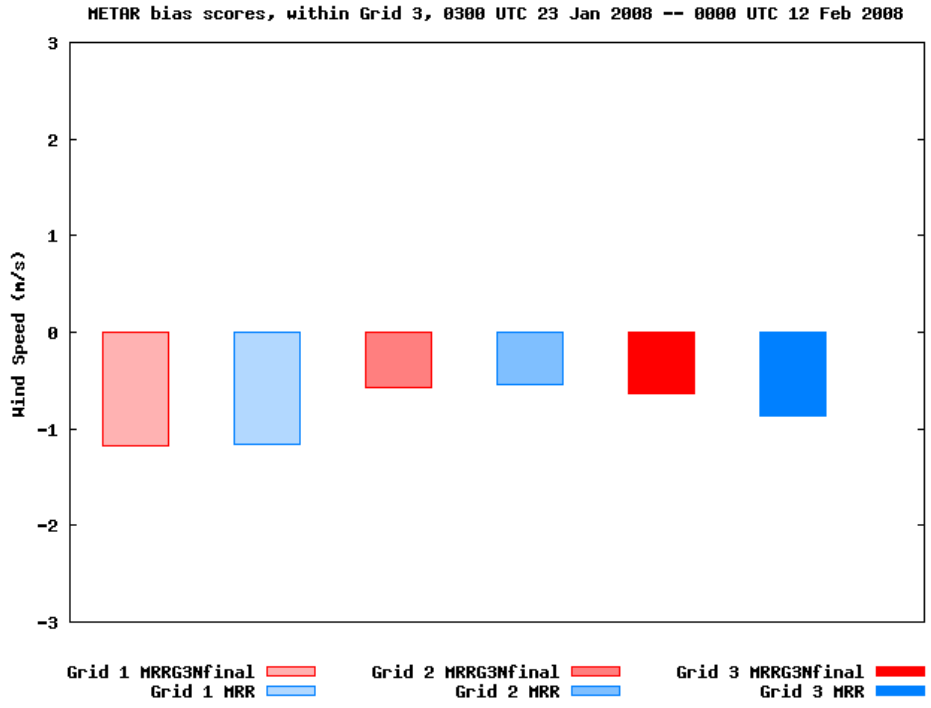


*Fig. 29: Same as Fig. 28, but for bias errors.*

## 6. CONCLUSIONS

### 6.1 Summary

The purpose of the project was to develop, adapt, and test a methodology for stable boundary layer representation (initial onset, space/time evolution, dissipation) in three-dimensional numerical models, with a specific focus on the dark, extremely cold environments such as those in the winter in the Fairbanks, AK region. A particular concern is the frequent occurrence of very high fine particular matter (PM2.5) concentrations within the stable boundary layers that form in these conditions.

Ten tasks were defined in the Statement of Work (SOW) for this project. A summary of these tasks and a brief overview of the work completed can be found in the Appendix to this report. Two twenty-day episodes were selected from the 2007-2008 winter season to study periods of extremely cold temperatures and high PM2.5 concentrations and to evaluate model performance: one in near total darkness (14 Dec 2007 – 03 Jan 2008), and the other in partial sunlight (23 Jan 2008 – 12 Feb 2008). One baseline physics configuration and three physics sensitivity experiments were performed for each episode. The physics sensitivity experiments were used to assess the impact of different planetary boundary layer (PBL) parameterizations, land surface models, and atmospheric radiation schemes on the simulations. Each simulation used three nested grids: Grid 1 (12-km horizontal grid spacing) and Grid 2 (4-km) utilized the multiscale multigrid data assimilation strategy of Stauffer and Seaman (1994) in order to ensure the model and observations remained close over the extended duration of the simulations. Grid 3 (1.3-km), centered over the Fairbanks region, did not use any direct data assimilation, and so was best-suited for quantifying the physics sensitivity; it also possesses sufficient horizontal resolution to be used by the EPA as meteorological input to chemical and air transport and dispersion models. From the different physics packages one was to be recommended to the EPA for further mesoscale modeling of the region.

The use of the three-grid configuration with a multiscale, multigrid four-dimensional data assimilation (FDDA) strategy on the outer two grids and no direct FDDA on Grid 3 consistently produced qualitatively plausible atmospheric fields throughout the variety of meteorological conditions found in the episodes, despite the relatively sparse data density. Quantitatively, the multiscale, multigrid FDDA strategy led to improved root-mean-square-error (RMSE) scores for both wind and temperature on all grids. The FDDA on the outer domains had the desired effect of improving the simulations of Grid 3 without FDDA and used for physics sensitivity tests, by providing improved lateral boundary conditions.

The best RMSE scores for the combination of both surface and sounding data required modification of the default FDDA procedure. These modifications included applying surface wind observational data to the third model vertical level instead of the lowest model level, because wind observations are normally taken at a height of 10 m which is the height of the third level in the high vertical resolution configuration used here. The influence of surface observations was also restricted to approximately the lowest 100 m, instead of to the top of the PBL, because the model-predicted PBL height in these simulations, based on the turbulent kinetic energy profile, was often found to be 1 km or higher. This

correction applied the surface innovation (observation minus model value) in these predominantly stable boundary layers over a much shallower layer than in the default FDDA procedure and produced improved statistical results in the lower troposphere.

All model physics combinations tended to have a positive temperature bias on Grid 3, especially during the most extremely cold periods. All of the physics sensitivity tests tended to reduce the warm bias in comparison with the selected baseline physics package. Switching from the RRTM longwave / Dudhia shortwave radiation package to the RRTMG longwave and shortwave radiation package led to significantly reduced warm biases and better RMSE statistics. RRTMG was then used in all future physics sensitivity tests. The reduced warm bias seemed to be due to the longwave component, both because of direct examination of surface fluxes in the partial sunlight case, and due to the fact that the difference was more pronounced in the near total darkness episode.

Though none of the four physics suites tested in the study was unambiguously superior to all of the others in terms of RMSE statistics, the simulation with the Rapid Update Cycle (RUC) land surface model, the Mellor-Yamada-Janjić (MYJ) PBL model, and the RRTMG radiation package was selected as the one to be recommended to EPA for modeling extremely cold SBLs and as the basis for producing the final atmospheric analysis. For both the near-total-darkness and partial sunlight episodes, the MYJ/RUC/RRTMG (henceforth MRR) physics suite had the lowest surface wind speed RMSE scores. For the partial sunlight episode the MRR configuration was one of two physics suites with the lowest surface temperature RMSE scores, and was among the lowest for the near-total-darkness episode. Of all the physics suites, the MRR package had the lowest warm bias during the most extremely cold periods, both when compared to the surface METAR stations and the Fairbanks sounding. The reason is not known for sure but is probably due to some combination of the effects of its snow model and top-level 'skin' layer. Since the extremely cold conditions are those with the potential for the highest PM2.5 concentrations, we took this as an additional reason to recommend the MRR physics suite for use by EPA.

However, there were periods in each episode, generally when the temperature was steadily decreasing in advance of an extremely cold period, during which all the physics configurations would tend to have a cold bias. During these periods the MRR configuration would still have colder temperatures than the other physics suites, and thus have worse magnitude temperature biases and RMSE scores. The relatively poorer performance of the MRR suite during a such a period accounts for the relatively poorer surface temperature statistics of the MRR suite compared to the MNR suite for the entire near-total-darkness episode. The reason for this behavior is not definitely known, but it is thought to be related to the interaction of radiation with the ice condensate that tends to occur during these periods. Also, the temperature biases of the MRR physics suite during the extremely cold period near the end of the partial sunlight episode were not quite as improved during daylight hours as during nighttime hours as compared to the other physics suites. Therefore, while overall we recommended the MRR configuration to EPA for these episodes, we also strongly recommended that the final fine-scale atmospheric data analysis (i.e., from Grid 3) to be provided to EPA should come from an additional simulation in which FDDA is performed directly on Grid 3, in order to reduce some of this error.

Use of obs nudging for temperature and humidity (and not surface wind) on Grid 3 produced large improvements in the mass fields as expected, and also improvements in the wind fields above the surface. Results were very encouraging and suggested that a smaller (larger) time window should be used for the surface (above-surface) data assimilation. This capability present in the Penn State MM5 FDDA system has been added to the new-release version of WRF.

In addition to this final report, deliverables to the EPA will include the full three-dimensional output at relatively fine temporal resolution (every 1 hour for Grid 1; every 12 minutes for Grids 2 and 3) for the final Grid 3 nudging simulation as well as all the baseline and physics sensitivity simulations. Model namelists, initialization files, and modifications to the model source code will also be provided.

The development and refinement of WRF FDDA capabilities and supporting software, including the surface analysis nudging, observation nudging and the OBSGRID objective analysis and obs-nudging pre-processing code, occurred concurrently with this project. This separate development effort led by PI Dave Stauffer and funded by the Defense Threat Reduction Agency (DTRA) allowed us rapid access to the most recent and robust versions of the WRF FDDA code, which greatly benefited this project.

The results of the default FDDA procedures not performing well here in this high vertical resolution modeling study of stable boundary layer environments motivated an additional FDDA code development effort to make the vertical influence functions of surface observations within the FDDA be a function of stability regime type, as well as to provide the user with greater flexibility in specifying the vertical influence functions. These modifications were not finalized in time to be used for this project but are scheduled to appear in the next official release of the WRF model.

An extended abstract and oral presentation were made at the 13$^{th}$ Conference on Mesoscale Processes (Gaudet et al. 2009), and a manuscript based on the project is in preparation.

**6.2 Limitations of the Study and Recommendations for Future Work**

Sensitivity to the microphysics parameterization was not performed here, but may be important to investigate further. In particular, results from this study suggested that both the occurrence of large negative RUC temperature biases and large differences between the RRTM and RRTMG longwave radiation schemes tended to occur when low-level ice condensate was present. Therefore, the microphysics / radiation interaction should probably be investigated further.

A fourth grid with 0.44-km horizontal grid spacing centered over Fairbanks was set up and initialized with topography, but it was not used in the sensitivity experiments here. Although this is finer horizontal resolution than the resolution requested by EPA, some of Penn State's past studies of SBLs (Stauffer et al. 2009) have suggested that the weak wind flows in these conditions may be sensitive to topographic features on these smaller scales, and it might be important to know if finer resolution is also required to resolve the topographic flows of the Fairbanks region.

The latest version of the WRF FDDA code has been designed to have more flexibility in how the temporal and spatial weighting functions are specified. Future simulations that use these new WRF FDDA options that were not yet available for this study should produce a further reduction of model error.

The availability of more meteorological observations from the immediate Fairbanks North Star Borough region, and in particular observations immediately above the surface, would allow one to make a more rigorous assessment of the accuracy of the different physics schemes (in particular, the PBL parameterizations).

More testing and analysis of the model physical parameterizations should be performed to determine the cause of the strong model biases often observed in the simulations, such as the generally persistent warm bias, and the cold RUC land surface model bias during falling temperature conditions.

## 7. REFERENCES


Benjamin, S.O., and N.L. Seaman, 1985: A simple scheme for objective analysis in curved flow. *Mon. Wea. Rev.*, **113**, 1184-1198.

Benson, C.S., 1970: Ice fog: Low temperature air pollution. Research Report 121. U.S. Army Corps of Engineers, Cold Regions Research and Engineering Laboratory, Hanover, NH, 118 pp.

Bromwich, D.H., J.J. Cassano, T. Klein, G. Heinemann, K.M. Hines, K. Steffen, and J.E. Box, 2001: Mesoscale modeling of katabatic winds over Greenland with the Polar MM5. *Mon. Wea. Rev*., **129**, 2290-2309.

Chen, F., and J. Dudhia, 2001: Coupling an advanced land-surface/hydrology model with the Penn State/NCAR MM5 modeling system. Part I: Model implementation and sensitivity. *Mon. Wea. Rev*., **129**, 569-585.

Deng, A., D. Stauffer, B. Gaudet, J. Dudhia, J. Hacker, C. Bruyere, W. Wu, F. Vandenberghe, Y. Liu, and A. Bourgeois, 2009: Update on WRF-ARW end-to-end multi-scale FDDA system. *10th Annual WRF Users' Workshop*, 23 Jun 2009, Boulder, CO.

Dudhia, J., 1989: Numerical study of convection observed during winter monsoon experiment using a mesoscale two-dimensional model. *J. Atmos. Sci*., **46**, 3077-3107.

Galperin, B., S. Sukoriansky, and P.S. Anderson, 2007: On the critical Richardson number in stably stratified turbulence. *Atmos. Sci. Let.*, **8**, 65-67.

Gaudet, B., D. Stauffer, N. Seaman, A. Deng, K. Schere, R. Gilliam, J. Pleim, and R. Elleman, 2009: Modeling extremely cold stable boundary layers over interior Alaska using a WRF FDDA system.

*13th Conference on Mesoscale Processes*, 17-20 Aug, Salt Lake City, UT, American Meteorological Society.

Girard, E., and J.-P. Blanchet, 2001: Microphysical parameterization of Arctic diamond dust, ice fog, and thin stratus for climate models. *J. Atmos. Sci.*, **58**, 1181-1198.

Hanna, S.R., 1983: Lateral turbulence intensity and plume meandering during stable conditions. *J. Appl. Meteor.*, **22**, 1424-1430.

Hines, K.M., and D.H. Bromwich, 2008: Development and testing of polar Weather Research and Forecasting (WRF) model. Part I: Greenland ice sheet meteorology. *Mon. Wea. Rev.*, **136**, 1971-1989.

Janjić, Z.I., 2002: Nonsingular implementation of the Mellor-Yamada Level 2.5 Scheme in the NCEP Meso model. NCEP Office Note 437, 61 pp.

Mahrt, L., 2009: Characteristics of submeso winds in the stable boundary layer. *Boundary-Layer Meteorology*, **130**, 1-14.

Mlawer, E.J., S.J. Taubman, P.D. Brown, M.J. Iacono, and S.A. Clough, 1997: Radiative transfer for inhomogeneous atmosphere: RRTM, a validated correlated-k model for the longwave. *J. Geophys. Res.*, **102**, 16663-16682.

Mölders, N. and G. Kramm, 2010: A case study on wintertime inversions in interior Alaska with WRF. *Atmos. Res.*, **95**, 314-332.

Morrison, H., J.A. Curry, and V.I. Khvorostyanov, 2005: A new double-moment microphysics parameterization for application in cloud and climate models. Part I: Description. *J. Atmos. Sci.*, **62**, 1665-1677.

Seaman, N.L., and S.A. Michelson, 2000: Mesoscale meteorological structure of a high-ozone episode during the 1995 NARSTO-Northeast study. *J. Appl. Meteor.*, **39**, 384-398.

Seaman, N.L., B. Gaudet, A. Deng, S. Richardson, D.R. Stauffer, J.C. Wyngaard, and L. Mahrt, 2008: Evaluation of meander-like wind variance in high-resolution WRF model simulations of the stable nocturnal boundary layer. *10th Conference on Atmospheric Chemistry*, 21-24 Jan, New Orleans, LA, American Meteorological Society.

Serreze, M.C., J.D. Kahl, and R.C. Schnell, 1992: Low-level temperature inversions of the Eurasian Arctic and comparison with Soviet drifting station data. *J. Climate*, **5**, 615-629.

Skamarock, W.C., J.B. Klemp, J. Dudhia, D.O. Gill, M. Barker, M.G. Duda, X.-Y. Huang, W. Wang, and J.G. Powers, 2008: A description of the Advanced Research WRF version 3. NCAR Technical Note NCAR/TN475+STR.

Smirnova, T.G., J.M. Brown, and D. Kim, 2000: Parameterization of cold-season processes in the MAPS land-surface scheme. *J. Geophys. Res.*, **105**, 4077-4086.

Stauffer, D.R., and N.L. Seaman, 1994: Multiscale four-dimensional data assimilation. *J. Appl. Meteor.*, **33**, 416-434.

Stauffer, D.R., N.L. Seaman, and F.S. Binkowski, 1991: Use of four-dimensional data assimilation in a limited-area mesoscale model. Part II: Effects of data assimilation with the planetary boundary layer. *Mon. Wea. Rev.*, **119**, 734-754.

Stauffer, D.R., B.J. Gaudet, N.L. Seaman, J.C. Wyngaard, L. Mahrt and S. Richardson, 2009: Sub-kilometer numerical predictions in the nocturnal stable boundary layer. *23rd Conference on Weather Analysis and Forecasting/19th Conference on Numerical Weather Prediction*, 1-5 Jun, Omaha, NE, American Meteorological Society.

Sukoriansky, S. B. Galperin, and V. Perov, 2005: Application of a new spectral theory of stably stratified turbulence to atmospheric boundary layers over sea ice. *Boundary-Layer Meteorology*, **117**, 231-257.

Vickers, D., and L. Mahrt, 2004: Evaluating formulations of stable boundary layer height. *J. Appl. Meteor.*, **43**, 1736-1749.

Wyngaard, J.C., 2004: Toward numerical modeling in the 'Terra Incognita'. *J. Atmos. Sci.*, **61**, 1816-1826.

## APPENDIX – SUMMARY OF TASKS

Ten tasks were included in the Statement of Work (SOW) for this project. An overview of the tasks and a summary of the work completed on each of these tasks are provided below:

- Task 1 – Participate in kick-off teleconference in accordance with the SOW.

This took place on 11 Sep 2008. The EPA was provided with the specifications of the nested grid configuration that we proposed in the SOW, and we received in turn particular information about the period and region of study from the EPA.

- Task 2 – Prepare workplan and QA/QC plan in accordance with the SOW.

This was submitted to the EPA during Nov. 2008, along with an updated timetable of deliverables provided during the next monthly teleconference. Included was a description of our proposed simulation plan, choice of baseline physics and grid configuration, and method of simulation.

- Task 3 – Participate in monthly project teleconferences.

We held hour-long teleconferences with the project manager and other scientists at Research Triangle Park and EPA Region 10 (which includes Alaska in its jurisdiction) near the beginning of every month between the kick-off meeting and Jan. 2010. These teleconferences were indispensible for coordinating the needs of EPA with our capabilities and adapting to unforeseen developments as they arose.

- Task 4 – Prepare brief monthly progress reports.

These reports provided to the EPA at the end of every month from Oct. 2008 – Dec. 2009, contained in total most of the information and task completion history found in this report.

- Task 5 – Set up meteorological model and conduct initial baseline testing.

After some minor modifications were made to the proposed model grid configuration to maximize the utility of available data, the final specifications of Grids 1, 2, and 3 were confirmed with the EPA in Feb. 2009; more precise coordination of these grids with a parallel emissions modeling project were completed in May 2009. The data assimilation procedures required for the multiscale multigrid procedure to be used for the project were still being developed for the WRF meteorological model, led by PI Dave Stauffer also working on this contract, which helped expedite the testing and validation of these procedures. Furthermore, the testing results had to be confirmed with the version 3.1 of WRF used for most of this study, released in Apr 2009. By Jun 2009 we determined that the model components were ready to begin physics sensitivity testing.

- Task 6 – Develop and/or adapt one or more stable boundary layer and land-surface models in accordance with the SOW.

For the choice of stable boundary model in the WRF baseline physics package, we used the Mellor-Yamada-Janjić (MYJ) parameterization that we had used for our previous studies of the stable boundary layer in Alaska, with a few modifications. For the land surface model, however, we decided that we should make use of the Noah model available in version 3.1 of WRF, since it included a number of adaptations to snow-covered terrain that would be critical in this study. Using the particular Noah adaptations in version 3.1 of WRF was one reason for using that model when it became available. After we confirmed that using the Noah land surface model initialized with Global Forecast System (GFS) model data produced reasonable results, we discovered that the default WRF data assimilation procedure needed to be modified to interact properly with the stable boundary layers generated by the high-resolution model. By Jul 2009 we had decided on the baseline physics package to be used for the main simulations.

- Task 7 – Conduct up to five sensitivity tests for the selected modeling periods and evaluate results in accordance with the SOW.

Two twenty-day episodes from the 2007-2008 winter season, both with periods of extremely cold temperatures and high PM2.5 concentrations, were selected for evaluation of model performance: one in near total darkness (14 Dec 2007 – 03 Jan 2008), and the other in partial sunlight (23 Jan 2008 – 12 Feb 2008). In addition to the baseline physics configuration that included the MYJ planetary boundary layer (PBL) scheme, the Noah land surface model, and the RRTM longwave / Dudhia shortwave radiation package, three other physics sensitivity tests were performed for the entirety of each twenty-day episode, which involved using the RRTMG radiation package (longwave and shortwave), the Quasi-Normal Scale Elimination (QNSE) PBL scheme, and the Rapid Update Cycle (RUC) land surface model. After some discussion, the specific combinations used, in addition to the baseline, were MYJ / Noah / RRTMG, QNSE/ Noah / RRTMG, and MYJ / RUC / RRTMG. After statistical comparison with available observations, there was no clearly superior model physics combination; however, the MYJ / RUC / RRTMG option seemed to do the best job at reproducing the extremely cold temperatures characteristic of the high exceedance episodes. However, all model configurations tended to have substantial warm surface temperature biases in these conditions on the innermost 1.3-km Grid 3 when no data assimilation was performed on it. (Data assimilation was performed on the outer Grids 1 and 2 for the physics sensitivity experiments to improve the lateral boundary conditions on Grid 3.) In Jan 2009 it was decided that the MYJ / RUC / RRTMG combination was to be recommended, but that final dynamic analyses using this physics package along with Grid 3 data assimilation should be performed for each episode in order to reduce the atmospheric model errors and biases before they are used in air transport and chemistry models.

- Task 8 – Participate in 1.5-day meeting with Project Officer and scientific staff at EPA/RTP in accordance with the SOW.

This meeting occurred 19-20 Nov 2009 at Research Triangle Park (RTP), NC, between one of the co-PI's (Brian Gaudet) and the Project Officer and other scientific staff at RTP. During this meeting scientific discussion of the results occurred, and a preliminary agreement that the MYJ/RUC/RRTMG combination was the most promising was reached. The main results of the project to date were presented, and plans for bringing the project to completion were made.

- Task 9 – Prepare final report and electronic data and computer code files in accordance with the SOW.

- Task 10 – Revise draft final report and data files.

This report serves to help complete Tasks 9 and 10. A pair of 2-Terabyte external hard drives were obtained from EPA for use for transferring the data, whose cumulative size is approximately 600 Gigabytes per episode simulation. The files to be transferred consist of a full three-dimensional set of model output files, generated every hour for the 12-km Grid 1, and every 12 minutes for the 4-km Grid 2 and 1.3-km Grid 3. The output for each episode from the final dynamic initialization (i.e., with data assimilation on Grid 3) using the best choice physics package will be transferred first; later, the output from the baseline and physics sensitivity studies without Grid 3 data assimilation will be transferred to EPA. In addition, the namelist specifications for each simulation, the WRF version 3.1 code as modified for the project, and the initial, boundary condition, and four-dimensional data assimilation (FDDA) files required for each WRF simulation will be included.

# Investigation of means for $PM_{2.5}$ mitigation through atmospheric modeling

Final report Phase I
12/1/08 – 12/31/10

Prepared for the Fairbanks North Star Borough

By

Nicole Mölders, Huy N.Q. Tran and Ketsiri Leelasakultum

Geophysical Institute and College of Natural Sciences and Mathematics
Department of Atmospheric Sciences

April 2011

## Summary

The Alaska adapted Weather Research and Forecasting model incline coupled with a chemistry package is used to assess the situation of $PM_{2.5}$ concentrations in the Fairbanks $PM_{2.5}$-nonattainment area in the winter months, to explore two mitigation scenarios and to assess the role of point-source emissions for the $PM_{2.5}$ concentrations at breathing level. The evaluation of the model results by the few data available suggests overall acceptable performance of WRF/Chem. WRF/Chem was chosen, as this research model was an air-quality model that was already adapted and tested for Alaska conditions.

Simulations were performed with WRF/Chem with and without consideration of point-source emissions for November 2005 to February 2006. The results suggest that point-source emissions contribute to the $PM_{2.5}$-nonattainment problem, but are not the main cause.

Two mitigations scenarios were performed for October 2008 to March 2009. The first mitigation scenario was a direct one as it assumed reduction of $PM_{2.5}$-emissions by replacing non-certified wood-burning devices with certified wood-burning devices while keeping emissions from all non-wood burning sectors the same. Comparison of the reference simulation that assumes business-as-usual, with the various simulations assuming replacement of non-certified wood-burning devices indicates that such replacements reduce the $PM_{2.5}$-concentrations at breathing level. However, a small replacement program that leads to only 6% reduction of $PM_{2.5}$-emissions on average is insufficient to achieve attainment. According to sensitivity studies, the magnitude of $PM_{2.5}$-concentration reductions at breathing level depends strongly on the number and kind of devices replaced, and the assumed partitioning of heating among devices in households with more than one heating device. Further uncertainty results from the unknown location of wood-burning devices.

Since $PM_{2.5}$ is not only emitted, but also can form by physio-chemical processes (gas-to-particle conversion) in the atmosphere from precursor gases, the second mitigation scenario addressed an indirect strategy to achieve mitigation of the $PM_{2.5}$ problem by reducing an important precursor of $PM_{2.5}$ namely sulfur. This emission-reduction scenario assumed the introduction of low sulfur fuel for domestic heating and use in all oil-burning facilities (e.g. oil-burning power plants) if they did not already use low sulfur fuel. This simulation was also performed for October 2008 to March 2009. Comparison of the results of the simulations suggest that on average over the entire winter and nonattainment area, a slightly higher reduction of $PM_{2.5}$-concentrations can be achieved when introducing low sulfur fuel than for the small wood-burning device replacement program assumed in the other emission reduction scenario. However, the results also suggest that locally and temporally $PM_{2.5}$-concentrations may increase after introduction of low sulfur fuel due to shifts in the equilibria of precursor concentrations. The increase is due to a shift towards more formation of nitrate that has a higher mass than sulfate. Note that introduction of low sulfur fuel not only changes the emissions of $SO_2$, but also the emissions of other species released during the combustion of oil and hence causes a shift in the distribution of precursors. The effect of such shifts in precursors on the equilibria depends on temperature, light and moisture conditions. The aforementioned meteorological conditions all affect gas-to-particle conversion and hence the production of $PM_{2.5}$ in the atmosphere. Since introduction of low sulfur fuel may, under certain conditions, lead to increased, instead of decreased $PM_{2.5}$-concentrations, a woodstove replacement program seems to be the safer way to achieve mitigation than a measure that tries to achieve mitigation indirectly.

Calculation of the relative response factors and new design values suggests that none of the scenarios assumed in this study may alone lead to attainment. Therefore, combined measures and/or other measures like enhancement of the use of gas should be examined in the future.

## 1. Brief description of Fairbanks' nonattainment problem

In 2006, the Environmental Protection Agency (EPA) tightened the previous 24h National Ambient Air Quality Standard (NAAQS) for particulate matter (PM)[1] with diameter <2.5µm ($PM_{2.5}$) from 65µg/m$^3$ to 35µg/m$^3$. The annual $PM_{2.5}$ standard of 15µg/m$^3$ remained. Data collected by the Fairbanks North Star Borough (FNSB) and faculty at the Geophysical Institute (GI) indicate that in the past years 24h-average $PM_{2.5}$ concentrations[2] exceeded the new standard frequently (cf. Fig. 1). Since in previous years, the measurements at the official PM measurement site of the FNSB at the State Building exceeded the new NAAQS for $PM_{2.5}$ repeatedly, a $PM_{2.5}$ nonattainment area was assigned.

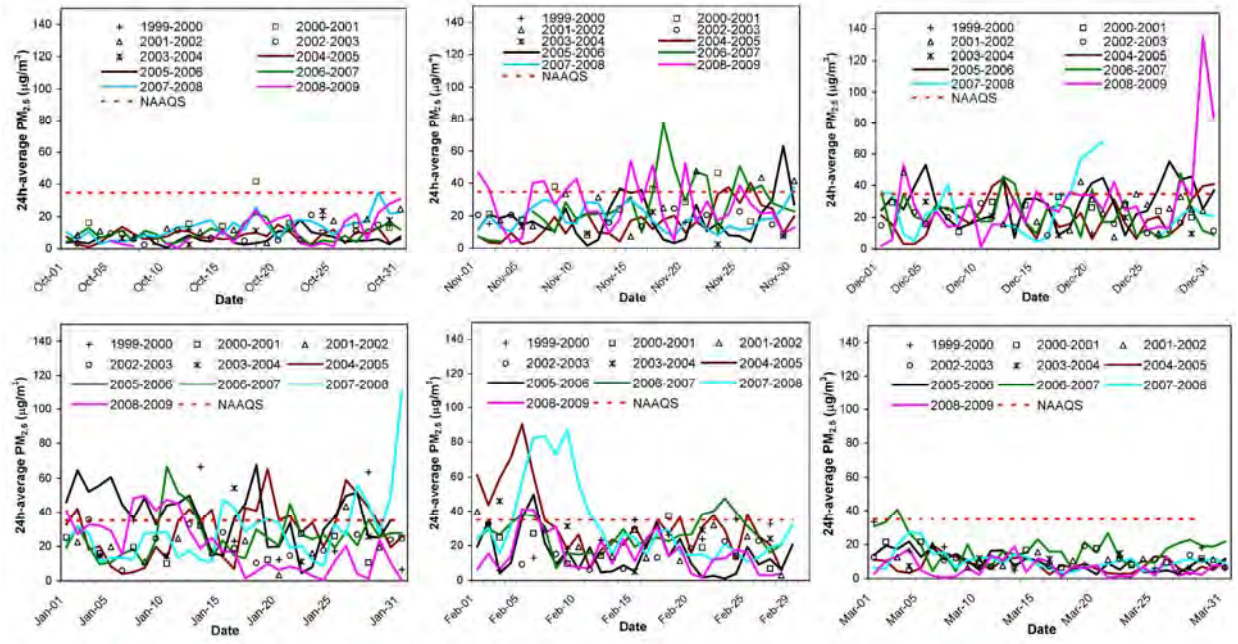


Fig. 1. $PM_{2.5}$ concentrations measured in downtown Fairbanks from October 1 to March 31 in various years from 1999 to 2009. Modified after *Tran and Mölders* [2011]

In Fairbanks, exceedances typically occur during the cold season (October to March) hereafter referred to as winter, and the fire season (summer) [*Tran and Mölders*, 2011]. In Alaska summer, fire events frequently create $PM_{2.5}$ concentrations well in excess of levels deemed "unhealthy". However, these events may be excluded from being considered as an exceedance if it can be proven that the exceedance was due to a particular event [*EPA*, 2007]. While exceedances due to fires may be considered as "natural events" under the aforementioned circumstances, the exceedances in winter are due to anthropogenic activity.

Analysis of available data showed that there are various factors contributing to the $PM_{2.5}$ exceedances in winter: topography, weather, and emissions[3] [*Tran and Mölders*, 2011].

[1] Particulate matter is often also called particulates. Here PM are tiny subdivisions of solid matter suspended in the atmosphere.
[2] Concentration refers to the amount of a substance per defined volume. Typically, concentration is expressed in terms of mass per unit volume (e.g. µg/m$^3$).
[3] Emission refers to the release of gases and/or particulate matter into the atmosphere, i.e. a flow. Typically, emissions are expressed in terms of mass per unit area per time (e.g. kg/(m$^2$s)).

Fairbanks' being located at the edge of an air-mass source region[4] yields low wind-speeds, and cold air that remains in place over long time [*Tran and Mölders*, 2011]. In addition, wintertime radiative cooling leads to inversions, i.e. a temperature increase with height[5]. Fairbanks experiences strong semi-permanent inversions with temperature differences of 5-10K from the basis close to the earth's surface to the top of the inversion during the period from November to February [*Bourne et al.*, 2010]. Such inversions hinder the vertical exchange of air. Consequently, if an inversion is present, $PM_{2.5}$ and other pollutants will accumulate in the air underneath the inversion, and will potentially lead to $PM_{2.5}$ exceedances [*Tran and Mölders*, 2011]. The fact that Fairbanks is surrounded by hills further contributes to the low exchange of polluted and clean air masses. Other meteorological factors affecting concentrations are mixing height, atmospheric stability, longevity and strength of inversions [*Mölders and Kramm,* 2010].

Heat and energy production as well as traffic are the main sources for $PM_{2.5}$ emissions. In winter, roughly 30% of the $PM_{2.5}$ in downtown Fairbanks may stem from traffic [*Johnson et al.*, 2009]. Pervious studies [*Davies et al.*, 2009] indicate that non-certified woodstoves and wood-boilers strongly contribute to the $PM_{2.5}$ emissions from the heating sector. Another source for $PM_{2.5}$ is gas-to-particle conversion a process that occurs naturally in the atmosphere [e.g. *Kumar et al.*, 2010].

Trace gases that are emitted are referred to as primary pollutants. Pollutants resulting from reaction of primary pollutants and other naturally available gases are called secondary pollutants. Particulate matter that is emitted is called primary PM. Secondary PM forms already in the plumes, but also elsewhere in the atmosphere, from gas-to particle conversion. Any $PM_{2.5}$ that results from gas-to-particle-conversion is called secondary $PM_{2.5}$ hereafter.

The term aerosol refers to solid and liquid particles suspended in the atmosphere. Aerosols can exist in the nucleation, accumulation and coarse mode. Aerosols in the coarse mode typically stem from mineral dust and ash fly from biomass burning. The terms *nucleation mode* and *accumulation* mode denote the mechanical and chemical processes that produce aerosol particles in these two size ranges.

In the nucleation mode, the aerosols are the smallest. They are produced by *gas-to-particle conversion*. Gas-to-particle conversion produces particles when trace gases react with other gases or particles that exist in the atmosphere or when trace gases absorb solar radiation that leads to photochemical reactions. In the nucleation mode, most aerosol particles consist of sulfuric compounds, and stem from the oxidation of sulfur containing precursor gases (like $SO_2$, $H_2S$, $CS_2$, COS, $CH_3SCH_3$, and $CH_3SSCH_3$) to sulfate ($SO_4^{2-}$), and subsequent condensation into particle form. This process is called homogenous gas-to-particle conversion. These tiny highly mobile sulfate aerosol particles can coagulate. Much of the sulfate aerosol from gas-to-particle conversion finally ends up in the 0.1-1.0μm size range. Sulfur dioxide ($SO_2$), for instance, can yield the formation of various sulfates in the presence of ammonia ($NH_3$) and water vapor via gas-to-particle conversion. Sources for $SO_2$ in the atmosphere are volcanic emissions, and emissions from fires, traffic, power-production and combustion for heating. Important anthropogenic sources for ammonia are domesticated animals and fertilizer.

[4] An air-mass source region is a region over which air remains frequently for a long enough time that the surface affects the air mass' temperature and moisture properties substantially.

[5] Under normal conditions, temperature decreases with height in the troposphere. Temperature inversion means that temperature increases with height. Inversion layer refers to the atmospheric layer within that such an increase exists.

Gas-to-particle-conversion forms ammonium ($NH_4^+$) $PM_{2.5}$ by the reaction of ammonia in the gas-phase with sulfur, nitrogen, and other acidic species forming ammonium nitrate and ammonium-sulfate particulate matter. $PM_{2.5}$ ammonium nitrate, for instance, forms from the $NO_x$-reaction by-product nitric acid and ammonia.

Nitrate ($NO_3^-$) containing aerosols typically exceed 1μm in diameter, i.e. they do not form by homogenous, but heterogeneous gas-to-particle conversion processes. They also may stem from evaporation of droplets, among other things.

In the accumulation mode (0.1-2.5μm in diameter), *coagulation* of smaller particles and/or *heterogeneous condensation* of gases onto existing particles produce particles. The largest mass and amount of particles occur in the accumulation mode due to the lack of efficient removal mechanisms for these particles.

The term secondary aerosol refers to particles that are produced by precursor gases, condensation and other processes in the atmosphere. This means that $PM_{2.5}$ can be released in the atmosphere from emissions, or be produced in the plume of stacks or in the atmosphere by gas-to-particle conversion. Primary aerosol refers to particles directly emitted into the atmosphere as particles. Primary aerosols produced by combustion span all three size ranges.

Measurements by the FNSB show a large spatial and temporal variability in $PM_{2.5}$ concentrations (e.g. Figs. 2, 3). The reasons for the observed spatial variability in $PM_{2.5}$ concentrations are manifold. In business districts dominated by central heating, traffic usually contributes more than in low-traffic residential areas dominated by heating with coal, wood or oil. $PM_{2.5}$ emissions from traffic, power plants and home heating with oil also depend on sulfur content [e.g. *Johnson et al.*, 2009]. $PM_{2.5}$ concentrations at breathing level depend on the emissions and meteorological factors like temperature, mixing height, atmospheric stability, longevity and strength of inversions [*Dawson et al.*, 2007; *Mölders and Kramm*, 2010; *Tran and Mölders*, 2011].


Fig. 2. $PM_{2.5}$ concentrations as measured in Fairbanks by the mobile platforms (lines of dots) on 12-29-2008 during the drive starting at 1523 AST (Alaska Standard Time). Measurements have been also made in the hills and the North Pole area (not shown here). Single dots are the $PM_{2.5}$ concentrations as measured at the stationary sites. Color code: deep green 0-35 $\mu g/m^3$, olive 35-105 $\mu g/m^3$, orange 105-210 $\mu g/m^3$, red 210-350 $\mu g/m^3$, and >350 $\mu g/m^3$ grey. Courtesy to *F. di Genova* [2009]

Due to the temperature dependency of chemical reaction [e.g. *Seinfeld and Pandis*, 1997] secondary pollutants, gas-to-particle-conversion and the emissions from energy and heat production differ for warm and cold atmospheric conditions. For $PM_{2.5}$ ammonium nitrate formation not only the $NO_x$ reaction by-product nitric acid and ammonia have to be available, but also temperatures must be low and relative humidity must be high [*Wexler and Seinfeld*, 1992]. This means that the local change rate $\partial[C]/\partial X$ in concentration [C] with changes in the meteorological quantity X can differ in winter from those in summer or in other words is different for Fairbanks' winter conditions as compared to winter conditions in a warmer climate.

As previously indicated, $PM_{2.5}$ is a complex mixture of components − nitrate, sulfate, organic carbon, elemental carbon (EC) other primary particulate matter, ammonium and water − that show strong seasonal variations (Fig. 3) due to differences in sources, temperature and humidity. Analysis of previous measurements suggests that the burning sector and especially wood-burning strongly contribute to the high $PM_{2.5}$ concentrations in the FNSB (e.g. Fig. 3).

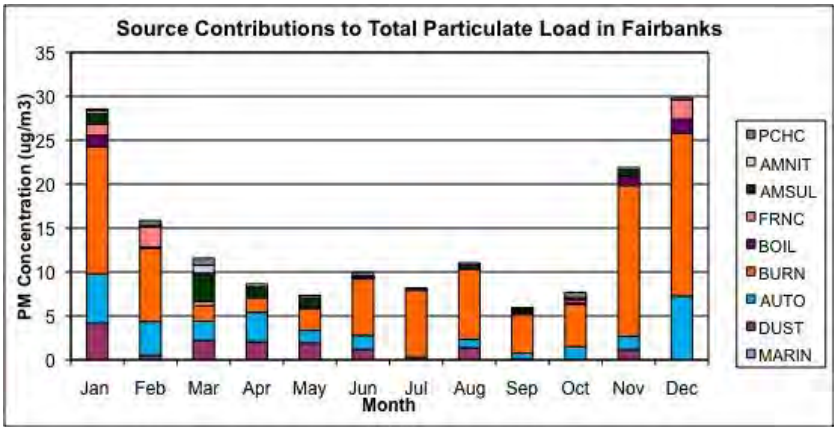


Fig. 3. $PM_{2.5}$ composition in Fairbanks. PCHC, AMNIT, AMSUL, FRNC, BOIL, BURN, AUTO, DUST and MARINE stand for coal-fired power plant, ammonium nitrate, ammonium sulfate, furnace, industrial boilers, biomass burning, automobiles, soils, and marine $PM_{2.5}$. Courtesy to *C.F. Cahill and A.N. Wallace* [2010]

If no action is taken to reduce the $PM_{2.5}$ concentrations in Fairbanks, Fairbanks will likely exceed the $PM_{2.5}$ standard in winters in the future. Such non-compliance is expected to have significant social, health and/or economic impacts on Fairbanks, the FNSB and their citizens.

The EPA, FNSB, Alaska Department of Environmental Conservation (DEC), Alaska Health & Social Services and scientists are concerned about the $PM_{2.5}$ concentrations in Fairbanks as $PM_{2.5}$ has various known health adverse effects. For instance, exposure to airborne $PM_{2.5}$ is associated with cardiovascular events and mortality in elderly and cardiac patients [*Riediker et al.*, 2004]. Various studies indicate that people − especially children − living in close proximity to roadways show more respiratory symptoms, decreased lung function, more respiratory hospitalizations and increased incidence of asthma than their peer groups in other environmental conditions [e.g. *McCreanor et al.*, 2007]. Climate-geographical location plays no role and a pre-existing family history of asthma is not required, i.e. living close to heavy traffic or heavily industrialized areas is the important factor [*Gordian* 2010; pers. communication]. Investigations on healthy young men who were exposed to $PM_{2.5}$ from road traffic suggest that these men experienced pathophysiological changes that involve inflammation, coagulation and cardiac rhythm [*Riediker et al.*, 2004].

## 2. Selection of the air quality model

Obviously, no exposure to any pollutants would avoid adverse health impacts from air pollution, but this is impossible to realize. The current NAAQS were set according to the best scientific knowledge to protect human health. These values are re-evaluated from time to time to adjust to newest scientific findings if required. Often tightening the NAAQS requires emission regulations. Such emission regulations may have enormous socio-economic impacts for both public and private stakeholders. Therefore, it is helpful to assess the effectiveness of a potential regulation and/or the contribution of an emission source sector being under suspicion to strongly contribute to the exceedance of the new NAAQS.

Photo-chemical models of various complexity have been used for a long time to examine (1) the relation between meteorological conditions and air quality, (2) the formation and distribution of acid rain, (3) air-quality issues, and (4) the role of long-range transport of pollutants for air quality [e.g. *Chang et al.*, 1989; *Mölders et al.*, 1994; *Grell et al.*, 2000, 2005; *Tetzlaff et al.*, 2002; *Otte et al.*, 2005; *Yu et al.*, 2008; *Eder et al.*, 2009; *Mölders et al.*, 2010]. The use of such air-quality models for emissions permits and/or for regulatory purposes has a long tradition not only at EPA [*EPA*, 2009]. Recently, ambient air-quality modeling has been used successfully to estimate individual and population exposure for human health research in mid-latitudes [e.g. *Bell* 2006].

The great advantage of photo-chemical models is that they permit easily to change emissions in the model world. The model then provides the atmospheric response, i.e. the concentrations that result in response to the altered emissions. This means photo-chemical models permit us to answer "What …if" questions like

- "What will happen to the $PM_{2.5}$ concentrations at breathing level if we replace a certain amount of non-certified wood-burning devices by EPA certified wood-burning devices?"
- "What will happen if we reduce the sulfur content in fuel used for domestic heating and power productions?"

They also permit us to assess the contribution of an emission source of interest to the $PM_{2.5}$ concentrations at breathing level, and answer questions like

- "What do the power plants contribute to the $PM_{2.5}$ concentrations at breathing level?"

Modeling is a useful tool to access in which direction emission-reduction efforts will go, how the altered emissions in combinations with the various chemical and meteorological processes affect the concentrations, and what the impact of emissions sources are. To answer such questions it is necessary to perform at least two simulations. One simulation considers the emissions as they are currently (business-as-usual). This simulation is the reference simulation and provides the baseline. The second simulation that is applied for the same meteorological condition as the first one, considers the emissions of the altered emission scenario (e.g. the change in emissions in response to a "woodstove exchange program"). Comparison of the results of the simulations permits us to assess how much the concentrations change in response to the altered emissions.

The goal of this study was to conduct photo-chemical model simulations with a complex state-of-the-art research model to quantify numerically the potential impacts of various emission reduction scenarios on the $PM_{2.5}$ concentrations at breathing level in Fairbanks, the Fairbanks nonattainment area and its adjacent land. These modeling studies in combination with various

other investigations related to Fairbanks' nonattainment problem [e.g. *Davies et al.*, 2009; *Carlson et al.*, 2010], ongoing studies and measurements are to help policy makers in the decision making process on which measures to apply to decrease the $PM_{2.5}$ levels in the future and to inform the public.

The Weather Research and Forecasting model inline coupled with a chemistry model commonly known as WRF/Chem [*Grell et al.*, 2005] is a state-of-the-art photo-chemical research model[6] based on the newest scientific knowledge. It simulates the meteorology and the trace-gas and aerosol cycles from emission, through a variety of chemical reactions, to transport, and finally removal from the atmosphere by wet or dry deposition. WRF/Chem can consider feedbacks between chemistry and meteorology.

WRF/Chem was chosen as it was the only photo-chemical model that was already adapted for application in Alaska [*Mölders et al.*, 2010, 2011]. These modifications, among other things, ensure Alaska-typical values of the vertical profiles of initial background concentrations (e.g., acetylene, $CH_3CHO$, $CH_3OOH$, CO, ethane, HCHO, $HNO_3$, $H_2O_2$, isoprene, $NO_x$, $O_3$, propene, propane, $SO_2$) and boundary conditions. The modifications also ensure that Fairbanks and other settlements are included in the land-use data and that winter typical vegetation parameters are used from Mid-October to Mid-April. In addition, modifications concerning the stomatal behavior of Alaska vegetation and dry deposition of trace gases on snow were included [*Mölders et al.*, 2010, 2011]. Furthermore, first evaluations studies of the Alaska adapted WRF/Chem already existed that showed accepatble performance for Alaska [*Mölders et al.*, 2010, 2011]. Such studies did not exist for other photo-chemical models yet.

We used the following model setup that was capable of capturing Alaska winter conditions well in previous studies [*Mölders*, 2008; *Mölders and Kramm*, 2010; *Mölders et al.*, 2010; *Yarker et al.*, 2010]. The WRF-Single-Moment six-class scheme that allows the coexistence of super-cooled water droplets and ice-crystals and processes among the solid and liquid phase cloud and precipitation components, served to simulate resolvable cloud- and precipitation-formation processes [*Hong and Lim*, 2006; *Hong et al.*, 2006]. It is able to simulate falling snow crystals and ice fog, which are of relevance for Fairbanks in winter. To consider the impact of the cumulus convection even though it rarely occurs in Fairbanks winters, we used the cumulus-ensemble scheme [*Grell and Dévényi*, 2002] as it is well suitable for the grid-resolution at which WRF/Chem was run for this study. The Goddard two-stream multi-band scheme was used to calculate shortwave radiation processes. It considers, among other things, the impacts of clouds and ice fog on shortwave radiation. This is important as the shortwave radiation affects photolysis rates. Long-wave radiation was calculated with the **R**apid **R**adiative **T**ransfer **M**odel [*Mlawer et al.*, 1997] that takes into account multiple spectral bands, trace gases, and cloud microphysical species (cloud-droplets, rain drops, ice-crystals, etc.), among other things. It allows considering the effects that pollution, ice fog and clouds have on long-wave radiation. The 1D-prognostic scheme by Janjić [2002] was applied to determine turbulent processes[7] in the atmospheric boundary layer[8] (ABL), i.e. the first 1000m or so above ground level (AGL). For the

[6] Note that WRF/Chem is a complex state-of-the-art research model, not a regulatory model.
[7] Turbulence refers to rapid fluctuations.
[8] The ABL is the lowest part of the atmosphere that is directly influenced by its contact with the surface. In the ABL, turbulence and vertical mixing can be strong.

atmospheric surface layer[9], i.e. the first 100m or so, Monin-Obukhov similarity hypotheses were used to describe the turbulent processes; the so-called Zilitinkevich thermal roughness-length concept was considered for the underlying viscous sublayer [*Janjić*, 1994]. Previous studies showed that out of various parameterizations available in WRF/Chem these parameterizations of ABL and surface layer processes provide the best results most of the time for Interior Alaska [e.g. *Mölders and Kramm*, 2010]. Simulating the ABL processes adequately is required to capture inversions and their strength and hence the accumulation of pollutants underneath. *Smirnova et al.*'s [2000] land-surface model (LSM) was used to determine the exchange of heat and moisture at the land-atmosphere interface. This LSM calculates, among other things, the soil-temperature and moisture states including frozen soil, snow conditions at various depths in the snow-pack, and vegetation impacts on the atmosphere. The LSM was chosen as it considers permafrost and snow processes. Simulating these processes adequately is important to capture the strength of inversions.

The chemical mechanism by *Stockwell et al.* [1990] served to calculate gas-phase chemistry, i.e. reactions among trace gases. This mechanism considers the chemical reactions that occur in the polluted and non-polluted atmosphere at day and night. Inorganic reactions and constants involve 14 stable inorganic compounds, four inorganic short-lived intermediates and three abundant stable species (oxygen, nitrogen, water). The organic chemistry scheme considers 26 groups of stable organic compounds and 16 groups of organic short-lived intermediates (peroxy radicals). Photolysis frequencies were calculated in accord with *Madronich* [1987] as even at winter solstice Fairbanks still experiences 3.7h of sunlight. These frequencies were used in the calculation of photochemical processes. Photolysis calculation considered 21 photo-chemical reactions. In mid latitudes, the chemical processes during daylight (daytime chemistry) differ from those at night (nighttime chemistry). In Fairbanks, however, the fraction of the day with daylight strongly differs over the winter. In Fairbanks, the sun is only a few hours above the horizon in January and December, while it is appreciably longer above the horizon to provide energy for photochemical processes in October, November, February and March. Thus, the importance of photochemical processes and their contribution to chemical transformations differs strongly over the winter due to the large differences in available shortwave radiation (see Fig. 11c). Thus, "daytime" and "nighttime" chemistry play a different role in January and December than the other winter months. Therefore, it was considered necessary to simulate several months rather than a short episode in the coldest month.

Various processes (transport, turbulence, evapotranspiration, sorption, desorption, biogenic activity, emission, settling, chemical reactions) are involved in the dry deposition process, i.e. the removal of trace gases from the atmosphere. Thus, dry deposition not only depends on the physical and chemical states of the atmosphere, but also on the surface on which the trace gases and particles deposit. The formulation of dry deposition [*Wesely*, 1989] with the modifications introduced by *Mölders et al.* [2011] considers these processes. The modifications serve to treat dry deposition of trace gases more realistically under low temperature conditions and consider dry deposition on snow. Since the stomata of Alaska vegetation often are still open at $-5^{o}\mathrm{C}$, the threshold for total stomata closure was lowered accordingly in the LSM and deposition module.

[9] In the atmosphere, surface layer refers to the layer where the turbulent air is most affected by interaction with the surface. The characteristics of the turbulence depend on the distance from the surface. The surface layer is characterized, among other things, by large concentration gradients of any substances transported to or from the surface.

Aerosol chemistry and physics was treated based on a modified version of the Regional Particulate Model [*Binkowski and Shankar*, 1995], where the vertical transfer of particulate matter is treated in accord with *Kramm et al.* [1992]. Among other things, the aerosol module considers aerosol chemistry and physics, and aerosol formation by gas-to-particle conversion, and Secondary Organic Aerosol (SOA) formation processes [*Schell et al.*, 2001] and the removal of particulate matter from the atmosphere by wet and dry deposition of aerosols. These aerosol chemistry modules have been well tested for mid latitudes. A through evaluation for Alaska is still missing due to lack of observational data. First evaluations with the limited data available [*Mölders et al.*, 2010, 2011] suggest acceptable performance most of the time.

## 3. Model domain, initial and boundary conditions

The Alaska Emission allocation Model (AkEM) [*Mölders* 2009, 2010] and WRF/Chem were set up for a domain covering most of Interior Alaska with a horizontal grid increment of $4\text{km} \times 4\text{km}$. Since Alaska available land-use data did not consider any urban areas, we introduced Fairbanks, North Pole, Eielson and the villages into the WRF/Chem land-use data file (Fig. 4) based on satellite data using Google Earth. Relevant WRF/Chem-simulated concentrations and meteorological quantities were written out hourly as a function of time and space for the domain of interest. The domain of interest for the analysis encompasses 89,600km$^2$ centered around Fairbanks up to 100hPa (Fig. 4).

WRF/Chem used logarithmically increasing vertical grid increments with the smallest increment being located above the ground and the largest increment reaching to the top of the model located at 100hPa. In total, there are 28 layers. In the lower troposphere, the tops of the layers were at 8, 16, 64, 113, 219, 343, 478, 632, and 824m AGL. The lowest atmospheric model layer represents the "breathing level". This vertical and horizontal grid is a compromise to ensure still sufficient vertical and horizontal resolution, and allow for several months long simulations in a reasonable amount of time.

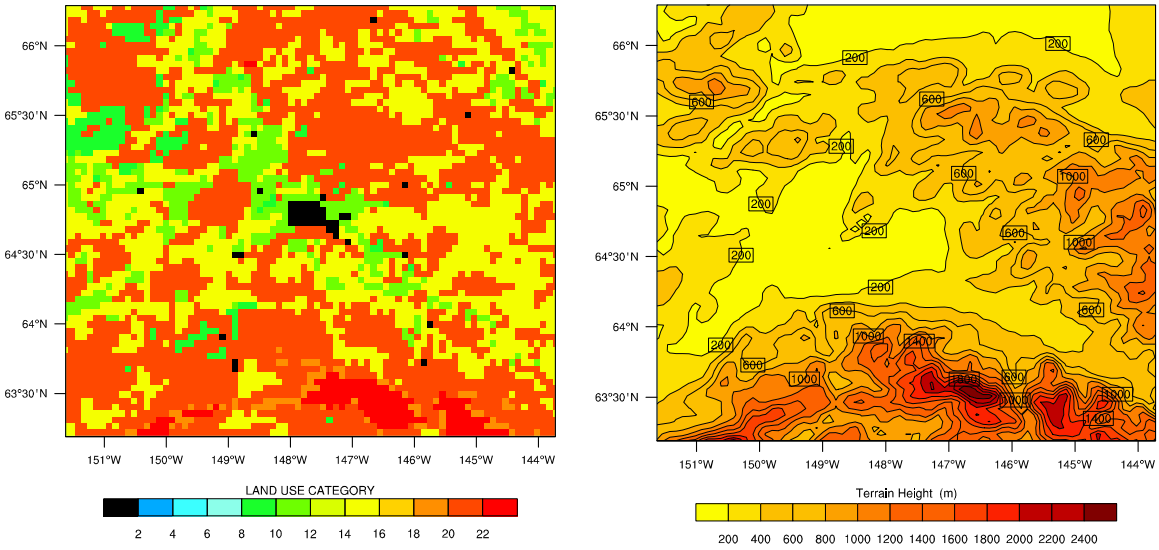


Fig. 4. Land-use (left) and topography (right) in the domain of interest for the analysis of this study. The land-use category code is 1 urban and built-up land, 2 dryland cropland and pasture, 3 irrigated cropland and pasture,4 mixed dryland/irrigated cropland and pasture, 5 cropland/grassland mosaic, 6 cropland/woodland mosaic, 7 grassland, 8 shrubland, 9 mixed shrubland/grassland, 10 savanna, 11 deciduous broadleaf forest, 12 deciduous needleleaf forest, 13 evergreen broadleaf, 14 evergreen needleleaf, 15 mixed forest, 16 water bodies, 17 herbaceous wetland, 18 wooden wetland, 19 barren or sparsely vegetated, 20 herbaceous tundra, 21 wooded tundra, 22 mixed tundra, 23 bare ground tundra, 24 snow or ice.

The meteorological fields were initialized every five days using data downscaled from the $1^o \times 1^o$, 6h-resolution National Centers for Environmental Prediction global final analyses (FNL). At the beginning of the simulations, WRF/Chem was initialized with idealized vertical profiles of Alaska background concentrations for each chemical specie (e.g., acetylene, $CH_3CHO$, $CH_3OOH$, CO, ethane, HCHO, $HNO_3$, $H_2O_2$, isoprene, $NO_x$, $O_3$, propene, propane, $SO_2$). For all further days, the simulated chemical fields of the previous day served as initial conditions to simulate the next day.

Since Fairbanks is far remote from any emission sources, Alaska background concentrations were used for the chemical lateral boundary conditions. The meteorological boundary conditions were downscaled and interpolated from the FNL-data.

WRF/Chem was run in forecast mode, i.e. no nudging or data assimilation was applied. The reference simulation and the simulation that was to assess the contribution of point sources to the $PM_{2.5}$ concentrations at breathing level, start with the same meteorological and chemical initial conditions on November 1, 2005 0000 UTC (see Table 1). In the mitigation investigations, the reference simulation and all mitigation scenarios start with the same meteorological and chemical initial conditions on October 1, 2008 0000 UTC (see Table 1). This procedure ensures that differences in simulated concentrations only result in response to the changes in assumed emissions.

Emissions were considered as a function of time (month, weekday, and hour) and space (latitude, longitude and height). Various types of emission sources are considered. Point sources are fixed (immobile) facilities that emit gaseous or particulate atmospheric pollutants (e.g. smokestacks, power plants, industrial plants, steel mills). A line source is one-dimensional emission source (e.g., vehicle traffic on a highway). An area source is a two-dimensional source of diffuse emissions (e.g. the emissions from domestic heating, landfills, fires). For more details, see e.g. *http://en.wikipedia.org/wiki/Air_pollution_dispersion_terminology* [2011].

In the case of point sources, emissions are released into the model levels that are calculated depending on stack parameters (stack height, stack diameter, flow temperature, flow velocity, etc.). WRF/Chem, among other things, also includes plume rise [*Peckham et al.*, 2009]. In the case of area and line sources, the model level in which the emissions are released depends on the kind of emission source. For instance, emissions from city or highway traffic are released into the first model layer above ground (Fig. 5).

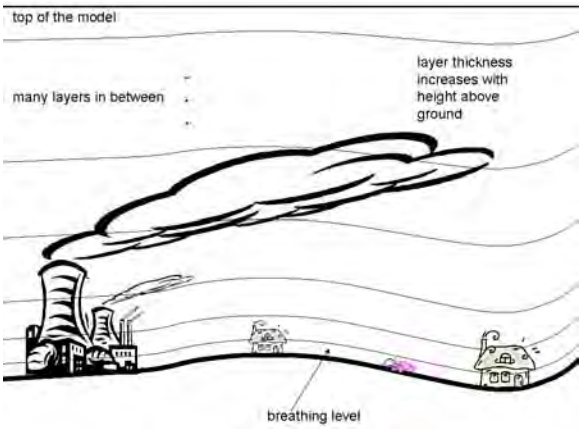


Fig. 5. Schematic view of the vertical grid structure and consideration of various emission sources. The spacing of vertical model layers increases logarithmically with height. Note that not all model layers and potential emission sources considered by WRF/Chem are pictured here.

Some Alaska plant species remain photosynthetically active up to temperatures as low as -5°C (23°F). Thus, we considered biogenic emissions of isoprenes, monoterpenes, and volatile organic compounds (VOC) by plants, and nitrogen emissions by soil as calculated by the **M**odel of **E**missions of **G**ases and **A**erosols from **N**ature [*Guenther et al.*, 1994; *Simpson et al.*, 1995] if the ground is not covered by snow.

## 4. Meteorological episodes simulated

At the start of the project in 2008, the most recent emission data available for the FNSB were the National Emission Inventory (NEI[10]) data of 2005. In December 2008, the FNSB expected that a gridded emission-data inventory with 400m spatial and hourly resolution representing the winter 2007/08 would be available for Fairbanks and its vicinity in April 2009 [*Conner* pers. communication, 2008]. Therefore, it was planned to switch to a more recent episode for the simulations on the impact of introduction of low sulfur fuel and a "woodstove replacement program" despite doing so would require producing an additional reference (baseline) simulation (Table 1).

### 4.1 Emissions

All NEI data were annual values for the various species and emission sectors in the FNSB. These emission data were allocated for use in WRF/Chem using the AkEM [*Mölders*, 2009; 2010]. Input data to AkEM are the EPA NEI data, stack parameters, data for the split of $PM_{2.5}$ and VOC, allocation data of annual, daily, hourly emission percentages for area, line, and point sources, population density data, land-use and street network data as well as meteorological data. The split of $PM_{2.5}$ emissions into ammonium ($NH_4$), carbon, nitrate ($NO_3$), potassium, sodium, and sulfate ($SO_4$) was made based on observations provided by the FNSB [*Conner,* 2009]. Due to the lack of observational data, we split the total anthropogenic VOC emissions into the various species like ethane, butane, formaldehyde, pentane, hexane, ethylene, propylene, acetylene, benzene, toluene, xylene, tri-methylbenzene, and other aromatics depending on emission-source types in accord with *Mölders et al.* [2011].

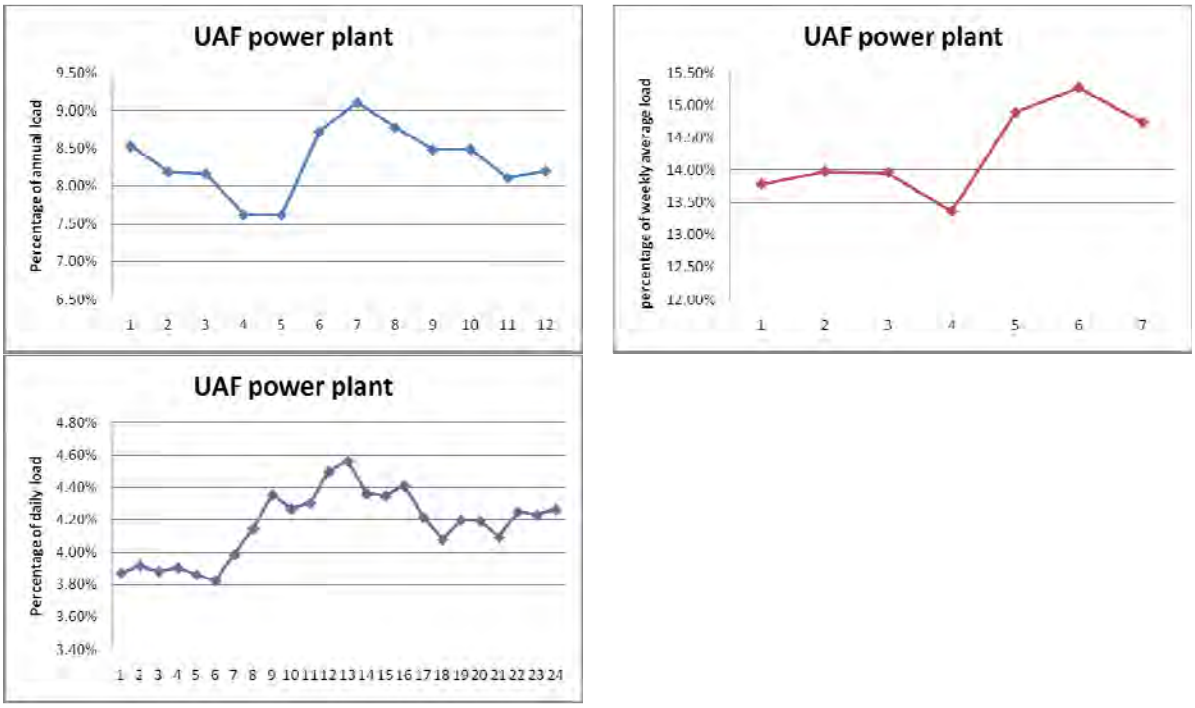


Fig. 6. Activity allocation as derived for the UAF power plant for (from upper left to lower left) monthly, weekday and hourly activity. Data courtesy by *Waard* [2008]

[10] Typically the National Emission Inventory is abbreviated as NEI and the year is added, e.g. NEI1999 would be the NEI for 1999.

AkEM calculates hourly emission rates for each grid-cell from the annual emission $E_{total}$ given by the NEI. In doing so, AkEM uses the spatial and temporal activity allocation functions for the various emission sources that have been recommended by EPA for Alaska with the modifications that have been derived in collaboration with local partners. Figure 6 exemplarily shows the emission-allocation functions as derived from data for the UAF power plant. Area emissions from the burning sector, for instance, are distributed spatially depending on specie, activity, population, and/or land-use, and time. The model level and grid cell into which point sources emit, depends on stack parameters, latitude, and longitude and plume raise that is calculated using Biggs formula [*Peckham et al.*, 2009].

### 4.1.1 Emission data for 2005/06

We performed a quality assessment and quality control (QA/QC) on the NEI2005 data for the FNSB. The QA/QC showed that for some point sources stack parameters were missing and/or the coordinates were incorrect or vice versa. We worked with the respective facility operators and EPA to fill in and/or replace the data with the correct data.

We worked with Golden Valley Electricity Association and UAF's power plant employees to obtain Alaska specific annually, daily and hourly emission profiles for 2005 (e.g. Fig. 6) and implemented them into the AkEM. We used the population-density data provided by the FNSB from the Census 2000 [data provided by *Duncan*, 2009] and projected them onto the model domain. AkEM requires these data for determining/distributing the area emissions.

For the winter 2005/06 simulations AkEM [*Mölders*, 2009] used allocations functions depending on space and time. Allocation differed with time of the day, day of the week and month. For 2006, an increase in annual emissions of 1.5% was assumed across the board.

### 4.1.2 Emission data for 2008/09

In December 2008, the FNSB expected that gridded spatially high resolved hourly emission data for winter 2007/08 would be available in April 2009 from SRL. The FNSB wanted to have the option to switch to a more recent episode (probably 2008/09) than 2005/06 for the "woodstove replacement" and "low sulfur emission" simulations. The reasons for this request were manifold. More observational data for model evaluation are available for this more recent winter. Moreover, since 2007, the number of woodstoves has increased notably and 2008 was discussed as a potential design year.

Early in 2010, the anticipated SRL-emission inventory for winter 2007/08 was still not available[11] due to unforeseen delays and difficulties in collecting the data that were beyond the control of SRL and/or the FNSB. Moreover, the QA/QC had still to be performed by EPA. Early, in 2010, the FNSB decided that we should perform the "woodstove replacement" and "low sulfur scenarios" for winter 2008/09. Meanwhile, namely, the NEI2008 became available except for point-source emissions. The NEI2008 more closely represents the current emission situation in the FNSB, as it considers emission changes between 2005 and 2008 and hence is more recent than the NEI2005. Therefore, we did a new reference simulation and the mitigation scenarios for winter 2008/09 (Table 1).

Note that the main difference between the emission data that we used for this study and those of the anticipated SRL-inventory is that the NEI2008 in combination with AkEM treat emission

[11] As of January 2011, we have no access to the SRL-compiled 2007/08 emission data.

data for the FNSB in a top-down approach, while the SRL-inventory treats emissions in a bottom-up approach. A top-down approach assesses emission rates based on aggregated-statistical methodologies, while the bottom-up approach compiles a site-specific emission inventory based on the detailed information for each area [e.g. *Kim et al.*, 2010]. Inter-comparison analysis suggests that standard emissions data from a top-down approach are appropriate for atmospheric model simulations [e.g. *Kannari et al.*, 2008]. The differences, advantages and disadvantages between these two types of approaches have been widely discussed in the literature [e.g. *Kannari et al.*, 2008; *Kim et al.*, 2010] and are therefore not repeated here.

Emissions of mobile and several nonpoint-emission sectors were available from the NEI2008. The NEI2008 considered aircraft emission as point sources. Other point-source sectors were not yet available in the NEI2008 and were not expected to be available before 2011. Therefore, we updated the point-source emission inventory (EI) by personal communications with the facilities holders in the FNSB whom we contacted with this request. Note that not all facilities contacted did respond. For those facilities without reported emission data, we used estimates on point-source emissions based on the previous inventory assuming a 1.5% increase per year.

The mobile emissions in the NEI2008 are less than what they were in the NEI2005, which is consistent with the lower traffic activity in 2008 as compared to 2005 [*DOT*, 2009]. Some nonpoint-emission sectors were required to be updated with the latest borough employment data. We performed these updates using the respective data from the Alaska Department of Labor and Workforce Development [*http://laborstats.alaska.gov/cgi/dataanalysis/?PAGEID=94*].

However, there were some nonpoint-emission sectors that EPA was not planning to estimate unless additional resources became available. Those sectors included industrial/commercial/ institutional fuel combustion and the residential wood combustion. The latter make up a large portion of the emission in the FNSB according to the NEI2005. Therefore, the emissions from these sectors were included in the emission database used for our simulations of winter 2008/09 to obtain realistic emission conditions. For industrial/commercial/institutional fuel combustion, we assumed the 2008 emissions to be the same as in NEI2005 because they were expected to have just marginally changed over 2005-2008. Emissions from residential wood combustions were taken from *Davies et al.* [2009] as was requested by the FNSB. The outcome showed much higher emissions from residential wood combustion in 2008 as compared to that category in the NEI2005. This increase in woodstove emissions, however, is expected given the situation in the FNSB in winter 2008/09. Note that in the NEI2005, EPA estimated emissions from residential wood combustions based on the small partition of wood-burning devices as obtained from the Census 2000. Meanwhile, in response to the increasing oil prices, many residents had added wood-burning devices to reduce heating costs. The wood-cutting permits have increased threefold in 2009 as compared to 2007 [*Conner* 2010, pers. communication]. To derive the annual emissions for 2009 from those of 2008, an increase in annual emissions of 1.5% was assumed across the board.

For allocation of the winter 2008/09 emissions a modified version of AkEM [*Mölders*, 2010] was used that applied allocations functions depending on space, time and temperature. Allocation differs with time of the day, day of the week; month and deviation of the daily mean temperature from the 30-year monthly average mean temperature. This modification (calibration) of the emission model was introduced to improve the allocation functions based on our experience with the simulations for winter 2005/06 and several sensitivity studies paid from other sources. This

modification of the emission allocation permits to better consider the temperature dependency of cold start enhanced emissions (CSEE) and the increase in energy consumption for heating for temperatures below 18°C (64.4°F) using a modified equation of *Hart and de Dear* [2004]. The temperature dependency for production of electrical power was determined assuming that freezers, refrigerators and hot water production consume equal amounts of energy. The same allocation functions and temperature correction as for power plants is assumed for emissions from fuel combustion for electricity production by nonpoint sources, but these emissions are considered dependent on population density [*Mölders*, 2010]. AkEM assumed that the non-temperature corrected allocation function is valid for the mean temperature of the month [*Mölders*, 2010]. Thus, the inclusion of temperature dependency increases (decreases) the emission factors for temperatures below (above) the monthly mean temperature. The temperatures used in these corrections are the 2m-temperatures read in from the WRF/Chem initialization data. Figure 7 exemplarily shows the impact of temperature-dependent emissions for March 3, 2005 where the domain average temperature was -22.1°C (-7.8°F).

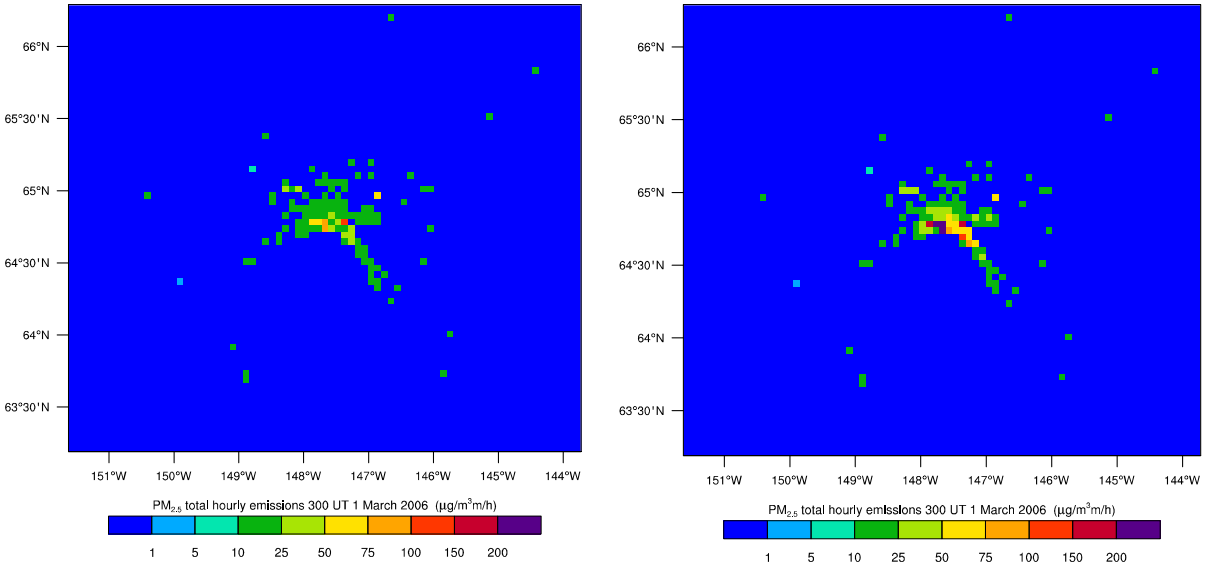


Fig. 7. Emissions of $PM_{2.5}$ without (left) and with consideration of temperature correction. This day is colder – the daily average temperature is 22.1°C (-7.8°F) - than the climatological average March temperature of -11.7°C (10.9°F) for which the original allocation functions were valid. As expected, emissions increase in response to the low temperatures. *Davies et al.*'s [2009] emission data were used.

## 4.2 Emission scenarios

This section describes the emission scenarios used in the mitigation simulations. Table 1 summarized the simulations performed for this study. Throughout this report, the simulations as their results are referred to as REF and NPE, or REF, WSR and LSF, respectively.

### 4.2.1 Emission scenario for investigation of point source contribution

The 2005/2006 winter was chosen because at the start of the project in 2008, the most recent available emission-data inventory was the NEI2005. Since the concentrations resulting from point-source (PS) emissions alone were so low that $PM_{2.5}$ concentrations were governed mainly by background chemistry, we performed simulations with emissions from all sectors as the reference simulation (REF). In a further simulation, we considered emissions from all sectors

except point-source emissions (NPE). This means emissions of all species emitted by point-sources were set to zero in the NPE scenario. Simulations with consideration of point-source emissions were performed for October 1, 2005 to February 28, 2006. The first 15 days performed for October 2005 served for calibration. The rest of October 2005 served to spin-up the chemical fields. Simulations without consideration of point sources were performed from November 1, 2005 to February 28, 2006. The simulations with and without consideration of point-source emissions start with the same initial conditions of the meteorological fields and chemical components on November 1, 2005 as obtained from the spin-up. Comparison of the concentrations obtained by the REF and NPE simulations for November 1, 2005 to February 28, 2006 served to quantify the contribution of the point sources (e.g. power plants) to the $PM_{2.5}$ concentrations at breathing level.

Table 1. List and names of simulations performed with WRF/Chem for this study. Note that LSF and WSR have the same reference simulation.

| Simulation name | Description | episode simulated |
|---|---|---|
| REF | Reference simulation with all emissions using the NEI2005 | October 1, 2005 to February 28, 2006 |
| NPE | Simulation using the NEI2005, but excluding emissions of all species from all point sources | November 1, 2005 to February 28, 2006 |
| REF | Reference simulation with all emissions using the NEI2008 with the updates as described in the emission section | October 1, 2008 to March 31, 2009 |
| WSS1 | "Woodstove replacement" sensitivity study that assumes non-certified wood-burning devices are replaced by modern EPA-certified woodstoves using *Davies et al.*'s [2009] numbers of wood-burning devices, while keeping emissions from all other emission sectors the same as in the respective reference simulation | October, 1 2008 to October 15, 2008 |
| WSS2 | as WSS1, but using the numbers wood-burning devices from SRL's draft report | October, 1 2008 to October 17, 2008 |
| WSR | as WSS2, but using the numbers of *Carlson et al.*'s [2010] final report | October 1, 2008 to March 31, 2009 |
| LSF | "Introduction of low sulfur fuel for heating and power generation", while keeping emissions from all other emission sectors the same as in the respective reference simulation | October 1, 2008 to March 31, 2009 |

### 4.2.2 Emissions for the "woodstove replacement" scenarios

A set of simulations addressed the influence of a "woodstove-replacement action" on the $PM_{2.5}$ concentrations at breathing level. The reference simulation (REF) considered emissions from all sectors available in the NEI2008 and the additional information described before. The simulation assuming "woodstove replacements" considered the same emissions as in REF minus the emissions from non-certified wood-burning devices that were assumed to be replaced plus the emissions that stem from the certified wood-burning devices that replaced the non-certified wood-burning devices. The reference and "woodstove replacement" simulations started with the same initial conditions of the meteorological fields and the same Alaska-typical chemical background concentrations for October 1, 2008.

To compile the emission data for the "woodstove-replacement" simulations, we analyzed *Davies et al.*'s [2009] results. We searched the literature and collected data on other species than $PM_{2.5}$ emitted by EPA-certified woodstoves and other wood-burning devices. These data were required as not only the $PM_{2.5}$ emissions from wood-burning devices, but also the emissions of the other species emitted by these devices will change if non-certified wood-burning devices are replaced by EPA-certified wood-burning devices. This means all species emitted by wood-burning were changed in the "woodstove-replacement scenarios". The consideration of changes for all species emitted by wood-burning devices is required because some $PM_{2.5}$ can form from gas-to-particle conversions once the species are in the atmosphere as explained before.

*Davies et al.*'s [2009] data only provide the total number of certified woodstoves (6912), but not the split between certified woodstoves with catalytic and non-catalytic equipment. The same is true for masonry heaters and pellet stoves. We assumed the same emission rates for wood-burning devices with catalytic and non-catalytic equipment.

Table 2. Number of households in Fairbanks. Data courtesy of *T. Duncan* [2010]

| Year | Pre-2005 | 2005 | 2006 | 2007 | 2008 | 2009 |
|---|---|---|---|---|---|---|
| Number of households | 33970 | 34946 | 35910 | 36952 | 37550 | 38292 |

The number of households changed over the years (Table 2). As obvious from the sum of the devices listed in *Davies et al*. [2009] report, some households have at least two heating devices. We assumed that in the case of households with more than one heating device, woodstoves co-exist with oil furnaces. For fire-safety reasons it is unlikely that a woodstove exists in a household with gas. It is unlikely that woodstoves co-exist with hydronic or masonry heaters or pellet stoves as well. The category "others" is most likely central heating which also has a low likelihood to co-exist with woodstoves. Coal and woodstoves are unlikely to co-exist as typically people who burn coal also burn wood in the same stove. To avoid double counting of households in their emission contribution, we determined the number of households with at least two heating devices

$$N_{two} = N_{devices} - N_{households} \quad (1)$$

Where $N_{devices}$ and $N_{households}$ are the number of heating devices and households in that particular year. After studying *Davies et al*.'s [2009] data, it seemed reasonable to assume that households with two devices use the woodstove to other device in a ratio 33.5:66.5 of the time. Sensitivity studies indicated that the total emission reduction is very sensitive to how households split their heating among their available devices. Thus, we recommend collecting data on the "split" behavior to reduce uncertainty in future modeling studies.

We determined the actual number of devices contributing at a time to wood-burning emission as

$$N_x^{'} = N_x\left(1 - 0.665\frac{N_{two}}{N_1 + N_2 + N_3}\right) \quad (2)$$

Where the x stands 1, 2 and 3, with 1 to 3 representing non-certified woodstoves, EPA-certified woodstoves with catalytic equipment, and EPA-certified woodstoves without catalytic equipment, respectively. Analogously, the number of devices contributing at a time to emissions from oil furnaces is determined as

$$N_7^{'} = N_7\left(1 - 0.335\frac{N_{two}}{N_7}\right) \quad (3)$$

Where the index 7 denotes oil furnaces. After this procedure, the sum $\sum_{k=1}^{11} N_k^{'}$ equals the number of households.

*Davies et al.*'s [2009] data for Fairbanks' wood-burning emissions differ from those assumed in the compilation of the NEI2008. We used *Davies et al.*'s [2009] data for all wood-burning devices and oil furnaces as requested by the FNSB. We used EPA's data for the other categories, as data for these devices were not included in *Davies et al.*'s [2009] report.

The total annual emission rate of the $i^{th}$ specie from heating after "woodstove replacement" is given by

$$E_{NEIyyyy,WSR} = E_{NEI,yyyy} + N_{exchange}E_2 - \sum_j N_j E_j \quad (4)$$

Where $N_{exchange}$ and $E_2$ are the number of wood-burning devices replaced and emission rates per certified wood-burning device, $E_j$ are $N_j$ the emission rates and numbers of noncertified wood-burning devices, and the index j stands for noncertified wood-burning devices, respectively.

In all "woodstove replacement" emission scenarios, we assumed emissions from all sectors to remain the same as in the reference simulation except for the heating sector. For the heating sector, we assumed the emissions from all heating devices but wood-burning devices to remain the same as in the reference simulation too. This means that in all "woodstove replacement" simulations, we only altered the emissions from the wood-burning sector.

In a first sensitivity study on "woodstove replacement", we determined the emissions remaining from wood-burning after the replacement of non-certified devices by assuming the number of residential wood-burning devices as reported in *Davies et al.* [2009]. We calculated the emissions from residential wood combustion, subtracted the contribution from non-certified devices (assumed to be replaced) and added the contribution that the certified device (that replaced the non-certified devices) would have. The simulation with this emission scenario is referred to as WSS1 hereafter. In total, 15 days (10-1-2008 to 10-15-2008) were simulated assuming this scenario.

In a second sensitivity study on "woodstove replacement", we determined the emissions remaining from wood-burning after the replacement of non-certified devices by assuming the number of wood-burning devices that became available from a draft by the Sierra Research Laboratories (SRL) group. This data based on a survey of 300 households in the nonattainment area carried out by SRL. The number of wood-burning devices reported in the draft and in the final report by *Carlson et al.* [2010] is lower than the estimates used in *Davies et al.*'s [2009] report. Note that there is high uncertainty in the actual number of wood-burning devices that exist in the nonattainment area [*Conner* 2011; pers. communication]. The draft SRL report did not include pellet stoves. *Carlson et al.*'s [2010] data only provide the total of certified woodstoves, but not the split between certified woodstoves with catalytic and non-catalytic equipment. We assumed the same emission rates for both. Again, we calculated the emissions from residential wood combustion, subtracted the contribution from non-certified devices

(assumed to be replaced) and added the contribution that the certified device (that replaced the non-certified devices) would have. The simulation performed using the emission scenario obtained this way is called WSS2 hereafter. We run this set of "woodstove-replacement" simulation from 10-01-2008 to 10-17-2008.

The final SRL report by *Carlson et al.* [2010] included pellet stoves as a separate category in the wood-burning sector. For the third "woodstove replacement" simulation, we determined the emissions remaining from wood-burning after the replacement of non-certified devices by assuming the number of wood-burning devices that were given in *Carlson et al.*'s [2010] final report. Using these numbers, we calculated the emissions from residential wood combustion, subtracted the contribution from non-certified devices (assumed to be replaced) and added the contribution that the certified device (that replaced the non-certified devices) would have. *Carlson et al.*'s [2010] data only provide the total of certified woodstoves, but not the split between certified woodstoves with catalytic and non-catalytic equipment. We assumed the same emission rates for both. A full winter simulation was performed assuming this emission scenario. This simulation is called WSR hereafter (Table 1).

Figure 8 exemplarily shows the hourly emission rates from all heating sectors for the Fairbanks area prior to and after the assumed three different "woodstove-replacement scenarios". In all "woodstove-replacement scenarios", we considered the impact on emissions of all species, not only $PM_{2.5}$.

The policy options recommended by *Davies et al.* [2009] estimated to reduce $PM_{2.5}$ emissions from residential heating from 874 tons/year to 422 tons/year, or 52% for their base year. The "woodstove replacement" scenario assuming *Davies et al.* [2009] numbers of wood-burning devices reduces the emissions for 2008 to 40%, while those with the SRL draft and *Carlson et al.*'s [2010] numbers reduce the emissions much less (Fig. 8). Note that changing out non-certified wood-burning devices to certified ones would reduce theoretically both primary and secondary $PM_{2.5}$ emission at the same order. In *Davies et al.* [2009], $PM_{2.5}$ accounts for both primary and secondary aerosol that forms after the emissions. WRF/Chem considers primary $PM_{2.5}$ from emissions and calculates the secondary $PM_{2.5}$ that builds in stacks and in air [*Peckham et al.*, 2009].

Note that if primary $PM_{2.5}$ emission were reduced greatly by changing noncertified wood-burning devices to oil furnaces, the secondary $PM_{2.5}$ emission might increase. Oil furnaces namely have higher emission rates of $SO_x$ and $NO_x$ than wood-burning devices. $SO_x$ and $NO_x$ are the main precursors of secondary $PM_{2.5}$ that forms through gas-to-particle conversion. Therefore, exchanging noncertified wood-burning devices to oil furnaces with current fuel sulfur content will be less effective in reducing $PM_{2.5}$ emission than exchanging them with certified wood-burning devices.

Obviously there is uncertainty in our study due to the unknown number of woodstoves that exist and that can be replaced. Unfortunately, no data were available, where what wood-burning devices are operated and when they were operated and how they were operated and how often. We simply assumed the distribution of wood-burning devices to be proportional to the distribution of population density. This assumption holds uncertainty in the spatial distribution that may affect local maximum concentrations as well as 24h-averages of $PM_{2.5}$ concentrations. *Fortun and Mölders* [2009] showed that uncertainty in the diurnal course of emission marginally affects the 24h-average $PM_{2.5}$ concentrations. However, uncertainty in the spatial distribution can

provide notable differences in the 24h-average $PM_{2.5}$ concentrations. Sensitivity studies on the emissions indicate that uncertainty in emission rates also results from the unknown partitioning of the use of wood-burning and other heating devices in households having more than one heating option. Note that the simulations on "woodstove replacement" do not consider that additional wood-burning devices have been added since 2008.

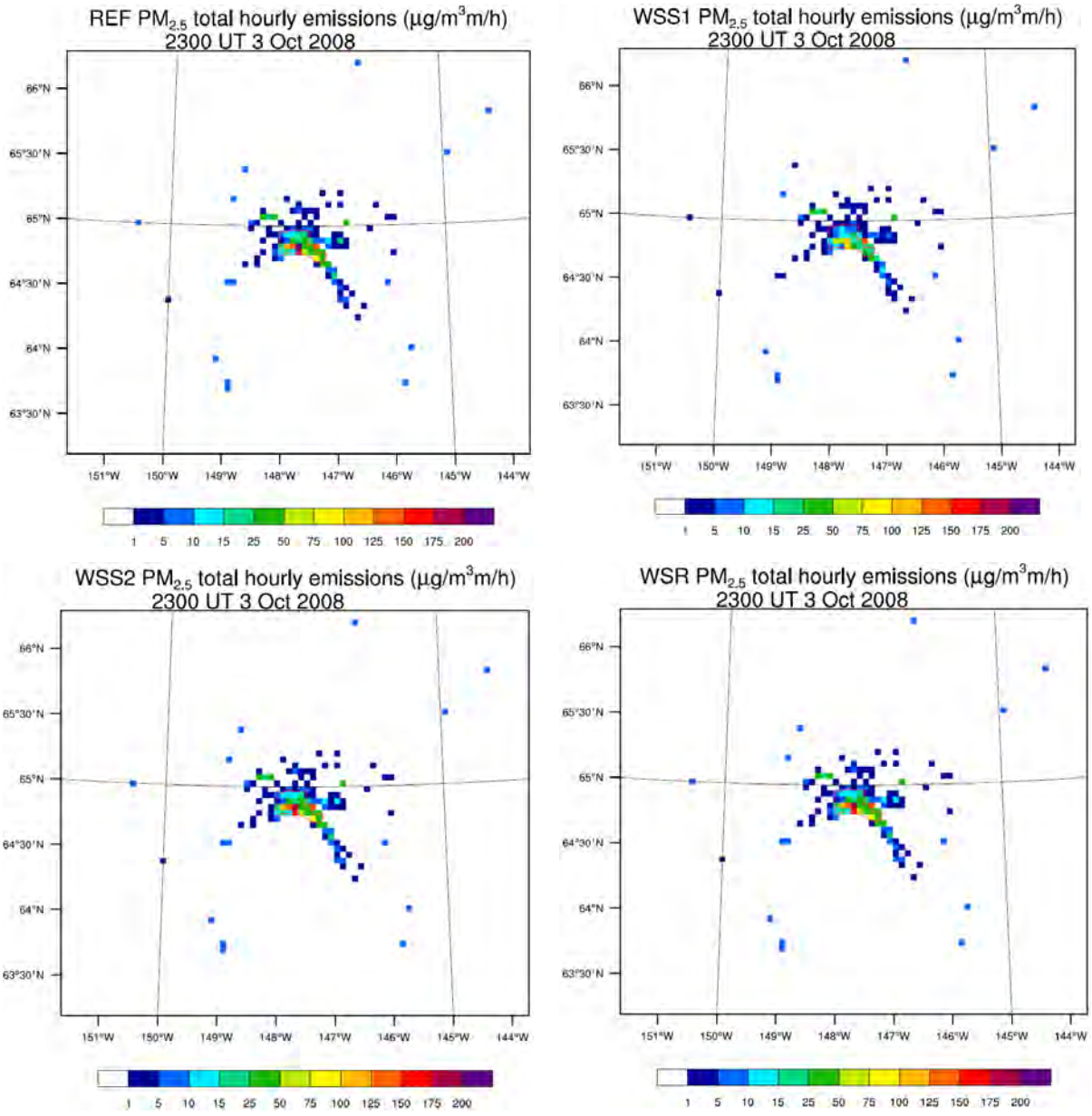


Fig. 8. Emissions of $PM_{2.5}$ as obtained with AkEM (upper left to lower right) before (REF) and after the assumed "woodstove replacement" assuming *Davies et al.*'s [2009] (WSS1), SRL's draft report (WSS2), and *Carlson et al.*'s [2010] (WSR) data on the numbers of heating devices. All "woodstove-replacement scenarios" result in reduced emissions over the nonattainment area. The nonattainment area is schematically superimposed in red.

As pointed out above, there is uncertainty in any emission data. This uncertainty is related to the approaches used and assumptions made. *Davies et al.* [2009] developed the emission rates for wood-burning devices using the operation-emission limits of the device (grams/hour) issued by EPA multiplied with the total hours of heating per year per household. Doing so, provided a

$PM_{2.5}$-emission rate of 60lb/yr.hh for noncertified and of 17lb/yr.hh for certified woodstoves. *Carlson et al.* [2010] list the amount of wood used annually as 3.95 cords wood/yr.hh. If one takes the EPA AP-42 emission factors of noncertified and certified woodstoves (30.6 and 14.6lb/short tons of dry wood, respectively), one obtains for the emission rates of noncertified and certified woodstoves 145lb/yr.hh and 69lb/yr.hh, respectively. *Davies et al.*'s [2009] study is based on heating hours and emission limits, while *Carlson et al.*'s [2010] study is based on fuel used. This means *Davies et al.*'s [2009] and *Carlson et al.*'s [2010] studies use different approaches. We used the AP-42 emission factors to compare their data. Depending on the approach, one will for each replaced woodstove reduce the emissions by (60-17) lb/yr.hh = 43lb/yr.hh and (145-69) lb/yr.hh = 76lb/yr.hh, respectively.

We used *Davies et al.*'s [2009] emission-rate data for all wood devices and oil furnaces as requested by the FNSB, but used *Carlson et al.*'s [2010] data for number of devices. Note that using this data seemed to be "safer" because the amount of reduction in response to a "woodstove replacement" program is smaller than using *Carlson et al.*'s [2010] emission rates. This means that the relative response factors that we obtained from our "woodstove replacement" simulations may underestimate the actual reduction that a woodstove replacement program can provide. In the sensitivity study WSS1, we used EPA's data for the "others" category, as data for these devices were not included in *Davies et al.*'s [2009] report. In the sensitivity study WSS2, we used *Carlson et al*.'s [2010] number of devices without consideration of pellet-stoves.

### 4.2.3 Emission scenario for introduction of low sulfur fuel for heating oil and power generation and other oil-burning point sources

The third scenario (LSF) represents a measure that aims at mitigation of $PM_{2.5}$ concentrations indirectly by reduction of precursors. As pointed out above sulfur can contribute to $PM_{2.5}$ formation in the atmosphere. Thus, the third emission scenario performed for winter 2008/09 assessed the impact of the introduction of low sulfur fuel for use as heating oil and in oil-burning power plants and other point-sources on the $PM_{2.5}$ concentrations at breathing level. The target emission categories that we considered in the "low sulfur fuel" scenario are heating oil, point source facilities and power plants that burn oil. The emissions from domestic and industrial combustion (including power plants) used in the reference simulation (REF) represent the emissions from relatively sulfur-rich fuel.

In the LSF simulation, the emissions from all sectors were kept the same as in the reference simulation except for emissions from domestic heating with heating oil, and oil-burning point sources and power plants with sulfur-rich fuel. The emissions from these sectors were replaced by emissions one would obtain with low sulfur content fuel for the same combustion amount.

To determine the amount of emission reduction due to a change from high to low sulfur-content fuels we reviewed the literature. Since the fuel-sulfur content may affect other emissions than just $PM_{2.5}$, we adjusted the emissions of these other species as well. Doing so is required as particles and hence $PM_{2.5}$ may form due to gas-to-particle conversion from various species as explained earlier.

*NESCAUM* [2005] reported the emission reduction due to reducing the sulfur content of No. 2 distilled heating oil from 2,000-3,000ppm to 500ppm for $SO_2$, PM and $NO_x$ as 75%, 80% and 10% respectively. In our study, we assumed the same transition of sulfur content in heating fuel in Fairbanks, and applied the same reduction found by *NESCAUM* [2005]. Since no reduction

benefits were reported for VOC and CO, we assumed that lowering of sulfur content in heating oil does not affect the VOC and CO emissions.

From personal communication with several power-plant operators in the FNSB, we learned that almost all power plants in the FNSB are burning No. 2 fuel oil having sulfur content about 4,000ppm. This fuel is similar to the fuel used for household heating. For the LSF simulations, we modified the point-source emissions with respect to low sulfur-fuel emissions for those oil-burning facilities that did not yet use low sulfur fuel already.

To our best knowledge, no report exists on the effects of low sulfur-fuel usage on the emissions of power plants. Therefore, we assumed a similar transition of sulfur content in heating fuel in the FNSB as reported in *NESCAUM* [2005] and applied the reduction given for power plants. Note that the actual reduction would be higher than the assumed reduction since the emission control devices in power plants become more effective as the sulfur content decreases.

In the low sulfur fuel (LSF) scenario, the emission reductions due to low sulfur fuel are only applied to those power plants and point sources that burn No. 2 fuel oil. For these facilities, a reduction rate of 75%, 80% and 10% was applied to the $SO_x$, PM and $NO_x$ emissions, respectively. For power plants burning both fuel oil and coal, only emissions from burning oil were subject to the emission reduction. We only got the break-down of the fuel-type consumption for the UAF power plant. Since the UAF power plant works on economic principles as the other power-plant operators do, we assumed a similar break-down of fuel types used for those facilities that burn different fuel types. No changes in emissions were made for power plants burning only coal.

### 4.3 Analysis methods

We compared the results of the simulations performed with modified emissions with the results of their respective reference simulation to assess the impact of the various emission mitigation measures or the contribution of point-source emissions on the $PM_{2.5}$ concentrations in the nonattainment area and in the grid-cell holding the FNSB official measurement site. This site is located on top of the State Building.

We used the Student t-test [*von Stroch and Zwiers*, 1999] to test the $PM_{2.5}$-concentration differences between REF and NPE for winter 2005/06, and REF and WSR or LSF for winter 2008/09 for their statistical significance at the 95% confidence level. The null hypothesis was that concentrations in REF and NPE, or REF and WSR or REF and LSF do not differ. In the following, we only use the word significant when data fail to pass this test.

Note that from a scientific point of view, it is important whether an emission source causes significant differences in the $PM_{2.5}$-concentrations. However, from a regulation point of view it is not of relevance whether or not, an emission source contributes significantly (in a statistical sense) to the concentrations of $PM_{2.5}$. Instead, it is important whether the emission-sources' contributions are the main contributor, i.e. dominate the concentration values, and whether reducing the emissions of these sources may lead to compliance.

If a certain kind of emission sources is the dominating one, regulation on the emission may help solve the exceedance problem. Here again distinctions have to be made. An emission source far away from the nonattainment area and/or far away from any settlements will typically dominate the concentrations in its surroundings, as it is most likely the only emission source out there. Thus, the large percentage contribution of such an emission source will not be worrisome as long

as the concentrations do not exceed the NAAQS. If an emission source is located in an unpopulated area close to populated areas, its contribution also may percentagewise be the main contributor. Then one has to consider how large the impact is on the adjacent populated areas and whether this impact leads to exceedances of the NAAQS. These facts have to be kept in mind in the following discussion.

For all scenarios, we determined the relative response factors and new design values.

### 4.3.1 Analysis of point source contribution

Differences between the highest 24h average $PM_{2.5}$-concentration obtained by REF and NPE were investigated to assess the impact of PS-emissions on the $PM_{2.5}$-concentrations at breathing level. The number, frequency and locations of grid-cells with 24h-average $PM_{2.5}$ exceedances were determined for both simulations to assess the contribution of PSs to exceedances. In addition, we examined the radius of impact of the point sources on the $PM_{2.5}$ concentrations at breathing level. Grid-cells affected by PS-emission will have non-zero $PM_{2.5}$-concentration difference between REF and NPE. Therefore, the influence of PS-emissions on the $PM_{2.5}$-concentration at breathing level was investigated by analyzing the correlation between the PS-emissions at each emitting level with the $PM_{2.5}$-concentration-difference. In the domain of interest, 27 PSs emit into the second (8-16m) to the seventh model layer (343-478m) due to plume raise.

The impact of each individual PS on the perturbation of $PM_{2.5}$-concentration is difficult to identify unambiguously because in WRF/Chem, like other photochemical models, all PSs located within the same grid cell are lumped but emit into the levels into which the individual PSs would emit. After lumping, there are nine grid columns holding PSs. Due to the lumping we cannot investigate individual PS impacts on $PM_{2.5}$-concentration at breathing level, but the cumulative impact of all PSs within a grid-column on the downwind $PM_{2.5}$ concentrations of that column. We examined the impact for each grid column holding PSs and denote these PS1 to PS9, hereafter. See Figure 14 for locations.

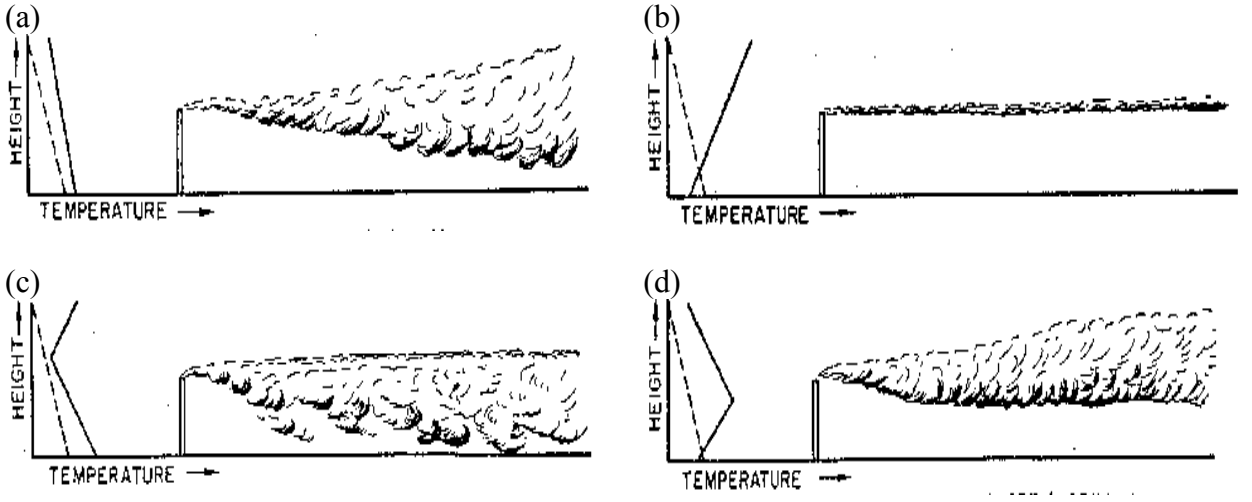


Fig. 10. Schematic view of temperature profiles and plume behavior for emissions in the case of (a) no inversion layer, (b) into an inversion layer, (c) below an inversion layer, and (d) above an inversion layer. From: *http://www.iitap.iastate.edu/gcp/acid/images/plume.gif.*

We only considered the $PM_{2.5}$-concentration-difference distribution at grid cells located downwind of a grid-cell with PSs. At each PS1 to PS9, we used the wind direction from the first level above ground to the uppermost emitting level to identify the downwind grid cells of each level in each simulation hour. This treatment ensured that not all grid cells around the PSs, but only the grid cells impacted by the PS are considered. These $PM_{2.5}$-concentration-difference values were used to calculate the correlation with the PS-emissions for November to February (NTF). All correlations were tested for their statistical significance at the 95% or higher confidence level using a Student-t test.

PSs in the downwind sectors of a PS-holding column may affect the $PM_{2.5}$-concentrations in its downwind. Therefore, the correlation behavior of each PS1 to PS9 was investigated under consideration of potential impacts by other PS holding grid-columns. As atmospheric temperature inversion and wind speed affects the dispersion of the PS emissions, we investigated separately the correlation between PS-emissions and $PM_{2.5}$-concentration-difference for different wind-speed classes at the emitting level and under conditions when PSs emitted below, above and into inversion layer (Fig. 10). We applied different time lags in determining the correlations to account for the lag in time between the actual emission and the time when the $PM_{2.5}$ reaches the downwind grid-cells at breathing level.

### 4.3.2 Analysis of the "woodstove replacement" scenario

We used the Student t-test to examine the $PM_{2.5}$-concentration differences (REF-WSR) for their significance at the 95% level of confidence. To verify that the differences are really due to replacing "woodstoves", we adopted a False Ensemble Analysis method (FEA) which was developed and applied successfully in climate model data analysis [*Carpenter et al.*, 1989; *Werth and Avissar*, 2002]. We performed the analysis for each month of the REF and WSR simulations. First, the true difference of 24h-average $PM_{2.5}$-concentration between REF and WSR was determined for each month. Secondly, a set of false "REF" and "WSR" ensembles was created by randomly replacing results of simulation days of REF (WSR) with the results of the corresponding simulation days of WSR (REF). Because the emission strengths are allocated depending on the hour of the day, day of the week and month of the year, and daily mean temperature [*Mölders,* 2010], each randomly selected REF-day had to be replaced by the corresponding WSR-day. In this way, emissions only differ with respect to the emission changes in response to the wood-burning devices exchanged. A random generator was used to create an index array, which days of the month were to be chosen to create the false ensemble, and REF (WSR) files were replaced accordingly. The replacement was completed as the number of WSR (REF) simulation days makes up 50% of the total days of the false "REF" ("WSR") ensemble by which the false "REF" and "WSR" can be considered as having no net difference in the mean emission.

Theoretically, $n!/[(n/2)!]\times 2$ numbers of false ensembles can be generated from n simulation days in the way described above. However, considering the time constrains and computational limitation, we generated 400 false "REF-WSR" ensembles randomly for each month. For each set of false "REF" and "WSR" ensemble the difference of 24h-average $PM_{2.5}$-concentration was determined as was done for the true difference REF-WSR. Finally, the true and 400 false concentration differences were ranked. The above procedure was applied for each grid cell. If at a grid cell, the true difference falls in the top 5% of all values, we can conclude that the true $PM_{2.5}$-concentration difference is real, i.e. the "woodstove replacement" actually reduced the $PM_{2.5}$-concentration in the grid cell of interest.

### 4.3.2 Analysis of the "low sulfur" scenario

Emissions of $PM_{2.5}$, $PM_{10}$, $SO_2$, NO and VOC from the current sulfur content fuel (REF) and the use of low sulfur fuel (LSF) were analyzed and compared on a monthly and daily basis. Note that these pollutants were selected as they are primary particular matter and precursors for secondary aerosols, i.e. they can affect the $PM_{2.5}$-concentrations at breathing level. Since the emissions were considered temperature-dependent, the mean temperatures and their deviation from the long-term mean temperature were analyzed and used to elucidate the variations in emission reductions.

Concentrations of $PM_{2.5}$ and other pollutants ($PM_{10}$, sulfate, nitrate, VOC) in the nonattainment area obtained by REF and LSF were compared. The monthly, daily, and hourly variations of $PM_{2.5}$-concentration reductions after introduction of low sulfur fuel were quantified and analyzed. The variations in the aerosol composition were also identified. Furthermore, mean meteorological quantities (temperature, dewpoint temperature, relative humidity, wind-speed, shortwave radiation fluxes, atmospheric boundary layer height, precipitation and cloudiness) were used in the analysis of $PM_{2.5}$-concentration reductions as there were feedbacks of aerosols on the meteorology.

Furthermore, we also applied the FEA to the REF and LSF data.

## 5. Evaluation

As pointed out above, we used the results of the WRF/Chem simulations of the first 15 days October 2005 for calibration. Within the framework of another project, WRF/Chem was evaluated by data from a Doppler SOund Detection And Ranging (SODAR) device, twice-daily radiosondes, 33 surface meteorological and four aerosol sites [*Mölders et al.* 2011].

The evaluation used the following performance skill-scores (root-mean-square error [RMSE], bias, standard deviation of error [SDE], correlation coefficient [R]) following *von Storch and Zwiers* [1999] for the meteorological quantities, and the fractional bias ($FB = \left(\overline{C_s} - \overline{C_o}\right) \Big/ \left[0.5\left(\overline{C_s} + \overline{C_o}\right)\right]$), normalized mean-square error ($NMSE = \left(\overline{C_s} - \overline{C_o}\right)^2 \Big/ \left(\overline{C_s} \cdot \overline{C_o}\right)$), geometric mean bias ($MG = \exp\left(\overline{\ln C_s} - \overline{\ln C_o}\right)$), and the fraction of simulated concentrations $C_s$ being within a factor of two of the observed concentrations $C_o$ (FAC2) following *Chang and Hanna* [2004] for the chemical quantities. These are standard measures typically used in the evaluation of photochemical models and hence allow us to assess how good the Alaska adapted WRF/Chem performs for Alaska winter relative to models applied for cases in mid latitudes.

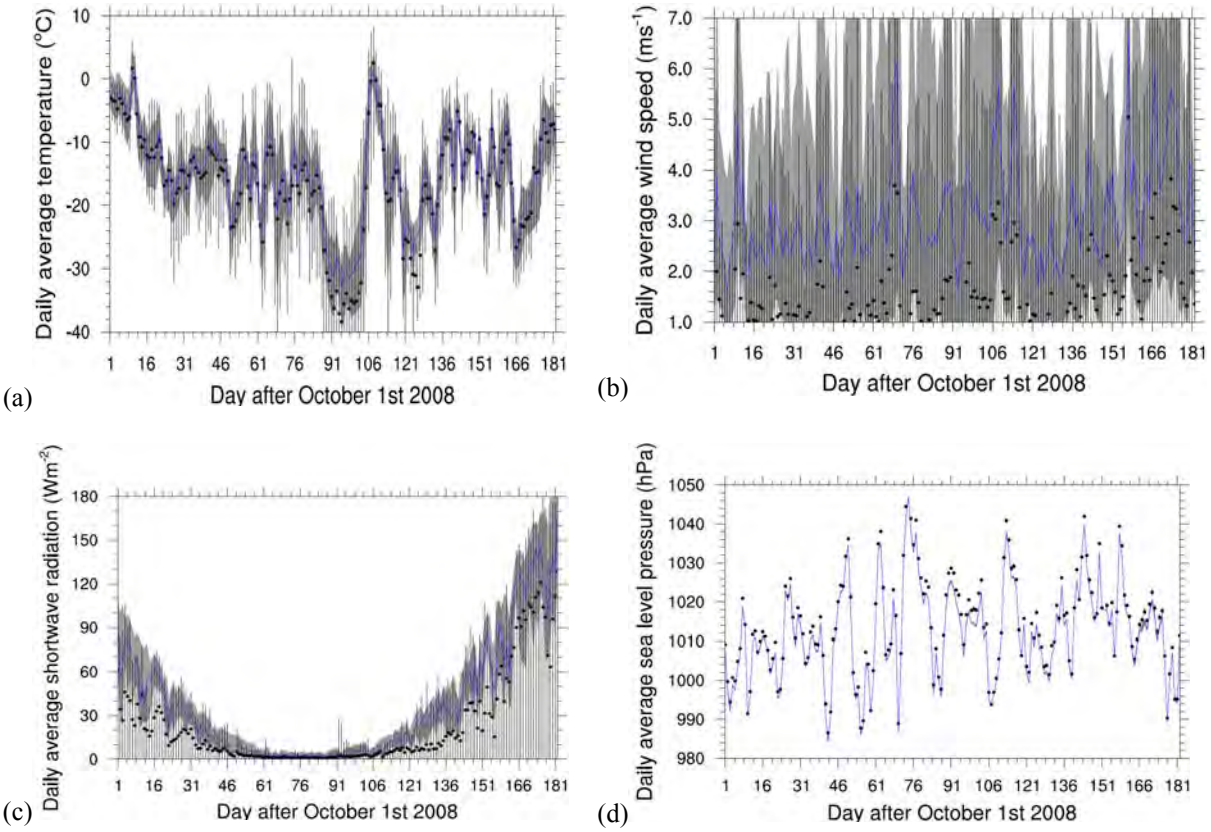


Fig.11. Temporal evolution of daily averaged of (a) air-temperature, (b) wind-speed, (c) downward shortwave radiation, and (d) pressure averaged over all sites for which data were available as simulated (blue line) and observed (dots). Plots for dewpoint (not shown) and air-temperatures look similar. Grey-shading and vertical bars indicate variance of simulated and observed quantities, respectively. Note that there were only two sites with pressure data Fairbanks International Airport and Eielson Air Force Base. Due to their relative close location, there is not much spatial variance. Therefore, no bars on the spatial variance of pressure are plotted.

All our simulations were run in"forecast" mode, i.e. no nudging or data assimilation was applied. *Mölders et al.* [2011] found that biases determined based on all available data from the 33 sites over NTF are 1.6K, 1.8K, 1.85m/s, -5$^{o}$, and 1.2hPa for temperature, dewpoint temperature, wind-speed, wind-direction, and sea-level pressure, respectively, in NTF 2005/06. Figure 11 shows the average temporal evolution of simulated and observed meteorological quantities as obtained for October 2008 to March 2009 (OTM) on average over all 23 sites within the domain of interest for which data were available for that time. Note that there were less meteorological sites operating in the area covered by the domain of interest for analysis in winter 2008/09 than 2005/06. Over OTM 2008/09, the overall biases over all sites are 1.3K, 2.1K, 1.55m/s, -4$^{o}$, and -1.9hPa for temperature, dewpoint temperature, wind-speed, wind-direction, and sea-level pressure, respectively. The 2005/06 temperature bias is only marginally higher than that reported by *Gaudet and Staufer* [2010] for their WRF short-term study with a 4km grid increment performed for Fairbanks using data assimilation. The wind-speed RMSE is slightly higher than the RMSE reported for their short study. Note that it is relatively easy to optimize a model for a short period of several days, while it is rather difficult to achieve a generally acceptable performance over an episode as long as four or six months like in our study.

The evaluation by means of SODAR-data revealed that WRF/Chem slightly over(under)estimates wind-speed in the lower (upper) ABL. WRF/Chem captures the frequency of low-level jets well, but overestimates the strength of moderate low-level jets [*Mölders et al.* 2011].

As aforementioned there are hardly any chemical data available for winter 2005/06. While $PM_{2.5}$ concentration data exist only at two sites (Fairbanks State Building, Denali Park) for winter 2005/06, measurements exist at 12 sites in Fairbanks for winter 2008/09. Based on the limited data available WRF/Chem simulated the maximum $PM_{2.5}$-concentration about 6% too low for winter 2005/06. Data from four aerosol sites suggest large underestimation of $PM_{10}$, and $NO_3$ at the remote sites outside of the nonattainment area and underestimation of $PM_{2.5}$ at the State Building in winter 2005/06 [*Mölders et al.* 2011].

Averaged over the two $PM_{2.5}$- and $SO_4$-sites, 41% and 50% of the simulated values, respectively, fell within ±50% of the observed concentration value for winter 2005/06. The low data density – for 2005/06 only one $PM_{2.5}$ observational site exists in the nonattainment area – may falsely indicate errors due to local effects [*Mölders et al.* 2011].

The hourly $PM_{2.5}$ evaluation of winter 2008/09 shows that 29%, and 36% of the simulated and observed concentrations agree within ±50% for the fixed sites FNSB (site at the State Building), and Peger Road, respectively. The performance for the 24h-average $PM_{2.5}$ is better – 46% of the fixed sites agree within ±50%. At the FNSB State Building, Peger Road, North Pole, Sadler and Denali site 35%, 58%, 38%, 39% and 58% of the simulated 24-average $PM_{2.5}$ concentrations are within ±50% of the observations, respectively. The scientific community considers photo-chemical models with fractional biases within ±30%, random scatter being within a factor of two or three of the mean, and 50% of the predictions falling within a factor of two of the observations to perform well [e.g. *Chang and Hanna* 2004]. Thus, our WRF/Chem simulations for 2005/06 fall in the lower end of acceptable performance, while those for 2008/09 are slightly better. The better performance for 2008/09 than 2005/06 may be due to the introduction of a temperature-dependency of traffic, power generation and domestic heating emissions in AkEM in response to the evaluation for 2005/06.

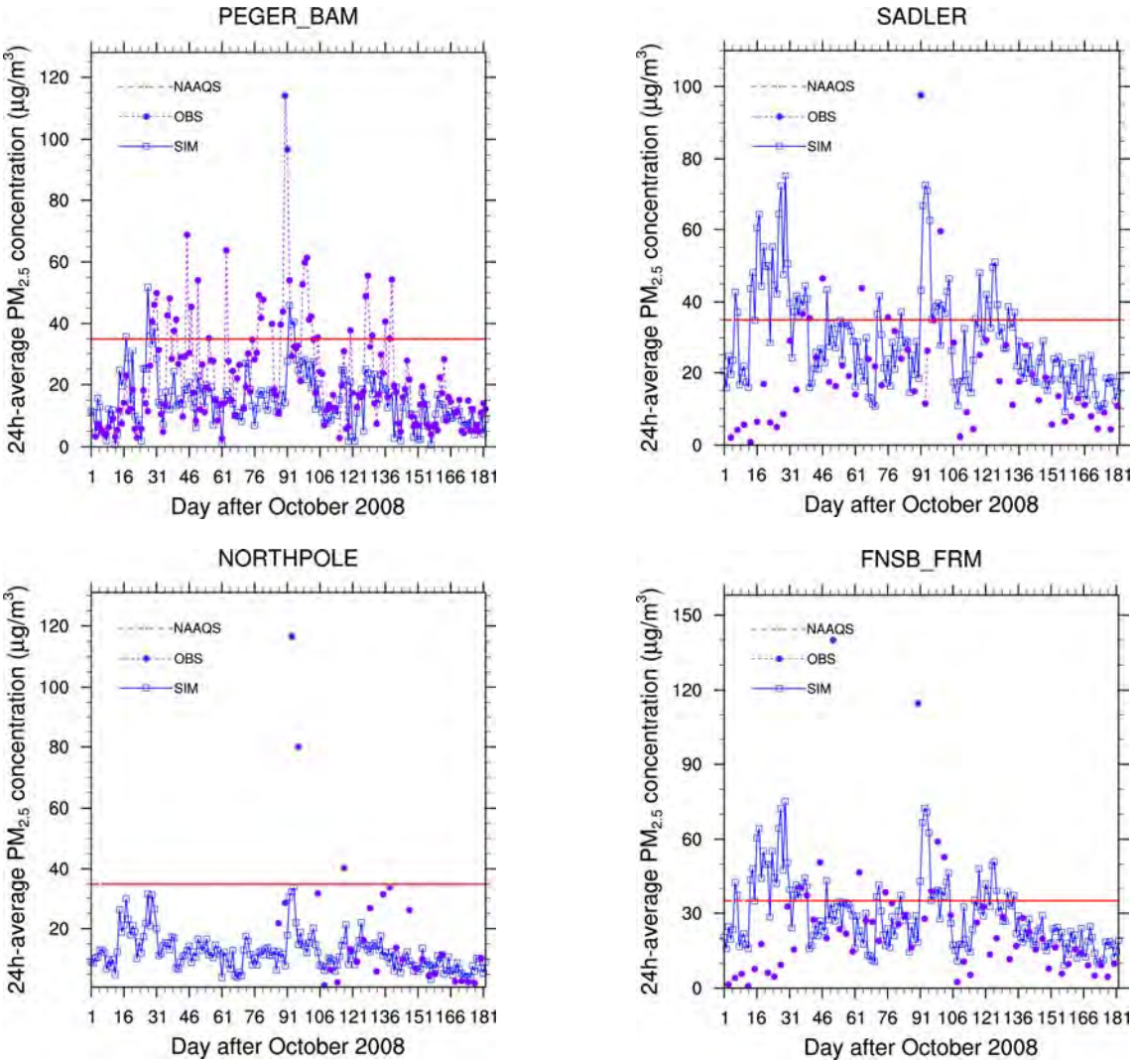


Fig. 12. Comparison of simulated and observed concentrations as obtained for winter 2008/09 for various sites. FNSB is the site at the State Building.

The evaluation of both winters indicates that WRF/Chem captures the temporal evolution of $PM_{2.5}$ concentrations well except during sudden temperature changes, underestimation of inversion-strengths and timing of frontal passages (e.g. Fig. 12). In October, WRF/Chem underestimates the $PM_{2.5}$ concentrations appreciably at all sites for which data are available. This behavior suggests that the assumed emissions for October 2008 are too low. Note that there are hardly any Alaska specific emission allocation functions. We used the allocation functions recommended by EPA for Alaska, which we modified to avoid obviously unreasonable emissions (e.g. emissions from lawn mowing in October), when no Alaska specific allocation functions could be obtained.

Errors in $PM_{2.5}$-concentrations relate strongly to temperature errors, i.e. to WRF rather than its chemical package [see also *Mölders et al.* 2011]. In October 2008, WRF/Chem underestimates the concentrations strongly at some sites (e.g. Sadler). It should be examined whether emissions are underestimated in October. On the contrary, in other months simulated and observed concentrations agree better in magnitude. The discrepancies found may also result from

channeling effects in streets or slight offsets of dispersion plumes. The occasional much higher observed than simulated concentrations are most likely due to contamination of the measurements by mobile sources at the site (e.g. busses idling at the Peger site upwind of the sampler). All these discrepancies are common in and known to occur for all photochemical models of the scale deployed here [e.g. *Chang and Hanna*, 2004].

The evaluation of winter 2005/06 suggested that simulated $PM_{2.5}$-concentrations may be slightly too low on average over the polluted and unpolluted site. However, averaging of polluted and non-polluted sites may be misleading due to the strong concentration differences of polluted and non-polluted sites. In both winters, WRF/Chem seems to overestimate the concentration slightly at the polluted sites. In winter 2005/06 and 2008/09, the mean biases over all available sites are 4.2 and 4.0$\mu g/m^3$, respectively. However, this bias affects the reference as well as the simulations with the emission scenarios. Since we are examining concentration differences in this study, the impact of the aforementioned errors can be considered as small.

## 6. Results

We examined the meteorological conditions on days with $PM_{2.5}$ exceedances. We found three distinct local circulation patterns at breathing level and five different circulation patterns higher above ground between 100 and 200 m that lead to exceedances of the NAAQS at breathing level (Fig. 13). If at breathing level, wind is very calm (<1m/s) and comes from various directions and the air remains in town, local exceedances will occur within the nonattainment area. The same will be true if slight drainage of the Fairbanks air occurs towards southwest, down the Tanana Valley or if air moves into town from southeast under calm wind conditions in Fairbanks. Obviously, in this case, advection of polluted air from the Salcha air shed and North Pole can contribute to causing the exceedances.

Exceedances are also related to what happens at heights between 100 and 200m or so. If at these levels, air moves out of town slowly down the Tanana Valley, air slowly travels through Fairbanks down the Tanana Valley, air moves towards North Pole and Eielson Air Force Base up the Tanana Valley, or air drains to both sides of the Tanana Valley (Fig. 13), exceedances will occur at some places in the nonattainment area at breathing level. This behavior is especially true when at the same time, winds are relatively calm over Fairbanks or the air circulates slowly over the town.

In the following, $PM_{2.5}$-concentrations at breathing level are discussed if not mentioned otherwise.

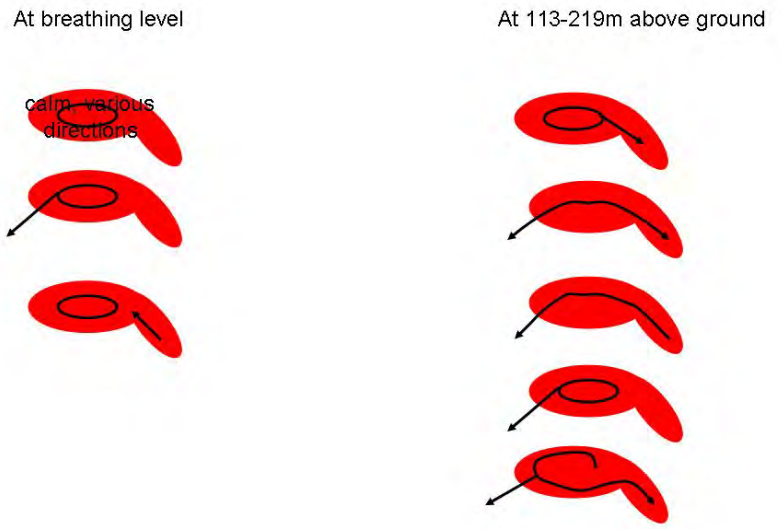


Fig. 13. Circulation pattern associated with violations at breathing level. The red area schematically illustrates Fairbanks, North Pole and Salcha air sheds. Wind-speeds must be very low.

Note that winter 2008/09 except for February and in particular October 2008 were colder than the 30-year average (Table 3).

Table 4 compares the results of the WSR, LSF and REF simulations. The results suggest that in October 2008, January, February and March 2009 the assumed "woodstove replacement" yields a stronger reduction of the $PM_{2.5}$-concentrations at breathing level than the introduction of low sulfur fuel. In November and December 2008, introduction of low sulfur fuel, on average,

provides the higher mitigation of the $PM_{2.5}$-concentrations. The results suggest that "woodstove replacement" provides a temporally more constant percentage reduction of around 6% averaged over the nonattainment area than does the introduction of low sulfur fuel (Table 4).

Table 3. Monthly mean temperatures at Fairbanks International Airport in Fahrenheit. Courtesy to *H. Angelhoff* [2011]. The 30-average for 1971-2000 is taken from *Shulski and Wendler* [2007]. Values for the episode simulated in this study are high-lighted.

| | Oct | Nov | Dec | Jan | Feb | Mar | Oct-Mar |
|---|---|---|---|---|---|---|---|
| 2007 | 21.2 | 11.5 | -3.4 | -6.6 | -6.7 | -6.5 | 1.6 |
| 2008 | 15.1 | -1.4 | -7.8 | -9.2 | -5.9 | 15.4 | 1.0 |
| 2009 | 30.7 | -1.2 | -2.8 | -12 | -1.5 | 5.6 | 3.1 |
| 2010 | 27.5 | 11.9 | -17.9 | -13.7 | 2.9 | 10.8 | 3.6 |
| 2007-2009 | 22.3 | 3.0 | -4.7 | -9.3 | -4.7 | 4.8 | 1.9 |
| 2008-2010 | 24.4 | 3.1 | -9.5 | -11.6 | -1.5 | 10.6 | 2.6 |
| 1971-2000 | 24 | 2 | -6 | -10 | -4 | 11 | 2.8 |

Table 4. Monthly average $PM_{2.5}$-concentration as obtained for the grid-cell holding the State Building and averaged over the nonattainment area for October 2008 to March 2009. The percentage reduction is given in brackets.

| | $PM_{2.5}$ ($\mu g/m^3$) | | | | | |
|---|---|---|---|---|---|---|
| | State Building | | | Nonattainment area | | |
| | REF | WSR | LSF | REF | WSR | LSF |
| OCT | 40.2 | 38.5 (4.2%) | 39.2 (2.5%) | 12.9 | 12.2 (5.4%) | 12.5 (3.1%) |
| NOV | 30.3 | 28.8 (5.0%) | 28.5 (5.6%) | 11.0 | 10.3 (6.3%) | 10.0 (9.0%) |
| DEC | 25.8 | 24.5 (5.0%) | 24.4 (5.4%) | 9.2 | 8.6 (6.5%) | 8.5 (7.6%) |
| JAN | 33.9 | 32.2 (5.0%) | 32.7 (3.5%) | 11.0 | 10.3 (6.4%) | 10.4 (5.5%) |
| FEB | 27.1 | 25.5 (5.9%) | 26.0 (4.1%) | 9.8 | 9.2 (6.1%) | 9.3 (5.1%) |
| MAR | 17.1 | 16.1 (5.8%) | 16.2 (5.3%) | 5.7 | 5.3 (6.4%) | 5.3 (7.0%) |

### 6.1 Impact of point-source emissions

This section discusses findings from the simulations performed for winter 2005/06. See Table 1 for details on the simulations.

The influence of emissions from elevated point sources on the $PM_{2.5}$ concentration at breathing level was investigated by analyzing the correlation between the PSs' emissions at each level with the $PM_{2.5}$-concentration at the breathing level. The highest effective level reached by the plume from point-source emissions is the model layer representing the conditions between 343 and 478m. Note that the buoyancy, depending on temperature of the plume, velocity at release etc. and the environmental conditions, determine which levels the emissions from PSs can reach.

Table 5. Monthly average of $PM_{2.5}$-concentration at the State Building and averaged over the nonattainment area as obtained from the simulations for winter 2005/06. The percentage reduction is given in brackets.

| | $PM_{2.5}$ ($\mu g/m^3$) | | | |
|---|---|---|---|---|
| | State Building | | Nonattainment area | |
| | REF | NPE | REF | NPE |
| NOV | 30.5 | 29.2 (4.2%) | 14.4 | 13.4 (6.9%) |
| DEC | 26.4 | 25.4 (3.8%) | 12.5 | 12.0 (4%) |
| JAN | 40.9 | 39.7 (2.9%) | 15.9 | 14.9 (6.3%) |
| FEB | 21.6 | 20.9 (3.2%) | 9.6 | 9.2 (4.2%) |

Since no emissions from PSs are considered in NPE, the monthly total emission strength does not differ between REF and NPE from November 2005 to February 2006 except at the locations of the PSs. Since most of the PS and the strongest PSs are located in the highly populated

Fairbanks area, here the largest differences between REF and NPE in emissions as well as concentrations occur. Emission and concentration differences are larger in December and January as during these months emissions from PSs are higher than in November and February. The majority of the PSs are facilities that emit more in December and January to cover the higher heating and/or energy demands during the darker, colder December and January than the relatively warmer and less dark November and February.

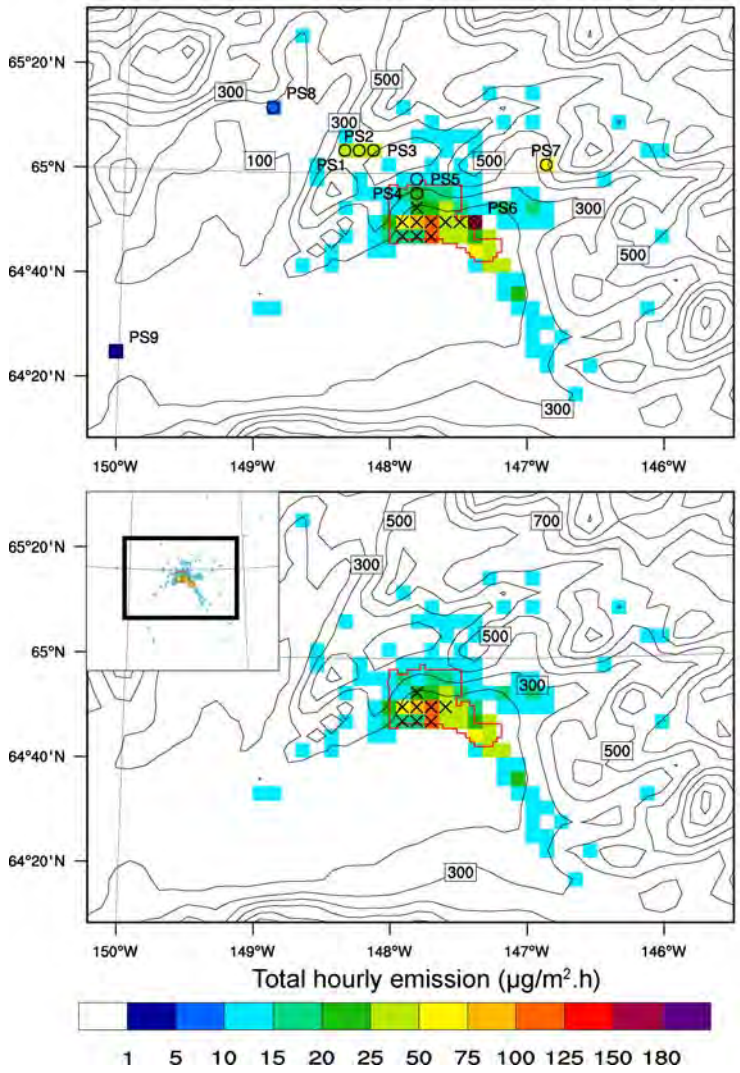


Fig. 14. Zoom-in on the spatial distribution of areas experiencing $PM_{2.5}$-concentration exceeding the NAAQS (grid cells with crosses) in REF (top) and NPE (bottom) exemplarily superimposed on the map of total hourly emission on 0200 UTC December 1, 2005. The black box indicates the location of the zoom-in area. PS1 to PS9 indicate locations of grid columns with point sources.

$PM_{2.5}$-concentration obtained by REF and NPE differ hardly with respect of the number of NAAQS exceedances. Within the domain of interest, the NAAQS is exceeded 10 (7), 6 (5), 22 (21) and 1(1) times in REF (NPE) in November, December, January, and February, respectively. The locations of exceedances within the nonattainment area are identical in both REF and NPE except at PS6 and the adjacent grid cell to its west (Fig. 14). Except for two events in November

2005 in REF, the grid-cell holding the State Building monitoring station experienced exceedances on all exceedance events in REF and NPE.

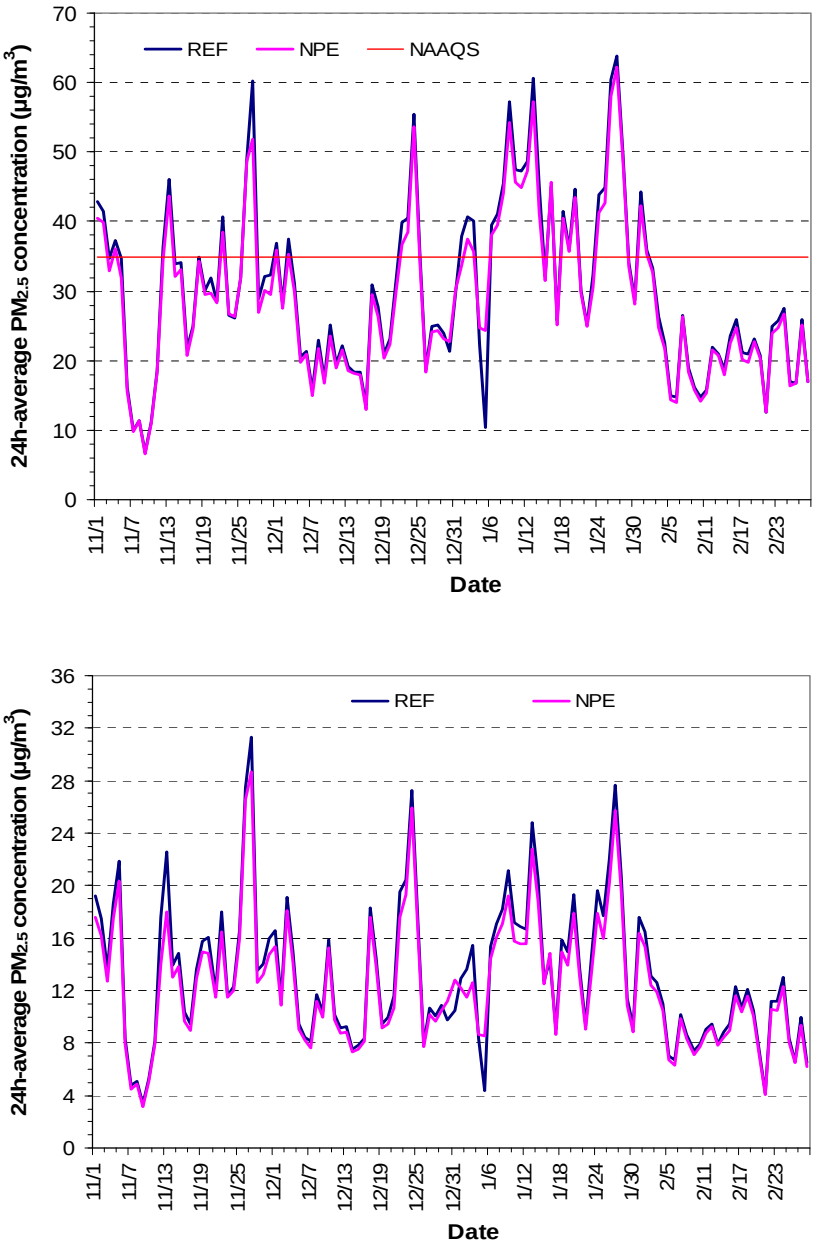


Fig. 15. Temporal evolution of 24h $PM_{2.5}$-concentrations as obtained for the grid-cell that holds the State Building (top) and the 24h $PM_{2.5}$-concentration averaged over the nonattainment area (bottom) for the simulations with (REF) and without (NPE) inclusion of point sources. NAAQS is the National Ambient Air Quality Standard of 35µg/m$^3$.

Despite the number of exceedances in REF exceeds that in NPE occasionally, the days with exceedances in REF, but not in NPE show almost the same magnitude of $PM_{2.5}$-concentration (Fig. 15). Over the entire simulation period, the average differences of between REF and NPE 24h-average $PM_{2.5}$-concentration are 0.04µg/m$^3$, 0.8µg/m$^3$ and 1.0µg/m$^3$ over the entire analysis domain, the nonattainment area and at the State Building, respectively. The average difference of

highest concentrations between REF and NPE were as low as 1.3µg/m$^3$ and barely exceeded 3µg/m$^3$. The most notable differences occurred at locations close to the PS-holding columns. The highest concentration differences occurred for PS6 and on 47% of 120 simulation days and amounted 7µg/m$^3$ on average. Note that PS6 has the strongest $PM_{2.5}$ emissions among the PS-holding columns.

These findings suggest that PS-emissions do not strongly increase the $PM_{2.5}$-concentration within the nonattainment area except for the grid-cell PS6. In the nonattainment area, on days and at the locations of exceedances, emission from PSs accounted for 4% of the 24h-average $PM_{2.5}$-concentration on average and barely exceeded 10%. These findings mean that emissions from area sources induced high $PM_{2.5}$-concentration in the nonattainment area and the emissions from the PSs just added the small amount needed to exceed the NAAQS. This also means that emissions from PSs play a minor role for the $PM_{2.5}$ exceedances in the nonattainment area.

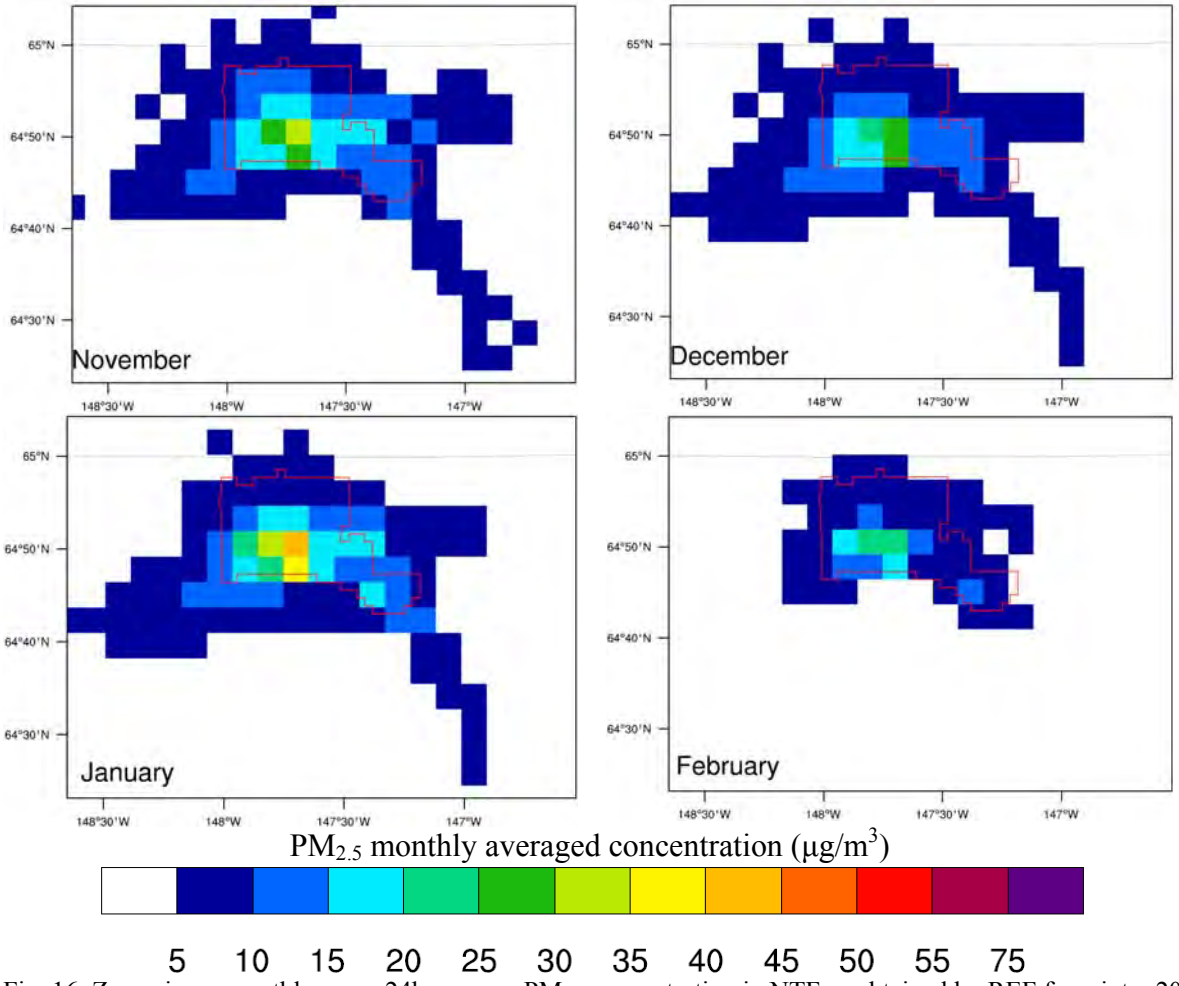


Fig. 16. Zoom-in on monthly mean 24h-average $PM_{2.5}$ concentration in NTF as obtained by REF for winter 2005/06.

Figure 16 shows a zoom on the spatial distribution monthly mean 24h-average $PM_{2.5}$-concentrations at breathing level. The hot spots remain the same over all four months, but with different magnitude. The hot spots remain the same in the simulation without consideration of point source emissions (Fig. 17). The concentrations are only slightly lower in the simulation without consideration of point source emissions. These facts indicate that area and line sources

(e.g. domestic combustion, traffic) are the main cause emission wise for the high $PM_{2.5}$ concentrations.

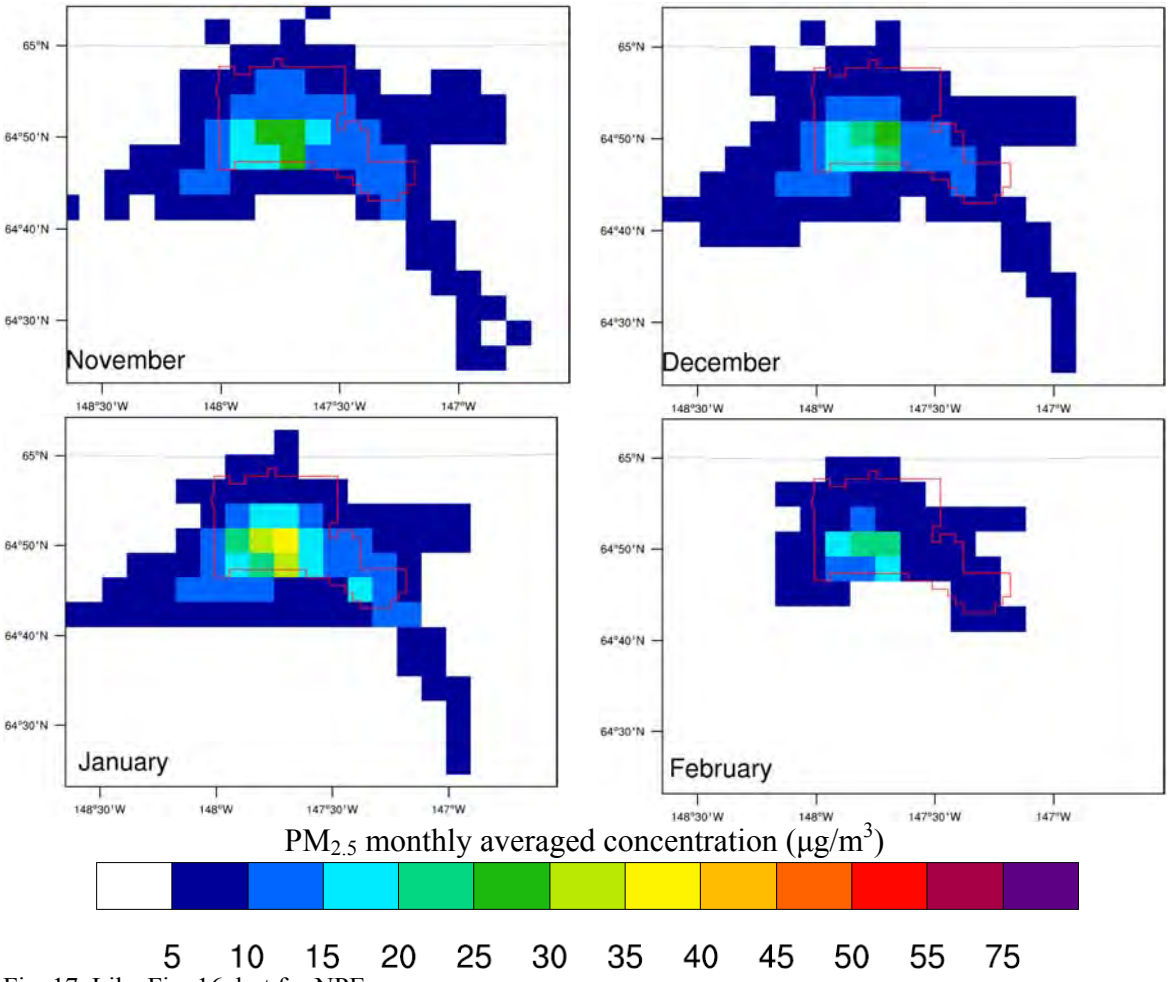


Fig. 17. Like Fig. 16, but for NPE.

Theoretically, higher $PM_{2.5}$-concentration at breathing level are expected with higher PS-emission rates, and under normal atmospheric conditions (no inversion), the location having the highest concentration at breathing level will be farther away from the PS as the effective emission level increases. Our analysis showed statistically significant correlations between emissions and $PM_{2.5}$-concentrations, but the correlation values are low and vary highly among PS-holding columns due to PS characteristics, location and co-location effects. In the downwind of PSs, the impact of point-source emissions on the $PM_{2.5}$-concentration decreases rapidly with increasing distance from the PS.

Investigations show that the total emissions within a grid-column and the simulated $PM_{2.5}$-concentrations at breathing level correlate highly in populated areas. This finding is true for both REF and NPE. The correlation between the total emissions within a grid-column and the simulated $PM_{2.5}$-concentrations at breathing level will only marginally differ if no point-source emissions are considered in the calculation of the $PM_{2.5}$ concentrations. This finding suggests that PS emissions are not the main causes for high $PM_{2.5}$ concentrations.

We evaluated the impact-radius of PS-emissions on the $PM_{2.5}$ concentrations at breathing level. Correlation values between PS-emissions and $PM_{2.5}$-concentration-differences at downwind grid-cells differ generally with wind-speed. Overall, under low wind-speed (<2ms$^{-1}$) conditions, the highest correlation values at breathing level occur within 2km from the PS; correlations under stronger wind-speed decrease, but are highest farther downwind (e.g. Fig. 18). The occurrence of highest correlation also shifts farther downwind when the emission-level height increases. Nevertheless, regardless of emission level and wind-speed, the highest correlations occurred within 10km from the PS. Beyond 10km from the PS, correlations are small and non-significant and small for low wind-speeds, but significant for moderate wind-speeds (≥5m/s). The strongest correlations are obtained typically with time lags of 0 or 1h.

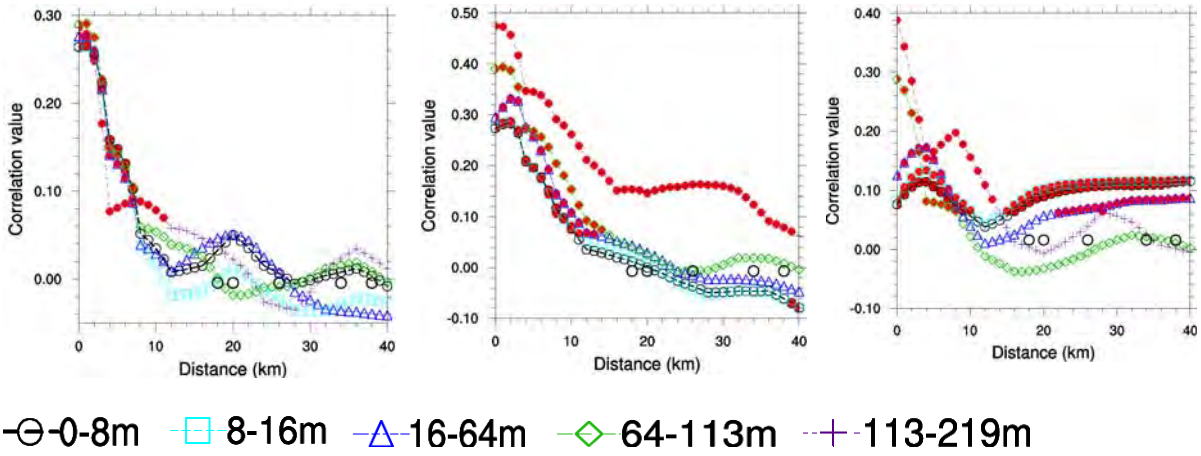


Fig. 18. Correlation of emissions at PS6 with the $PM_{2.5}$-concentration-difference (REF-NPE) at downwind grid-cells in subsequently lower levels from the emitting level (113-219m) to the breathing level (0-8m) under wind-speeds <2m/s (left), 2-5m/s (middle) and ≥5m/s (right). The emitting level is the highest level displayed in the figure. Open black circles indicate the relative position of grid columns holding other PSs near the PS-holding grid-column of interest. Closed red circles represent statistically significant (at the 95% confidence level) correlations.

Atmospheric temperature inversions influence the dispersion of PS-emissions (Fig. 10). As can be easily derived from Figure 10, theoretically, PS-emissions emitting into levels above, in-between and below inversion layers would have their impact on the breathing level from the lowest to highest magnitude, respectively. In the following, we talk about "no-inversion conditions" when the bottom of any inversion layer aloft is 200m above the emitting-level. "Below-inversion" refers to when the bottom of any inversion aloft is less than 50m above the highest emitting-level. On average, WRF/Chem predicted in-between-inversion, above-inversion, below-inversion and no-inversion conditions for PS-emissions in 64%, 18%, 10% and 8% of the time, respectively. Note that WRF/Chem for 2005/06 predicted the frequency of inversions acceptably [*Mölders et al.*, 2011].

In general, WRF/Chem reproduced successfully the emission-inversion relationship at all PSs. Here we only show the correlation at PS6 as an example. The strongest and significant correlations between PS-emissions and $PM_{2.5}$-concentration-difference at breathing level occurred under "below-inversion" conditions and the highest correlation values typically occurred at 8-10km downwind depending on emission level and wind speed (e.g. Fig. 19). The second strongest (significant) correlations occurred under "in-between-inversion" conditions. Then the highest correlation values occurred within 0-12km downwind depending on wind-speed, emission level and inversion strength. The location of highest correlation typically shifts

farther downwind as the inversion strength increases and vice versa. Under both "no-inversion" and "above-inversion" conditions, PS-emissions correlate marginally and insignificantly with the breathing level $PM_{2.5}$-concentration. Based on these finding we conclude that PSs have their highest impact on the $PM_{2.5}$-concentration at breathing level within 10km of their location.

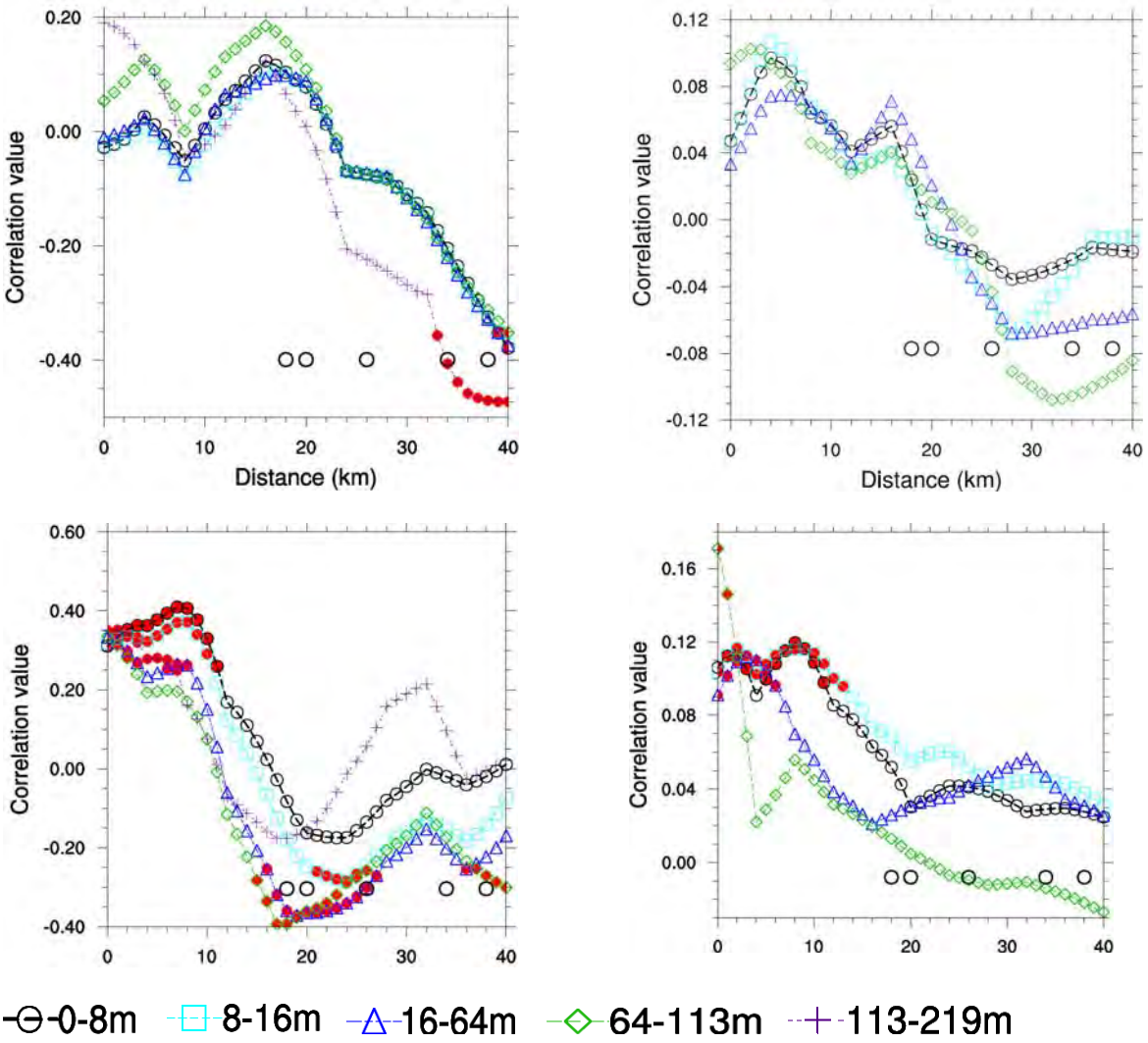


Fig. 19. Correlation of $PM_{2.5}$ emissions at PS6 with $PM_{2.5}$-concentration-difference at downwind grid-cells in subsequently lower levels from the emitting-level to the breathing level (0-8m) under conditions when there was "no inversion", emission into levels above, just below and in between inversion layers (top-left to bottom-right, respectively). The emitting-level is the highest level displayed in the figure. Open black circles indicate the relative position of grid columns holding other PSs in the vicinity of the PS-holding grid-column of interest. Closed red circles represent statistically significant (at the 95% confidence level) correlations.

### 6.2 Potential impact of "woodstove replacement" programs

As pointed out above, WSR is a very moderate "woodstove replacement" scenario in comparison with the sensitivity simulation that assumed a replacement of all non-certified wood burning devices based on the number of devices given in *Davies et al.*'s [2009] report (WSS1). The emission reduction in WSR was much lower than in WSS1 (cf. section 4). Within the nonattainment area, the emission strength in WSR was 6$\mu gm^{-2}h^{-1}$ (6%) less than in REF on

average whereas in WSS1 the emission strength was 40% lower than in REF. Because of the comparably small emission difference between REF and WSR, simulated $PM_{2.5}$-concentration of REF and WSR differ typically only slightly (Figs. 20, 21).

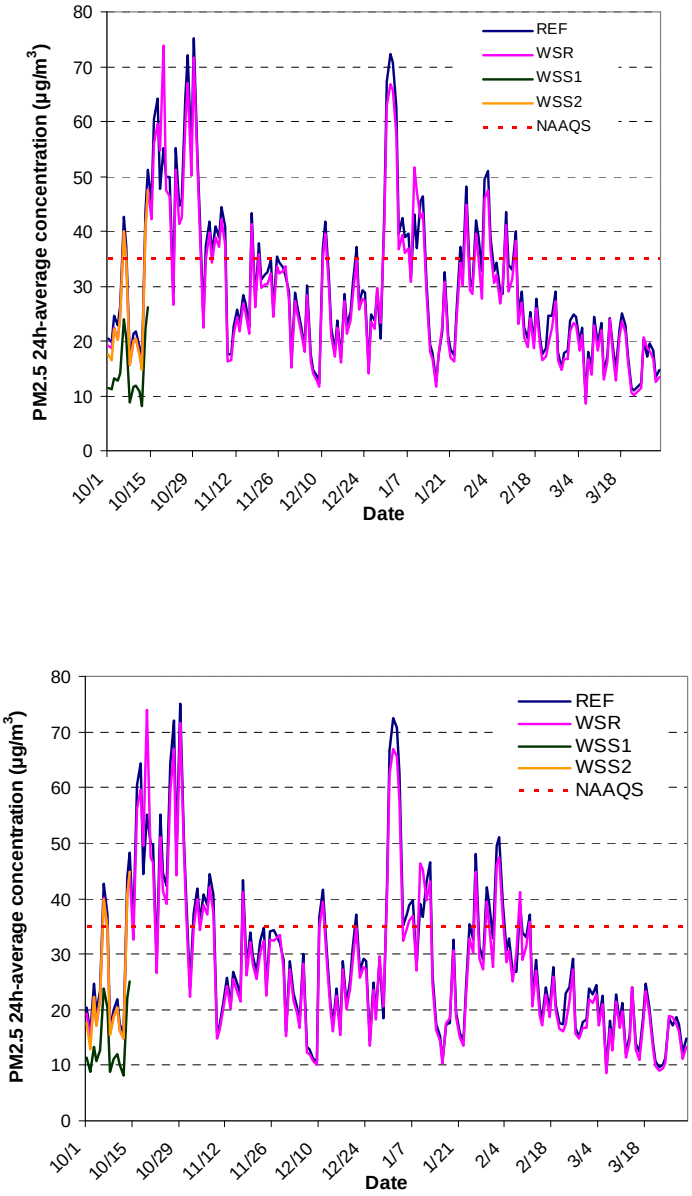


Fig. 20. Highest 24h-average $PM_{2.5}$ concentration as obtained anywhere in the model domain (top) and the 24h-average concentration at the grid-cell holding the State Building (bottom) in REF, WSR, WSS1, and WSS2. Note that the highest concentrations within the model domain occurred in the nonattainment area.

In comparison with the emissions in REF, the average $PM_{2.5}$-emission reductions in the nonattainment area are 6%, 36%, and 7% in WSR, WSS1, WSS2, respectively. The highest 24h-average $PM_{2.5}$-concentration difference anywhere in the domain amounts 5.7µgm$^{-3}$ on February 22, 2009 (Fig. 20). Averaged over the nonattainment area, the highest (2.1µg/m$^3$) and the second highest (2.0µg/m$^3$) difference in 24h-averaged $PM_{2.5}$-concentrations were simulated for October 27, 2008 and January 1, 2009, respectively, and the average difference over time and the nonattainment area amounts 0.6µg/m$^3$. About 45% and 33% of the concentration differences fall

between 0.5-1μg/m$^3$ and 0-0.5 μg/m$^3$, respectively (Fig. 22). All grid-cells with the highest concentrations are located in the nonattainment area.

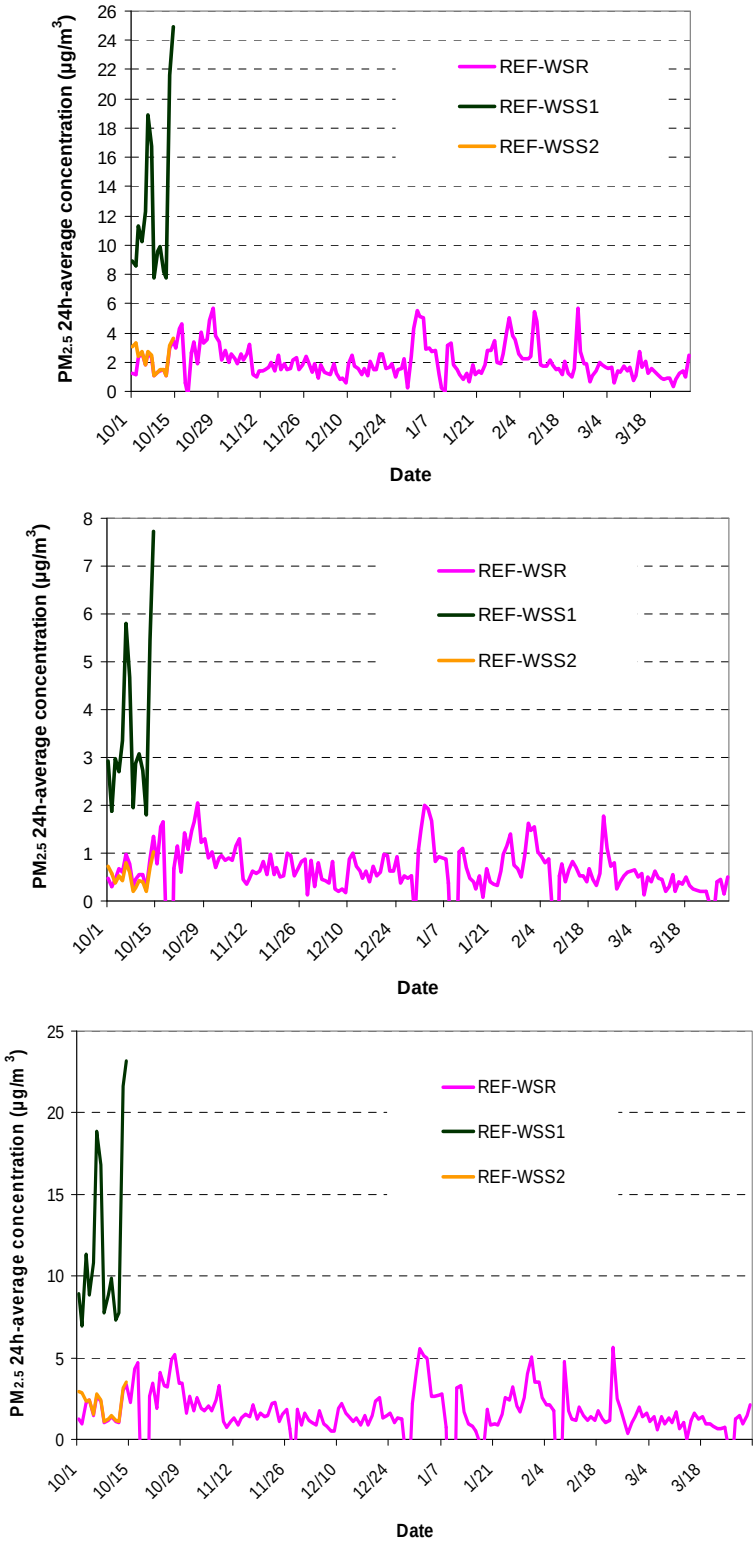


Fig. 21. Highest 24h-average $PM_{2.5}$-concentration difference from REF for WSR, WSS1, WSS2 as obtained in the domain (top), on average over the nonattainment area (middle) and the grid-cell with the State Building (bottom).

In the nonattainment area, the monthly average $PM_{2.5}$-concentration differences amount to 0.7µg/m$^3$, 0.7µg/m$^3$, 0.6µg/m$^3$, 0.7µg/m$^3$, 0.6µg/m$^3$ and 0.3µg/m$^3$ in October, November, December, January, February and March, respectively. We calculated the 24h-averaged $PM_{2.5}$-concentration difference for each day of the 182 simulation days and sorted them from high to low differences. We picked the 20% highest and 20% lowest concentration differences from this list. Note that 20% corresponds to 36 days in our study. The investigation showed that 14 and 13 of the top 20% highest and lowest concentration differences occurred in October and January, respectively. Off the 20% lowest, nine days occurred in March. This means the highest differences typically occurred in October and January whereas the lowest differences occurred in March. This finding means that the highest mitigation of $PM_{2.5}$-concentrations can be achieved in the months that are coldest.

The Student t-test showed statistically significant $PM_{2.5}$-concentration differences only within the nonattainment area and some adjacent grid-cells (Fig. 23). Outside the nonattainment area, the $PM_{2.5}$-concentration differences are very low and non-significant. Although the Student t-test shows that the concentration differences are significant, there is still a possibility that the $PM_{2.5}$-concentration difference at a given grid-cell is not due to the reduced emission, but rather due to some variable random effects between the two simulations (e.g. truncation errors, model sensitiveness). This is especially true for very small differences in $PM_{2.5}$-concentration. We adopted the FEA analysis [*Carpenter et al.*, 1989; *Werth and Avissar*, 2002] to verify that the differences are really due to the "woodstove replacement".

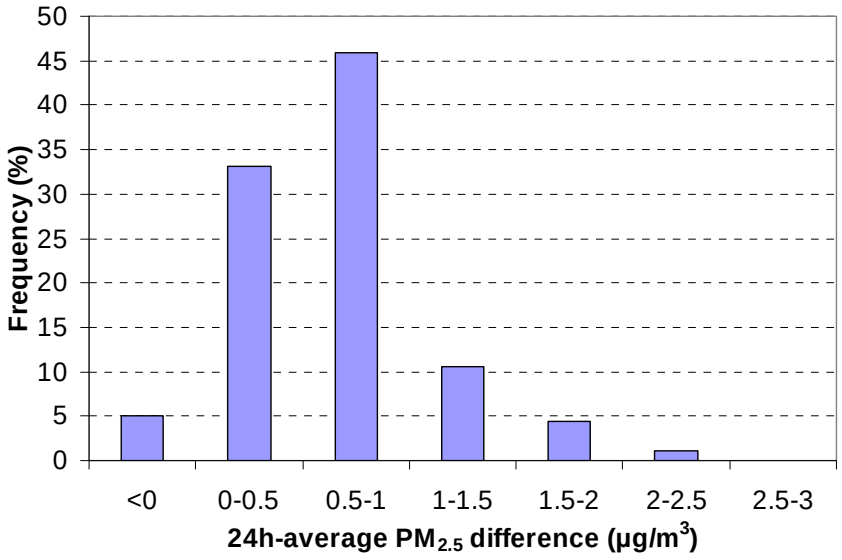


Fig. 22. Frequency distribution of 24h-average $PM_{2.5}$-concentration difference as obtained for WSR.

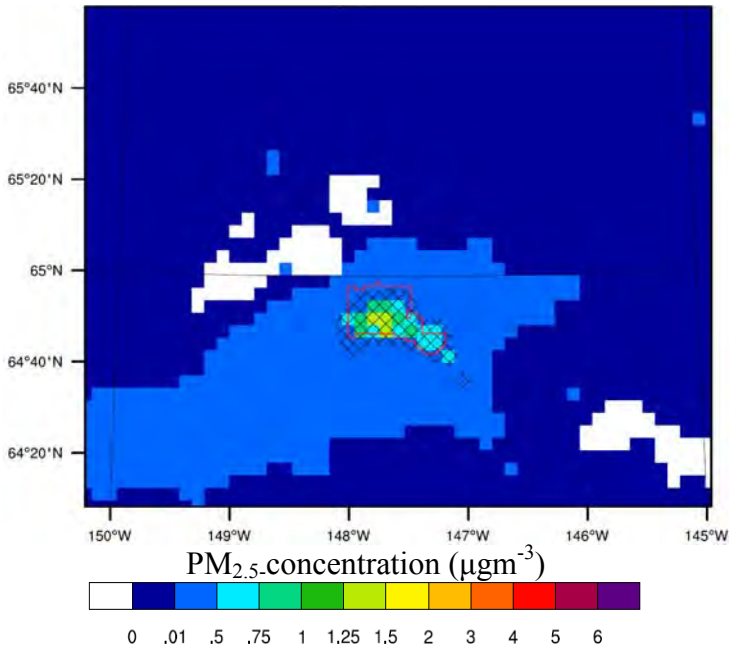


Fig. 23. Zoom-in showing the average difference of $PM_{2.5}$-concentration between REF and WSR for October 1, 2008 to March 31, 2009. The hashed shading indicates grid cells where the difference is statistically significant at 95% or higher level of confidence

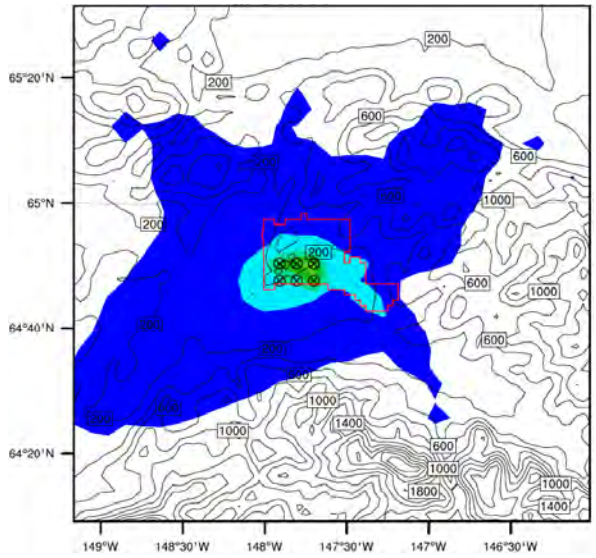


Fig. 24. Zoom-in map of grid-cells for which exceedances were simulated during October 1, 2008 to February 28, 2009 in REF. The 24h-average $PM_{2.5}$ concentration on October 1, 2008 is superimposed. The crossed circles indicate grid cells for which exceedance were simulated during OTM; the red polygon indicates schematically the nonattainment area. Grid-cells for which exceedances were simulated in WSR are identical to those for which exceedances occurred in REF (therefore not shown).

In February 2009, several grid-cells exist in the northwest of the nonattainment area that have ranks lower than the top 5%. Some of them have non-significant concentration-differences according to the Student-t test (Fig. 24). For November and December 2008, the ranks of true

concentration differences are relatively uniform anywhere in the whole model domain whereas they vary strongly in other months. This behavior coincides with the temporal evolution of the 24h-average $PM_{2.5}$-concentration difference (Fig. 21) that indicates low variation of the difference in November and December 2008, but strong variation in the other months.

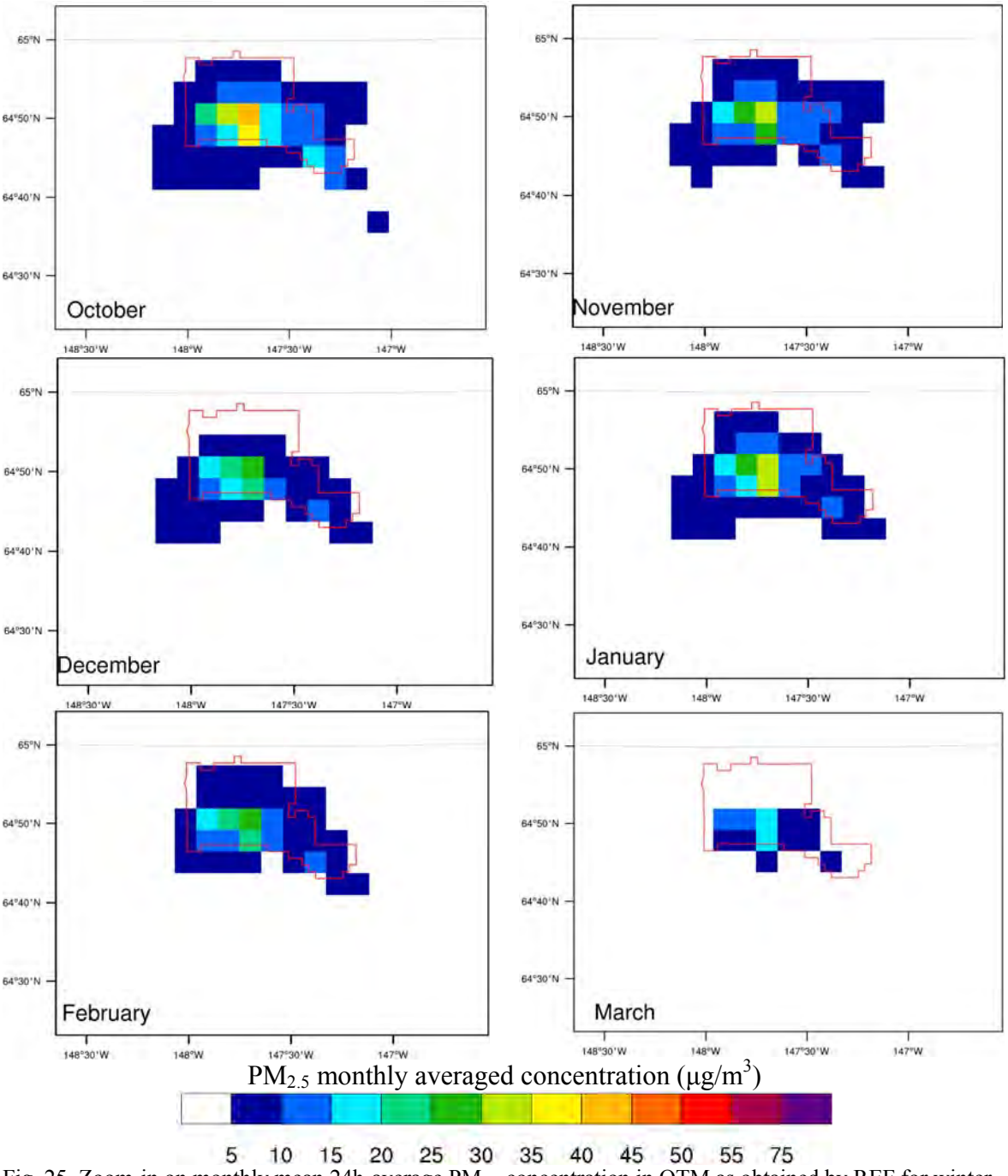


Fig. 25. Zoom-in on monthly mean 24h-average $PM_{2.5}$ concentration in OTM as obtained by REF for winter 2008/09.

According to the FEA, exchanging the noncertified wood-burning devices helped to reduce the number of exceedance days during OTM. The number of exceedance days anywhere in the nonattainment area are 20 (19), 10 (7), 5 (3), 15 (14), and 5 (5) in REF (WSR) for October,

November, December, January, February respectively. All exceedance events of OTM occurred at grid-cells in the nonattainment area. At the grid-cell holding the State Building monitoring site, exceedances were simulated for 52 (44) days in REF (WSR). At grid-cells other than that holding the official site, exceedances were simulated for 40 (34) days by REF (WSR). Despite the different number of exceedance days, locations (grid-cells) that experienced exceedances are identical in REF and WSR during OTM (Fig. 25). Days and grid-cells having the highest $PM_{2.5}$-concentrations during simulated exceedance events during OTM are also identical. This fact indicates that there are no offsets in the temporal and spatial distribution of exceedance events between REF and WSR.

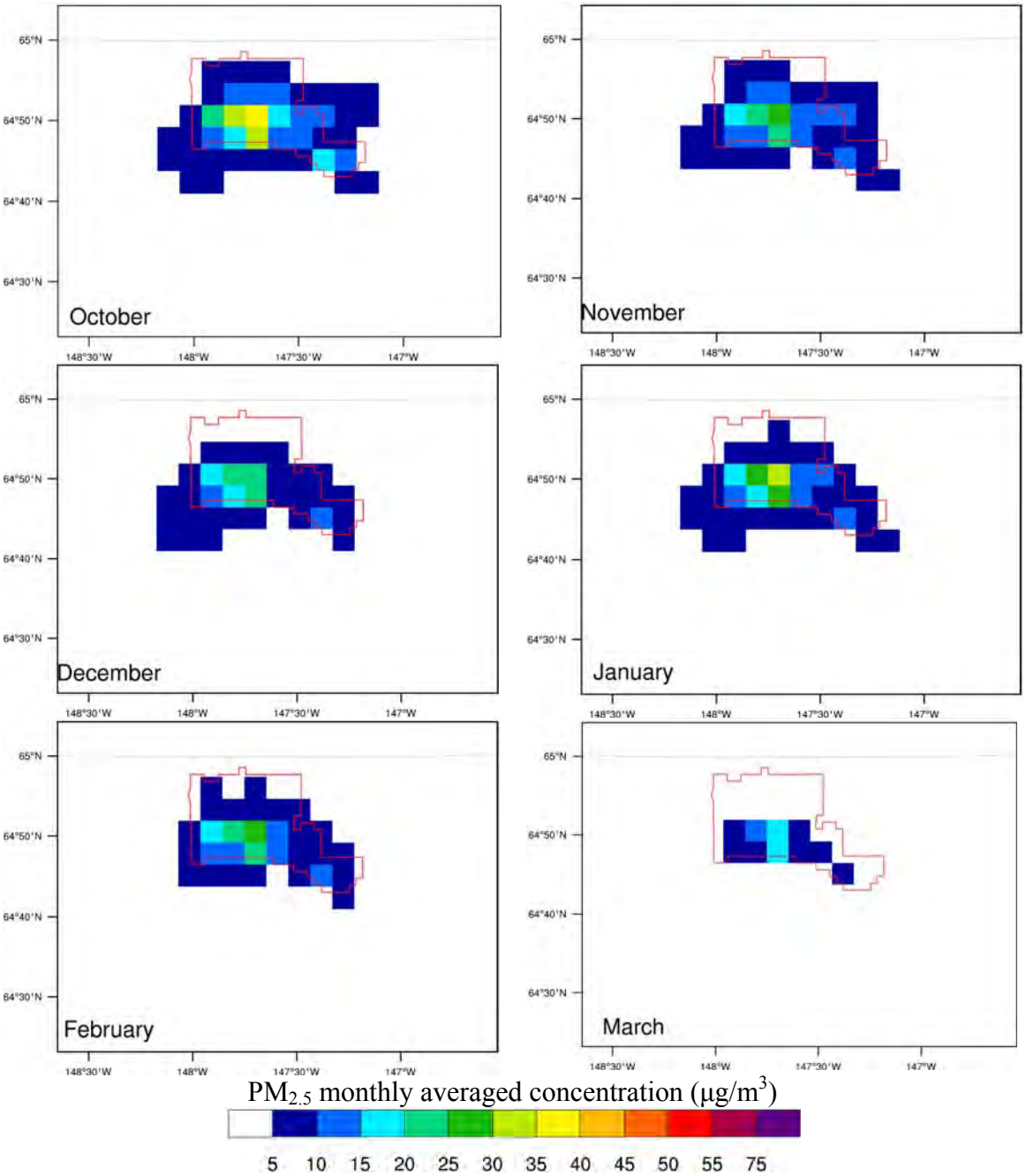


Fig. 26. Like Fig. 25, but for WSR.

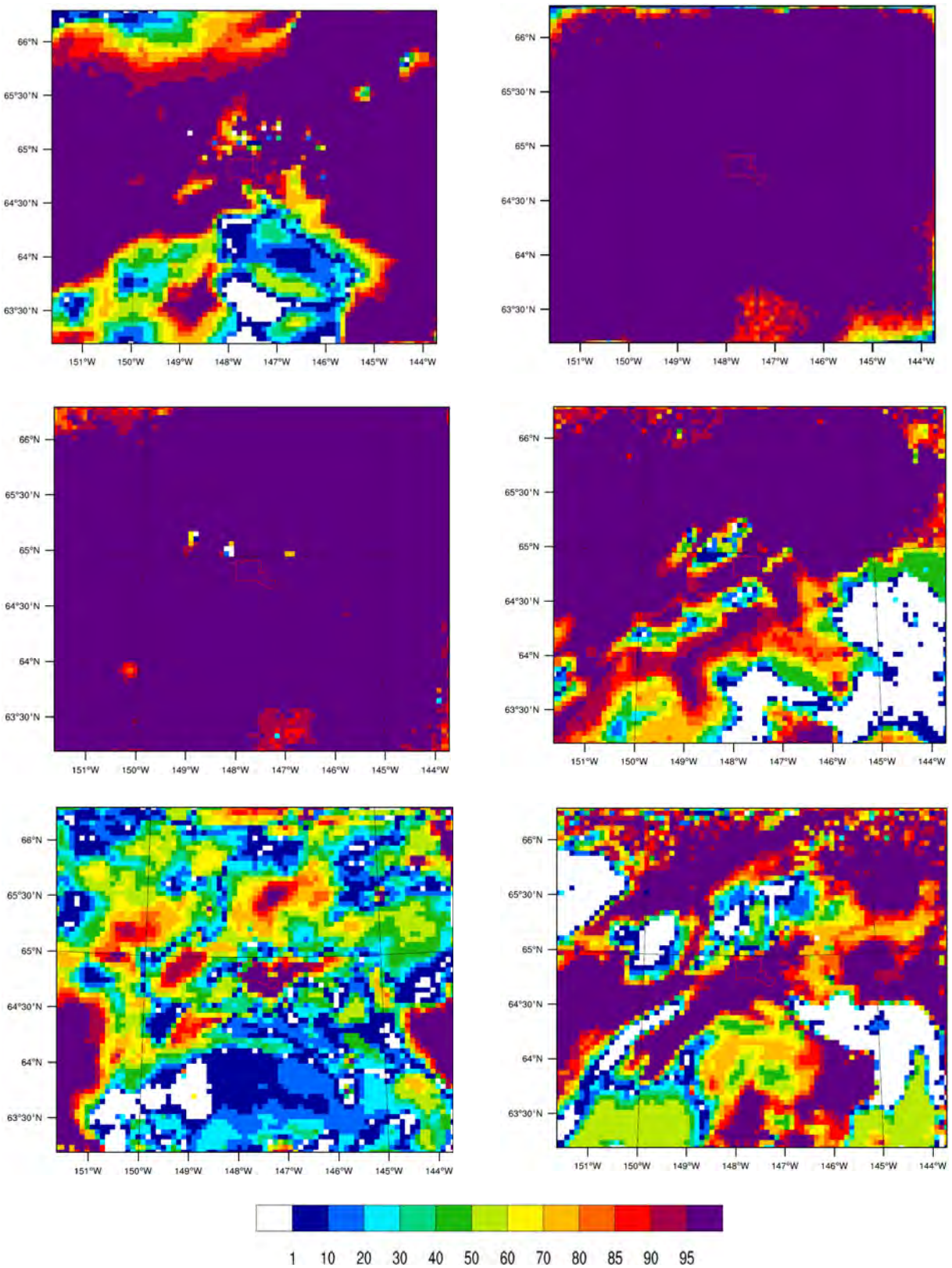


Fig. 27. Monthly rank of "true" differences over "false" differences of $PM_{2.5}$-concentration for October 2008 to March 2009 (from top left to bottom right). At grid-cells ranking higher than the 95% percentile, the "woodstove replacement" can be considered as the factor that actually reduced the $PM_{2.5}$ concentrations at breathing level.

Comparison of the monthly mean 24h-average $PM_{2.5}$ concentrations obtained with REF and WSR (Figs. 25, 26) indicates that the hot spots remain the same, but with slightly lower concentrations.

The FEA was applied for every month from October 2008 to March 2009. The ranks of the true-difference concentrations varied highly at all grid-cells throughout OTM except for those in the nonattainment area (Fig. 27). The ranks of true concentration difference at grid-cells in the nonattainment area lay consistently in the top 5% of the false ensembles. This means that exchanging the non-certified wood-burning devices does really help to reduce the $PM_{2.5}$-concentrations in the nonattainment area.

The results of the Student-t test and FEA (Fig. 27) indicate that exchanging the noncertified wood-burning devices does really help to reduce the $PM_{2.5}$-concentration in the nonattainment area. This outcome results from the fact that wood-burning devices emit into low levels of the atmosphere. Therefore, the emitted species are not transported far away from their sources. This behavior is especially true for conditions with low wind-speeds, as they frequently exist during winter in Fairbanks [cf. *Tran and Mölders*, 2010]. Thus, the impact of emissions from wood-burning on the $PM_{2.5}$-concentrations at breathing level remains local compared to the impacts of elevated point sources.

### 6.2.1 Sensitivity studies on "woodstove replacements"

We compared the emission reductions that related only to the different numbers of heating devices in WSS1, WSS2 and WSR with each other as well as with the reference simulation. Recall that the reference simulation, and the simulations assuming the "woodstove replacement" using *Davies et al.*'s number of devices, and the "woodstove replacement" using the SRL draft report and *Carlson et al.*'s number of devices were denoted as REF, WSS1, WSS2, and WSR, respectively (Table 1). Due to the tremendous CPU time required for a half-year long simulation the WSS1 and WSS2 simulations were carried out only for a limited time. While WSS1 reduces the $PM_{2.5}$ concentrations in the nonattainment area greatly, WSS1 is much less doing so (Figs. 20, 21). Within the 15 days of simulation, WSS2 reduces the 24h-average $PM_{2.5}$ concentrations by 3.6μg/m$^3$ to the highest, while WSS1 reduces them by as much as 25μg/m$^3$. WSS1's reduction helped efficiently to avoid four exceedances encountered locally in REF. On the contrary, the reduction in WSS2 was not sufficient to do so. The locations of exceedances do not differ between REF, WSS1 and WSS2 and they all occur in the nonattainment area. The reduction benefit of WSS1 was higher when local exceedances existed, while the reduction obtained in WSS2 differed marginally with time.

The sensitivity studies suggested large uncertainty in the magnitude of the efficiency of a "woodstove replacement" program. This uncertainty mainly results from (1) the unknown number of wood-burning devices that exist in the nonattainment area and could be replaced, (2) the unknown partitioning of the use of wood-burning and other heating devices in households with more than one heating option, (3) the unknown temporal use of wood-burning devices, and (4) the unknown spatial distribution of wood-burning devices.

## 6.3 Potential impact of usage of low sulfur fuel for heating oil, power generation and in oil-burning facilities

Introducing low sulfur fuel decreased the total monthly $PM_{2.5}$-emissions in the nonattainment area from October to March by 15.666, 17.448, 15.407, 15.447, 14.294, and 13.381 kg/km$^2$,

respectively from 140.130, 94.184, 94.118, 101.265, and 98.398 kg/km$^2$, respectively. The percentage total daily $PM_{2.5}$-emission reductions from October to March were 11.1%, 18.5%, 16.4%, 13.0, 14.1, and 13.6%, respectively. The decreases in monthly emissions of $SO_2$, NO and VOC were approximately 23%, 1% and 0%, respectively.

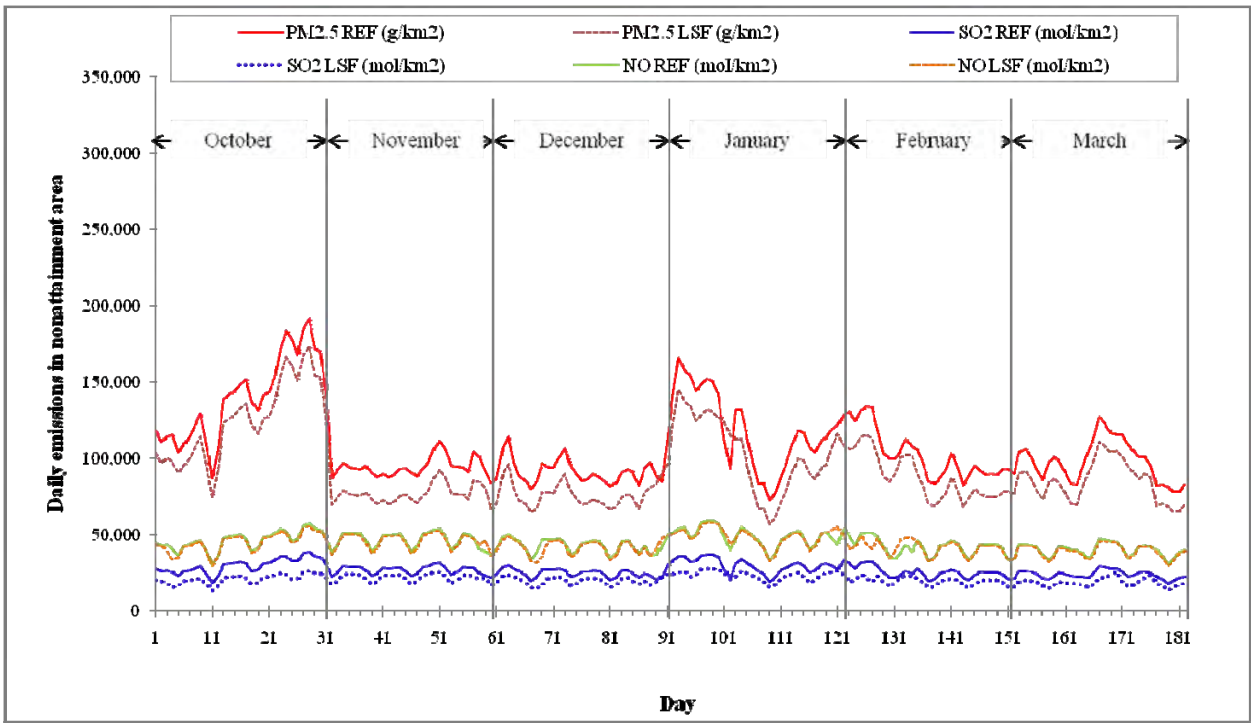


Fig. 28. Temporal evolution of daily emissions averaged over the nonattainment area for October 2008 to March 2009 as assumed in REF and LSF. The day refers to the day since start of the simulation (1 October 2008).

The daily mean temperatures are a main factor that affects the efficiency of utilizing low sulfur fuel. Low temperatures cause incomplete combustion and support the gas-to-particle conversion. During OTM, October 2008 had the highest frequency of days with daily near-surface temperatures below the 1971-2000 30-year monthly mean temperature (Table 3). Consequently, October 2008 had high emissions of particulate matter. Daily emissions in the nonattainment area with the current fuel sulfur content and after introduction of low sulfur fuel are compared in Figure 28.

In the nonattainment area, the monthly average $PM_{2.5}$-concentration amounted to 13.0, 11.6, 9.2, 11.0, 9.8 and 5.7μg/m$^3$, respectively, and 9.9μg/m$^3$ on average over OTM. The monthly average $PM_{2.5}$-concentration difference (REF-LSF) amounts to 0.4, 1.0, 0.7, 0.6, 0.5 and 0.4μg/m$^3$ in October, November, December, January, February and March, respectively, and 0.6μg/m$^3$ on average over the entire winter. The percentage reductions varied from 3% to 9% (Table 4). November had the highest assumed emission reduction and simulated concentration reductions. The daily reduction in emissions does not yield to a linearly corresponding reduction in the daily average $PM_{2.5}$ concentrations at breathing level in the nonattainment area (cf. Figs. 28, 29).

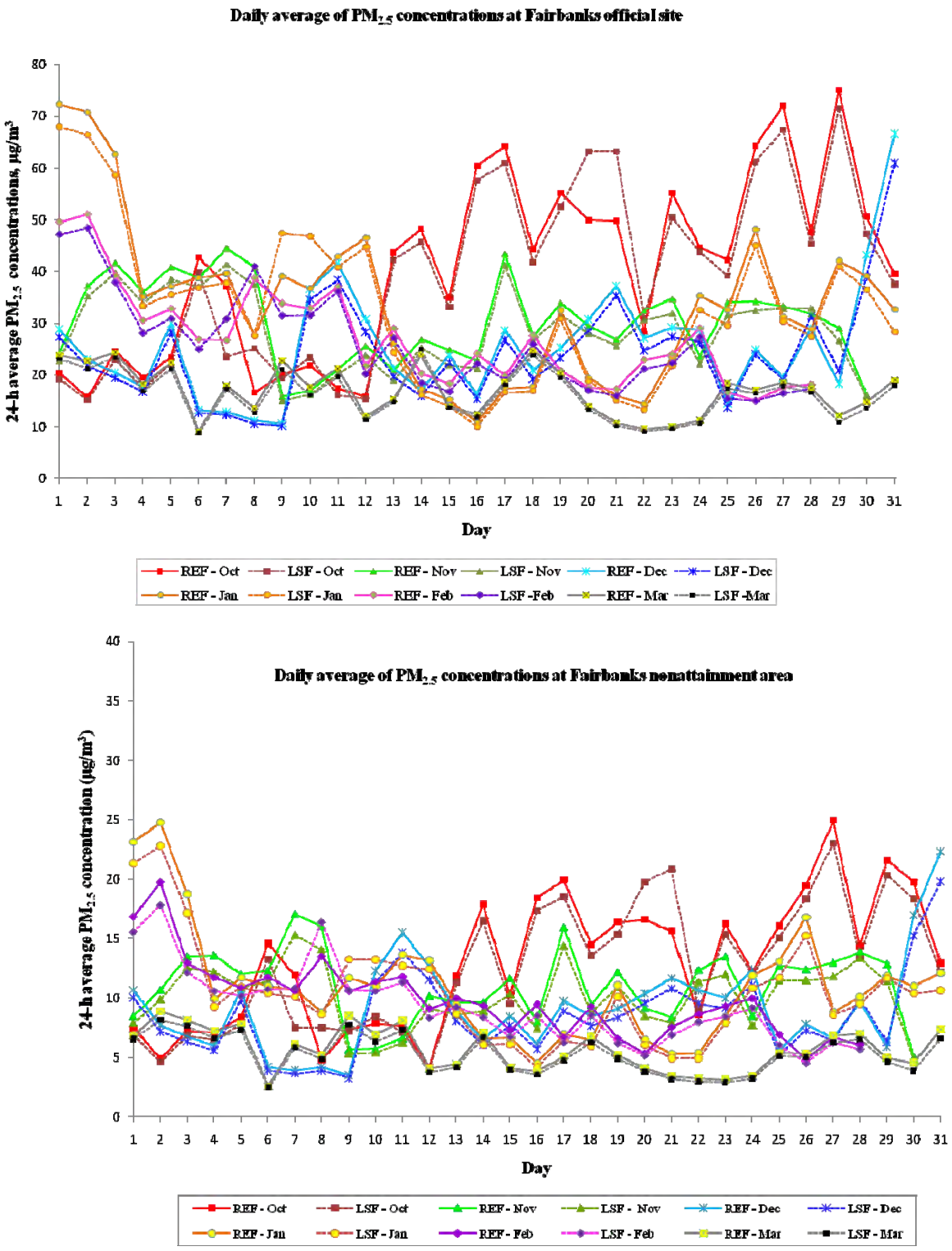


Fig. 29. Temporal evolution of simulated 24h-average $PM_{2.5}$ concentrations as obtained for the grid-cell that holds the State Building (top) and the 24h-average $PM_{2.5}$ concentrations averaged over the nonattainment area (bottom) in the various months of winter 2008/09. REF and LSF refer to the reference simulation and the simulation assuming the introduction of low sulfur fuel for heating oil, power generation and facilities burning oil (see Table 1).

On average, the simulated reduction of 24h-average $PM_{2.5}$ concentrations during OTM was 0.6µg/m$^3$. The maximum 24h-average $PM_{2.5}$-concentrations reduction of 4.4µg/m$^3$ occurred in October (Fig. 29). Focusing on the values simulated for the grid-cell holding the official $PM_{2.5}$-monitoring site in the nonattainment area at the State Building, the average daily concentrations reduction was 1.2µg/m$^3$ for OTM. The maximum 24h-average $PM_{2.5}$-concentration reduction at the State Building site was 13.6µg/m$^3$ and was simulated for October 2008. In comparison with the $PM_{2.5}$-concentrations obtained for other grid-cells in the nonattainment area, this site had the highest frequency of exceedance days (19, 8, 5, 15, 5, and 0 exceedance days for October to March, respectively), and most of them had the highest $PM_{2.5}$-concentrations, when compared to other grid-cells in the nonattainment area on the same day.

We calculated the 24h-averaged $PM_{2.5}$-concentration difference between REF and LSF for each day of the total 182 simulation days and sorted them from high to low differences. We picked the 20% highest and 20% lowest concentration differences from this list. Note that 20% corresponds to 36 days in this case. Investigation of the top 20% showed that 14 of the highest concentration differences occurred in November. Off the 20% lowest, most days (14) occurred in March. This means the highest differences typically occurred in November whereas the lowest differences occurred in March. The highest differences were mainly due to the concentration values. In this scenario, high monthly average concentrations mostly translated into high monthly average reductions. Table 4 shows that high $PM_{2.5}$ concentrations occurred in October, January, and November from the first to the third rank, respectively. In October and January, the concentrations were high, but there were some days for which $PM_{2.5}$ concentrations increased after introduction of low sulfur fuel. Therefore, in October and January, the $PM_{2.5}$-concentration reduction was not as high as in November. The lowest difference for $PM_{2.5}$-concentrations occurred for March as this month had the lowest $PM_{2.5}$-concentrations.

The daily reductions in $PM_{2.5}$-concentrations vary strongly with the meteorological conditions and over the months (Fig. 29). By reducing the fuel sulfur content of oil, the number of simulated exceedance days in October 2008 to March 2009, which amounted to 20, 10, 5, 15, 5 and 0 in REF were reduced to 19, 8, 4, 14, 5 and 0 in LSF, respectively. The simulations suggested that in total, five exceedance days could have been avoided by introduction of low sulfur fuel.

Remarkably, on several days, the 24h-average $PM_{2.5}$-concentrations increased in the nonattainment area after introduction of low sulfur fuel. Note that similar was found also in another sulfur reduction study carried out over the North Pacific for January with another configuration of WRF/Chem [*T.T. Tran*, 2011; pers. communication]. In our study, on some simulated days, the increase of $PM_{2.5}$-concentrations stemmed from the increase of $PM_{2.5}$ emissions, for example at the end of December and in mid-January (Fig. 28). The emissions increased due to the non-linear temperature dependency of emissions from power generation and domestic combustion considered in AkEM.

However, the increase of $PM_{2.5}$ concentrations on October 8, 10, 20-22, and February 7-9 and March 14 did not coincide with increased $PM_{2.5}$ emissions. These increases despite of decreased $PM_{2.5}$ emissions are due to gas-to-particle conversion. Recall that the usage of low sulfur fuel leads to a different emission spectrum for various other species. Increases of $PM_{2.5}$ concentrations occurred both inside and outside the nonattainment area (e.g. Fig. 30). The increases were related to the atmospheric chemistry of $NO_x$ that affected the thermodynamic equilibria of sulfate-nitrate-ammonia-water in aerosols.

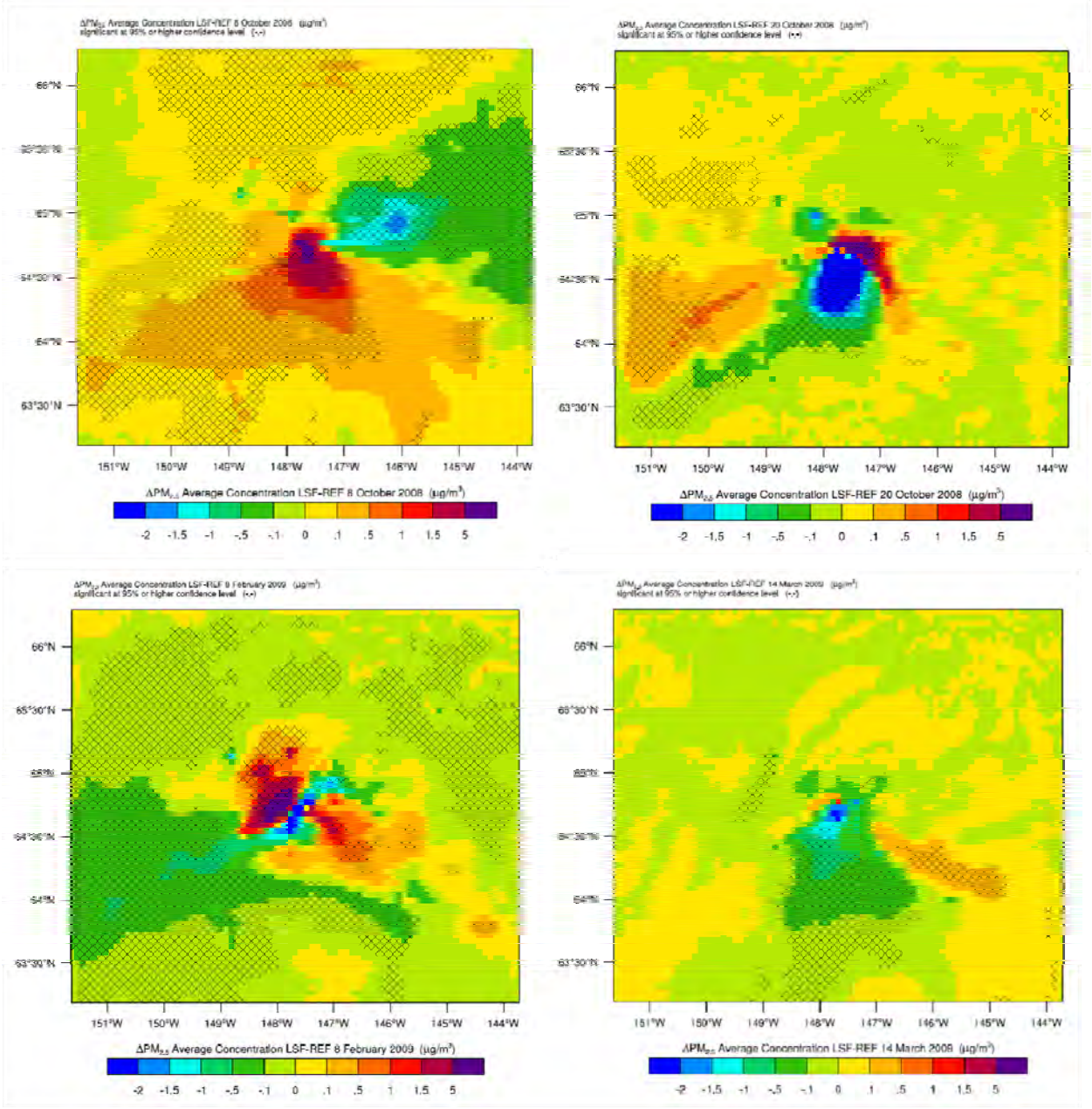


Fig. 30. Examples of $PM_{2.5}$-concentration difference distributions on days with days with locally increased $PM_{2.5}$ concentrations after introduction of low sulfur fuel. The hashed shading indicates grid cells wherein the difference (REF-LSF) is statistically significant at 95% or higher level of confidence.

The large number of days (12 days in the nonattainment area, 13 days for the grid-cell holding the State Building) with increased $PM_{2.5}$-concentrations and the emission-concentration relationship (Figs. 28, 29) suggest that the locally increased $PM_{2.5}$-concentrations after introduction of low sulfur fuel are most likely not a model artifact, but real. The reduction of $SO_2$ emissions and lower $SO_2$-concentrations in LSF reduced the sulfate-aerosol concentrations. This circumstance further resulted in partial replacement of the reduced aerosol mass by available nitric acid. The percent fraction of nitrate increased, but sulfate decreased on days with increased $PM_{2.5}$ concentrations (Fig. 31). Note that nitrate has more mass than sulfate.

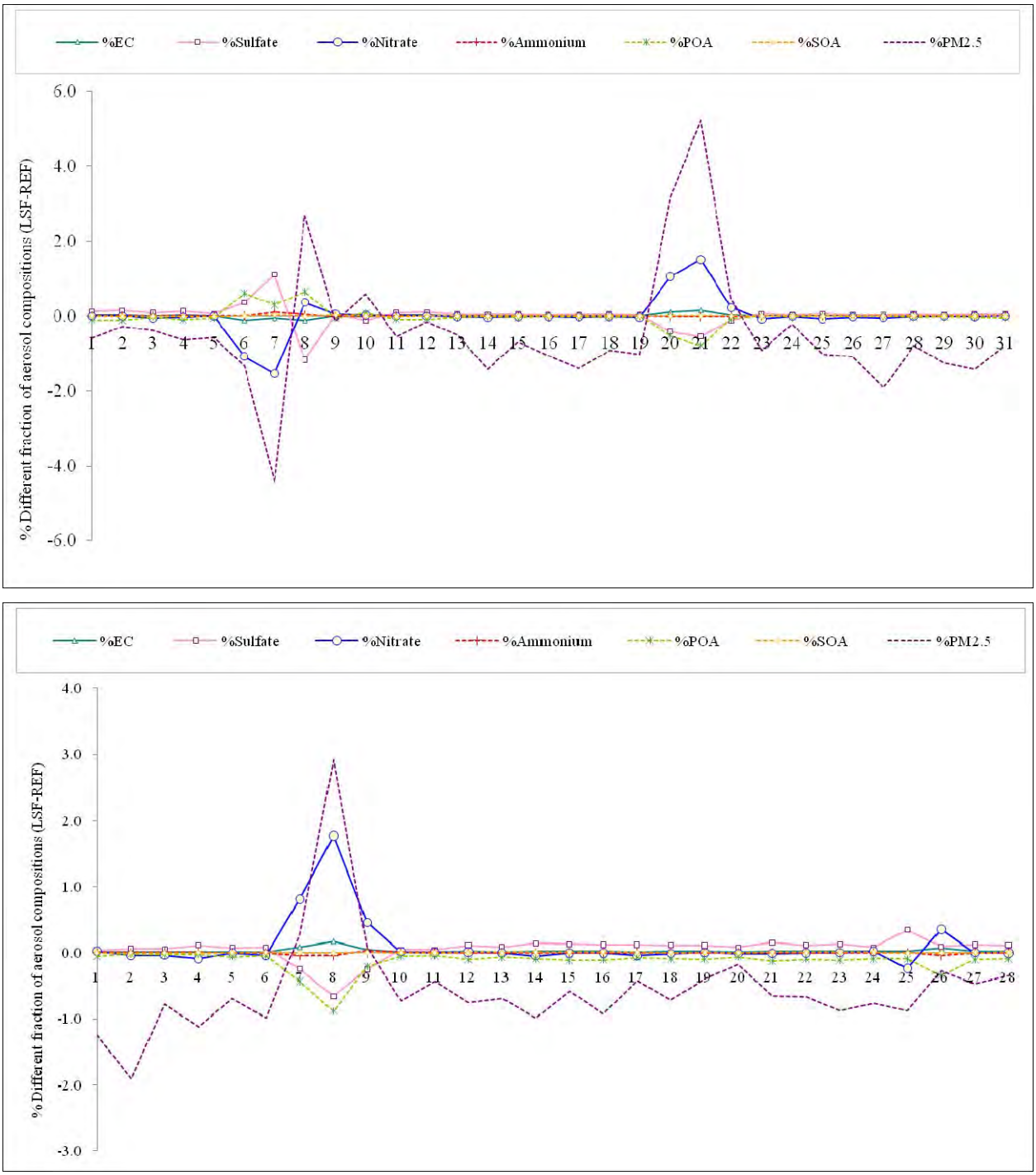


Fig. 31. Temporal evolution of daily average percentage difference of aerosol composition in the nonattainment area as obtained for October (top) and February (bottom).

The investigation of the reasons is beyond the scope of this study. However, preliminary analysis within the framework of a PhD thesis suggests that less transformation and removal of $NO_x$ after introduction of low sulfur fuel during months with still relatively high solar radiation led to an increase of the nitrate concentrations, and increased the particulate matter concentrations accordingly (Fig. 31). The replacement of nitrate brought about a shift of the $NH_4NO_3$ equilibrium toward the gas-phase. Consequently, the $NO_3$-concentrations increased in the

atmosphere after introducing low sulfur fuel. The fact that no such increase occurs during the months with lowest insolation (e.g. December, January) suggests that chemical processes initiated by photolysis play an important role. As explained earlier, during October, February, and March, photolysis plays a stronger role as photolysis rates are higher than in December or January. Consequently, NO, $NO_2$ and $NO_3$ concentrations increase during October, February, and March, and $PM_{2.5}$ concentrations increased accordingly. The high aerosol concentrations fed back to meteorology. The simulated atmosphere became more stable and air quality became worse in the Fairbanks nonattainment area. The increase of nitrate, which means an increase of aerosols in the atmosphere, and the effect of chemistry on meteorology, should be analyzed for full understanding, but both tasks are beyond the scope of this study.

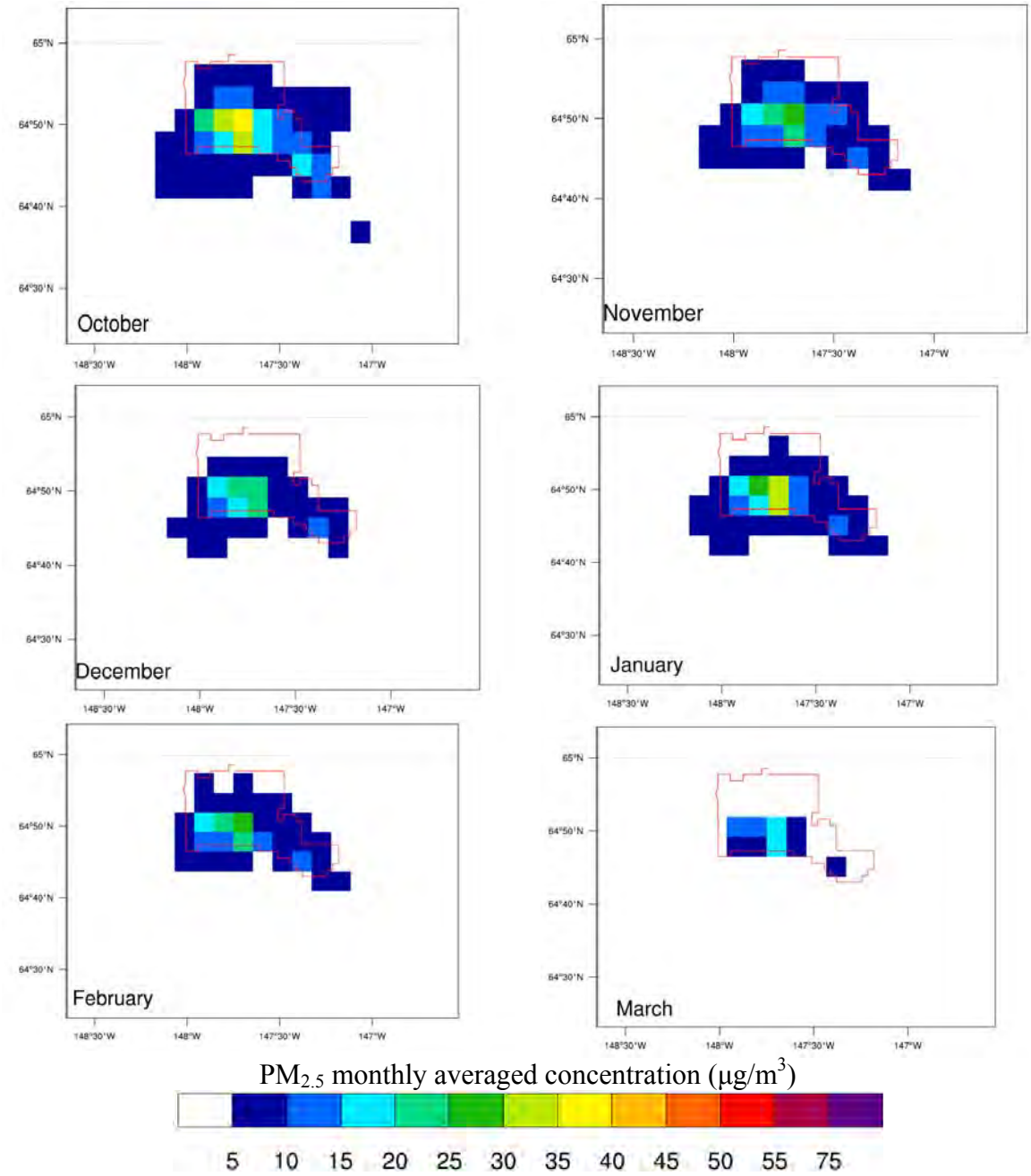


Fig. 32. Like Fig. 25 but for LSF.

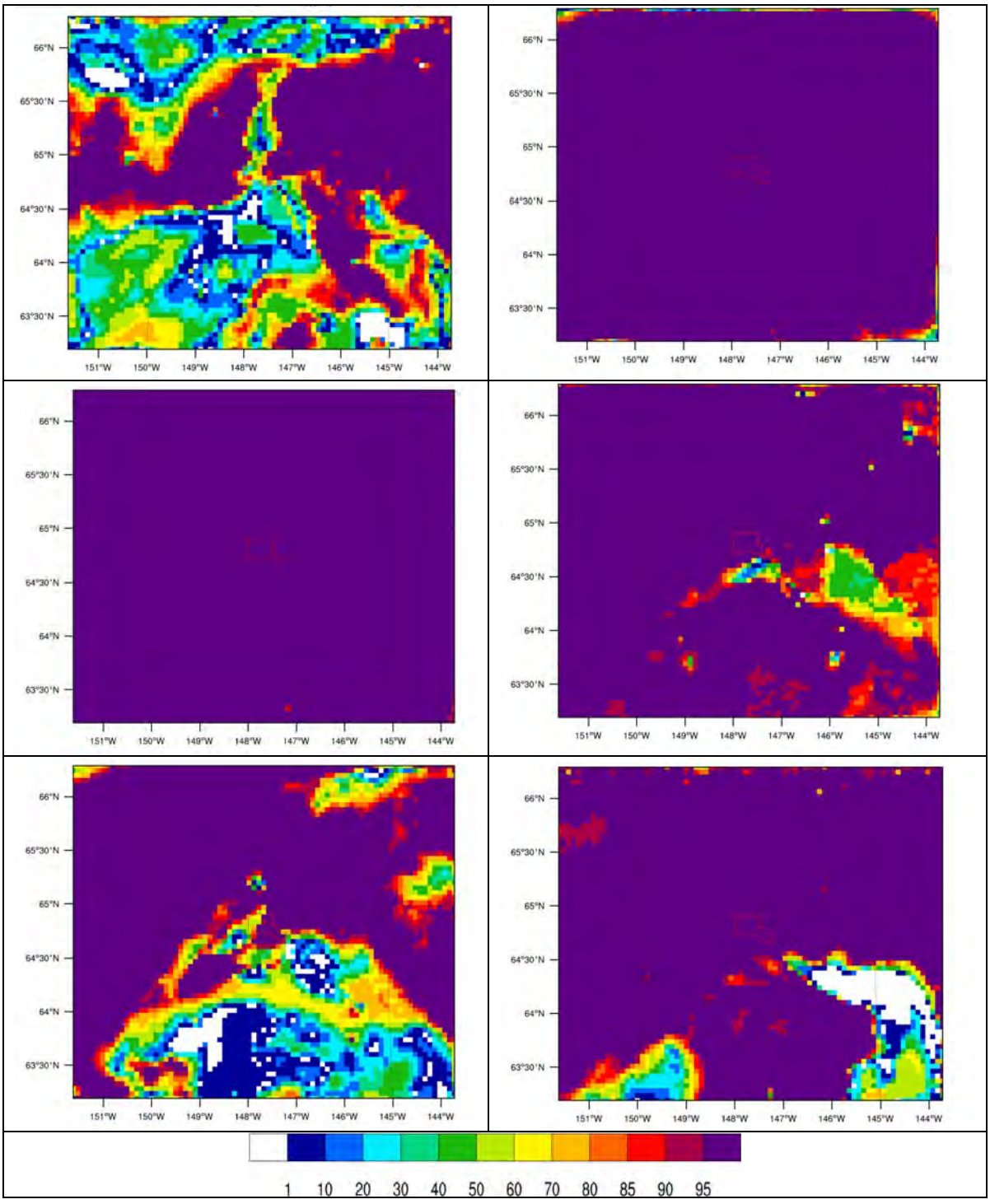


Fig. 33. Monthly rank of "true" differences over "false" differences of $PM_{2.5}$-concentration for October 2008 to March 2009 (from top left to bottom). At grid-cells ranking higher than the 95% percentile, the low sulfur fuel scenario has high efficiency in reducing concentrations in nonattainment area only in November, December, January and March.

Comparison of the monthly mean 24h-average $PM_{2.5}$ concentrations (Figs. 25, 32) shows the same hot spots in October, January, February and March than for REF, but these hotspots have

lower values in LSF. The local reduction is smaller in February and March than in the relatively cold October. The distribution-patterns of $PM_{2.5}$ concentrations change notably for November and December. These spatial changes suggest that gas-to-particle conversion to changes in the concentrations. Note that these processes depend on the concentrations of precursor gases, photolysis rates, temperature and humidity in non-linear ways. Thus, small changes in the concentrations of precursors may lead to much higher or lower gas-to-particle conversion rates.

Like for NPE and WSR we applied the FEA method to the data of LSF and REF. The FEA results indicate that the concentration differences (REF-LSF) in November, December, January, February and March are due to the introduction of low sulfur fuel (Fig. 33). In October, obviously random effects may play a role.

### 6.3 Comparison of the mitigation measures relative to each other

EPA's Office of Air Quality Planning and Standards in conjunction with the EPA Regional Offices compute design values based on observations in previous years, and review and publish them annually [*EPA*, 2011]. Design values are expressed as a concentration instead of an exceedance. These design values describe the air-quality status of a given area relative to the NAAQS. Consequently, design values can be used to classify nonattainment areas, develop control strategies, and assess progress towards meeting the NAAQS [*EPA*, 2011]. The design value for the baseline year 2008 for the Fairbanks nonattainment area is 44.5μg/m$^3$ [*Huff,* 2011; pers. communication]. The design values of 2005-2007, 2006-2008, and 2007-2009 were 39, 41, and 57, respectively [*EPA*, 2011]. These values partly reflect the decreasing air quality in response to the increase in wood burning.

Emissions are temperature dependent – more heating is required when it is colder than warmer outside. The winter episode 2007-2009 was about 0.7$^o$F colder than that of 2008-2010 (Table 3). This fact explains why the 2008-2010 design value is smaller than the 2007-2009 design value. The average temperature OTM for winter 2008/09 was 0.3$^o$F, i.e. much colder than winter 2007/08 (4.9$^o$F) or winter 2009/10 (4.5$^o$F).

An easy way to compare the impacts of the altered emissions on the $PM_{2.5}$ concentrations and their composition at breathing level is to determine the relative response factors (RRF). The RRF for each simulated particulate matter component j at site i is given by [*EPA*, 2007]

$$RRF_{ij} = \frac{\lfloor C_{j,projected} \rfloor}{\lfloor C_{j,current} \rfloor} \qquad (5)$$

Where in our study $\lfloor C_{j,projected} \rfloor$ is the mean concentration obtained from the various simulations with altered emissions (e.g. WSR or LSF), and $\lfloor C_{j,current} \rfloor$ is the respective mean concentration obtained from the reference simulation for the episode simulated. Note that the lower the RRF value is the higher is the response to the measure (e.g. “woodstove replacement”, “introduction of low sulfur fuel”).

Table 6 summarizes the RRFs for the grid-cell holding the State Building, i.e. the official monitoring site. The RRFs suggest that point sources contribute slightly to the $PM_{2.5}$ concentration and its composition at the State Building. This finding is not surprising because several point sources are in the immediate vicinity of this site. However, as discussed above, on average over the non-attainment area, the contribution of point sources to the total $PM_{2.5}$ concentration is relatively low. The very low RRF for $NH_4$ obtained for January results from the

very low $NH_4$ concentrations in both REF and NPE as compared to the other months. Speciation data did not become available before the end of this project. Therefore, no through analysis and interpretation of simulated vs. observed speciation is included in this report. A first screen of this data, however, supports that simulated $NH_4$ concentrations are too low (Fig. 34). A detailed analysis of simulated speciation was beyond the scope of our study, but should be done in the future to improve forecasts. Future studies should investigate the role of $NH_4$ and the emission sources of $NH_3$ that seem to be missing in the NEI2008 for Fairbanks.

Table 6. Relative response factors for $PM_{2.5}$ and the particulate matter composition as obtained for the scenarios without point source emissions (NPE), with woodstove replacement (WSR) and low sulfur fuel (LSF) at the grid-cell holding the official $PM_{2.5}$ site at the State Building for various periods. EC, ORG and PBW stand for elemental carbon, organic compounds, and particle bound water, respectively. Note that for the NPE scenario investigations were only to be carried out for November through February (cf. Table 1). Note that the baseline (reference) for the response factors of NPE (winter 2005/06) differs from that of WSR and LSF. WSR and LSF both use the same baseline of winter 2008/09.

| | $PM_{2.5}$ | $SO_4$ | $NO_3$ | $NH_4$ | EC | ORG | PBW |
|---|---|---|---|---|---|---|---|
| | | | NPE | | | | |
| Nov | 0.957 | 0.961 | 0.858 | 0.976 | 0.961 | 0.961 | 0.949 |
| Dec | 0.964 | 0.963 | 0.954 | 1.019 | 0.962 | 0.962 | 0.971 |
| Jan | 0.973 | 0.978 | 0.849 | 0.247 | 0.977 | 0.977 | 0.959 |
| Feb | 0.970 | 0.971 | 0.954 | 0.810 | 0.970 | 0.970 | 0.971 |
| Nov-Dec | 0.960 | 0.962 | 0.901 | 0.996 | 0.961 | 0.961 | 0.960 |
| Jan-Feb | 0.972 | 0.976 | 0.865 | 0.254 | 0.975 | 0.975 | 0.963 |
| Winter 05/06 | 0.966 | 0.969 | 0.892 | 0.965 | 0.969 | 0.969 | 0.961 |
| | | | WSR | | | | |
| Oct | 0.958 | 0.959 | 0.865 | 1.003 | 0.959 | 0.959 | 0.954 |
| Nov | 0.950 | 0.952 | 0.898 | 1.005 | 0.951 | 0.951 | 0.948 |
| Dec | 0.950 | 0.952 | 1.001 | 1.001 | 0.950 | 0.951 | 0.949 |
| Jan | 0.953 | 0.952 | 0.887 | 1.075 | 0.952 | 0.952 | 0.951 |
| Feb | 0.944 | 0.940 | 1.041 | 0.891 | 0.939 | 0.939 | 0.944 |
| Mar | 0.941 | 0.943 | 0.855 | 1.005 | 0.941 | 0.941 | 0.941 |
| Oct-Dec | 0.954 | 0.955 | 0.880 | 1.004 | 0.954 | 0.954 | 0.951 |
| Jan-Mar | 0.946 | 0.947 | 0.935 | 0.976 | 0.945 | 0.945 | 0.946 |
| Winter 08/09 | 0.950 | 0.951 | 0.897 | 0.991 | 0.950 | 0.950 | 0.949 |
| | | | LSF | | | | |
| Oct | 0.975 | 0.974 | 1.023 | 1.016 | 0.973 | 0.973 | 0.976 |
| Nov | 0.943 | 0.944 | 0.937 | 0.998 | 0.943 | 0.943 | 0.944 |
| Dec | 0.945 | 0.946 | 0.925 | 0.999 | 0.944 | 0.944 | 0.945 |
| Jan | 0.966 | 0.966 | 0.947 | 1.074 | 0.965 | 0.965 | 0.965 |
| Feb | 0.957 | 0.955 | 1.129 | 0.887 | 0.955 | 0.955 | 0.961 |
| Mar | 0.953 | 0.954 | 0.926 | 1.002 | 0.952 | 0.952 | 0.953 |
| Oct-Dec | 0.957 | 0.957 | 0.970 | 1.004 | 0.956 | 0.956 | 0.958 |
| Jan-Mar | 0.960 | 0.959 | 1.006 | 0.973 | 0.959 | 0.959 | 0.961 |
| Winter 08/09 | 0.958 | 0.958 | 0.981 | 0.990 | 0.957 | 0.957 | 0.959 |

The RRFs also indicate that there is not much wiggle room related to point-source emission. Recall that in the real world, point sources cannot be “switched off”. Power plants, for instance, ensure the supply of energy. Thus, if “switching them off” in the model world does not reduce the concentration much – as indicated by the RRFs – introduction of filters to reduce the point-source emissions will not solve the problem either as the point sources still will emit even though at a lower rate.

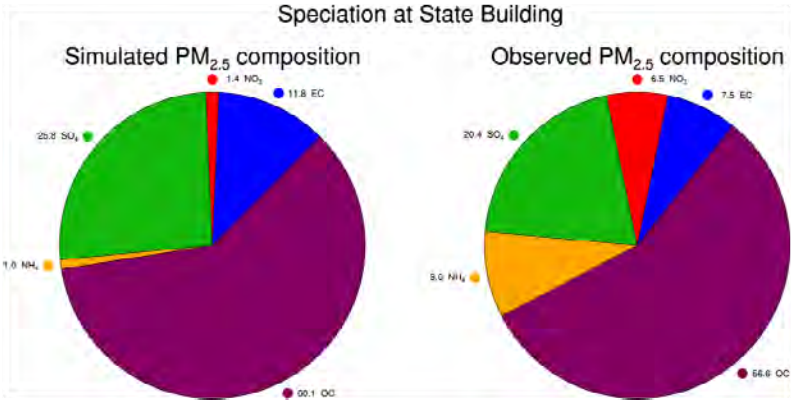


Fig. 34. Comparison of simulated and observed $PM_{2.5}$ components for winter 2005/06. Observed data courtesy of *D. Huff* [2011].

The RRFs for the "low sulfur fuel" and "woodstove replacement" scenarios are of similar magnitude, but on average over the entire winter slightly favor a "woodstove replacement" program. The RRFs to the introduction of low sulfur fuel show a higher variability among months than to the woodstove replacement. This means that for individual months "introduction of low sulfur fuel" may yield a stronger mitigation than "woodstove replacement". However, the latter seems to be the more temporally reliable measure as it more stably provides similar RRFs.

The RRFs of the various compounds of $PM_{2.5}$ indicate shifts in the composition in response to the altered emissions (Table 6). This means that both measures ("woodstove replacement", "introduction of low sulfur fuel" for heating and use in oil burning facilities) strongly affect the atmospheric chemistry and secondary aerosol formation via gas-to-particle conversion. The composition changes differ for the two measures. The "woodstove replacement" yields a shift towards more $NH_4$ and less $NO_3$ aerosols in most months. The composition shifts in response to "introduction of low sulfur fuel" vary more strongly among months than in response to "woodstove replacement".

To calculate the future design values we multiplied the observed design value with the RRFs obtained for the various measures tested. The resulting new design values are listed in Table 7.

Table 7. Calculated $PM_{2.5}$ "design values" ($\mu g/m^3$) in response to the tested measures for the grid-cell holding the State Building for various periods. Here "winter" refers to November 2005 to February 2006 for the NPE scenario and October 2008 to March 2009 for the "woodstove replacement" and "low sulfur fuel" scenarios.

| | No point source emissions | small woodstove replacement program | introduction of low sulfur fuel |
|---|---|---|---|
| Oct | -.- | 42.6 | 43.4 |
| Nov | 42.6 | 42.3 | 42.0 |
| Dec | 42.9 | 42.3 | 42.1 |
| Jan | 43.3 | 42.4 | 43.0 |
| Feb | 43.2 | 42.0 | 42.6 |
| Mar | -.- | 41.9 | 42.4 |
| Oct-Dec | -.- | 42.5 | 42.6 |
| Jan-Mar | -.- | 42.1 | 42.7 |
| Nov-Dec | 42.7 | -.- | 42.6 |
| Jan-Feb | 43.3 | -.- | 43.4 |
| Winter | 43.0 | 42.3 | 42.0 |

The introduction of low sulfur fuel results in a slightly lower new design value than the small "woodstove replacement program" assumed in WSR. The results also showed that such a small "woodstove replacement program" reduces the design value already by 2.2μg/m$^3$. The sensitivity studies performed on "woodstove replacement" suggested that a more rigorous replacement (WSS1) than assumed in WSR may yield much higher mitigation. Since the introduction of low sulfur fuel is very expensive, since a further reduction of sulfur content costs even more, and since the RRF and resulting new design values vary strongly among months when introducing low sulfur fuel, it seems that a rigorous replacement of non-certified wood-burning devices is the more promising way to achieve compliance.

Comparison of Figs. 25, 26, and 32 suggests that both "woodstove replacement" as well as "introduction of low sulfur fuel" reduce the concentrations in the nonattainment area. However, while hot spots remain in the same areas in the case of a "woodstove replacement" for all months, this is not the case when introducing low sulfur fuel.

## 7. Conclusions

We performed simulations for November 2005 to February 2006 with and without consideration of point-source emissions (Table 1) using the Alaska-adapted WRF/Chem[12] to assess the contribution of point-source emissions on the $PM_{2.5}$-concentrations at breathing level. The emission data for the reference simulation (business-as-usual) based on the NEI2005. The simulation without consideration of point-source emissions was run with the same meteorological input data and same emission data except that all point-source emissions were set to zero (NPE). Based on the comparison of the results of these simulations, we conclude that point sources are not the major cause for Fairbanks' wintertime $PM_{2.5}$-pollution problem. This conclusion is also supported by the results of the other mitigation scenarios. Eliminating the point-source emissions – as it is practically done in the NPE simulation – only led to marginal decreases in $PM_{2.5}$ concentrations at breathing level and only five avoidances of exceedances at locations in the nonattainment area. The highest $PM_{2.5}$-concentrations obtained in REF and NPE only differ 1.3μg/m$^3$ on average. The locations where simulated $PM_{2.5}$ exceeds the NAAQS occur in the nonattainment area. According to the results of REF and NPE, PS6[13] is the point source that often contributes to exceedances in the nonattainment area. However, in these cases concentrations without that point source were already high. Note that this point source has the highest emission rate. Emissions from point sources located in the nonattainment area may influence the $PM_{2.5}$-concentration at breathing level within 10km or so from the point-source-holding air column. This phenomenon is a combined effect of extreme atmospheric stable condition, weak circulation, and for some point sources the low-level in which they emit. These meteorological conditions altogether inhibit transport of the pollutants out of the area. It would be worth examining how increases in stack height and emission temperature (which also would lead to emissions into higher levels) would affect the point-sources' radius of impact and the $PM_{2.5}$ concentrations at breathing level.

Based on or simulations with and without consideration of point-source emissions we conclude that when "switching off" of the point sources does not solve the problem, reducing point-source emissions by new techniques will not solve the problem either as the point sources still emit even though at a lower rate. For days that are close to the NAAQS, just a marginal increase in area emission would lead to an exceedance.

Some of the $PM_{2.5}$ in the air is formed in the air from gases that transform to particles via physico-chemical processes called gas-to-particle conversion. Since gas-to-particle conversion non-linearly depends on temperature and vapor pressure of species and introducing measures to further clean the exhausts of point sources alters the composition of the point-source emission plumes, it may be worth examining whether in combination with other measures such additional filtering may nevertheless be beneficial.

In addition to the investigation on the impact of point sources on $PM_{2.5}$-concentrations in the nonattainment area, we performed a suit of simulations for October 2008 to March 2009 with the Alaska optimized WRF/Chem (Table 1). This suit of simulations assumed the same meteorological initial input data and boundary conditions. The reference simulation (REF) used the NEI2008 updated with point-source emissions (for details see section on emissions). Two scenarios were run. One scenario assumed a replacement program for non-certified wood-

[12] Note that WRF/Chem is a complex state-of-the-art research model, not a regulatory model.
[13] Privacy law forbids naming facilities.

burning devices. With the assumptions made on how households with several heating devices partition heating among devices and the burning behavior and number of non-certified burning devices replaced, the $PM_{2.5}$ emissions from heating were reduced by 4% on average over the nonattainment area over the six months (WSR). Two sensitivity studies were performed assuming different numbers of non-certified wood-burning devices that could be replaced (WSS1, WSS2). In addition, sensitivity analysis was made how emissions change with the assumptions on the burning behavior (partitioning among devices, time of burning). The second scenario mitigation for winter 2008/09 assumed the use of low sulfur fuel for domestic combustion, oil-burning point-source facilities and that part of power generation that used oil-fuel in accord with the 2008 allowances for fuel-sulfur content (LSF).

The LSF and WSR mitigation studies (like the study on the contribution of point-source emissions on the $PM_{2.5}$-concentrations at breathing level) suggest that emissions from area sources (e.g. domestic heating) and/or traffic are the main contributors to the $PM_{2.5}$ NAAQS exceedances occurring in the nonattainment area.

The "woodstove replacement" simulations indicate that a program for replacement of wood-burning devices can reduce the $PM_{2.5}$-concentrations at breathing level in the Fairbanks $PM_{2.5}$-nonattainment area. The study suggests that the highest mitigation of $PM_{2.5}$-concentrations with a "woodstove replacement" can be achieved in the months that are coldest. The sensitivity studies suggest that the reduction effectiveness depends on the number of wood-burning devices exchanged and on what kinds of devices are replaced (see results of WSR, WSS1, WSS2). The average emission reduction in the heating sector calculated for October 1 to October 15, 2008 amounts 40%, 7% and 6% on average over the nonattainment area under the assumption made for the "woodstove replacement" in WSS1, WSS2, and WSR, respectively. Note that we are here talking about the emission reduction of primary $PM_{2.5}$, not the emission reductions for other species (e.g. $SO_2$, $NO_x$, VOC) that go along with a "woodstove replacement".

Unfortunately, no data are available, where and what wood-burning devices are operated and when and how intensively. In our study, we simply assumed the distribution of wood-burning devices as being proportional to the population density. This assumption holds uncertainty in the spatial distribution that may affect local maximum concentrations as well as 24h-averages of $PM_{2.5}$-concentrations according to sensitivity studies. Further uncertainty is due to the unknown number of wood-burning devices that exist and that can be replaced. Sensitivity studies on the emissions indicated that uncertainty results from the unknown partitioning of the use of wood-burning and other heating devices in households with more than one heating option. Despite these uncertainties, all simulation studies on "woodstove replacement" show in common a mitigation of $PM_{2.5}$-concentrations on average at breathing level. Note that the simulations on "woodstove replacement" do not consider that additional wood-burning devices may have been added since 2008 or might be added in the future.

Based on the studies performed on the replacement of wood-burning devices we can conclude that exchanging noncertified wood-burning devices can help to reduce the number of exceedance days during October to March. The full benefit of exceedance reduction due to the "woodstove replacement" may be underestimated by WSR because the number of woodstoves exchanged may be on the lower end of the number of woodstoves that actually could/will be exchanged. Nevertheless, the concentration offsets between the baseline simulation REF and the "future" simulation WSR (Table 6, Figs. 25, 26) imply that replacement of non-certified wood-burning devices alone when only preformed in low numbers will not be sufficient to avoid all $PM_{2.5}$

exceedances. If emissions of area and point sources only slightly increase due to increasing of traffic, population, etc. the benefit due to the "woodstove replacement" will be set off quickly. This means a high number of non-certified wood-burning devices has to be replaced.

We further conclude that there is an urgent need to collect data on the location and kind of wood-burning devices used in the nonattainment area and to obtain additional information on how households with wood-burning devices and another heating device partition their heating among these heat sources. Information is also needed on the diurnal burning behavior on weekdays, weekends and holidays. Since emissions also depend on the dryness of the wood, data on the fraction of seasoned and non-seasoned wood typically burned will be helpful in better assessing the contribution from wood-burning devices to the $PM_{2.5}$-concentrations at breathing level. Furthermore, it would be good to know how accurate data from surveys may be if people fear, their information could later lead to measures that may be of disadvantage to them. This means it has to be examined whether we do obtain the correct information in surveys.

Our study suggests that the introduction of low sulfur fuel can reduce the number of exceedance days. The simulations suggest that introduction of low sulfur fuel as assumed in LSF leads occasionally to higher reductions than achieved by the "woodstove replacement" (WSR) assumed in this study. However, the results also suggest that up to 20% of the days in months with relatively long daylight hours (October, February, March) may experience increases in $PM_{2.5}$-concentrations at breathing level in response to introduction of low sulfur fuel due to gas-to-particle conversion. This increase is related to shifts in the thermodynamic equilibrium of sulfate-nitrate-ammonia-water in aerosol during months with still or already again enough daylight. The highest temporal and local differences in simulated $PM_{2.5}$ concentrations in response to introducing low sulfur fuel typically occurred in November whereas the lowest differences occurred in March. The reason is that October had high and February, March small increases in $PM_{2.5}$-concentrations after introducing low sulfur, while there were no increases in November.

The results of the simulation on the introduction of low sulfur fuel also suggest that in the case of measures aiming at mitigation indirectly by reduction of precursors it is important to simulate an entire winter emission season. Otherwise one could by accident just be lucky to have chosen a period where reduction occurs and oversee that there may be cases where despite reduced emissions of precursors the concentrations go up. Moreover, only in the case of the statistics over the entire winter it is possible to judge whether, on average, mitigation can be reached. Our study also suggests that care has to be taken in the judgment of the representativeness of the winter examined.

The simulation results showed that "introduction of low sulfur fuel" (LSF) results in a slightly lower new design value than the small "woodstove replacement program" assumed in WSR. The results also showed that a small "woodstove replacement program" such as assumed in WSR already reduces the design value by 2.2$\mu g/m^3$. The sensitivity studies performed on "woodstove replacement" (WSS1, WSS2) suggested that a more rigorous replacement of wood-burning devices (WSS1) may yield much higher mitigation than the small exchange program assumed in WSR. Since the introduction of low sulfur fuel is very expensive and further reduction costs even more, and since the relative response factors and new design values vary strongly among months when introducing low sulfur fuel, it seems that a rigorous replacement of non-certified wood-burning devices is much more promising to achieve compliance.

The results of all the simulations performed for this study suggest that a single pollution-control policy may not be sufficient to help comply with the 24h-average $PM_{2.5}$ NAAQS. Due to the high nonlinearity of chemical processes, we cannot assume that a combined "woodstove replacement" and "low sulfur fuel" program will lead to the goal. An additional study considering both measures would be required because precursors for gas-to-particle conversion are changed by both measures and interaction among the impacts of the two measures may yield to diminution or enhancement of wanted or even unwanted effects. Since changes in emissions of precursors lead to changes in gas-to-particle conversion, combinations of different control methods (i.e. "woodstove replacement" and concurrent "low sulfur fuel" programs) and other mitigation strategies (i.e. replacement of oil furnaces by gas, replacement of oil furnaces and wood-burning devices by gas) should be investigated. Future studies should also examine the impact of introducing other energy sources and/or expansion the use of gas for heating and energy generation.

The results of our study also show a stronger percentage mitigation of $PM_{2.5}$-concentrations on average over the entire nonattainment area than at the grid cell holding the State Building. In the future, it should be examined whether observations also show differences in changes of air quality at various sites in the nonattainment area. If so, local sources may play a role and they should be identified.

Unfortunately, the speciation data did not become available during the time of the project. Thus, an evaluation of the simulated composition of $PM_{2.5}$ is still pending, but planned for the future. Such an evaluation of simulated speciation is an urgent need to assess the role of ammonia. Based on speciation data of prior years and a first screen of the data that became available after the end of the project (Fig. 34), various scientists are concerned that the NEI2008 may underestimate the $NH_4$ emissions in the FNSB.

**Personnel who worked on this study:**

Nicole Mölders, Ph.D., Ph.D.

Huy N.Q. Tran, M.S.

Ketsiri Leelasakultum, M.S.

Kelcy Brunner, undergraduate student

Todd Fortun, undergraduate student

## References:


Bell, M.L. (2006) The use of ambient air quality modeling to estimate individual and population exposure for human health research: A case study of ozone in the Northern Georgia Region of the United States. *Environment International, 32*, 586–593.

Binkowski, F. S., and U. Shankar (1995), The regional particulate matter model, 1. Mode description and preliminary results, *Journal Geophysical Research*, *100*, 26191-26209.

Bourne, S. M., U. S. Bhatt, J. Zhang, and R. Thoman (2010), Surface-based temperature inversions in Alaska from a climate perspective, *Atmospheric Research*, *95*, 353-366.

Carlson, T. R., S.-H. Yoon, and R. G. Diulla (2010), Fairbanks home heating survey*Rep.*, 63 pp, Sacramento, CA.

Carpenter, S., T. Frost, D. Heisey, and T. Kratz (1989), Randomized intervention analysis and the interpretation of whole-ecosystem experiments, *Ecology*, *70*, 1142– 1152.

Chang, J. C., and S. R. Hanna (2004), Air quality model performance evaluation, *Meteorol Atmos Phys*, *87*, 167–196.

Dawson, J.P., P.J. Adams, and S.N. Pandis (2007), Sensitivity of PM2.5 to climate in the Eastern U.S.: a modeling case study, *Atmos. Chem. Phys.*, *7*, 6487-6525.

Davies, J., D. Misiuk, R. Colgan, and N. Wiltse (2009), Reducing PM2.5 emissions from residential heating sources in the Fairbanks North Star Borough: Emission estimates, policy options, and recommendations*Rep.*, 56 pp, Cold Climate Housing Research Center.

DOT (2009), Northern Region Annual Traffic Volume Report - Volume I 2009*Rep.*, 200 pp, Department of Transport and Public Facilities, Alaska.

Eder, B., D. Kang, R. Mathur, J. Pleim, S. Yu, T. Otte, G. Pouliot (2009), A performance evaluation of the National air quality forecast capability for the summer of 2007. *Atmos. Environ., 43,* 2312-2320.

EPA (2007) http://www.epa.gov/glo/SIPToolkit/documents/20070322_72fr_13560-13581_exceptional_events_data.pdf.

EPA (2009) http://www.epa.gov/.

EPA (2011) *http://www.epa.gov/airtrends/values.html.*

Fortun, T., and N. Mölders (2009), Investigations on the sensitivity of predicted air quality to the uncertainty in anthropogenic emissions.*Rep.*, 18 pp, ARSC, Fairbanks, AK.

Gaudet, B.J., D.R. Stauffer (2010) Stable boundary layers representation in meteorological models in extremely cold wintertime conditions, EPA report, pp. 60.

Grell, G.A., S. Emeis, W.R. Stockwell, T. Schoenemeyer, R. Forkel, J. Michalakes, R. Knoche, W. Seidl (2000), Application of a multiscale, coupled MM5/chemistry model to the complex terrain of the VOTALP valley campaign. *Atmos. Environ. 34,* 1435-1453.

Grell, G. A., and D. Dévényi (2002), A generalized approach to parameterizing convection, *Geophysical Research Letters*, *29*.

Grell, G.A., S.E. Peckham, R. Schmitz, S.A. McKeen, G. Frost, W.C. Skamarock, B. Eder (2005), Fully coupled "online" chemistry within the WRF model. *Atmos. Environ. 39,* 6957-6975.

Guenther, A., et al. (1994), A global model of natural volatile organic compound emissions, *Journal Geophysical Research*, *100D*, 8873-8892.Mölders, N. (2009), Alaska Emission Model (AkEM) description. *Rep.*, 10 pp, Fairbanks.

Hart, M., and R. de Dear (2004), Weather sensitivity in household appliance energy end-use, *Energy and Buildings*, *36*(2), 161-174.

Hong, S.-Y., and J.-O. J. Lim (2006), The WRF Single-Moment 6-class microphysics scheme (WSM6), *Journal Korean Meteorological Society*, *42*, 129-151.

Hong, S.-Y., Y. Noh, and J. Dudhia (2006), A new vertical diffusion package with an explicit treatment of entrainment, *Mon. Wea. Rev.* , *134*, 2318-2341.

Janjić, Z. I. (1994), The step-mountain eta coordinate model: further developments of the convection, viscous sublayer and turbulence closure schemes, *Mon. Wea. Rev.*, *122*, 927-945.

Janjić, Z. I. (2002), Nonsingular implementation of the Mellor-Yamada level 2.5 scheme in the NCEP meso model*Rep.*, 61pp

Johnson, R., T. Marsik, M. Lee, and C.F. Cahill (2009), Helping Fairbanks meet new air quality requirements: Developing ambient PM-2.5 management strategies, in *Transportation safety, security, and innovation in cold regions*, p. 1.

Kannari, A., D. G. Streets, Y. Tonooka, K. Murano, and T. Baba (2008), MICS-Asia II: An inter-comparison study of emission inventories for the Japan region, *Atmospheric Environment*, *42*, 3584-3591.

Kim, J., B. Kwak, H.-S. Park, N. Kim, K. Choi, and J. Yi (2010), A GIS-based national emission inventory of major VOCs and risk assessment modeling: Part I — methodology and spatial pattern of emissions, *Korean Journal of Chemical Engineering*, *27*(1), 129-138.

Kramm, G., K.-D. Beheng, and H. Müller (1992), *Vertical transport of polydispersed aerosol particles in the atmospheric surface layer*, 1125-1141 pp., The Semonin Vol. Hemisphere Publ., Washington/Philadelphia/London.

Kumar, P., A. Robins, S. Vardoulakis, and R. Britter (2010), A review of the characteristics of nanoparticles in the urban atmosphere and the prospects for developing regulatory controls, *Atmospheric Environment*, *44*, 5035-5052.

Madronich, S. (1987), Photodissociation in the atmosphere, 1, actinic flux and the effects of ground reflections and clouds, *Journal Geophysical Research*, *92*, 9740-9752.

McCreanor, J., et al. (2007), Respiratory Effects of Exposure to Diesel Traffic in Persons with Asthma, *New England Journal of Medicine*, *357*, 2348-2358.

Mlawer, E. J., S. J. Taubman, P. D. Brown, M. J. Iacono, and S. A. Clough (1997), Radiative transfer for inhomogeneous atmospheres: RRTM, a validated correlated-k model for the longwave, *Journal of Geophysical Research*, *102D*, 16663-16682.

Mölders, N., H. Hass, H. J. Jakobs, M. Laube, and A. Ebel (1994), Some effects of different cloud parameterizations in a mesoscale model and a chemistry transport model, *J. Appl. Meteor.*, *33*, 527-545.

Mölders, N. (2008), Suitability of the Weather Research and Forecasting (WRF) model to predict the June 2005 fire weather for Interior Alaska, *Wea. Forecast.*, *23*, 953-973.

Mölders, N. (2009), Alaska Emission Model (AkEM) description*Rep.*, 10 pp, Fairbanks.

Mölders, N. (2010), Alaska Emission Model (AkEM) - version 1.01 description. *Rep.*, 16 pp, Fairbanks.

Mölders, N., and G. Kramm (2010), A case study on wintertime inversions in Interior Alaska with WRF, *Atmospheric Research*, *95*, 314-332.

Mölders, N., S. E. Porter, C. F. Cahill, and G. A. Grell (2010), Influence of ship emissions on air quality and input of contaminants in southern Alaska National Parks and Wilderness Areas during the 2006 tourist season, *Atmospheric Environment*, *44*, 1400-1413.

Mölders, N., S. E. Porter, T. T. Tran, C. F. Cahill, J. Mathis, and G. B. Newby (2011), The effect of unregulated ship emissions for aerosol and sulfur dioxide concentrations in southwestern Alaska, in *North by 2020: Perspectives on a Changing North*, edited by K. Criddle, H. Eicken, A. Lovecraft and A. Metzger, p. 14, Alaska University Press, Fairbanks, in press.

NESCAUM (2005), Low Sulfur Heating Oil in the Northeat States: An Overview of Benefits, Costs and Implementation Issues*Rep.*, Boston, MA:NESCAUM.

Otte, T.L., G. Poulliot, J.E. Pleim, J.O. Young, K.L. Schere, D.C. Wong, P.C.S. Lee, M. Tsidulko, J.T. McQueen, P. Davidson, R. Mathur, H.-Y. Chuang, G. DiMego, N.L. Seaman, (2005), Linking the Eta Model with the Community Multiscale Air Quality (CMAQ) modeling system to build a national air quality forecasting system. *Wea. Forecast., 20*, 367-384.

Peckham, S. E., et al. (2009), WRF/ChemVersion 3.1 User's Guide*Rep.*, 78 pp.

Riediker, M., W. E. Cascio, T. R. Griggs, M. C. Herbst, P. A. Bromberg, L. Neas, R. W. Williams, and R. B. Devlin (2004), Particulate Matter Exposure in Cars Is Associated with Cardiovascular Effects in Healthy Young Men, *Am. J. Respir. Crit. Care Med.*, *169*(8), 934-940.

Schell, B., I. J. Ackermann, H. Hass, F. S. Binkowski, and A. Ebel (2001), Modeling the formation of secondary organic aerosol within a comprehensive air quality model system, *J. Geophys. Res.*, *106*(D22), 28275-28293.

Seinfeld, J. H., and S. N. Pandis (1997), *Atmospheric Chemistry and Physics, from Air Pollution to Climate Change* John Wiley & Sons.

Shulski, M., and G. Wendler (2007), *The Climate of Alaska*, 216 pp., University of Alaska Press, Fairbanks.

Simpson, D., A. Guenther, C. N. Hewitt, and R. Steinbrecher (1995), Biogenic emissions in Europe 1. Estimates and uncertainties, *Journal Geophysical Research*, *100D*, 22875-22890.

Smirnova, T. G., J. M. Brown, S. G. Benjamin, and D. Kim (2000), Parameterization of cold season processes in the MAPS land-surface scheme, *Journal Geophysical Research*, *105D*, 4077-4086.

Stockwell, W. R., P. Middleton, J. S. Chang, and X. Tang (1990), The second-generation regional acid deposition model chemical mechanism for regional air quality modeling, *Journal Geophysical Research*, *95*, 16343-16367.

Tetzlaff, G., R. Dlugi, K. Friedrich, G. Gross, D. Hinneburg, U. Pahl, M. Zelger, and N. Mölders (2002), On modeling dry deposition of long-lived and chemically reactive species over heterogeneous terrain, *J. Atm. Chem.*, *42*, 123-155.

Tran, H. N. Q., and N. Mölders (2011), Investigations on meteorological conditions for elevated $PM_{2.5}$ in Fairbanks, Alaska, *Atmospheric Research*, *99*(1), 39-49.

von Storch, H., and F. W. Zwiers (1999), *Statistical Analysis in Climate Research*, 484pp. pp., Cambridge University Press.

Werth, D., and R. Avissar (2002), The local and global effects of Amazone deforestation, *Journal of Geophysical Research*, *107*, 8.

Wesley, M. L. (1989), Parameterization of surface resistances to gaseous dry deposition in regional-scale numerical models, *Atmospheric Environment 23*, 1293-1304.

Wexler, A. S., and J. H. Seinfeld (1992), Analysis of aerosol ammonium nitrate: departures from equilibrium during SCAQS, *Atmos. Environ.* , *26A*, 579–591.

Yarker, M. B., D. PaiMazumder, C. F. Cahill, J. Dehn, A. Prakash, and N. Mölders (2010), Theoretical investigations on potential impacts of high-latitude volcanic emissions of heat, aerosols and water vapor and their interactions on clouds and precipitation, *The Open Atmospheric Science Journal*, *4*, 24-44.

Yu, S., R. Mathur, K. Schere, D. Kang, J. Pleim, J. Young, D. Tong, G. Pouliot, S.A. McKeen, S.T. Rao (2008), Evaluation of real-time PM2.5 forecasts and process analysis for PM2.5 formation over the eastern United States using the Eta-CMAQ forecast model during the 2004 ICARTT study. *J. Geophys. Res., 113,* D06204, doi:10.1029/2007JD009226.

Final Report

To

Alaska Department of Environmental Conservation (ADEC)

Grant Number 127617

Reporting Period: 8 March 2011 – 31 January 2012

# 'Fairbanks, North Star Borough AK PM2.5 Non-Attainment Area WRF-ARW'

Dr. Brian J. Gaudet, PI

Dr. David R. Stauffer, co-PI

The Pennsylvania State University

Dept. of Meteorology

University Park, PA 16802

bjg20@met.psu.edu

2 Apr 2012

## EXECUTIVE SUMMARY

This final report describes work performed by the Department of Meteorology at the Pennsylvania State University under Grant Number 127617, 'Fairbanks North Star Borough PM2.5 Non-Attainment Area WRF-ARW Modeling', supported by the Alaska Department of Environmental Conservation (ADEC) and the Fairbanks / North Star Borough. The purpose of this project was to perform meteorological modeling of the region around Fairbanks and North Pole, AK, as part of the State Implementation Plan for fine particulate matter (PM2.5) analysis of the region. The Fairbanks / North Star region was designated a non-attainment area for the daily National Ambient Air Quality Standard (NAAQS) for PM2.5 by the Environmental Protection Agency (EPA); high PM2.5 concentrations for the area predominantly occur within stable boundary layers during periods of extreme cold and weak winds during the winter season. The air quality modeling component of the SIP utilizes atmospheric analyses generated by a meteorological model; therefore it is important to select a meteorological model configuration that can properly represent the structure and evolution of the local stable boundary layer in these conditions.

The simulations were to be performed with the Weather Research and Forecasting (WRF), Advanced Research WRF (WRF-ARW) model, a globally used and freely-available meteorological model. Initial WRF-ARW simulations for a period in Jan. – Feb. 2008 were performed by Penn State under the Regional Applied Research Effort (RARE) project funded by the EPA. During the RARE project an optimal set of physics options, grid configuration, and data assimilation strategy was developed and tested. For physics sensitivity tests data assimilation was only performed on the coarser two domains (12-km and 4-km horizontal grid spacing), while the finest domain (1-km horizontal grid spacing) was used for assessing sensitivity. It was concluded, however, that a final meteorological analysis to be provided to EPA should also have data assimilation on the finest domain, to provide a better fit to the observations.

For the current contract, the model setup from the RARE project was to be applied to the production of a new meteorological analysis covering the period 2-17 Nov. 2008. As in the final meteorological analysis of the RARE project, data assimilation for the current project uses data assimilation on all three domains. However, a few modifications to the data assimilation procedure were implemented to take advantage of data and source code not used in the RARE project: 1) the effective vertical resolution of the observations as seen by the data assimilation modules was increased; 2) a more vertically-consistent objective analysis procedure was used; 3) additional surface observations from non-standard sources (i.e., stations not present in the standard METAR-format database typically used for hourly meteorological reporting) were used

both for verification and in the data assimilation, in order to supplement the METAR observations in this relatively data-sparse region.

A test period (5 – 9 Nov 2008) was used to perform some initial evaluations of possible modified procedures. In particular, during the RARE project the data assimilation on Grid 3 for the final meteorological analysis only used the temperatures from the METAR surface stations, and not the winds. For the RARE project it was thought that, since the surface winds during the coldest episode would be expected to be weak and poorly sampled, and since the surface winds in these conditions might be expected to be thermally-driven, the best chance of accurately reproducing existing flows would be to only use the temperature (and moisture) fields from surface observations in data assimilation, while relying on the model itself to generate the proper wind fields. This led to realistic low-level flow patterns and generally satisfactory wind error statistics at non-calm locations. There did tend to be a positive near-surface temperature bias during periods of extreme cold and weak winds, which could have been a result of overestimated vertical mixing due to the model's positive near-surface wind speed bias. The extended surface dataset used in the current study provided an opportunity to determine if improved statistics could result if 1-km grid data assimilation of near-surface winds was included. This was one of the initial sensitivity tests performed for the test period.

The major findings of the current project are as follows:

- The use of near-surface winds in data assimilation during the test period, when compared to a control simulation, led to about a 20 degree improvement in the mean absolute error (MAE) of wind direction. Temperature and wind speed statistics were also improved, but the improvements were modest. The modest size of these improvements was hypothesized to be due to either insufficient horizontal resolution of the model topography, or too large of a region of influence of particular observations in the data assimilation procedure.

- A new simulation was performed in which the radius of influence of observations on the 1-km grid was reduced from 75 km to 30 km, and the strength of the relaxation coefficient was doubled. These experiments produced slightly better temperature statistics on average, but slightly worse wind speed statistics. Wind direction errors, however, were further reduced by the new simulation procedure by a substantial amount (about 19 degrees in MAE). It was decided to make this model configuration (experiment TWIND2X30) the basis of a simulation of the entire 2-17 Nov. 2008 episode.

- Previous experiments did not make use of calm wind observations in the data assimilation procedure; the possible presence of missing data or high instrument response thresholds imply that it might be preferable to retain model-generated flows in weak-

wind conditions rather than relax the flows towards a zero-magnitude wind vector by data assimilation. However, because it was desired to further reduce the model positive wind speed bias, an additional set of simulations over the 2-17 Nov. 2008 episode was performed, for which data assimilation did make use of calm wind reports (henceforth experiment TWIND2X30CALM). While the use of calm wind reports did reduce the positive near-surface wind bias of the model, the improvement was only on the order of 0.1 m $s^{-1}$. Meanwhile, TWIND2X30CALM had wind direction MAE scores that were about 14 degrees worse. Since wind direction by necessity can only be verified with non-calm wind observations, the implication was that the use of near-surface calm wind observations in data assimilation was degrading wind direction statistics at other observation locations without making a substantial improvement in wind speed statistics. Therefore, it was decided to deliver the results of TWIND2X30, rather than TWIND2X30CALM, to ADEC for use in subsequent air quality modeling.

- The Jan-Feb 2008 episode simulated during the RARE study was re-simulated using the TWIND2X30 procedure, and compared with corresponding statistics using the RARE configuration. Little statistical difference was found between the RARE and TWIND2X30 for variables other than wind direction, for which the TWIND2X30 configuration was about 12 degrees better in terms of MAE.

- Qualitatively, it was found that the meteorological analysis produced realistic topographical flows, and was capable of reproducing observed surface temperatures below -40 °C in locations such as Woodsmoke. However, the model did tend to have a positive near-surface temperature bias during the coldest episodes at valley locations that could not be well-resolved by the model (e.g., Goldstream Creek). This was counteracted by periods when the model had a negative temperature bias, such as during the initial precipitation event of the 2-17 Nov. 2008 episode, such that the overall model temperature bias was quite small (less than a degree Celsius) for both simulated episodes.

## 1. INTRODUCTION

The region around Fairbanks and North Pole, AK, was designated by the Environmental Protection Agency (EPA) as a non-attainment area for fine particulate matter (PM2.5, referring to particles with aerodynamic diameters equal to or less than 2.5 microns). This designation required that a State Implementation Plan (SIP) be developed. The violations occur predominantly during the cold season, when the meteorological conditions frequently become ideal for achieving high concentrations of any tracer released into the atmosphere. These ideal conditions, often present in combination, include the presence of extremely strong inversions capping a shallow layer of extremely cold air, light and variable winds, and very weak, intermittent turbulence (e.g., Benson 1970; Serreze et al. 1992; Mölders and Kramm 2010). These conditions, which frequently occur in the winter over inland Alaska, can be exacerbated in the region around Fairbanks, where a rough semicircle of ridges tends to isolate the airflow around Fairbanks from its surroundings, restricting the dispersal of pollutants.

## 2. EPA RARE STUDY BACKGROUND

The Regional Applied Research Effort (RARE) study was sponsored by the EPA to help the Fairbanks North Star Borough and the Alaska Department of Environmental Conservation (ADEC) develop a State Implementation Plan for the Fairbanks / North Pole PM2.5 non-attainment area. This project included meteorological modeling, meteorological observational, and trace gas and aerosol analysis modeling components. Penn State conducted the meteorological modeling component of this study from 1 Sep 2008 – 31 Jan 2010, with the specific focus being the extremely cold stable boundary layers in winter in the Fairbanks region. The meteorological portion of the project consisted of selecting and performing two twenty-day simulations down to 1-km horizontal grid spacing for two episodes from the 2007-2008 winter season characterized by high PM2.5 exceedance events in the Fairbanks region. One episode was to be characterized by near total darkness, while the second was to contain partial sunlight.

There were two components of the atmospheric modeling portion of the study. One was to produce the best possible analysis of the atmosphere (at approximately 1-km grid spacing) that could be used in conjunction with the parallel chemical and emissions modeling efforts to better understand the nature of the PM2.5 exceedance events of the Fairbanks / North Star Borough area. The other was to perform physics sensitivity studies on turbulence and land surface model parameterizations to determine the best-performing modeling configuration and physics suite for representing the stable atmospheric boundary layers in these conditions.

The tool used for the meteorological modeling component of the RARE project was the Weather Research and Forecasting (WRF) model (Skamarock et al. 2008), more specifically, the Advanced Research WRF dynamic core (WRF-ARW, henceforth simply called WRF). WRF contains separate modules to compute different physical processes such as surface energy budgets and soil interactions, turbulence, cloud microphysics, and atmospheric radiation. Since turbulent eddies in the SBL are typically much smaller than mesoscale model horizontal grid spacing (e.g., ten meters vs. a thousand or more meters), they cannot be modeled directly (e.g., Wyngaard 2004), but typically their effect is parameterized by a planetary boundary layer (PBL) scheme that predicts turbulent kinetic energy (TKE). Within WRF the user has many options for selecting the different schemes for each type of physical process. There is also a WRF Preprocessing System (WPS) that generates the initial and boundary conditions used by WRF, based on topographic datasets, land use information, and larger-scale atmospheric and oceanic models.

The RARE simulations used three one-way nested horizontal grids with horizontal grid spacing of 12 km, 4 km and 1.3 km, respectively. Grid 1 covers the entirety of Alaska and extends from Siberia to the northwestern continental United States (Figure 1). Grid 2 closely coincides with the extent of the Alaskan landmass south of the Brooks range; it includes the Anchorage region and the Gulf of Alaska in the south (Figure 2). Grid 3, centered around Fairbanks and extending south to the Alaska Range and north past the White Mountains and other uplands just north of Fairbanks, includes all of the non-attainment area within the Fairbanks North Star Borough (Figure 3 - Figure **4**).

Many of the WRF namelist parameters used in the RARE study were taken directly from modeling studies performed by Penn State for studying the nocturnal stable boundary layers of central Pennsylvania (Stauffer et al. 2009; Seaman et al. 2012) using version 3.1 of WRF-ARW. Many of the grid-independent parameters are listed in Table 1. In particular, the extremely fine vertical grid spacing of the model levels near the surface is in order to adequately resolve the depth of stable boundary layers that may be only tens of meters deep, and within which the scale of the turbulent eddies may be even less. However, the near-surface vertical grid spacing in the RARE study was coarsened slightly from that of the central Pennsylvania studies both in order to prevent numerical instabilities from occurring over the extremely steep elevation gradients on the north edge of the Alaska Range, and to alleviate concerns about the model atmospheric grid spacing being on the order of the vegetation canopy height. The final near-surface vertical grid spacing was 4 m, increasing gradually with height above the surface (refer to Gaudet and Stauffer 2010).

Grid-dependent namelist parameters and WRF Preprocessing System (WPS) namelist parameters are listed in Table 2 and Table 3, respectively.

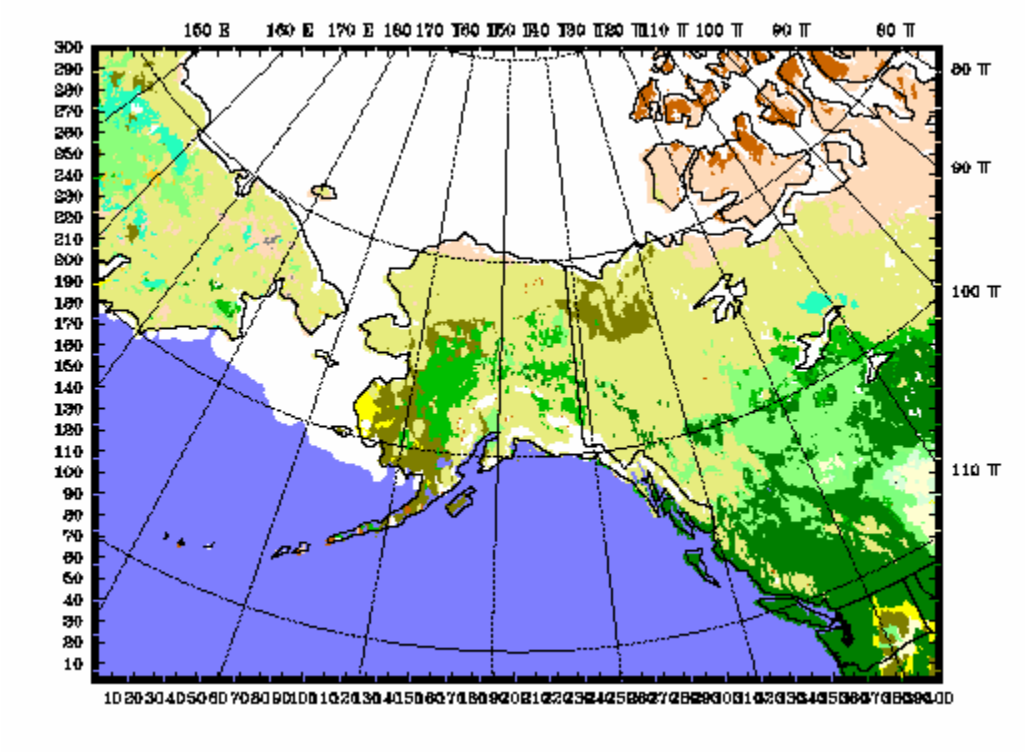

Figure 1: Grid 1 domain, showing land use variation. Colors indicate: light green – cropland/woodland mosaic; yellow – grassland; dark yellow – shrubland; mustard – mixed shrubland/grassland; leaf green – deciduous broadleaf forest; dark green – deciduous or evergreen needleleaf forest; forest green – mixed forest; light blue – water body; brown – herbaceous wetland; surf green – wooded wetland; tan – barren or sparsely vegetated; light gray – herbaceous tundra; avocado – wooded tundra; peach – mixed tundra; medium gray – bare ground tundra; white – snow or ice.

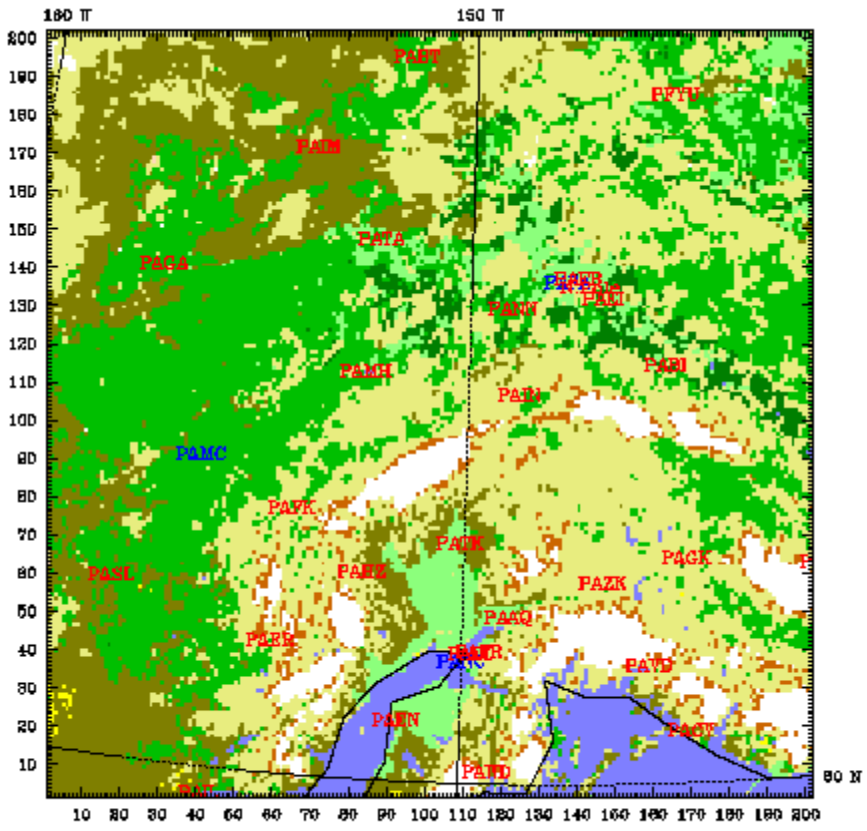


Figure 2: Grid 2 domain, showing land use variation. Color scale same as in Figure 1.

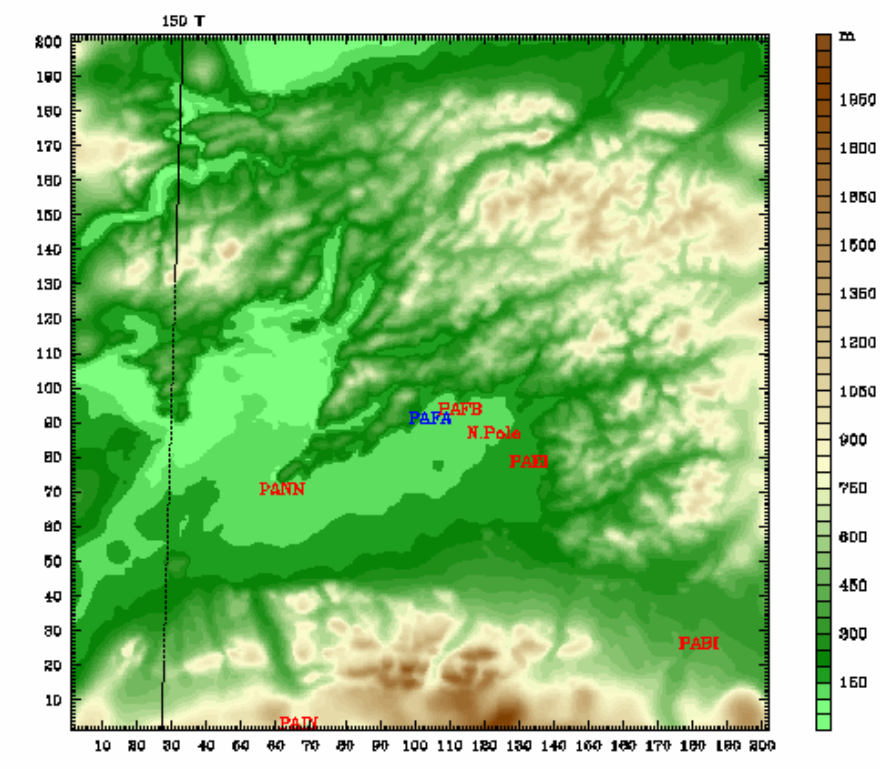


Figure 3: Grid 3 domain, showing topographic relief. METAR stations are shown in red; rawinsonde stations are shown in blue. Eielson AFB is denoted by PAEI; Fort Wainwright is denoted by PAFB. Location of community of North Pole is also indicated.

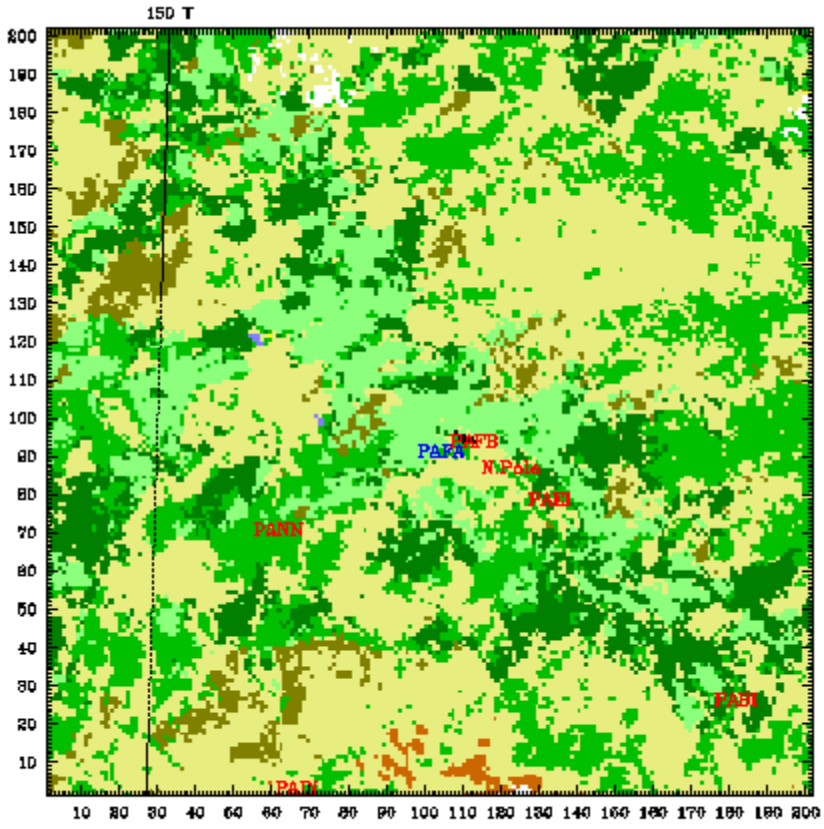


Figure 4: Grid 3 domain, showing land use variation. Color scale same as in Figure 1.

Table 1: Grid-independent features of WRF simulations.

| | |
|---|---|
| nesting procedure | one-way concurrent |
| model top (hPa) | 50 |
| number of vertical layers | 39 |
| eta value of full levels | 1.0, 0.9995, 0.999, 0.9984, 0.99705, 0.99415, 0.99155, 0.986, 0.78, 0.966, 0.95, 0.034, 0.918, 0.902, 0.886, 0.866, 0.842, 0.814, 0.78, 0.74, 0.694, 0.648, 0.602, 0.556, 0.51, 0.464, 0.418, 0.372, 0.326, 0.282, 0.24, 0.2, 0.163, 0.128, 0.096, 0.066, 0.04, 0.018, 0 |
| approximate height above ground level of half levels (m) | 2.0, 6.0, 10.5, 18.4, 35.5, 57.8, 90.9, 146.2, 228.3, 344.5, 478.7, 614.8, 752.7, 892.5, 1052.3, 1251.1, 1491.2, 1785.4, 2148.4, 2587.7, 3079.8, 3598.2, 4146.0, 4727.3, 5346.7, 6010.4, 6725.8, 7502.6, 8333.4, 9208.6, 10135.5, 11190.6, 12139.8, 13234.2, 14408.4, 15652.1, 16921.7, 18193.7 |
| exclude nudging from the boundary layer | no |
| *G* for analysis nudging, when used ($s^{-1}$) | 0.0003 |
| *G* for obs nudging, when used ($s^{-1}$) | 0.0004 |
| obs nudging half-time window (hr) | 2 |
| specified, relaxed zone width | 1, 9 |

Table 2: Grid-Dependent features of baseline model configuration

| | Grid 1 | Grid 2 | Grid 3 |
|---|---|---|---|
| horizontal extent | 401 x 301 | 202 x 202 | 202 x 202 |
| horizontal Δx (km) | 12 | 4 | 1.33 |
| i parent start | - | 156 | 103 |
| j parent start | - | 106 | 106 |
| time step (s) | 24 | 8 | 4 |
| sound step ratio | 8 | 8 | 4 |
| dampcoef | 0.0 | 0.0 | 0.0 |
| analysis nudging | yes | no | no |
| obs nudging | yes | yes | yes |
| surface obs nudging xy radius (km) | 100 | 100 | 75 |
| topographic dataset | USGS<br>10 m | USGS<br>2 m | USGS<br>30 s |

Table 3: Grid-independent WRF Preprocessor System (WPS) features

| | |
|---|---|
| projection | Lambert conformal |
| reference latitude, longitude | 64.8, -148.0 |
| true latitudes | 50.0, 70.0 |
| standard longitude | -148.0 |
| initial conditions | 0.5 degree GFS analyses |
| analysis interval (hr) | 6 |

Two twenty-day episodes from the 2007-2008 winter season were selected in the RARE study. One episode was from 14 Dec 2007 to 03 Jan 2008, a time of year when there is little solar radiation in the Fairbanks area (approximately three hours of daylight per day near the solstice). During this episode the temperature rapidly decreased to near -40°C by 21 Dec, accompanied by rapid increases in PM2.5 concentrations, and then temperatures generally increased and PM2.5 decreased for the remainder of the episode. The second episode was from 23 Jan 2008 to 12 Feb 2008, when solar insolation was more significant (between five and eight hours of sunlight per day), and provides an example of 'partial sunlight' conditions. During this episode temperatures were initially relatively warm (near 0°C), decreased briefly to near -35°C by 27 Jan, rebounded slightly, and then decreased during the most extensive period of sub -35°C weather of the season. Consistent with the prolonged period of cold temperatures were recurring violations of the PM2.5 standard in the Fairbanks area.

In the initial period of a regional model simulation there is generally a period of several hours when the atmospheric state, whose initial conditions are usually provided by a global or coarser regional model, is still dynamically adjusting to the finer scale resolution and topography of the regional model. Therefore the model output from this initial 'spin-up' period is not completely reliable as an indicator of the true atmospheric state. However, if a regional model simulation is allowed to progress for too long without re-initialization (normally several days), it tends to drift away from the actual observed atmospheric state. Therefore, our method of obtaining realistic regional atmospheric analyses over an entire twenty-day episode was to divide each episode into four overlapping simulation segments. Each segment was around five days long with a twelve-hour overlap between each segment to avoid spin-up effects. (Specifically, the near total darkness episode was divided into successive segments of 6 days, 5.5 days, 5.5 days, and 4.5 days; the partial sunlight episode was divided into successive segments of 5 days, 5.5 days, 5.5 days, and 5.5 days). Initial conditions and most of the Grid 1 lateral boundary conditions were obtained from the half-degree Global Forecast System (GFS) zero-hour analyses (except for a few particular times during the near total darkness episode when the half-degree GFS product was unavailable, when one-degree GFS analysis was used).

Even with the overlapping simulation segment strategy, it is difficult to ensure that the interior of a regional model simulation remains close to observations for simulations of more than a day or so. Therefore, dynamic analyses of historical cases are often performed, in which a Four-Dimensional Data Assimilation (FDDA) strategy is applied throughout the model integration. Relaxation terms based on the differences between actual observations and the corresponding model fields at the observation sites (also known as the 'innovations') are added to the model's predictive equations. In this way the model error is constrained based on available observations while the model still provides dynamic consistency and finer mesoscale structure not present in the observations. The version of FDDA used in these simulations is the multiscale, multigrid

nudging FDDA strategy developed by Stauffer and Seaman (1994) for the MM5 mesoscale model, and implemented in WRF as described in Deng et al. (2009). Nudging is also known as Newtonian relaxation, where the nudging relaxation terms are proportional to the innovation divided by a characteristic e-folding time inversely proportional to a nudging coefficient *G*. Nudging does not perform a direct insertion of observational information at a single point in space and time, but rather it applies the correction or innovation gradually in time and space based on the model terrain influences and prescribed / assumed weighting functions. For example, when a well-mixed PBL is present, one would generally want the influence of surface observations to be extended throughout the PBL, because in these conditions there is high correlation between errors in atmospheric fields at the surface and those anywhere within the PBL.

The multiscale multigrid FDDA method uses a combination of two forms of nudging: analysis nudging and observation ('obs') nudging. Analysis nudging is performed in model grid space where an objective analysis of observations (e.g., a modified Cressman scheme, Benjamin and Seaman 1985) is performed using the interpolated global analyses (e.g., from the GFS) as a background field. The resultant 'enhanced analysis' can then be used as the basis for analysis nudging. Analysis nudging is generally applied on coarser model domains where synoptic data can be used to produce a reasonable gridded analysis. Obs nudging is more attractive for finer-scale domains and asynoptic data. It is particularly effective where observational data density is sparse and corrections are applied only in the neighborhood of the observations, allowing the model to still add value in regions without any data by advecting observation information into the data-sparse regions and creating mesoscale structure not in the observations. In this case the nudging is performed in observation space, and the model field is interpolated to the observation site to compute the innovation that is then analyzed back to the model grid over some three-dimensional neighborhood in space, and over some time window. Quality control (QC) of observations is critically important for the success of both analysis nudging and observation nudging.

In the multiscale multigrid FDDA method applied in the RARE study, 3D-analysis nudging, as well as surface analysis nudging using higher temporal frequency surface data within the PBL (e.g., Stauffer et al. 1991), were performed on the outermost 12-km domain. Obs nudging is applied on at least the 12-km and 4-km domains. (Obs nudging is not applied on the finest 1.33-km model nest for the physics sensitivity studies described further below.) The finer domains thus have the benefit of improved lateral boundary conditions from the coarsest 12-km domain using both types of nudging, as well as the obs nudging performed directly on the 4-km nested domain. This project was one of the first applications of the multiscale FDDA strategy of Stauffer and Seaman (1994) in WRF. The newly developed OBSGRID module was used to produce gridded objective analyses similar to those produced by Rawins / Little_r in the MM5 system. The output files of OBSGRID can be used for 3D and surface analysis nudging and obs

nudging within WRF. OBSGRID takes as input raw WMO observations (both surface and upper air) and the output from WPS, which consists of large-scale gridded data (e.g., GFS output) horizontally interpolated to the model grid to be used in WRF. The outputs of OBSGRID relevant to this study include 1) pressure-level and surface objective analyses of the WMO observations (passing internal QC checks) using the GFS output interpolated to the model grid as background fields; the resultant analyses are then vertically interpolated to the WRF terrain-following "sigma" layers to be used for 3D analysis nudging; 2) surface analysis nudging files that can be directly used by WRF; 3) observation nudging files usable by WRF, and 4) files of the WMO observations including those passing the QC tests for use in the statistical verification software.

As mentioned above, for the physics sensitivity portion of the RARE study, 3D analysis nudging, surface analysis nudging, and obs nudging were performed on the 12-km domain (Grid 1); obs nudging was performed on the 4-km domain (Grid 2); and no nudging was performed on the 1.33- km domain (Grid 3). Thus Grid 3 has no direct FDDA tendencies and could be used to determine physics sensitivities, while still benefiting from improved lateral boundary conditions derived from the coarser grids that did have FDDA.

The following modifications were made to the WRF FDDA schemes for use in the baseline Alaska simulations. 1) The verification software was rewritten so that surface wind observations are verified against the third model half-layer from the ground (level closest to the 10-m observation level), while surface moisture and temperature observations are verified against the lowest model half-layer (level closest to the 2-m observation level). 2) A portion of the verification software that uses an assumed lapse rate to adjust model temperatures based on the difference between modeled and actual elevation was disabled, because this can lead to large errors in very stable conditions. 3) The surface analysis nudging and obs nudging codes were modified so that surface innovations for wind are computed and applied directly at the third model level. 4) Because surface wind observations directly relate to the third model layer and surface temperature and moisture observations directly relate to the lowest model layer, the similarity-based adjustments normally performed on model output for surface innovation computation was also disabled. 5) Hardwired vertical weighting functions for surface innovations were implemented into the surface analysis nudging and obs nudging codes, replacing the default functions that extend surface corrections to the model-predicted PBL height. The new functions had a vertical extent hardwired at about 150 m, which is a reasonable order of magnitude estimate for the maximum depth of nocturnal radiatively-driven stable boundary layers (SBL).

As a result of the physics sensitivity studies, the selected physics parameterizations included the Morrison cloud microphysics scheme (specifically designed for high-latitude simulations; Morrison et al. 2005 ), the RRTMG longwave / shortwave radiation package (Mlawer et al. 1997; Chen and Dudhia 2001), the Mellor-Yamada-Janjic PBL turbulence parameterization

(Janjic 2002) (as modified to be appropriate for the weak-turbulence conditions of very stable boundary layers), and the Rapid Update Cycle (RUC) land surface model (Smirnova et al. 2000). In particular, this physics suite seemed to have the best (least positive) temperature bias and best statistics during the periods when the surface temperatures were coldest and PM2.5 concentrations were the greatest. However, even with this physics configuration, the model's positive temperature bias could not be completely removed; furthermore, during other periods (such as the falling temperature periods in advance of a number of extremely cold episodes) the selected model physics suite seemed to have a negative temperature bias. It was thus strongly suggested that the actual meteorological analysis provided to the EPA be obtained from a final dynamic analysis simulation in which FDDA was also used to constrain the 1.33-km Grid 3 to the observations. However, there was concern that data assimilation of wind fields on Grid 3 would produce spurious low-level circulations in the model; furthermore, it was expected that the low-level circulations in both the actual atmosphere and the model would be driven by the low-level temperature fields. Thus, it was decided that in the delivered final dynamic analysis, that FDDA on Grid 3 would be done within all layers for temperature and moisture fields, but only within layers more than 150 m above the surface for wind fields. Also, the radius of influence for obs nudging on Grid 3 was reduced from the 100 km used on Grids 1 and 2 to 75 km. This value was obtained by computing the characteristic Grid 3 surface temperature innovation length scale through a correlation procedure that will be described in more detail in the next section.

## 3. WORK PLAN FOR NOV 2008 EPISODE

The current study covers the period 2-17 Nov 2008. Temperatures were relatively mild during the initial portion of this period (Figure 5), but then decreased to -17 °F (-27.2 °C) by the 7$^{th}$, as recorded by a portable Beta Attenuation Mass (BAM) monitoring unit in the Fairbanks / North Star Borough region. Temperatures then rebounded for about 5 days before the next cold outbreak which bottomed out again at (-11 °F) (-24 °C )by the 14$^{th}$. The low temperature periods corresponded to high PM2.5 concentrations as expected, especially towards the end of the study episode. However, the extremely cold temperatures, below (-22 °F) -30 °C, recorded during the Jan-Feb 2008 RARE episode did not occur during the Nov 2008 episode, and so the extreme effect of ice fog was not a factor. The final simulation of the episode was divided into four overlapping segments (12 UTC 01 Nov – 00 UTC 05 Nov; 12 UTC 04 Nov – 12 UTC 09 Nov; 00 UTC 09 Nov – 00 UTC 14 Nov; 12 UTC 13 Nov – 12 UTC 18 Nov). In order to facilitate the performance of initial sensitivity studies, an initial test period of 00 UTC 05 Nov – 12 UTC 09 Nov, encompassing one of the colder times during the Nov 2008 episode, was chosen.

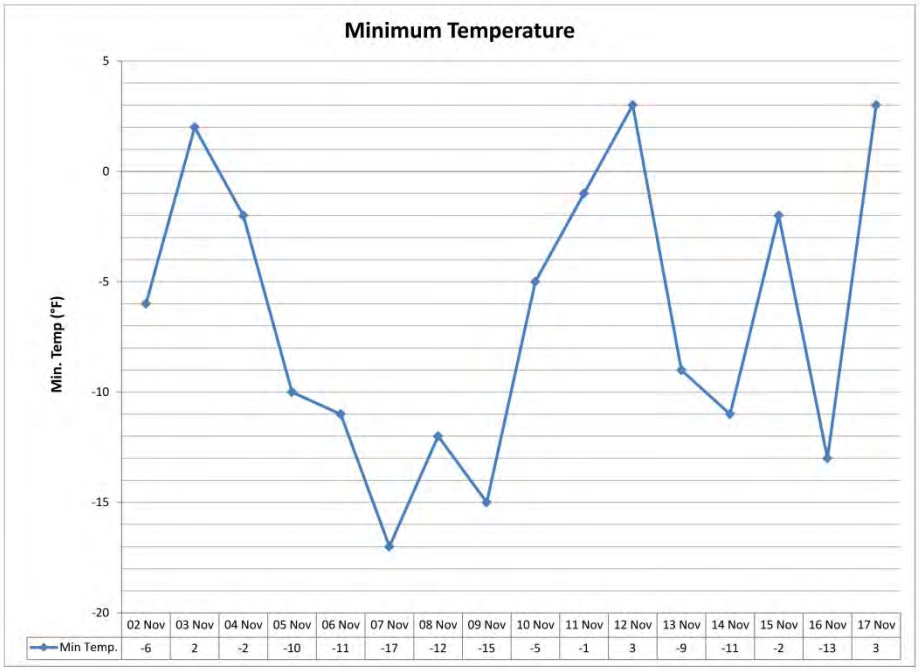


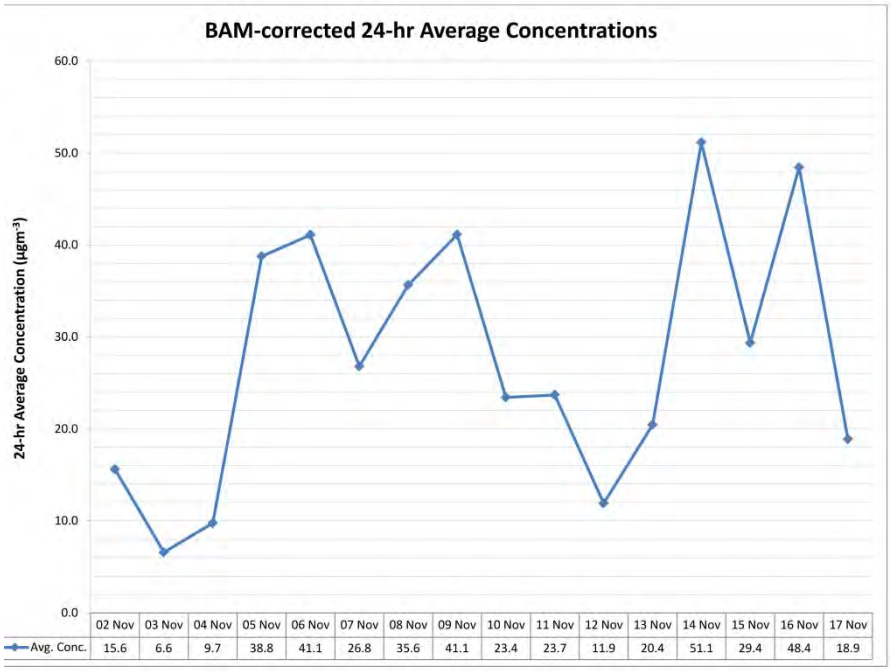


Figure 5 – Plot showing the daily minmun temperatures for the November episode in the Fairbanks region in Farenheit (top) and the BAM-corrected 24-hr average concentration of PM2.5 (bottom). Courtesy Bob Dulla, Sierra Research.

The grid configuration was taken directly from the EPA RARE study, although there are a few modifications relating to the use of observations for the November case as compared to the RARE study. The first involves the effective vertical resolution of the quality control procedure performed on the observations. The OBSGRID pre-processing software package compares point observations of a field such as temperature (either at a single level such as the surface or at multiple levels such as in a sounding) to the background analysis values of that field. For surface observations a direct comparison is performed between observed values of temperature and the background surface values. For sounding observations, if a vertical pressure level of the background analysis does not correspond to one of the pressure levels of that sounding, the observed sounding is interpolated in pressure space to the background pressure levels prior to the objective analysis and the values at the original observed sounding pressure levels are not retained. The result of this procedure is that the effective vertical resolution of sounding observations in the verification dataset and as used in the model is limited by the vertical resolution of the background analysis. In the GFS background fields the pressure levels are spaced 25 hPa apart near the surface, which corresponds to a distance in physical space of approximately 250 m. To alleviate this issue for the current study, a modified version of the GFS decoder, obtained from NCAR, permitted the generation of a background analysis with enhanced vertical resolution, with pressure levels spaced 5 hPa (~50 m) apart near the surface. It was hoped that the increased vertical resolution would improve the representation of the extremely shallow stable boundary layers characteristic of the winter season.

Another modification dealt with the specific objective analysis procedure used by OBSGRID. During the RARE project OBSGRID used either a Cressman scan procedure or a multiquadric analysis (Nuss and Titley 1994) depending on the number of observations at each vertical level. Since the RARE project, NCAR modified the OBSGRID code to provide the user with more flexibility in the objective analysis procedure. It was decided to use the Cressman method at each vertical level in order to produce more vertical consistency in the analysis; furthermore, each successive scan radius was set using the same method present in the Mesoscale Model version 5 (MM5) developed by the co-PI and others at Penn State.

Finally, a decision was made to make use of observations beyond those from the standard METAR observational dataset, in order to enhance the sparse local observational dataset. The total number of surface METAR stations within the Grid 3 domain is eight: Fairbanks (code PAFA), Eielson Air Force Base (PAEI), Ft. Wainwright (PAFB), Nenana (PANN), Delta Junction / Ft. Greely (PABI), McKinley Park (PAIN), Healy (PAHV), and Manley Hot Springs (PAML). Of these, only three could be said to lie in the focus region of the non-attainment area (Fairbanks, Eielson AFB, Ft. Wainwright). However, data from non-METAR surface stations for the period of Nov 2008 were located in the focus region during this project. The data quality from these stations is sometimes uncertain, and often standard METAR meteorological fields

(such as dewpoint) may be absent, but some of the data may be quite valuable, and many of them are used in the Meteorological Assimilation Data Ingest System (MADIS) that is run operationally by the National Weather Service. Stations from the non-METAR database are shown in Table 4.

Table 4: Non-METAR stations used for data assimilation and verification in current study. APRSWXNET – Automatic Position Reporting System as a WX NETwork; RAWS – Remote Automated Weather Station; AKDOT – AK Department of Transportation; MADIS – Meteorological Assimilation Data Ingest System

| Station | Database | Latitude | Longitude | Elevation (m) |
|---|---|---|---|---|
| Woodsmoke | Other MADIS | 64.781 | -147.284 | 145 |
| Goodpasture | RAWS | 64.238 | -145.267 | 463 |
| Healy (near Otto Lake Rd.) | APRSWXNET | 63.839 | -149.068 | 594 |
| Two Rivers | APRSWXNET | 64.873 | -147.174 | 229 |
| Fairbanks, near Farmer's Loop Rd. & Ballaine Rd. | APRSWXNET | 64.879 | -147.824 | 152 |
| Goldstream Creek | APRSWXNET | 64.894 | -147.876 | 176 |
| Livengood | RAWS | 65.424 | -148.722 | 137 |
| Ester Dome | APRSWXNET | 64.879 | -148.055 | 708 |
| Parks Hwy at Antler Creek | AKDOT | 63.810 | -148.965 | 462 |

A qualitative examination of the data from the non-METAR stations suggested that the temperature data are quite reasonable, although data gaps are more common than for most of the METAR stations. Most of these stations also provide wind data; while the actual values often seem quite plausible, the non-METAR stations overwhelmingly report zero wind speeds during the time period of this study. This is probably due to the relatively high start-up measurement threshold of the instruments used, making them inadequate to measure the very weak winds in the stable meteorological conditions. The one exception to this is Ester Dome, located 710 m above sea level on a ridge to the west of Fairbanks, which normally records a stronger flow. Many of the non-METAR stations also report pressure, but it was discovered that in some cases the pressure seemed to be reduced to the 1000-hPa level, whereas in other cases actual pressure was used. The value of pressure has some significance in that WRF uses potential temperature

as an internal variable, which is the temperature that would result if an air parcel is adiabatically compressed or expanded from its current pressure to the standard sea level pressure. An incorrect or misinterpreted pressure would lead to an erroneous potential temperature and thus an erroneous sense of the 'warmth' of a station. Thus, a decision was made to disregard any reported pressures from the non-METAR surface stations, and effectively use the model-predicted surface pressures to generate a self-consistent potential temperature field from the surface observations.

## 4. NEAR-SURFACE WIND ASSIMILATION

In the original RARE project a decision was made not to assimilate low-level wind data from surface stations on the 1.33-km (Grid 3). The reasoning was that the near-surface flow in these conditions was weak and predominantly thermally-forced (i.e., much of the existing wind circulation likely consists of topographically-forced drainage flows induced by air masses of varying temperatures). Thus, a numerical model may actually do a better job at capturing these flows than an observational network, especially a sparse observational network, and any data assimilation of observed near-surface winds within the model may erroneously override the development of these flows. The use of this data assimilation strategy in the RARE project did lead to realistic low-level flow patterns and produced generally satisfactory wind error statistics. However, the reported wind speed and wind directions statistics excluded cases where the observation wind report was calm. Including calm wind reports in the wind speed verification, by necessity, makes the wind speed bias more positive, because the model generated wind is never exactly zero. On the one hand, calm or near-calm conditions are common in extremely cold stable boundary layers, so representing them properly is of importance to this study. On the other hand, it is not clear how much of the positive model wind speed bias during calm wind reports is an artifact of insufficient instrument sensitivity. (More discussion on this issue will appear in the next section.) The reported surface temperature biases in the RARE project were also reasonable, but did tend to be positive during the periods of the weakest winds, which could be a direct consequence of positive model wind speed biases leading to too much turbulent mixing in the model. Because the extended dataset to be used in Nov 2008 case provided the potential for more surface data coverage over the Fairbanks region than that used in the Jan-Feb 2008, the possible use of near-surface wind data assimilation was revisited.

A comparison for the 5-9 Nov test period was performed between a simulation that used the RARE FDDA strategy on Grid 3, only nudging temperature and moisture near the surface (henceforth experiment T), and a simulation where additionally nudging of winds near the surface was performed (henceforth experiment TWIND). Statistics for the three local METAR stations are shown in Table 5. The wind speed statistics here include calm wind observations, but the wind direction statistics still do not, because wind direction cannot be defined in calm conditions. It can be seen that in experiment TWIND the wind speed RMSE statistics for all stations are reduced in comparison with experiment T; the reduction is modest but is about 10%

for Ft. Wainwright. The positive wind speed biases are also reduced, though their reduction is even more modest (no more than 0.02 m $s^{-1}$). Temperature statistics show a small sensitivity, although again Ft. Wainwright shows the greatest improvement in RMSE score. The biggest statistical difference between experiments T and TWIND resides in the wind direction RMSE scores, for which there is a 20 degree improvement for TWIND relative to T when the statistics for all stations are combined.

Table 5: Surface METAR statistics for experiments T and TWIND

| Temperature (°C) | T RMSE (MAE for wind direction) | TWIND RMSE (MAE for wind direction) | T Bias | TWIND Bias |
|---|---|---|---|---|
| Fairbanks | 1.71 | 1.72 | -0.07 | -0.15 |
| Eielson AFB | 1.83 | 1.80 | 1.20 | 1.18 |
| Ft. Wainwright | 1.36 | 1.32 | 0.05 | -0.05 |
| Three Stations | 1.70 | 1.68 | 0.42 | 0.36 |
| Relative Humidity (%) | | | | |
| Fairbanks | 4.21 | 4.31 | -0.54 | -0.59 |
| Eielson AFB | 7.39 | 7.50 | 3.59 | 3.70 |
| Ft. Wainwright | 17.55 | 17.89 | -16.59 | -16.96 |
| Three Stations | 9.31 | 9.49 | -2.06 | -2.11 |
| Wind Speed (m $s^{-1}$) | | | | |
| Fairbanks | 0.98 | 0.95 | 0.54 | 0.16 |
| Eielson AFB | 1.20 | 1.16 | 0.71 | 0.70 |
| Ft. Wainwright | 0.82 | 0.75 | 0.18 | 0.53 |
| Three Stations | 1.05 | 1.01 | 0.54 | 0.53 |
| Wind Direction (degrees) | | | | |
| Fairbanks | 49.1 | 32.6 | 26.2 | 22.4 |
| Eielson AFB | 66.2 | 37.6 | 42.0 | 16.7 |
| Ft. Wainwright | 93.1 | 74.2 | 35.8 | 36.2 |
| Three Stations | 73.1 | 53.8 | 33.2 | 28.4 |

This statistical improvement in wind direction statistics suggested that using near-surface wind FDDA on the 1.33-km Grid 3 should be recommended, once a subjective analysis of the wind field in simulation TWIND revealed no irregularities.

Though the wind direction improvement in experiment TWIND was encouraging, the relatively small improvement in surface wind speed statistics, and the lack of substantial improvement in surface temperature statistics, was puzzling. An examination of the time series of the statistics during the test period (Figure 6 - Figure **13**) suggests that while at Eielson AFB positive temperature biases are the norm during the early morning hours, this is not true at Fairbanks on 06 Nov, within one of a couple of prolonged periods of negative surface temperature biases at Fairbanks. (The time axes on the plots are in Coordinated Universal Time (UTC), so 00 UTC is 1500 Alaska Standard Time while 12 UTC is 0300 Alaska Standard Time, which correspond closely to the typical times of daily maximum and minimum temperatures, respectively.) Note that the location of the Fairbanks METAR is at the airport near the west end of the semi-circular topographical bowl in the region, while Eielson AFB is at the east end of this bowl and somewhat more distant from the neighboring ridges (Figure 3). If the time series of actual observed and modeled surface temperatures at the METARs are examined (Figure 14), it can be seen that for Eielson AFB and apparently for Ft. Wainwright the model is significantly too warm during the night (approximately -22 °C versus the observed -25 °C), consistent with the findings from the RARE study. (The gap during the night in the Ft. Wainwright observations is due to the fact that observations from that location are not typically reported during the night or on weekends.) However, on 06 Nov the Fairbanks observation reports a much warmer temperature (near -18 °C) than the other stations, and it shows significant oscillations but no trend of decreasing temperatures during the night. The modeled temperature time series in Figure 14 shows much less variability among the three stations; however, there is a warm spike in the modeled temperature at Fairbanks near 12 UTC 06 Nov that is reflective of the observations.

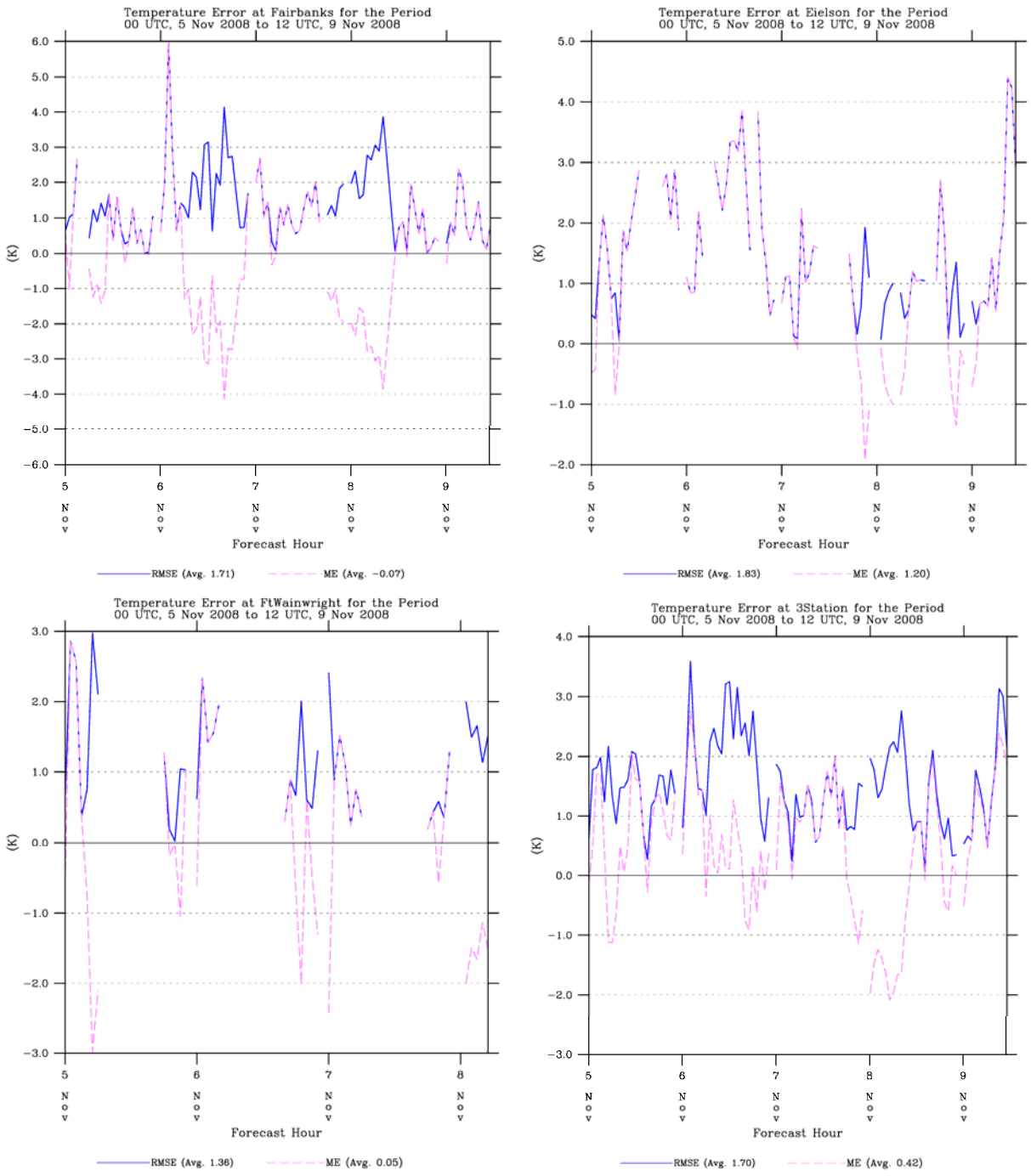


Figure 6: Temperature root mean square error (RMSE) and bias or mean error (ME) statistics for experiment T during the 00 UTC 5 Nov 2008 – 12 UTC 9 Nov 2008 test period at the local METAR surface stations. Statistics are for Fairbanks (top left), Eielson AFB (top right), Ft. Wainwright (bottom left) and all three stations combined (bottom right).

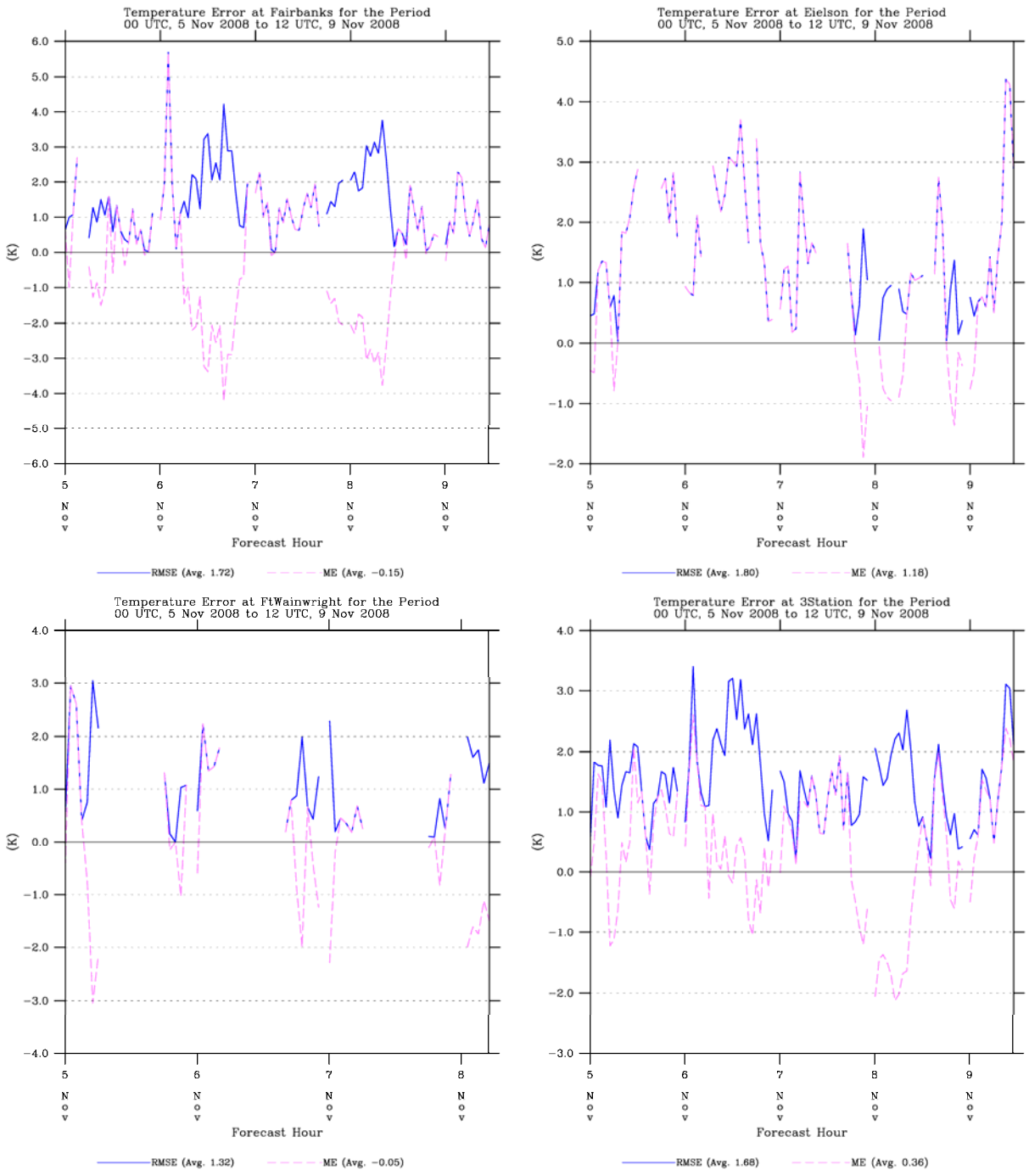


Figure 7: Same as Figure 6, but for experiment TWIND.

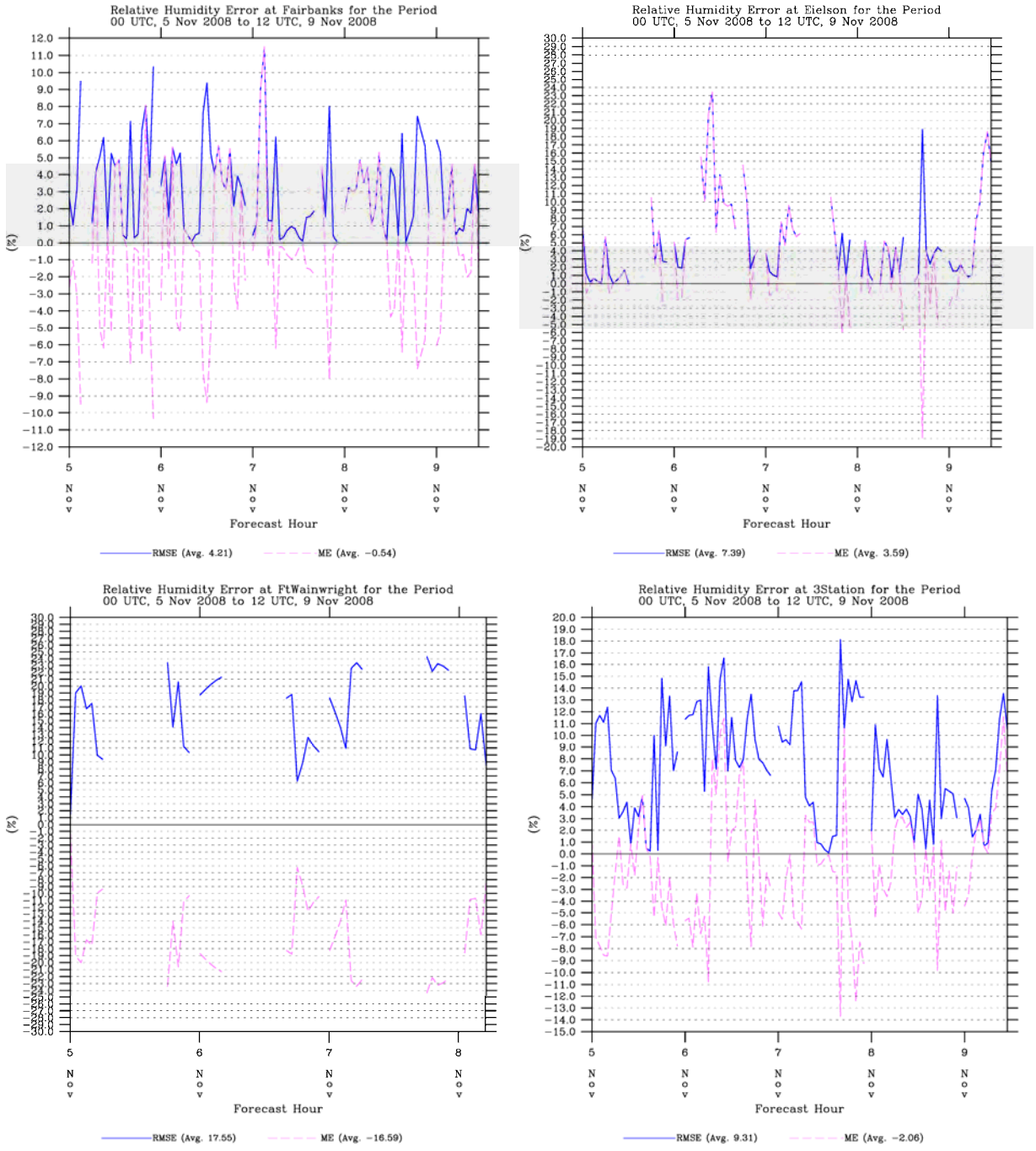


Figure 8: Relative humidity root mean square error (RMSE) and bias or mean error (ME) statistics for experiment T during the 00 UTC 5 Nov 2008 – 12 UTC 9 Nov 2008 test period at the local METAR surface stations. Statistics are for Fairbanks (top left), Eielson AFB (top right), Ft. Wainwright (bottom left) and all three stations combined (bottom right).

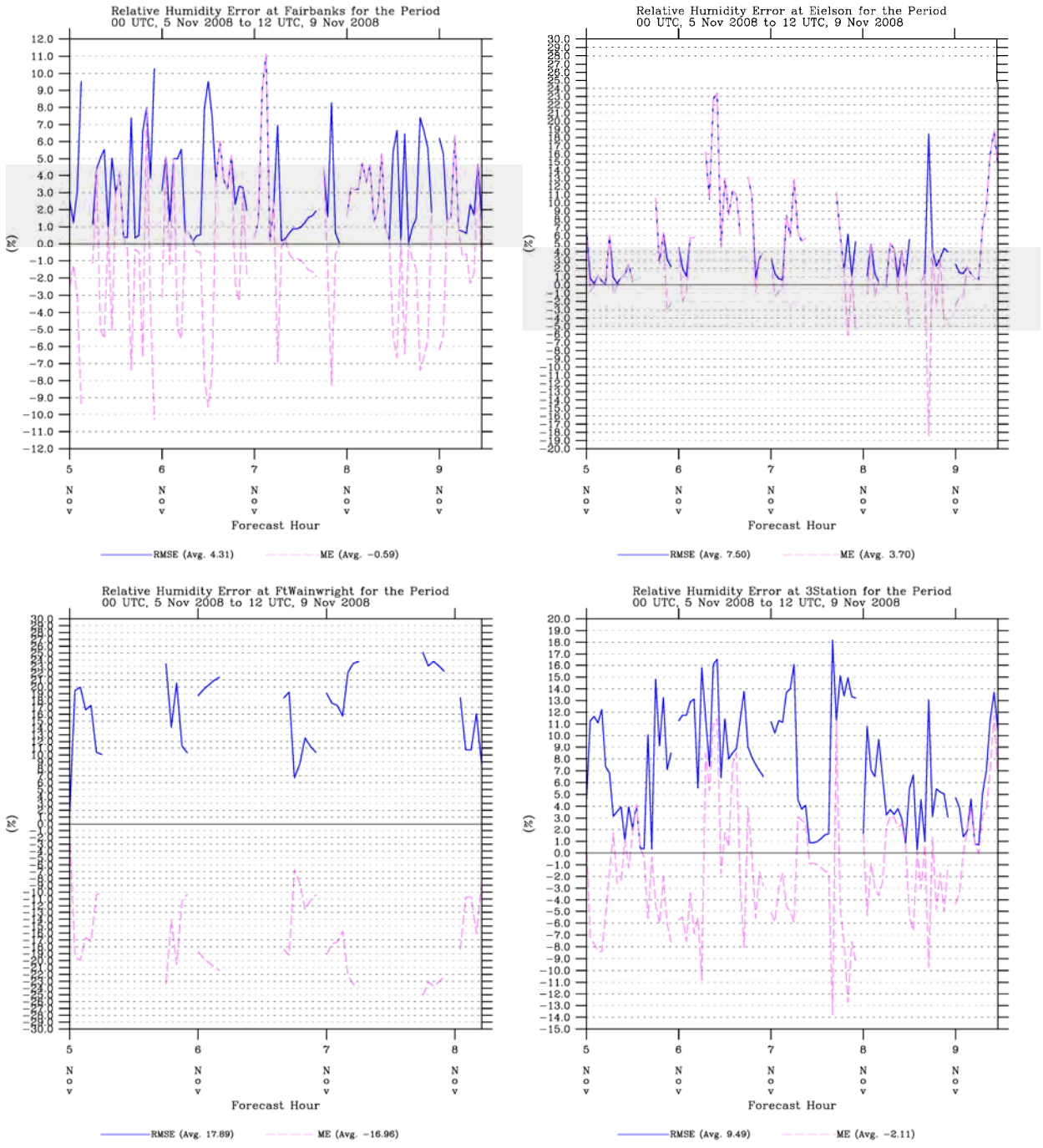


Figure 9: Same as Figure 8, but for experiment TWIND.

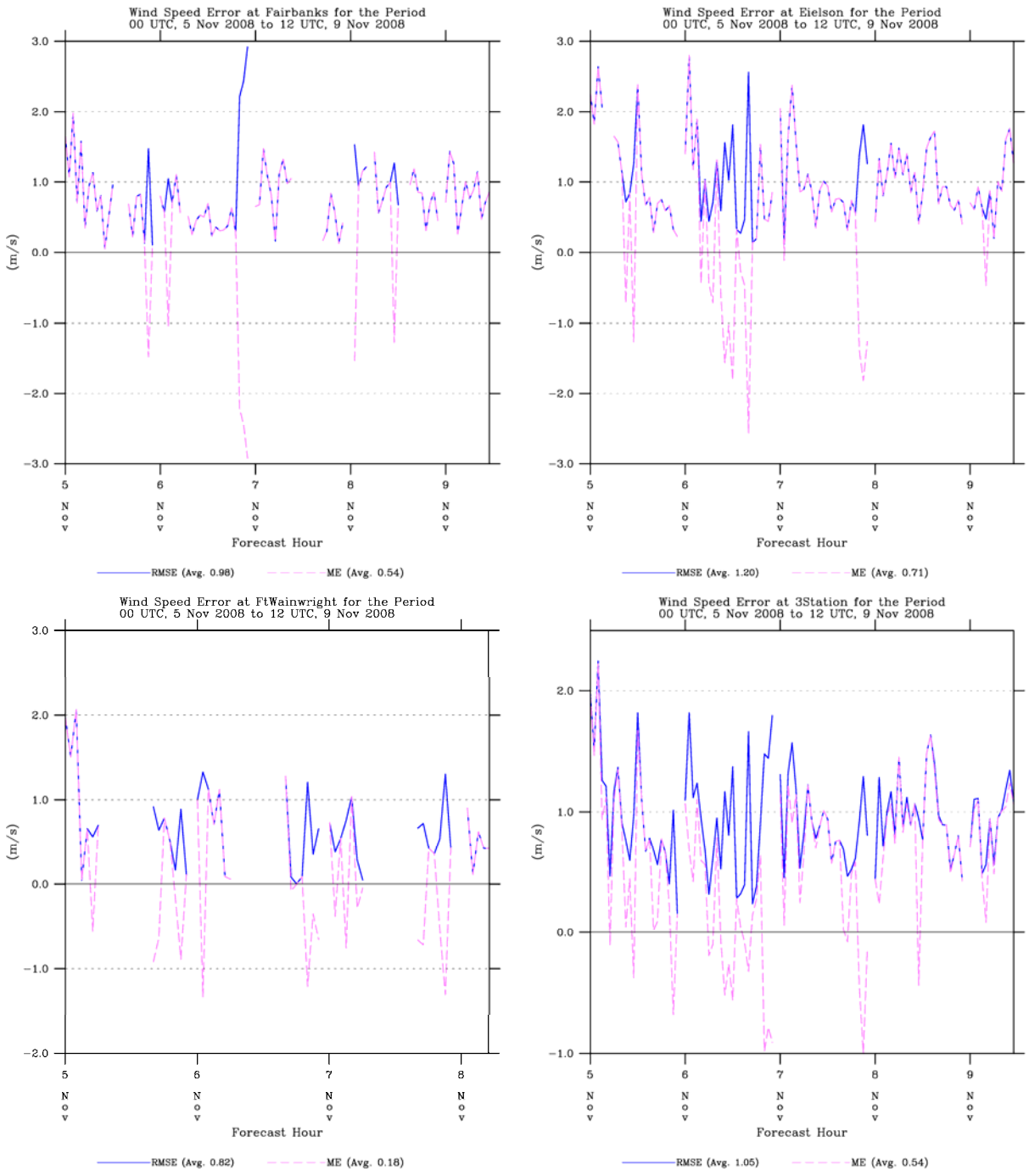


Figure 10: Wind speed root mean square error (RMSE) and bias or mean error (ME) statistics for experiment T during the 00 UTC 5 Nov 2008 – 12 UTC 9 Nov 2008 test period at the local METAR surface stations. Statistics are for Fairbanks (top left), Eielson AFB (top right), Ft. Wainwright (bottom left) and all three stations combined (bottom right).

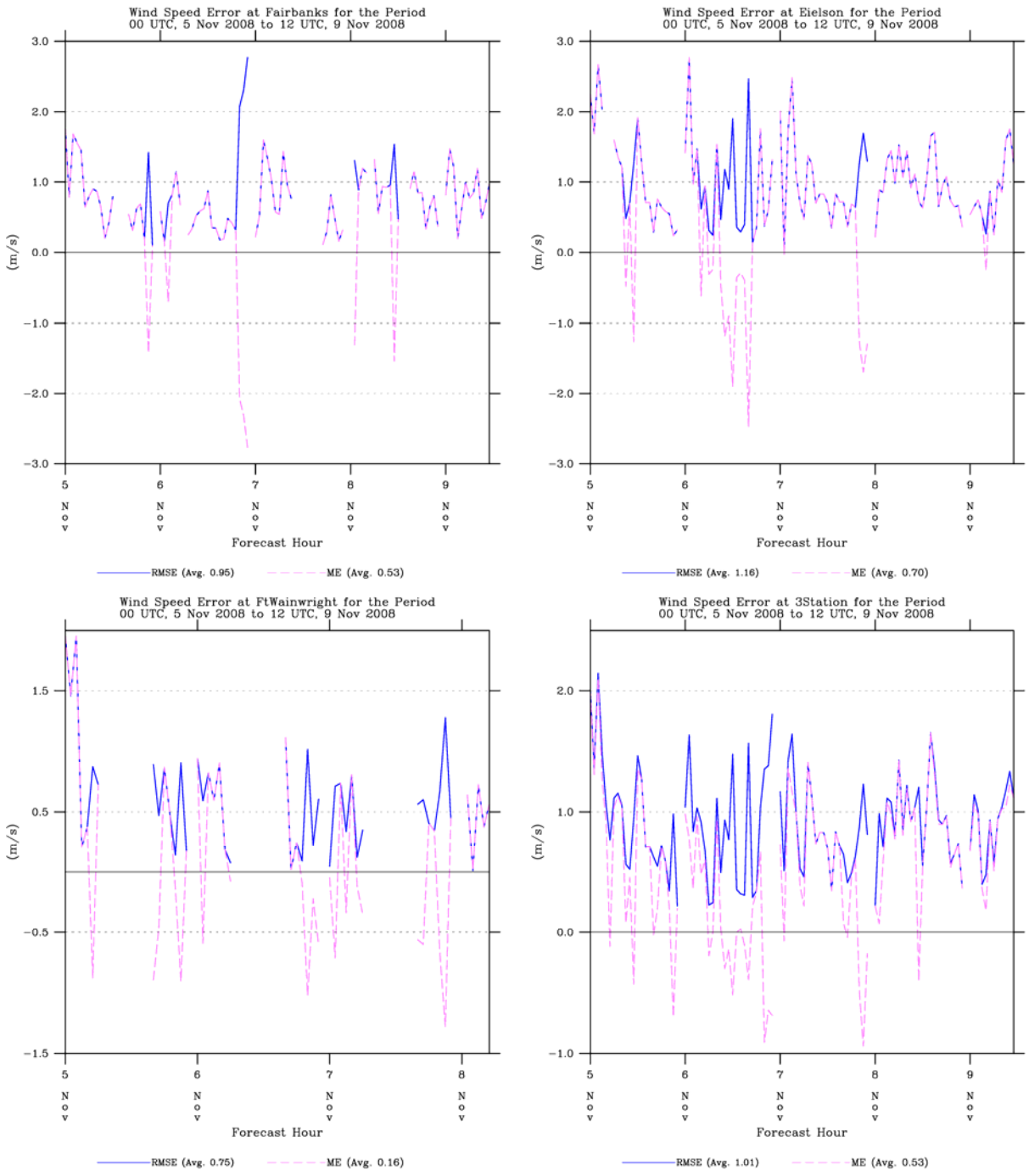


Figure 11: Same as Figure 10, but for experiment TWIND.

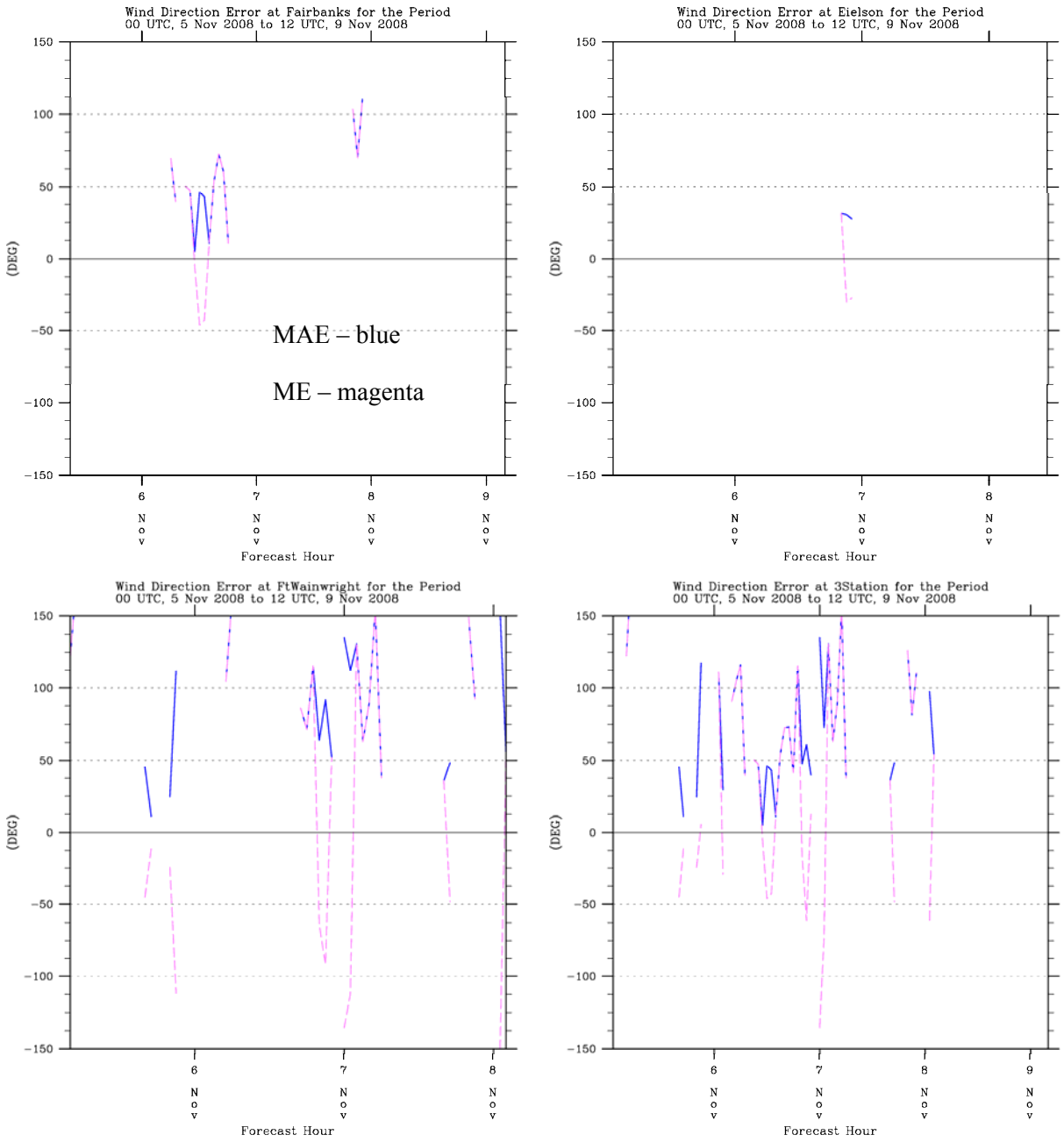


Figure 12: Wind direction mean absolute error (MAE) and bias or mean error (ME) statistics for experiment T during the 00 UTC 5 Nov 2008 – 12 UTC 9 Nov 2008 test period at the local METAR surface stations. Statistics are for Fairbanks (top left), Eielson AFB (top right), Ft. Wainwright (bottom left) and all three stations combined (bottom right).

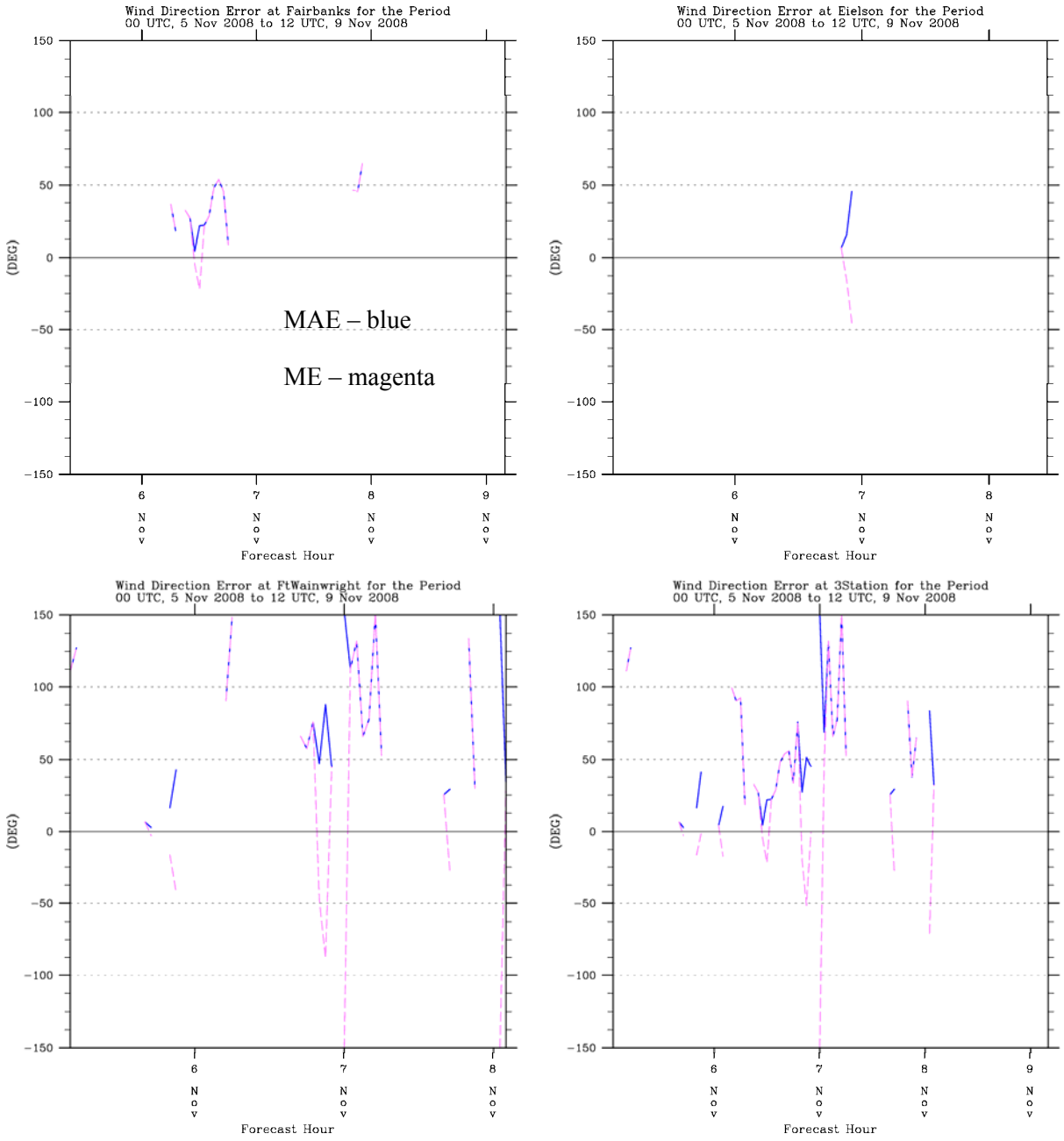


Figure 13: Same as Figure 12, but for experiment TWIND.

The corresponding time series of observed and modeled wind speeds (Figure 15) reveal that 06 Nov exhibits fairly strong wind speeds at Fairbanks (to about 4 m $s^{-1}$ or about 8 knots), especially compared to the other stations, which is probably due to the fact that the Fairbanks station is

closest to the perimeter of the stagnant air within the topographic semicircle. The model successfully reproduces some of the increased wind speed at Fairbanks at this time (2.2 – 2.8 m $s^{-1}$), but the maximum wind speed of 4.0 m $s^{-1}$ is underestimated. It is plausible that the anomalously warm temperatures at Fairbanks for this case are a direct consequence of increased wind speeds at this location, which lead to increased turbulent mixing and prevent the occurrence of the cold surface temperatures shown at the more stagnant locations at Ft. Wainwright and Eielson AFB. A plausible explanation of the errors in the model predictions is that the model is insufficiently resolving the differences in topography and location among the three stations, and effectively blending the effects of the observations of all three stations. The conclusion, then, is that surface wind data assimilation on Grid 3 seems to be beneficial, especially for wind direction, but that the radius of influence of wind observations should probably be reduced.

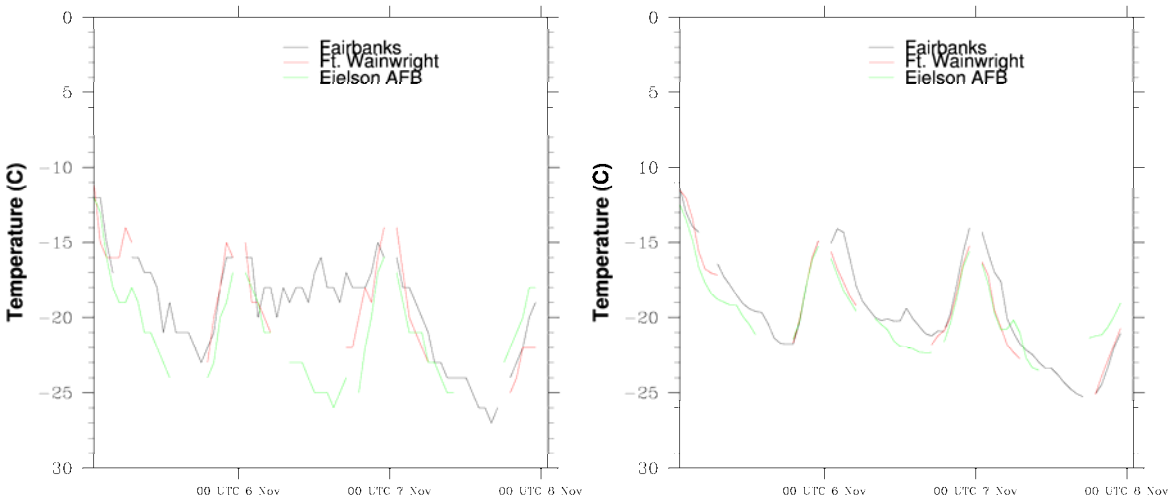


Figure 14: Time series of temperature for Fairbanks, Ft. Wainwright, and Eielson AFB from observations (left) and experiment TWIND (right)

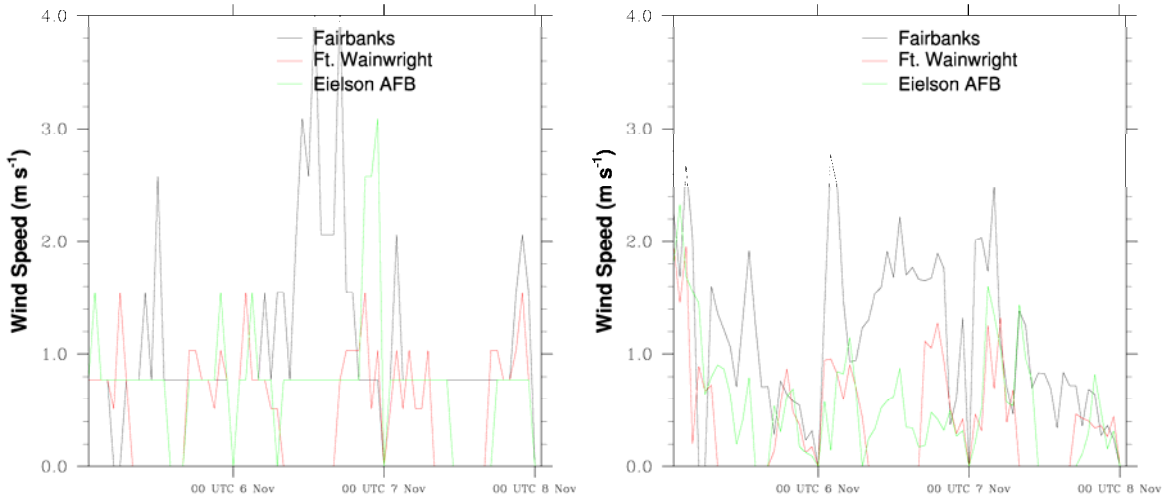


Figure 15: Same as Figure 14, but for wind speed

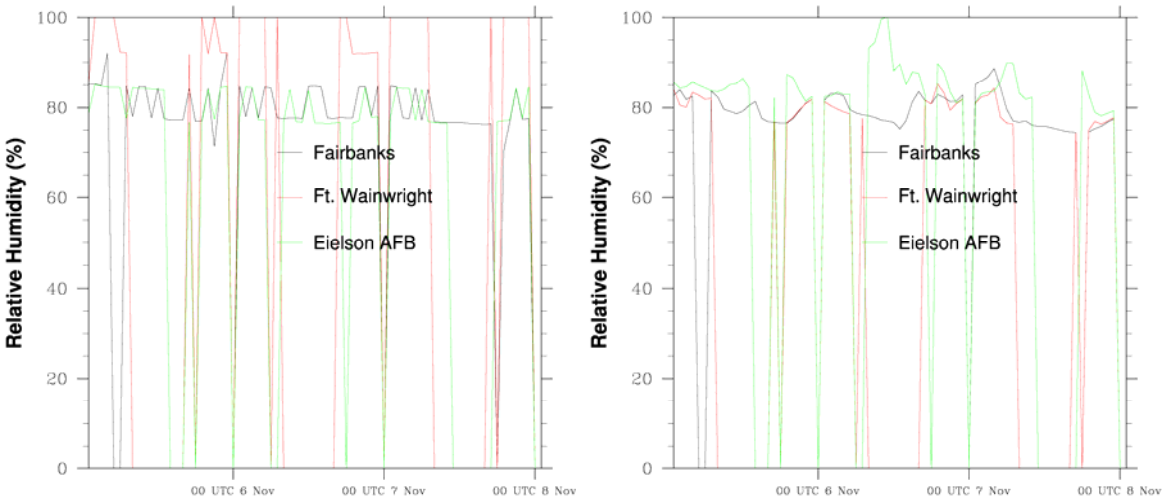


Figure 16: Same as Figure 14, but for relative humidity

Some insight into the characteristics of the relative humidity statistics can be found in Figure 16. The observations for stations other than Ft. Wainwright indicate relative humidity values are consistently near 80%. This is consistent with conditions near saturation with respect to ice but with relative humidity reported with respect to water saturation, when temperatures are on the order of -20 °C. However, Ft. Wainwright always reports relative humidity near 100% in these conditions. The model output at the Ft. Wainwright location tends to be closer to 80%, leading to the large positive relative humidity bias found in the Ft. Wainwright relative humidity

statistics. This could reflect the fact that Ft. Wainwright is erroneously reporting 100% relative humidity, based on the occurrence of ice crystals and other water condensate in the atmosphere, when in reality the atmosphere is ice saturated. However, it is interesting that the model does in fact produce conditions closer to water saturation near Eielson AFB during the day of 07 Nov, though the observations do not reflect this. Water saturation at temperatures as cold as -20 °C is difficult to maintain because of the large numbers of ice nuclei at these temperatures; after nucleation, ice crystals tend to deplete all water vapor above the ice saturation value and deplete all remaining liquid water via the Bergeron-Findeisen process. However, it is possible to maintain water saturation at these temperatures if the air is pristine. So a full explanation of these differences is not known at present.

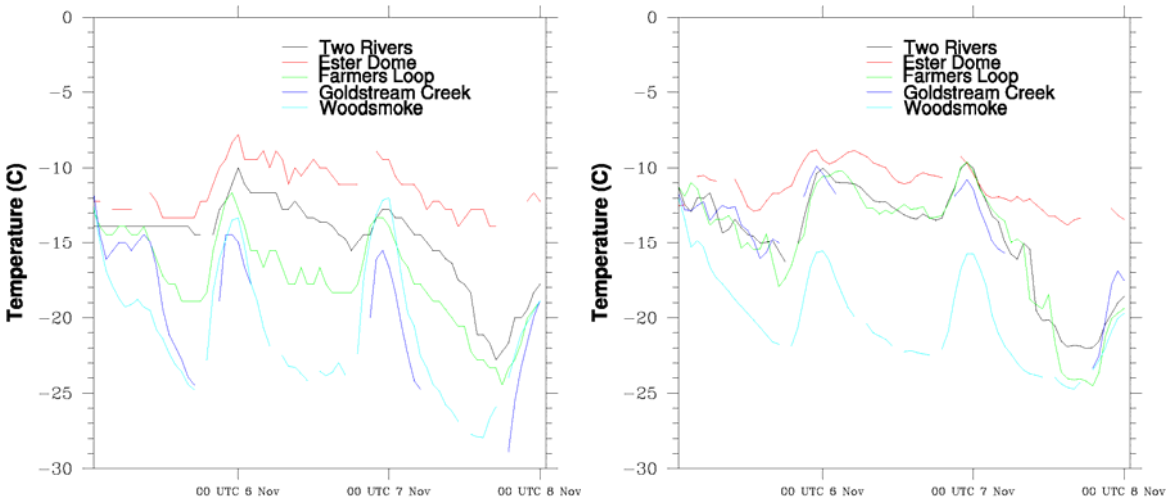


Figure 17: Time series of temperature for the local non-METAR surface stations from observations (left) and experiment TWIND (right).

Figure 17 shows the time series of observed and TWIND temperature at five non-METAR surface stations in the immediate Fairbanks region. The observed temperatures show that Woodsmoke and presumably Goldstream Creek behave like Eielson AFB and Ft. Wainwright, approaching -25 °C at night. The location near Farmer's Loop Rd. behaves somewhat like the Fairbanks METAR station in that it has temperatures decreasing to only about -18 °C at night. Two Rivers has even less of a nocturnal decrease of temperature, while Ester Dome remains near -10 °C for most of the period. This seems to confirm that the warmest temperatures during these episodes occur on the ridges while the coldest temperatures occur within the low spots of local valleys. Of these stations, Ester Dome is predicted very well by the model, helping corroborate the model skill for the atmosphere above the near-surface stable boundary layer. Two Rivers and Woodsmoke are also fairly well predicted by the model; the latter performance is notable because it confirms that the model configuration is capable of reproducing observed surface

temperatures at least as low as about -23 °C. These two stations also happen to be located at the east end of the Fairbanks / North Star Borough valley, near Eielson AFB. The model predicts approximately the same temperatures at Goldstream Creek and Farmer's Loop Rd. as at Two Rivers, but for Farmer's Loop Rd. and Goldstream Creek the resultant temperature is much too warm. It should be pointed out that these two stations are only about 2 km apart in physical distance, so it cannot be expected that a numerical model with 1.33-km horizontal grid spacing would be able to differentiate the temperature behavior between the two. All of the results considered together suggest that the model is able to predict the temperature evolution well in places both along the ridges and in the valley, but in other places the model is insufficiently resolving the actual difference in meteorological conditions between stations, whether the insufficient resolution is in the model terrain or in the way the model is treating observations in the data assimilation.

Statistics for wind speed are shown in Figure 18 for the non-METAR stations. This is an example of the fact that, other than Ester Dome, the wind instrumentation at these stations is generally not capable of recording what little wind is present. For Ester Dome itself, however, the magnitude of the wind speed peaks are well represented at the beginning of the test period. It can be seen that at the Woodsmoke station, the appropriately low model temperatures are accompanied by model wind speeds generally about 1 m $s^{-1}$ or less, while the other stations have model wind speeds that are usually above 1 m $s^{-1}$.

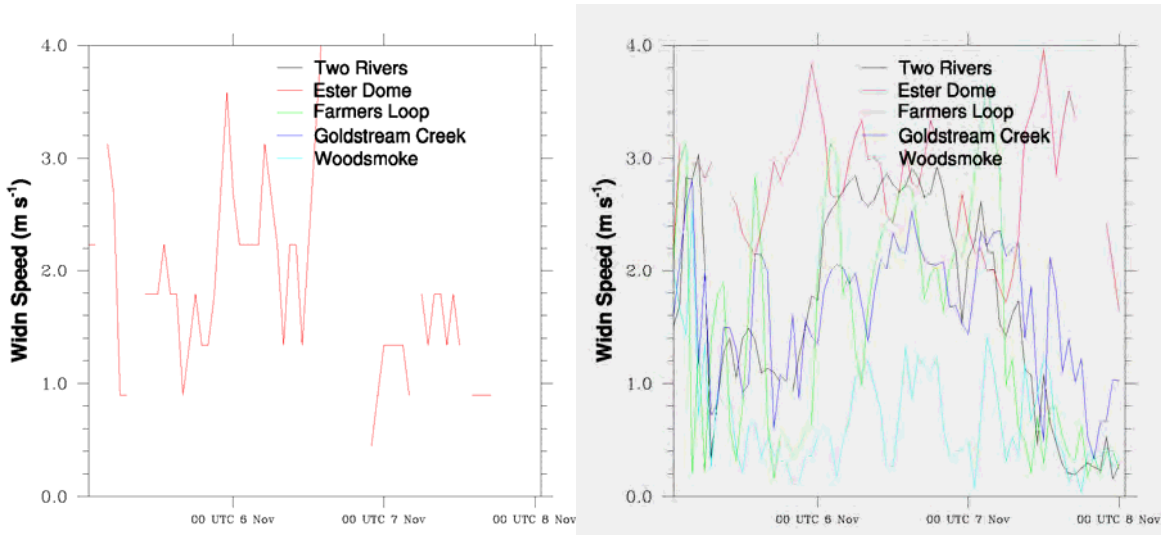


Figure 18: Same as Figure 17, but for wind speed.

Based on these results, it was decided to re-apply a procedure performed during the RARE study to derive an observation nudging correlation length scale based on the near-surface temperature field, and to use that radius of influence in subsequent model simulations. The procedure

consists of repeating the simulation with the same configuration, but with no FDDA of any sort performed on Grid 3. For each station on Grid 3, the temperature innovation (value of the observation minus the value of the model at that location) is computed at one hour increments. The correlation coefficient was then calculated between pairs of stations separated by known horizontal distances. Since the innovation for a variable is proportional to the nudging tendency for that variable, the typical distance over which innovations are correlated gives an indication of what the radius of influence should be. When this analysis was performed for the November case, it was discovered that the typical correlation distance was on the order of 30 km, substantially smaller than the 75 km value derived in the RARE project. (The ability to calculate a smaller radius of influence for the current study was aided by the presence of a denser surface observational network after the inclusion of the non-METAR stations.) It was thus decided to try a combination of a reduced radius of influence from 75 km to 30 km on Grid 3, along with a doubled value of the wind nudging strength on Grid 3 (from $4 \times 10^{-4}$ $s^{-1}$ to $8 \times 10^{-4}$ $s^{-1}$). The temperature nudging strength was left unaltered, because the extreme horizontal variability in the temperature field and its strong dependence on the local topography argue for a more conservative approach.

When the new experiment (henceforth TWIND2X30) was run on the test period, the results (Table 6 and Figure 19 - Figure **22**) showed even more improvement in surface wind direction errors for the three local METAR stations, with an average decrease in MAE of 19 degrees. Temperature RMSE scores were slightly better for Fairbanks, somewhat worse for Ft. Wainwright, but substantially better for Eielson AFB. Since Eielson AFB is relatively distant from most of the other stations, this is an indication that the reduced radius of influence was in fact an improvement. Relative humidity errors are also generally improved. On the other hand, wind speed RMSE scores were made slightly worse, by up to 0.16 m $s^{-1}$ for Ft. Wainwright.

Though there was no completely unambiguous choice, based on the test period results, for the optimal model configuration to produce the dynamic analysis for the entire 2-17 Nov 2008 episode, it was decided that, since the degradation in wind speed errors was slight while the improvement in wind direction errors was substantial, we would select the TWIND2X30 setup as the basis for further simulations.

Table 6: Surface METAR statistics for experiments TWIND and TWIND2X30

| Temperature (°C) | TWIND RMSE (MAE for wind direction) | TWIND2X30 RMSE (MAE for wind direction) | TWIND Bias | TWIND2X30 Bias |
|---|---|---|---|---|
| Fairbanks | 1.72 | 1.68 | -0.15 | 0.33 |
| Eielson AFB | 1.80 | 1.45 | 1.18 | 0.95 |
| Ft. Wainwright | 1.32 | 1.43 | -0.05 | 0.63 |
| Three Stations | 1.68 | 1.55 | 0.36 | 0.62 |
| Relative Humidity (%) | | | | |
| Fairbanks | 4.31 | 4.46 | -0.59 | -0.61 |
| Eielson AFB | 7.50 | 5.43 | 3.70 | 2.49 |
| Ft. Wainwright | 17.89 | 16.22 | -16.96 | -15.33 |
| Three Stations | 9,49 | 8.36 | -2.11 | -2.26 |
| Wind Speed ($m\ s^{-1}$) | | | | |
| Fairbanks | 0.95 | 1.01 | 0.16 | 0.60 |
| Eielson AFB | 1.16 | 1.24 | 0.70 | 0.82 |
| Ft. Wainwright | 0.75 | 0.91 | 0.53 | 0.27 |
| Three Stations | 1.01 | 1.10 | 0.53 | 0.63 |
| Wind Direction (degrees) | | | | |
| Fairbanks | 32.6 | 21.0 | 22.4 | 9.5 |
| Eielson AFB | 37.6 | 19.3 | 16.7 | 3.1 |
| Ft. Wainwright | 74.2 | 48.9 | 36.2 | 10.7 |
| Three Stations | 53.8 | 34.5 | 28.4 | 9.2 |

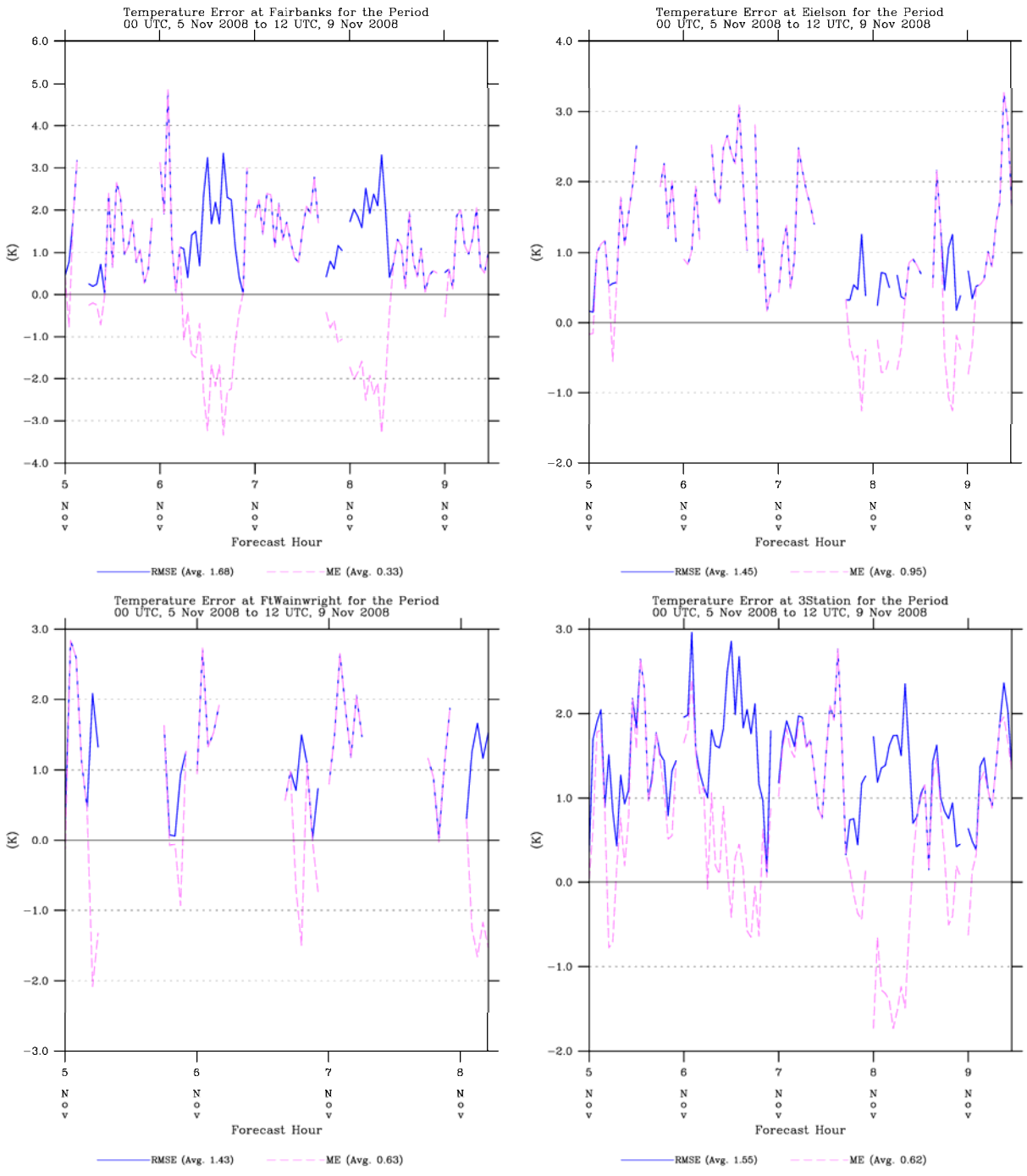


Figure 19: Same as Figure 6, but showing temperature statistics for experiment TWIND2X30.

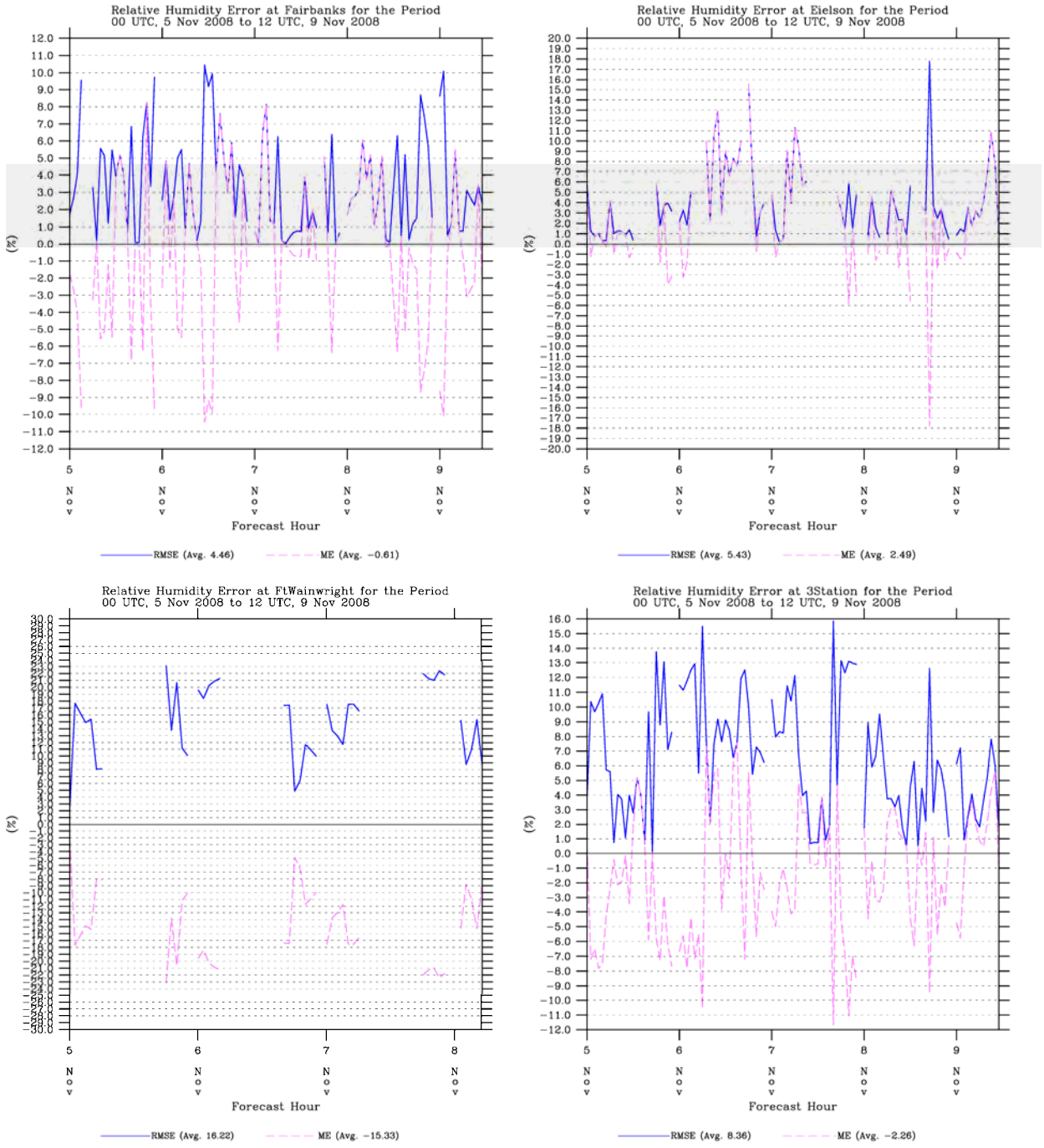


Figure 20: Same as Figure 8, but showing relative humidity statistics for experiment TWIND2X30.

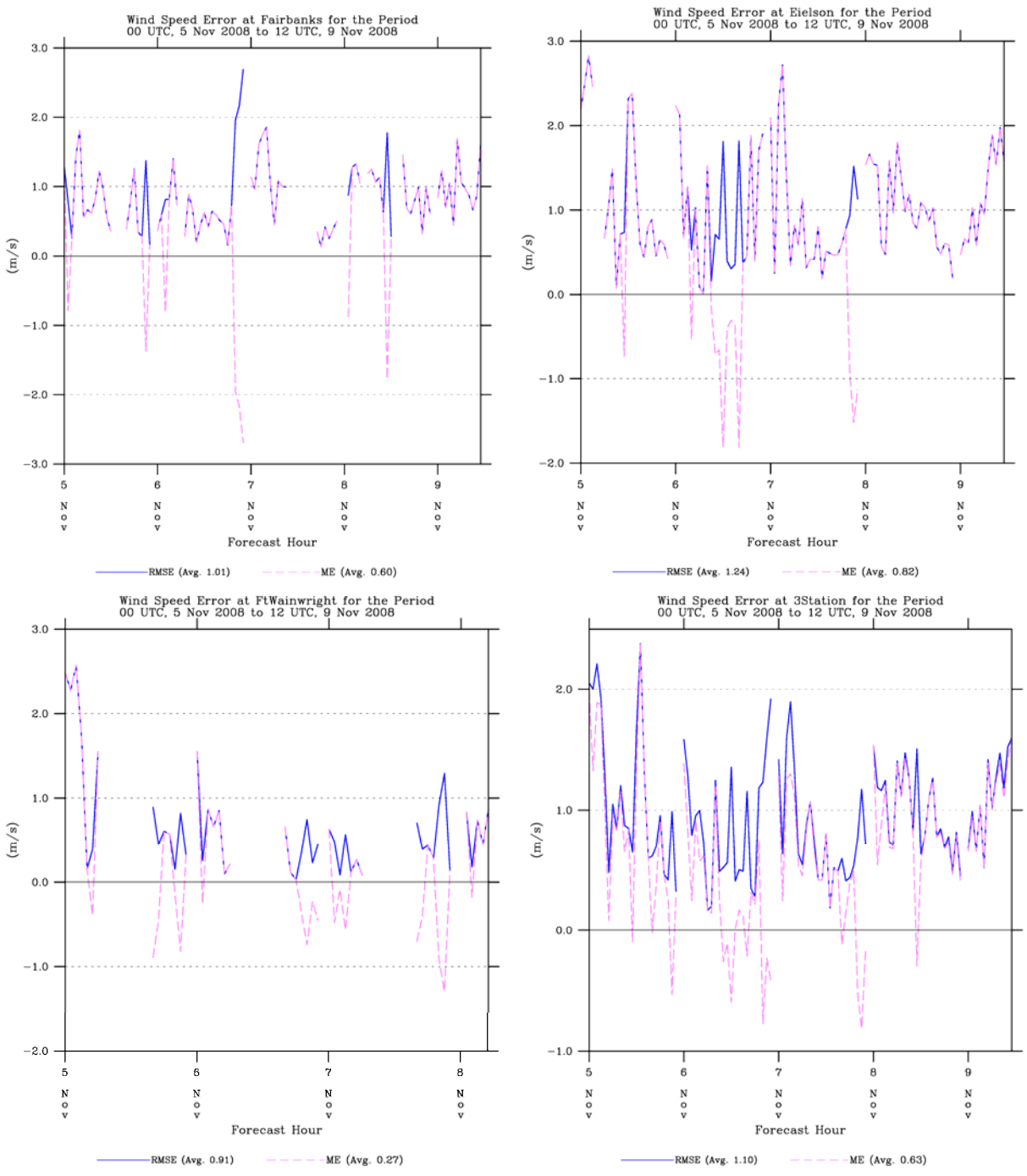


Figure 21: Same as Figure 10, but showing wind speed statistics for experiment TWIND2X30.

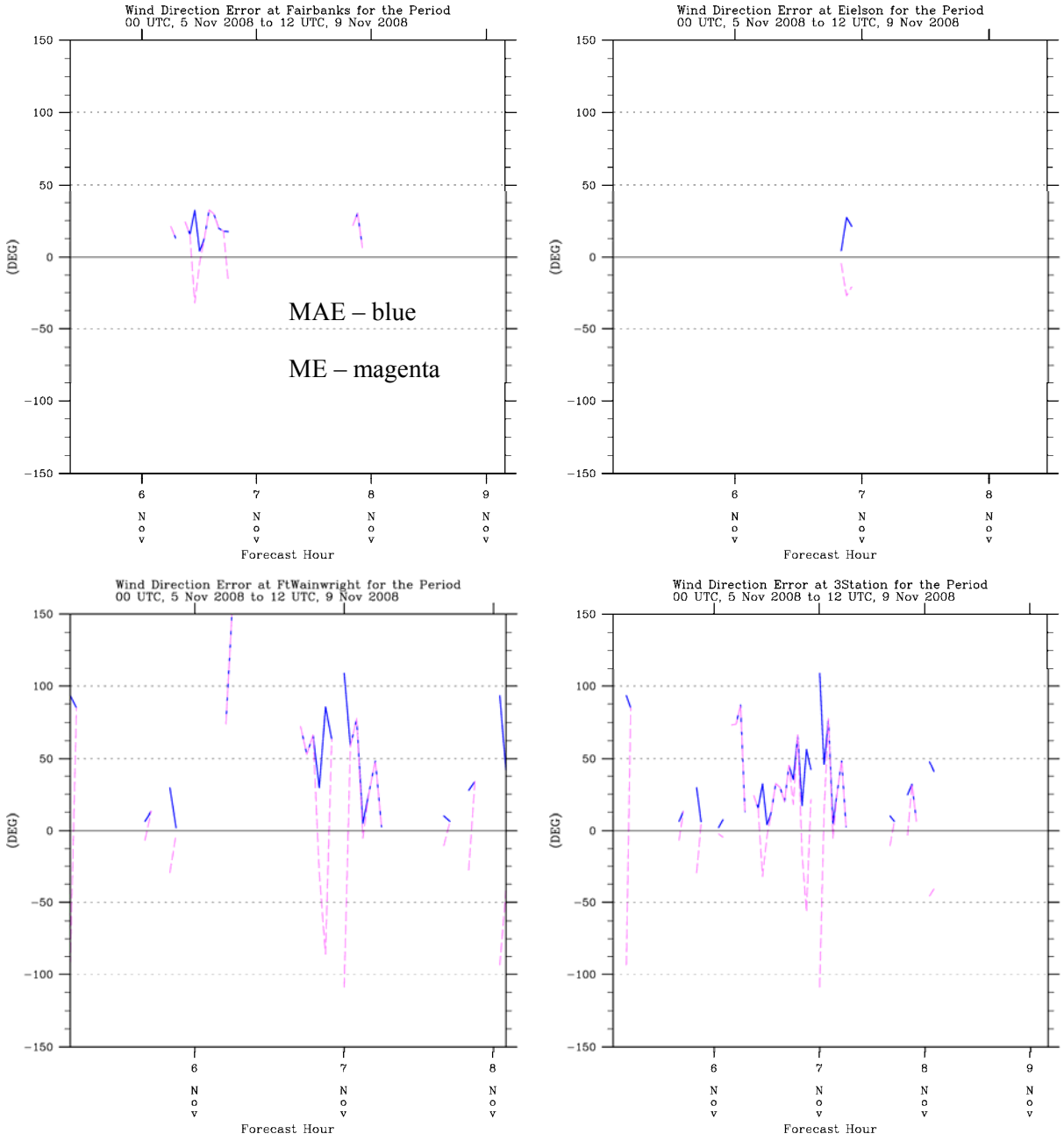


Figure 22: Same as Figure 12, but showing wind direction MAE and ME statistics for experiment TWIND2X30.

## 5. USE OF CALM WIND OBSERVATIONS

One issue of particular importance lies in the treatment of observations that report zero wind speed. It is often not clear, especially for non-METAR data, whether a report of zero wind speed indicates calm conditions, or indicates missing or faulty data. Furthermore, even if it is accepted that the data correctly represents calm conditions, in practice a report of calm generally indicates an actual wind speed that could have any value up to some minimum detection threshold. For automated METAR surface stations such as Fairbanks this threshold is 3 knots (=1.543 m $s^{-1}$). This is on the order of the model positive wind speed biases, which suggests that a (not-well-known) component of the model positive wind speed bias may be due to the model capturing actual atmospheric flows that are below the observational threshold. Furthermore, observations of calm winds do not provide usable guidance on the direction of the flow that does exist, which is of great importance for dispersion applications, and for which the model may be the only reliable source of information.

Because of these considerations, the default obs nudging data assimilation strategy is not to use calm wind reports. For the typical case of dense surface observing networks and non-stagnant meteorological conditions, this is entirely satisfactory. However, in the particular application of near-surface transport under very stable conditions, when only a few meters per second of flow can have a great effect on the transport of pollutants, and where the presence of non-calm surface wind observations are infrequent, the assimilation of near-surface calm winds should be considered.

As noted above, the great majority of the surface wind observations for these stable episodes are calm reports. Since the model appears to have a positive wind speed bias in these conditions, nudging towards a zero velocity wind vector near the surface may have a beneficial effect on reducing a positive wind speed bias. On the other hand, also as noted above, an unknown portion of the positive wind speed bias in near-calm conditions is an artifact of the model always having a wind speed above zero while observations indicate a wind speed of exactly zero when the wind speed is below the instrument threshold. Furthermore, since a calm wind observation does not provide guidance as to the wind direction, within the radius of influence of a calm surface observation there is the potential to degrade model predictions of wind direction at locations where the wind speed is not actually calm.

Table 7: Surface METAR statistics for experiments TWIND2X30CALM and TWIND2X30 for the November test period.

| Temperature (°C) | TWIND2X30CALM RMSE (MAE for wind direction) | TWIND2X30 RMSE (MAE for wind direction) | TWIND2X30CALM Bias | TWIND2X30 Bias |
|---|---|---|---|---|
| Fairbanks | 1.51 | 1.68 | 0.22 | 0.33 |
| Eielson AFB | 1.43 | 1.45 | 0.93 | 0.95 |
| Ft. Wainwright | 1.50 | 1.43 | 0.70 | 0.63 |
| Three Stations | 1.48 | 1.55 | 0.57 | 0.62 |
| Relative Humidity (%) | | | | |
| Fairbanks | 4.55 | 4.46 | -0.87 | -0.61 |
| Eielson AFB | 5.44 | 5.43 | 2.46 | 2.49 |
| Ft. Wainwright | 16.21 | 16.22 | -15.30 | -15.33 |
| Three Stations | 8.37 | 8.36 | -2.38 | -2.26 |
| Wind Speed (m $s^{-1}$) | | | | |
| Fairbanks | 0.97 | 1.01 | 0.54 | 0.60 |
| Eielson AFB | 1.18 | 1.24 | 0.72 | 0.82 |
| Ft. Wainwright | 0.96 | 0.91 | 0.29 | 0.27 |
| Three Stations | 1.07 | 1.10 | 0.57 | 0.63 |
| Wind Direction (degrees) | | | | |
| Fairbanks | 31.4 | 21.0 | 20.9 | 9.5 |
| Eielson AFB | 31.0 | 19.3 | 4.97 | 3.1 |
| Ft. Wainwright | 83.7 | 48.9 | 5.9 | 10.7 |
| Three Stations | 57.1 | 34.5 | 11.3 | 9.2 |

A final sensitivity test to the effect of including calm wind reports in the data assimilation procedure of experiment TWIND2X30, henceforth experiment TWIND2X30CALM, was performed. Statistics for the two experiments performed over the test period are shown in Table 7. The assessment of the comparison is mixed. Overall temperature biases and wind speed biases are improved by about 10% in experiment TWIND2X30CALM (note however that a 10% improvement of wind speed bias in this case amounts to less than 0.1 m $s^{-1}$ which is certainly less than the instrumentation precision), and temperature RMSE scores are improved by about 5%. However, both statistics are actually degraded for the Ft. Wainwright station. Furthermore, overall wind direction MAE statistics are over 20 degrees worse in experiment TWIND2X30CALM than in experiment TWIND2X30. Recall that in wind direction statistics calm wind observations are excluded from the verification dataset; therefore, a degradation of wind direction statistics in experiment TWIND2X30CALM means that the inclusion of calm wind reports in the data assimilation is having an adverse affect on the model-generated winds at other locations that are not reporting calm winds.

The decision between using simulation TWIND2X30CALM and TWIND2X30 was even more challenging than the decision between simulation TWIND and TWIND2X30. However, despite the beneficial reduction in the positive wind speed bias in TWIND2X30CALM, because of the importance of wind direction prediction to dispersion calculations in these conditions, and because wind direction was the variable that showed the most statistical variability between different experiments, a final decision was made to simulate the whole 2-17 Nov 2008 episode using the TWIND2X30 setup (although a parallel simulation of the entire episode using TWIND2X30CALM was also performed). The time series of the entire episode are presented in Figure 23 - Figure **26**. It appears that the statistics for the whole 2-17 Nov 2008 episode are somewhat worse than the statistics for just the test period, particularly for the temperature statistics during 2-5 Nov, 13-14 Nov, and 17-18 Nov. These three periods of greater-than-typical temperature RMSE scores are actually characterized by negative temperature biases, and meteorologically are characterized by extensive cloudiness and frequent reports of snow. Failure of the model to properly represent these events and the cloudiness in particular could explain the negative temperature biases. The periods of coldest temperatures adjacent to these events have positive temperature biases at these stations, but these are generally of the order of 2 °C or less. The overall three-station temperature bias for the whole episode is negative (-0.9 °C), and the overall temperature RMSE of 2.4 °C is comparable to what was obtained in the RARE project. The overall wind speed bias for the whole Nov 2008 episode for the three METAR stations is almost exactly the same as it is for just the test period (+1.0 m $s^{-1}$). The overall wind direction MAE of 41 degrees for these stations is slightly better than what we have observed in SBLs over central Pennsylvania using unfiltered wind data. These results give us confidence that our general model configuration is performing as intended, though possibilities for improvement still exist.

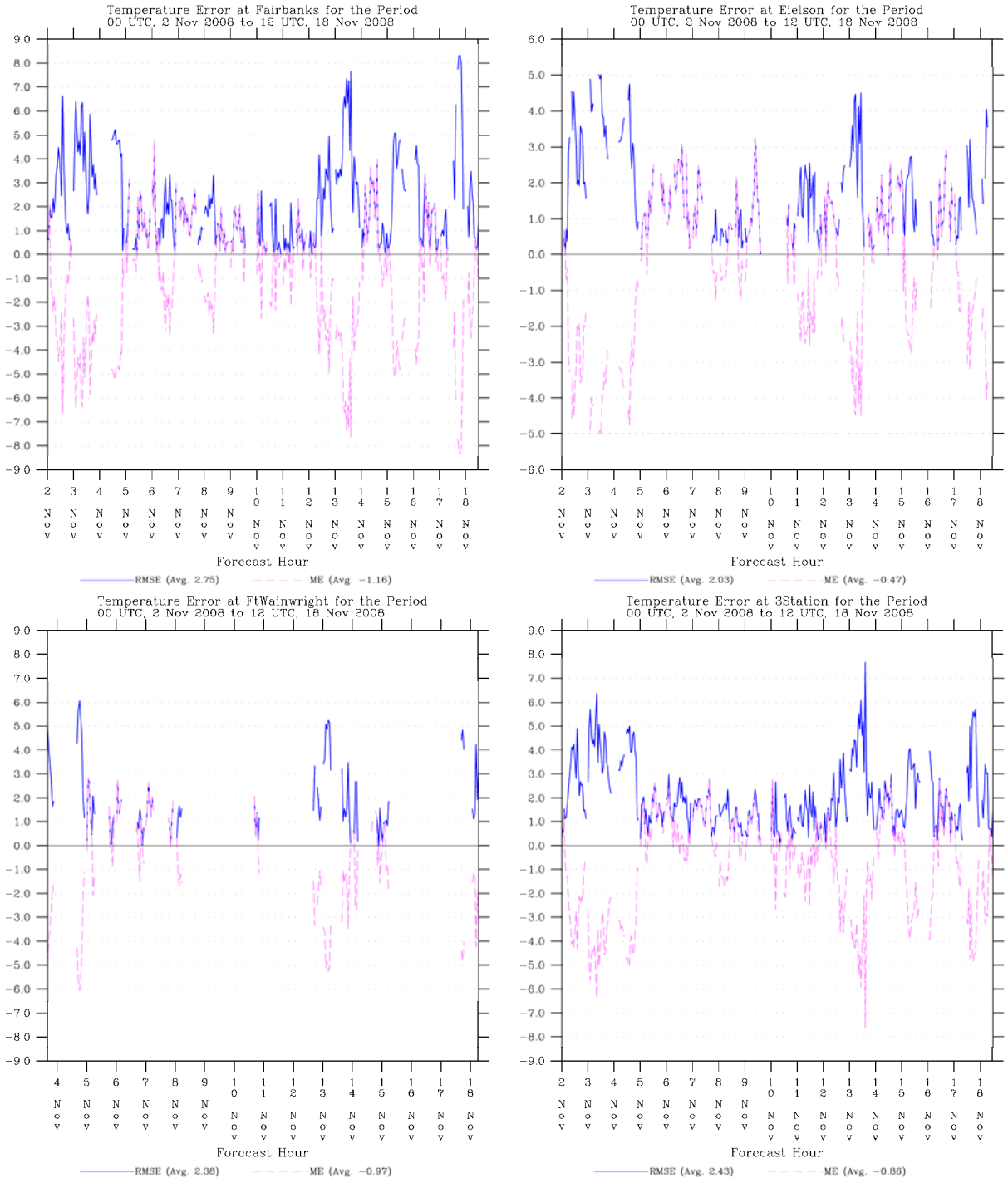


Figure 23: Temperature statistics for experiment TWIND2X30 over the entire 00 UTC 2 Nov 2008 – 12 UTC 18 Nov 2008 test episode at the local METAR surface stations.

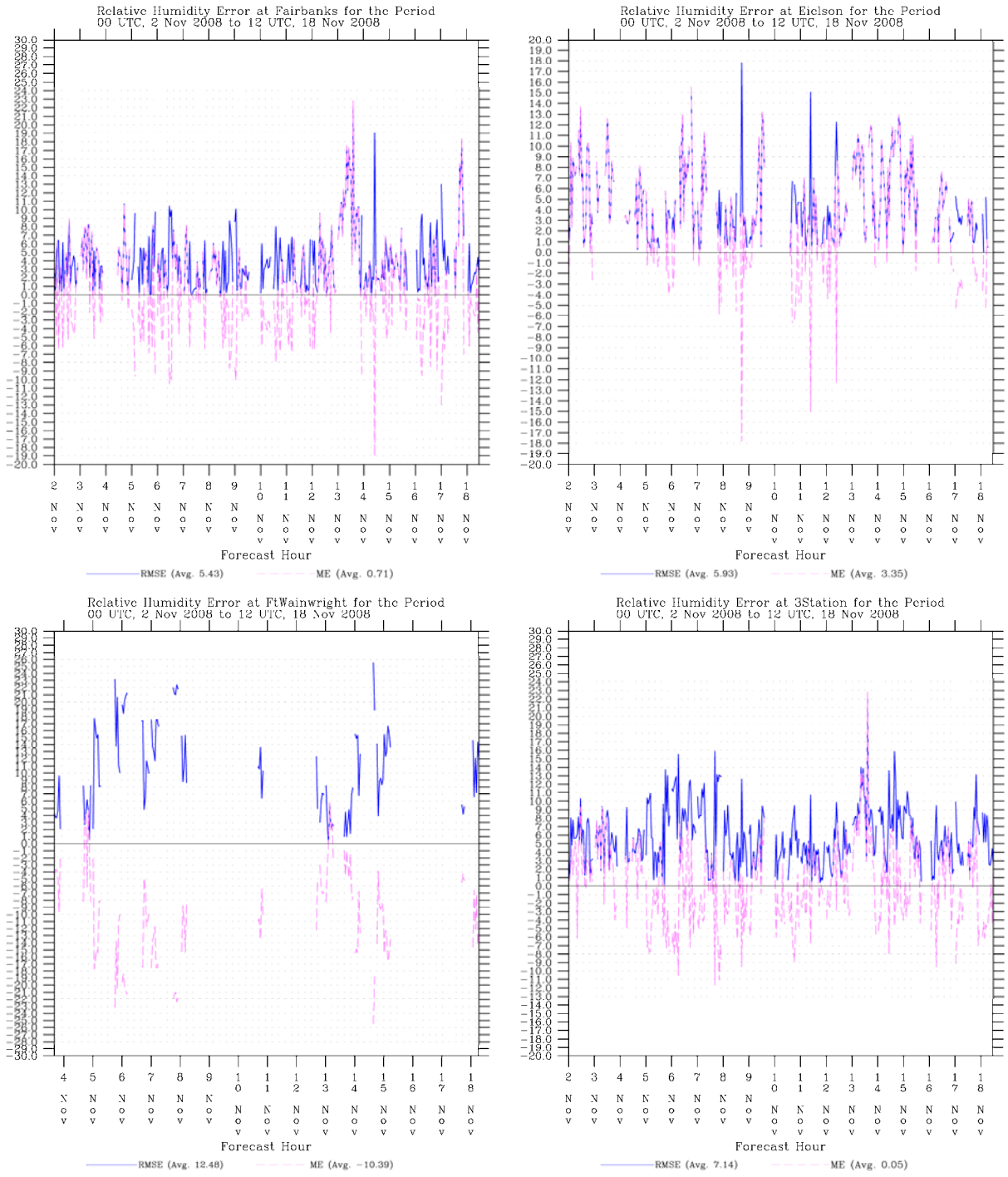


Figure 24: Same as Figure 23, but showing relative humidity statistics.

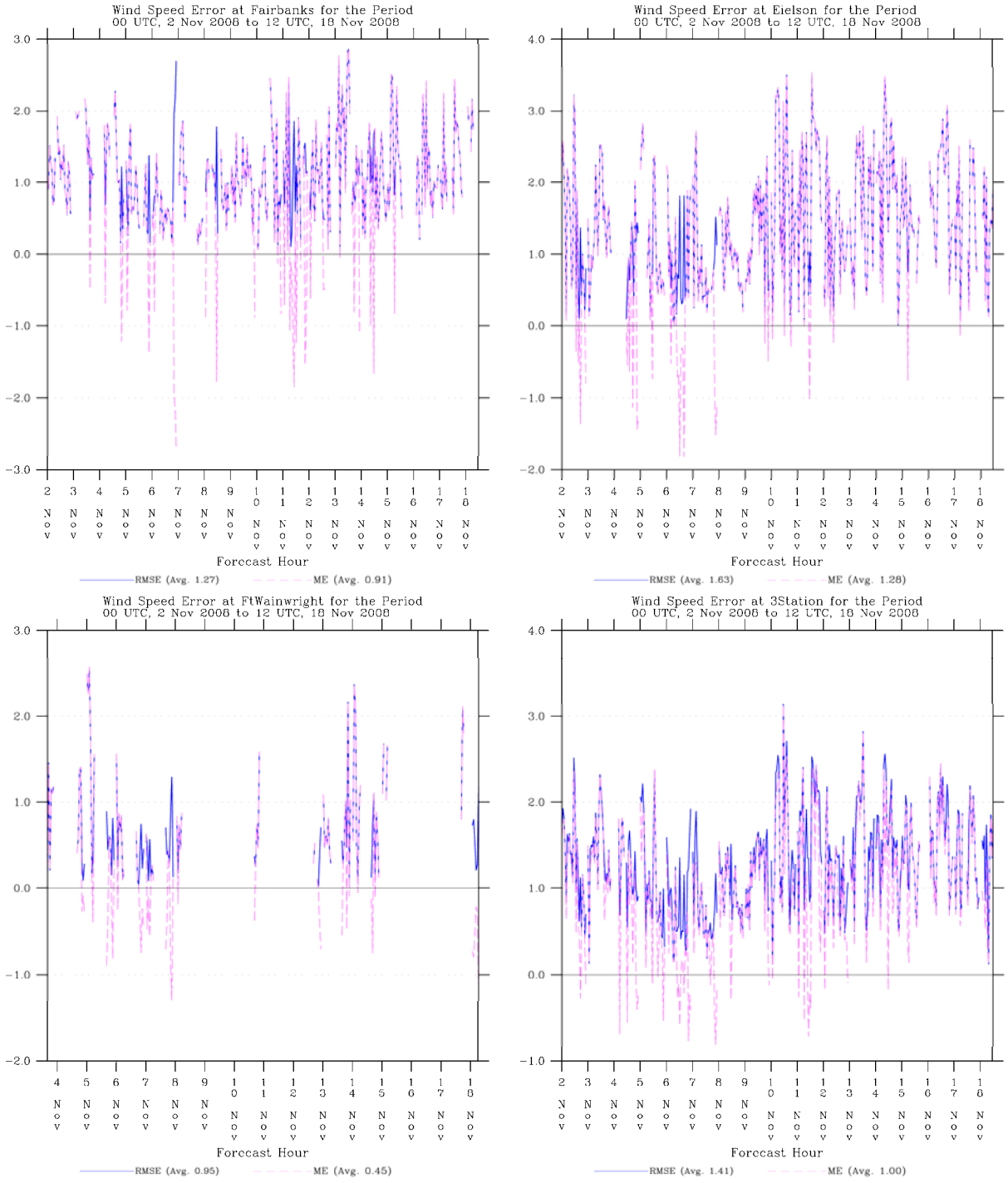


Figure 25: Same as Figure 23, but showing wind speed statistics.

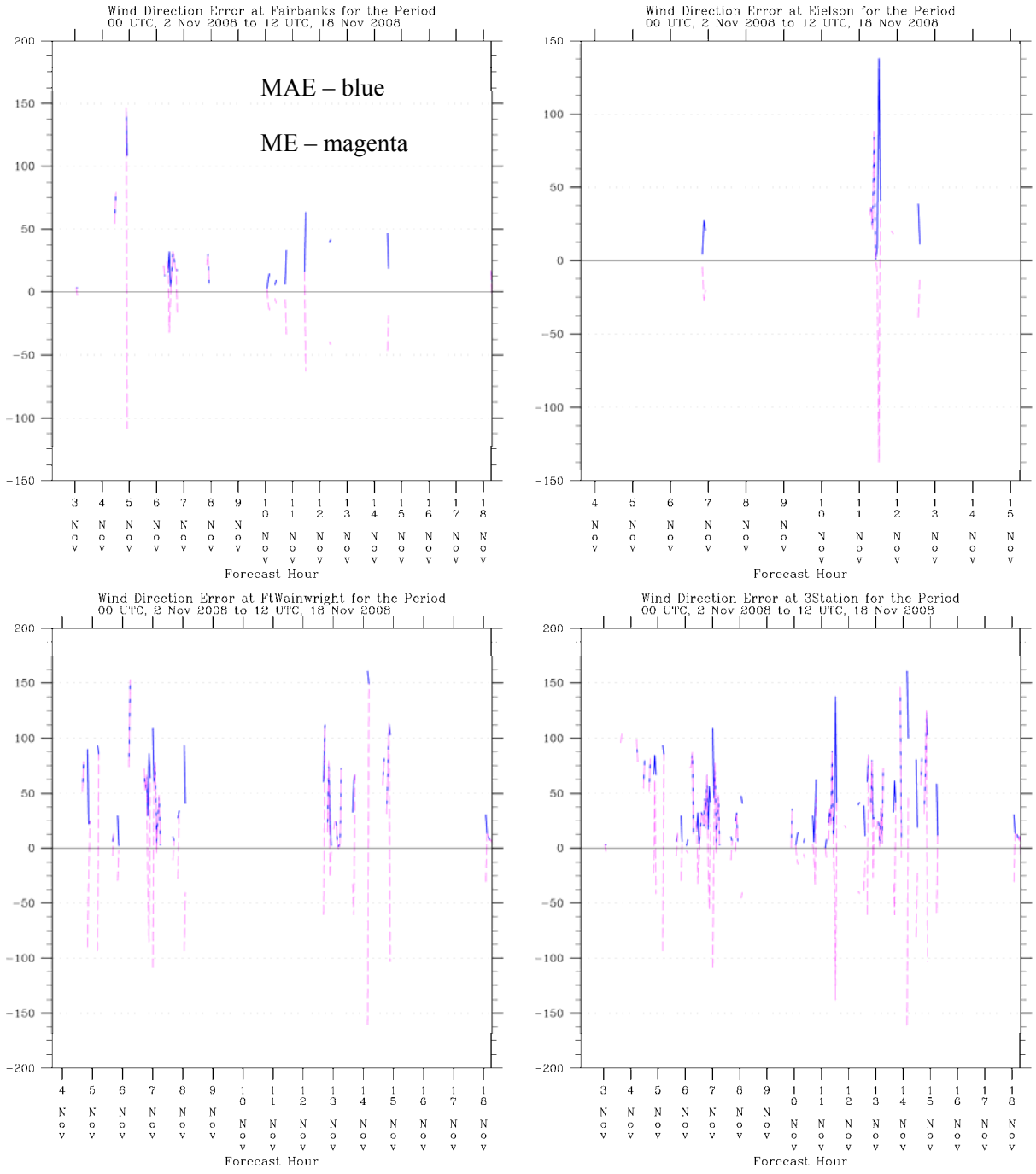


Figure 26: Same as Figure 23, but showing wind direction statistics.

For reference, a comparison between the statistics for the TWIND2X30CALM and TWIND2X30 model configurations for the entire November episode are presented in Table 8. Essentially, the same tendencies found for the November test period apply to the entire November episode as a whole. The superior configuration for temperature depends on statistic and station, and in all cases the sensitivity to calm wind inclusion is never more than about 0.15 °C. Positive wind speed biases are reduced by the inclusion of calms by on the order of 0.1 m $s^{-1}$ for Fairbanks and Eielson, but are actually increased at Ft. Wainwright. Again, the one substantial sensitivity is in wind direction error, for which TWIND2X30 has the better performance.

Finally, detailed time series of the statistics and modeled and observed values of surface meteorological variables, for both METAR and non-METAR stations, are presented in Appendix A for the TWIND2X30 simulation of the November episode that was provided to ADEC.

Table 8: Same as Table 7, but over entire November episode.

| Temperature (°C) | TWIND2X30CALM RMSE (MAE for wind direction) | TWIND2X30 RMSE (MAE for wind direction) | TWIND2X30CALM Bias | TWIND2X30 Bias |
|---|---|---|---|---|
| Fairbanks | 2.64 | 2.75 | -1.30 | -1.16 |
| Eielson AFB | 2.03 | 2.03 | -0.46 | -0.47 |
| Ft. Wainwright | 2.44 | 2.38 | -0.94 | -0.97 |
| Three Stations | 2.38 | 2.43 | -0.92 | -0.86 |
| Relative Humidity (%) | | | | |
| Fairbanks | 5.49 | 5.43 | 0.75 | 0.71 |
| Eielson AFB | 6.01 | 5.93 | 3.42 | 3.35 |
| Ft. Wainwright | 12.39 | 12.48 | -10.40 | -10.39 |
| Three Stations | 7.17 | 7.14 | 0.10 | 0.05 |
| Wind Speed (m $s^{-1}$) | | | | |
| Fairbanks | 1.22 | 1.27 | 0.84 | 0.91 |
| Eielson AFB | 1.51 | 1.63 | 1.16 | 1.28 |
| Ft. Wainwright | 1.00 | 0.95 | 0.49 | 0.45 |
| Three Stations | 1.33 | 1.41 | 0.93 | 1.00 |
| Wind Direction (degrees) | | | | |
| Fairbanks | 46.6 | 32.8 | 6.5 | 6.1 |
| Eielson AFB | 45.7 | 38.6 | 22.0 | 18.2 |
| Ft. Wainwright | 69.7 | 50.8 | 17.1 | 17.9 |
| Three Stations | 55.7 | 41.3 | 14.2 | 13.6 |

## 6. JAN-FEB 2008 EPISODE

The episode from 23 Jan – 12 Feb 2008 was re-simulated using the final model setup used for the 2-17 Nov 2008 episode (i.e., model configuration TWIND2X30, using the supplemental surface stations and enhanced vertical resolution in data assimilation). As mentioned previously, the Jan-Feb 2008 episode was considerably colder than the Nov 2008 case, with an extended period of temperatures reaching -35°C (see Figure 27**)**. A comparison between the METAR station statistics for the TWIND2X30 re-simulation with the statistics from the original RARE project simulation is shown in Table 9. Generally the difference between the re-simulated and original statistics were slight for temperature, wind speed, and relative humidity (although at Ft. Wainwright the temperature RMSE increased by 0.5 °C in the re-simulated case). Wind direction errors were substantially reduced in the re-simulated Jan – Feb 2008 episode, though, because in the original RARE configuration there was no assimilation of any surface wind observations on the finest domain. It appears that either model configuration has little, if any, overall temperature bias for the Jan-Feb episode. However, this reflects a cancellation between periods of positive temperature bias (generally the coldest temperature episodes) and periods of negative temperature bias (generally before the coldest episodes, often when precipitation is occurring).

A comparison of the METAR statistics between the TWIND2X30 versions of the Nov 2008 and Jan-Feb 2008 episodes (Table 10) shows that the TWIND2X30 version of the Jan-Feb 2008 episode arguably has better statistics than the Nov 2008 episode, despite the more extreme cold present in the former. However, the more negative temperature bias in the Nov 2008 versus the Jan-Feb 2008 episode is consistent with the relative absence of extreme cold periods in Nov 2008 and the configurations general tendency to have a negative temperature bias in milder winter conditions for the Fairbanks region. While the model tends to be too warm during the periods of the coldest temperatures, the coldest temperature periods also tend to be of short duration.

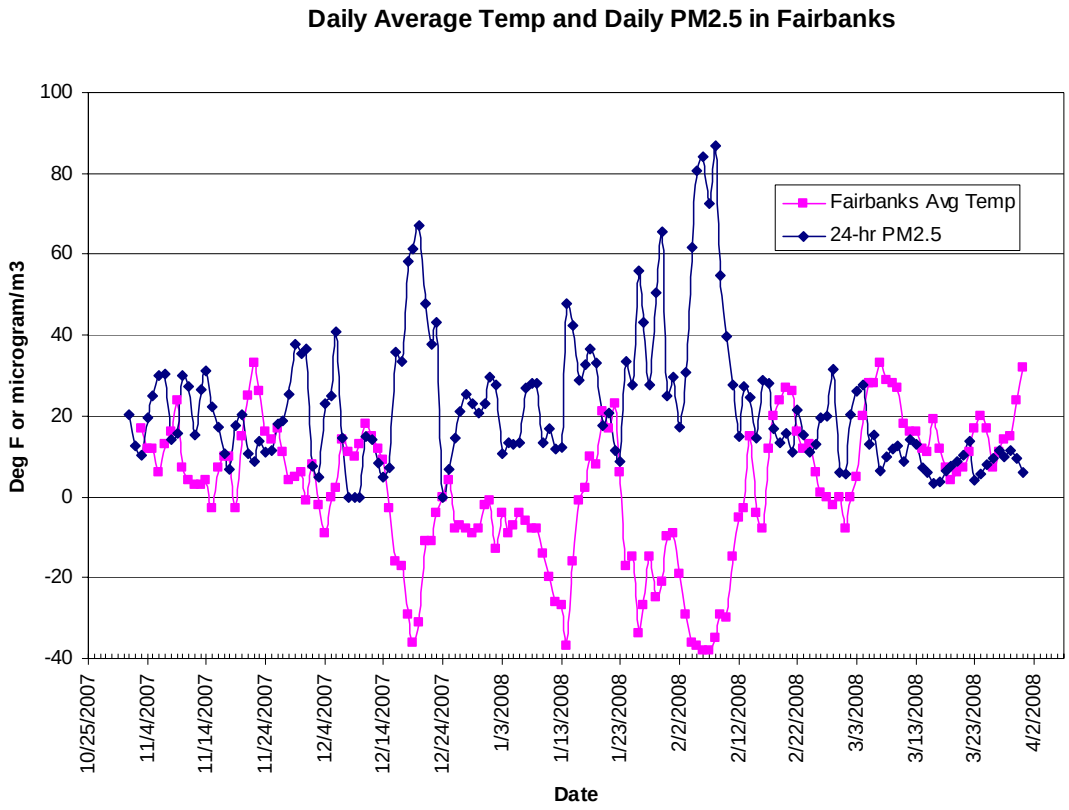


Figure 27: Measured daily average temperature (Fahrenheit) and 24-hr PM2.5 concentration in Fairbanks region during 2007-2008 winter season. Courtesy Robert Dulla, Sierra Research.

Temperatures for some of the local non-METAR stations are shown in Figure 28. Although the data record is a bit erratic, it is apparent that for the coldest period between 00 UTC on the 4$^{th}$ and 00 UTC on the 9$^{th}$, the temperatures in Woodsmoke can be 10 °C or more colder than those in Two Rivers, which in turn can be 10 °C colder than those on Ester Dome. While the model surface temperature forecasts are not perfect (daytime temperatures at Two Rivers in particular seem to be too warm) the model configuration is certainly capturing a large part of the temperature variability and magnitude across these stations

Time series of statistics for the METAR stations for the rerun of the Jan – Feb 2008 case are shown in Figure 29 – Figure **32**. While there are significant gaps in the data, it seems clear that the period from about 28 January through 31 January, as well as from about 4 – 11 February, exhibit positive temperature bias, corresponding to periods of low actual temperatures, while other periods tend to have a negative temperature bias (Figure 29). The largest temperature RMSE values for the positive and negative temperature bias periods are roughly comparable (exceeding 4 °C at times, but usually less than 3 °C). Wind speed biases tend to be positive

(Figure 31), but wind speed RMSE values seem to vary little on average between the warm and cold periods. These results are broadly consistent with those from the RARE project.

Appendix B contains more detailed time series of the statistics and modeled and observed surface field values for the Jan-Feb 2008 episode.

Table 9: Comparison of statistics for Jan-Feb 2008 between RARE configuration and TWIND2X30 configuration.

| Temperature (°C) | Jan-Feb RARE RMSE (MAE for wind direction) | Jan-Feb RARE Bias | Jan-Feb TWIND2X30 RMSE (MAE for wind direction) | Jan-Feb TWIND2X30 Bias |
|---|---|---|---|---|
| Fairbanks | 2.20 | -0.03 | 2.22 | -0.12 |
| Eielson AFB | 1.81 | -0.07 | 2.05 | -0.23 |
| Ft. Wainwright | 1.33 | 0.23 | 1.83 | 0.51 |
| Three Stations | 1.87 | 0.02 | 2.07 | 0.00 |
| Relative Humidity (%) | | | | |
| Fairbanks | 8.07 | 2.74 | 8.15 | 2.55 |
| Eielson AFB | 11.45 | -1.38 | 12.45 | -2.49 |
| Ft. Wainwright | 16.85 | -13.87 | 17.09 | -13.67 |
| Three Stations | 11.98 | -2.89 | 12.44 | -3.32 |
| Wind Speed (m $s^{-1}$) | | | | |
| Fairbanks | 1.58 | 0.87 | 1.51 | 0.86 |
| Eielson AFB | 1.17 | 0.69 | 1.18 | 0.69 |
| Ft. Wainwright | 1.31 | 0.32 | 1.21 | 0.25 |
| Three Stations | 1.38 | 0.69 | 1.34 | 0.68 |
| Wind Direction (degrees) | | | | |
| Fairbanks | 43.6 | 0.3 | 21.6 | -5.6 |
| Eielson AFB | 55.7 | -19.4 | 26.0 | -10.3 |
| Ft. Wainwright | 66.4 | 18.9 | 40.3 | 3.4 |
| Three Stations | 54.6 | 1.9 | 29.2 | -3.6 |

Table 10: Comparison of statistics for Nov 2008 and Jan-Feb 2008 episodes for TWIND2X30 model configuration.

| Temperature (°C) | Nov 2008 RMSE (MAE for wind direction) | Nov 2008 Bias | Jan-Feb 2008 RMSE (MAE for wind direction) | Jan-Feb 2008 Bias |
|---|---|---|---|---|
| Fairbanks | 2.75 | -1.16 | 2.22 | -0.12 |
| Eielson AFB | 2.03 | -0.47 | 2.05 | -0.23 |
| Ft. Wainwright | 2.38 | -0.97 | 1.83 | 0.51 |
| Three Stations | 2.43 | -0.86 | 2.07 | 0.00 |
| Relative Humidity (%) | | | | |
| Fairbanks | 5.43 | 0.71 | 8.15 | 2.55 |
| Eielson AFB | 5.93 | 3.35 | 12.45 | -2.49 |
| Ft. Wainwright | 12.48 | -10.39 | 17.09 | -13.67 |
| Three Stations | 7.14 | 0.05 | 12.44 | -3.32 |
| Wind Speed (m $s^{-1}$) | | | | |
| Fairbanks | 1.27 | 0.91 | 1.51 | 0.86 |
| Eielson AFB | 1.63 | 1.28 | 1.18 | 0.69 |
| Ft. Wainwright | 0.95 | 0.45 | 1.21 | 0.25 |
| Three Stations | 1.41 | 1.00 | 1.34 | 0.68 |
| Wind Direction (degrees) | | | | |
| Fairbanks | 32.8 | 6.1 | 21.6 | -5.6 |
| Eielson AFB | 38.6 | 18.2 | 26.0 | -10.3 |
| Ft. Wainwright | 50.8 | 17.9 | 40.3 | 3.4 |
| Three Stations | 41.3 | 13.6 | 29.2 | -3.6 |

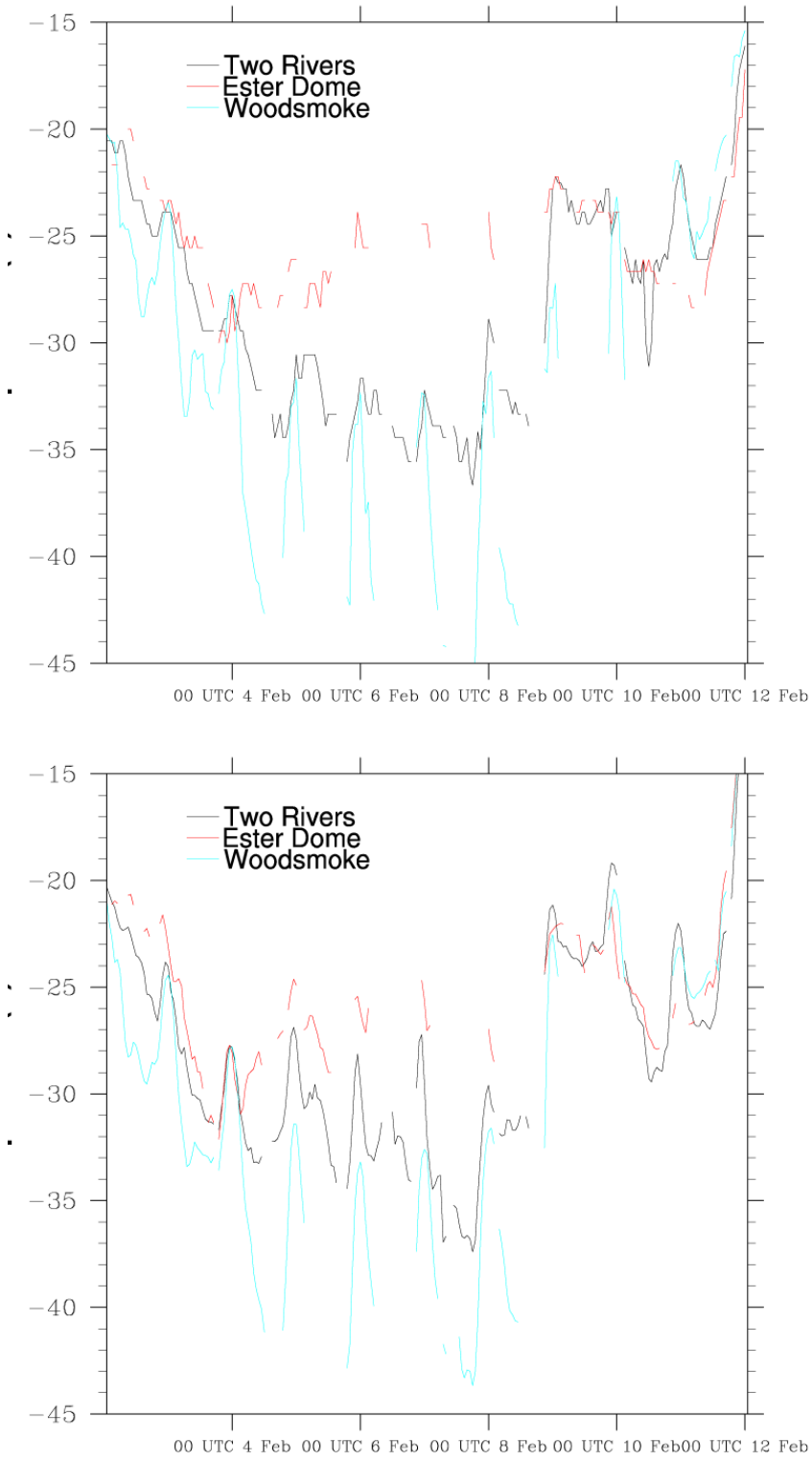


Figure 28: Observed (top) and model (bottom) surface temperatures (degrees Celsius) at non-METAR stations for 00 UTC 3 Feb -- 00 UTC 12 Feb

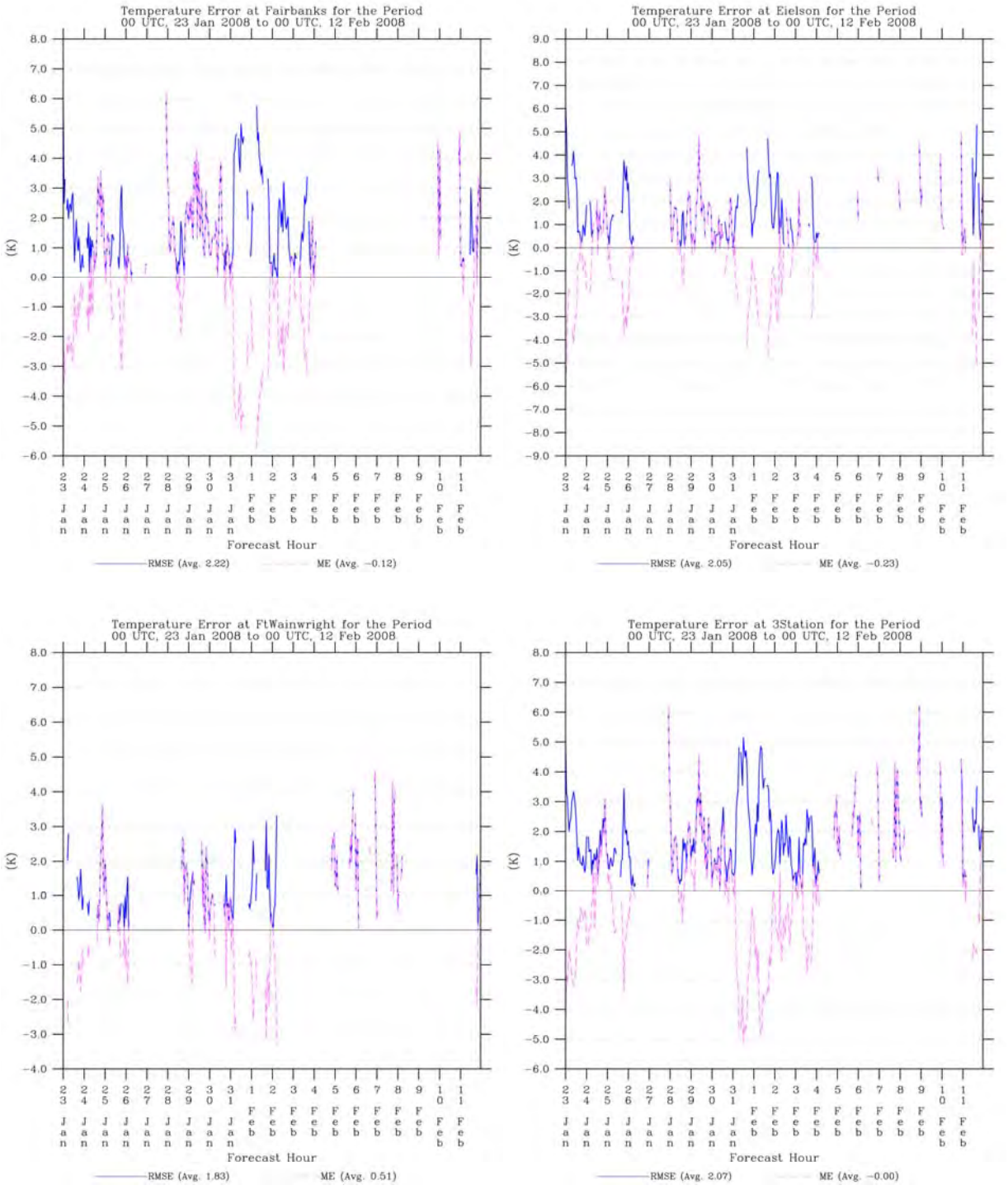


Figure 29: Temperature RMSE and Bias statistics for Jan-Feb 2008 episode at the local METAR surface stations using TWIND2X30 configuration.

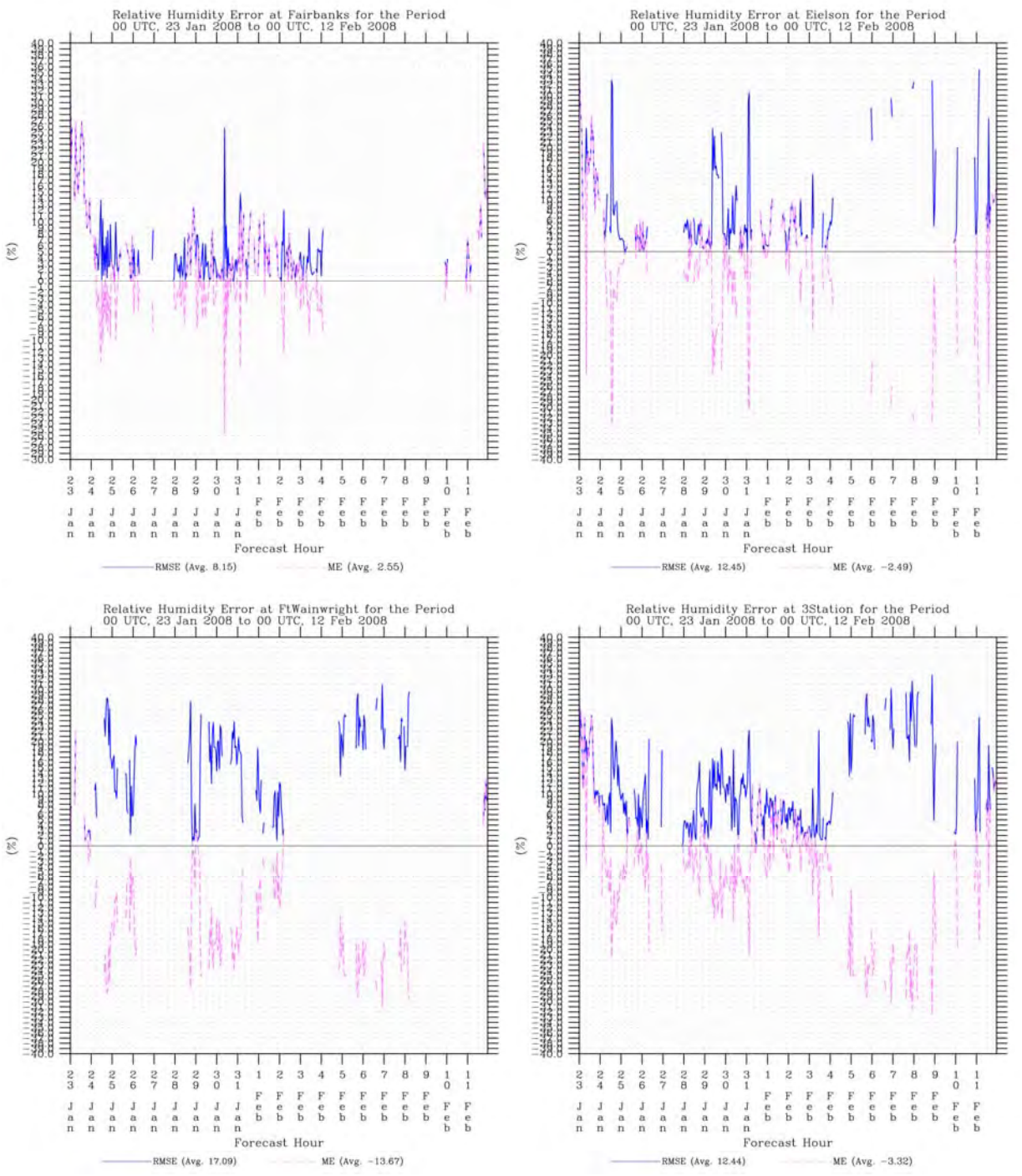


Figure 30: Same as Figure 29, but for relative humidity.

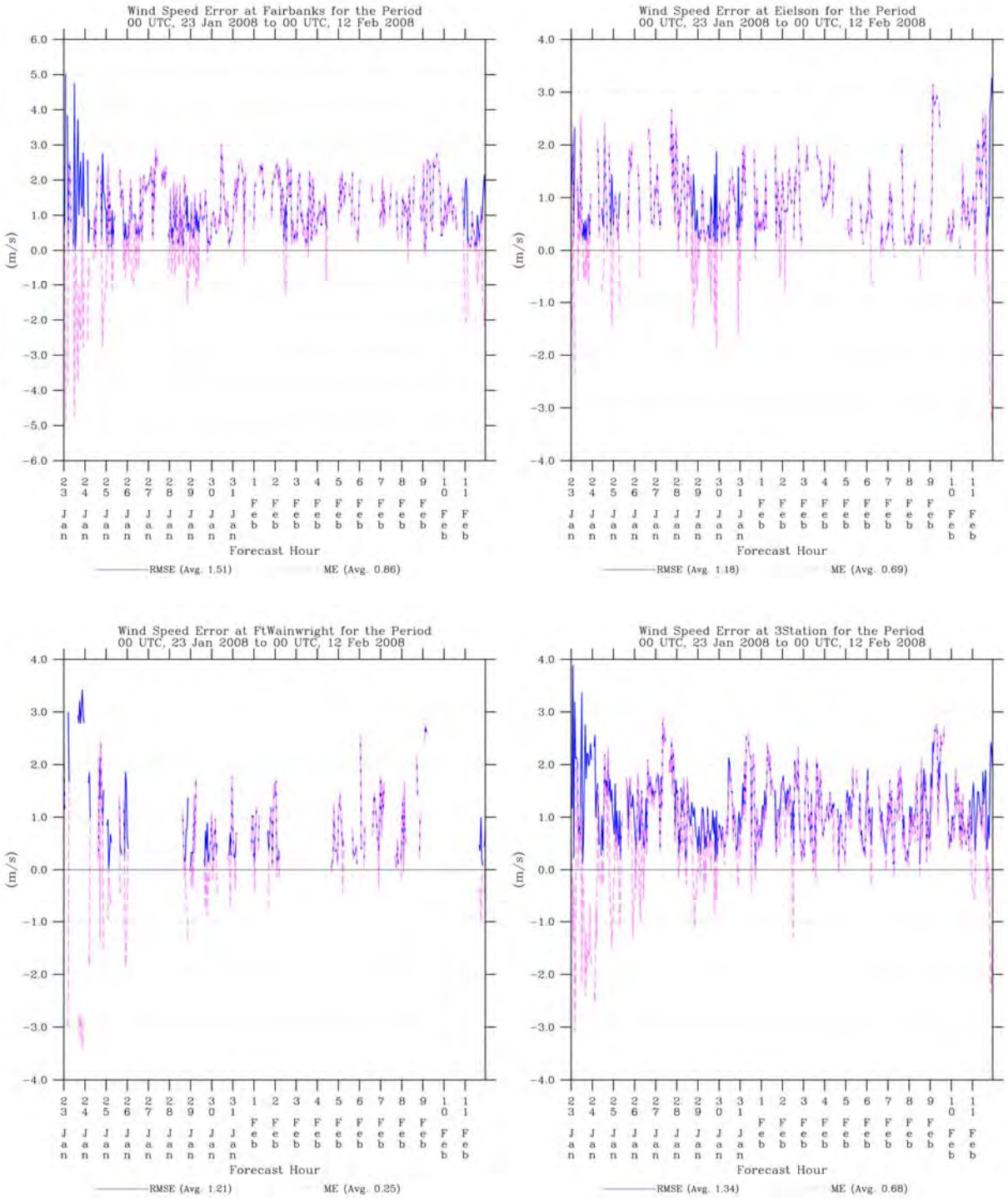


Figure 31: Same as Figure 29, but for wind speed.

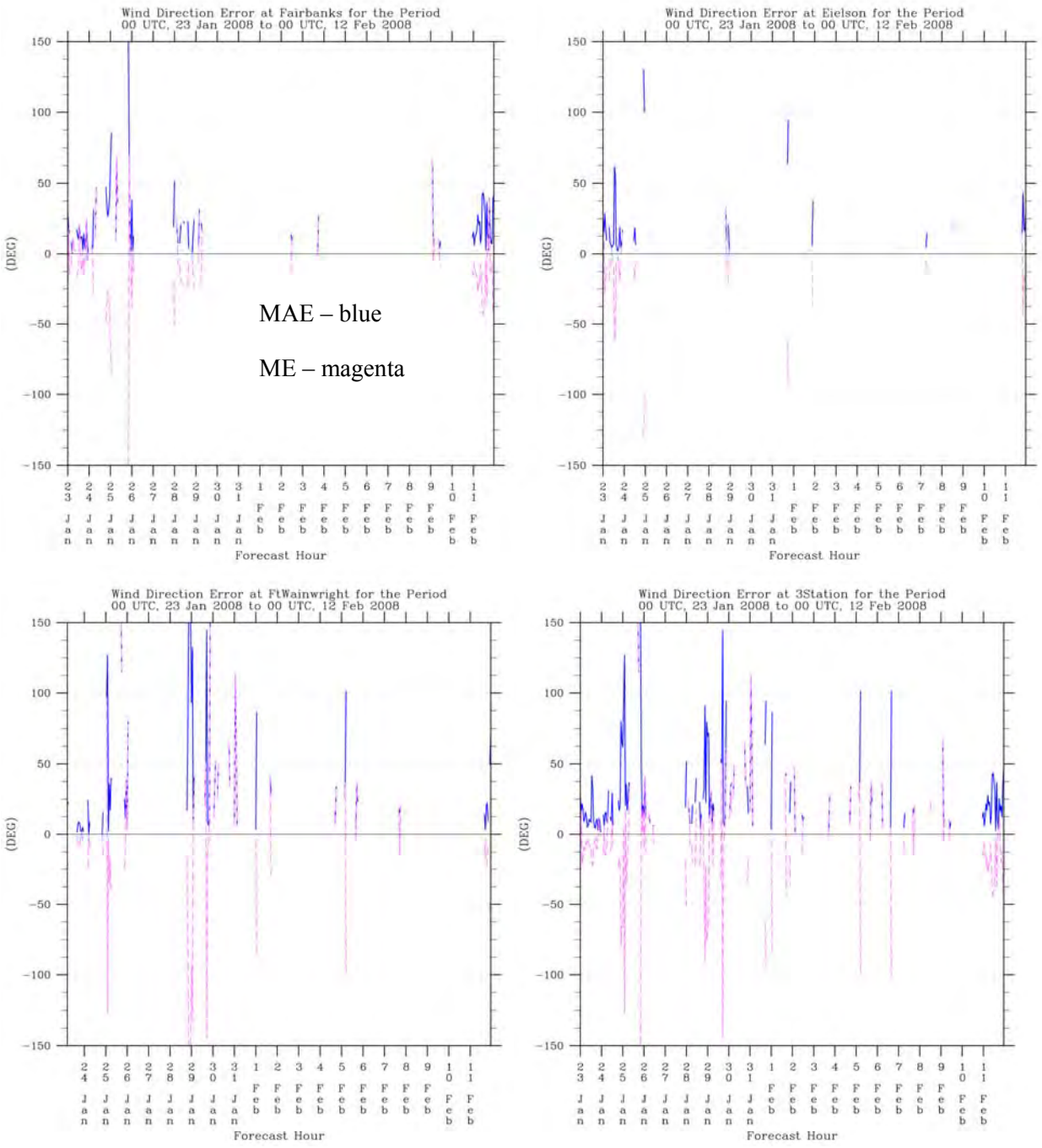


Figure 32: Same as Figure 29, but for wind direction MAE and ME statistics.

## 7. CONCLUSIONS

An episode extending from 2-17 November 2008 was simulated as part of the State Implementation Plan for the Fairbanks / North Star non-attainment region. The simulations were performed using the WRF-ARW model with essentially the same configuration as that used in the preliminary RARE study. However, initial decisions were made to increase the effective vertical resolution of the data assimilation near the surface, to use observation nudging towards surface wind observations even on the 1.33-km finest grid, and to make use of both standard METAR and non-METAR surface observations that were available for the period. These alterations to the procedure of the RARE study were made because, even though the statistics from that study were reasonably good, the model displayed a warm bias during the coldest, most stagnant conditions from that study, and concurrently the model wind speed bias was consistently positive. It was felt that these modifications would lead to the creation of a dynamic analysis that would be a closer fit to the actual state of the atmosphere.

The November episode was divided into four overlapping simulation segments using the discussed model configuration. A test period from 5-9 November was chosen for model sensitivity tests, including a comparison between the RARE study methodology and the proposed method of enhancing the data assimilation capabilities. Statistics indicated the benefits of the new data assimilation configuration, especially for wind direction. This configuration was then used for all subsequent simulations. However, the statistics also suggested that the model data assimilation was effectively blending the influence of neighboring observations in the Fairbanks region, leading to model simulations that did not possess all of the horizontal variability of the observations. A procedure taken from the RARE study was performed to determine an effective correlation length scale for surface temperature observation innovations; this led to new simulations in which the radius of influence was reduced from 75 km to 30 km, while the strength of the nudging coefficients was doubled. The new configuration (indicated by the label TWIND2X30) was then used to simulate the entire November episode, and generated the atmospheric analysis delivered to ADEC.

A positive wind speed model bias remained during stagnant, cold temperature conditions, though a portion of that bias is an artifact of the threshold of instrument detection, causing observations to frequently report dead calm conditions while model simulations produce non-zero wind speeds near the surface. While one procedure to reduce the positive wind speed bias would be to explicitly nudge towards the calm wind observations, it was found that this led to only minimal reductions in the wind speed bias, and using these reports in nudging had the undesirable effect of creating large increases in wind direction error at nearby stations not reporting dead calm conditions. Therefore, the decision was made to use the default procedure of not making explicit use of calm surface wind observations in the data assimilation procedure.

The Jan-Feb 2008 episode was then re-simulated using the TWIND2X30 configuration. Wind direction statistics for the METAR stations were improved with respect to the original simulations from the RARE project. Other fields did not show much change statistically. While model output at the location of the non-METAR station at Woodsmoke confirmed that the model could produce temperatures (nearly) as cold as observed temperatures around -45 °C, at other locations the model had difficulty producing sufficient cooling, especially if the horizontal resolution was insufficient (e.g., Goldstream Creek).

At the METAR stations, overall temperature bias for both episodes was quite low (less than a degree Celsius), while the temperature RMSE was on average 2 – 2.5 °C, which seemed reasonable given the occasionally extreme meteorological conditions. Wind speed RMSE values seemed to be fairly consistent at 1.3 – 1.4 m $s^{-1}$, while wind direction MAE values were on the order of 30 – 40 degrees with the TWIND2X30 configuration.

# APPENDIX A – Detailed Time-Series Figures of 2-17 November 2008 Episode, for TWIND2X30 Configuration

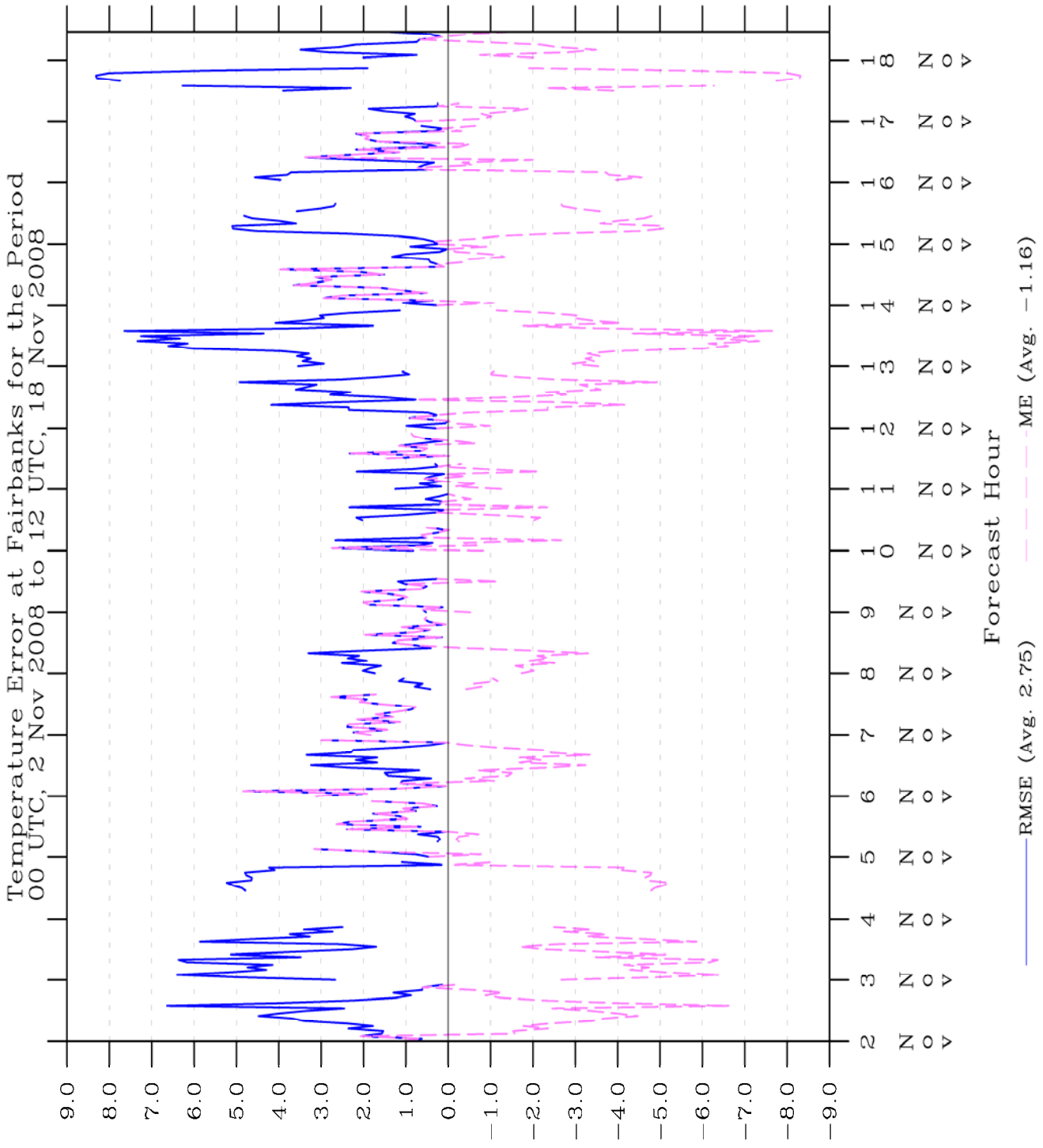


Figure 33: Time series of temperature statistics for Fairbanks in TWIND2X30.

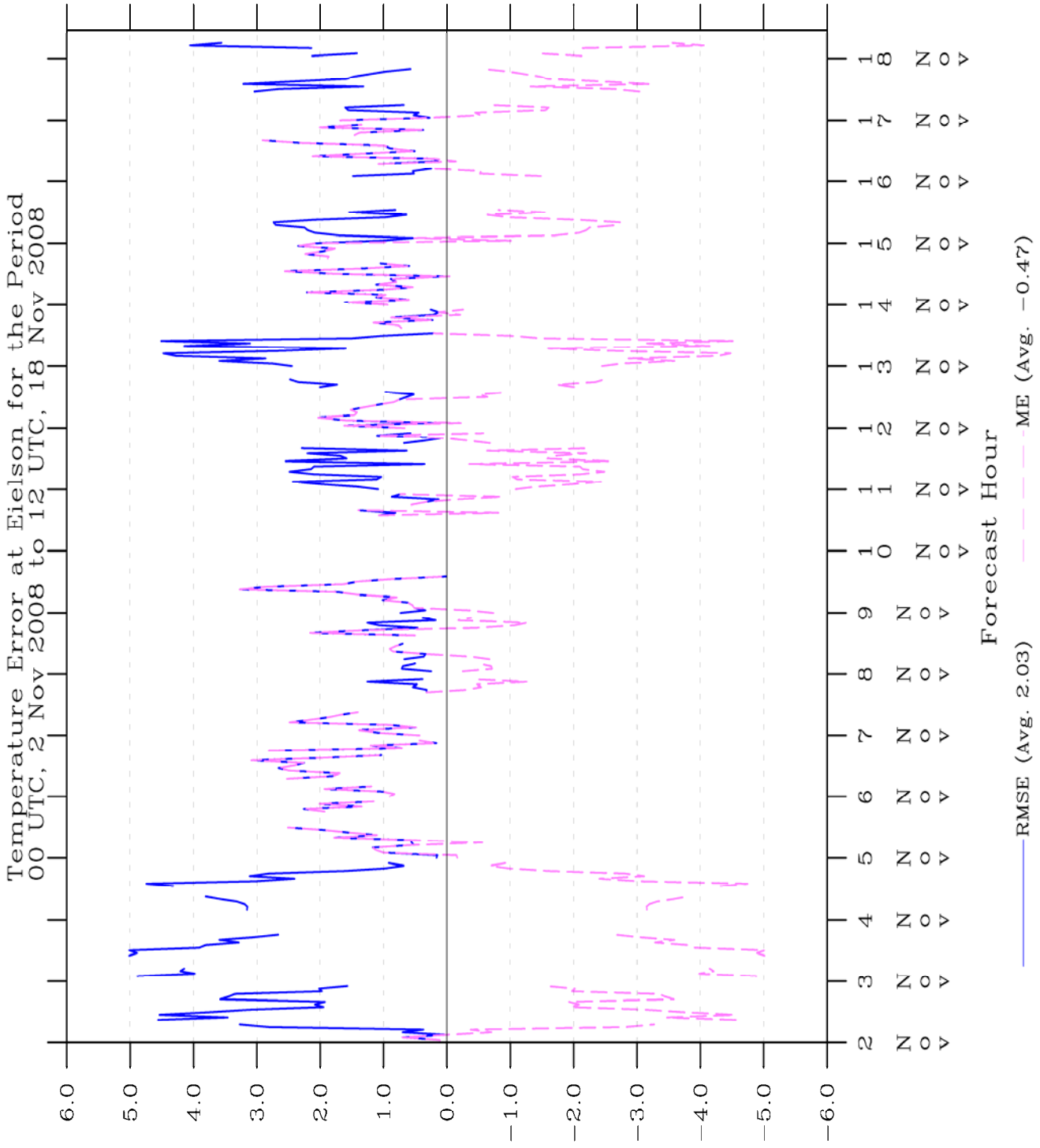


Figure 34: Time series of temperature statistics for Eielson in TWIND2X30.

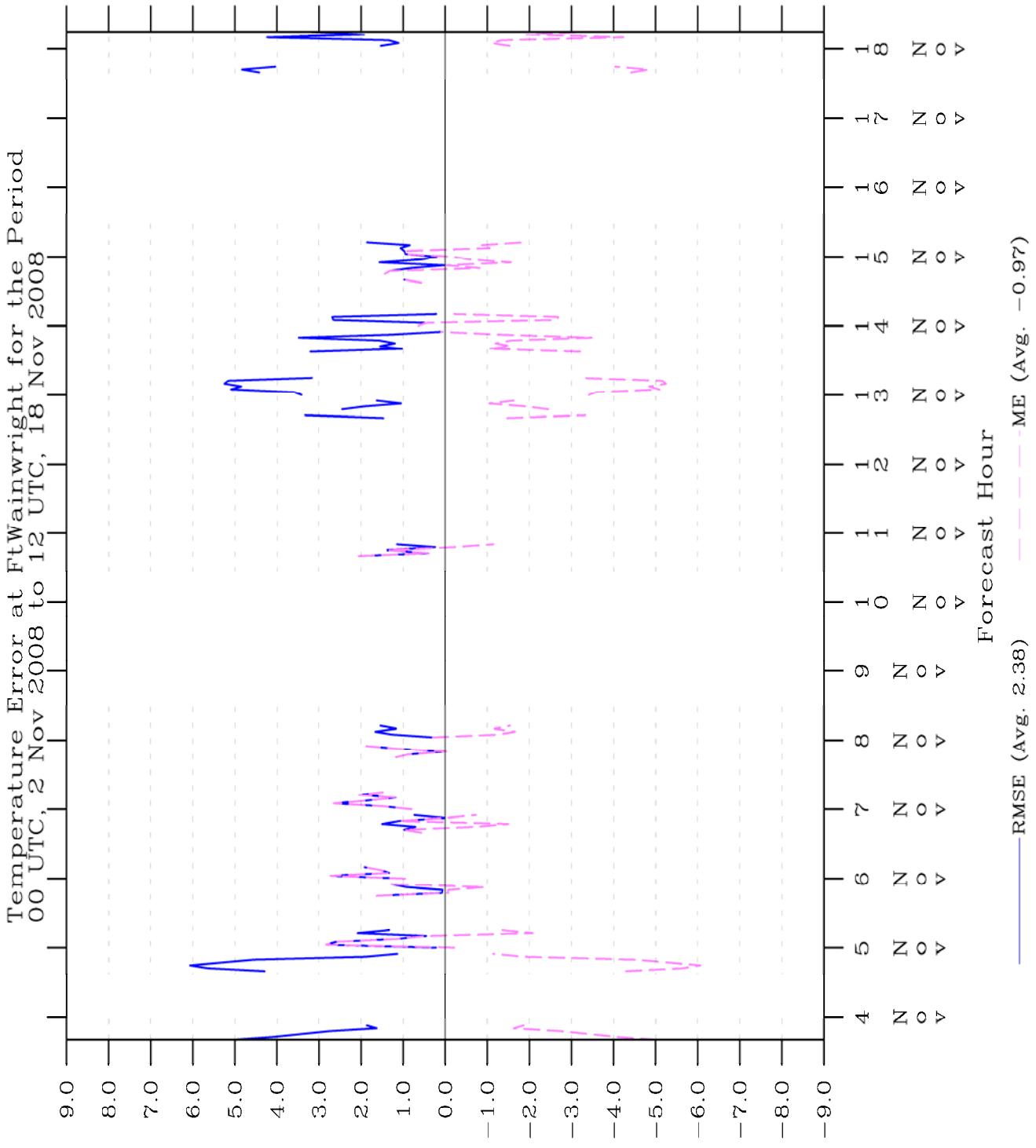


Figure 35: Time series of temperature statistics for Ft. Wainwright in TWIND2X30.

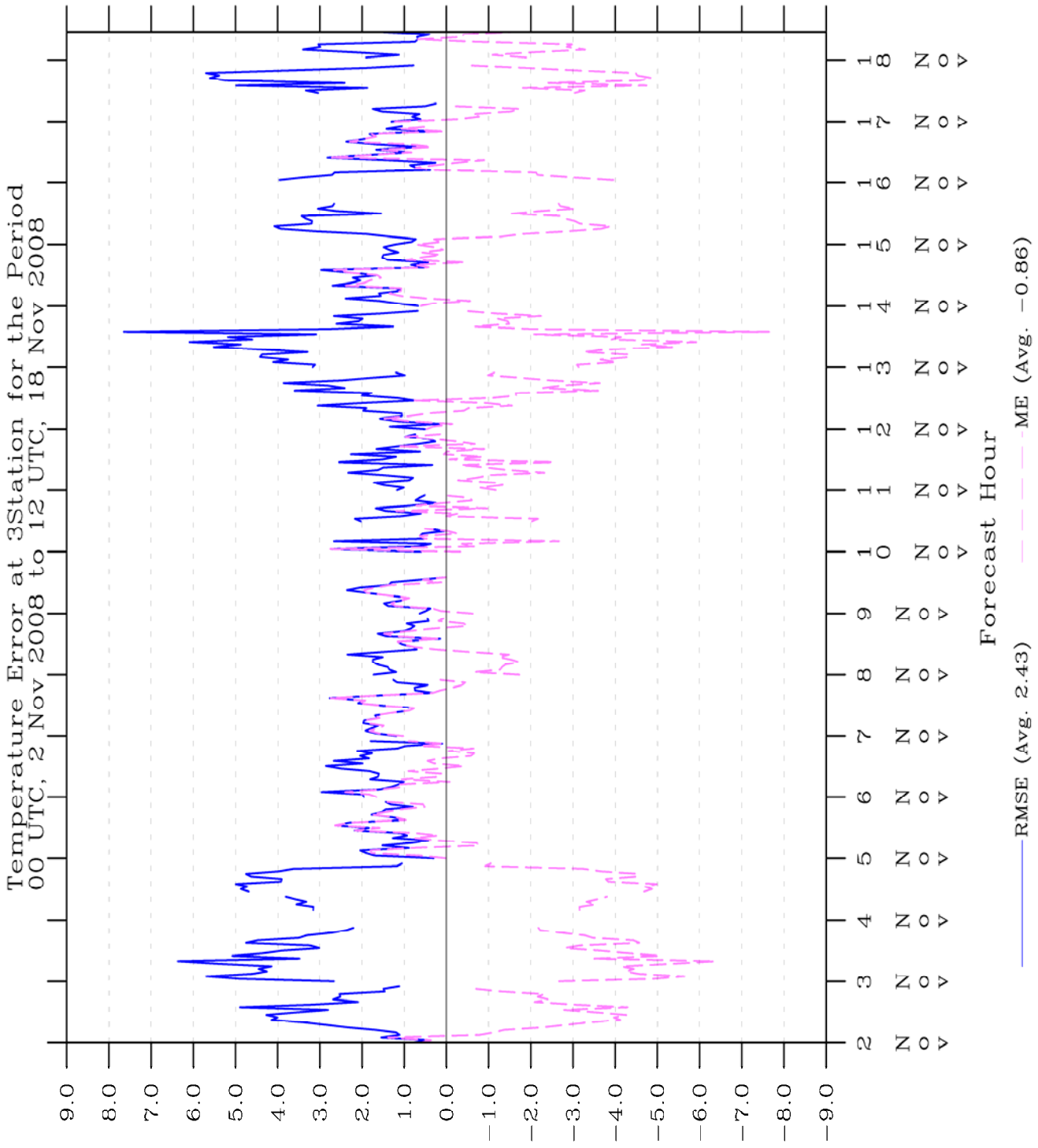


Figure 36: Time series of temperature statistics for all three stations in TWIND2X30.

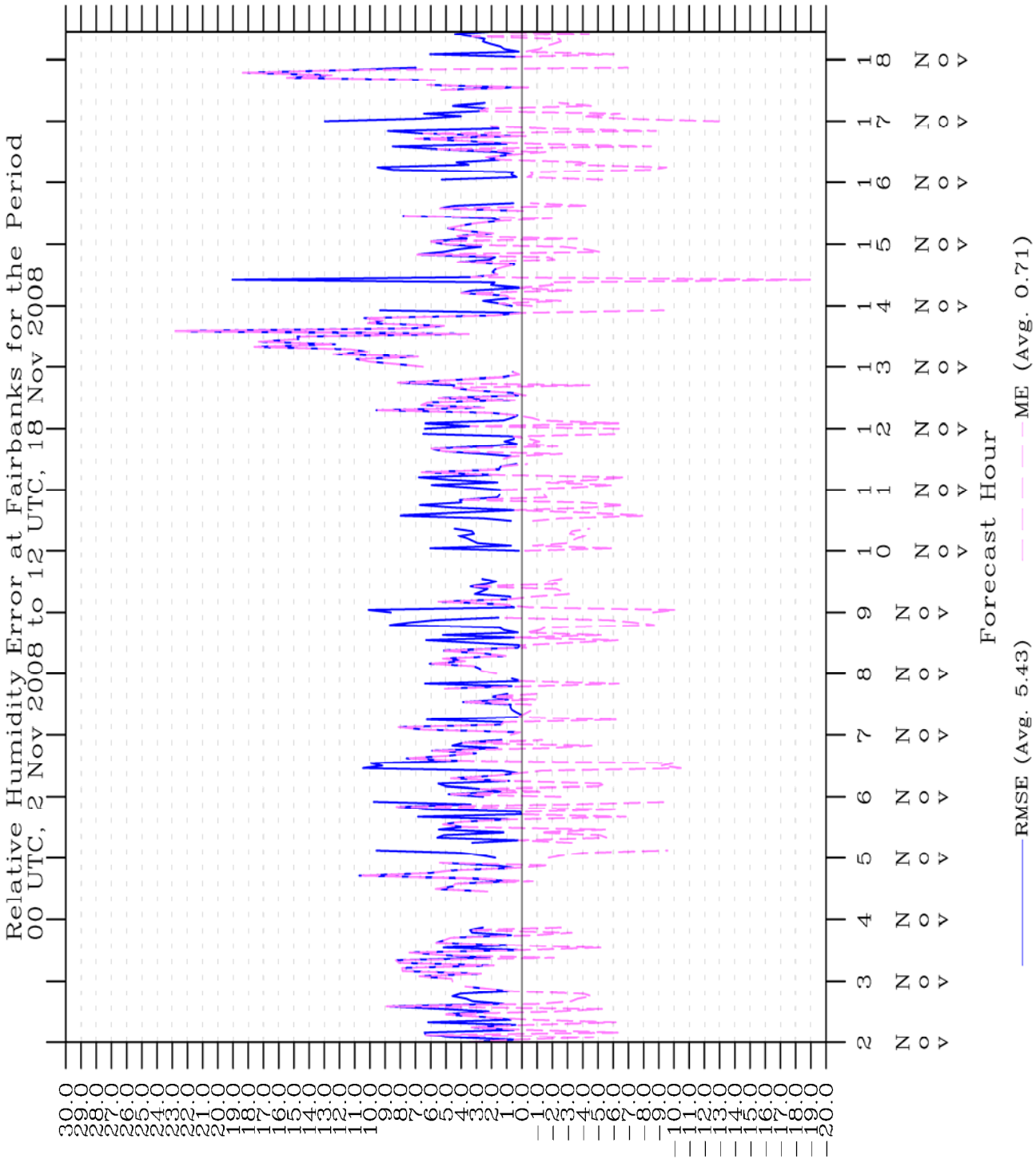


Figure 37: Time series of relative humidity statistics for Fairbanks in TWIND2X30.

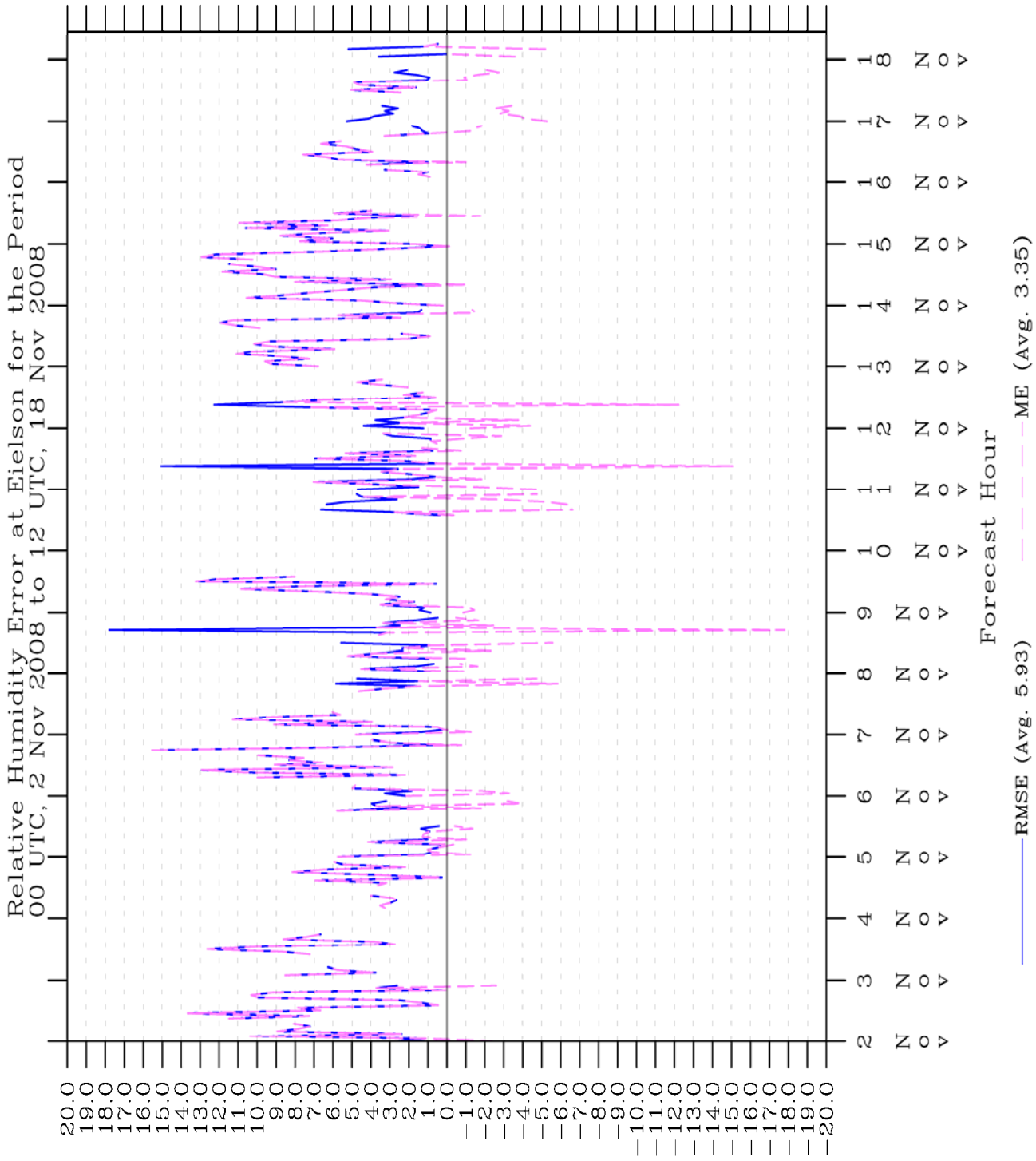


Figure 38: Time series of relative humidity statistics for Eielson in TWIND2X30.

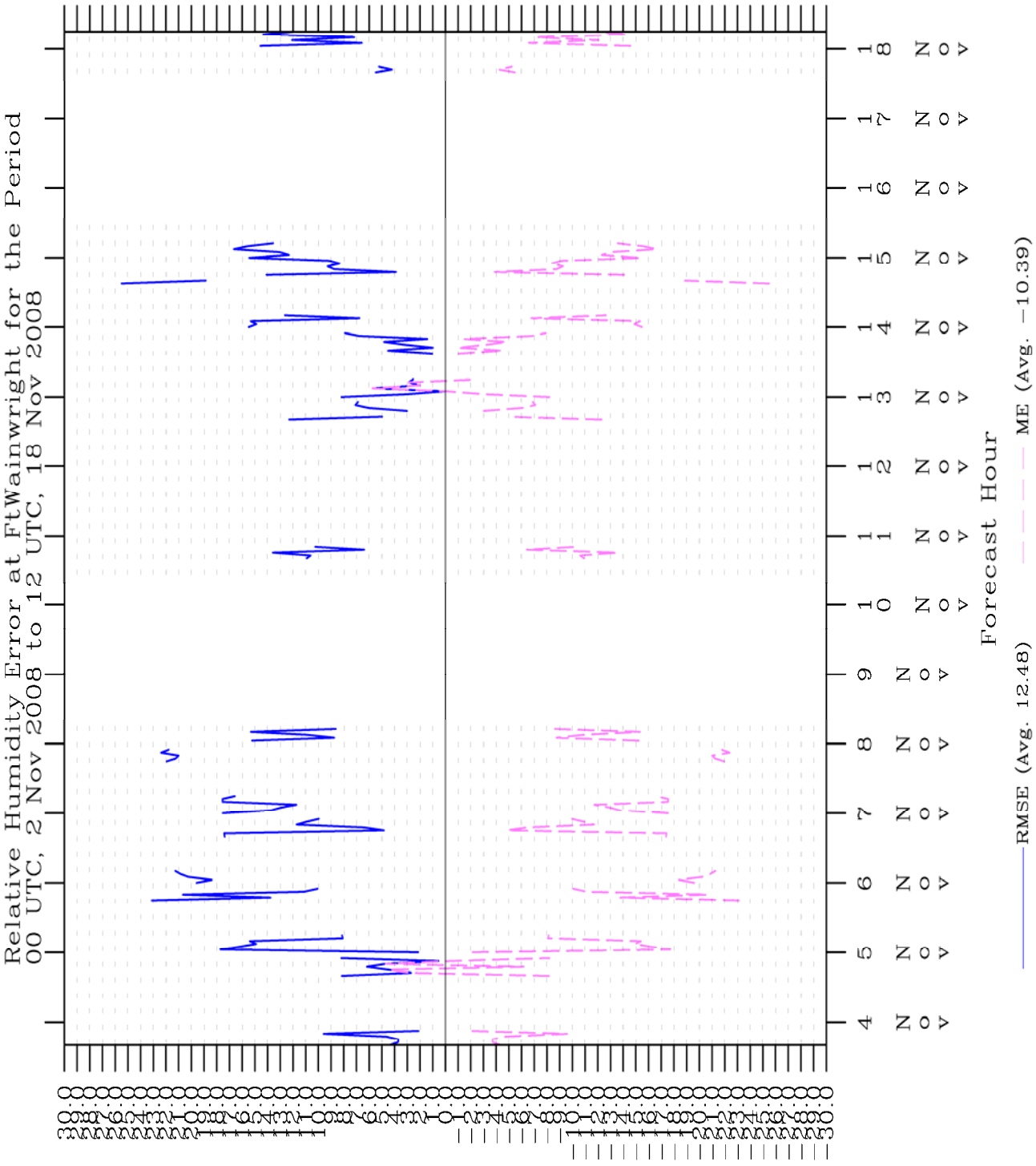


Figure 39: Time series of relative humidity statistics for Ft. Wainwright in TWIND2X30.

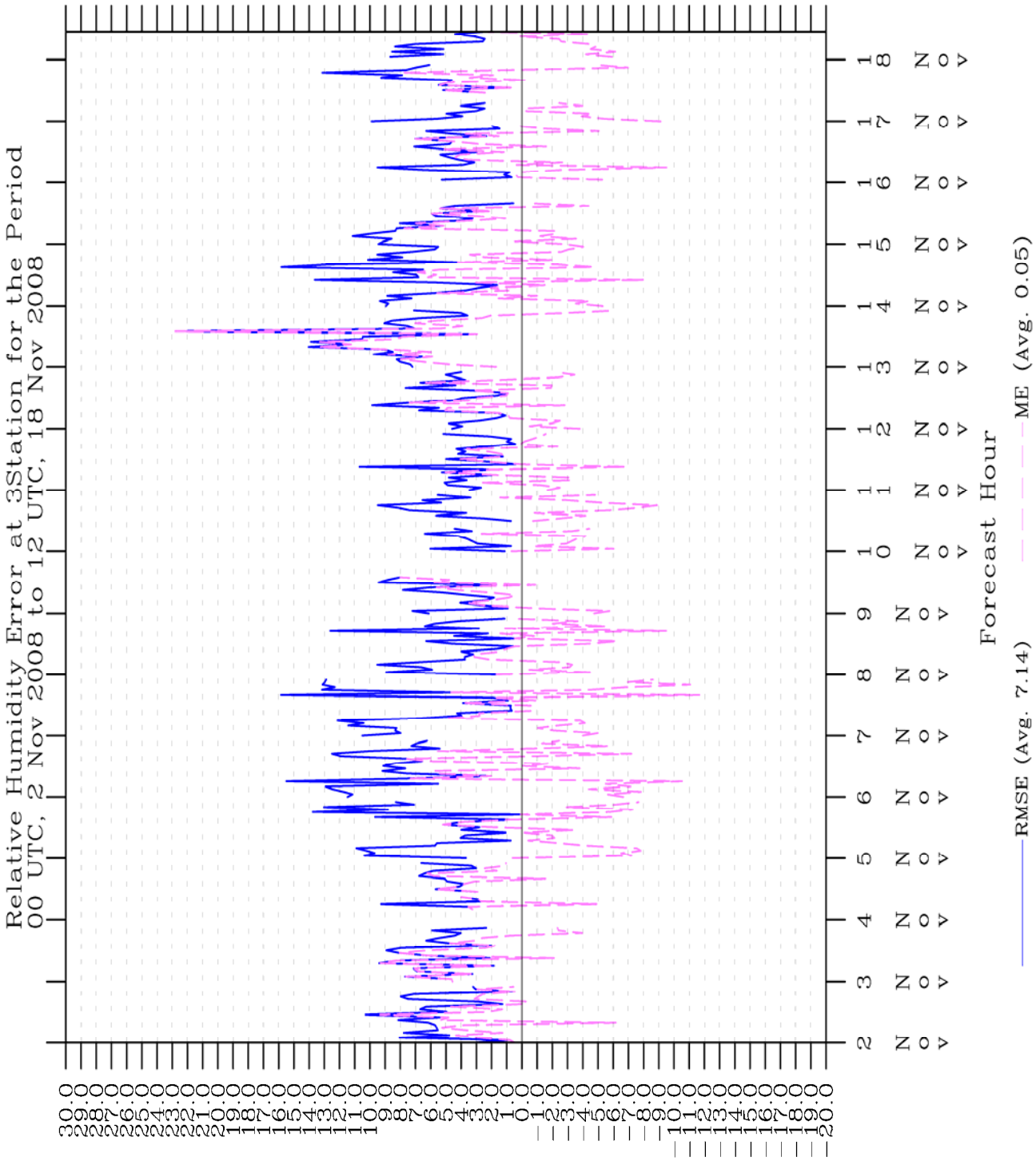


Figure 40: Time series of relative humidity statistics for all three stations in TWIND2X30.

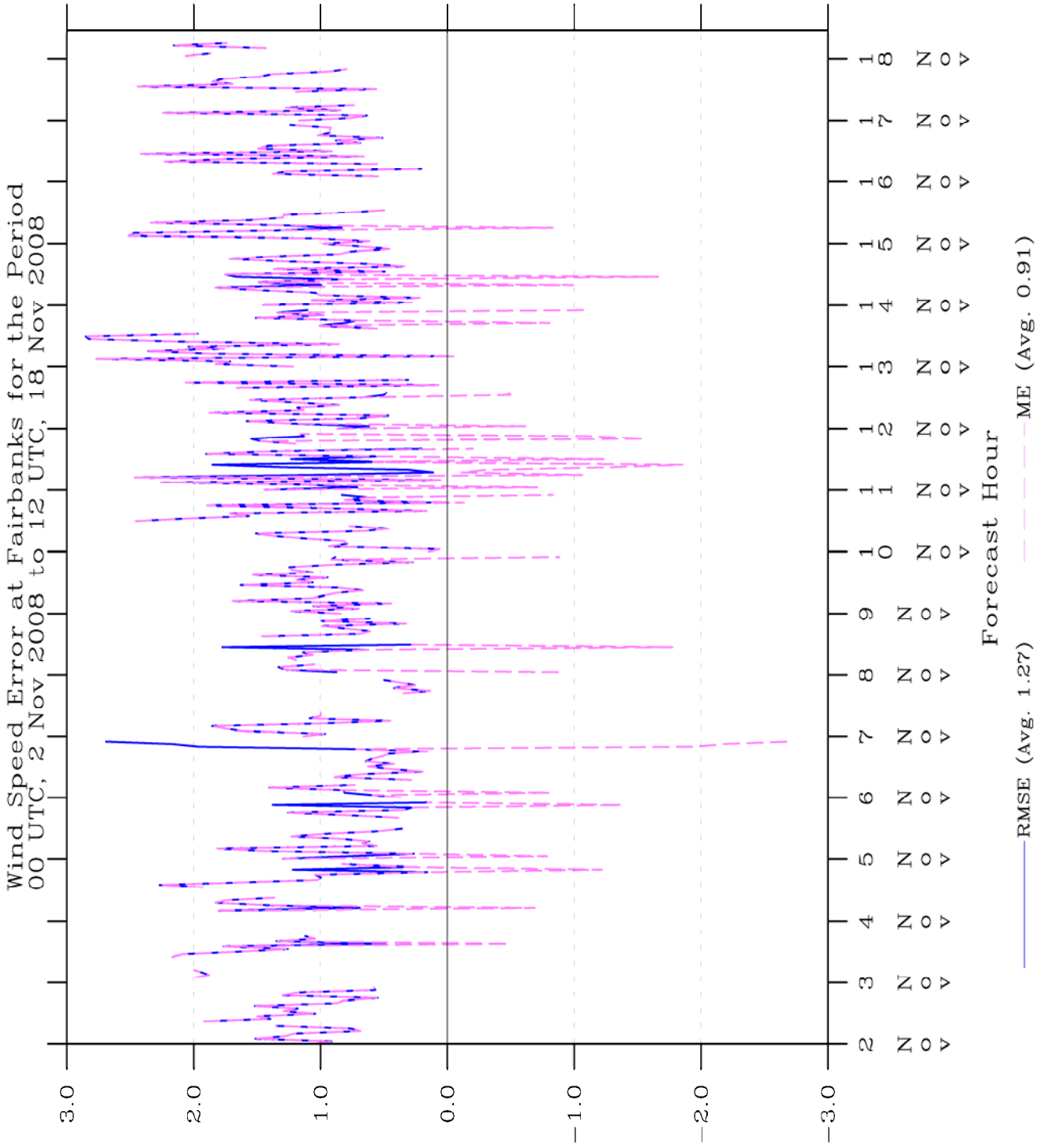


Figure 41: Time series of wind speed statistics for Fairbanks in TWIND2X30.

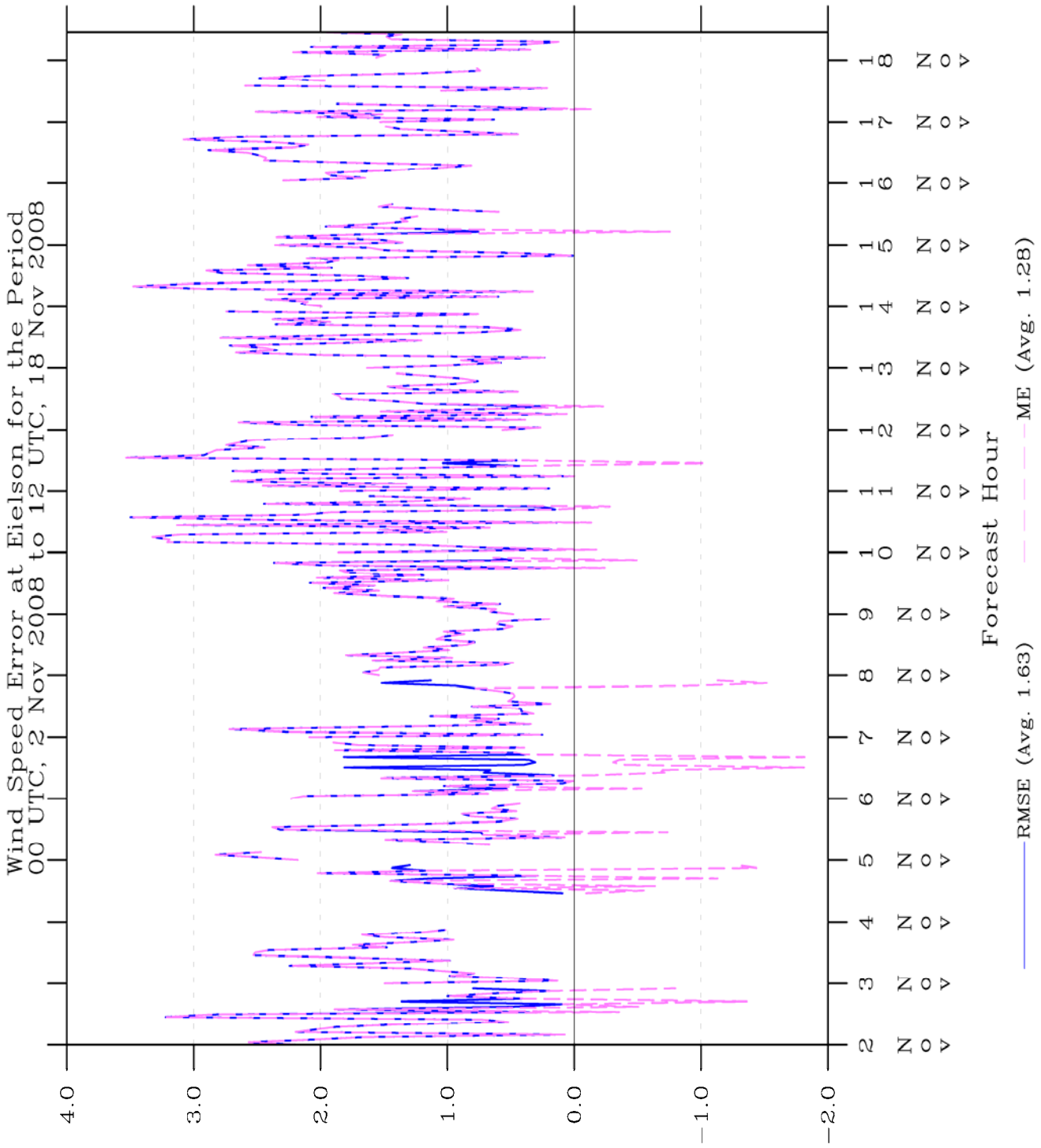


Figure 42: Time series of wind speed statistics for Eielson in TWIND2X30.

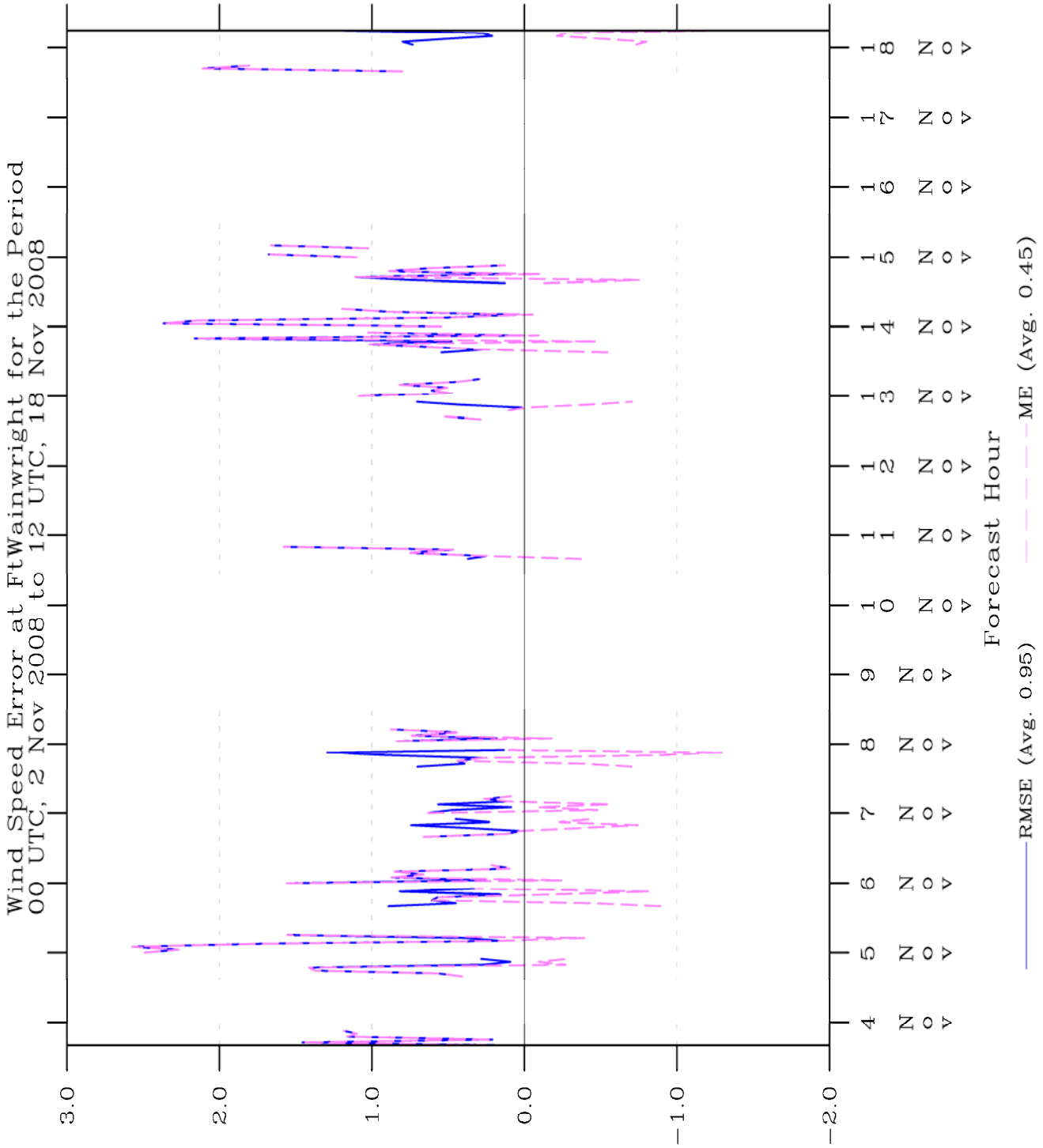


Figure 43: Time series of wind speed statistics for Ft. Wainwright in TWIND2X30.

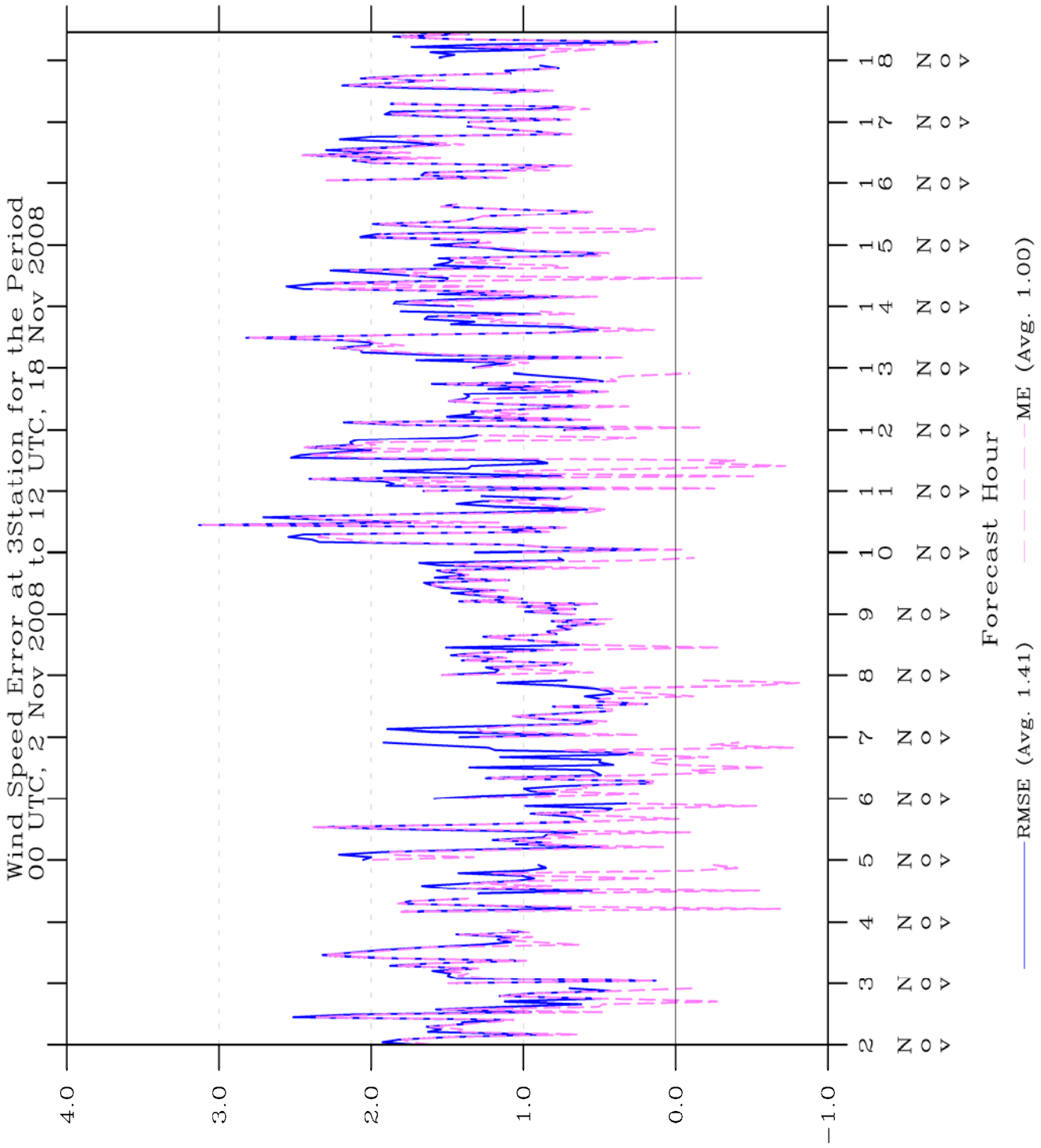


Figure 44: Time series of wind speed statistics for all three stations in TWIND2X30.

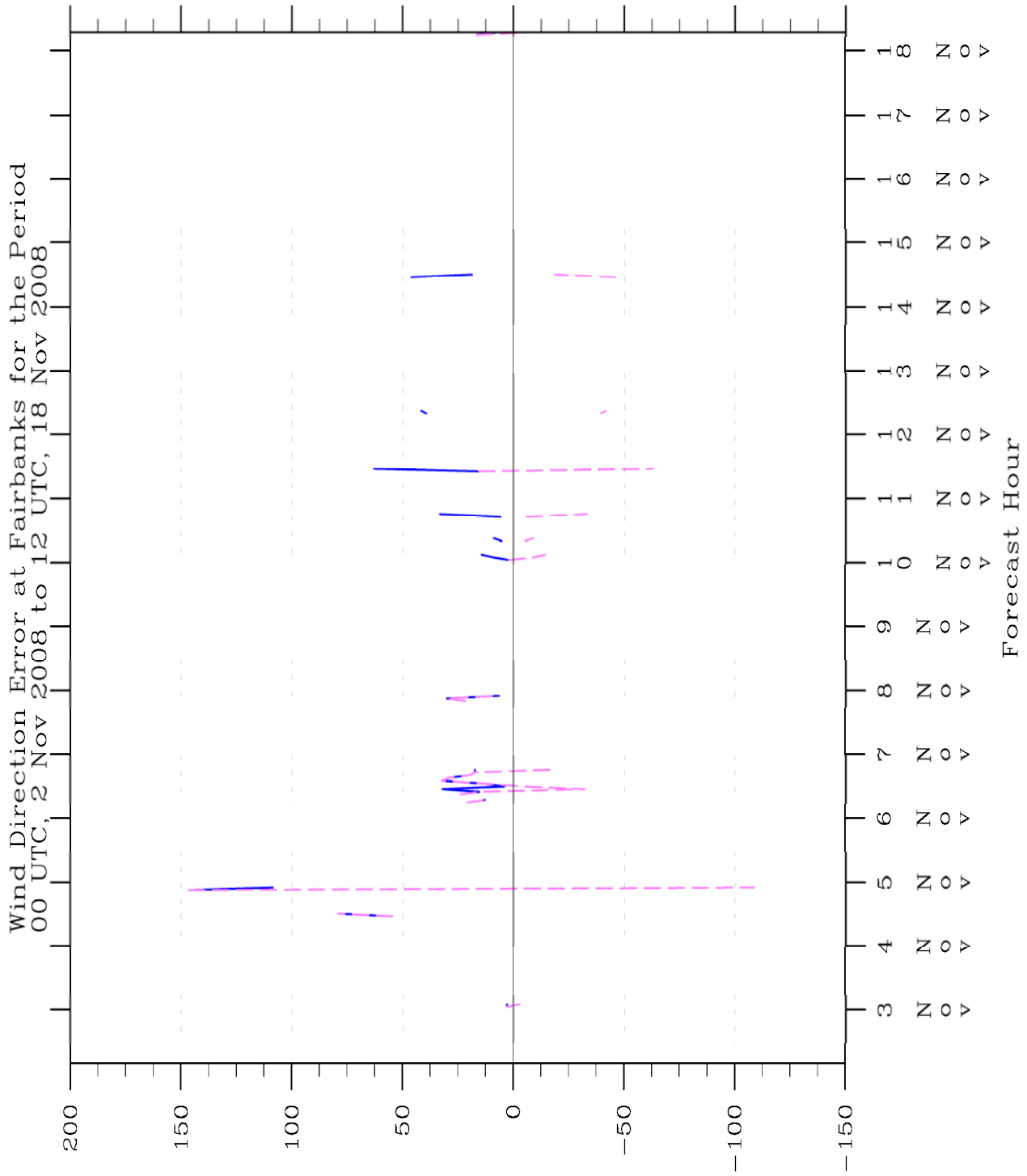


Figure 45: Time series of wind direction mean absolute error (blue) and mean error (magenta) statistics for Fairbanks in TWIND2X30.

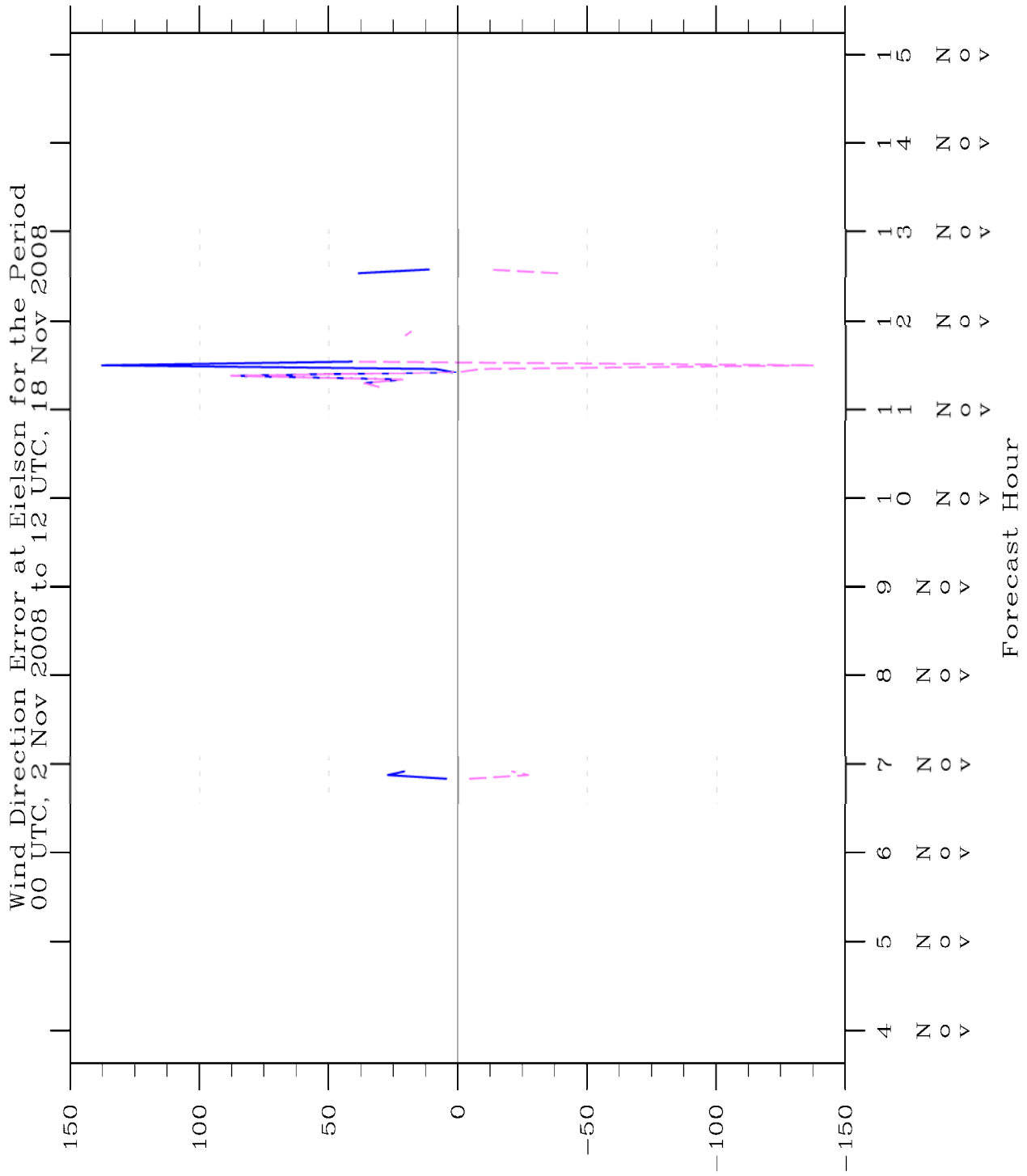


Figure 46: Time series of wind direction mean absolute error (blue) and mean error (magenta) statistics for Eielson in TWIND2X30.

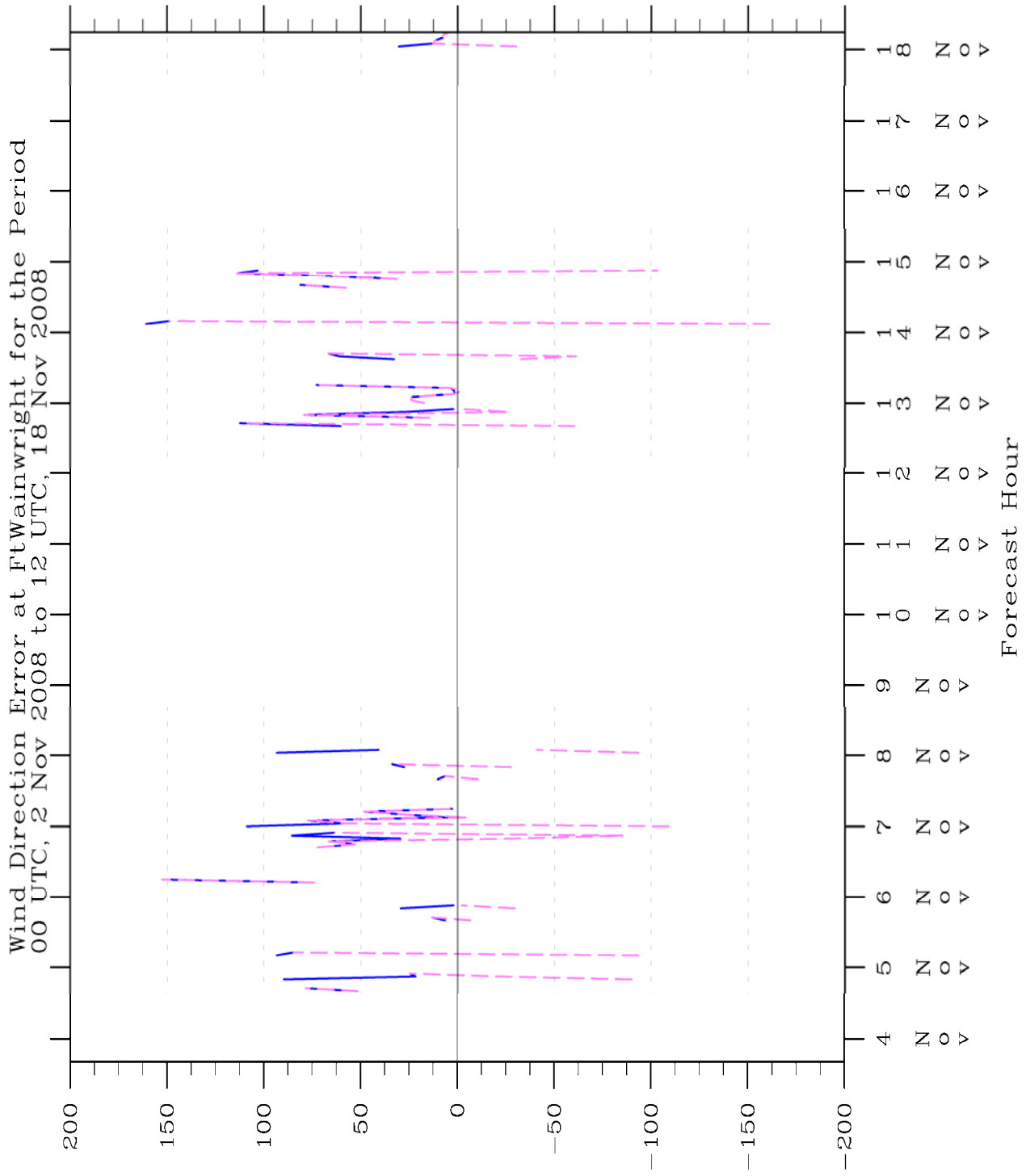


Figure 47: Time series of wind direction mean absolute error (blue) and mean error (magenta) statistics for Ft. Wainwright in TWIND2X30.

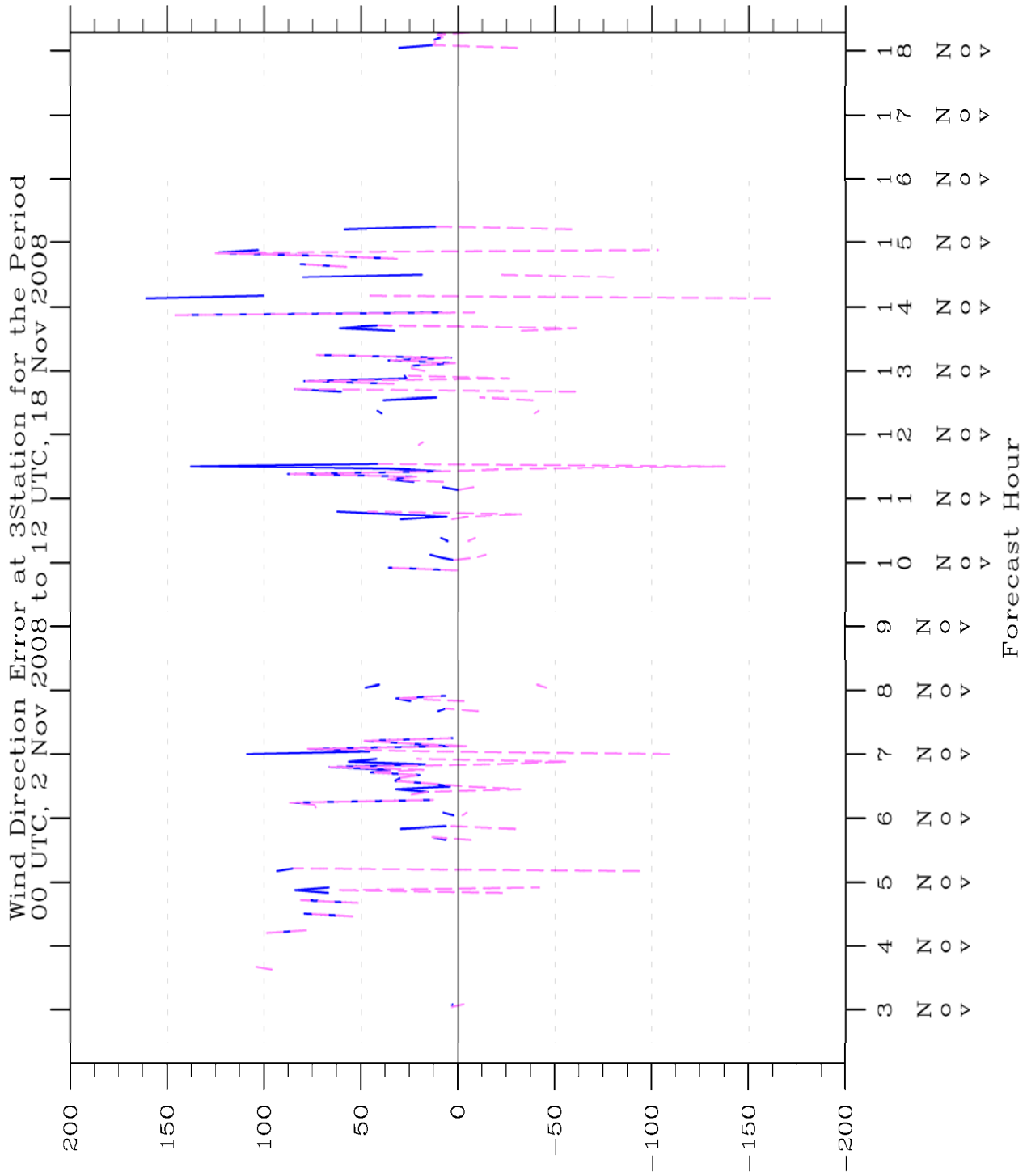


Figure 48: Time series of wind direction mean absolute error (blue) and mean error (magenta) statistics for all three stations in TWIND2X30.

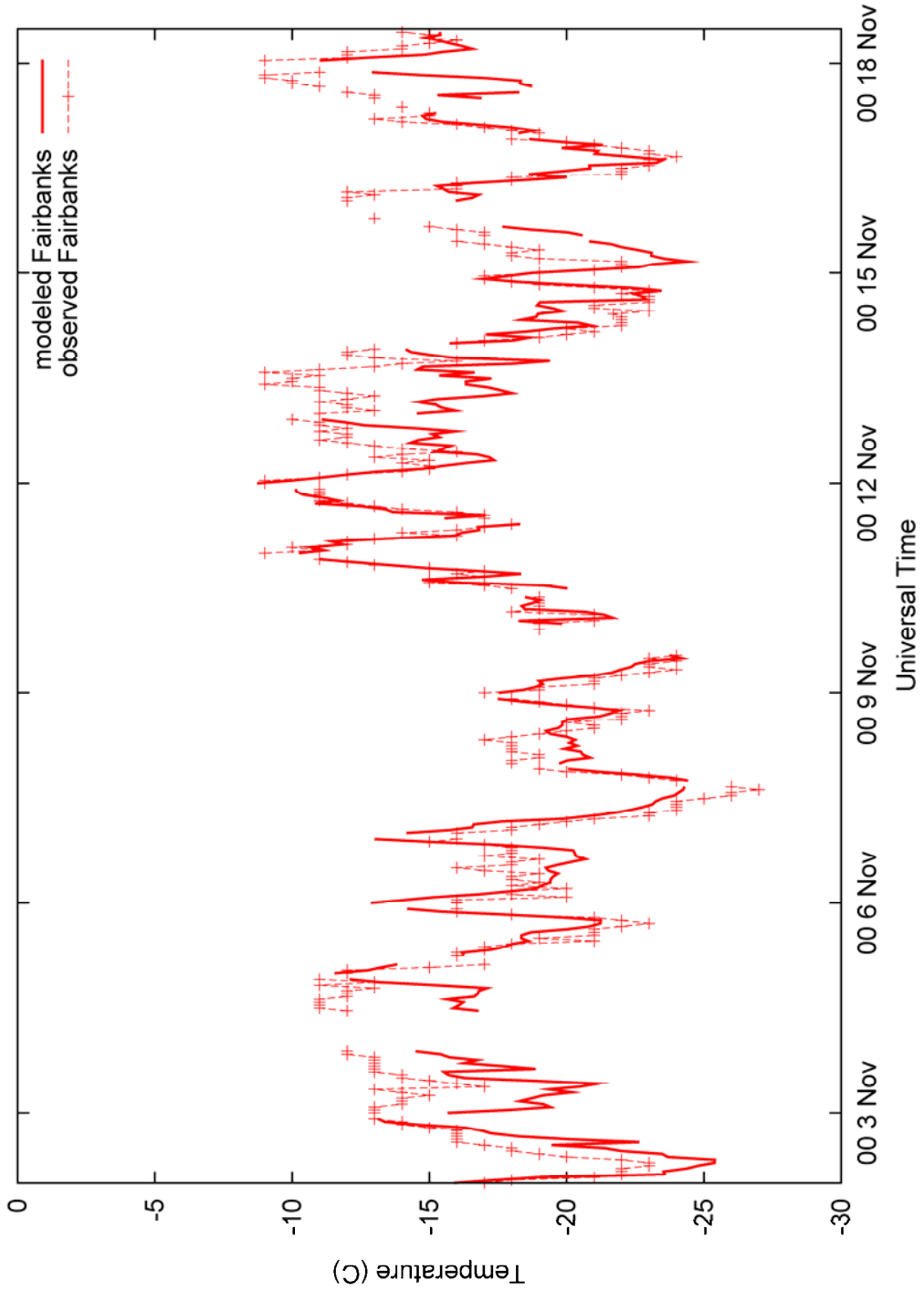


Figure 49: Time series of modeled and observed temperature for Fairbanks in TWIND2X30.

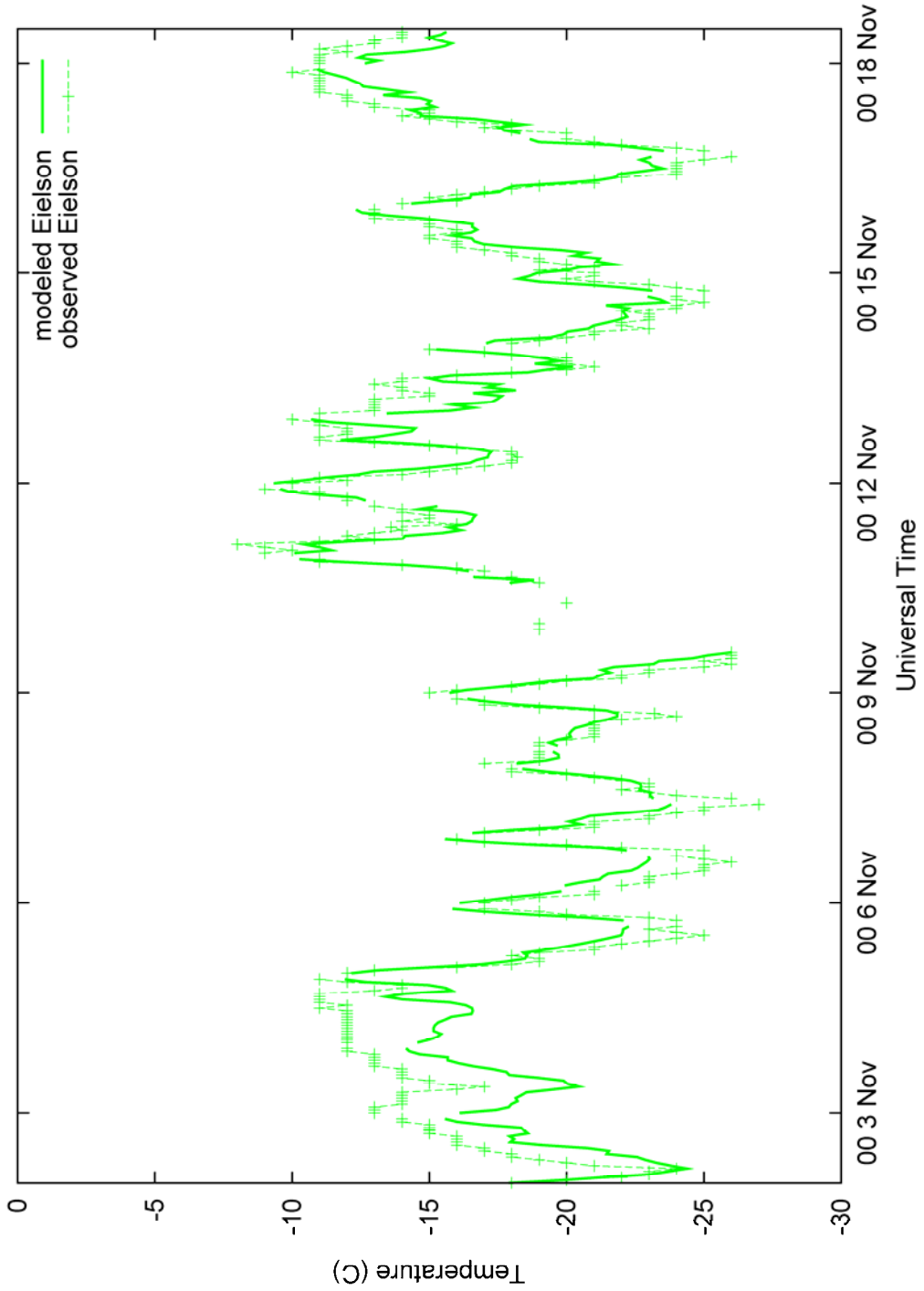


Figure 50: Time series of modeled and observed temperature for Eielson in TWIND2X30.

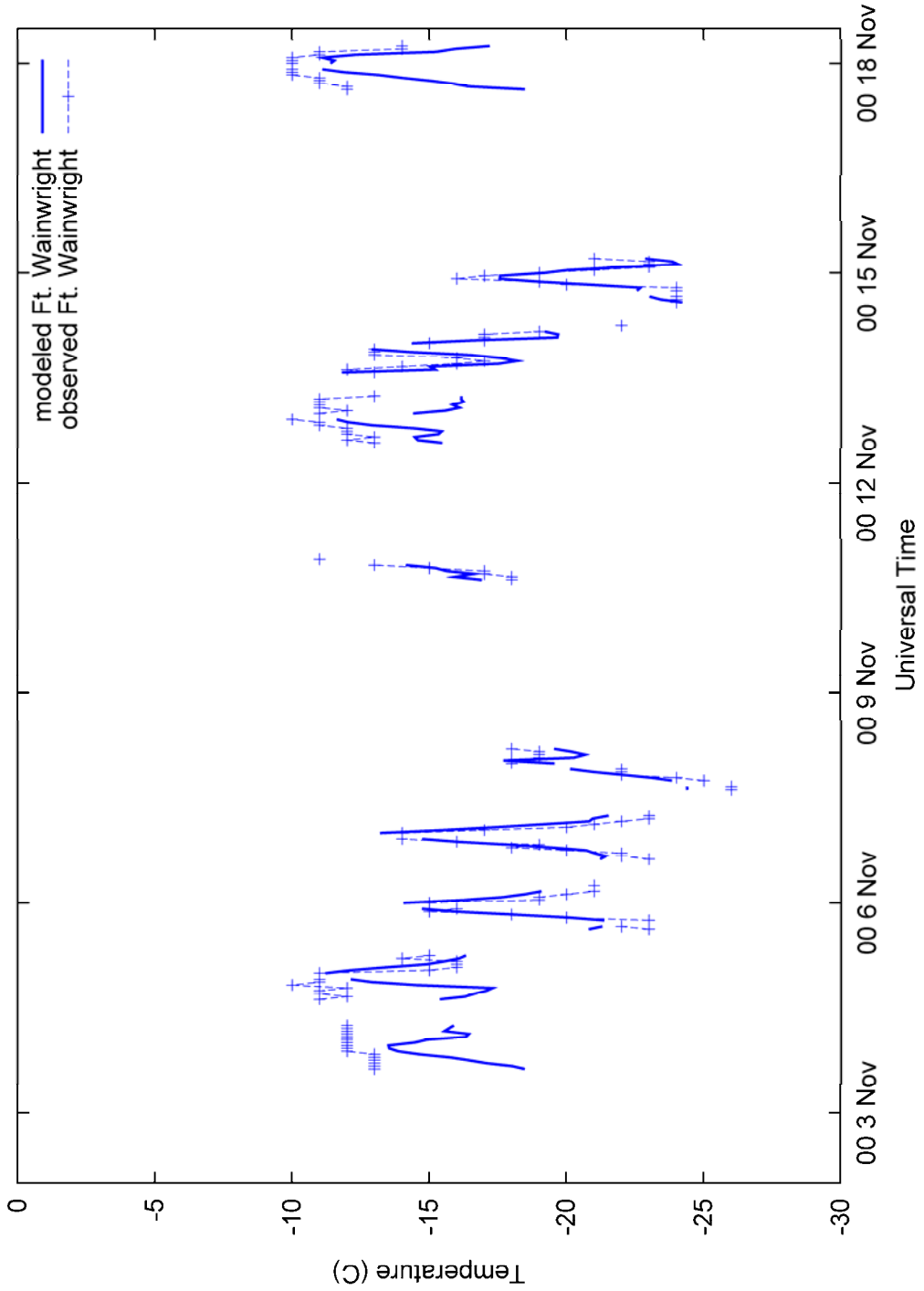


Figure 51: Time series of modeled and observed temperature for Ft. Wainwright in TWIND2X30.

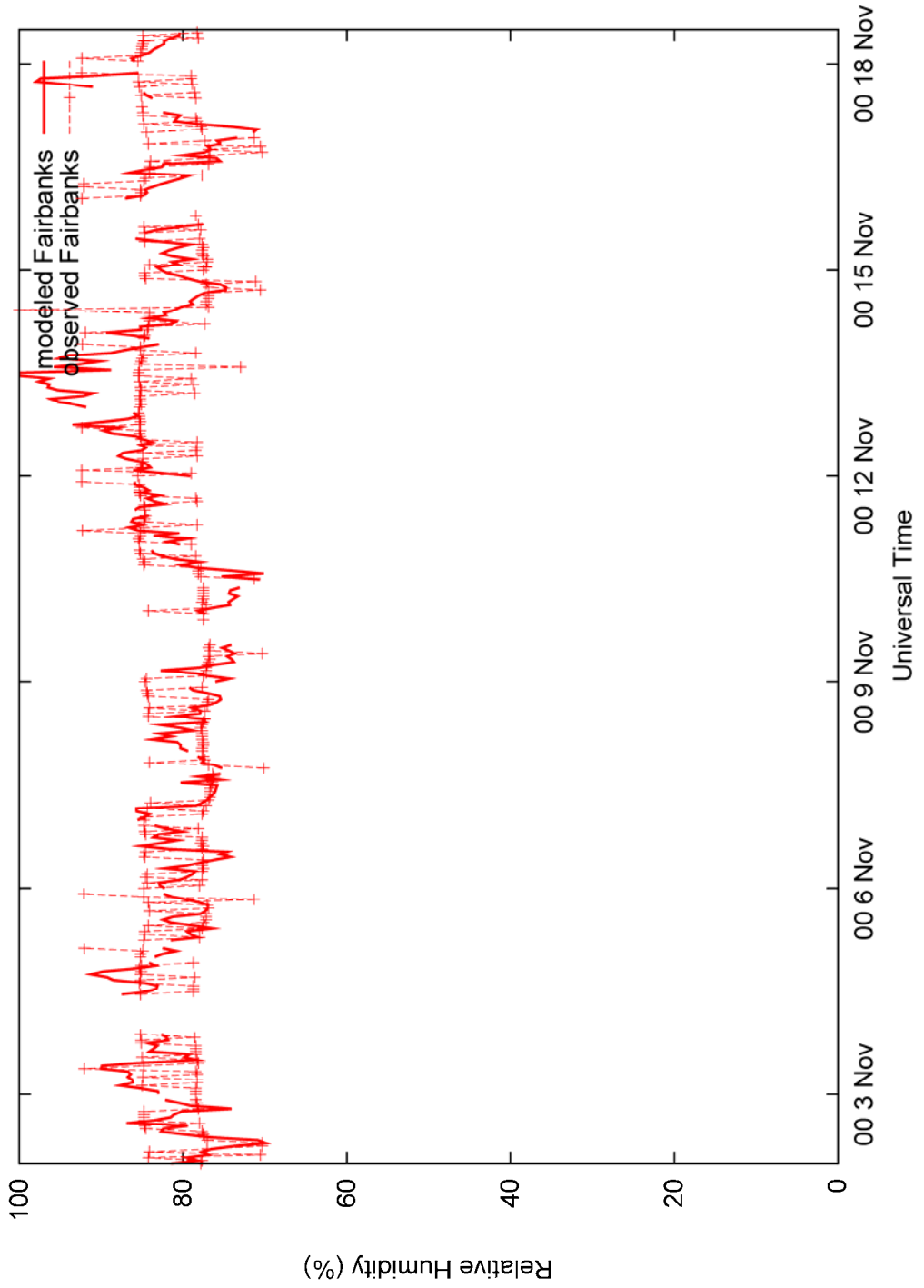


Figure 52: Time series of modeled and observed relative humidity for Fairbanks in TWIND2X30.

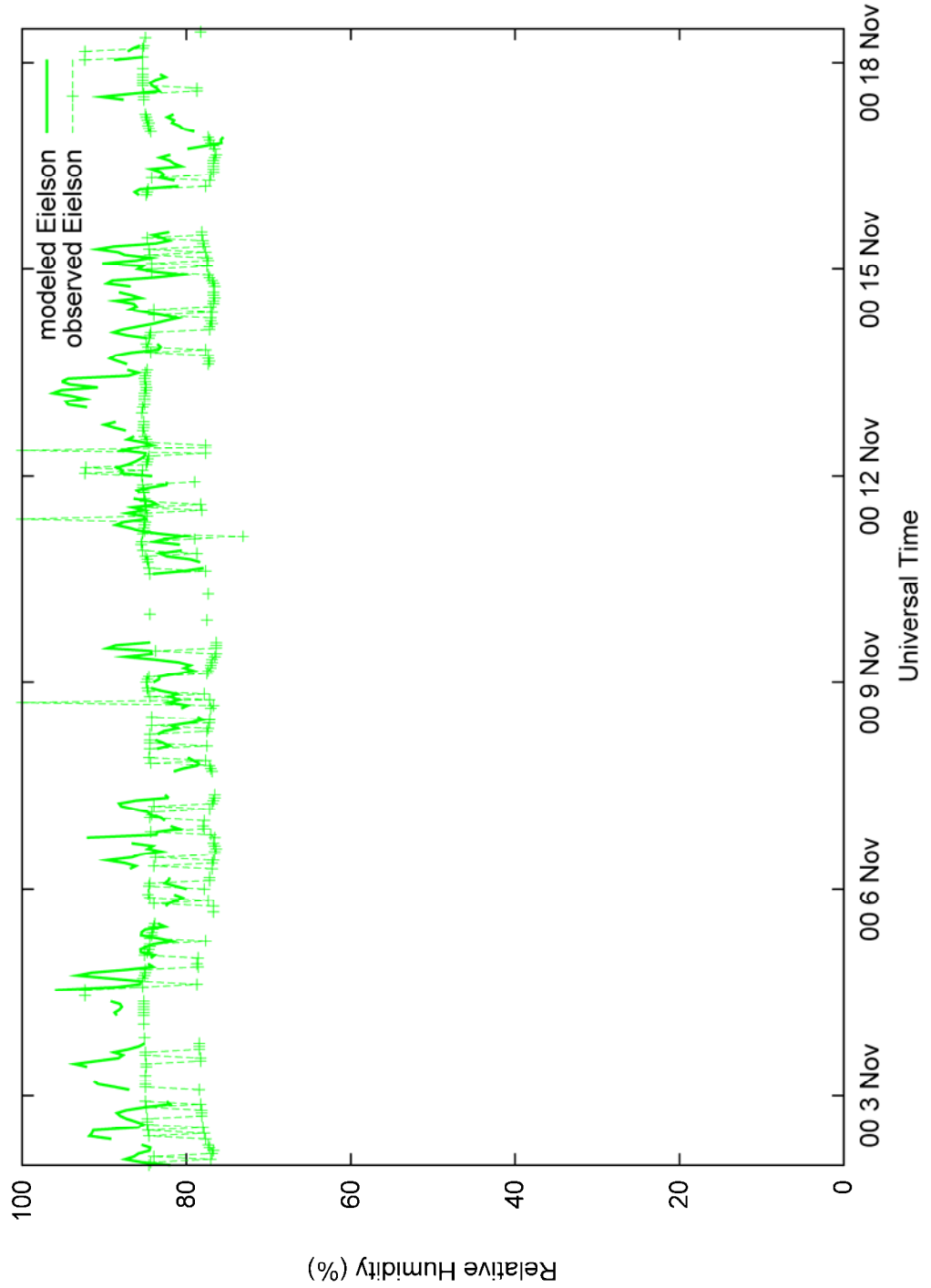


Figure 53: Time series of modeled and observed relative humidity for Eielson in TWIND2X30.

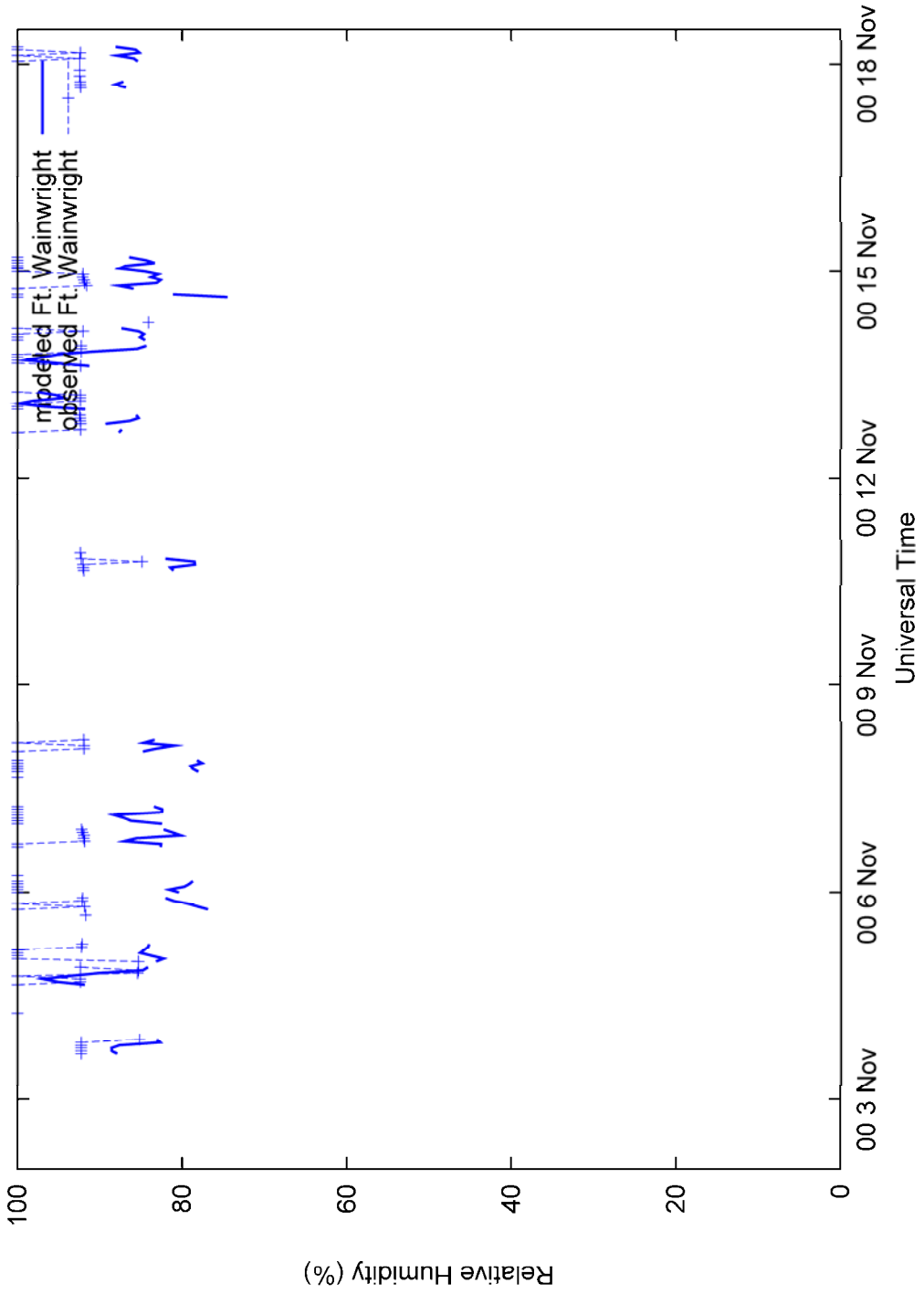


Figure 54: Time series of modeled and observed relative humidity for Ft. Wainwright in TWIND2X30.

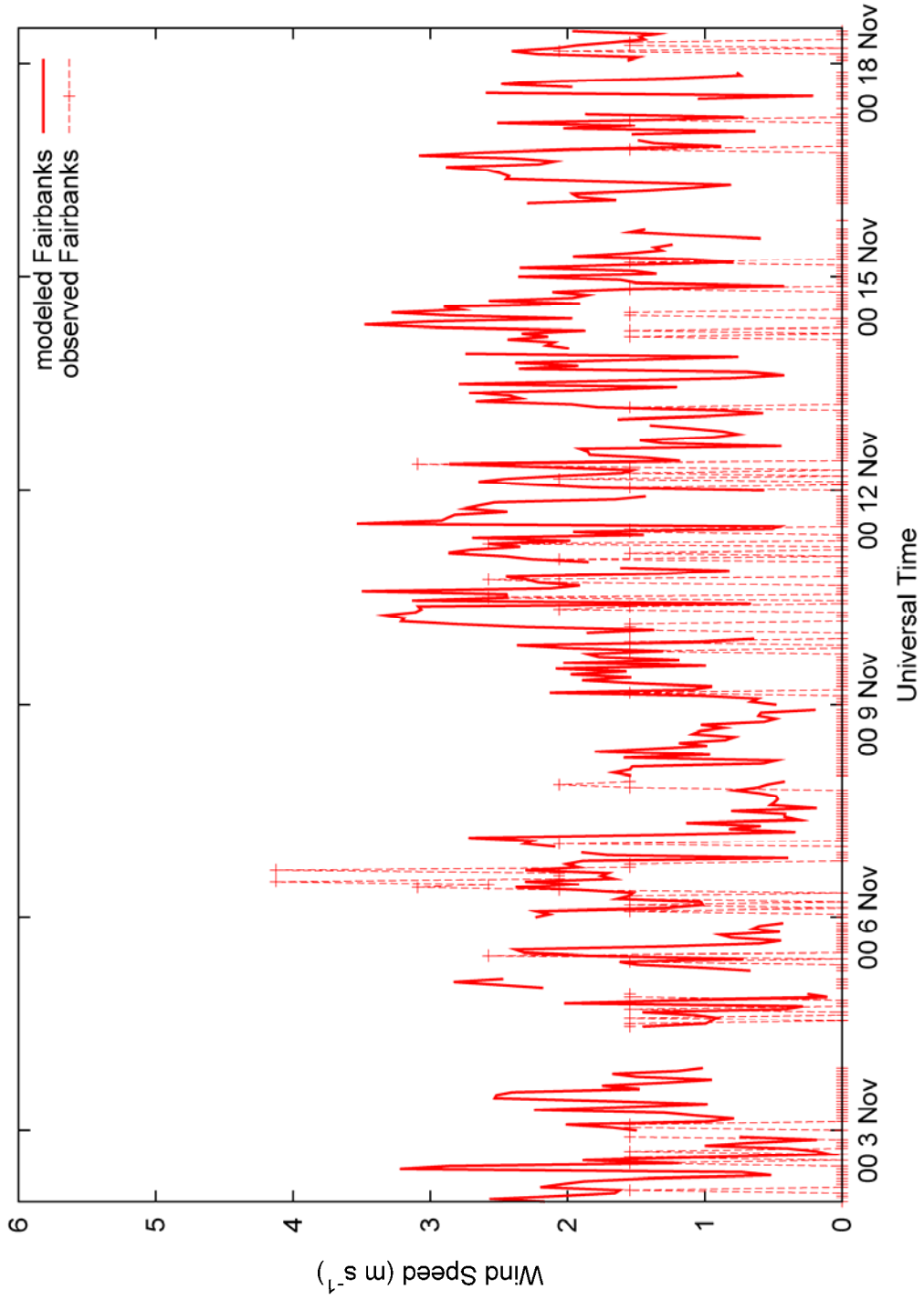


Figure 55: Time series of modeled and observed wind speed for Fairbanks in TWIND2X30.

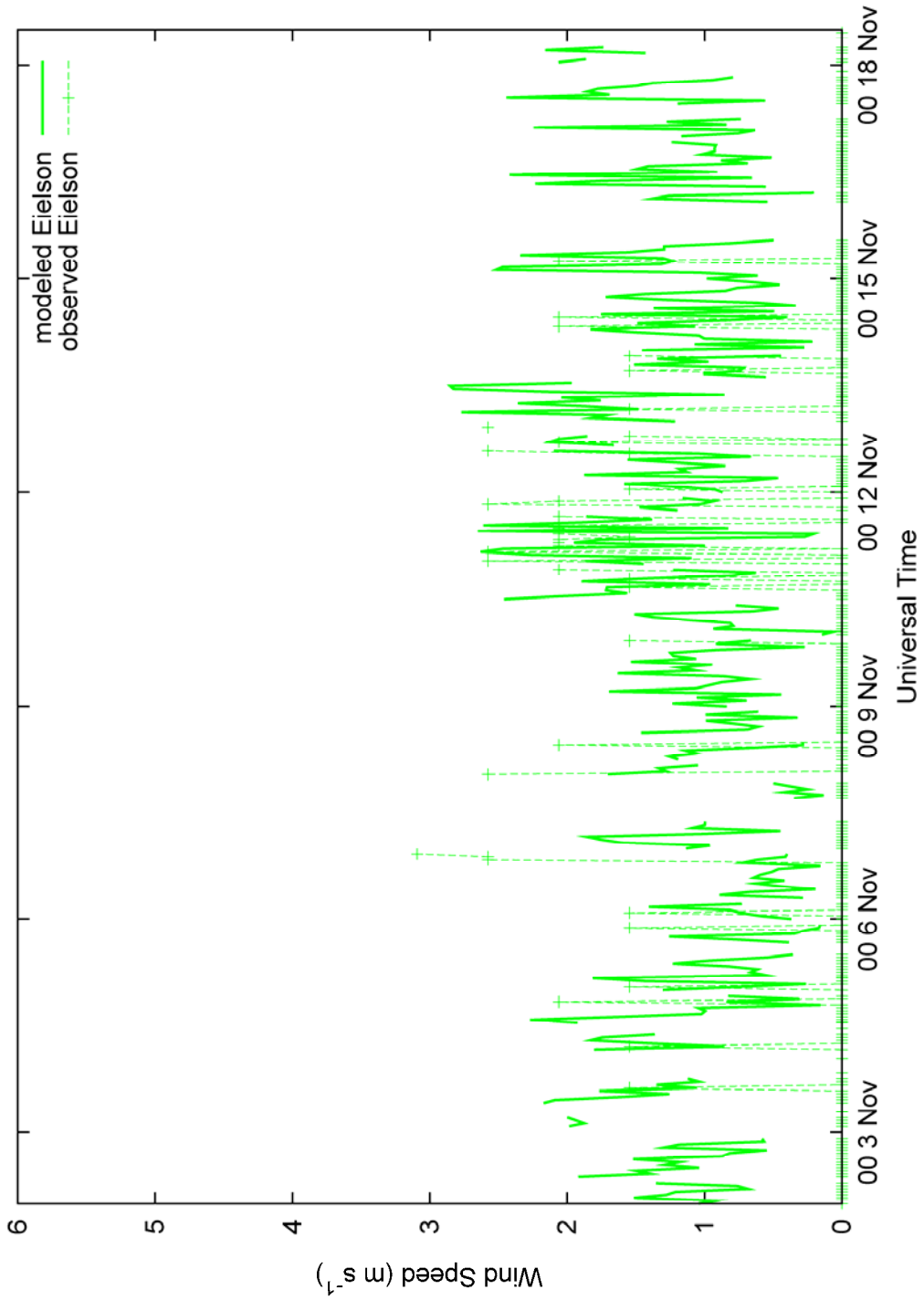


Figure 56: Time series of modeled and observed wind speed for Eielson in TWIND2X30.

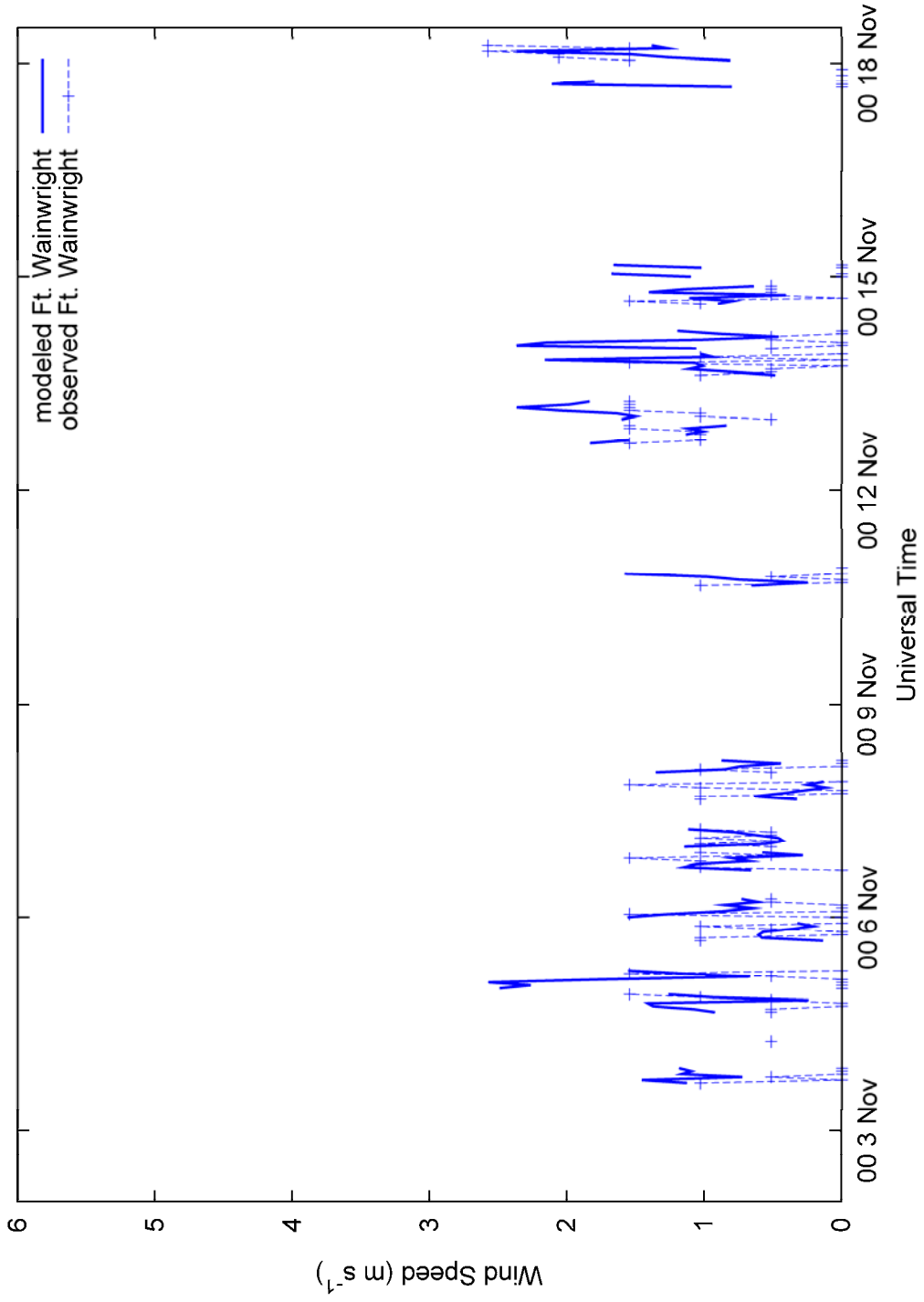


Figure 57: Time series of modeled and observed wind speed for Ft. Wainwright in TWIND2X30.

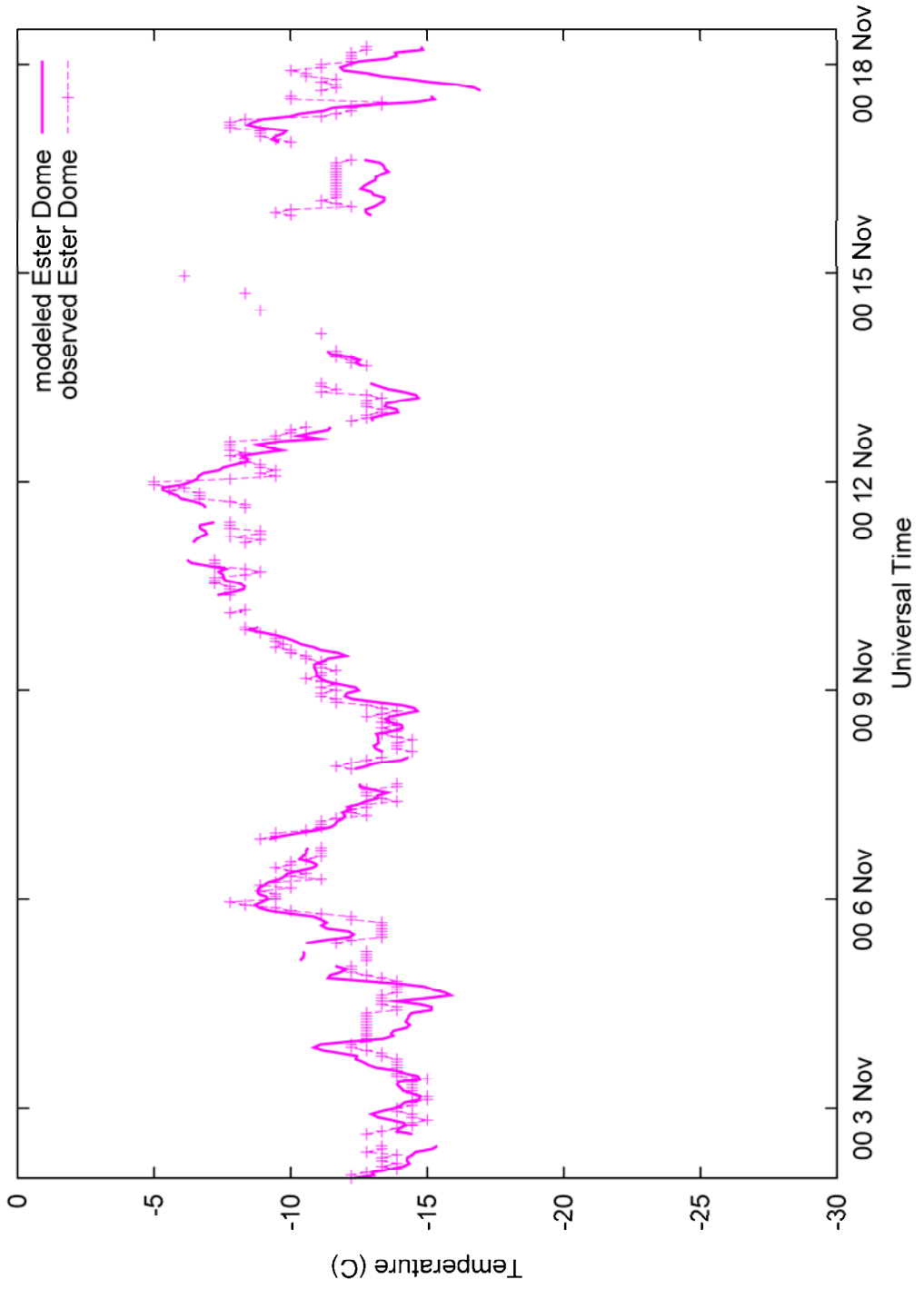


Figure 58: Time series of modeled and observed temperature for Ester Dome in TWIND2X30.

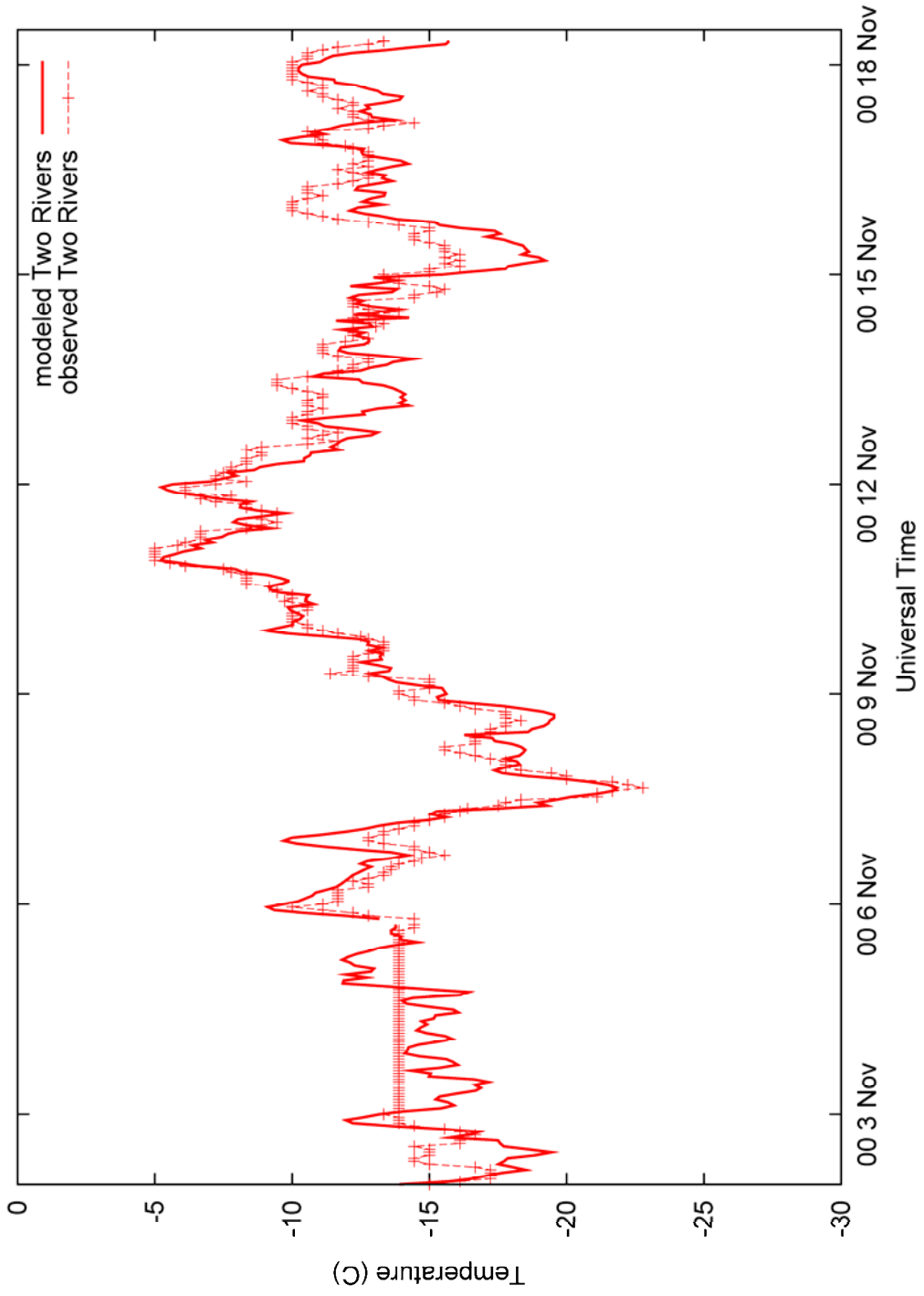


Figure 59: Time series of modeled and observed temperature at Two Rivers in TWIND2X30.

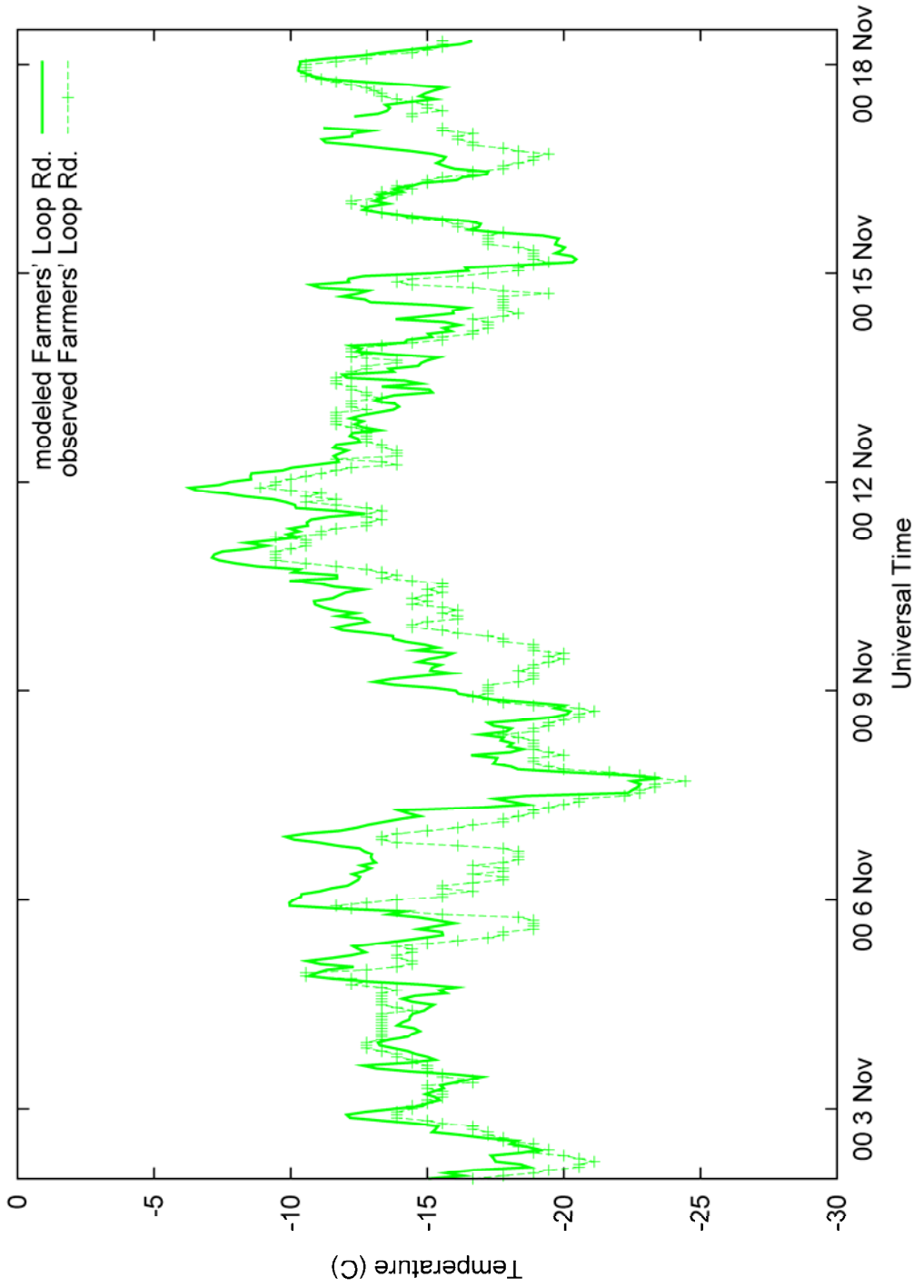


Figure 60: Modeled and observed time series of temperature for Farmers' Loop Rd. in TWIND2X30.

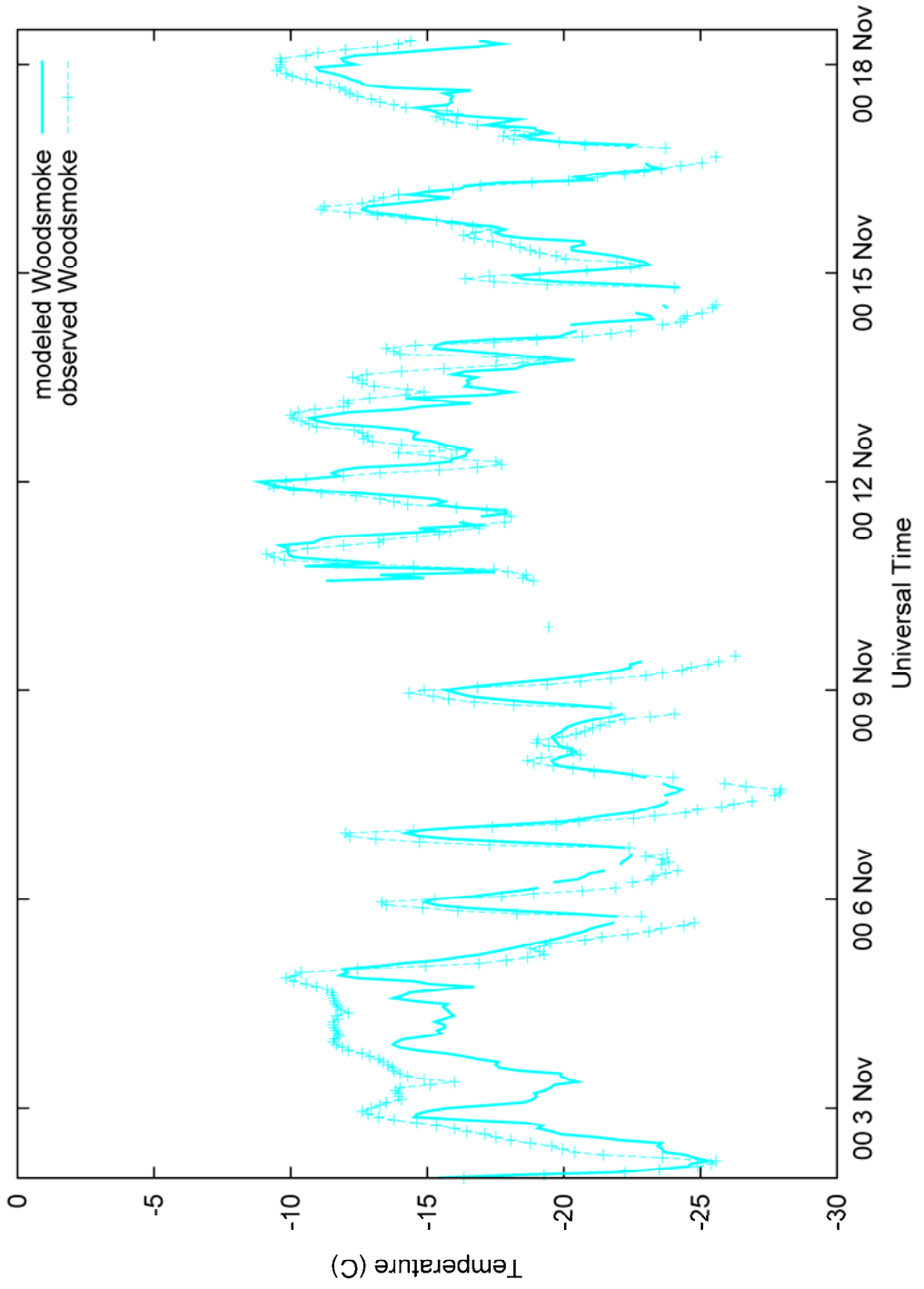


Figure 61: Time series of modeled and observed temperature for Woodsmoke in TWIND2X30.

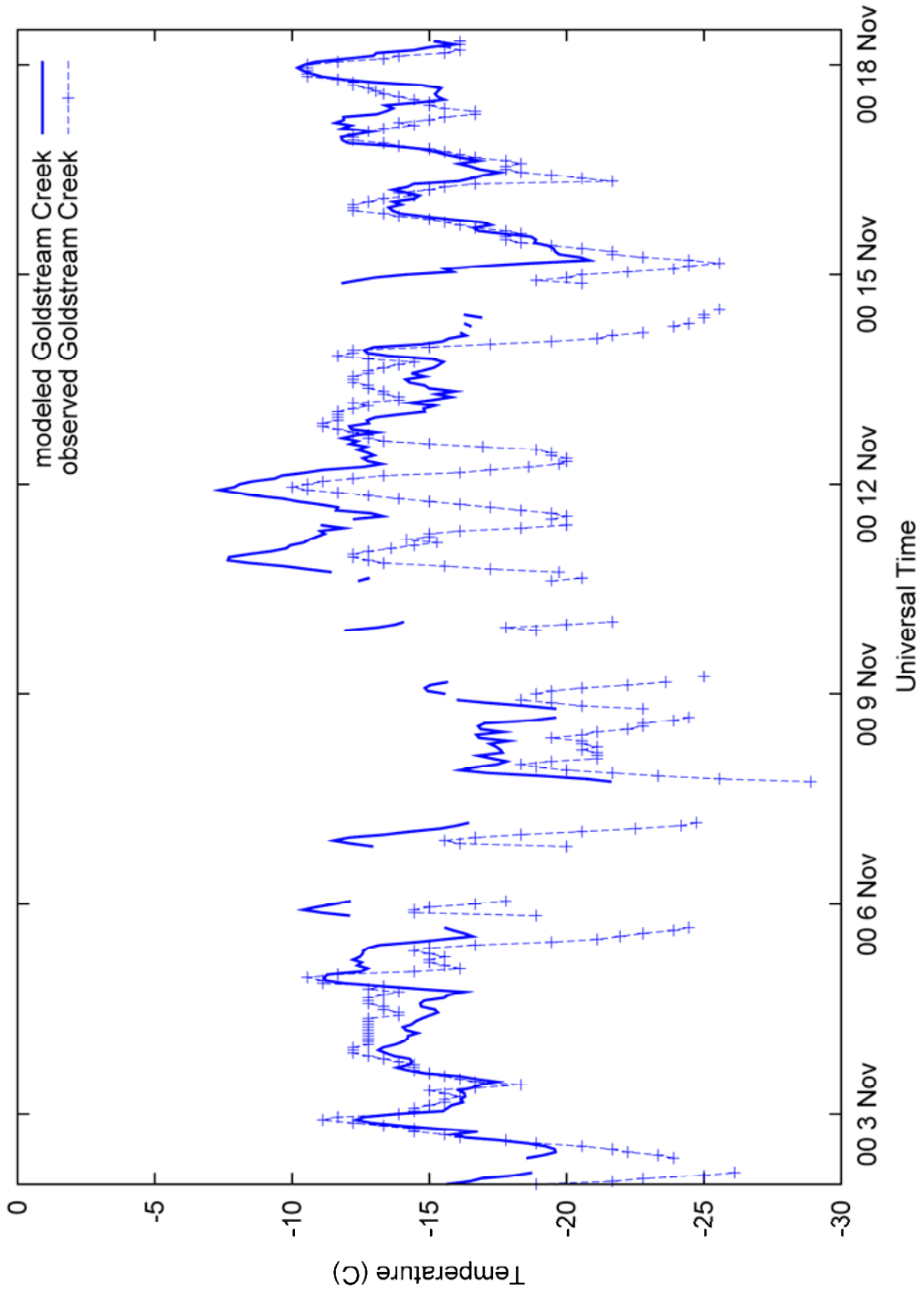


Figure 62: Time series of modeled and observed temperature for Goldstream Creek in TWIND2X30.

# APPENDIX B – Detailed Time-Series Figures of 23 Jan – 12 Feb 2008 Episode, for TWIND2X30 Configuration

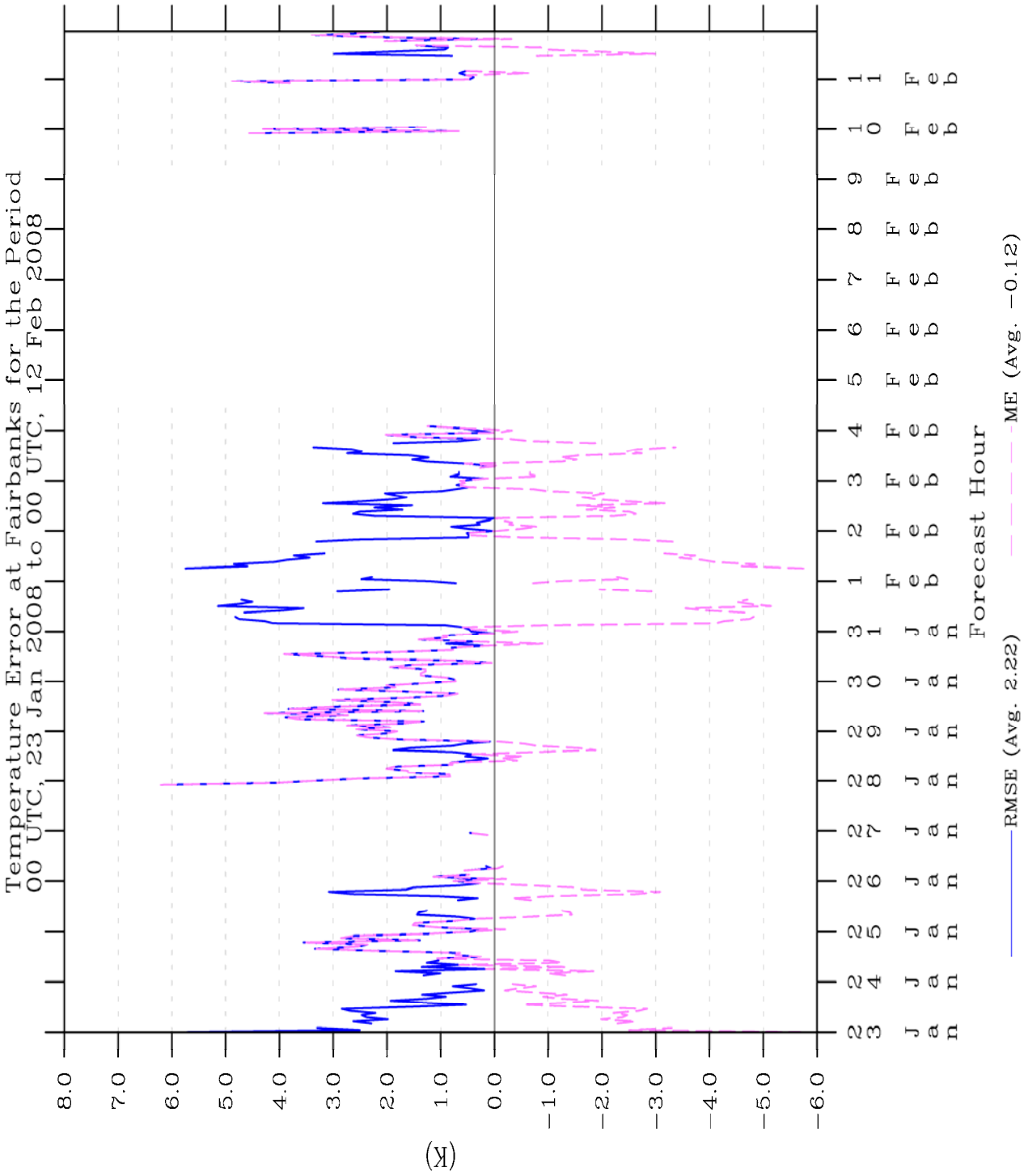


Figure 63: Time series of temperature statistics for Fairbanks in TWIND2X30

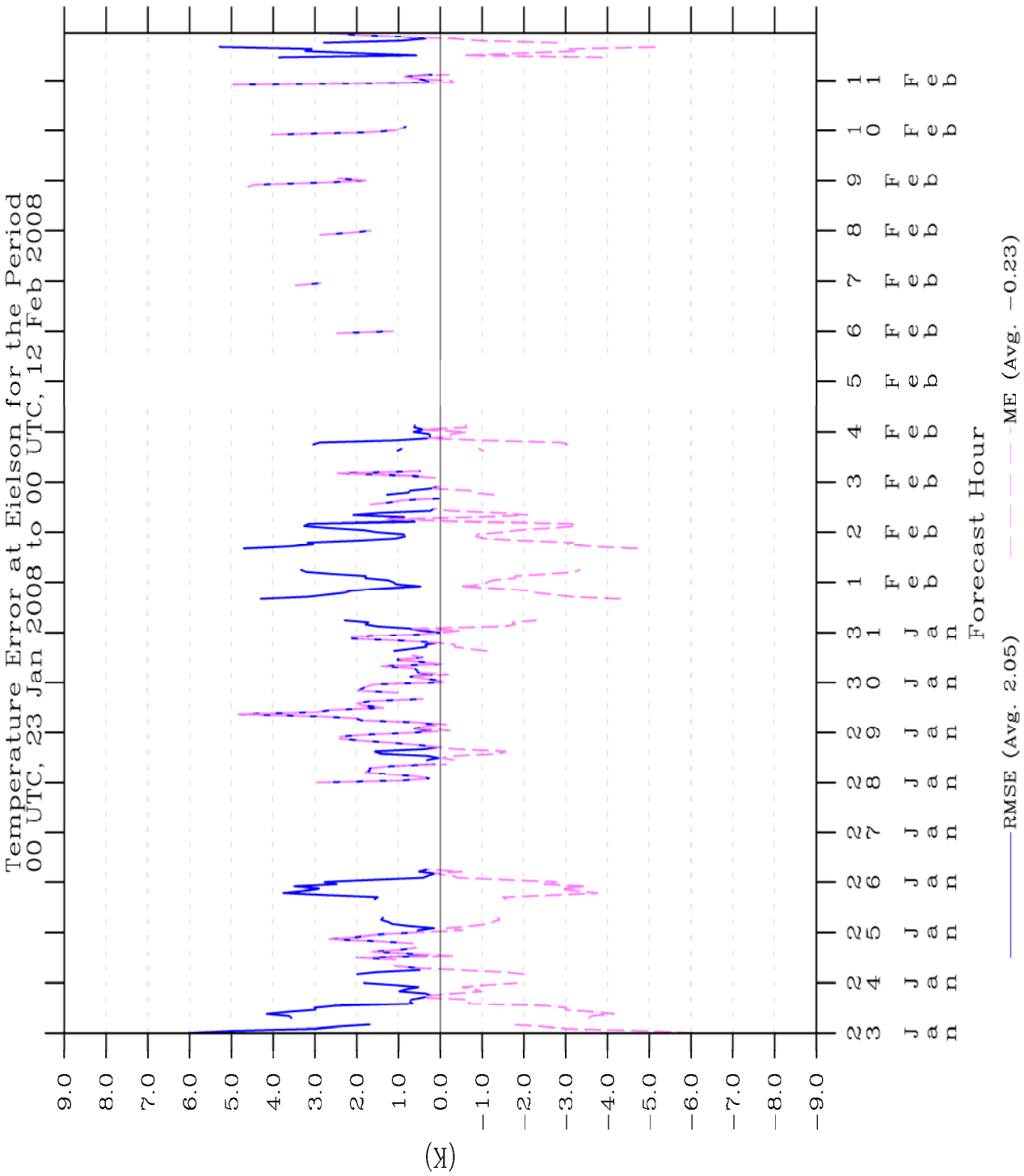


Figure 64: Time series of temperature statistics for Eielson in TWIND2X30.

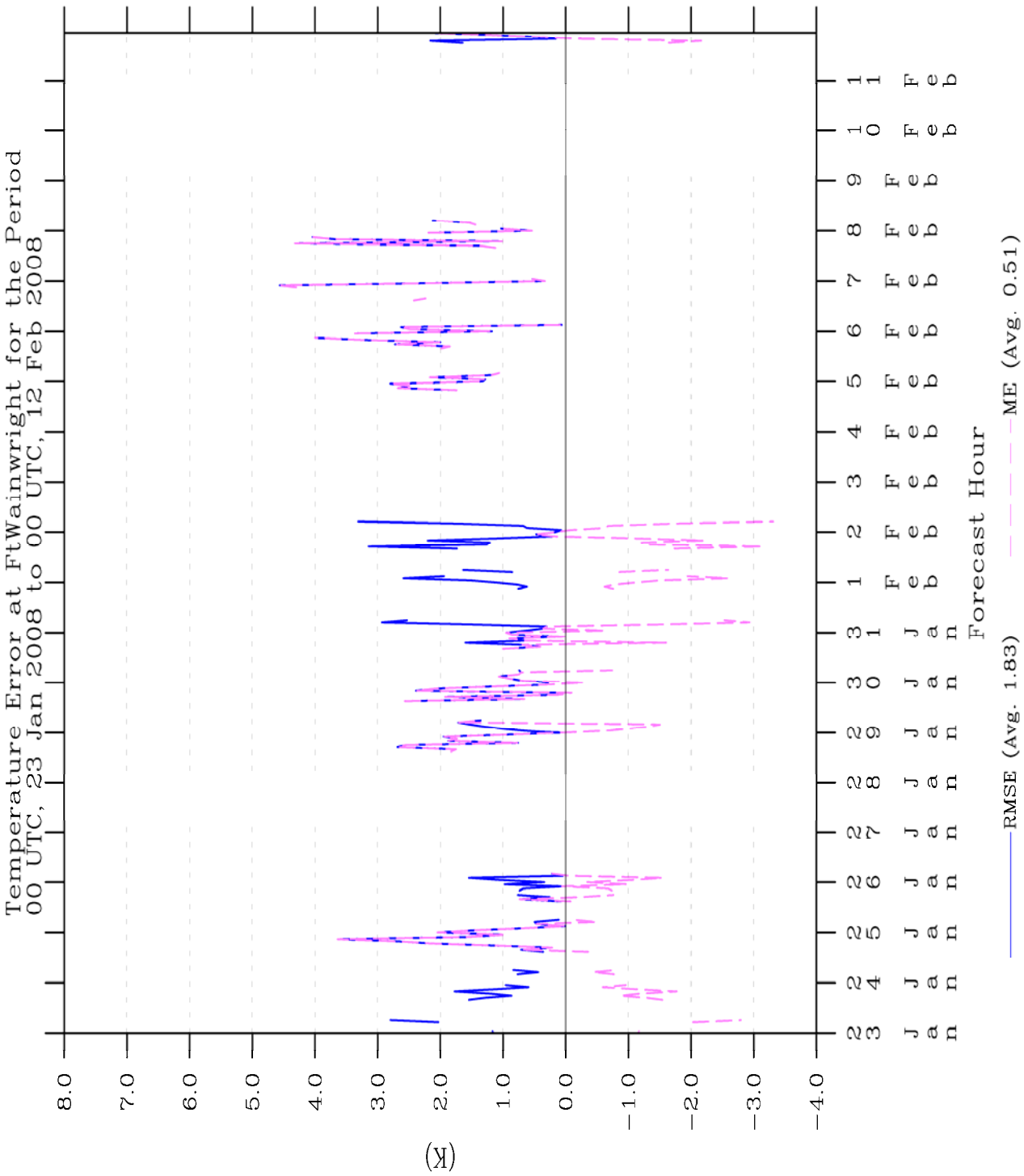


Figure 65: Time series of temperature statistics for Ft. Wainwright in TWIND2X30.

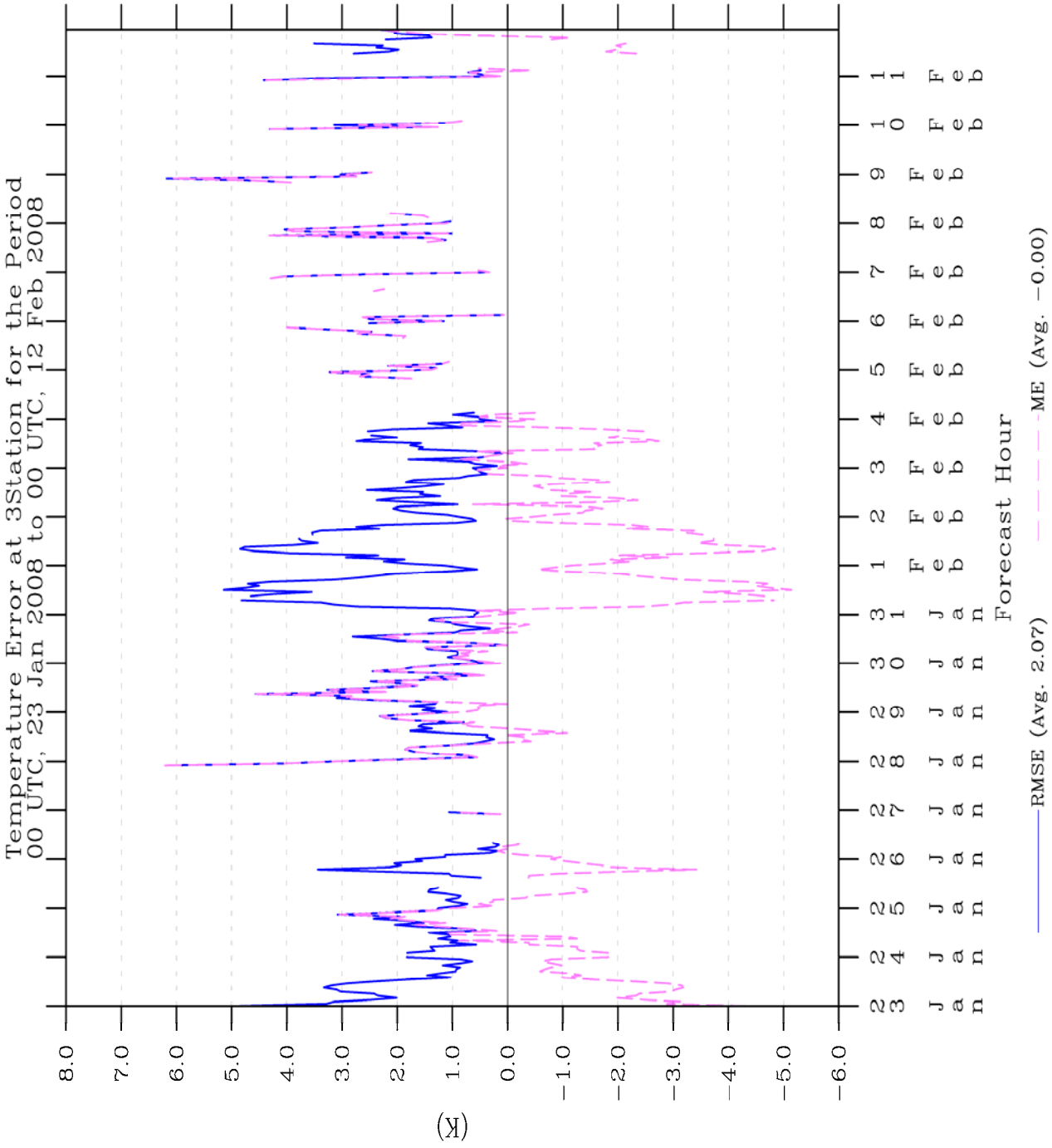


Figure 66: Time series of temperature statistics for all three stations in TWIND2X30.

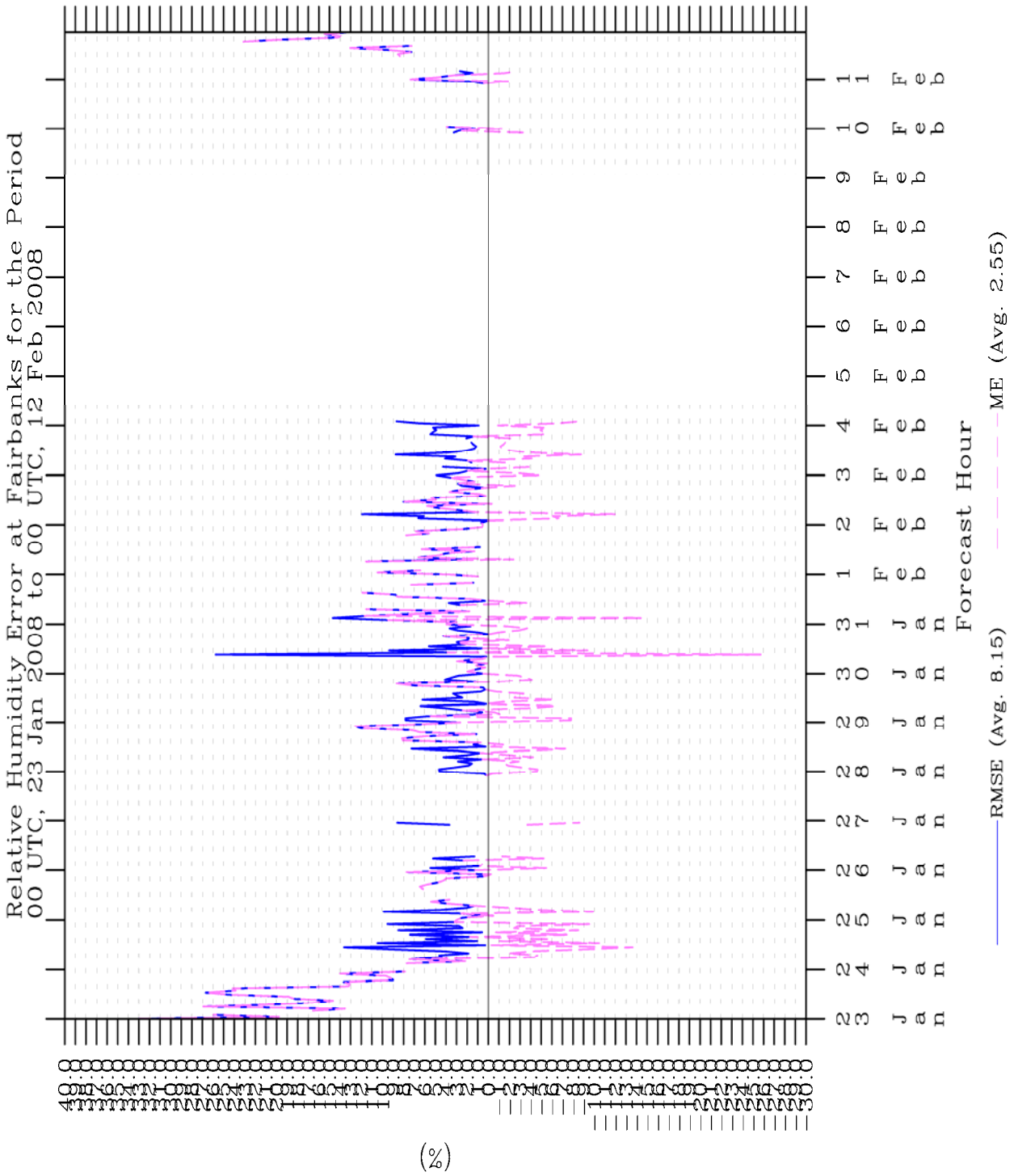


Figure 67: Time series of relative humidity statistics for Fairbanks in TWIND2X30.

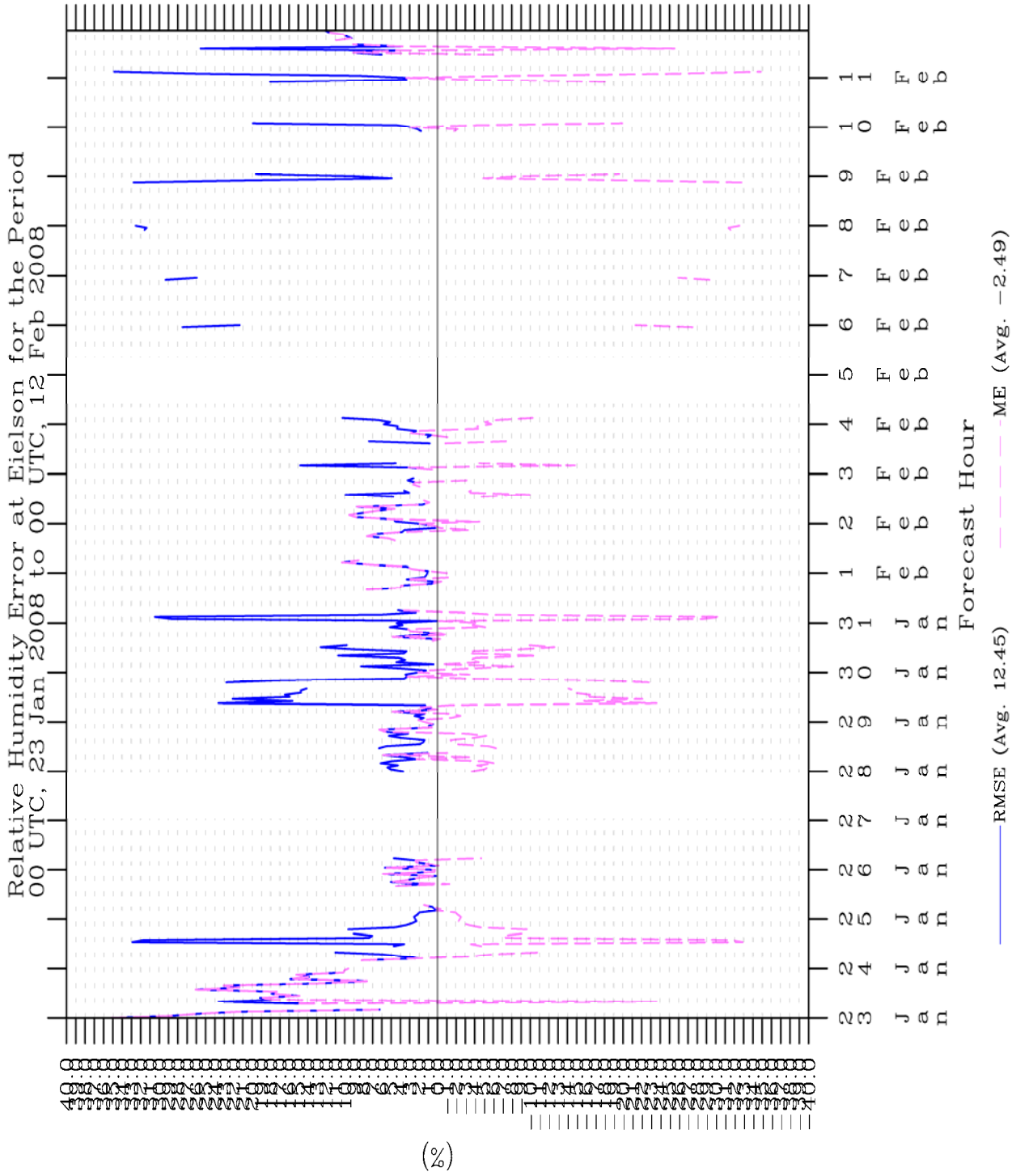


Figure 68: Time series of relative humidity statistics for Eielson in TWIND2X30.

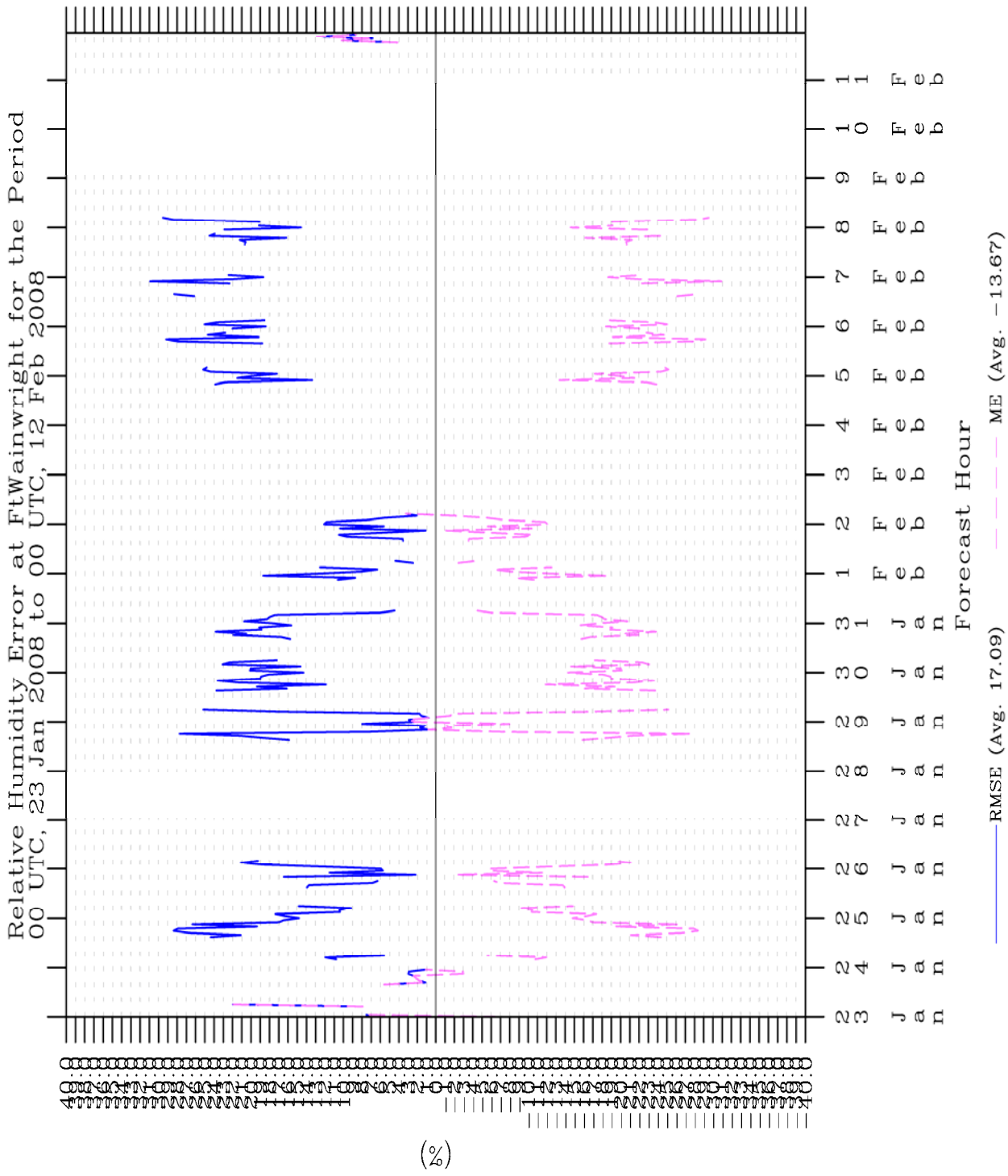


Figure 69: Time series of relative humidity statistics for Ft. Wainwright in TWIND2X30.

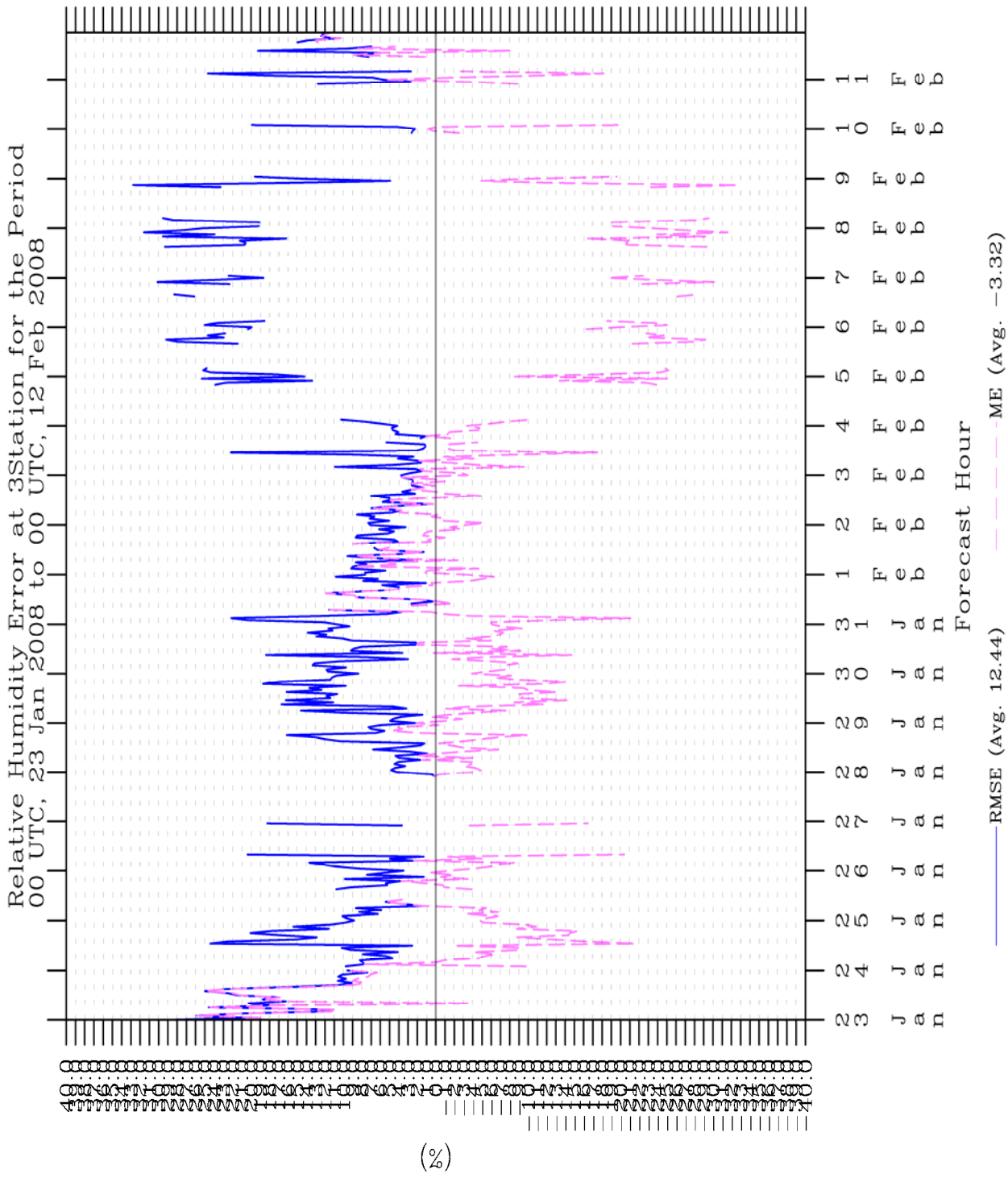


Figure 70: Time series of relative humidity statistics for all three stations in TWIND2X30.

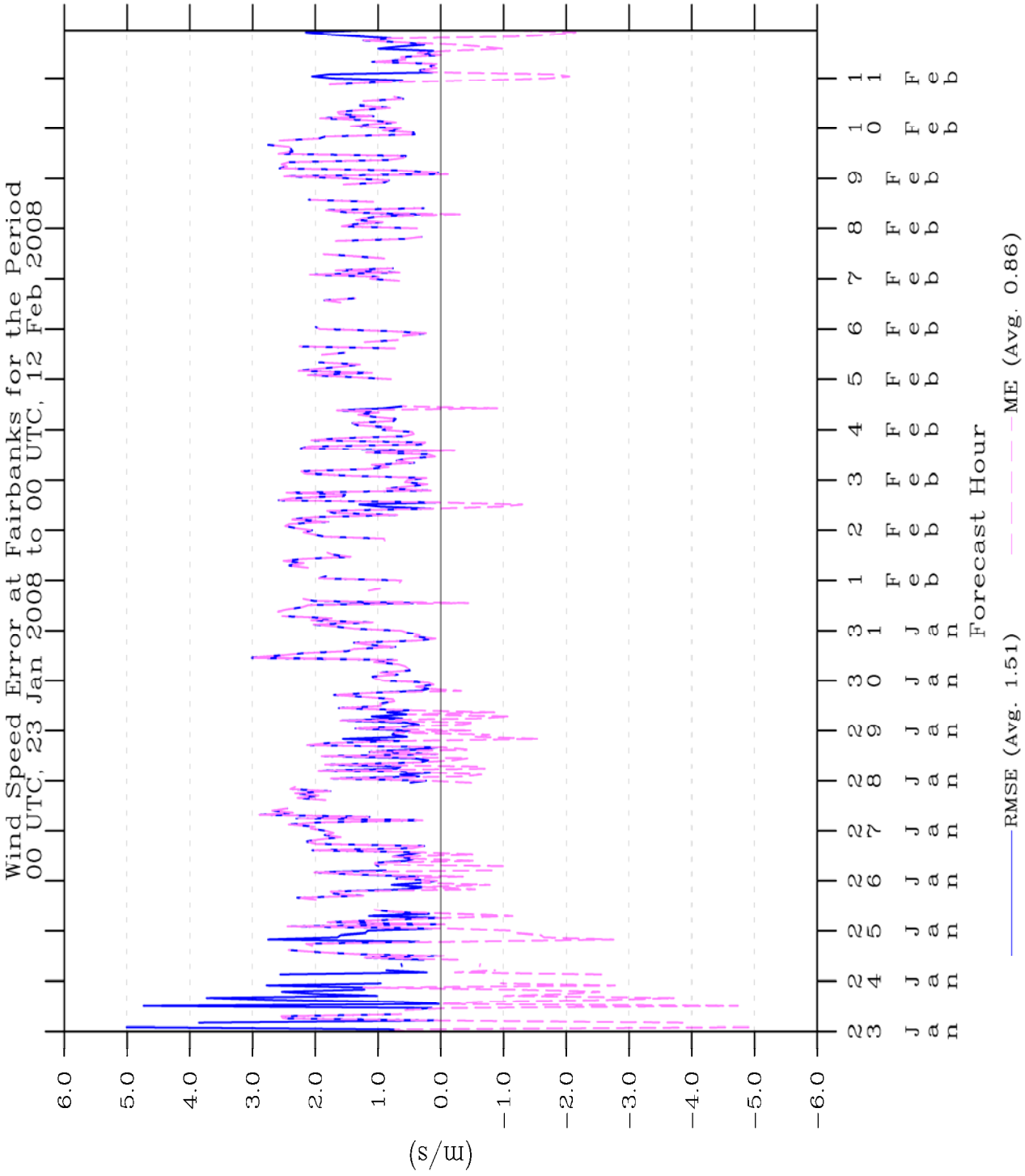


Figure 71: Time series of wind speed statistics for Fairbanks in TWIND2X30.

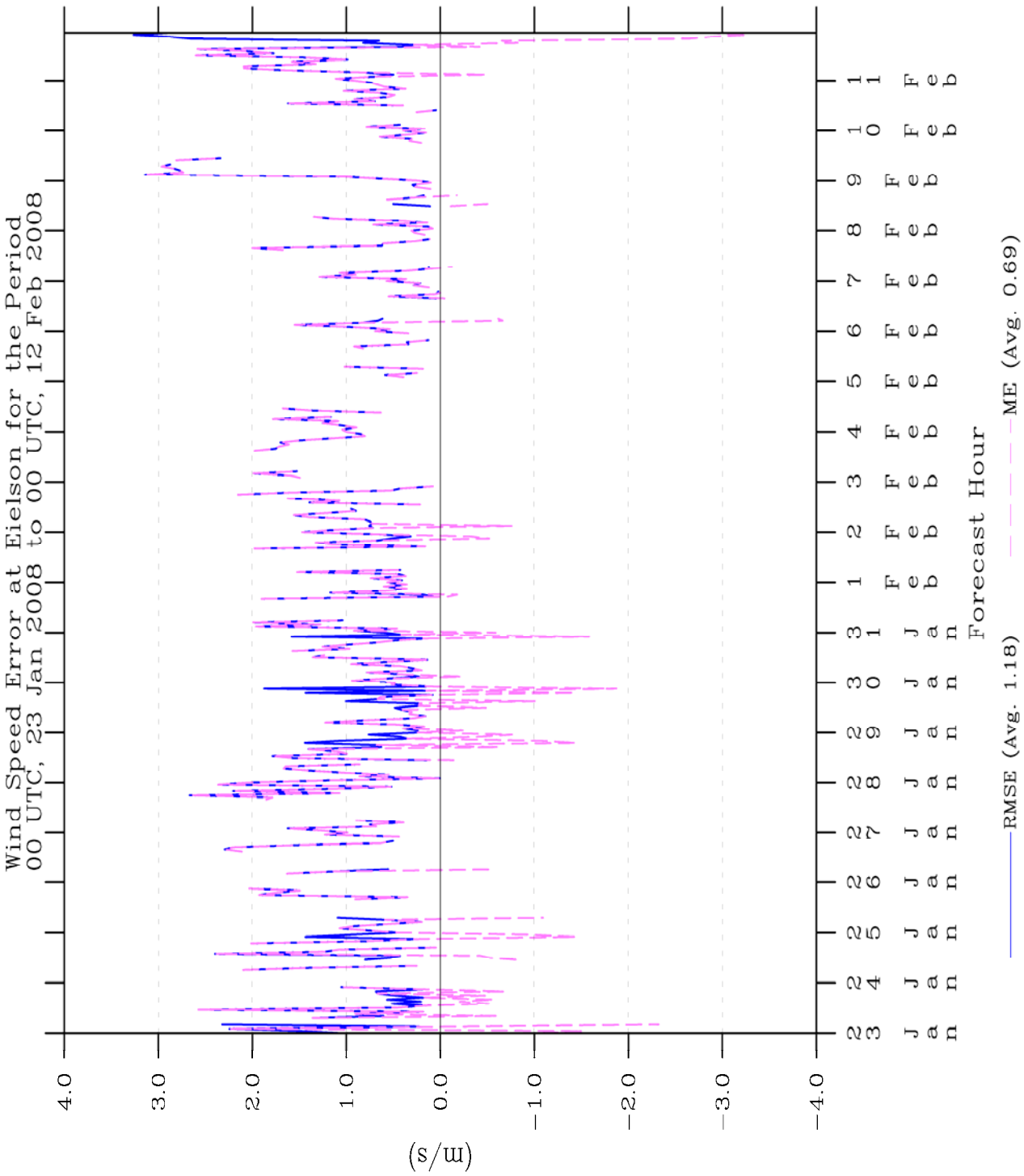


Figure 72: Time series of wind speed statistics for Eielson in TWIND2X30.

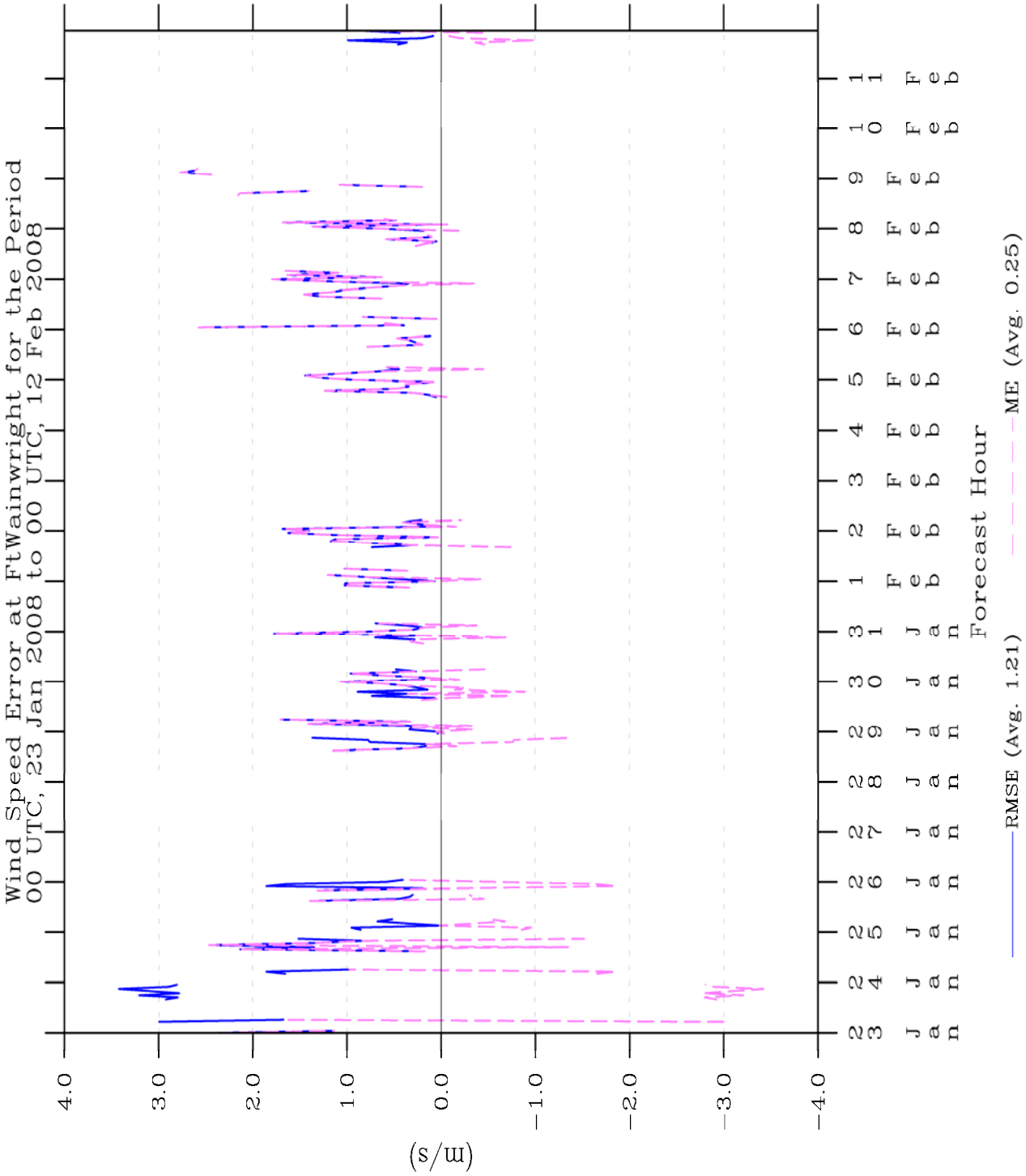


Figure 73: Time series of wind speed statistics for Ft. Wainwright in TWIND2X30.

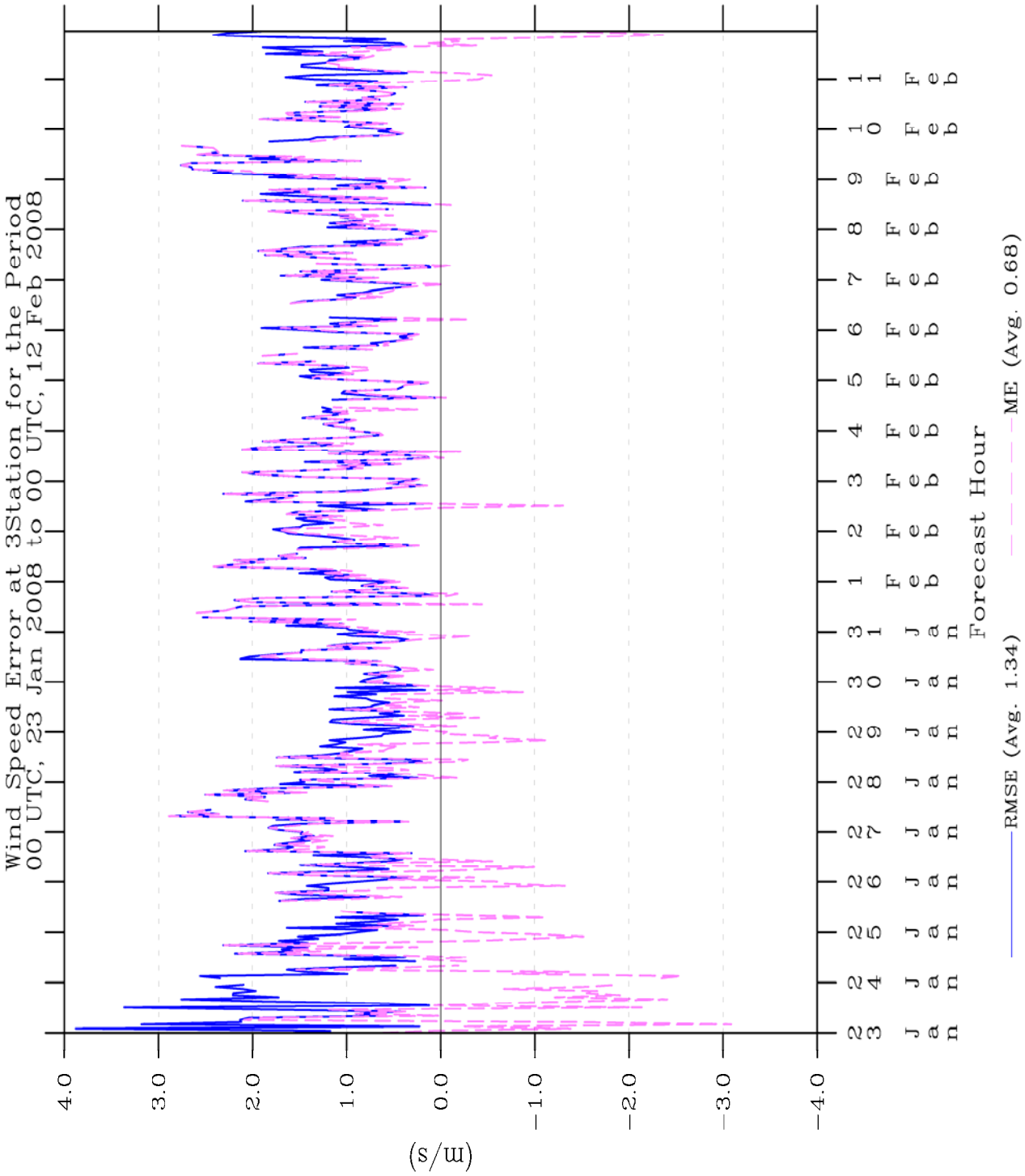


Figure 74: Time series of wind speed statistics for all three stations in TWIND2X30.

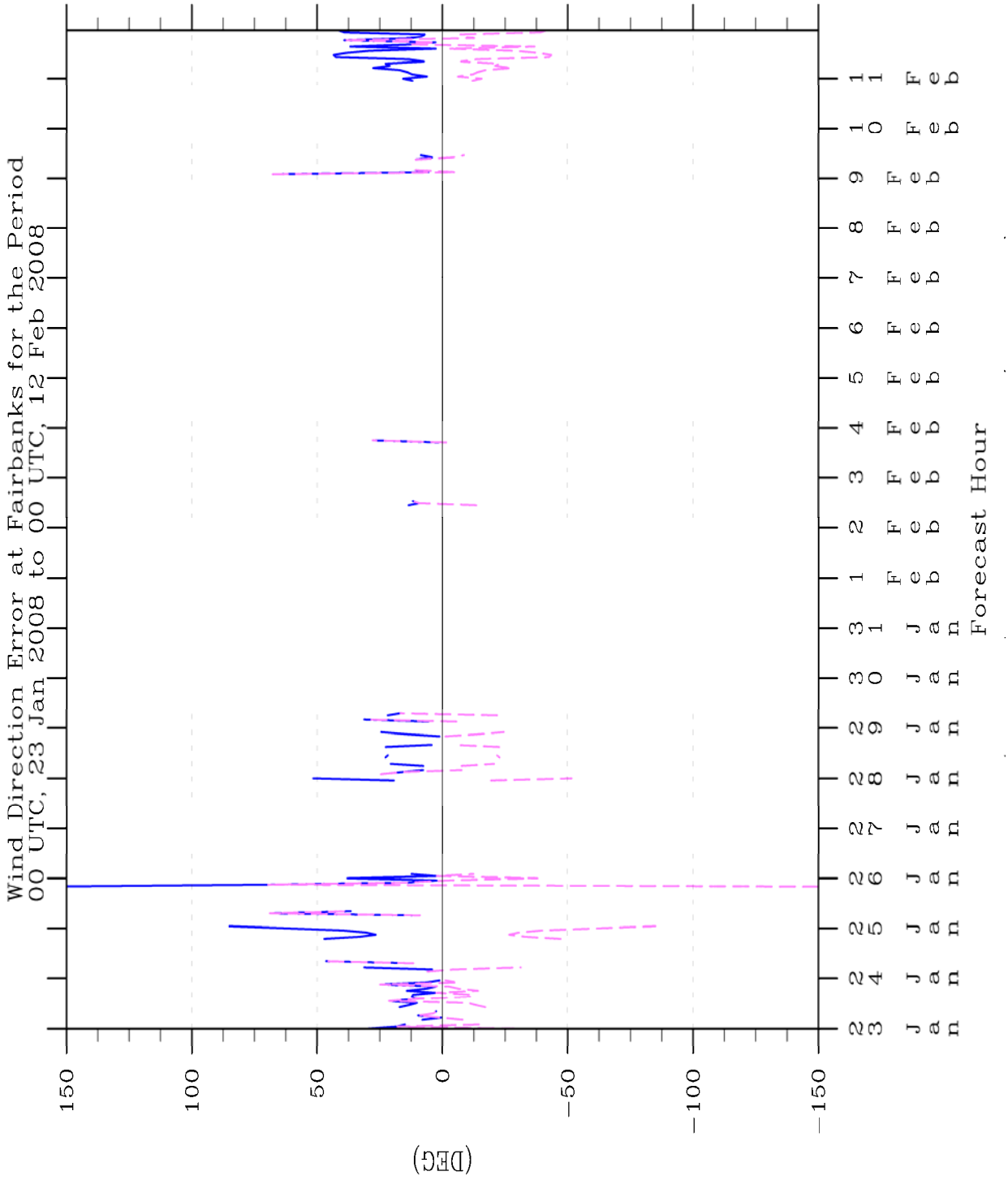


Figure 75: Time series of wind direction mean absolute error (blue) and mean error (magenta) statistics for Fairbanks in TWIND2X30.

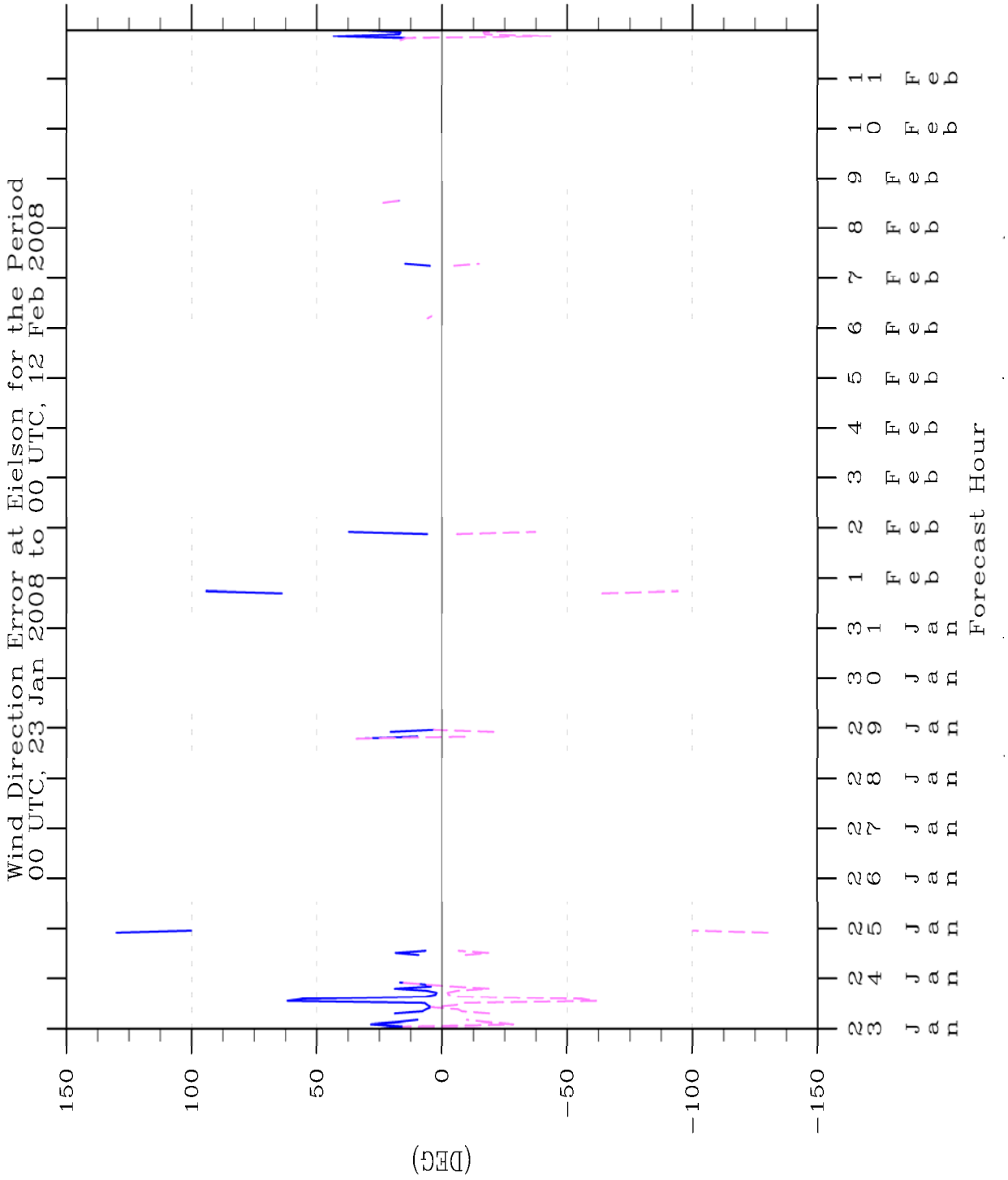


Figure 76: Time series of wind direction mean absolute error (blue) and mean error (magenta) statistics for Eielson in TWIND2X30.

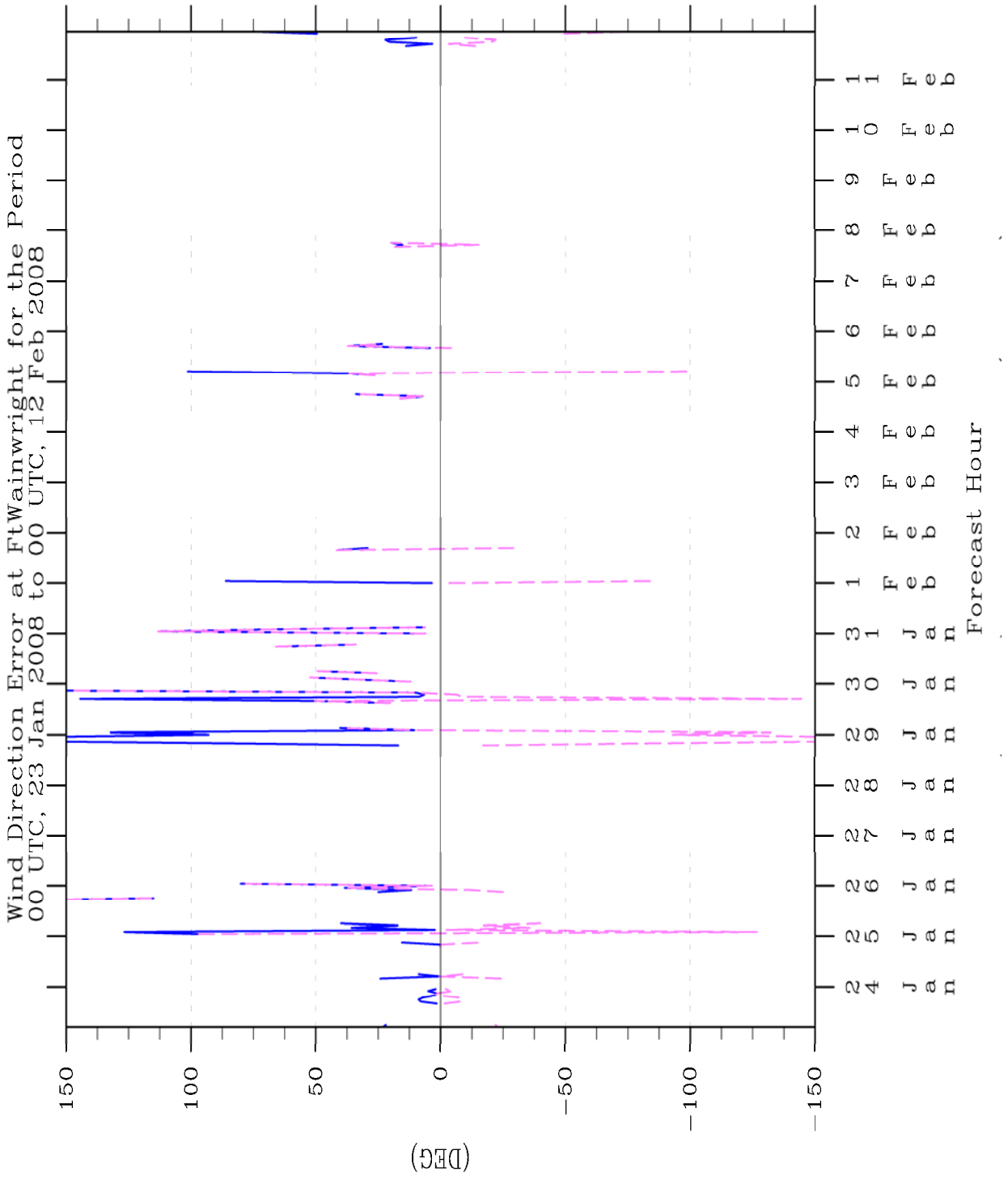


Figure 77: Time series of wind direction mean absolute error (blue) and mean error (magenta) statistics for Ft. Wainwright in TWIND2X30.

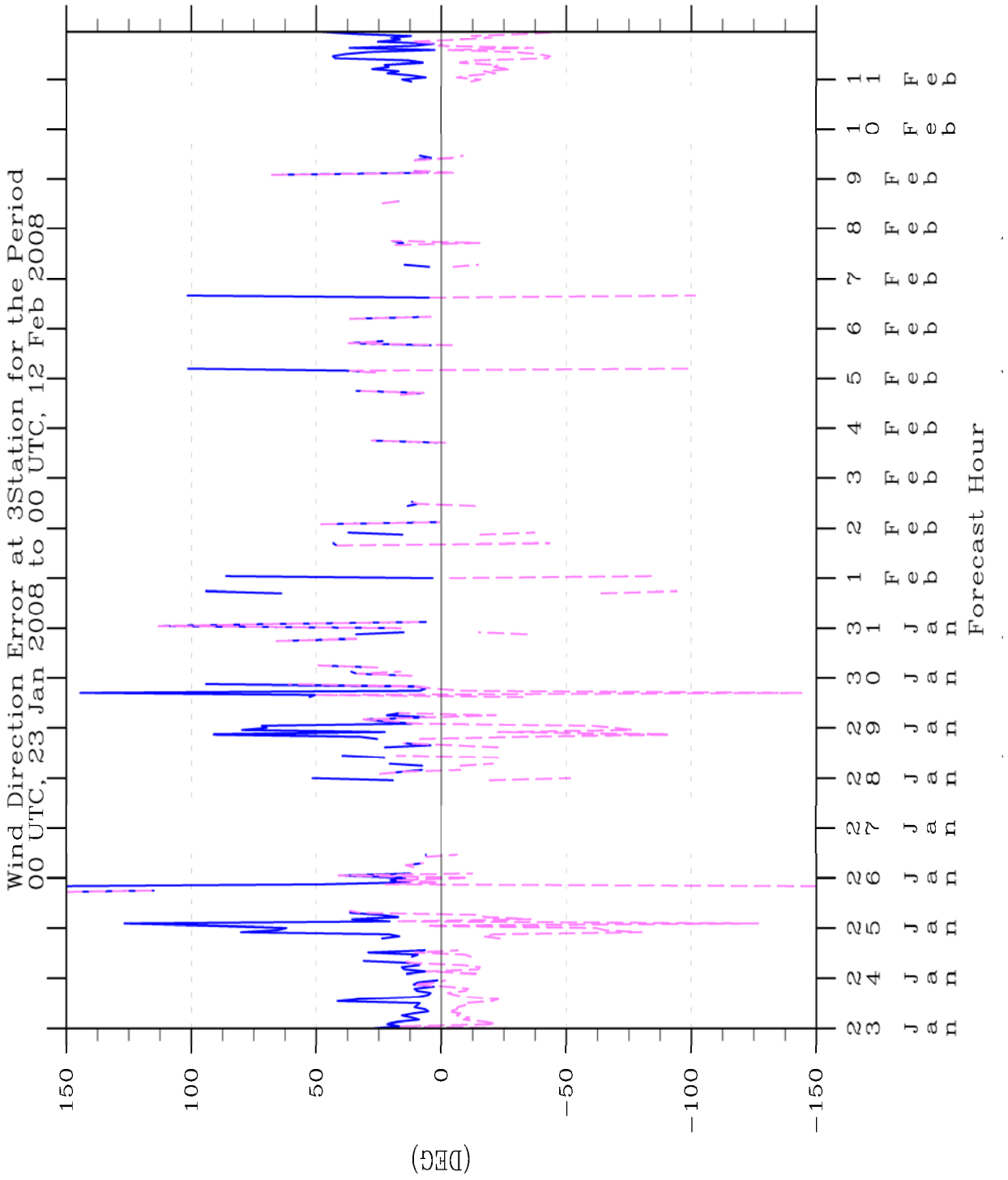


Figure 78: Time series of wind direction mean absolute error (blue) and mean error (magenta) statistics for all three stations in TWIND2X30.

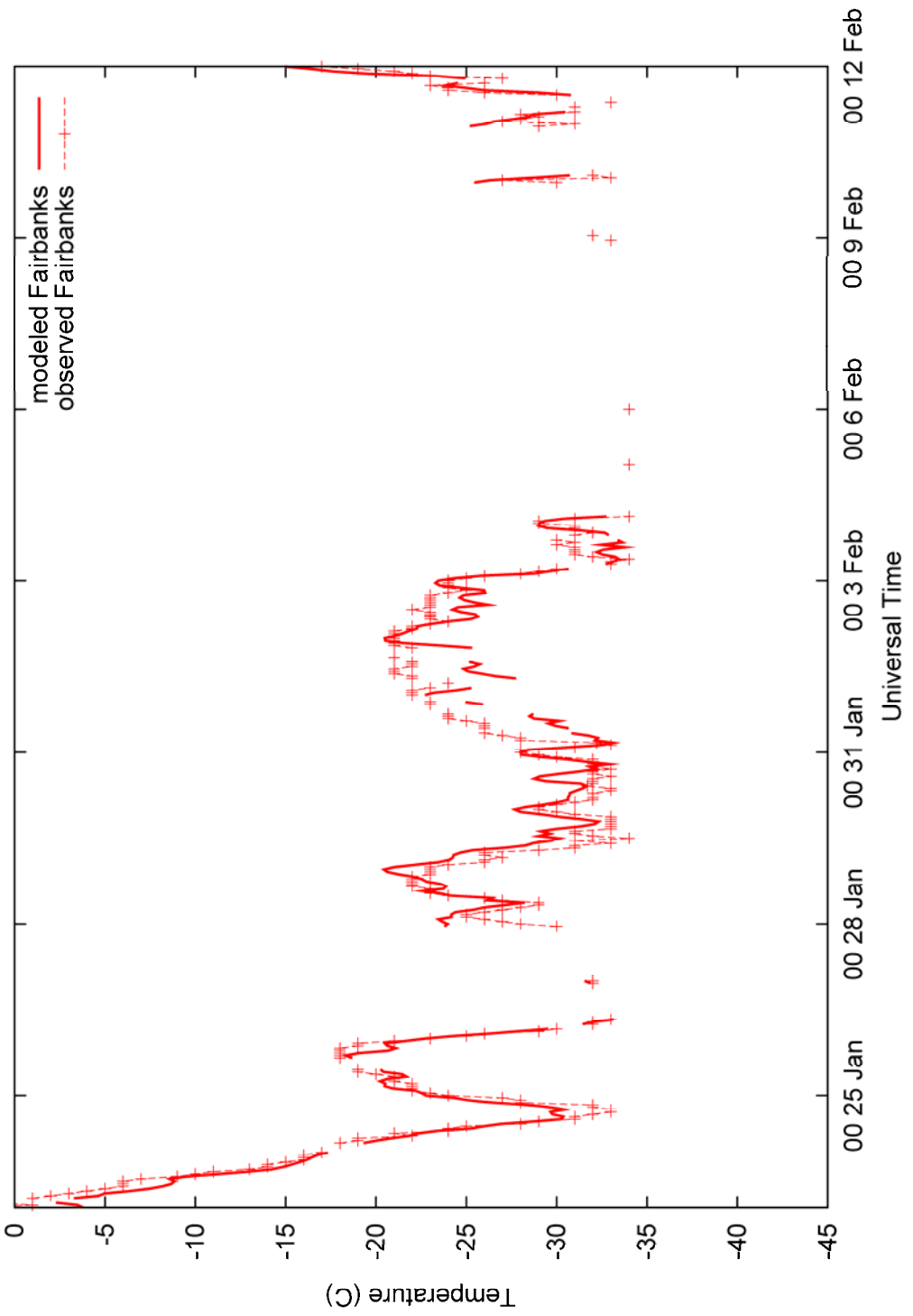


Figure 79: Time series of modeled and observed temperature for Fairbanks in TWIND2X30.

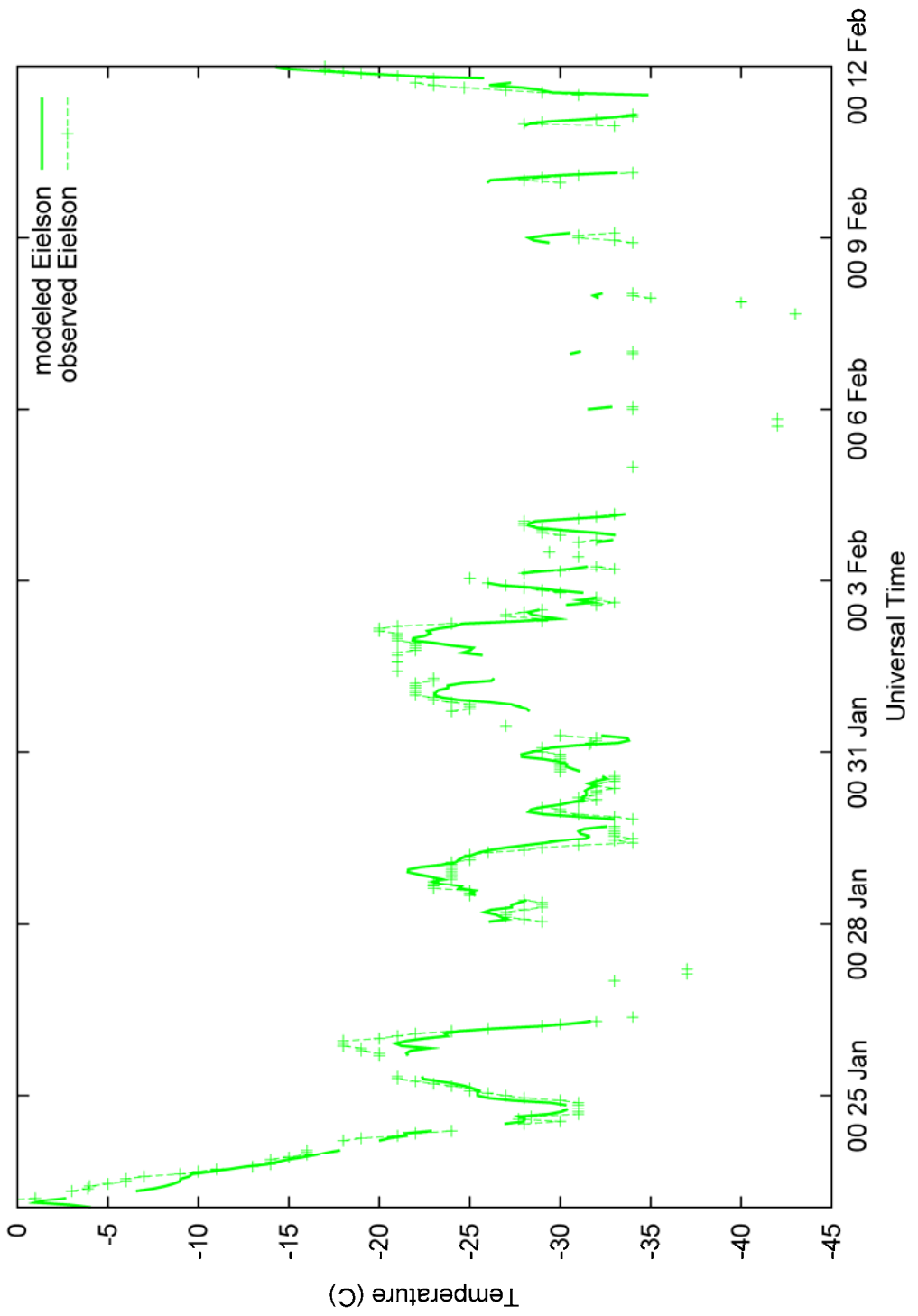


Figure 80: Time series of modeled and observed temperature for Eielson in TWIND2X30.

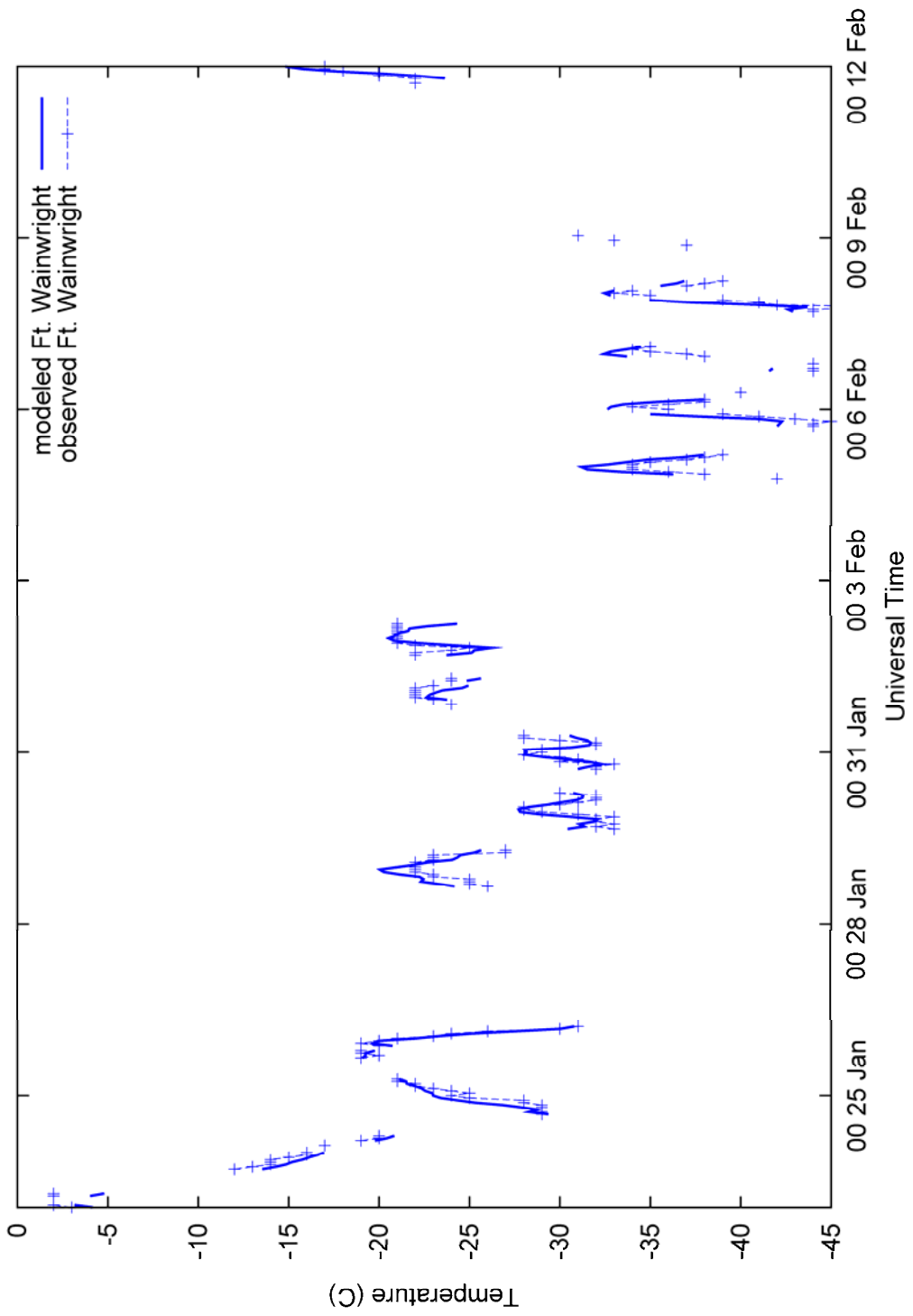


Figure 81: Time series of modeled and observed temperature for Ft. Wainwright in TWIND2X30.

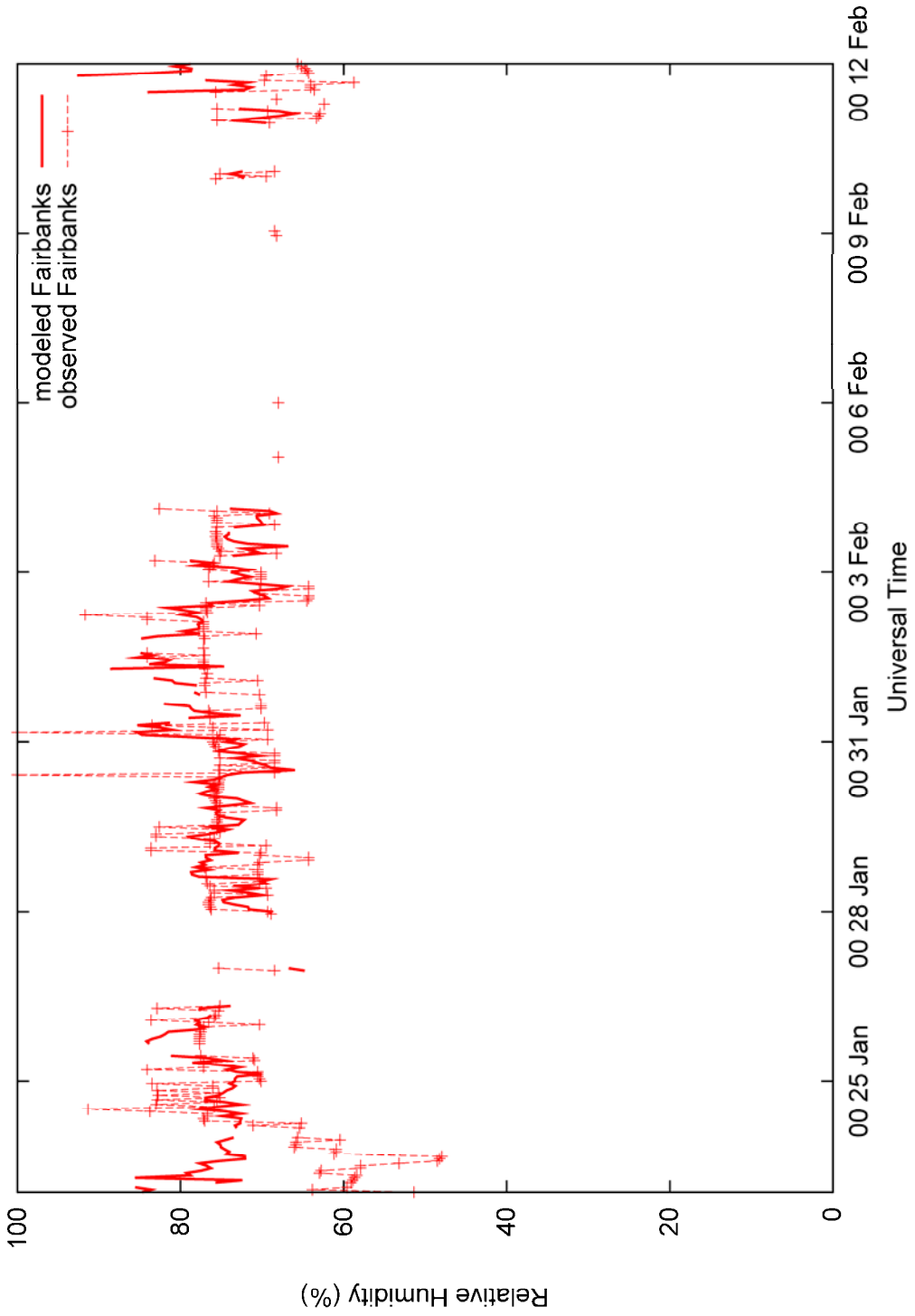


Figure 82: Time series of modeled and observed relative humidity for Fairbanks in TWIND2X30.

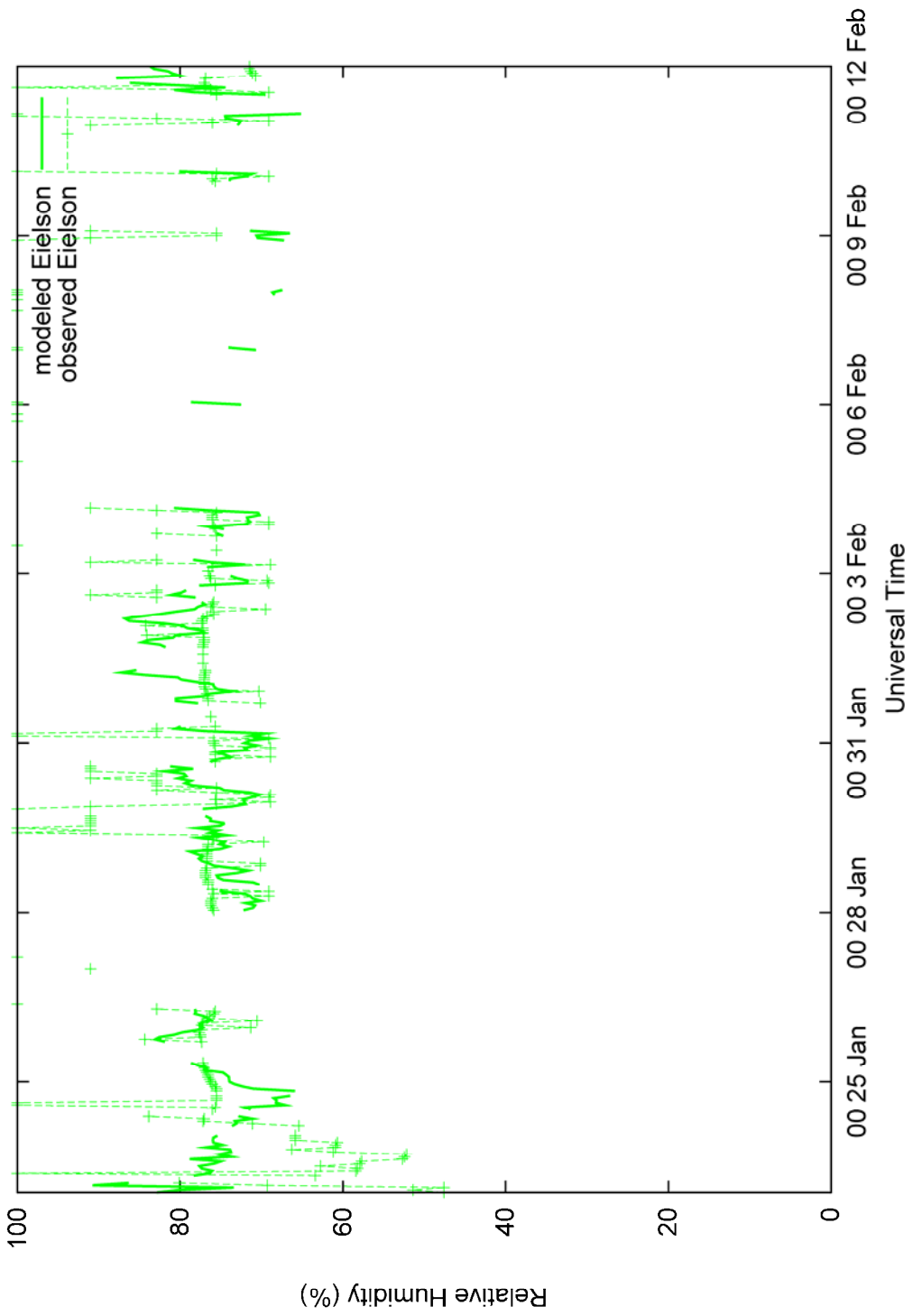


Figure 83: Time series of modeled and observed relative humidity for Eielson in TWIND2X30.

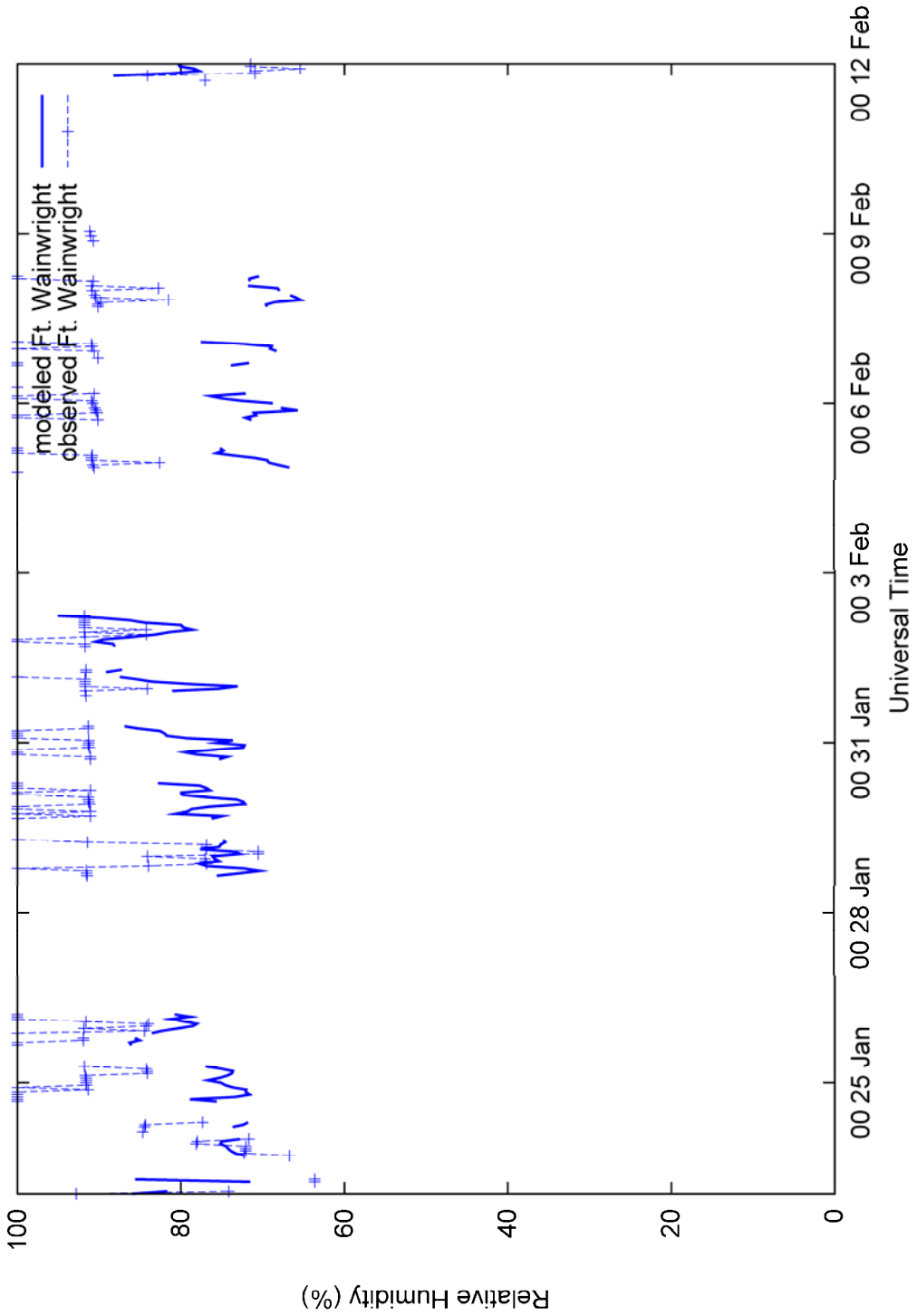


Figure 84: Time series of relative humidity for Ft. Wainwright in TWIND2X30.

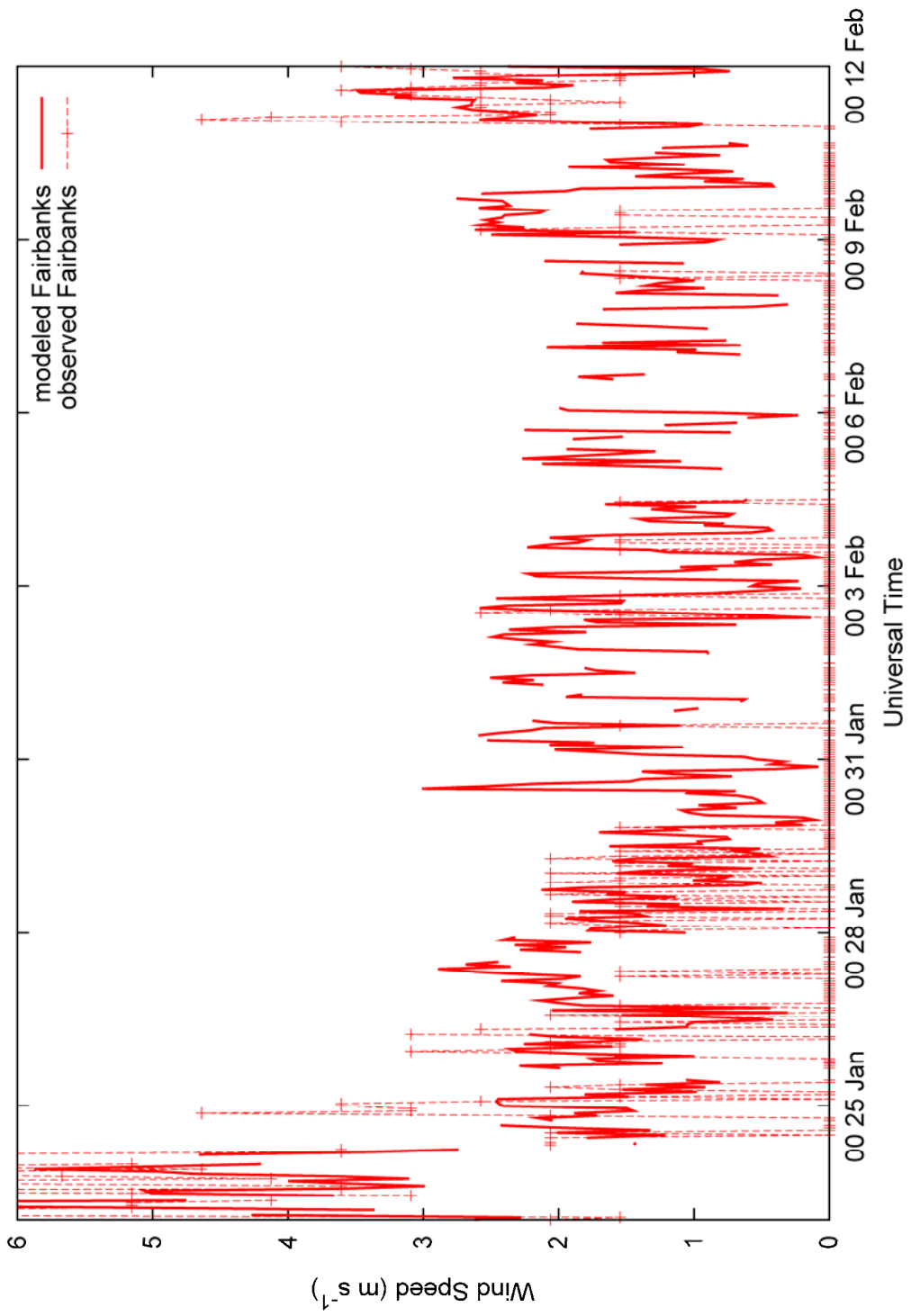


Figure 85: Time series of modeled and observed wind speed for Fairbanks in TWIND2X30.

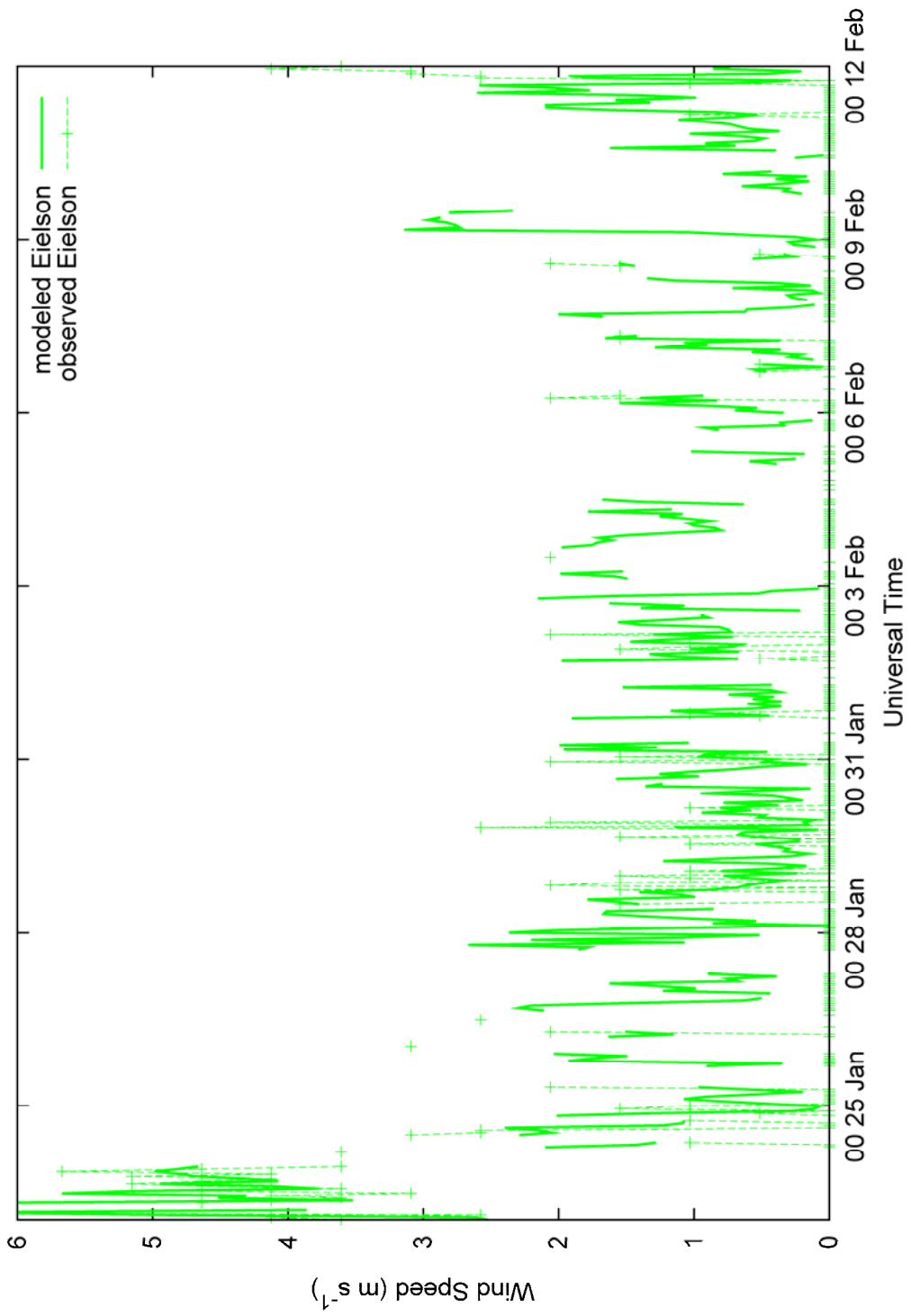


Figure 86: Time series of modeled and observed wind speed for Eielson in TWIND2X30.

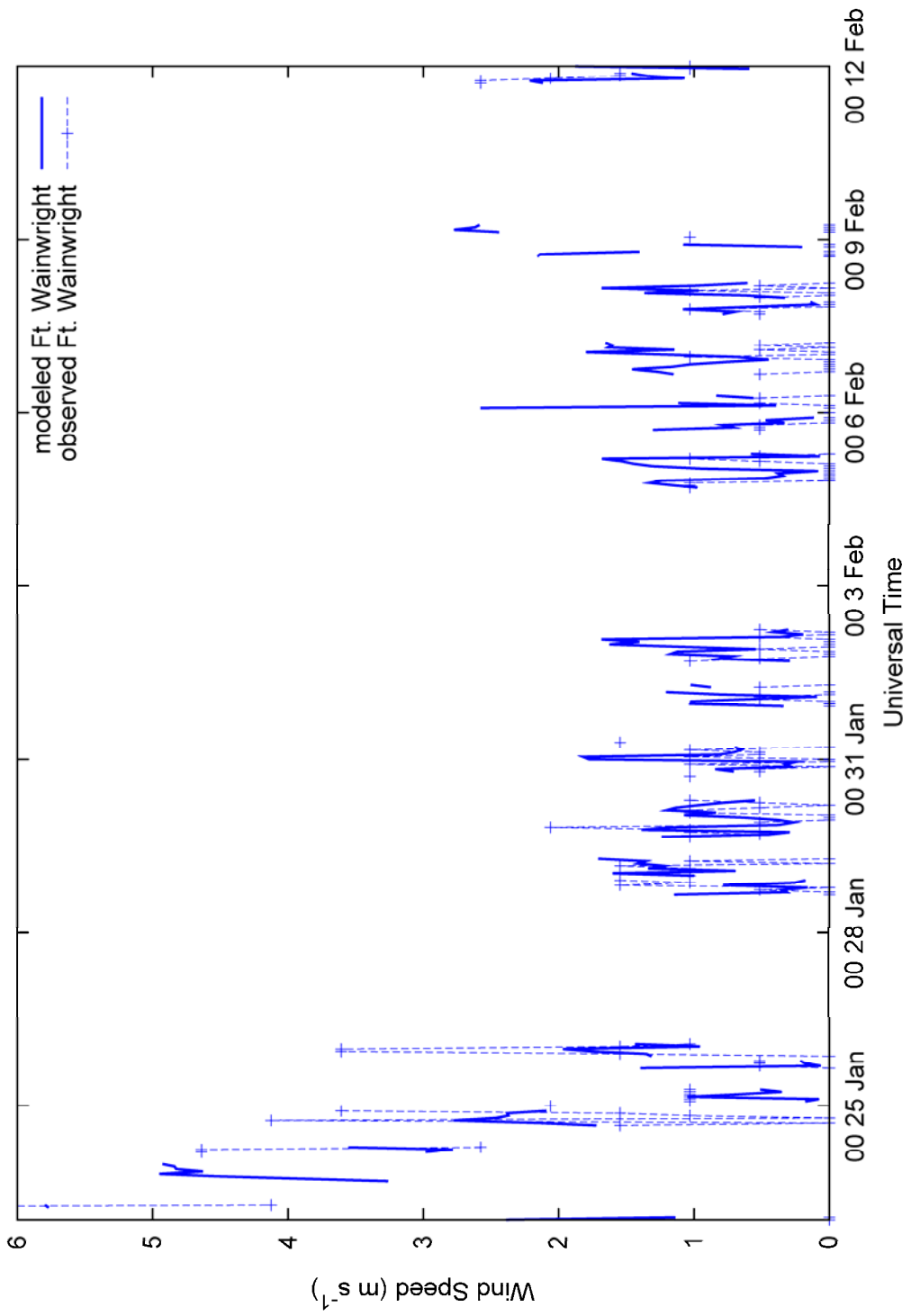


Figure 87: Time series of modeled and observed wind speed for Ft. Wainwright in TWIND2X30.

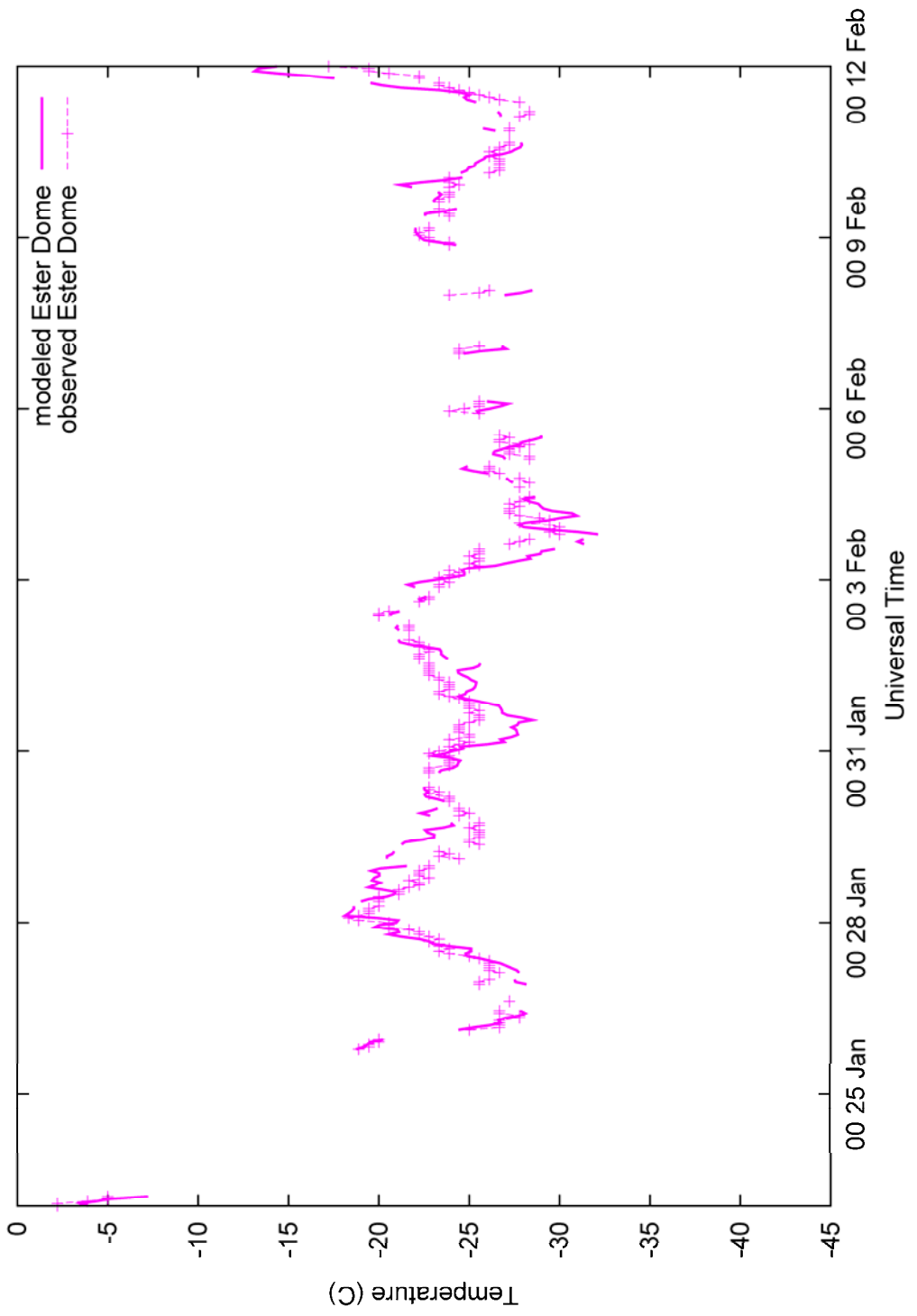


Figure 88: Time series of modeled and observed temperature for Ester Dome in TWIND2X30.

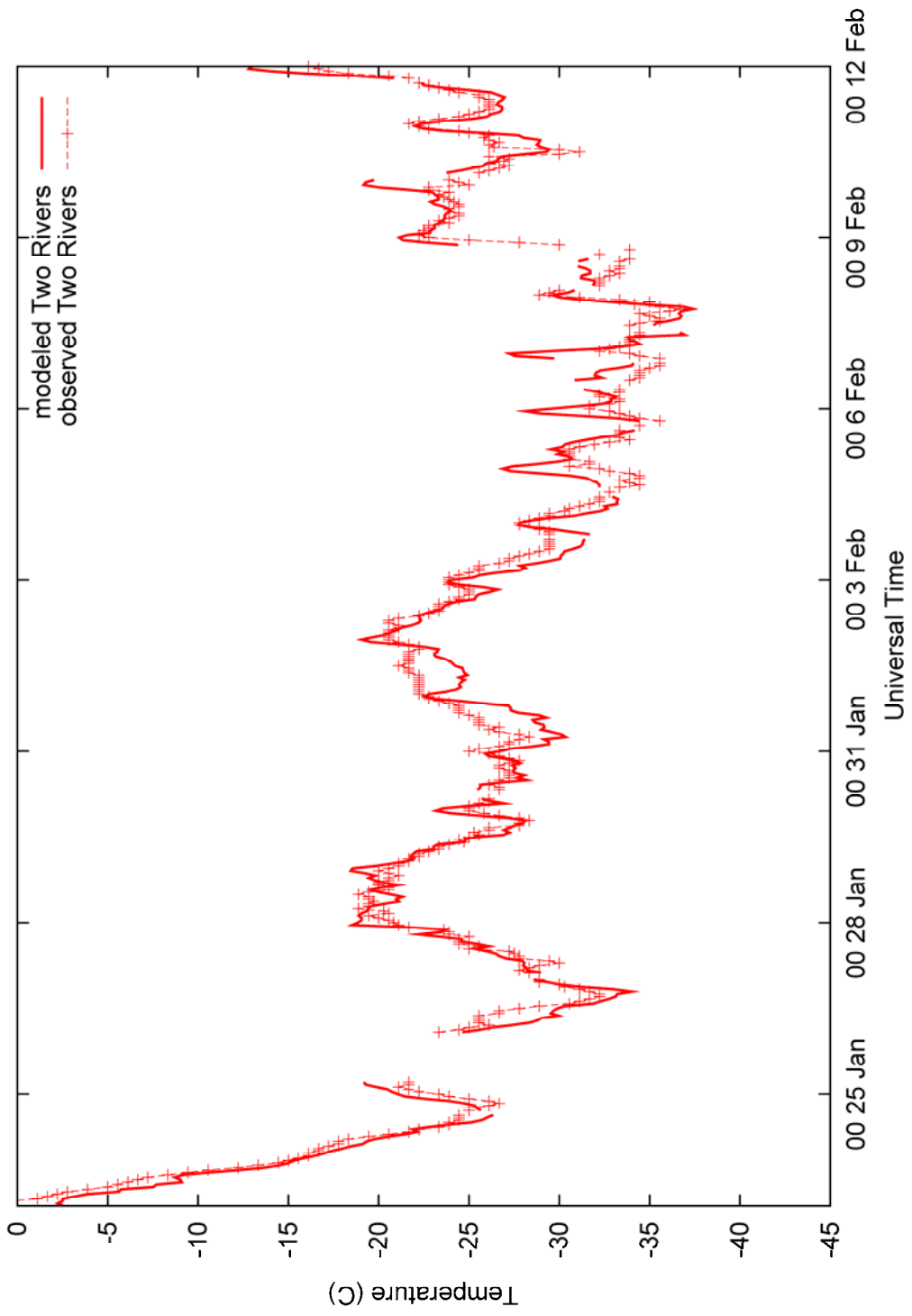


Figure 89: Time series of modeled and observed temperature for Two Rivers in TWIND2X30.

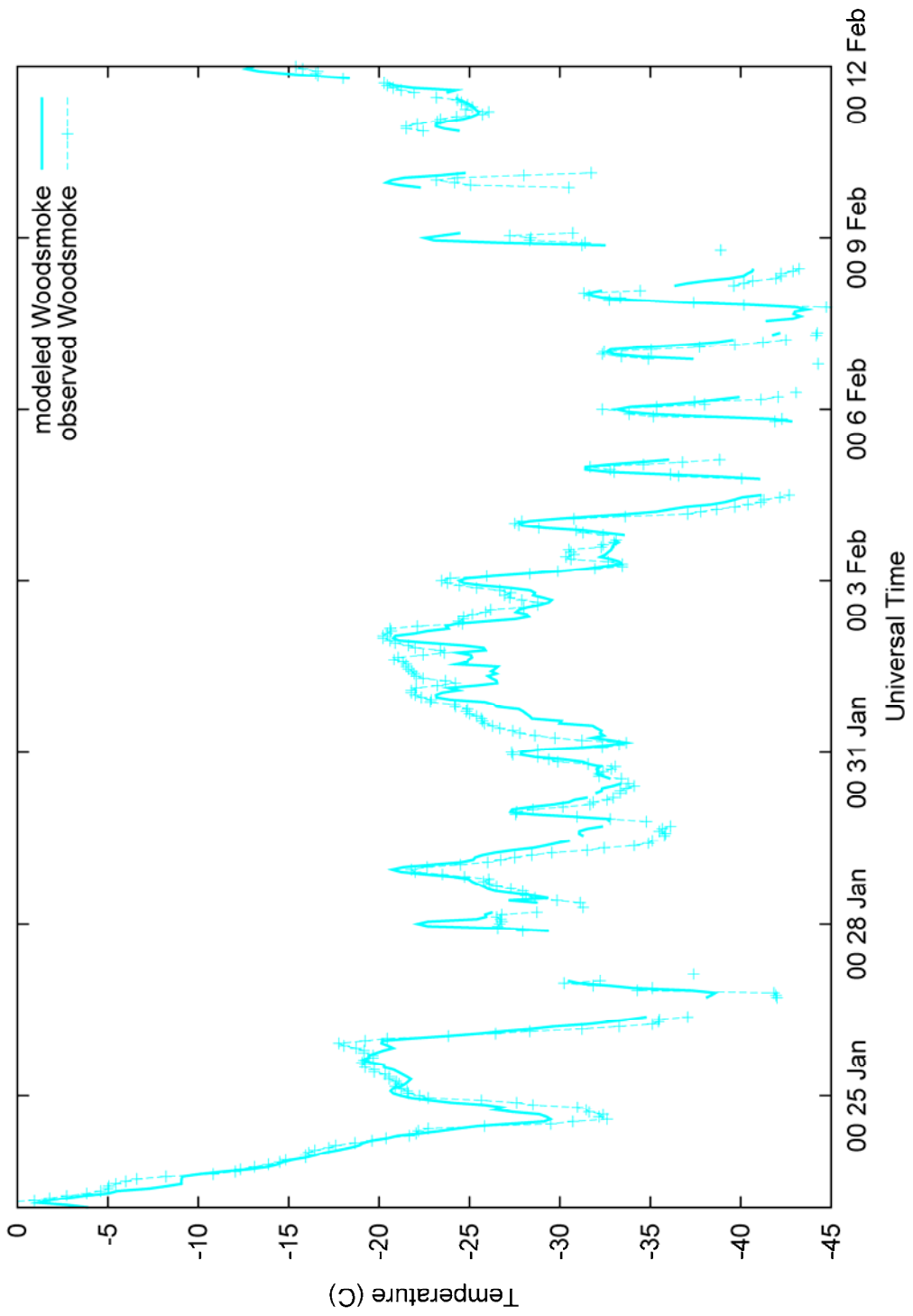


Figure 90: Time series of modeled and observed temperature for Woodsmoke in TWIND2X30.

## REFERENCES


Benjamin, S.O., and N.L. Seaman, 1985: A simple scheme for objective analysis in curved flow. *Mon. Wea. Rev.*, **113**, 1184-1198.

Benson, C.S., 1970: Ice fog: Low temperature air pollution. Research Report 121. U.S. Army Corps of Engineers, Cold Regions Research and Engineering Laboratory, Hanover, NH, 118 pp.

Chen, F., and J. Dudhia, 2001: Coupling an advanced land-surface/hydrology model with the Penn State/NCAR MM5 modeling system. Part I: Model implementation and sensitivity. *Mon. Wea. Rev*., **129**, 569-585.

Deng, A., D. Stauffer, B. Gaudet, J. Dudhia, J. Hacker, C. Bruyere, W. Wu, F. Vandenberghe, Y. Liu, and A. Bourgeois, 2009: Update on WRF-ARW end-to-end multi-scale FDDA system. *10th Annual WRF Users' Workshop*, 23 Jun 2009, Boulder, CO.

Gaudet, B.J., and D.R. Stauffer, 2010: Stable boundary layer representation in meteorological models in extremely cold wintertime conditions. Final Report, Purchase Order EP08D000663, Environmental Protection Agency, 54 pp.

Gaudet, B., D. Stauffer, N. Seaman, A. Deng, K. Schere, R. Gilliam, J. Pleim, and R. Elleman, 2009: Modeling extremely cold stable boundary layers over interior Alaska using a WRF FDDA system. *13th Conference on Mesoscale Processes*, 17-20 Aug, Salt Lake City, UT, American Meteorological Society.

Janjić, Z.I., 2002: Nonsingular implementation of the Mellor-Yamada Level 2.5 Scheme in the NCEP Meso model. NCEP Office Note 437, 61 pp.

Mlawer, E.J., S.J. Taubman, P.D. Brown, M.J. Iacono, and S.A. Clough, 1997: Radiative transfer for inhomogeneous atmosphere: RRTM, a validated correlated-k model for the longwave. *J. Geophys. Res.*, **102**, 16663-16682.

Mölders, N. and G. Kramm, 2010: A case study on wintertime inversions in interior Alaska with WRF. *Atmos. Res.*, **95**, 314-332.

Morrison, H., J.A. Curry, and V.I. Khvorostyanov, 2005: A new double-moment microphysics parameterization for application in cloud and climate models. Part I: Description. *J. Atmos. Sci.*, **62**, 1665-1677.

Nuss, W.A., and D.W. Titley, 1994: Use of multiquadric interpolation for meteorological objective analysis. *Mon. Wea. Rev*., **122**, 1611-1631.

Seaman, N.L., B.J. Gaudet, D.R. Stauffer, L. Mahrt, S.J. Richardson, J.R. Zielonka, and J. C. Wyngaard, 2012: Numerical prediction of submesoscale flow in the nocturnal stable boundary layer over complex terrain. *Mon. Wea. Rev.*, **140**, 956-977.

Serreze, M.C., J.D. Kahl, and R.C. Schnell, 1992: Low-level temperature inversions of the Eurasian Arctic and comparison with Soviet drifting station data. *J. Climate*, **5**, 615-629.

Skamarock, W.C., J.B. Klemp, J. Dudhia, D.O. Gill, M. Barker, M.G. Duda, X.-Y. Huang, W. Wang, and J.G. Powers, 2008: A description of the Advanced Research WRF version 3. NCAR Technical Note NCAR/TN475+STR.

Smirnova, T.G., J.M. Brown, and D. Kim, 2000: Parameterization of cold-season processes in the MAPS land-surface scheme. *J. Geophys. Res.*, **105**, 4077-4086.

Stauffer, D.R., and N.L. Seaman, 1994: Multiscale four-dimensional data assimilation. *J. Appl. Meteor.*, **33**, 416-434.

Stauffer, D.R., N.L. Seaman, and F.S. Binkowski, 1991: Use of four-dimensional data assimilation in a limited-area mesoscale model. Part II: Effects of data assimilation with the planetary boundary layer. *Mon. Wea. Rev.*, **119**, 734-754.

Stauffer, D.R., B.J. Gaudet, N.L. Seaman, J.C. Wyngaard, L. Mahrt and S. Richardson, 2009: Sub-kilometer numerical predictions in the nocturnal stable boundary layer. *23rd Conference on Weather Analysis and Forecasting/19th Conference on Numerical Weather Prediction*, 1-5 Jun, Omaha, NE, American Meteorological Society.

Wyngaard, J.C., 2004: Toward numerical modeling in the 'Terra Incognita'. *J. Atmos. Sci.*, **61**, 1816-1826.

Atmospheric Pollution Research 4 (2013) 238-244

Atmospheric Pollution Research

www.atmospolres.com

# The impact of a community–wide woodstove changeout intervention on air quality within two schools

**Tony J. Ward [1], Christopher P. Palmer [2], Kathi Hooper [3], Megan Bergauff [1], Curtis W. Noonan [1]**

[1] *The University of Montana, Center for Environmental Health Sciences, Missoula, MT 59812, U.S.A.*
[2] *The University of Montana, Department of Chemistry, Missoula, MT 59812, U.S.A.*
[3] *Lincoln County Environmental Health Department, Libby, Montana, U.S.A.*

## ABSTRACT

Due to temperature inversions and widespread residential woodstove use, Libby, Montana historically experienced elevated levels of ambient woodsmoke $PM_{2.5}$ throughout the winter months. In an effort to reduce wintertime $PM_{2.5}$, a large community–wide woodstove changeout was conducted between 2005 and 2007, removing nearly 1 200 old polluting stoves from service. To determine the impact of this intervention on indoor air quality, $PM_{2.5}$ sampling was conducted in the gymnasiums of an elementary and middle school before, during, and after the woodstove changeout over a four–year period. Throughout the program, results showed that indoor $PM_{2.5}$ concentrations at the elementary school were moderately high regardless of year or season (mean±sd, 31.9±14.1 μg/m$^3$), ranging from 11.0 μg/m$^3$ to 79.3 μg/m$^3$. At the middle school, the mean was 12.2±11.2 μg/m$^3$, with no differences by season. Although there was an overall improvement in ambient air quality (and reduction of woodsmoke–$PM_{2.5}$) when comparing pre– and post–changeout $PM_{2.5}$ concentrations, results suggest that the community–wide woodstove changeout did not have a significant impact on indoor air quality within the gymnasiums over this same time period. These findings are supported by the results of selected chemical markers of woodsmoke measured from indoor PM (including levoglucosan) at both schools, which also demonstrated no significant reductions throughout the four–year sampling program.

***Keywords:*** *$PM_{2.5}$, smoke, woodstove, school, gymnasium*

***Corresponding Author:***
*Tony J. Ward*
☎ : *+1-406-243-4092*
🖷 : *+1-406-243-2807*
✉ : *tony.ward@umontana.edu*

***Article History:***
*Received: 30 November 2012*
*Revised: 23 March 2013*
*Accepted: 23 March 2013*

**doi:** 10.5094/APR.2013.025

## 1. Introduction

Studies conducted throughout the United States (Sexton et al., 1984; Fairley, 1990; McDonald et al., 2000; Schauer and Cass, 2000; Fine et al., 2001; Polissar et al., 2001; Maykut et al., 2003; Larson et al., 2004; Chow et al., 2007) and world (McGowan et al., 2002; Luhar et al., 2006; Puxbaum et al., 2007; Alfarra et al., 2007; Szidat et al., 2007; Lanz et al., 2008) have identified woodsmoke as a major component of ambient particulate matter. This is especially true in valley locations located throughout the northern Rocky Mountains of western Montana, where $PM_{2.5}$ from woodstoves have been shown to be the predominant source of $PM_{2.5}$ throughout the winter months (Ward and Lange, 2010).

Libby is a small mountain valley community in northwestern Montana (Lincoln County) with a population of approximately 2 600. Temperature inversions are common throughout the winter months, contributing to elevated levels of ambient $PM_{2.5}$. Before a community–wide woodstove changeout was implemented, the winter $PM_{2.5}$ concentrations were so high that Libby exceeded the annual $PM_{2.5}$ National Ambient Air Quality Standard (NAAQS) of 15 μg/m$^3$, resulting in Libby being designated as a nonattainment area for the fine fraction. With the exception of some areas of southern California, Libby was the only $PM_{2.5}$ nonattainment area in the mid and western states prior to the revised 24–hour $PM_{2.5}$ NAAQS in 2007.

Residential woodstoves are a common source of home heating in many areas of the Northern Rocky Mountains, and many other areas throughout the world, and remain a cheap alternative to burning fossil fuels. This is especially true in Libby, where upwards of 80% of the wintertime ambient $PM_{2.5}$ came from residential woodsmoke (Ward et al., 2006). In a 2005 emission inventory conducted by the Montana Department of Environmental Quality, ~2 264 wood burning devices were identified within Libby. This included fireplaces (no insert), pre–certified woodstoves, EPA catalytic certified stoves, EPA non–catalytic stoves, cord wood furnaces, masonry furnaces, and pellet stoves/inserts (Carlin, 2008).

In an effort to lower wintertime ambient $PM_{2.5}$, woodstove emissions were targeted through a community wide woodstove changeout program. From 2005 through 2007, nearly 1 200 old woodstoves were changed out, modified, or surrendered (Eagle and Houck, 2007a; Eagle and Houck, 2007b). Although the woodstove changeout improved ambient air quality in Libby by lowering the woodsmoke–related $PM_{2.5}$ during the winter months (Ward et al., 2010), perhaps a more important question is what impact the changeout had on indoor air quality. Most people spend the majority of their time indoors (Fishbein and Henry, 1991; Jenkins et al., 1992), as much as 95% in some areas. When considering children, they spend at least a third of their total time inside school buildings (ISIAQ, 2001), and up to several hours per week within the school gymnasiums exercising.

To expand our investigation into the effectiveness of the woodstove changeout beyond ambient air quality and residential indoor environments, the overall goal of this sampling program

was to quantify the potential indoor air quality improvements within two Libby–area schools. To this end, we present results from a $PM_{2.5}$ air sampling program conducted in the gymnasiums of an elementary and middle school before, during, and after the woodstove changeout over a four–year period.

## 2. Experimental

### 2.1. Woodstove changeout program

From June 2005 through June 2007, a community–wide woodstove changeout was conducted in Libby, Montana. In this context, changeout refers to the removal of older, high–emitting woodstoves and replacement with U.S. EPA–certified woodstoves that meet $PM_{2.5}$ emissions standards of less than 7.5 g/h. The conventional model woodstoves utilize firebox insulation, a longer, hotter gas flow path, and pre–heated combustion air to yield more complete combustion. Other residences chose not to receive a new woodstove, and instead opted for the following heating appliance types: gas stoves/heaters/furnaces, wood inserts, pellet stoves, pellet inserts, pellet furnaces, oil stoves/furnaces, electric heaters, and wood furnaces. At the conclusion of the woodstove changeout program in 2007, nearly 1 200 old woodstoves were changed out, modified, or surrendered in an effort to lower the ambient $PM_{2.5}$ during the winter heating season (Eagle and Houck, 2007a; Eagle and Houck, 2007b). As a result of this community–wide intervention, ambient wintertime $PM_{2.5}$ concentrations were reduced by ~25–30% (Bergauff et al., 2009; Ward et al., 2010).

### 2.2. Periods of air sampling

Starting in January 2006, $PM_{2.5}$ samples were collected during the winter (January through March), spring (May), and fall (September through October) seasons within two Libby schools throughout the duration of the woodstove changeout. In this school sampling program, please note that the winter of 2005/2006 is considered the baseline winter of the woodstove changeout program, while the winter of 2008/2009 is considered the first winter after the changeout program was completed.

### 2.3. Sampling sites

$PM_{2.5}$ samples were simultaneously collected within two school gymnasiums throughout the duration of the woodstove changeout, with Figure 1 showing the locations of these schools within Libby. During the periods of sampling (winter 2005/2006 through winter 2008/2009), the elementary school had approximately 400 students in grades pre–kindergarten through 4$^{th}$ grade, while the middle school had approximately 600 students in grades 5–8. Sampling sites within the two school gymnasiums were dictated by practical considerations (i.e., security of sampling equipment and access to power source) and consultation with school administrators. At the elementary school, the $PM_{2.5}$ sampling site was located within the school gymnasium (~300 m$^2$ in size) approximately 6.1 meters from an exterior door (the only exterior door in the entire gymnasium, which was kept closed the majority of the time), and in proximity to a storage room containing a copying machine. Samples within the elementary school gymnasium were collected at a height of approximately 1.5 meters above the ground.

At the middle school gymnasium (~790 m$^2$ in size), air samplers were placed on a balcony located approximately 4.6 meters above the gymnasium floor along a side wall approximately 61 meters from the nearest door. In total, there were eight exterior doors in the middle school gymnasium, with doors kept closed the majority of the time. The elementary school was built in 1953, and the middle school was built in 1970. As illustrated in Figure 1, the schools were located approximately 2.5 kilometers from one another.

Both gymnasiums were heated by electricity and mechanically ventilated using Class 2, 40P1, R12347ND air filters. The air–exchange rate for the elementary school gymnasium was 11 900 m$^3$/h and operated as needed. The air–exchange rate for the middle school gymnasium was 54 400 m$^3$/h, and operated 05:30 to 16:30 Monday through Friday. Both gymnasiums were heavily used throughout the weekdays and evenings, and sporadically used during the weekends for community recreational activities. Weekday activity patterns were consistent between both school gymnasiums, with ~25–50 students within the gymnasiums at any one time.

For comparison with indoor $PM_{2.5}$ values, ambient $PM_{2.5}$ data were collected on the roof of the Lincoln County Environmental Health Department in downtown Libby on the same days as school sampling. This is the primary $PM_{2.5}$ compliance monitoring site for the city of Libby, and is located approximately 1.6 kilometers from the elementary school, and 3.2 kilometers from the middle school (Figure 1). Daily temperature, wind speed, relative humidity, and precipitation data collected in Libby throughout the time period were obtained from an archived database (WRCC, 2010).

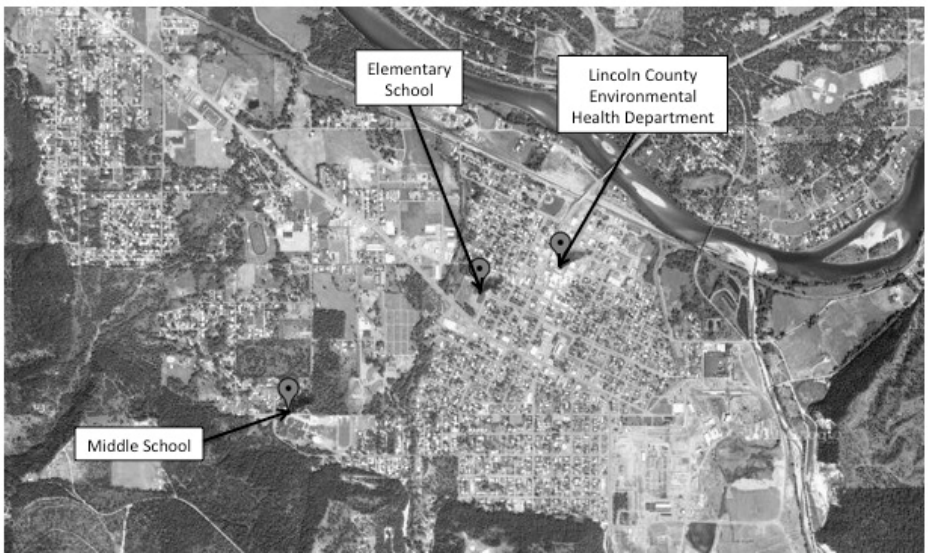


***Figure 1.*** *Map of Libby, Montana, including schools and ambient $PM_{2.5}$ monitoring site.*

### 2.4. Sampling procedures

At each of the two indoor school sites, 24–hour samples were simultaneously collected approximately once per week (during the weekdays throughout the winter, spring, and fall seasons, respectively) using three individual $PM_{2.5}$ samplers. Two Leland Legacy pumps (SKC Inc., Eighty Four, PA, USA) were used to pull air sample through Personal Environmental Monitors (PEMs). One of the PEMs was fitted with a 37–mm $PM_{2.5}$ Teflon filter to collect information on the indoor $PM_{2.5}$ mass, while a second PEM was fitted with a pre–fired 37–mm quartz filter to quantify $PM_{2.5}$–assoicated levels of Organic Carbon (OC) and Elemental Carbon (EC). A 47–mm quartz filter was also collected during each event using a BGI cyclone (BGI, Inc., Waltham, MA, USA) for subsequent analyses of $PM_{2.5}$–associated chemical markers of woodsmoke such as levoglucosan. The flow rates were set at 10 Liters per Minute (LPM) for the Leland/PEM samplers and ~16.7 LPM for the BGI cyclone.

At the Lincoln County Environmental Health Department, continuous ambient $PM_{2.5}$ was measured with a MetOne BAM–1020 (MetOne Instruments Inc., Grants Pass, OR, USA) to investigate the relationship between ambient and indoor levels of $PM_{2.5}$ at each of the two schools. As the BAM data reported hourly $PM_{2.5}$ measurements, ambient hourly concentrations were averaged to match up with the 24–hour sampling events within each of the schools.

### 2.5. Analytical procedures

A gravimetric analysis was conducted on the 37–mm Teflon filters, while levels of OC and EC were measured from the 37–mm quartz filters by Thermal Optical Reflectance. Both analyses were conducted by a contracted laboratory (Chester LabNet, Tigard, OR, USA). From the 47–mm quartz filter, chemical markers of woodsmoke (levoglucosan, abietic acid, and dehydroabietic acid) were quantified. These compounds are all known chemical markers of biomass combustion, and were tracked based on their elevated concentrations measured in the ambient environment during a 2003/2004 Libby $PM_{2.5}$ source apportionment program (Ward et al., 2006).

The woodsmoke markers were analyzed at the University of Montana following a method described in Bergauff et al. (2008). This method was adapted from methods reported previously by Schauer et al. (2001) and Simpson et al. (2005). Briefly, half of each filter was spiked with deuterated recovery standards, placed in a vial, and extracted by ultrasonication using ethyl acetate containing 3.6 mM triethylamine. The extract was filtered, reduced in volume to approximately 500 µL and split into two equal fractions. One fraction was evaporated to dryness and derivatized with N–*O*–bis (trimethylsilyl) trifluoroacetamide, trimethylchlorosilane and trimethylsilylimidazole to convert the sugar anhydrides and the abietic acids to their trimethylsilyl derivatives. The second fraction was treated with a 2:3 mixture of acetic anhydride:triethyl amine to generate the acetate derivatives of the methoxyphenols. Both sample fractions were analyzed by GC/MS on a Hewlett–Packard GC/MSD (GC Model 6890, MSD Model 5973) using an HP–5MS capillary column or equivalent.

### 2.6. Data analysis and statistical procedures

In an effort to determine the impact of the woodstove changeout on indoor air quality, we have separated the sampling days into winter (wood burning season) and non–winter seasons (the non–burning seasons of fall and spring) for comparison. As mentioned previously, winter samples included sampling days in January through March. Non–winter samples were characterized by samples collected during fall (September through October) and spring (May). Non–detects was assigned a value of ½ the detection limit for the corresponding analyses. Pearson product correlation coefficients were calculated for indoor $PM_{2.5}$, ambient $PM_{2.5}$, and meteorological measures on the corresponding sample days. For each school, differences in indoor $PM_{2.5}$ concentrations between the first year of the sampling program (winter 2005/2006) and the fourth year (winter 2008/2009) were evaluated by generalized linear models, adjusting for ambient $PM_{2.5}$ and meteorological variables as appropriate. Differences by season (winter versus non–winter) were also evaluated in a similar manner. All analyses were conducted using SAS v9.2 (Cary, NC).

### 2.7. Quality assurance/quality control (QA/QC)

A comprehensive QA/QC program was employed throughout the sampling program. Using a certified Bios DryCal (SKC Inc., Eighty Four, PA, USA) flow meter, the flow rate on the Leland pump/PEM was measured both before and after each sampling event, while a certified DeltaCal (BGI, Inc., Waltham, MA, USA) was used to measure the flow rates of the cyclone. Teflon and quartz filter field blanks were collected for approximately every 10 samples (10%) to address artifact contamination. Field personnel followed the recommended maintenance and cleaning schedules for the samplers as described in their respective manuals throughout the program.

Filters were always transported in coolers to and from the sampling sites. Clean Teflon and quartz filters were stored in a refrigerator at approximately 2 °C prior to sample collection. Following sample collection, the filter samples were stored in a freezer at –20 °C until analysis. Within the University of Montana laboratory, the QA/QC program for the woodsmoke marker analyses included the analysis of blank filters (one blank filter is analyzed for every 10 samples), spikes, instrument calibration checks, and routine instrument maintenance.

## 3. Results and Discussion

### 3.1. Ambient $PM_{2.5}$, indoor $PM_{2.5}$, and meteorology

Ambient characteristics on the school indoor sampling days are presented in Table 1. As anticipated, ambient $PM_{2.5}$ was higher on winter sampling days compared to non–winter sampling days. When we look specifically at the non–winter seasons, there was little difference in ambient $PM_{2.5}$ mean±sd concentrations when comparing fall sampling days, (8.0±5.0 µg/m$^3$) and spring sampling days (5.7±2.5 µg/m$^3$, $p$=0.15). Winter sampling days demonstrated lower temperature, less wind, and higher relative humidity, with no significant difference in precipitation compared to non–winter sampling days. Across all seasons, average ambient temperature was highly correlated with average wind speed ($r$=0.50, $p$<0.0001) and maximum wind gust ($r$=0.46, $p$<0.0001), and inversely correlated with relative humidity ($r$=–0.41, $p$<0.0001).

Ambient $PM_{2.5}$ sampling conducted on days corresponding to the scheduled indoor school sample days did not demonstrate a significant reduction across the winter years. When adjusted for ambient temperature, the difference (and 95% CI) in ambient $PM_{2.5}$ between the first winter 2005/2006 and the winter of 2008/2009 (winter following the completion of the changeout) was –2.0 µg/m$^3$ (–7.4, +3.4). Table 2 presents the correlations between $PM_{2.5}$ concentrations (including both schools and ambient) and the meteorological variables on the sampling days. Ambient $PM_{2.5}$ was inversely correlated with temperature, wind, and precipitation, while positively correlated with relative humidity. By contrast, indoor $PM_{2.5}$ at the elementary school was positively associated with temperature and wind, and inversely associated with relative humidity and precipitation. Indoor $PM_{2.5}$ at the elementary school was also inversely correlated with ambient $PM_{2.5}$. Results from the middle school showed no correlations between indoor $PM_{2.5}$ and ambient conditions.

***Table 1**. Average (sd) ambient characteristics on school sampling days*

| School Year | Sample Days | $PM_{2.5}$ ($\mu g/m^3$) | Temp (°C) | Wind Speed (km/h) | Max Wind Gust (km/h) | Relative Humidity (%) | Precipitation (cm) |
|---|---|---|---|---|---|---|---|
| **Winter** | | | | | | | |
| All years | 46 | 18.0 (6.8) | –0.68 (4.5) | 0.6 (0.5) | 7.8 (4.1) | 77.7 (14.6) | 0.7 (1.1) |
| 2005/06 | 15 | 19.4 (5.7) | –0.03 (3.1) | 0.6 (0.5) | 8.3 (5.1) | 70.1 (15.7) | 0.5 (1.1) |
| 2006/07 | 10 | 17.2 (7.7) | 1.4 (2.6) | 0.5 (0.9) | 6.8 (4.5) | 82.7 (18.0) | 0.5 (1.1) |
| 2007/08 | 11 | 16.1 (6.9) | –2.2 (6.2) | 0.6 (0.4) | 8.0 (2.7) | 76.5 (9.6) | 0.9 (1.3) |
| 2008/09 | 10 | 18.8 (7.7) | –2.0 (5.1) | 0.6 (0.4) | 7.9 (3.7) | 85.5 (8.1) | 0.8 (1.2) |
| **Non–Winter** | | | | | | | |
| All years | 35 | 6.9 (4.1) | 11.2 (4.5) | 1.0 (0.6) | 11.5 (5.0) | 67.2 (13.5) | 1.0 (1.3) |
| 2005/06 | 6 | 5.8 (1.7) | 14.5 (4.4) | 1.2 (0.2) | 10.7 (1.7) | 58.5 (9.1) | 0.8 (1.3) |
| 2006/07 | 12 | 9.2 (5.8) | 10.9 (4.7) | 0.9 (0.7) | 11.0 (5.7) | 66.8 (15.7) | 1.1 (1.3) |
| 2007/08 | 11 | 5.2 (1.8) | 10.4 (3.9) | 1.0 (0.6) | 12.4 (4.8) | 69.3 (14.2) | 1.4 (1.3) |
| 2008/09 | 6 | 6.2 (3.5) | 10.1 (4.7) | 0.9 (0.9) | 11.8 (7.2) | 73.2 (7.7) | 0.4 (1.0) |

*Note: Winter samples included sampling days in January through March. Non-winter samples are characterized by samples collected during fall (September through October) and spring (May).*

***Table 2.** Pearson correlation coefficients (p–value) for ambient characteristics and indoor $PM_{2.5}$ mass on indoor sample days*

| | Ambient $PM_{2.5}$ ($n$=79) | Elementary School Indoor $PM_{2.5}$ ($n$=73)[a] | Middle School Indoor $PM_{2.5}$ ($n$=69)[b] |
|---|---|---|---|
| Ambient $PM_{2.5}$ ($\mu g/m^3$) | | –0.252 (0.032) | 0.053 (0.663) |
| Temperature (°C) | –0.687 (<0.001) | 0.491 (<0.001) | 0.056 (0.643) |
| Wind Speed (km/h) | –0.512 (<0.001) | 0.301 (0.009) | –0.005 (0.969) |
| Wind Gust (km/h) | –0.542 (<0.001) | 0.241 (0.038) | –0.084 (0.489) |
| Relative Humidity (%) | 0.246 (0.029) | –0.426 (<0.001) | 0.027 (0.821) |
| Precipitation (cm) | –0.433 (<0.001) | –0.186 (0.110) | –0.117 (0.332) |

[a] *n=75 for bivariate comparisons with meteorological variables.*
[b] *n=71 for bivariate comparisons with meteorological variables.*

### 3.2. Elementary school

Table 3 presents the indoor results from the elementary school. Indoor $PM_{2.5}$ concentrations at the elementary school were moderately high regardless of year or season (mean±sd, 31.9±14.1 $\mu g/m^3$), with individual 24–hour sampling results ranging from 11.0 $\mu g/m^3$ to 79.3 $\mu g/m^3$. The proportion of Total Carbon (TC) comprised of the OC component ranged from 88.8% to 99.7%. Significant differences were observed between the first winter (2005/2006) and the fourth, post–changeout winter (2008/2009), but these differences did not change as expected (i.e. overall reduction across years), nor were the changes in a consistent direction across all years. EC was slightly higher during winter versus non–winter sampling days ($p$=0.025), but all other results did not demonstrate a strong seasonal response.

### 3.3. Middle school

Table 4 presents the indoor results for the middle school. Overall, indoor $PM_{2.5}$ concentrations were lower at this school compared to the elementary school. The mean±sd was 12.2±11.2 $\mu g/m^3$, and there were no differences by season. Despite the lower overall averages at this site, there were four sampling days with $PM_{2.5}$ concentrations above 30 $\mu g/m^3$, with one sample day yielding an average of 83.3 $\mu g/m^3$. The proportion of TC comprised from the OC component ranged from 95.0% to 99.9%. Middle school concentrations of $PM_{2.5}$ mass, OC, EC, and abietic acid were actually more elevated during the winter 2008/2009 compared to the initial winter of 2005/2006. Adjusting for year and ambient $PM_{2.5}$, indoor levoglucosan at the middle school was higher in the winter versus non–winter sampling days ($p$=0.004), whereas the OC fraction was lower in winter versus non–winter sampling days ($p$<0.001).

### 3.4. Comparison with pre–changeout results (Winter 2004/2005)

During January through March 2005, we conducted PM sampling within Libby's elementary and middle schools to establish baseline indoor PM concentrations (in five distinct size fractions) before the start of the woodstove changeout program (Ward et al., 2007). During this winter 2004/2005 baseline study, $PM_{2.5}$ mass averaged 35.6 $\mu g/m^3$ at the elementary school and 6.9 $\mu g/m^3$ at the middle school. It is important to note that different sampling equipment was used in the baseline program (Sioutas 5–stage impactors) as was a different sampling location for the middle school site (inside the main school compared to inside the gymnasium in this study). Unfortunately, due to these fundamental differences in the sampling programs, we cannot use these baseline data for comparison with the during/post–changeout results presented in this manuscript. Therefore, we have used the winter 2005/2006 results to serve as our baseline winter for comparison with results collected during the winters of 2006/2007, 2007/2008, and 2008/2009.

### 3.5. Impact of the woodstove changeout on indoor air quality

We have previously reported on an overall successful reduction in wintertime ambient $PM_{2.5}$ concentrations (Ward et al., 2010) as well as indoor residential $PM_{2.5}$ concentrations (Ward et al., 2008; Noonan et al., 2012) as a result of the Libby woodstove changeout program. However, we did not see corresponding improvements in indoor air quality measured within the two

school gymnasiums investigated in this program. In addition to $PM_{2.5}$, we did not measure large reductions in levels of OC and EC when comparing the four winter periods. A more revealing finding is the results of the levoglucosan analyses, which are indicative of woodsmoke–related $PM_{2.5}$. At both the elementary and middle schools, there was no consistent reduction in levoglucosan throughout the four–year winter sampling program. These findings are not consistent with what was observed in the ambient air throughout the duration of the changeout, where there was a 50% reduction in levoglucosan when comparing the winters of 2004/2005 and 2007/2008 (Bergauff et al., 2009). There was a reduction in dehydroabietic acid at each of the schools, but this pattern was not mirrored by the levels of abietic acid, where levels actually increased throughout the program within the schools.

### 3.6. Comparison between schools, and with other school sampling programs

Throughout the four year program, $PM_{2.5}$ concentrations were much higher at the elementary school compared to the middle school. As noted earlier, there were physical differences between the two sampling sites. At the elementary school, the $PM_{2.5}$ sampling site collected air samples at a height of approximately 1.5 meters above the ground. At the middle school, air samplers were placed on a balcony located approximately 4.6 meters above the gym floor. It is unknown how this difference in sampling heights influenced results (if at all), and it is likely that the difference in measured $PM_{2.5}$ concentrations between schools was likely due to other factors. For example, these factors might include air exchange, ventilation conditions (Rojas–Bracho et al., 2000), and particle deposition (He et al., 2005). Indeed, the unit ventilators within the smaller elementary school gymnasium ran with much less frequency compared to the larger middle school gymnasium, partly explaining the higher levels of $PM_{2.5}$ within the elementary school gymnasium. Other things that may have influenced concentrations of $PM_{2.5}$ inside the school gymnasiums include building design, number and age of occupants, their activities, and other sources inside the buildings. This includes a copying machine within the elementary gymnasium, as well as greater frequency/quantities of tracked–in dirt within the elementary school gymnasium compared to the middle school gymnasium.

The $PM_{2.5}$ levels reported in this Libby study can be compared to findings reported in other school sampling programs. In a study conducted in three elementary schools in Central and Southeast Ohio, $PM_{2.5}$ concentrations ranged from ~15–18 μg/m$^3$ (John et al., 2007). In Munich, indoor air quality within 64 schools was evaluated. The median indoor $PM_{2.5}$ concentration during the winter was 37.0 μg/m$^3$ (range of 4.3 to 73.1 μg/m$^3$), with the median in summer of 22.1 μg/m$^3$ (range of 9.8 and 55.1 μg/m$^3$) (Fromme et al., 2006). In another study conducted in Germany, samples were collected within two classrooms for a period of six weeks. Median indoor $PM_{2.5}$ concentrations were 37.4 μg/m$^3$ (Fromme et al., 2008). $PM_{2.5}$ concentrations measured in these programs were consistent with the concentrations measured throughout the Libby school sampling program.

Large indoor sources of $PM_{2.5}$ within the schools and infiltration of ambient particles to the indoor environment can lead to elevated indoor $PM_{2.5}$ concentrations. This partly explains the results measured in other school studies conducted across the world in places such as Delhi City, India (Goyal and Khare, 2009), Tehran, Iran (Halek et al., 2009), Antwerp, Belgium (Stranger et al., 2008), Istanbul, Turkey (Ekmekcioglu and Keskin, 2007), and Athens, Greece (Diapouli et al., 2008). Each of these studies reported much higher indoor school $PM_{2.5}$ levels compared to what was measured in this program.

***Table 3.*** *Mean (sd) for indoor $PM_{2.5}$ mass (μg/m$^3$), and $PM_{2.5}$–associated OC/EC (μg/m$^3$) and selected organics (ng/m$^3$) at the elementary school by season and year*

| | Winter Sampling | | | | | Non–winter Sampling | | | | | Season[c] |
|---|---|---|---|---|---|---|---|---|---|---|---|
| | 2005/06 (*n*=15) | 2006/07 (*n*=7) | 2007/08 (*n*=11) | 2008/09 (*n*=10) | Year[a] *p*-value | 2005/06 (*n*=6) | 2006/07 (*n*=9) | 2007/08 (*n*=11) | 2008/09 (*n*=6) | Year[b] *p*-value | *p*–value (*n*=73) |
| $PM_{2.5}$ | 27.1 (5.8) | 26.6 (16.4) | 21.5 (8.5) | 30.5 (11.3) | <0.001 | 25.6 (4.3) | 52.7 (12.8) | 36.1 (12.9) | 39.2 (15.7) | 0.012 | 0.378 |
| Organic carbon | 13.9 (1.3) | 12.1 (1.3) | 12.0 (1.3) | 17.5 (4.2) | <0.001 | 11.6 (0.9) | 16.7 (4.1) | 13.2 (2.4) | 16.2 (3.4) | 0.002 | 0.160 |
| Elemental carbon | 0.4 (0.12) | 0.5 (0.24) | 0.4 (0.23) | 1.0 (0.65) | <0.001 | 0.2 (0.04) | 0.4 (0.14) | 0.2 (0.11) | 0.5 (0.22) | <0.001 | 0.025 |
| Levoglucosan | 264 (116) | 163 (128) | 706 (285) | 410 (145) | 0.551 | 107 (86.3) | 74.2 (90.7) | 422 (207) | 167 (28.3) | 0.871 | 0.709 |
| Dehydroabietic acid | 134 (35.9) | 74.5 (21.4) | 162 (39.6) | 50.4 (22.9) | <0.001 | 86.3 (13.7) | 79.0 (31.5) | 109 (18.5) | 12.5 (5.6) | <0.001 | 0.595 |
| Abietic acid | 8.4 (3.6) | 4.5 (4.7) | 20 (13) | 73 (41) | <0.001 | 2.1 (1.0) | 1.6 (4.0) | 90 (157) | 25 (9.6) | 0.944 | 0.088 |

[a] *Least squares mean model for first versus last year differences during winter sampling, adjusted for ambient $PM_{2.5}$, temperature and relative humidity. Observation numbers may vary from crude data due to missing ambient data.*
[b] *Least squares mean model for first versus last year differences during non-winter sampling, adjusted for ambient $PM_{2.5}$, temperature and relative humidity. Observation numbers may vary from crude data due to missing ambient data.*
[c] *Least squares mean model for winter versus non–winter differences, adjusted for year, ambient $PM_{2.5}$, temperature and relative humidity.*

***Table 4.*** *Mean (sd) for indoor $PM_{2.5}$ mass (μg/m$^3$), and $PM_{2.5}$–associated OC/EC (μg/m$^3$) and selected organics (ng/m$^3$) at the middle school by season and year*

| | Winter Sampling | | | | | Non–winter Sampling | | | | | Season[c] |
|---|---|---|---|---|---|---|---|---|---|---|---|
| | 2005/06 (*n*=12) | 2006/07 (*n*=8) | 2007/08 (*n*=10) | 2008/09 (*n*=9) | Year[a] *p*–value | 2005/06 (*n*=5) | 2006/07 (*n*=11) | 2007/08 (*n*=10) | 2008/09 (*n*=6) | Year[b] *p*-value | *p*–value (*n*=69) |
| $PM_{2.5}$ | 7.7 (1.9) | 15.2 (6.9) | 6.5 (2.0) | 20.4 (24.1) | 0.022 | 10.1 (2.1) | 19.8 (10.9) | 9.9 (4.8) | 5.6 (3.3) | 0.342 | 0.778 |
| Organic carbon | 8.3 (1.5) | 7.3 (0.7) | 6.8 (0.9) | 9.8 (1.4) | 0.002 | 7.4 (1.0) | 9.4 (2.3) | 7.5 (1.6) | 8.9 (1.3) | 0.175 | <0.001 |
| Elemental carbon | 0.2 (0.11) | 0.2 (0.08) | 0.1 (0.11) | 0.3 (0.16) | 0.009 | 0.1 (0.04) | 0.2 (0.14) | 0.0 (0.06) | 0.1 (0.11) | 0.809 | 0.086 |
| Levoglucosan | 573 (223) | 341 (185) | 598 (120) | 405 (120) | 0.068 | 225 (359) | 130 (83.3) | 412 (37.2) | 149 (116) | 0.385 | 0.004 |
| Dehydroabietic acid | 163 (46.2) | 113 (71.9) | 132 (13.6) | 27.4 (9.3) | <0.001 | 94.7 (24.2) | 67.4 (13.4) | 129 (21.7) | 10.6 (3.0) | <0.001 | 0.163 |
| Abietic acid | 7.1 (2.3) | 6.9 (7.9) | 11.3 (4.2) | 37.6 (26.9) | <0.001 | 1.8 (1.6) | 1.6 (1.6) | 14.7 (7.0) | 0.3 (0.0) | 0.500 | 0.739 |

[a] *Least squares mean model for first versus last year differences during winter sampling, adjusted for ambient $PM_{2.5}$. Observation numbers may vary from crude data due to missing ambient data.*
[b] *Least squares mean model for first versus last year differences during non-winter sampling, adjusted for ambient $PM_{2.5}$. Observation numbers may vary from crude data due to missing ambient data.*
[c] *Least squares mean model for winter versus non–winter differences, adjusted for year and ambient $PM_{2.5}$.*

### 3.7. Indoor $PM_{2.5}$ correlations with ambient $PM_{2.5}$

Some of the school sampling studies have reported a strong correlation between ambient and indoor levels of $PM_{2.5}$. In a school study conducted in biomass–smoke impacted Christchurch, New Zealand, results showed a close relationship between the fine fraction of indoor and outdoor particles (Kingham et al., 2008). In a study conducted in Prague (Czech Republic) from November 2005 to August 2006, 24–hour indoor concentrations of $PM_{2.5}$ averaged 24.03 μg/m$^3$ in the studied gymnasium. In addition, these levels were closely correlated to ambient levels, suggesting a high outdoor–to–indoor penetration rate (Branis et al., 2009). We did not observe a positive correlation between the ambient and indoor $PM_{2.5}$ concentrations at the two schools in this study – even with wood burning residences in proximity to the schools (especially the elementary school as shown in Figure 1). Indeed, one of our schools demonstrated a strong inverse correlation between indoor and ambient $PM_{2.5}$ concentrations.

## 4. Conclusions

Results from the Libby woodstove changeout program have shown that targeting woodstoves can have a positive impact on ambient air quality throughout the winter months. Between 2005 and 2007, nearly 1 200 older model woodstoves were replaced with newer, cleaner burning models in an effort to reduce winter-time ambient $PM_{2.5}$ concentrations. A secondary (but perhaps more important) benefit was discovered from sampling conducted within wood burning residences in the area, where modest improvements to indoor air quality were measured (Ward et al., 2008; Noonan et al., 2012). These residential improvements were likely due to the replacement of woodstoves (and chimney packages) within each of the residences, directly influencing indoor air quality. To determine the impact of this community–wide intervention on indoor air quality within the local schools, $PM_{2.5}$ sampling was conducted in the gymnasiums of an elementary and middle school throughout the woodstove changeout over a four–year period.

Results from this study suggest that the changeout did not result in a measurable improvement on school indoor air quality. Overall, none of the chemical markers of woodsmoke (levoglucosan or resin acids), OC/EC, or $PM_{2.5}$ measures at either school showed a pattern that would be consistent with the timing of the woodstove intervention program. Even though compliance monitoring of $PM_{2.5}$ showed a ~20% reduction in ambient wintertime $PM_{2.5}$ as a result of the community–wide changeout over the same time period (Bergauff et al., 2009), crude ambient $PM_{2.5}$ measured on our scheduled winter indoor sample days was only 0.6 μg/m$^3$ lower in the fourth, post–changeout winter (2008/2009) compared to the 2005/2006 winter. Comparing these years after adjusting for ambient temperature indicated no significant differences.

These ambient results on the scheduled indoor sampling days could help explain why there was not an improvement in indoor air quality at the conclusion of the woodstove changeout. However, we did not observe a positive correlation between the ambient and indoor $PM_{2.5}$ concentrations at the two schools in this study – even with wood burning residences in proximity to the schools. This suggests the presence of indoor sources of $PM_{2.5}$ within the schools throughout the duration of the changeout. It is also possible that concentrations were dependent on the presence and/or absence of students in the gymnasiums, though this activity was not tracked in this study. Looking ahead to future studies, additional sampling can be used within these school gymnasiums to evaluate the effectiveness of indoor interventions, such as frequent mopping of the gym floors, as well as increased ventilation strategies.

## Acknowledgments

The authors would like to thank Kirby Maki, Ken Foss, and Ron Goodman for their cooperation and for providing access to the elementary and middle schools in Libby. This work was funded in part by the Health Effects Institute (#4743–RFA04–4/06–4), and NIH COBRE grant P20 RR01760 from NCRR.

## References

Alfarra, M.R., Prevot, A.S.H., Szidat, S., Sandradewi, J., Weimer, S., Lanz, V.A., Schreiber, D., Mohr, M., Baltensperger, U., 2007. Identification of the mass spectral signature of organic aerosols from wood burning emissions. *Environmental Science & Technology* 41, 5770–5777.

Bergauff, M.A., Ward, T.J., Noonan, C.W., Palmer, C.P., 2009. The effect of a woodstove changeout on ambient levels of $PM_{2.5}$ and chemical tracers for woodsmoke in Libby, Montana. *Atmospheric Environment* 43, 2938–2943.

Bergauff, M., Ward, T., Noonan, C., Palmer, C.P., 2008. Determination and evaluation of selected organic chemical tracers for wood smoke in airborne particulate matter. *International Journal of Environmental Analytical Chemistry* 88, 473–486.

Branis, M., Safranek, J., Hytychova, A., 2009. Exposure of children to airborne particulate matter of different size fractions during indoor physical education at school. *Building and Environment* 44, 1246–1252.

Carlin, J., 2008. Libby, Montana $PM_{2.5}$ Annual Standard, 2005 $PM_{2.5}$ emission inventory, Montana Department of Environmental Quality, 141 pages.

Chow, J.C., Watson, J.G., Lowenthal, D.H., Chen, L.W.A., Zielinska, B., Mazzoleni, L.R., Magliano, K.L., 2007. Evaluation of organic markers for chemical mass balance source apportionment at the Fresno Supersite. *Atmospheric Chemistry and Physics* 7, 1741–1754.

Diapouli, E., Chaloulakou, A., Mihalopoulos, N., Spyrellis, N., 2008. Indoor and outdoor PM mass and number concentrations at schools in the Athens area. *Environmental Monitoring and Assessment* 136, 13–20.

Eagle, B., Houck, J.E., 2007a. Phase I of the Libby, Montana Woodstove Changeout Program, OMNI Environmental Services, Inc, Beaverton, 91 pages.

Eagle, B., Houck, J.E., 2007b. Phase II of the Libby, Montana woodstove changeout program, OMNI Environmental Services, Inc, Denver, 100 pages.

Ekmekcioglu, D., Keskin, S.S., 2007. Characterization of indoor air particulate matter in selected elementary schools in Istanbul, Turkey. *Indoor and Built Environment* 16, 169–176.

Fairley, D., 1990. The relationship of daily mortality to suspended particulates in Santa–Clara County, 1980–1986. *Environmental Health Perspectives* 89, 159–168.

Fine, P.M., Cass, G.R., Simoneit, B.R.T., 2001. Chemical characterization of fine particle emissions from fireplace combustion of woods grown in the northeastern United States. *Environmental Science & Technology* 35, 2665–2675.

Fishbein, L., Henry, C.J., 1991. Workshop on the methodology for assessing health risks from complex–mixtures in indoor air – introduction. *Environmental Health Perspectives* 95, 3–5.

Fromme, H., Diemer, J., Dietrich, S., Cyrys, J., Heinrich, J., Lang, W., Kiranoglu, M., Twardella, D., 2008. Chemical and morphological properties of particulate matter ($PM_{10}$, $PM_{2.5}$) in school classrooms and outdoor air. *Atmospheric Environment* 42, 6597–6605.

Fromme, H., Dietrich, S., Twardella, D., Heitmann, D., Schierl, R., Kiranoglu, M., Liebl, B., 2006. Indoor air concentrations of particulate matter ($PM_{10}$ and $PM_{2.5}$) in German schools. *Air Pollution XIV* 86, 393–399.

Goyal, R., Khare, M., 2009. Indoor–outdoor concentrations of RSPM in classroom of a naturally ventilated school building near an urban traffic roadway. *Atmospheric Environment* 43, 6026–6038.

Halek, F., Kavousi, A., Hassani, F., 2009. Evaluation of indoor–outdoor particle size distribution in Tehran's elementary schools. *World Academy of Science, Engineering and Technology* 33, 463–466.

He, C.R., Morawska, L., Gilbert, D., 2005. Particle deposition rates in residential houses. *Atmospheric Environment* 39, 3891–3899.

ISIAQ (International Society of Indoor Air Quality and Climate), 2001. Creation of Healthy Indoor Environment in Schools. ISIAQ Task Force on Schools – A Nordic Approach, 45 pages.

Jenkins, P.L., Phillips, T.J., Mulberg, E.J., Hui, S.P., 1992. Activity patterns of Californians – use of and proximity to indoor pollutant sources. *Atmospheric Environment Part A–General Topics* 26, 2141–2148.

John, K., Karnae, S., Crist, K., Kim, M., Kulkarni, A., 2007. Analysis of trace elements and ions in ambient fine particulate matter at three elementary schools in Ohio. *Journal of the Air & Waste Management Association* 57, 394–406.

Kingham, S., Durand, M., Harrison, J., Cavanagh, J., Epton, M., 2008. Temporal variations in particulate exposure to wood smoke in a residential school environment. *Atmospheric Environment* 42, 4619–4631.

Lanz, V.A., Alfarra, M.R., Baltensperger, U., Buchmann, B., Hueglin, C., Szidat, S., Wehrli, M.N., Wacker, L., Weimer, S., Caseiro, A., Puxbaum, H., Prevot, A.S.H., 2008. Source attribution of submicron organic aerosols during wintertime inversions by advanced factor analysis of aerosol mass spectra. *Environmental Science & Technology* 42, 214–220.

Larson, T., Gould, T., Simpson, C., Liu, L.J.S., Claiborn, C., Lewtas, J., 2004. Source apportionment of indoor, outdoor, and personal $PM_{2.5}$ in Seattle, Washington, using positive matrix factorization. *Journal of the Air & Waste Management Association* 54, 1175–1187.

Luhar, A.K., Galbally, I.E., Keywood, M., 2006. Modelling $PM_{10}$ concentrations and carrying capacity associated with woodheater emissions in Launceston, Tasmania. *Atmospheric Environment* 40, 5543–5557.

Maykut, N.N., Lewtas, J., Kim, E., Larson, T.V., 2003. Source apportionment of $PM_{2.5}$ at an urban IMPROVE site in Seattle, Washington. *Environmental Science & Technology* 37, 5135–5142.

McDonald, J.D., Zielinska, B., Fujita, E.M., Sagebiel, J.C., Chow, J.C., Watson, J.G., 2000. Fine particle and gaseous emission rates from residential wood combustion. *Environmental Science & Technology* 34, 2080–2091.

McGowan, J.A., Hider, P.N., Chacko, E., Town, G.I., 2002. Particulate air pollution and hospital admissions in Christchurch, New Zealand. *Australian and New Zealand Journal of Public Health* 26, 23–29.

Noonan, C.W., Navidi, W., Sheppard, L., Palmer, C.P., Bergauff, M., Hooper, K., Ward, T.J., 2012. Residential indoor $PM_{2.5}$ in wood stove homes: follow–up of the Libby changeout program. *Indoor Air* 22, 492–500.

Polissar, A.V., Hopke, P.K., Poirot, R.L., 2001. Atmospheric aerosol over vermont: chemical composition and sources. *Environmental Science & Technology* 35, 4604–4621.

Puxbaum, H., Caseiro, A., Sanchez–Ochoa, A., Kasper–Giebl, A., Claeys, M., Gelencser, A., Legrand, M., Preunkert, S., Pio, C., 2007. Levoglucosan levels at background sites in Europe for assessing the impact of biomass combustion on the European aerosol background. *Journal of Geophysical Research–Atmospheres* 112, art. no. D23S05.

Rojas–Bracho, L., Suh, H.H., Koutrakis, P., 2000. Relationships among personal, indoor, and outdoor fine and coarse particle concentrations for individuals with COPD. *Journal of Exposure Analysis and Environmental Epidemiology* 10, 294–306.

Schauer, J.J., Cass, G.R., 2000. Source apportionment of wintertime gas–phase and particle–phase air pollutants using organic compounds as tracers. *Environmental Science & Technology* 34, 1821–1832.

Schauer, J.J., Kleeman, M.J., Cass, G.R., Simoneit, B.R.T., 2001. Measurement of emissions from air pollution sources. 3. $C_1$–$C_{29}$ organic compounds from fireplace combustion of wood. *Environmental Science & Technology* 35, 1716–1728.

Sexton, K., Spengler, J.D., Treitman, R.D., Turner, W.A., 1984. Winter air–quality in a wood–burning community – a case–study in Waterbury, Vermont. *Atmospheric Environment* 18, 1357–1370.

Simpson, C.D., Paulsen, M., Dills, R.L., Liu, L.J.S., Kalman, D.A., 2005. Determination of methoxyphenols in ambient atmospheric particulate matter: tracers for wood combustion. *Environmental Science & Technology* 39, 631–637.

Stranger, M., Potgieter–Vermaak, S.S., Van Grieken, R., 2008. Characterization of indoor air quality in primary schools in Antwerp, Belgium. *Indoor Air* 18, 454–463.

Szidat, S., Prevot, A.S.H., Sandradewi, J., Alfarra, M.R., Synal, H.A., Wacker, L., Baltensperger, U., 2007. Dominant impact of residential wood burning on particulate matter in Alpine valleys during winter. *Geophysical Research Letters* 34, art. no. L05820.

Ward, T., Lange, T., 2010. The impact of wood smoke on ambient $PM_{2.5}$ in northern Rocky Mountain valley communities. *Environmental Pollution* 158, 723–729.

Ward, T.J., Palmer, C.P., Noonan, C.W., 2010. Fine particulate matter source apportionment following a large woodstove changeout program in Libby, Montana. *Journal of the Air & Waste Management Association* 60, 688–693.

Ward, T., Palmer, C., Bergauff, M., Hooper, K., Noonan, C., 2008. Results of a residential indoor $PM_{2.5}$ sampling program before and after a woodstove changeout. *Indoor Air* 18, 529–529.

Ward, T.J., Noonan, C.W., Hooper, K., 2007. Results of an indoor size fractionated PM school sampling program in Libby, Montana. *Environmental Monitoring and Assessment* 130, 163–171.

Ward, T.J., Rinehart, L.R., Lange, T., 2006. The 2003/2004 Libby, Montana $PM_{2.5}$ source apportionment research study. *Aerosol Science and Technology* 40, 166–177.

WRCC (Western Regional Climate Center), 2010., http://www.wrcc.dri.edu/cgi–bin/rawMAIN.pl?mtMLIB, accessed in July, 2010.

Atmos. Chem. Phys., 14, 7601–7616, 2014
www.atmos-chem-phys.net/14/7601/2014/
doi:10.5194/acp-14-7601-2014


Atmospheric Chemistry and Physics
Open Access

# The fate of $NO_x$ emissions due to nocturnal oxidation at high latitudes: 1-D simulations and sensitivity experiments

**P. L. Joyce[1,2], R. von Glasow[3], and W. R. Simpson[1,2]**

[1]Department of Chemistry and Biochemistry, University of Alaska, Fairbanks, AK, USA
[2]Geophysical Institute, University of Alaska, Fairbanks, AK, USA
[3]Centre for Ocean and Atmospheric Sciences, School of Environmental Sciences, University of East Anglia, Norwich, UK

*Correspondence to:* W. R. Simpson (wrsimpson@alaska.edu) and R. von Glasow (r.von-glasow@uea.ac.uk)

Received: 29 January 2014 – Published in Atmos. Chem. Phys. Discuss.: 18 March 2014
Revised: 6 June 2014 – Accepted: 13 June 2014 – Published: 29 July 2014

**Abstract.**

The fate of nitrogen oxide pollution during high-latitude winter is controlled by reactions of dinitrogen pentoxide ($N_2O_5$) and is highly affected by the competition between heterogeneous atmospheric reactions and deposition to the snowpack. MISTRA (MIcrophysical STRAtus), a 1-D photochemical model, simulated an urban pollution plume from Fairbanks, Alaska to investigate this competition of $N_2O_5$ reactions and explore sensitivity to model parameters. It was found that dry deposition of $N_2O_5$ made up a significant fraction of $N_2O_5$ loss near the snowpack, but reactions on aerosol particles dominated loss of $N_2O_5$ over the integrated atmospheric column. Sensitivity experiments found the fate of $NO_x$ emissions were most sensitive to NO emission flux, photolysis rates, and ambient temperature. The results indicate a strong sensitivity to urban area density, season and clouds, and temperature, implying a strong sensitivity of the results to urban planning and climate change. Results suggest that secondary formation of particulate ($PM_{2.5}$) nitrate in the Fairbanks downtown area does not contribute significant mass to the total $PM_{2.5}$ concentration, but appreciable amounts are formed downwind of downtown due to nocturnal $NO_x$ oxidation and subsequent reaction with ammonia on aerosol particles.

## 1 Introduction

The high-latitude winter is a unique chemical environment characterized by extreme cold, extended periods of darkness, and constant snow cover. As the world's population increases, high latitudes are likely to see increased population, enhanced urbanization, and increased resource extraction, all leading to increased pollution emissions including nitrogen-containing species. Anthropogenic nitric oxide (NO) emissions react to form nitrogen dioxide ($NO_2$), and together they form the chemical family of $NO_x$, which is ultimately removed through further oxidation to form nitric acid ($HNO_3$). Nitric acid can acidify aerosol particles in the atmosphere or deposit to the ground where it has been found to affect ecosystems adversely (Fenn et al., 2003). In sunlit conditions, the principal removal pathway of $NO_2$ is reaction with OH (Seinfeld and Pandis, 2006) which can form significant amounts of $HNO_3$ during the day, particularly in polluted regions (Finlayson-Pitts and Pitts, 2000). In the absence of photolysis, the "dark" reaction pathway forms the intermediate species nitrate radical ($NO_3$) and dinitrogen pentoxide ($N_2O_5$), which have both been measured in the nocturnal boundary layer (e.g., Brown et al., 2003; Wood et al., 2005; Ayers and Simpson, 2006; Osthoff et al., 2008; Chang et al., 2011; Riedel et al., 2012; Wagner et al., 2013). The dark reaction pathway includes Reactions (R1) to (R3), followed by either Reaction (R4a) or (R4b):

$$NO + O_3 \rightarrow NO_2 + O_2, \quad \text{(R1)}$$

$$NO_2 + O_3 \rightarrow NO_3 + O_2, \quad \text{(R2)}$$

$$NO_2 + NO_3 \rightleftharpoons N_2O_5, \quad \text{(R3)}$$

$$N_2O_5 + H_2O \xrightarrow{\text{surface}} 2HNO_3, \quad \text{(R4a)}$$

$$N_2O_5 + Cl^- \xrightarrow{\text{surface}} ClNO_2 + NO_3^-. \quad \text{(R4b)}$$

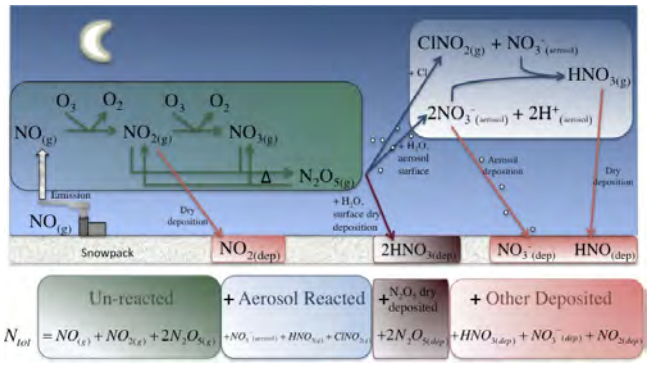


**Figure 1.** A nocturnal nitrogen schematic with emphasis on $N_2O_5$ reactivity. The total nitrogen equation ($N_{tot}$) is a sum of the total column-integrated nitrogen from emitted $NO_x$, divided into speciation fractions.

The absence of photolysis allows $NO_3$ to exist in sufficient concentration for Reaction (R3) to occur, and cold temperatures hinder the dissociation of $N_2O_5$, making the cold and dark conditions of high-latitude winter ideal for $N_2O_5$ formation. Upon formation, $N_2O_5$ can undergo heterogeneous hydrolysis through Reaction (R4a) on the surface of an aerosol particle in the atmosphere or the snowpack surface on the ground to form $HNO_3$. Alternatively, $N_2O_5$ can react with $Cl^-$ (Reaction R4b) after uptake in an aerosol particle to form nitryl chloride ($ClNO_2$), which is volatile and quickly enters the gas phase. Figure 1 outlines the dark oxidation pathway reaction sequence and the competing removal of $N_2O_5$ by reactions on aerosol particles and the snowpack. Cold and dark conditions of high-latitude winter encourage loss of $NO_x$ via the dark oxidation pathway. In a modeling study, Dentener and Crutzen (1993) found that 80 % of high latitude $NO_x$ is lost through the dark oxidation pathway in winter. Measurements by Wood et al. (2005) at midlatitudes found that total $HNO_3$ produced by $N_2O_5$ hydrolysis during the night can be comparable to ambient $NO_2$ concentrations, suggesting total $HNO_3$ produced by heterogeneous hydrolysis may be greater at high latitudes during winter.

The probability of a heterogeneous reaction of $N_2O_5$ to occur upon a molecular collision with an aerosol particle is described by the reactive uptake coefficient, $\gamma$. Laboratory and field studies have shown $\gamma$ can be affected by aerosol particle chemical composition (Hanson and Ravishankara, 1991; Van Doren et al., 1991; Chang et al., 2011; Gaston et al., 2014). In a midlatitude flight campaign, Brown et al. (2007a) observed a strong dependence of $\gamma$ on particle acidity and composition. Laboratory analysis has found that high concentrations of $NO_3^-$ in aerosol particles can hinder uptake of $N_2O_5$ and suppress $\gamma$ in a phenomena known as the "nitrate effect" (Mentel et al., 1999). Additionally, Reaction (R4b) was presented by Graedel and Keene (1995) as a sink of $N_2O_5$ and the product, $ClNO_2$, has been observed in the atmosphere (Osthoff et al., 2008; Thornton et al., 2010). Bertram and Thornton (2009) found that trace amounts of $Cl^-$, when the molar $Cl^-/NO_3^- > 0.1$, can negate the nitrate effect. They have characterized $\gamma$'s dependence on aerosol liquid water content, aqueous $Cl^-$ concentration, and aqueous $NO_3^-$ concentration in a parameterization for mixed organic and inorganic aerosol particles in the laboratory.

Other methods for parameterizing gamma have been developed. Chang et al. (2011) wrote an excellent review article on $N_2O_5$ heterogeneous hydrolysis that describes various models for $\gamma$, comparison to ambient measurements, and size and chemical composition effects on $\gamma$. The nitrate effect and production of nitryl chloride are well documented by Chang et al. (2011) and cited references, as well as the effect of organic aerosol particle components, which generally is indicated to reduce $\gamma$, as described below. Evans and Jacob (2005) parameterized $\gamma$ based upon aerosol particle type, and for some types $\gamma$ was a function of temperature and relative humidity and performed global model simulations resulting in a global mean $\gamma = 0.02$, which is lower than Dentener and Crutzen (1993), but often larger than predicted by the Bertram and Thornton (2009) model. Anttila et al. (2006) described a resistor model for how organic coatings on inorganic core / organic shell aerosol particles could slow heterogeneous hydrolysis and Riemer et al. (2009) found that inclusion of these coatings slowed nitrate formation in a modeling study. Gaston et al. (2014) performed laboratory studies of the reduction of $\gamma$ due to addition of organic to ammonium bisulfate aerosol particles. They found that low O : C ratios (atomic O : C ratio $< 0.5$) suppressed $\gamma$, while more highly oxygenated (O : C ratio $> 0.8$) species had little effect on $\gamma$. Ambient observations of $\gamma$ (Bertram et al., 2009; Riedel et al., 2012; Ryder et al., 2014) or modeling of ambient levels of $N_2O_5$ where $\gamma$ is varied in the model to constrain its value (Brown et al., 2009; Wagner et al., 2013) have generally found that field measured $\gamma$ values are lower by factors of 2 or more than the Bertram and Thornton (2009) parameterization. More recent studies have indicated that the inclusion of organic aerosol information and the particle mixing state improved the agreement between modeled and observed $\gamma$, but an $\sim 2\times$ overprediction still exists in polluted air masses (Ryder et al., 2014). Only one study of $\gamma$ during wintertime has been reported upon by Wagner et al. (2013). This study supports the nitrate effect, but unlike the other studies finds that the wintertime observed $\gamma$ can be larger than that of the Bertram and Thornton (2009) model.

Because pollution is typically emitted at or near ground level, vertical gradients of reactive nitrogen species can easily form in nocturnal boundary layers, especially in cold and stable conditions. Observations of vertical distributions of $NO_3$ and $N_2O_5$ demonstrated that nocturnal mixing ratios can vary widely over vertical scales of 10 m or less, implying that $NO_3$ and $N_2O_5$ occupy distinctly different chemical regimes as a function of altitude (Brown et al., 2007b; Wagner et al., 2013). Aircraft observations of $NO_3$ and $N_2O_5$ show that these species occur at larger concentrations and are

longer lived aloft than they are near the ground (Brown et al., 2007a). A modeling study by Geyer and Stutz (2004) found that slow upward transport of NO emitted near the ground, and the simultaneously occurring chemistry, controlled the vertical structure of the chemistry of $NO_x$, $NO_3$, and $N_2O_5$.

Such observations of vertical gradients of nocturnal nitrogen species may be due to competition between the removal of $N_2O_5$ through Reaction (R4a) or (R4b) on aerosol particle surfaces aloft vs. deposition to the ground. Measurements of $N_2O_5$ near Fairbanks in winter by our group found that sinks of $N_2O_5$ (presumably heterogeneous chemistry) were an efficient mechanism for $NO_x$ removal near ground level (Ayers and Simpson, 2006). Apodaca et al. (2008) found that dry aerosol surface area was insufficient to explain the loss of $N_2O_5$ observed, suggesting loss to other surfaces plays a key role. To characterize the loss to the snowpack, Huff et al. (2011) found the deposition velocity of $N_2O_5$ to be $0.59 \pm 0.47\,\mathrm{cm\,s^{-1}}$ and that dry deposition represents at least $1/8$ of the total chemical removal of $N_2O_5$ near the ground. Theoretical studies of Kramm et al. (1995) calculated a somewhat higher $N_2O_5$ deposition velocity that is towards the high end of our sensitivity studies. Understanding the magnitude of relative loss rates is essential for interpretation of $N_2O_5$ measurements performed at ground level since air parcels near the ground surface will undergo loss both to aerosol particles and the snowpack.

Here we use a 1-D atmospheric chemistry model to address the fate of emitted $NO_x$ in high-latitude winter. A 1-D model allows for analysis of a theoretical atmospheric column composition versus height over time and comparison of loss processes, such as reaction of $N_2O_5$ on aerosol particles versus the snowpack. Timescales for removal of $NO_x$ are analyzed and model sensitivities to parameters and constraints are examined.

## 2 Model description

### 2.1 General features

The meteorological and microphysical part of MISTRA (MIcrophysical STRAtus) was originally a cloud-topped boundary layer model used for microphysical simulations of stratus clouds (Bott et al., 1996). MISTRA has been adapted as a marine and polar boundary layer model for studies of halogen chemistry (von Glasow et al., 2002; Piot and von Glasow, 2008) and includes gas-phase, liquid-phase, and heterogeneous chemistry, as well a microphysical module that explicitly calculates particle growth and treats interactions between radiation and particles. The full gas-phase reaction mechanism is available in the supplemental materials of Sommariva and von Glasow (2012), the aqueous mechanism is described in Pechtl et al. (2006), and photolysis rates are calculated online by the method of Landgraf and Crutzen (1998). Aerosol particles are initialized as the sum of three log-normal modes based on the Jaenicke (1993) "urban" model and distributed into 70 bins by diameter. We note that these particles show a peak in the surface area distribution in the submicron range, where mass transport (diffusion) limitations to heterogenous reactivity are less important than the reactive uptake coefficient. Calculations of kinetic rates are governed by IUPAC (International Union of Pure and Applied Chemistry) rate constants. Mixing is driven by turbulent heat exchange coefficient calculations. The model has 150 vertical layers from the bottom layer centered at a height of 5 m to the model top at 2000 m. The bottom 100 layers are spaced with a 10 m vertical resolution while the top 50 layers are spaced logarithmically. The model runs have a 10 s integration time with output every 15 min. For a more detailed description of the model see von Glasow et al. (2002).

MISTRA treats dry deposition of gases to the snowpack as an irreversible removal from the lowest atmospheric layer (5 m) to the snowpack below using a resistance model presented by Wesely (Wesely, 1989; Seinfeld and Pandis, 2006). The parameterization includes aerodynamic, quasi-laminar, and surface resistance and utilizes gas–aqueous equilibrium coefficients explicitly calculated for each species by MISTRA. Parameters for a mixed forest with wetland in a winter, sub-freezing environment were chosen (Wesely, 1989) and include resistance to deposition by buoyant convection and a lower ground "canopy" to simulate resistance to uptake by leaves, twigs, and other exposed surfaces. No resistance to deposition by large vegetation resistance is included. A dry deposition velocity of $0.59\,\mathrm{cm\,s^{-1}}$ is explicitly specified for $N_2O_5$, based on the field study by Huff et al. (2011), while all other dry deposition velocities are calculated using the parameterization by (Wesely, 1989). Significant dry deposition in the model occurs for species of interest: $NO_2$, $O_3$, $N_2O_5$, and $HNO_3$. The dry deposition velocity for NO is calculated in MISTRA with the Wesely formulation but is unimportant, as found by Wesely and Hicks (2000).

The parameterization presented by Bertram and Thornton (2009) is used to calculate the accommodation coefficient, $\alpha$, which is used in Eq. (4) of von Glasow et al. (2002) to calculate the heterogeneous uptake rates of $N_2O_5$ for each aerosol particle size bin in each model layer as a function of time. The difference in the resulting heterogeneous rate coefficient between this approach and using $\gamma$ in the simple equation $k = \gamma \bar{v} A/4$ is less than 10% but it allows us to use a model-consistent way to calculate heterogeneous rate coefficients. Compared to the old approach as used in von Glasow et al. (2002), where $\alpha = 0.1$, the heterogeneous uptake rates of $N_2O_5$ are now slower by a factor of up to 20. The Bertram and Thornton (2009) parameterization is dependent on aqueous $NO_3^-$ concentration, aqueous $Cl^-$ concentration, and aerosol particle liquid water content. This parameterization was chosen because it includes the nitrate effect and formation of nitryl chloride through chemical concentrations available in the model's aerosol formulation. Although the organic component of aerosol particles is significant, we have

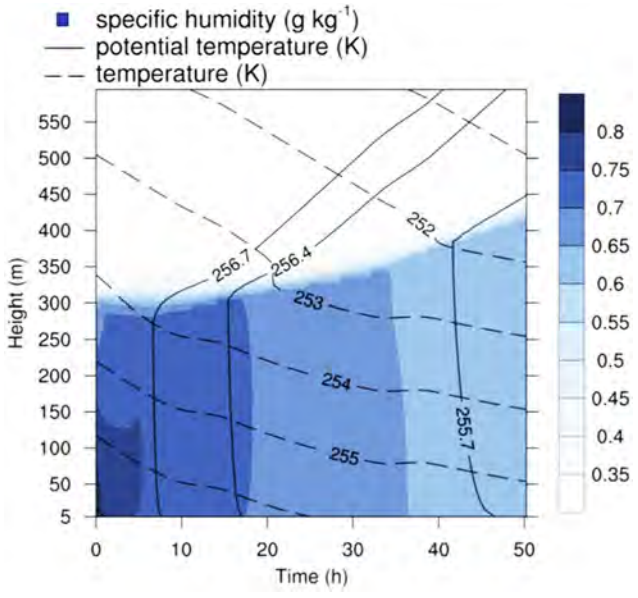


**Figure 2.** Modeled meteorological parameters include temperature (dashed contours), potential temperature (solid contours), and specific humidity (blue). The boundary layer height is initialized to be 300 m.

few observational details about the properties of this organic matter; for instance, we do not have the O : C ratio characterized, nor do we have any detailed information about the mixing state. Therefore, it was not possible to model the effect of the organic component of aerosol particles on $\gamma$. The only wintertime study of $\gamma$ (Wagner et al., 2013) indicated that the Bertram and Thornton (2009) model was reasonably close to observations, sometimes underpredicting observed $\gamma$ values. This cold-climate study's findings differ from the warmer-climate studies (e.g. Bertram et al., 2009; Riedel et al., 2012; Ryder et al., 2014), which found that organics poison $N_2O_5$ heterogenous reactivity.

To simulate a high-latitude atmospheric column moving in space, MISTRA is initialized with a clean Arctic air mass that then receives a pollution injection for 2 hours, corresponding to the contact time of an air parcel moving over Fairbanks at a speed of about 1 m s$^{-1}$. Model runs begin at local midnight ($t = 0$ h), with the pollution injection period beginning at $t = 2$ h and ending at $t = 4$ h. Injection occurs as a positive flux from the ground surface into the lowest model layer (5 m). No additional injection occurs after $t = 4$ h and simulations continue until $t = 50$ h for analysis 2 days "downwind" of the pollution source to focus on the fate of emitted $NO_x$.

### 2.2 Observational constraints

Model runs did not attempt to simulate a specific day for comparison with observations, but rather typical conditions are presented to study the detailed chemical processes occurring under idealized conditions. The "base case" scenario is initialized as an average November day with a clear sky and snow covered ground with an albedo of 0.8. Photolysis rate calculations are performed online for 10 November at latitude 64.76° N, with a sunrise of 08:03 AKST and a sunset of 15:57 AKST. Both daytime and nighttime chemistry occur in the model. Photolysis rate calculations use a total column ozone of 401 Dobson units based the average of November 2009 observations over Fairbanks from the Total Ozone Mapping Spectrometer (TOMS, 2011). An initial temperature at ground level of 257 K (Fig. 2) is an observational average from 1929–2010 for November (ACRC, 2011). Relative humidity (RH) is initialized to 78 % in the mixed layer for the base case (Fig. 2) based on the average of November 2009 observations from the meteorological station located at the Fairbanks International Airport courtesy of the National Climate Data Center (NCDC, 2011).

Vertical mixing at high latitudes can become extremely hindered due to temperature inversions caused by strong radiative cooling from the ground surface at night. We know of no nocturnal vertical profiles of $NO_x$ species above Fairbanks in November, but a nocturnal in situ vertical profile of $NO_2$ was obtained in early April from the Arctic Research of the Composition of the Troposphere from Aircraft and Satellites (ARCTAS) campaign was available and also represents typical wintertime (inverted) conditions. Therefore, the ARCTAS $NO_2$ profile is used to constrain chemical vertical profiles in such conditions (ARCTAS, 2008). The flight originated at Fairbanks International Airport and took off at 02:23 AKST on 8 April 2008. $NO_2$ was detected from the surface up to an altitude of 300 m along a flight path to the southwest, downwind from downtown Fairbanks. The temperature profile obtained from the 8 April 2008 flight showed a surface inversion at an altitude of 50 m and a capping inversion at an altitude of 300 m. Vertical mixing in stable conditions often presents problems in model simulations (e.g., Anderson and Neff, 2008) and our simulations suffer from this as well. Attempts to simulate chemical profiles based on temperature profile observations did not yield results that agreed with the chemical profiles. Therefore, a mixed layer of 300 m is initialized using a dry-adiabatic lapse rate from the ground capped by a small isothermal layer (Fig. 2). The modeled vertical temperature profile allows for mixing of $NO_2$ to agree with the observed chemical vertical profile.

The chemical composition of the modeled atmospheric column at $t = 0$ h represents an unpolluted Arctic air mass. Ambient ozone mixing ratios from Barrow, Alaska are 35 nmol mol$^{-1}$ on average from 2000–2010 in November, with peak abundances of 42 nmol mol$^{-1}$ (ESRL, 2011) and concentrations of polar aerosols found close to the surface

are generally very low (Seinfeld and Pandis, 2006). Therefore, the background chemical composition of the model is initialized as devoid of anthropogenic pollutants with an $O_3$ mixing ratio of 40 nmol mol$^{-1}$ and an aerosol particle loading of $< 1\,\mu g\,m^{-3}$.

The pollution injection during the "emission period" consists of NO, sulfur dioxide ($SO_2$), ammonia ($NH_3$), and aerosol particles containing organic matter, trace chloride ($Cl^-$), and $SO_3$ that rapidly hydrolyzes to sulfuric acid ($H_2SO_4$) (Table 1). Sufficient NO emissions can "titrate" an air mass through Reactions (R1) and (R2), depleting $O_3$ and leading to an environment with excess NO, which is observed almost nightly during winter months in downtown Fairbanks (State of Alaska, 2008). The modeled NO flux is the smallest emission rate possible to titrate ozone to near zero through Reactions (R1) and (R2). This yields a modeled $NO_x$ mixing ratio of 58 nmol mol$^{-1}$ at the end of the pollution injection period ($t = 4$ h), which is within the first quartile (Q1) to third quartile (Q3) range of 31–103 nmol mol$^{-1}$ from observations in downtown Fairbanks (State of Alaska, 2008) and simultaneously brings $O_3$ down to 1 nmol mol$^{-1}$ at ground level. Emission of $SO_2$ is constrained by November 2008 average abundance observed in downtown Fairbanks (State of Alaska, 2008).

Ammonia and aerosol particle emissions are interrelated. Modeled aerosol particles are emitted as liquid particles containing organic material, highly oxidized sulfur species (e.g., $SO_3$ that rapidly hydrolyzes to sulfuric acid, $H_2SO_4$), and trace amounts of chloride and are constrained by $PM_{2.5}$ (aerosol particles with aerodynamic diameter $< 2.5\,\mu m$) observations of particulate organic matter, sulfate, and chloride from downtown Fairbanks (ADEC, 2007) (Table 1). To obtain an appropriate aerosol number density and surface area, the number density of a standard tri-modal urban aerosol distribution (Jaenicke, 1993) is scaled to agree with the average $PM_{2.5}$ mass observation for November (ADEC, 2007). Sulfate ($SO_4^{2-}$) concentrations from emitted highly oxidized sulfur species (e.g., $SO_3$ leading to $H_2SO_4$) are constrained on a percent-mass basis based on total $PM_{2.5}$. The remaining observed aerosol particulate mass is primarily composed of organic carbon, elemental carbon, and heavy metals and is accounted for in the model using chemically inert dissolved organic matter.

Currently, there are no known ammonia observations in Fairbanks. Ammonia mixing ratios in remote areas can be $< 50$ pmol mol$^{-1}$ (Finlayson-Pitts and Pitts, 2000), so background $NH_3$ is initialized as 0.05 nmol mol$^{-1}$. Biomass burning is a well documented source of ammonia emission (Yokelson et al., 1996, 1997; Akagi et al., 2011), suggesting combustion in woodstoves is a significant $NH_3$ source. Emission of ammonia is constrained based on ratios of CO and $NO_x$ emissions using Environmental Protection Agency (EPA) emission inventories and calculations based on previous studies. Carbon monoxide is produced from both automotive emissions and smoldering combustion in woodstoves. The automotive fraction comes at least partially from cold starts and poor operation at cold temperatures. These cold-weather-related emissions have been targeted and the automotive CO source has decreased, with the last exceedance of National Ambient Air Quality standards for CO in 1999, implying that woodstove emissions are now a larger fraction of CO emissions. Studies of smoldering combustion composition by Yokelson et al. (1997) have shown ammonia is the primary nitrogen emission from a smoldering fire and estimate $NH_3$ emissions from burning wood to be 10.8 % of the CO emissions for white spruce harvested in Alaska. Recent southern California emissions of ammonia related to automotive operations have been found to be somewhat smaller at $3.3 \pm 1.3$% mol $NH_3$/mol CO (Nowak et al., 2012). However, emissions of CO in Fairbanks are related to cold weather not experienced in California, so the emissions ratio may be different. Therefore, we used the larger smoldering combustion emissions ratio as an estimate of combustion-related ammonia emissions. The EPA emissions inventory for Fairbanks in 2005 listed 1325 tons year$^{-1}$ (TPY) of CO (ADEC, 2008). Assuming all smoldering combustion emissions are produced in the winter, 6 months out of the year, this yields an estimate of 221 tons month$^{-1}$ (TPM) of CO. Assuming local fuel is consumed in woodstoves, the estimation using Yokelson et al. (1997) would yield 24 TPM $NH_3$, currently not accounted for in the emissions inventory. For mobile sources, the emissions inventory reports 71 TPM $NO_x$ and 4 TPM $NH_3$ from annually occurring on-road, gasoline-powered sources. Calculations based on results from a study by Kean et al. (2000) suggest the magnitude of $NH_3$ emissions are 25 % that of $NO_x$ from automobiles due to use of three-way catalyst systems in gas-powered vehicles. By this estimate, on-road $NH_3$ from gas-powered vehicles is 18 TPM, an estimate $4.5\times$ higher than the $NH_3$ value listed in the inventory. Together, these estimates of $NH_3$ emissions from woodstoves and automotive sources make for 42 TPM $NH_3$, which is 4.8 % of the total reported $NO_x$ emission of 872 TPM. Therefore, the ammonia flux during the emission period in the base case is constrained to be 4.8 % by mass of $NO_x$ emissions. Using the Nowak et al. (2012) California automotive ammonia / carbon monoxide emissions ratio and associating all wintertime CO with automotive emissions and no woodstove ammonia would lead to about 7 TPM automotive $NH_3$, again significantly higher than in the inventory, but with lower total emissions than in the base case. We will address this uncertainty in ammonia emissions through sensitivity studies.

Another constraint on ammonia emissions comes from observed aerosol particle ammonium. Ammonia ($NH_3$) readily protonates in acidic particles to form ammonium ($NH_4^+$), increasing the pH. The molar ratio of $NH_4^+/SO_4^{2-}$ in aerosol particles can be used to determine aerosol acidity, where a value above 2 indicates that all sulfuric acid has been neutralized. Data from downtown Fairbanks shows the first

**Table 1.** Emissions of pollutants in the base model case (at end of emissions, $t = 4$ h) and observations from downtown Fairbanks. Q1–Q3 refers to first to third quartile range.

| Emission Parameter | Base case 5 m, $t = 4$ h | Observed Q1–Q3 or average | Reference |
|---|---|---|---|
| $NO_x$ (nmol mol$^{-1}$) | 58 | 31–103 | downtown Fairbanks, November 2008 (State of Alaska, 2008) |
| $SO_2$ (nmol mol$^{-1}$) | 12 | 8.8–20.6 | downtown Fairbanks, November 2008 (State of Alaska, 2008) |
| $NH_3$ (nmol mol$^{-1}$) | 1.5 | – | no known observations |
| $PM_{2.5}$ (µg m$^{-3}$) | 19 | 19 | downtown Fairbanks, November 2008 average (ADEC, 2007) |
| $PM_{2.5}$ $SO_4^{2-}$ (% mass) | 0.18 % | 0.18 % | downtown Fairbanks, November 2008 average (ADEC, 2007) |
| $PM_{2.5}$ $Cl^-$ (% mass) | 0.4 % | 0.5 % | downtown Fairbanks, November average (State of Alaska, 2011) |
| $PM_{2.5}$ $NH_4^+/SO_4^{2-}$ (mol mol$^{-1}$) | 1.5 | 1.5–2.4 | downtown Fairbanks, annual average (State of Alaska, 2011) |

to third quartile range of molar $NH_4^+/SO_4^{2-}$ to be 1.5–2.4 (State of Alaska, 2011). The modeled $NH_3$ emission from the ground, as explained above, is $\sim 3\times$ the molar $H_2SO_4$ emission, thus enough $NH_3$ is emitted to neutralize the sulfuric acid. Smaller emissions of ammonia become insufficient to neutralize sulfate aerosol particles, although sensitivity studies are carried out down to levels of ammonia emission $5\times$ below the base case.

## 3 Results

### 3.1 The urban pollution plume

The evolution of modeled primary emissions, destruction of ozone, and resulting products are shown in Figs. 3 and 4. All pollutants rapidly mix upon emission to 100 m at $t = 4$ h, reaching 300 m at approximately $t = 8$ h, then slowly diluting higher for the duration of the model run. The $NO_x$ vertical profile (Fig. 3a) shows a strong decrease with height at the end of the emission period due to ground-level emissions. Emitted $NO_x$ reaches 100 m altitude at the end of the emission period ($t = 4$ h) and 300 m, the top of the initialized mixed layer, within 2 h after emissions cease ($t = 6$ h).

Modeled total $PM_{2.5}$ (Fig. 3b) shows a vertical profile similar to $NO_x$ in the first 2 hours after the emission period ends ($t = 6$ h) due to vertical dilution. No observations of aerosol number density and surface area are available for downtown Fairbanks for model evaluation. Modeled values at ground level at $t = 4$ h reach a number density of $2 \times 10^4$ cm$^{-3}$ and aerosol surface area density of 380 µm$^2$ cm$^{-3}$. Modeled nitrate produced through secondary formation by Reaction (R4a) and (R4b) in aerosol particles is 2 % of total $PM_{2.5}$ mass at $t = 4$ h, compared to an average observed value of 4.4 % total $PM_{2.5}$ mass in November (ADEC, 2007). Background and emitted ammonia rapidly react with emitted acidic aerosol particles, forming particulate ammonium (Fig. 4f). Modeled ammonium in aerosol particles is 5 % by mass at $t = 4$ h, and closely resembles ammonium observations comprising 6.4 % of total $PM_{2.5}$ mass (State of Alaska, 2011). Particulate ammonium formation leads to values of $NH_4^+/SO_4^{2-} = 1.5$ (Table 1) at the end of the emission period ($t = 4$ h) through aerosol particle uptake and increases the molar ratio of $NH_4^+/SO_4^{2-}$ to 2.1 one hour after the emission period ($t = 5$ h). Column-integrated $SO_2$ remains constant in time, indicating that the model does not produce significant amounts of sulfate from oxidation of $SO_2$ in the base case, and the only loss mechanism of $SO_2$ from the atmosphere is dry deposition (not shown).

### 3.2 Plume evolution in the base case

Previous field studies in Fairbanks were performed outside of the downtown area in order to observe un-titrated air masses that allow for formation of $N_2O_5$. Ayers and Simpson (2006) conducted measurements on the edge of the populated area of Fairbanks and observed both titrated and un-titrated air masses. Modeled dilution of $NO_x$ (Fig. 3a) agrees well with various field measurements in the greater Fairbanks area (Table 2), where abundances of $NO_x$ reduce with distance from downtown.

Background ozone (Fig. 4a) is depleted ($< 2$ nmol mol$^{-1}$) at ground level at $t = 4$ h and is significantly reduced in the

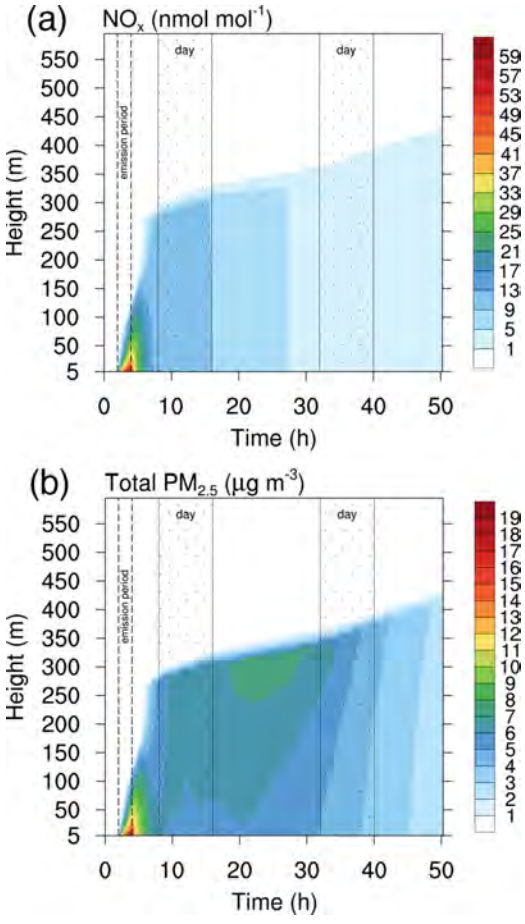


**Figure 3.** Modeled evolution of primary emission $NO_x$ and total $PM_{2.5}$ beginning at local midnight. Daytime regions are indicated by the dotted region and the emission period is indicated by the dashed lines. Emitted species dilute throughout the mixed layer. $NO_x$ undergoes chemical loss **(a)** while total $PM_{2.5}$ increases **(b)**, primarily due to formation of particulate nitrate.

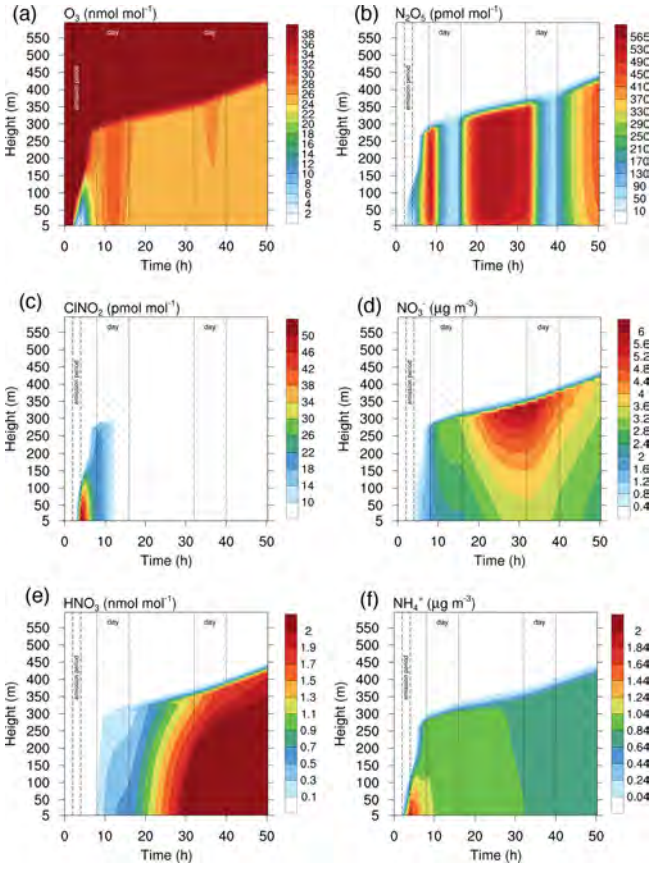


**Figure 4.** Contour plots of important gas-phase species. Modeled $NO_3^-$ and $NH_4^+$ are total aerosol mass density (sum of all aerosol particle sizes). Daytime regions are indicated by the dotted region and the emission period is indicated by the dashed lines.

mixed layer due to titration of the air mass through Reactions (R1) and (R2). Ozone abundance returns to near-background levels approximately 4 hours after the pollution injection due to vertical mixing and photolysis of $NO_2$ in daylight hours.

Abundance of $N_2O_5$ in the model (Fig. 4b) peaks aloft in the early morning of the first day ($t = 9$ h) and in the middle of the second night (beginning $t = 21$ h). The diurnal cycle of $N_2O_5$ shows it is not produced during daylight hours, but peak levels can be maintained for about 1 day after NO emissions cease from the remaining $NO_x$ in the atmosphere. A reduction in the mixing ratio of $N_2O_5$ near the ground occurs due to dry deposition to the snowpack. Modeled abundance of $N_2O_5$ agrees well with observations by Ayers and Simpson (2006), but modeled $N_2O_5$ near the ground is overestimated at longer distances (Table 2). This result is consistent with enhanced $N_2O_5$ deposition to vegetation and enhanced turbulence due to surface vegetation and is discussed in Sect. 5.1.

Formation of $ClNO_2$ (Fig. 4c) occurs immediately upon formation of $N_2O_5$ through Reaction (R4b) and removes trace $Cl^-$ in emitted aerosol particles (not shown) in less than 1 hour after emissions end ($t = 5$ h). A reduction in $N_2O_5$ mixing ratio below 50 m can be seen (Fig. 4b) from $t = 4$ h to $t = 5$ h that is due to $ClNO_2$ formation. Once formed, $ClNO_2$ dilutes through the mixed layer and abundances of $\sim 20$ pmol mol$^{-1}$ throughout the mixed layer are lost through photolysis during the first day resulting in peak Cl radical concentrations of $2.6 \times 10^3$ radicals cm$^{-3}$. Formation of $ClNO_2$ is limited by aqueous $Cl^-$ concentrations in this simulation.

Particulate nitrate (Fig. 4d) is primarily formed through Reaction (R4a) and peaks $\sim 24$ h after the emission period at the end of the second night, corresponding to reactive uptake of $N_2O_5$ formed during the second night. Total nitrate (all aerosol particle sizes) peaks at a concentration of 6.0 µg m$^{-3}$ at an altitude of 325 m at $t = 30$ h, where 4.2 µg m$^{-3}$ of the nitrate is in the $PM_{2.5}$ size fraction. Concentrations of nitrate at ground level reach a maximum of 2.2 µg m$^{-3}$ about 16 h after emission ends, showing a delay in secondary formation

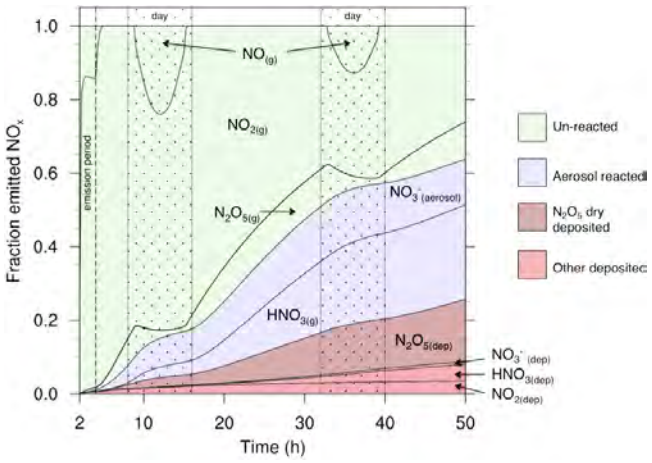


**Figure 5.** Speciation diagram of reactive nitrogen species showing column-integrated concentrations plus time integrated depositional loss as a function of time. Color categories correspond to Fig. 1.

of nitrate through the dark oxidation pathway. Gas-phase nitric acid (Fig. 4e) mixing ratio peaks within hours after the nitrate aerosol peaks and is outgassed by particles made acidic through Reaction (R4a). Larger aerosol particles are able to uptake greater amounts of $NO_3^-$. The peak number density of large aerosol particles ($d > 2.5\,\mu m$) occurs aloft, leading to increased $NO_3^-$ aloft (Fig. 4d) and decreased abundance of gas-phase $HNO_3$ aloft (Fig. 4e). The modeled $HNO_3$ does not react readily with other species and will be ultimately removed through aerosol uptake upon mixing or deposition to the snowpack.

Formation of $NH_4^+$ (Fig. 4f) occurs during the emission period and 1 hour immediately following emission due to aerosol particle uptake of $NH_3$ and neutralization of emitted sulfuric acid aerosol particles. This process depletes background ammonia and emitted ammonia throughout the column (not shown) and forms ammonium sulfate $[(NH_4)_2SO_4]$ or ammonium nitrate ($NH_4NO_3$) in the particles. Once ammonium in-formed in the aerosol particles they are well-mixed throughout the mixed layer and no losses from the atmosphere exist except aerosol particle deposition to the snowpack. Some additional ammonium is produced after the emission period due to entrainment from background ammonia above the mixed layer.

### 3.3 Fate of $NO_x$ in the base case

Nitrogen speciation is divided into four categories (Fig. 1) to characterize the state of emitted $NO_x$ in time. Gas-phase nitrogen oxide species that have not yet undergone heterogenous reaction on aerosol particles (R4a and R4b) are grouped into the term "un-reacted", which is not meant to imply no reaction but simply no irreversible heterogenous conversion to nitrate-type species. The un-reacted fraction includes $NO_x$, $NO_3$ (which is very small due to reactivity), $N_2O_5$, and other reactive nitrogen species present in sub-pmol $mol^{-1}$ range: HONO and $HNO_4$. The "aerosol-reacted" fraction includes any aqueous-phase $NO_3^-$, $HNO_3$ formed by nighttime chemistry then outgassed from acidic particles, and $ClNO_2$ that remains suspended in the atmosphere. The "$N_2O_5$ dry-deposited" fraction represents dry deposition of $N_2O_5$ only. The "other deposited" fraction includes dry deposition of $NO_2$ and $HNO_3$ and deposition of $NO_3^-$ aerosol. Reduced species $NH_3$ and $NH_4^+$ are not oxidized under simulation conditions and are not included in the speciation analysis.

Figure 5 presents a time series of speciation of emitted $NO_x$, depicted as the column-integrated fraction of each species out of the total emitted $NO_x$. Diurnal cycles discernible include the formation of NO and destruction of $N_2O_5$ during the day. A vertical transect at any point in time depicts the current state of emitted $NO_x$. Most apparent is the trend of the un-reacted fraction decreasing with time. In the base case, only 36 % of un-reacted nitrogen remains in the atmosphere 2 days after the beginning of emissions ($t = 50$ h), with the remaining 63 % partitioned among the other categories (Fig. 5). The large fraction of gas-phase $HNO_3$ (33 % at $t = 50$ h) is due to acidic aerosol conditions and represents a significant fate of emitted $NO_x$. Nighttime formation of $HNO_3$ dominates gas-phase $HNO_3$ production, but a small amount of $HNO_3$ production can be seen in the afternoon periods due to the daytime oxidation pathway. Dry deposition of $HNO_3$ through the aerosol-reacted pathway is the fate of 5 % of the total emitted NO after 2 days, but is less than the $N_2O_5$ dry-deposited fraction of 17 %. Dry deposition of $N_2O_5$ makes up a discernable fraction 2 hours after the emission period ends while $NO_3^-$ aerosol deposition and $HNO_3$ dry deposition does not build until 16 h after the emission period ends. A slight increase in dry deposition occurs during the day due to increased turbulent mixing. Other reactive nitrogen species such as HONO, $HNO_4$, and $N_2O_4$ are included with the $NO_2$ fraction and make up an insignificant portion (< 1 %).

## 4 Sensitivity of the fate of $NO_x$ to model parameters

Experiments were performed to analyze the sensitivity of the fate of $NO_x$ to model constraints by modifying parameters over ranges based on realistic conditions. These experiments are presented as demonstrations of model performance as well as representations of the base case under changing scenarios. The sensitivities found to be most significant are described below and are depicted in Fig. 6a–h. Analysis of each experiment is conducted by relative comparison of total nitrogen fractions in each speciation category 2 days after the emission period ends ($t = 50$ h).

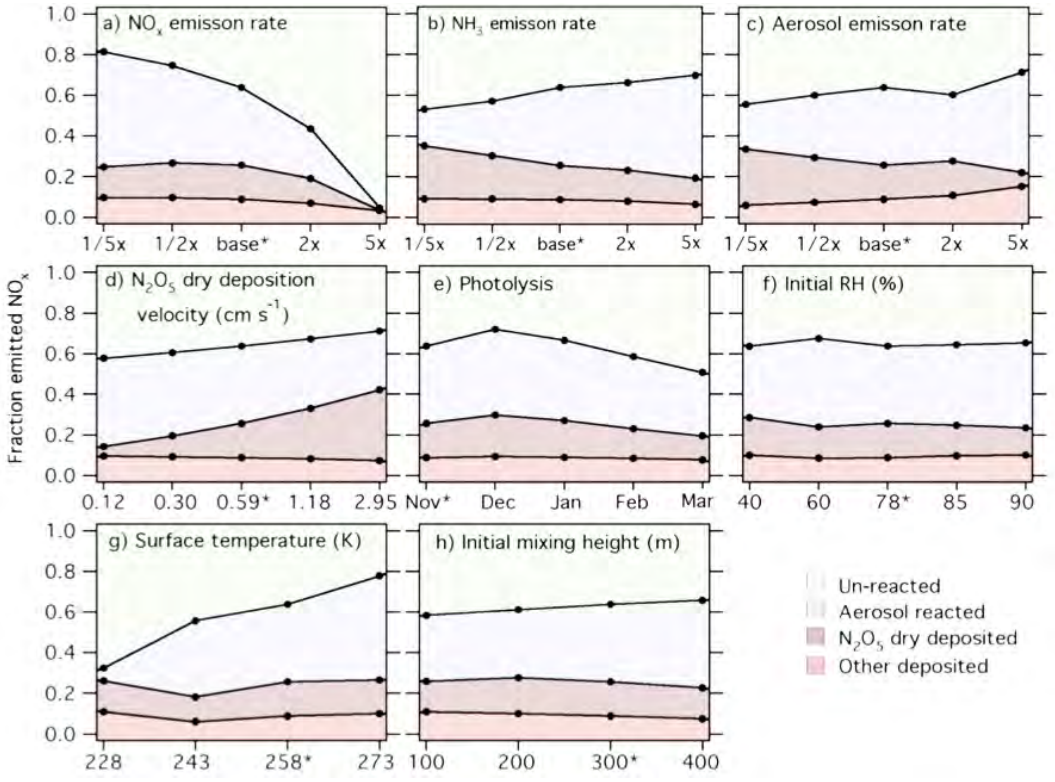


**Figure 6.** Sensitivity of the fate of emitted $NO_X$ to model parameters was investigated by variations of constraints on the base case. Shown are speciation fractions of total column nitrogen emitted as $NO_X$ at $t = 50$ h, corresponding to 2 days after the emission period begins. Base case runs are marked by an asterisk (*).

### 4.1 NO emission rate

Increased flux of NO during the emission period leads to increased $NO_x$ abundance, most intensely near the ground. Increased mixing ratio of NO depletes $O_3$ in the mixed layer, slowing Reactions (R1) and (R2) and $N_2O_5$ formation. This slowing of $N_2O_5$ formation causes the un-reacted fraction to remain dominant. The 5×-NO-case represents a strongly titrated air mass. In this case, modeled $NO_x$ reaches 300 nmol mol$^{-1}$ at $t = 4$ h, within the range of downtown observations (Table 1), leaving excess NO and depleted ozone at night throughout the mixed layer for the entire duration of the run, suppressing $N_2O_5$ formation and slowing nocturnal oxidation of $NO_x$. Alternatively, under a lower NO emission rate, $NO_x$ is efficiently removed through the dark oxidation pathway, with preference for the aerosol-reacted fraction.

### 4.2 $NH_3$ emission rate

Increased emissions of $NH_3$ lead to greater amounts of $NO_3^-$ retention in the particulate phase, giving increased particulate surface area and thus a greater aerosol-reacted fraction. This result was somewhat surprising because we expected that the increased nitrate effect from enhanced $NO_3^-$ retention would

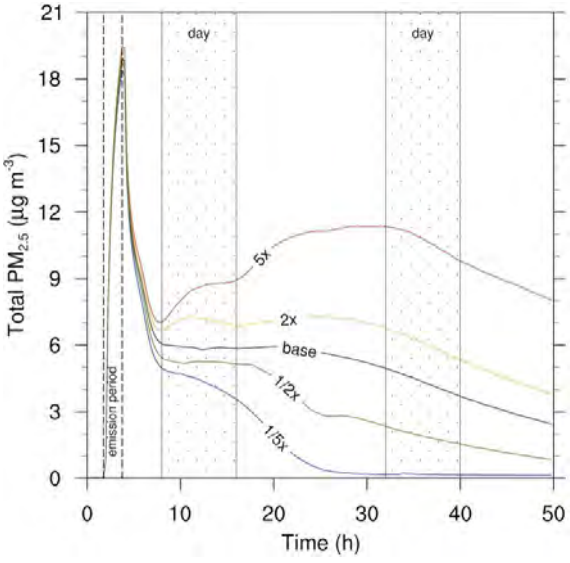


**Figure 7.** Secondary formation of ammonium nitrate begins at $t = 8$ h and is controlled in magnitude by $NH_3$ abundance. The delay of ammonium nitrate formation after emissions end is due to the slowness of nocturnal oxidation caused by ozone titration present during the first night. Pictured above is total $PM_{2.5}$ for the lowest model layer (5 m) for each $NH_3$ sensitivity experiment.

decrease the reactive uptake coefficient, according to the parameterization by Bertram and Thornton (2009), and reduce the aerosol particle reactivity. However, the heterogeneous uptake rate is not only determined by reactive uptake limitations, and in this case the larger available reactive surface area outweighs the reduction in the reactive uptake coefficient due to the nitrate effect. This sensitivity is discussed further in Sect. 5.3.

### 4.3 Aerosol emission rate

In general, increased aerosol flux from the surface leads to greater aerosol particle number density, surface area, and mass density of sulfate particles. Primary sulfate emissions do not leave the particles and thus lead to increased total aerosol particle mass. The increase in aerosol particle surface area allows for more surface reactivity and increases the aerosol-reacted fraction and aerosol particle deposition in the other deposited fraction over the $1/5\times$–$5\times$ factor sensitivity experiments. Additionally, the $N_2O_5$ dry-deposited fraction is decreased due to the enhanced aerosol uptake. The decrease of the aerosol-reacted fraction in the $2\times$ experiment requires further examination, but is likely a feedback based on $NO_x$ emission and time of analysis ($t = 50$ h).

As discussed in the introduction, the reactive uptake coefficient calculation model (Bertram and Thornton, 2009) may overestimate reactive uptake rates, particularly in the case where organic components coats particulate surfaces. Because the rate of $N_2O_5$ heterogeneous hydrolysis is dependent upon both the aerosol particle surface area and the reactive uptake coefficient, the effect of increasing the latter is likely to be similar to increased aerosol particulate emissions. Therefore, we would expect that if the actual reactive uptake coefficient is lower than calculated by Bertram and Thornton (2009), as has been observed in the presence of organic coatings (Bertram et al., 2009; Riedel et al., 2012; Ryder et al., 2014), the aerosol-reacted fraction would decrease. Alternatively, if the actual $\gamma$ is larger than modeled, as has been observed at times during the wintertime study of Wagner et al. (2013), the aerosol-reacted fraction would be expected to increase.

### 4.4 $N_2O_5$ dry deposition velocity

The empirical value of dry deposition velocity of $N_2O_5$ was found to be between 0.12 and 1.06 cm s$^{-1}$ (Huff et al., 2011) and covered by the range of the $1/5\times$–$2\times$ sensitivity experiments. The total fraction of $N_2O_5$ dry deposited varies from 5 % to 25 % over this range. Increases in the dry deposition velocity of $N_2O_5$ lead to an increase in the $N_2O_5$ dry-deposited fraction, a corresponding decrease in all other fractions, and a reduction of $N_2O_5$ mixing ratio at ground level, near the snowpack.

### 4.5 Photolysis

In this experiment, photolysis calculations are carried out for 10 November, 21 December, 22 January, 21 February, and 20 March. The lowest photolysis rate (21 December) corresponds to the smallest un-reacted fraction. Under the weakest photolysis conditions, $N_2O_5$ is present at all hours and reaches a minimum value of 200 pmol mol$^{-1}$ throughout the mixed layer during the day. This $N_2O_5$ abundance allows for nitrate formation via the dark oxidation pathway through Reaction (R3) for 24 h per day. Increased photolysis and longer periods of daylight (20 March) leads to an increased unreacted fraction due to limitation of Reaction (R3) during the shorter nights and weak daytime oxidation of $NO_x$. Monthly average temperatures in winter in Fairbanks are very similar due to large temperature fluctuations over a monthly time period, and each month is likely to have days near the base case temperature of 258 K. For a sensitivity experiment with respect to temperature, see (Sect. 4.7).

### 4.6 Initial RH

This experiment modifies the initial RH in the mixed layer. Increases in RH lead to increases in aerosol surface area from water vapor to particle equilibrium, which is calculated by the model. Most substantial in a relatively dry mixed layer, a 20 % increase in RH from 40 % to 60 % increase the aerosol-reacted fraction by 9 %.

### 4.7 Surface temperature

For this experiment, temperature at the bottom layer of the atmosphere ranges from 228 K to 273 K, which could occur on any given day during the months of November to March. Decreasing temperatures produce a significantly greater unreacted fraction due to kinetic limitation of reactions.

### 4.8 Initial mixing height

The mixed layer in the model gradually rises in time (Fig. 2) due to mixing from above. Due to the time needed to mix air throughout the 300 m mixed layer ($\sim$ 6 h), the height of the mixed layer is nearly constant at 100 m at the end of the emission period for all runs (100–400 m) and therefore does not affect constrained mixing ratios of emissions. Thus, this experiment shows variation of the dilution downwind of the emission source due to a variable mixed layer height. Increases in the height of the mixed layer decrease both $N_2O_5$ dry deposited and other deposited fractions while increasing the amount of aerosol-reacted fraction retained in the atmosphere due to less contact with the snowpack surface.

### 4.9 Chloride concentration (not shown)

In this experiment, the aqueous concentration of emitted chloride in aerosol particles varies from zero–$5\times$ base to

determine the effect on $NO_x$. This range leads to a particulate chloride concentrations of 0.00–0.56 µg $m^{-3}$ at $t = 4$ h near the ground. These trace amounts of $Cl^-$ present in the particles slightly reduce the aerosol-reacted fraction, while the aerosol-reacted fraction increases by 3 % when no $Cl^-$ is included. This weak sensitivity of the fate of $NO_x$ to particulate chloride is likely due to analysis occurring 2 days after emission. Analysis undertaken less than 8 hours after emissions end yields a larger sensitivity to $Cl^-$ due to the presence of $ClNO_2$ in the aerosol-reacted fraction. Significant reductions in $N_2O_5$ mixing ratio and nitrate production are seen (Fig. 4b) in the first hours after emission ends due to the production of $ClNO_2$. Therefore, aerosol chloride concentrations may have a much greater impact on the local scale.

### 4.10 Time of day (not shown)

The start of the emission period was varied to analyze the effect of photolysis on the fresh or aged plume. With respect to local impacts (under 8 h), the time of day has a significant effect on column composition by hindering or allowing the dark oxidation pathway to occur immediately after emission. Therefore, the time of day of $NO_x$ emission is found to have a significant effect on $N_2O_5$ deposition on a local scale, where $NO_x$ emissions in daylight are likely to travel farther from the source before undergoing oxidation, and $NO_x$ emissions at night will enhance local deposition. By $t = 50$ h, however, the plumes are exposed to approximately equal amounts of sunlight and there is no significant effect on the fate of $NO_x$.

### 4.11 $SO_2$ emission (not shown)

Weak photolysis conditions in the base case do not allow for significant secondary formation of sulfate by $SO_2$ oxidation by the OH radical. Therefore, $SO_2$ is virtually inert in these simulations and does not affect the fate of $NO_x$.

### 4.12 Deposition to canopy (not shown)

An additional experiment was performed to include the "upper canopy" term (see Seinfeld and Pandis, 2006) of mixed forest in the dry deposition parameterization to simulate deposition to trees. The addition of an upper canopy parameter in the dry deposition equation leads to increases of dry deposition velocity of 10 % for $HNO_3$, 16 % for $NO_3$, and by 1 order of magnitude for $NO_2$. The explicitly set value for dry deposition velocity of $N_2O_5$ is scaled up by 10 % for this experiment, based on the result for $HNO_3$. Including the upper canopy results in a 4 % increase in the other deposited fraction, primarily due to increased $NO_2$ deposition, and a $< 1$ % increase in the $N_2O_5$ dry-deposited fraction. In this 1-D model, the addition of deposition to the upper canopy of trees has an insignificant effect on the fate of $NO_x$. However, air transport over horizontally varying trees causes mixing of surface and near-surface layers that may enhance deposition in a way we cannot model in this 1-D simulation. This point is discussed below.

## 5 Discussion

### 5.1 Local effects vs. long-range transport

Results from the base case speciation analysis (Fig. 5) have implications for local and long-range deposition effects. Dry deposition of $N_2O_5$ begins immediately upon formation of $N_2O_5$ and dominates the nitrogen flux to the snowpack during the night. Snowpack deposition of aerosol nitrate and gas-phase $HNO_3$ does not occur in significant amounts until 16 h after emissions have ended. This indicates dry deposition of $N_2O_5$ dominates nitrogen deposition to the snowpack on a local scale, while particulate nitrate deposition is minimal. Alternatively, particulate nitrate can remain suspended in the local atmosphere, undergo long-range transport, be diluted in transit, and removed by a precipitation event.

Observations of both titrated and un-titrated air masses in studies such as Ayers and Simpson (2006) indicate a wide variability of the oxidation capacity of the mixed layer. Sensitivity experiments presented here have shown NO emissions in the absence of photolysis can transform the lower atmosphere from an oxidizing environment rich in ozone to a reduced environment with no oxidation capacity. Some values of $NO_x$ observed in downtown Fairbanks are even greater than the modeled 5×-$NO_x$ experiment (Fig. 6a) in which ozone was titrated in the mixed layer for 2 days. In reality, horizontal mixing may reduce the timescale of titration as background ozone is mixed in, but ozone reduction may linger for well over 24 h downwind. Ozone titration is likely to be enhanced under stable meteorological conditions.

The photolysis experiment (Fig. 6e) has implications for environments at higher latitudes than Fairbanks, which is located at 64.76° N. The month of December, with the weakest photolysis and longest periods of darkness, shows the smallest un-reacted fraction. Dry deposition of $N_2O_5$ and aerosol-reacted fractions are enhanced by extended darkness. Locations north of the Arctic Circle (66.56° N) will have days on which no photolysis will occur and $N_2O_5$ formation occurs continuously, allowing the dark oxidation pathway of $NO_x$ to be active 24 h per day. Under total darkness conditions, local deposition of $N_2O_5$ is likely to be enhanced.

The drastic dependence of the fate of $NO_x$ on temperature (Fig. 6g) shows that ambient temperatures are the most important naturally occurring factor controlling the chemistry of the nocturnal $NO_x$ plume. The primary reason for the increased un-reacted fraction is that the formation rate of $NO_3$ slows at colder temperatures, leaving a larger fraction of $NO_x$ un-reacted at the $t = 50$ h analysis time. Interestingly, dry deposition rates of $N_2O_5$ remain fairly constant over this temperature range. The range of temperatures studied are not uncommon in Fairbanks for the months of November to March.

For temperatures lower than 228 K and stable meteorological conditions, $NO_x$ may be near the snowpack for extended periods of time, possibly enhancing dry deposition.

### 5.2 Vertically varying chemistry

Modeled vertical profiles of $N_2O_5$ have implications for interpreting field measurements. Modeled $N_2O_5$ mixing ratio at 105 m one hour immediately following the emission period ($t = 5$ h) is over 2× greater than at the surface and consistently 10–15 % greater for the duration of the model run. This suggests that observations carried out near the snowpack may yield abundances of $N_2O_5$ significantly lower than those aloft. More importantly, positive vertical gradients of $N_2O_5$ reaffirm the result found by Huff et al. (2011) that dry deposition is a significant loss mechanism of $N_2O_5$ near the snowpack.

Additionally, loss of $N_2O_5$ near the ground may be underestimated. Modeled values of $N_2O_5$ aloft in the first hour after emissions end ($t = 5$ h) are in good agreement with measurements performed 80 m above the valley floor (Table 2). This suggests the model properly captures loss of $N_2O_5$ aloft on short timescales (a few hours). At longer distances and near the ground, the model predicts ∼ 4× observed abundances of $N_2O_5$ (Table 2). The measured dry deposition velocity of $N_2O_5$ used to constrain the model was based on aerodynamic methods and measured above a treeless, flat snowpack. Under this constraint, the model assumes a flat ground surface for the entire model run, whereas Fairbanks is surrounded by densely wooded terrain, which enhances turbulence due to roughness. This turbulence is expected to enhance deposition of $N_2O_5$ and thus reduce observed $N_2O_5$ when compared to modeled values, which is a treeless environment free of mechanical turbulence.

The effect of enhanced turbulence near the ground would increase air parcel transport to the ground surface, with a result similar to that of a sensitivity experiment with enhanced dry deposition velocity of $N_2O_5$. The model scenario with an enhanced value of 2.95 cm $s^{-1}$ (Fig. 6d) still predicts $N_2O_5$ abundance near the ground ∼ 2× greater than observed values. This method is not the correct way to address enhanced deposition because deposition velocity is increased rather than air parcel contact with the snowpack. It does, however, suggest that deposition of $N_2O_5$ may be significantly underestimated in the treeless model scenario. Modeling enhanced deposition due to mechanical turbulence induced by a 3-D object such as tree cover is a limitation of the 1-D model. Airborne observations of $N_2O_5$ aloft, away from Fairbanks, would verify if the model properly captures loss of $N_2O_5$ away from the ground and would verify that loss to ground surface is underestimated. Such observations are necessary to fully understand the vertical and spatial distribution of the nocturnal nitrogen plume.

### 5.3 Ammonium nitrate formation

Downtown Fairbanks lies in a US Environmental Protection Agency non-attainment area for $PM_{2.5}$ (ADEC, 2008). A common concern in reducing total $PM_{2.5}$ lies in a nonlinearity present in aerosols containing ammonium, nitrate, and sulfate. When excess ammonia is available (molar ratio of $NH_4^+/SO_4^{2-} > 2$), reductions in particulate sulfate may be replaced by particulate nitrate, leading to an increase of ammonium nitrate in the aerosol particles (Seinfeld and Pandis, 2006, p. 483). Modeled particulate nitrate concentrations in the polluted area ($t = 4$ h) are $< 0.5\,\mu g\,m^{-3}$ and agree with observations (ADEC, 2007), but concentrations of $> 2\,\mu g\,m^{-3}$ $NO_3^-$ are modeled within 6 hours after emissions end. These results suggest that secondary particulate nitrate formation due to $NO_x$ oxidation within Fairbanks urban core is not a major contributor to $PM_{2.5}$ non-attainment because titration of $O_3$ slows $N_2O_5$ formation and thus formation of $NO_3^-$ and $HNO_3$. Enhanced secondary formation of particulate nitrate, however, may have implications further downwind of the polluted area.

In the $NH_3$ emission rate sensitivity experiment (Fig. 6b), the aerosol-reacted fraction increases with increased ammonia emissions. This effect can be seen in total $PM_{2.5}$ concentrations near the ground (Fig. 7) beginning 2 hours after the end of emissions due to the formation of ammonium nitrate ($NH_4NO_3$). During the emission period, primary emissions of fully oxidized sulfur leading to $H_2SO_4$ and organic matter dominate total mass and are similar for each experiment. During the emission period and for ∼ 2 h afterward, $NH_4NO_3$ concentrations are zero and $NH_4^+/SO_4^{2-} < 2$ in the particle and sulfuric acid is not fully neutralized. Base case emissions of $NH_3$ are sufficient to bring the molar ratio of $NH_4^+/SO_4^{2-}$ at the surface to 1.5 at $t = 4$ h, which gradually increases to 2.1 at $t = 5$ h. Values of $NH_4^+/SO_4^{2-} > 2$ are possible as $NO_3^-$ is formed and available to react with $NH_4^+$ to form $NH_4NO_3$ (Seinfeld and Pandis, 2006, p. 479). Increases in the $NH_3$ flux bring the $NH_4^+/SO_4^{2-}$ ratio at the end of the emission period ($t = 4$ h) to 1.9 for the 5× $NH_3$ run. Divergence of total $PM_{2.5}$ mass at $t = 8$ h (Fig. 7) between the sensitivity studies is controlled by $NH_3$ emission and subsequent formation of $NH_4NO_3$. In this manner, secondary formation of nitrate particles is controlled in magnitude by ammonia flux and the rate of nocturnal $NO_x$ oxidation, which is strongly affected by ozone titration. In all cases, secondary aerosol mass continues to form during the first day while $N_2O_5$ is still present from nighttime formation (Fig. 7). Dry deposition of ammonia gas competes with uptake of ammonia by aerosol particles and neutralization of particulate acidity, so in cases where vertical mixing is hindered, deposition of ammonia may also limit the uptake to aerosol particles.

The slow timescale of $NH_4^+$ uptake by aerosol forming $NH_4NO_3$ makes it impossible to infer $NH_3$ abundances

**Table 2.** Field observations of $NO_x$ from downtown Fairbanks, University of Alaska Fairbanks (UAF), and the Quist Farm as well as related model results. A wind speed of $1\,m\,s^{-1}$ and distance from downtown was used to calculate corresponding model time. Observations at UAF were performed at an elevation 80 m above the valley floor ([1]) and compared to modeled values in layer centered at 75 m ([2]).

| | Downtown | UAF | Quist Farm |
|---|---|---|---|
| Distance from downtown (km, direction) | 0 | 5, WNW | 20, WSW |
| Corresponding model time (h) | 4 | 5 | 8 |
| Modeled $NO_x$ ($nmol\,mol^{-1}$) | 58 | 24[2] | 12 |
| Observed $NO_x$ range ($nmol\,mol^{-1}$) | 1–390 | 0–100[1] | 0–15 |
| Modeled $N_2O_5$ ($pmol\,mol^{-1}$) | 38 | 182[2] | 412 |
| Observed $N_2O_5$ range ($pmol\,mol^{-1}$) | – | 0–250[1] | 0–80 |
| Reference | State of Alaska (2008) | Ayers and Simpson (2006) | Huff et al. (2011) |

downtown based on $NH_4^+$ measurements. Due to the slow timescale of nitric acid and particle nitrate formation, a decrease in primary sulfate emissions should reduce total $PM_{2.5}$ and not be replaced by an increase in particulate nitrate in the downtown area. However, this $NO_x$ is later oxidized to $HNO_3$ and particulate $NO_3^-$, which later reacts with $NH_3$ forming $NH_4NO_3$ that could result in soil fertilization downwind of Fairbanks.

Constrained by emissions inventories and calculations, $NH_3$ emissions yielded a value of $0.96\,\mu g\,m^{-3}$ $NH_4^+$ and $1.6\,nmol\,mol^{-1}$ excess $NH_3$ near the ground at the end of the emission period ($t = 4$ h). In order to achieve the measured November average of $0.97\,\mu g\,m^{-3}$ $NH_4^+$ (State of Alaska, 2011) through aerosol uptake, we estimate that a minimum of $1.2\,nmol\,mol^{-1}$ $NH_3$ needs to be available for uptake into aerosol particles. The base-case-emitted $NH_3$ was sufficient to reach $NH_4^+$ observations and yield excess $NH_3$. We believe automotive and woodsmoke sources of $NH_3$ are sufficient to account for the measured $NH_4^+/SO_4^{2-}$ ratio. Results of sensitivity experiments have shown $NH_3$ could be greater than modeled in the base case with no indication present in $NH_4^+$ observations downtown due to slow $NH_4NO_3$ formation caused by titration. However, if there are larger than the base case ammonia emissions, significantly enhanced formation of $NH_4NO_3$ is modeled outside of the primarily polluted area. Therefore, observations of $NH_3$ emissions would be highly valuable for understanding Fairbanks air quality and possible downwind ecosystem impacts through ammonium nitrate deposition.

The origin and chemistry of sulfate aerosol in Fairbanks winter is currently unknown. The emissions used in this simulation, constrained by gas-phase $SO_2$ and $PM_{2.5}$ $SO_4^{2-}$ observations, estimate column-integrated total sulfur is in the form of 93 % $SO_2$ and 7 % fully oxidized sulfur (e.g., $SO_3$) that rapidly reacts to form $SO_4^{2-}$. A value of 7 % is likely too high to be purely primary sulfate emission, but the modeled base case scenario produces no secondary sulfate from $SO_2$, which would be expected in an atmosphere with weak OH photochemistry and reduced oxidants (due to titration of ozone). Sulfur oxidation catalysis by transition metals has been presented as a sulfate formation mechanism (Brandt and van Eldik, 1995; Hoffman and Boyce, 1983) and could be a significant secondary $SO_4^{2-}$ source during winter. If the formation of $SO_4^{2-}$ by metal catalysis is fast, the sulfate could appear like true primary emissions, as we have modeled them in this study. The fate of $NO_x$ emissions is found to be insensitive to $SO_2$, but this may not have been the case if secondary sulfate was formed by pathways alternative to photochemistry. Additional study would be useful for understanding the sulfate chemistry in Fairbanks and identifying possible remedies for $PM_{2.5}$ non-attainment.

### 5.4 Model limitations

The simulations in this experiment presented for analysis of the fate of anthropogenic $NO_x$ pollution in a high-latitude environment are not without a few limitations. The meteorological conditions in the model were chosen such that cloud formation is avoided, primarily because microphysical and chemical feedbacks would hinder the main focus of this study, which was the fate of emitted $NO_x$ in a high-latitude winter environment. Clear skies dominate synoptic conditions in the greater Fairbanks area in the winter months, supporting that the base case simulation is not weakened by the absence of clouds. Observations by Sommariva et al. (2009) found that $N_2O_5$ removal by fog droplets was dominant when fog was present. Cloud formation would likely lead to dominance of $N_2O_5$ uptake aloft in large cloud particles, leading to less gas-phase $HNO_3$ and more nitrate aloft which could undergo long-range transport. Cloud formation would also affect photolysis rates in model layers below the clouds.

The temperature profile used to initialize the model was not taken from an individual measured profile but rather an idealized case because this idealized case better replicated the ARCTAS $NO_2$ profile. This model deficiency is a common problem for numerical models of the stable boundary layer (see discussion in Anderson and Neff, 2008). The $NO_2$ detected by the ARCTAS aircraft at 300 m was 14 km from downtown Fairbanks (ARCTAS, 2008). Assuming column motion of about $1\,m\,s^{-1}$, 14 km would correspond to the modeled $NO_x$ profile at $t = 8$ h, which shows vertical dilution to $\sim 290$ m. The modeled temperature profile of the base case is applicable for conditions with relatively high mixed layers and weak inversions, which are common in the "shoulder" months of October, November, March and April. Mixing due to the modeled temperature gradient is suitable for this study; however, mixing forced by eddy-diffusivity has been performed to match observed vertical profiles (Geyer and Stutz, 2004) and may be more appropriate for thermally inverted and stratified boundary layer simulations. However, vertically resolved chemical observations are required to apply the Geyer and Stutz (2004) method.

As MISTRA is a 1-D model, horizontal mixing is not included. This lack of horizontal mixing ensures that column-integrated abundances conserve mass, allowing the analysis shown here, while still explicitly allowing vertical mixing that is necessary to consider the competition between surface and aloft chemical processes. Horizontal mixing over the duration of the model runs will depend strongly on the prevailing synoptic situation so that a quantification of the effect of horizontal mixing is not possible. Horizontal mixing with background ozone would lead to less limitation of Reactions (R1) and (R2) and more efficient removal of $NO_x$.

Aerosol particles in the simulations were represented as purely aqueous constituents. With respect to frozen water, observations by LIDAR in Fairbanks indicate presence of super-cooled droplets in high-latitude environments at temperatures as low as 240 K, suggesting aqueous-phase aerosols are present in temperatures well below the freezing temperature of water (Fochesatto et al., 2005). The freezing of particles would have complex and currently poorly understood effects on reactivity. However, freezing could potentially occur on the 2-day timescale, implying that more study of the structure and reactivity of ice particles is needed.

Field observations have shown that the reactive uptake coefficient parameterization of (Bertram and Thornton, 2009) often results in $\gamma$ values larger than observed in the field, which has been associated with organic aerosol content (Bertram et al., 2009; Riedel et al., 2012; Ryder et al., 2014). We had no observational constraints on the properties of the organic matter in the aerosol particles (internal/external mixing state, O : C ratio, etc.), so we could not enhance the $\gamma$ calculation model. However, $\gamma$ observed under wintertime conditions in the study of Wagner et al. (2013) was comparable to and sometimes exceeded the calculation method used here, possibly indicating that the Bertram and Thornton (2009) model is reasonably accurate under the conditions simulated here. The significant uncertainties that exist in the proper calculation of $\gamma$ need further study, and the study we report here indicates that airborne observations of $N_2O_5$ should be particularly sensitive to $\gamma$ and aerosol particle properties.

## 6 Conclusions

Simulations have shown that approximately two-thirds of $NO_x$ is lost in the 2 days after emission in high-latitude winter conditions mostly through the dark oxidation pathway. Observed pollution fluxes commonly produce a reduced environment with excess NO and near-zero ozone, slowing secondary oxidation chemistry that removes $NO_x$. The fraction of emitted $NO_x$ that remains in the atmosphere was found to be most sensitive to the NO emission flux and temperature. Winter months with relatively warm temperatures and high mixing heights are likely to have the greatest nitrate aerosol particulate loading. Alternatively, cold days with low mixed layers are likely to have the greatest dry deposition rates and greatest local nitrogen deposition impact. Dry deposition rates of $N_2O_5$ were found to be most sensitive to aerosol surface area and dry deposition velocity, illustrating the competition between dry deposition and aerosol reactivity for the removal of $N_2O_5$. Due to ground contact only occurring in the bottom model layer, greater amounts of total emitted $NO_x$ were removed from the column via aerosol particle reactions (38 %) than through dry deposition (17 %) two days after emission in the base case scenario. Modeled abundances of $N_2O_5$ showed diurnal variations of over 1000 % and positive vertical gradients from the snowpack, showing the need for further study to understand vertical distribution of the emission plume and estimate potential impacts.

*Acknowledgements.* The authors would like to thank NOAA for use of the Ferret program for analysis of model output and UCAR for the use of NCL plotting software, which was used to generate the figures in this manuscript. The authors would like to thank Deanna Huff and Barbara Trost with the Alaska Department of Environmental Conservation and Jim Connor with the Fairbanks North Star Borough Air Quality Division for collaboration and providing observational data. Thanks to Catherine Cahill, Tom Trainor, and the two reviewers for helpful comments. This project was funded by the NSF under grant ATM-0926220. We also thank Flora Grabowski at the Keith Mather Library in the Geophysical Institute for supporting open access publication of this article.

Edited by: R. Sander

## References


ACRC: Alaska Climate Research Center Climate data for Fairbanks, AK, http://climate.gi.alaska.edu/Climate/Location/TimeSeries/Fairbanks.html, 2011.

ADEC: Alaska Department of Environmental Conservation Supplemental information: $PM_{2.5}$ Designation and Bounadry Recommendations, http://dec.alaska.gov/air/doc/PM25_info.pdf, 2007.

ADEC: Alaska Department of Environmental Conservation Fairbanks non-attainment area boundary comments. Emissions Inventory 2005, http://www.dec.state.ak.us/air/doc/DEC_EPA_Fbks_NA_20oct08.pdf, 2008.

Akagi, S. K., Yokelson, R. J., Wiedinmyer, C., Alvarado, M. J., Reid, J. S., Karl, T., Crounse, J. D., and Wennberg, P. O.: Emission factors for open and domestic biomass burning for use in atmospheric models, Atmos. Chem. Phys., 11, 4039—4072, doi:10.5194/acp-11-4039-2011, 2011.

Anderson, P. S. and Neff, W. D.: Boundary layer physics over snow and ice, Atmos. Chem. Phys., 8, 3563–3582, doi:10.5194/acp-8-3563-2008, 2008.

Anttila, T., Kiendler-Scharr, A., Tillmann, R., and Mentel, T. F.: On the Reactive Uptake of Gaseous Compounds by Organic-Coated Aqueous Aerosols: Theoretical Analysis and Application to the Heterogeneous Hydrolysis of $N_2O_5$, The Journal of Physical Chemistry A, 110, 10435–10443, doi:10.1021/jp062403c, http://pubs.acs.org/doi/abs/10.1021/jp062403c, pMID: 16942049, 2006.

Apodaca, R., Huff, D., and Simpson, W.: The role of ice in $N_2O_5$ heterogeneous hydrolysis at high latitudes, Atmos. Chem. Phys, 8, 7451–7463, doi:10.5194/acp-8-7451-2008, 2008.

ARCTAS: Arctic Research of the Composition of the Troposphere by Aircraft and Satellites NASA DC-8 aircraft data, http://www-air.larc.nasa.gov/cgi-bin/arctas-c, 2008.

Ayers, J. D. and Simpson, W. R.: Measurements of $N_2O_5$ near Fairbanks, Alaska, J. Geophys. Res., 111, D14309, doi:10.1029/2006JD007070, 2006.

Bertram, T. and Thornton, J.: Toward a general parameterization of $N_2O_5$ reactivity on aqueous particles: The competing effects of particle liquid water, nitrate and chloride, Atmos. Chem. Phys, 9, 8351–8363, doi:10.5194/acp-9-8351-2009, 2009.

Bertram, T. H., Thornton, J. A., Riedel, T. P., Middlebrook, A. M., Bahreini, R., Bates, T. S., Quinn, P. K., and Coffman, D. J.: Direct observations of $N_2O_5$ reactivity on ambient aerosol particles, Geophys. Res. Lett., 36, n/a–n/a, doi:10.1029/2009GL040248, http://dx.doi.org/10.1029/2009GL040248, 2009.

Bott, A., Trautmann, T., and Zdunkowski, W.: A numerical model of the cloud topped planetary boundary layer: Radiation, turbulence and spectral microphysics in marine stratus, Q. J. R. Meteorol. Soc., 122, 635–667, 1996.

Brandt, C. and van Eldik, R.: Transition metal-catalyzed oxidation of sulfur (IV) oxides Atmospheric-relevant processes and mechanisms, Chem. Rev., 95, 119–190, 1995.

Brown, S., Stark, H., Ryerson, T., Williams, E., Nicks, D., Trainer, M., Fehsenfeld, F., and Ravishankara, A.: Nitrogen oxides in the nocturnal boundary layer: Simultaneous in situ measurements of $NO_3$, $N_2O_5$, $NO_2$, NO, and $O_3$, J. Geophys. Res., 108, 2917, doi:10.1029/2002JD002917, 2003.

Brown, S., Dubé, W., Osthoff, H., Stutz, J., B., R. T., Wollny, A. G., Brock, C. A., Warneke, C., de Gouw, J. A., Atlas, E., Neuman, J. A., Holloway, J. S., Lerner, B. M., Williams, E. J., Kuster, W. C., Goldan, P. D., Angevine, W. M., Trainer, M., Fehsenfeld, F. C., and Ravishankara, A. R.: Vertical profiles in $NO_3$ and $N_2O_5$ measured from an aircraft: Results from the NOAA P-3 and surface platforms during the New England Air Quality Study 2004, J. Geophys. Res., 112, doi:10.1029/2007JD008883, 2007a.

Brown, S. S., Dubé, W. P., Osthoff, H. D., Wolfe, D. E., Angevine, W. M., and Ravishankara, A. R.: High resolution vertical distributions of $NO_3$ and $N_2O_5$ through the nocturnal boundary layer, Atmos. Chem. Phys., 7, 139–149, doi:10.5194/acp-7-139-2007, 2007b.

Brown, S. S., Dubé, W. P., Fuchs, H., Ryerson, T. B., Wollny, A. G., Brock, C. A., Bahreini, R., Middlebrook, A. M., Neuman, J. A., Atlas, E., Roberts, J. M., Osthoff, H. D., Trainer, M., Fehsenfeld, F. C., and Ravishankara, A. R.: Reactive uptake coefficients for $N_2O_5$ determined from aircraft measurements during the Second Texas Air Quality Study: Comparison to current model parameterizations, J. Geophys. Res.-Atmos., 114, n/a–n/a, doi:10.1029/2008JD011679, http://dx.doi.org/10.1029/2008JD011679, 2009.

Chang, W. L., Bhave, P. V., Brown, S. S., Riemer, N., Stutz, J., and Dabdub, D.: Heterogeneous Atmospheric Chemistry, Ambient Measurements, and Model Calculations of $N_2O_5$: A Review, Aerosol Sci. Technol., 45, 665–695, doi:10.1080/02786826.2010.551672, http://dx.doi.org/10.1080/02786826.2010.551672, 2011.

Dentener, F. J. and Crutzen, P. J.: Reaction of $N_2O_5$ on Tropospheric Aerosols: Impact on the Global Distributions of NOx, $O_3$, and OH, J. Geophys. Res, 98, 7149–7163, 1993.

ESRL: Earth System Research Laboratory, Global Monitoring Division, Surface ozone, in-situ hourly averages, Barrow, AK, http://www.esrl.noaa.gov/gmd/dv/data/index.php?site=brw&category=Ozone&parameter_name=SurfBOzone, 2011.

Evans, M. J. and Jacob, D. J.: Impact of new laboratory studies of $N_2O_5$ hydrolysis on global model budgets of tropospheric nitrogen oxides, ozone, and OH, Geophys. Res. Lett., 32, n/a–n/a, doi:10.1029/2005GL022469, http://dx.doi.org/10.1029/2005GL022469, 2005.

Fenn, M., Baron, J., Allen, E., Rueth, H., Nydick, K., Geiser, L., Bowman, W., Sickman, J., Meixner, T., and Johnson, D.: Ecological effects of nitrogen deposition in the western United States,, BioScience, 53, 404–420, 2003.

Finlayson-Pitts, B. and Pitts, J.: Chemistry of the Upper and Lower Atmosphere, Academic Press, 2000.

Fochesatto, J., Collins, R., Yue, J., Cahill, C., and Sassen, K.: Compact eye-safe backscatter lidar for aerosol studies in urban polar environment, Vol. 5887, 58870U–58870U–9, SPIE, 2005.

Gaston, C. J., Thornton, J. A., and Ng, N. L.: Reactive uptake of $N_2O_5$ to internally mixed inorganic and organic particles: the role of organic carbon oxidation state and inferred organic phase separations, Atmos. Chem. Phys., 14, 5693–5707, doi:10.5194/acp-14-5693-2014, 2014.

Geyer, A. and Stutz, J.: Vertical profiles of $NO_3$, $N_2O_5$, $O_3$, and $NO_x$ in the nocturnal boundary layer: 2 Model studies on the altitude dependence of composition and chemistry, J. Geophys. Res., 109, D12307, doi:10.1029/2003JD004211, 2004.

Graedel, T. E. and Keene, W. C.: Tropospheric budget of reactive chlorine, Global Biogeochem. Cycles, 9, 47, doi:10.1029/94GB03103, 1995.

Hanson, D. R. and Ravishankara, A. R.: The Reaction Probabilities of $ClONO_2$ and $N_2O_5$ on 40 to 75% Sulfuric Acid Solutions, J. Geophys. Res., 96, 17307–17314, doi:10.1029/91JD01750, 1991.

Hoffman, M. R. and Boyce, S. D.: Catalytic autooxidation of aqueous sulfur dioxide in relationship to atmospheric systems, Adv. Environ. Sci. Technol., 12, 148–189, 1983.

Huff, D. M., Joyce, P. L., Fochesatto, G. J., and Simpson, W. R.: Deposition of dinitrogen pentoxide, $N_2O_5$, to the snowpack at high latitudes, Atmos. Chem. and Phys., 11, 4929–4938, doi:10.5194/acp-11-4929-2011, 2011.

Jaenicke, R.: Tropospheric aerosols, chap. Chapter 1: Aerosol-Cloud-Climate Interactions, 1993.

Kramm, G., Dlugi, R., Dollard, G., Foken, T., Mölders, N., Müller, H., Seiler, W., and Sievering, H.: On the dry deposition of ozone and reactive nitrogen species, Atmos. Environ., 29, 3209–3231, doi:10.1016/1352-2310(95)00218-N, 1995.

Landgraf, J. and Crutzen, P.: An Efficient Method for "On-Line" Calculations of Photolysis and Heating Rates, J. Atmos. Sci., 55, 863–878, 1998.

Mentel, T. F., Sohn, M., and Wahner, A.: Nitrate effect in the heterogenous hydrolysis of dinitrogen pentoxide on aqueous aerosols, Phys. Chem. Chem. Phys., 2, 5451–5457, doi:10.1039/A905338G, 1999.

NCDC: National Climate Data Center, Relative humidity from Fairbanks, AK station (PAFA), ftp://ftp.ncdc.noaa.gov/pub/data/asos-fivemin/6401-2009/, 2011.

Nowak, J. B., Neuman, J. A., Bahreini, R., Middlebrook, A. M., Holloway, J. S., McKeen, S. A., Parrish, D. D., Ryerson, T. B., and Trainer, M.: Ammonia sources in the California South Coast Air Basin and their impact on ammonium nitrate formation, Geophys. Res. Lett., 39, n/a–n/a, doi:10.1029/2012GL051197, http://dx.doi.org/10.1029/2012GL051197, 2012.

Osthoff, H., Roberts, J., Ravishankara, A., Williams, E., Lerner, B., Sommariva, R., Bates, T., Coffman, D., Quinn, P., Dibb, J., Stark, H., Burkholder, J. B., Talukdar, R. K., Meagher, J., Fehsenfeld, F. C., and Brown, S. S.: High levels of nitryl chloride in the polluted subtropical marine boundary layer,, Nat. Geosci., 1, doi:10.1038/ngeo177, 2008.

Pechtl, S., Lovejoy, E. R., Burkholder, J. B., and von Glasow, R.: Modeling the possible role of iodine oxides in atmospheric new particle formation, 6, 503–523, 2006.

Piot, M. and von Glasow, R.: The potential importance of frost flowers, recycling on snow, and open leads for ozone depletion events, Atmos. Chem. Phys., 8, 2437–2467, doi:10.5194/acp-8-2437-2008, 2008.

Riedel, T. P., Bertram, T. H., Ryder, O. S., Liu, S., Day, D. A., Russell, L. M., Gaston, C. J., Prather, K. A., and Thornton, J. A.: Direct $N_2O_5$ reactivity measurements at a polluted coastal site, Atmospheric Chemistry and Physics, 12, 2959–2968, doi:10.5194/acp-12-2959-2012, http://www.atmos-chem-phys.net/12/2959/2012/, 2012.

Riemer, N., Vogel, H., Vogel, B., Anttila, T., Kiendler-Scharr, A., and Mentel, T. F.: Relative importance of organic coatings for the heterogeneous hydrolysis of $N_2O_5$ during summer in Europe, J. Geophys. Res.-Atmos., 114, n/a–n/a, doi:10.1029/2008JD011369, http://dx.doi.org/10.1029/2008JD011369, 2009.

Ryder, O. S., Ault, A. P., Cahill, J. F., Guasco, T. L., Riedel, T. P., Cuadra-Rodriguez, L. A., Gaston, C. J., Fitzgerald, E., Lee, C., Prather, K. A., and Bertram, T. H.: On the Role of Particle Inorganic Mixing State in the Reactive Uptake of $N_2O_5$ to Ambient Aerosol Particles, Environ. Sci. Technol., 48, 1618–1627, doi:10.1021/es4042622, http://pubs.acs.org/doi/abs/10.1021/es4042622, 2014.

Seinfeld, J. H. and Pandis, S. N.: Atmospheric Chemistry and Physics, 2nd ed., 2006.

Sommariva, R. and von Glasow, R.: Multi-phase halogen chemistry in the tropical Atlantic Ocean, Environ. Sci. Technol., 46, 10429–10437, 2012.

State of Alaska: Measurements of $NO_x$ and $SO_2$ from downtown Fairbanks, 2008–2009, personal communication with Alaska Department of Environmental Conservations, 2011, 2008.

State of Alaska: Aerosol particle composition from downtown Fairbanks, 2006–2010, personal communication with Alaska Department of Environmental Conservations, 2011.

Thornton, J. A., Kercher, J. P., Riedel, T. P., Wagner, N. L., Cozic, J., Holloway, J. S., Dubé, W. P., Wolfe, G. M., Quinn, P. K., Middlebrook, A. M., Alexander, B., and Brown, S. S.: A large atomic chlorine source inferred from mid-continental reactive nitrogen chemistry, Nature, 464, 271—274, doi:10.1038/nature08905, 2010.

TOMS: Total Ozone Mapping Spectrometer (TOMS). What is the total column ozone over your house?, http://toms.gsfc.nasa.gov/teacher/ozone_overhead_v8.html, 2011.

Van Doren, J., Watson, L., Davidovits, P., Worsnop, D., Zahniser, M., and Kolb, C.: Uptake of $N_2O_5$ and $HNO_3$ by aqueous sulfuric acid droplets, J. Phys. Chem., 95, 1684–1689, 1991.

von Glasow, R., Sander, R., Bott, A., and Crutzen, P.: Modeling halogen chemistry in the marine boundary layer 1. Cloud-free MBL, J. Geophys. Res., 107, 4352, doi:10.1029/2001JD000942, 2002.

Wagner, N. L., Riedel, T. P., Young, C. J., Bahreini, R., Brock, C. A., Dubé, W. P., Kim, S., Middlebrook, A. M., Öztürk, F., Roberts, J. M., Russo, R., Sive, B., Swarthout, R., Thornton, J. A., VandenBoer, T. C., Zhou, Y., and Brown, S. S.: $N_2O_5$ uptake coefficients and nocturnal $NO_2$ removal rates determined from ambient wintertime measurements, J. Geophys. Res.-Atmos., 118, 9331–9350, doi:10.1002/jgrd.50653, 2013.

Wesely, M.: Parameterization of surface resistances to gaseous dry deposition in regional-scale numerical models, Atmos. Environ., 23, 1293–1304, 1989.

Wesely, M. and Hicks, B.: A review of the current status of knowledge on dry deposition, Atmos. Environ., 34, 2261–2282, 2000.

Wood, E., Bertram, T., and Wooldridge, P.: Measurements of $N_2O_5$, $NO_2$, and $O_3$ east of the San Francisco Bay, Atmos. Chem. Phys., 5, 483–491, doi:10.5194/acp-5-483-2005, 2005.

Yokelson, R. J., Griffith, D. W. T., and Ward, D. E.: Open-path Fourier transform infrared studies of large-scale laboratory biomass fires, J. Geophys. Res., 101, 21067–21080, doi:10.1029/96JD01800, 1996.

Yokelson, R. J., Susott, R., Ward, D. E., Reardon, J., and Griffith, D. W. T.: Emissions from smoldering combustion of biomass measured by open-path Fourier transform infrared spectroscopy, J. Geophys. Res., 102, 18865–18877, doi:10.1029/97JD00852, 1997.


IanJohnson
www.ianajohnson.com

# Spatial and Temporal Analysis of the Composition of Fine Particulates in Fairbanks, Alaska

*Final Results*

Authors: KC Nattinger[1], Deanna Huff[2], William R. Simpson[1]

[1]Geophysical Institute and Department of Chemistry and Biochemistry
University of Alaska, Fairbanks, Fairbanks, AK 99705
knattinger@alaska.edu

State of Alaska Department of Environmental Conservation,
Juneau, AK, 99802

# Spatial and Temporal Analysis of the Composition of Fine Particulates in Fairbanks, Alaska

I. Background
II. Processing of Data
III. Past Modeling Work
IV. Research Questions and Results

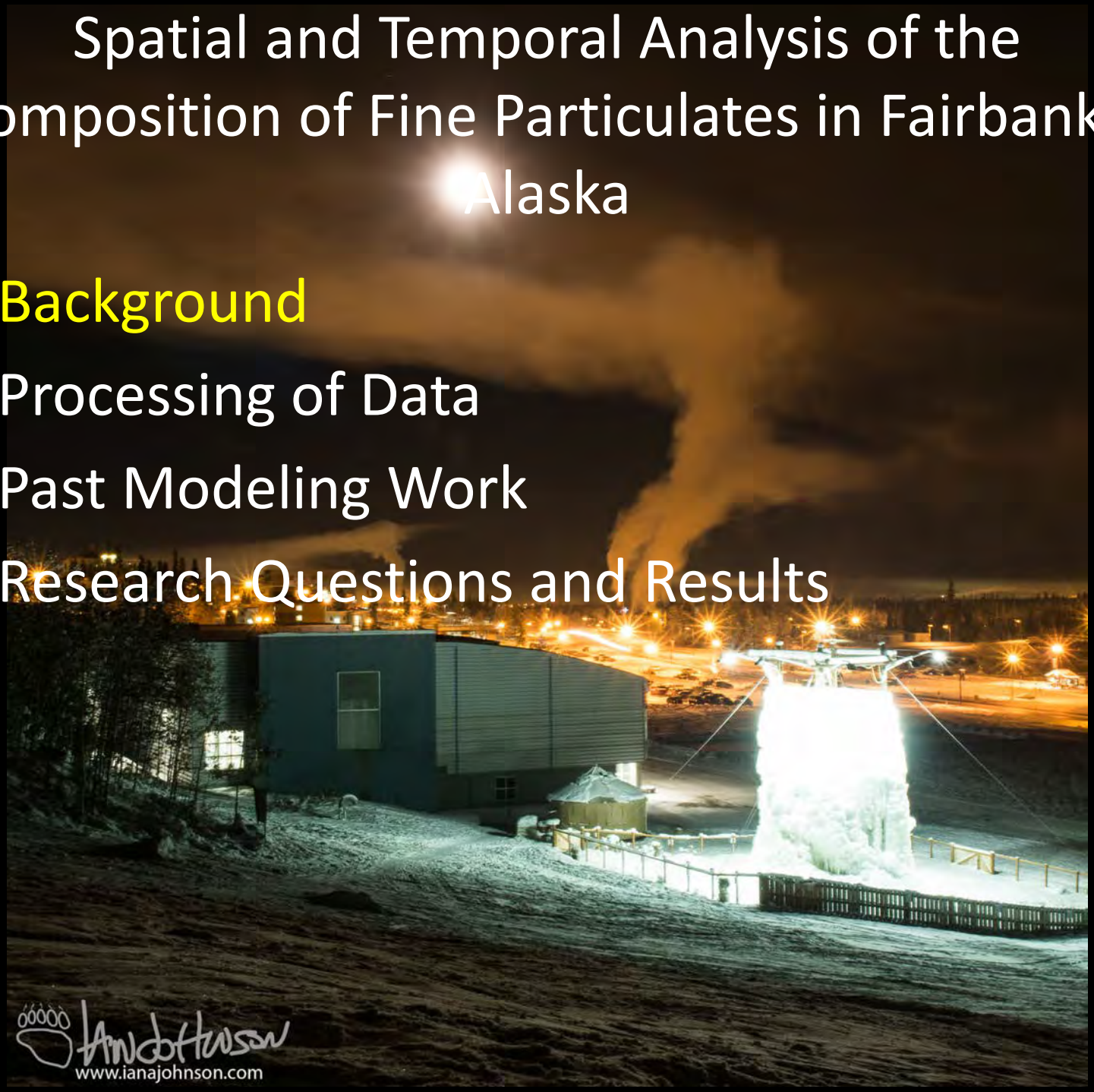

# Fairbanks Winter Air Pollution Events

Highest measured 24 hour concentrations of Fine Particulate Matter ($PM_{2.5}$) in U.S.

(Ward, 2013) Apportionment Research Study Final Report

# $PM_{2.5}$ Mass Concentration

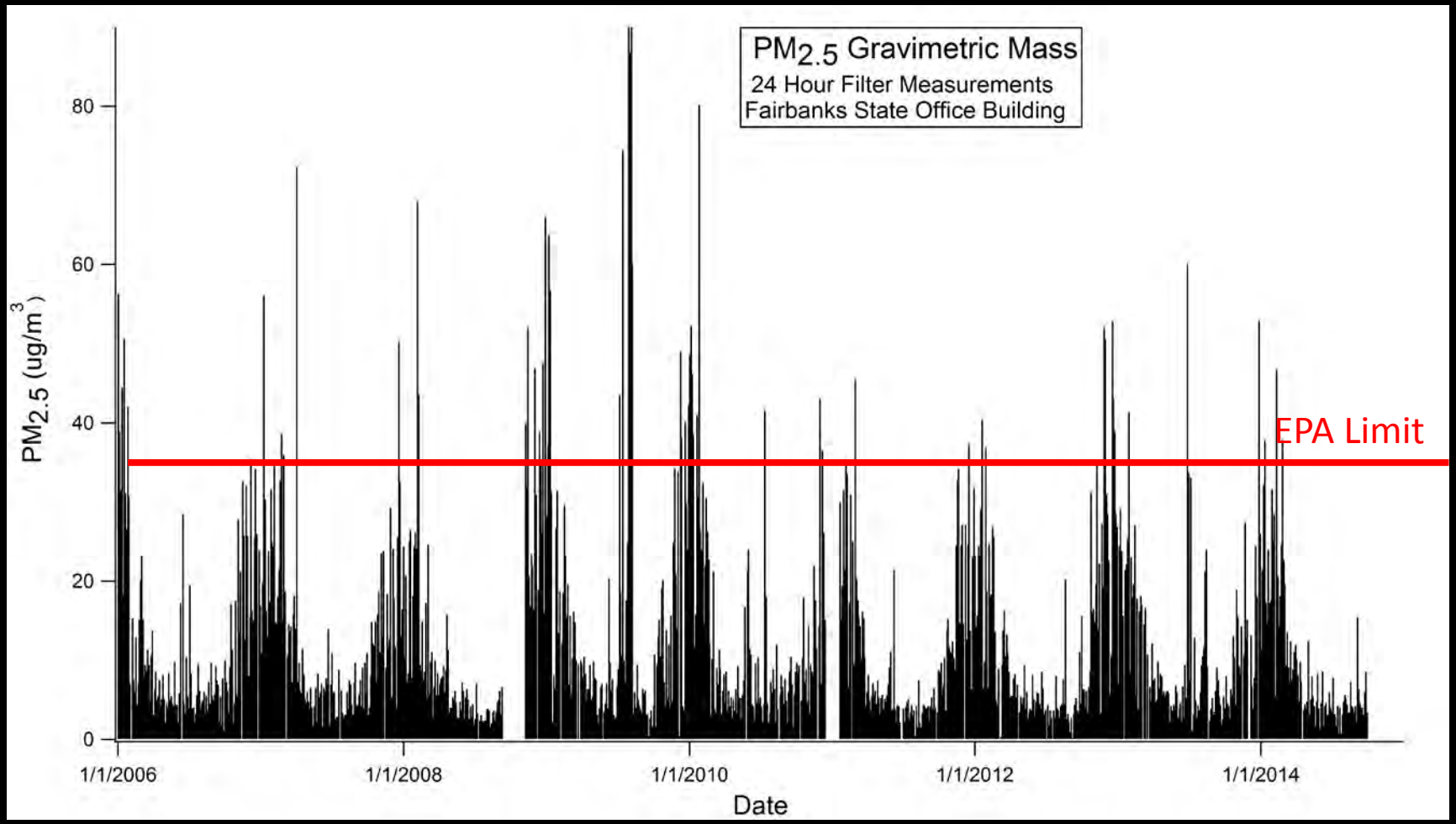


Data from (US EPA Website, Air Quality System Database, 2014))

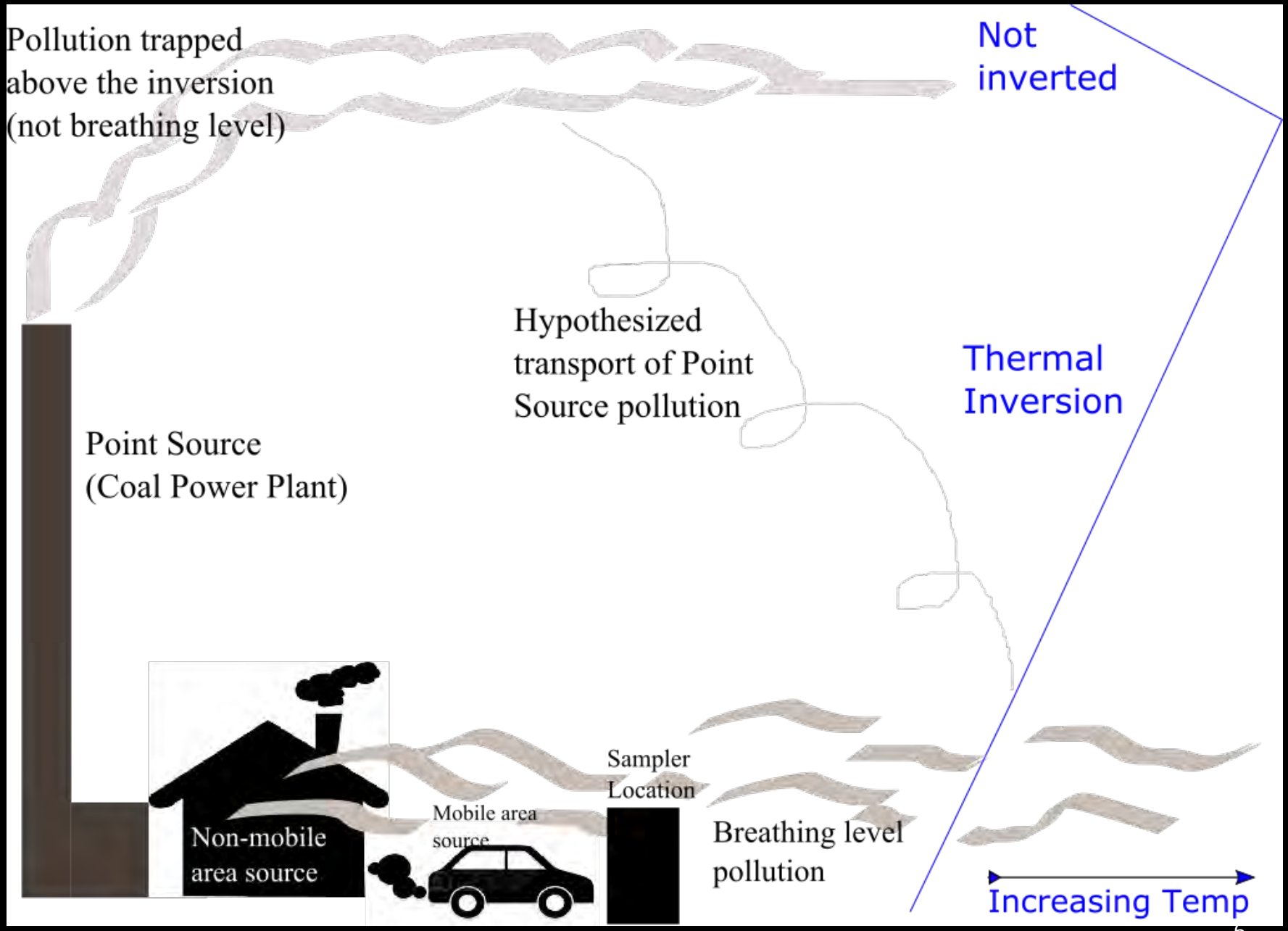
Pollution trapped above the inversion (not breathing level)
Not inverted
Hypothesized transport of Point Source pollution
Thermal Inversion
Point Source (Coal Power Plant)
Non-mobile area source
Mobile area source
Sampler Location
Breathing level pollution
Increasing Temp

# Fairbanks Example Radiosonde

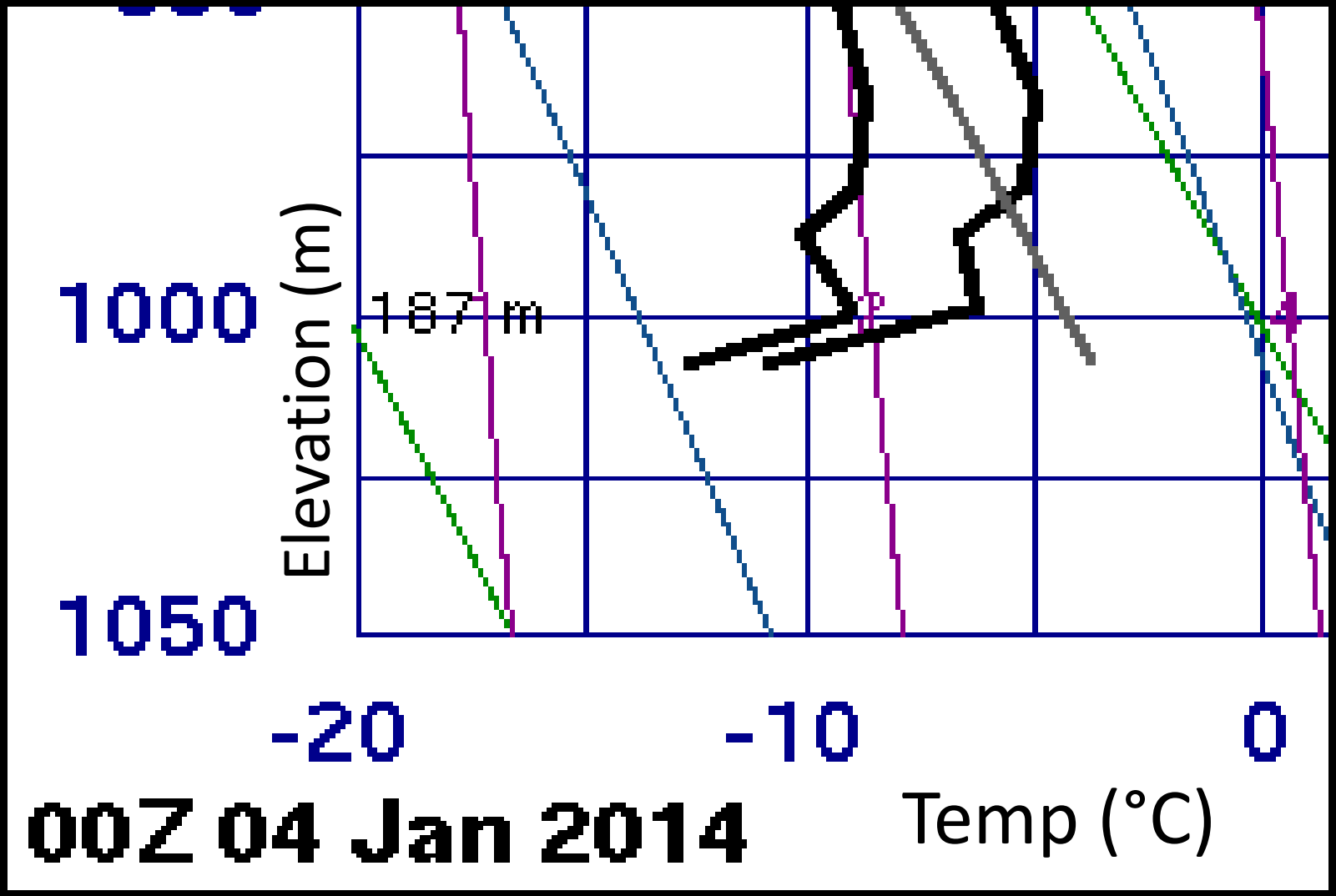


(University of Wyoming Department of Atmospheric Science, 2014)

# Health Effects

**3.2 million deaths annually** due to particulate pollution

(Holstius et al., 2014) doi:10.5194/amt-7-1121-2014

# Health Effects

*Fairbanks:*

**6%** increase in cerebrovascular hospitalizations and respiratory tract infections

(Alaska Department of Health and Social Services, 2010)
http://dhss.alaska.gov/dph/Epi/eph/Documents/bulletins/docs/b2010_26.pdf

# How this research may help Fairbanks

- Understanding trends and chemistry can inform policy
- Alternative approaches to analysis may help with outreach efforts

# Data Source:  EPA Website


# Air Quality System Data

## Downloaded as Ambient Concentration

- Ion Chromatograph – Inorganic Ions
- X-Ray Fluorescence – Elemental
- Thermal Optical Analysis – Carbon
- Gravimetric Analysis – $PM_{2.5}$ Mass

# Mean $PM_{2.5}$ Composition 2006-2014

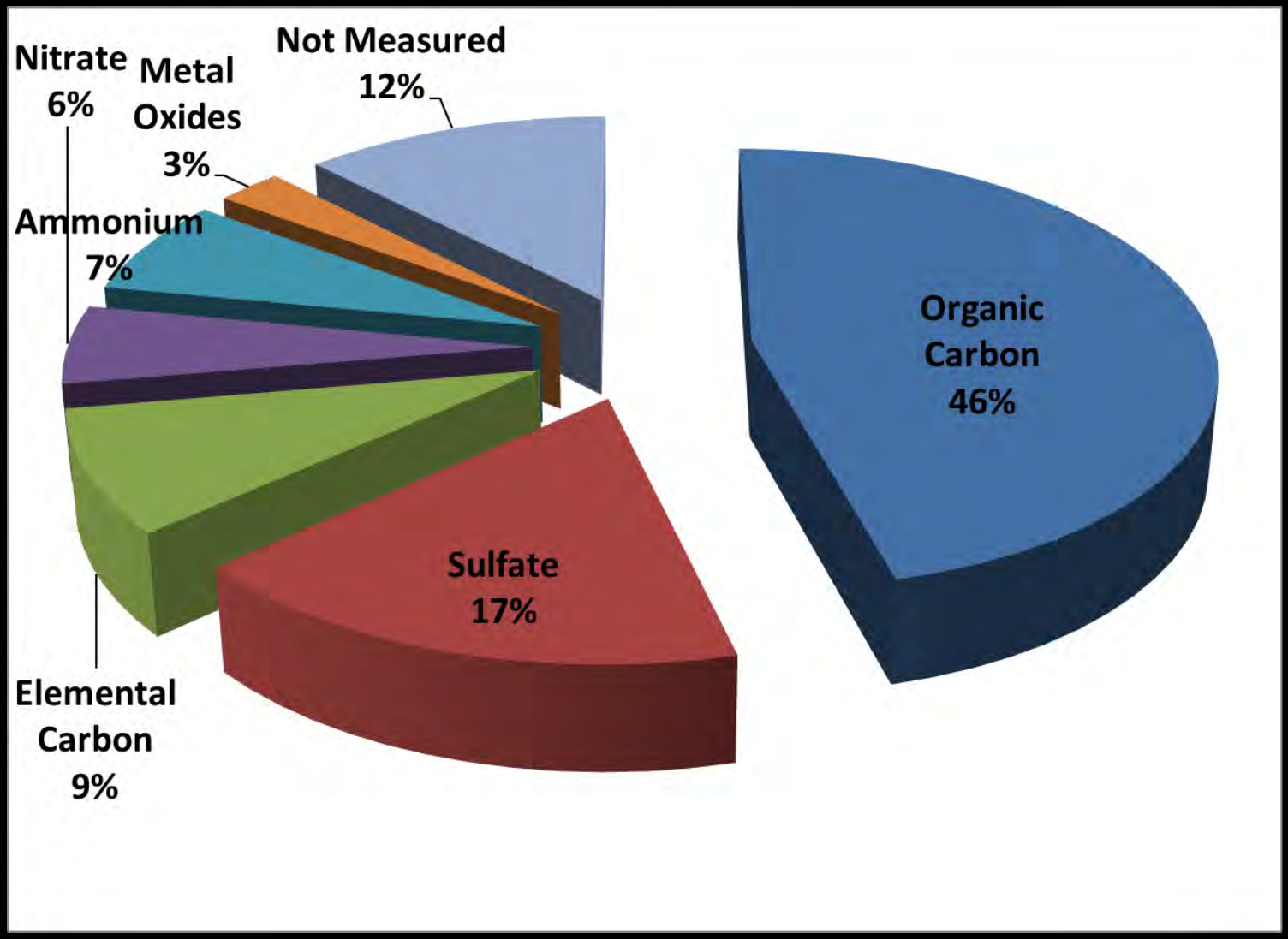


Data from (US EPA Website, Air Quality System Database, 2014)

# Can’t measure the O and the H….

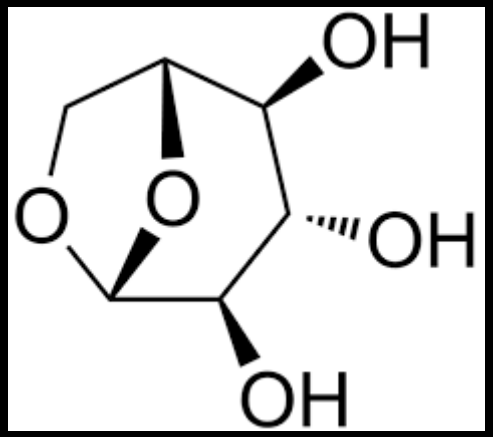


…and everyone else just estimates them.

Organic Carbon Mass = 1.4 * Organic Carbon

(Chow et al., 2010) doi:10.5194/acp-10-5223-2010
(Lim and Turpin, 2002) doi:10.1021/es0206487

# Mean $PM_{2.5}$ Composition 2006-2014

*Organic Carbon Mass Estimated*

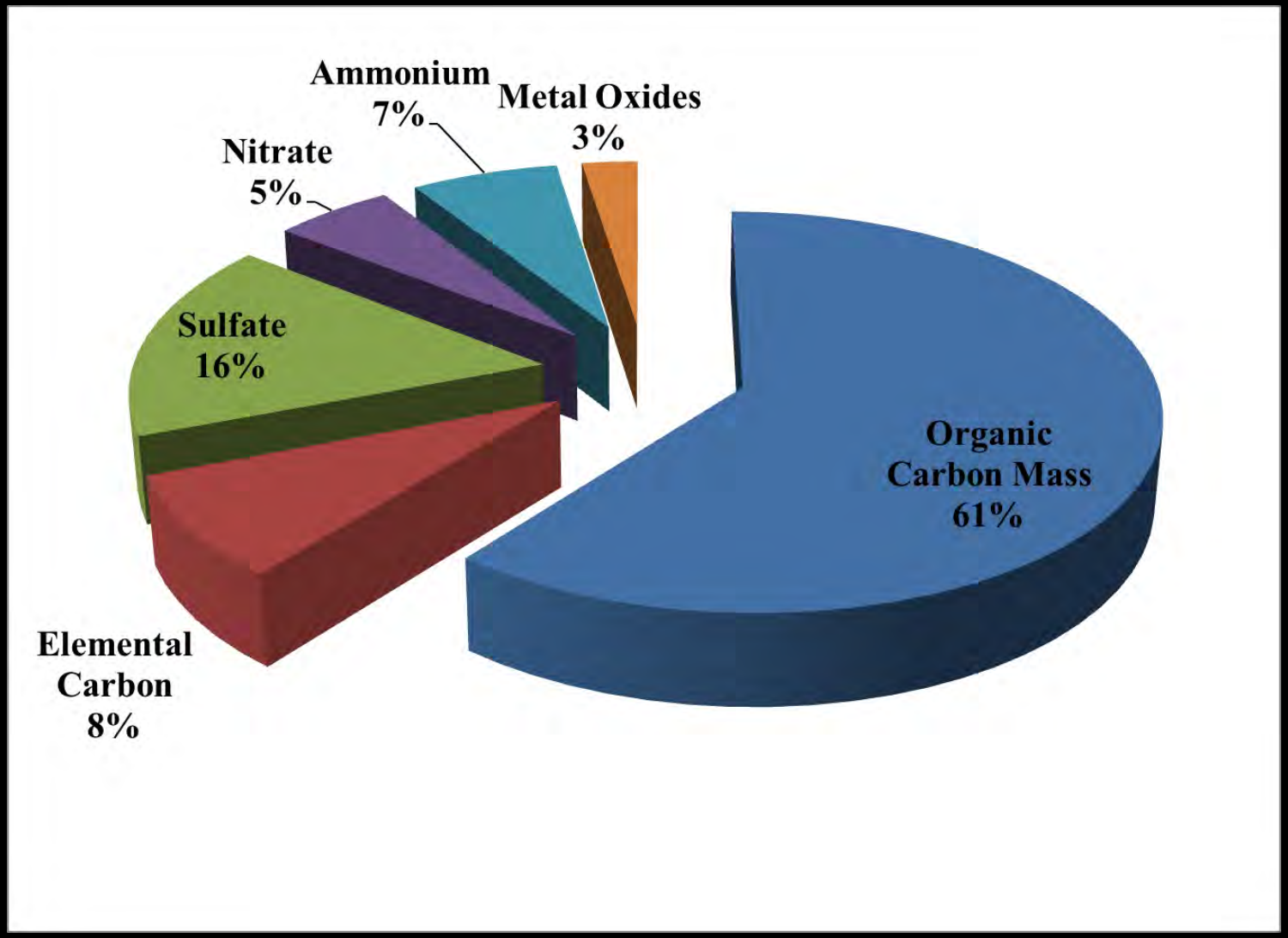


Data from (US EPA Website, Air Quality System Database, 2014)

# 2006-2010 $PM_{2.5}$ Composition

## *Mass Balance Modeling*

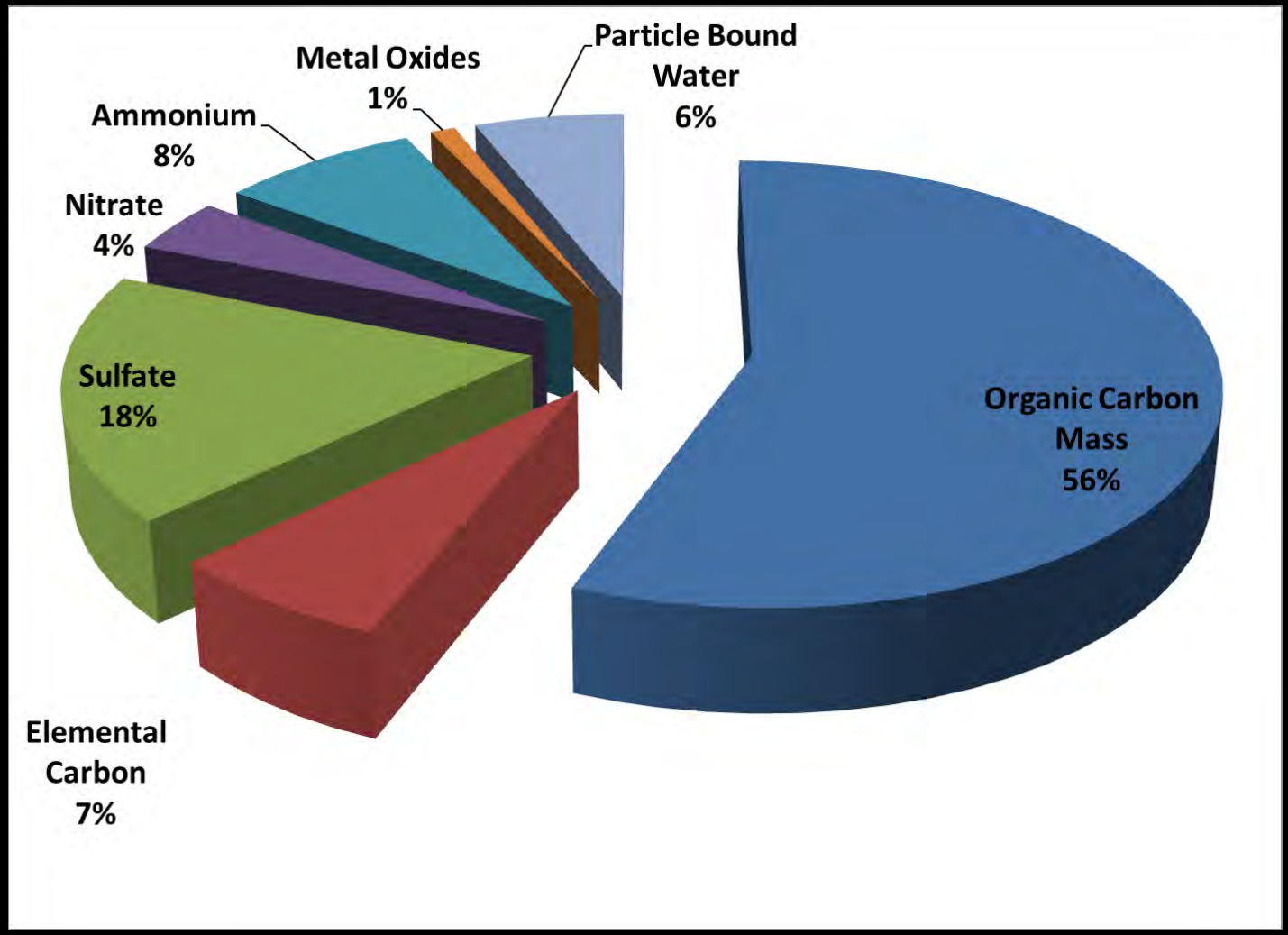


(Huff, 2014) SIP IIID5.6, Alaska State Department of Environmental Conservation

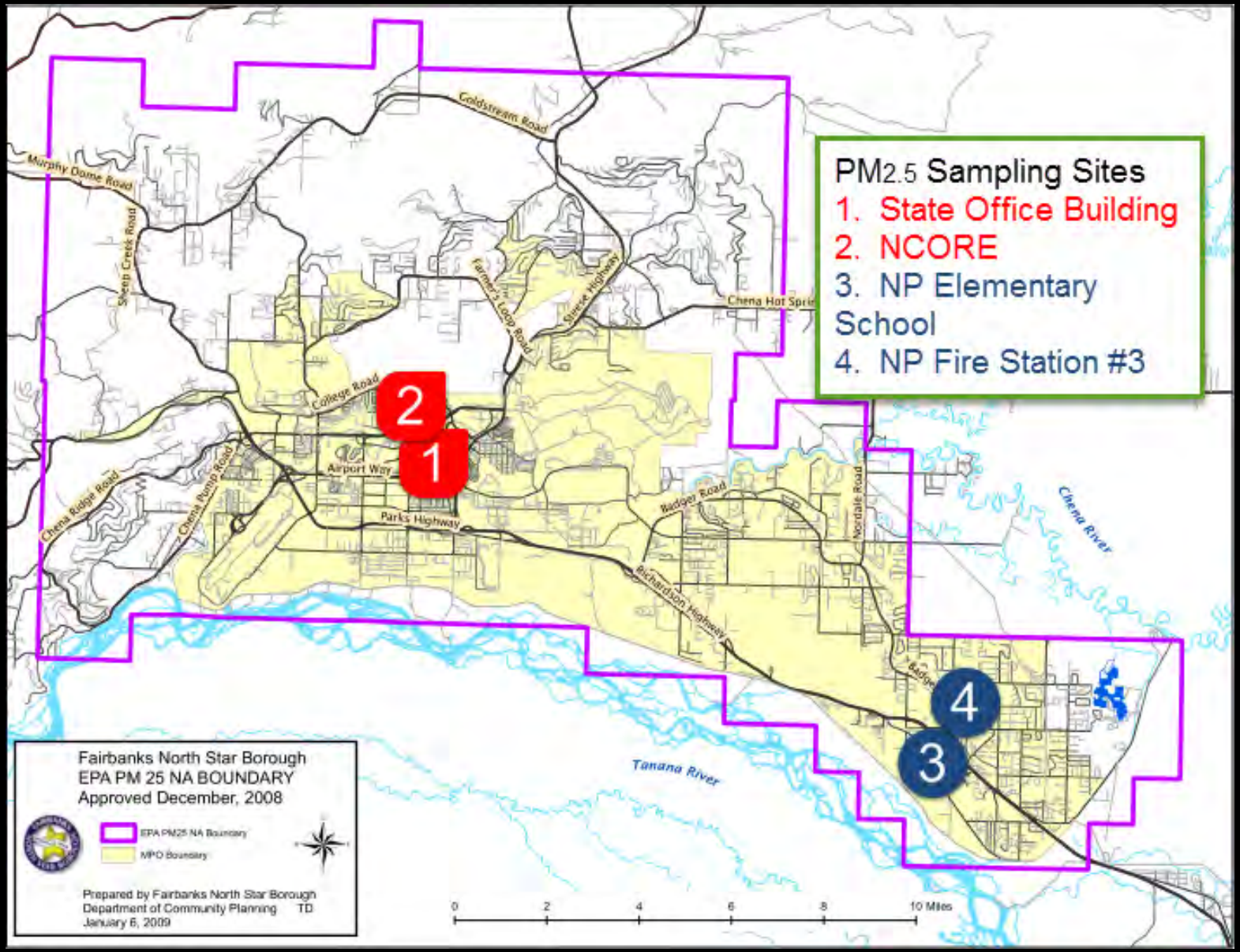
PM2.5 Sampling Sites
1. State Office Building
2. NCORE
3. NP Elementary School
4. NP Fire Station #3
Fairbanks North Star Borough
EPA PM 25 NA BOUNDARY
Approved December, 2008
EPA PM25 NA Boundary
MPO Boundary
Prepared by Fairbanks North Star Borough
Department of Community Planning TD
January 6, 2009
0 2 4 6 8 10 Miles
Goldstream Road
Murphy Dome Road
Sheep Creek Road
Farmer's Loop Road
Steese Highway
College Road
Airport Way
Parks Highway
Chena Ridge Road
Chena Pump Road
Badger Road
Nordale Road
Richardson Highway
Chena River
Tanana River
1
2
3
4

# Analysis of Fine Particulate Composition Data

I. Background
II. Processing of Data
III. Past Modeling Work
IV. Research Questions and Results

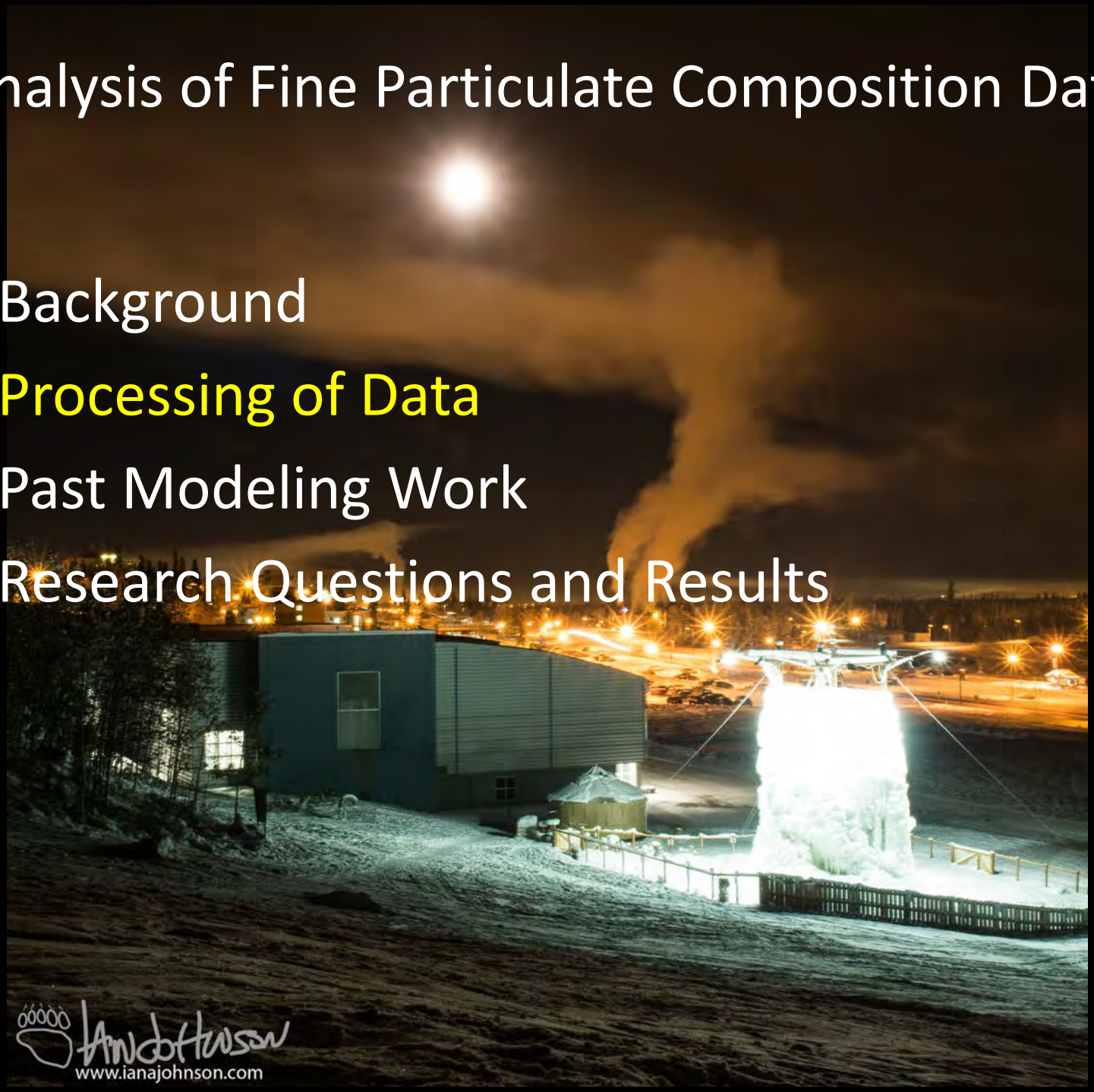

# Confounding Factors

- Meteorology
- Variability in human behavior
- Wildfires (seasonal change)
- Analytical Error

# Normalization to $PM_{2.5}$ Mass Concentration

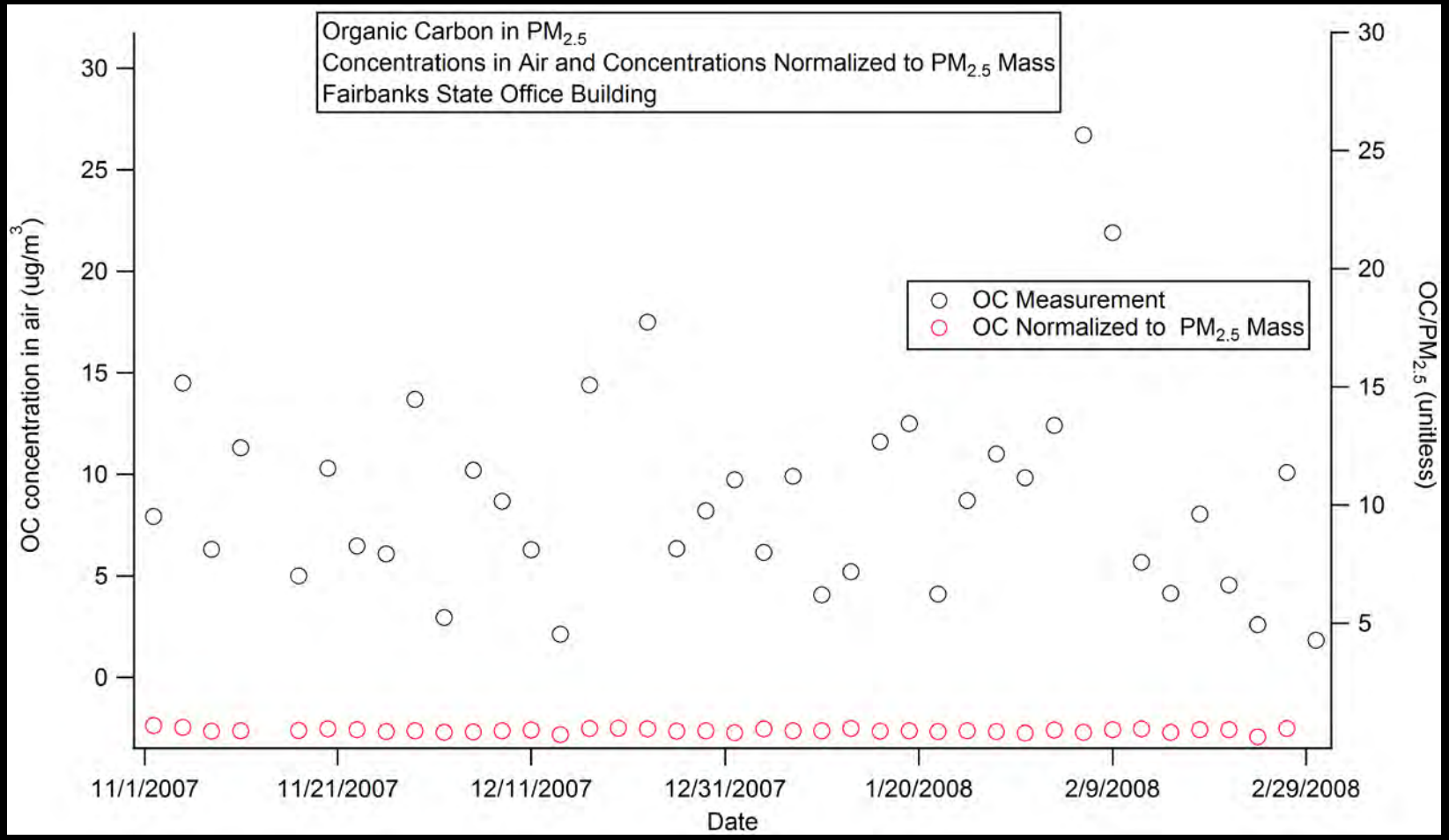


Data from (US EPA Website, Air Quality System Database, 2014)

# EPA Data - What an amazing mess!

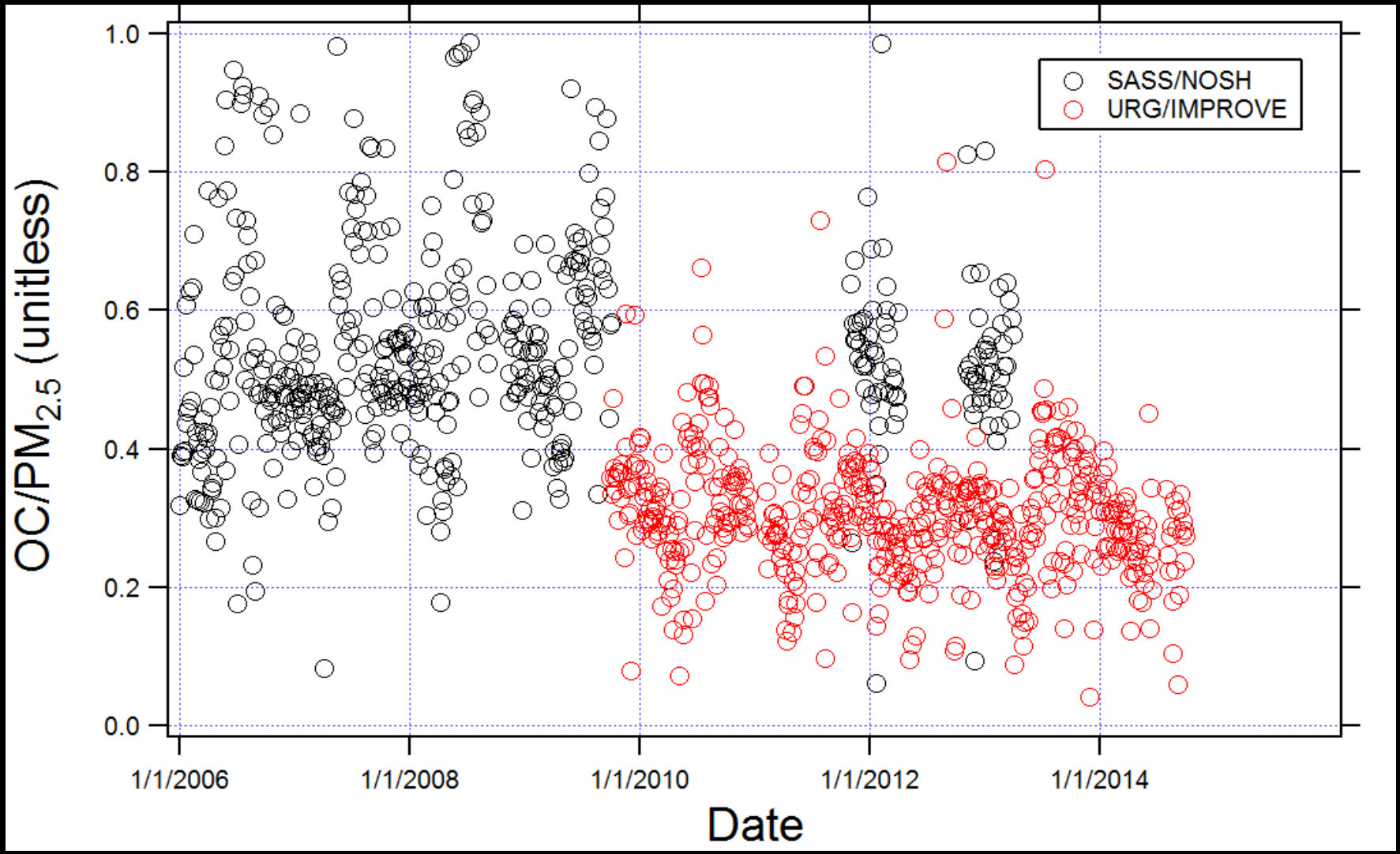


Data from (US EPA Website, Air Quality System Database, 2014)

# Method Corrected, QC'd, Blank Subtracted, Season Sorted Data

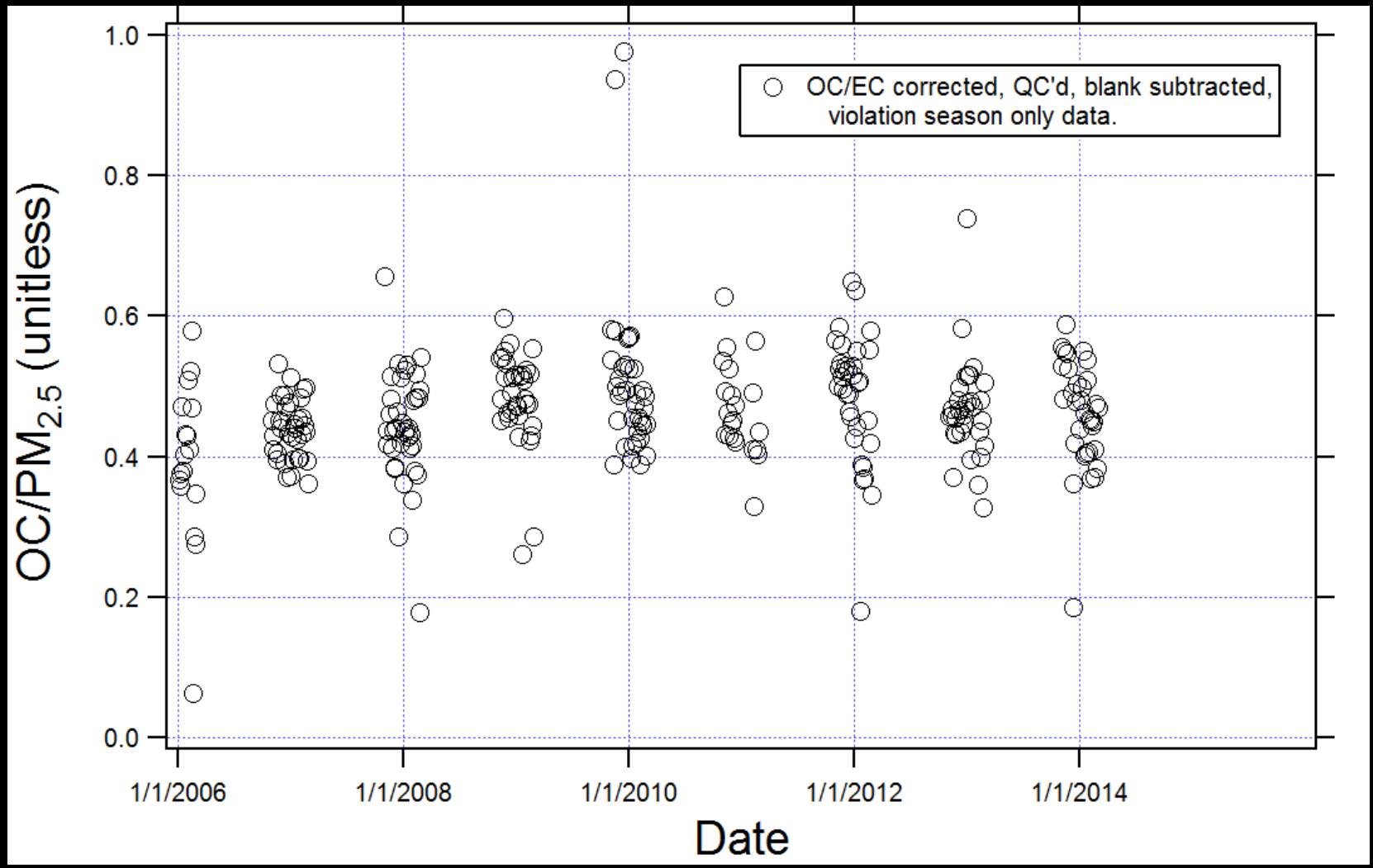


Data from (US EPA Website, Air Quality System Database, 2014)

# Reconstruction Succeeds!

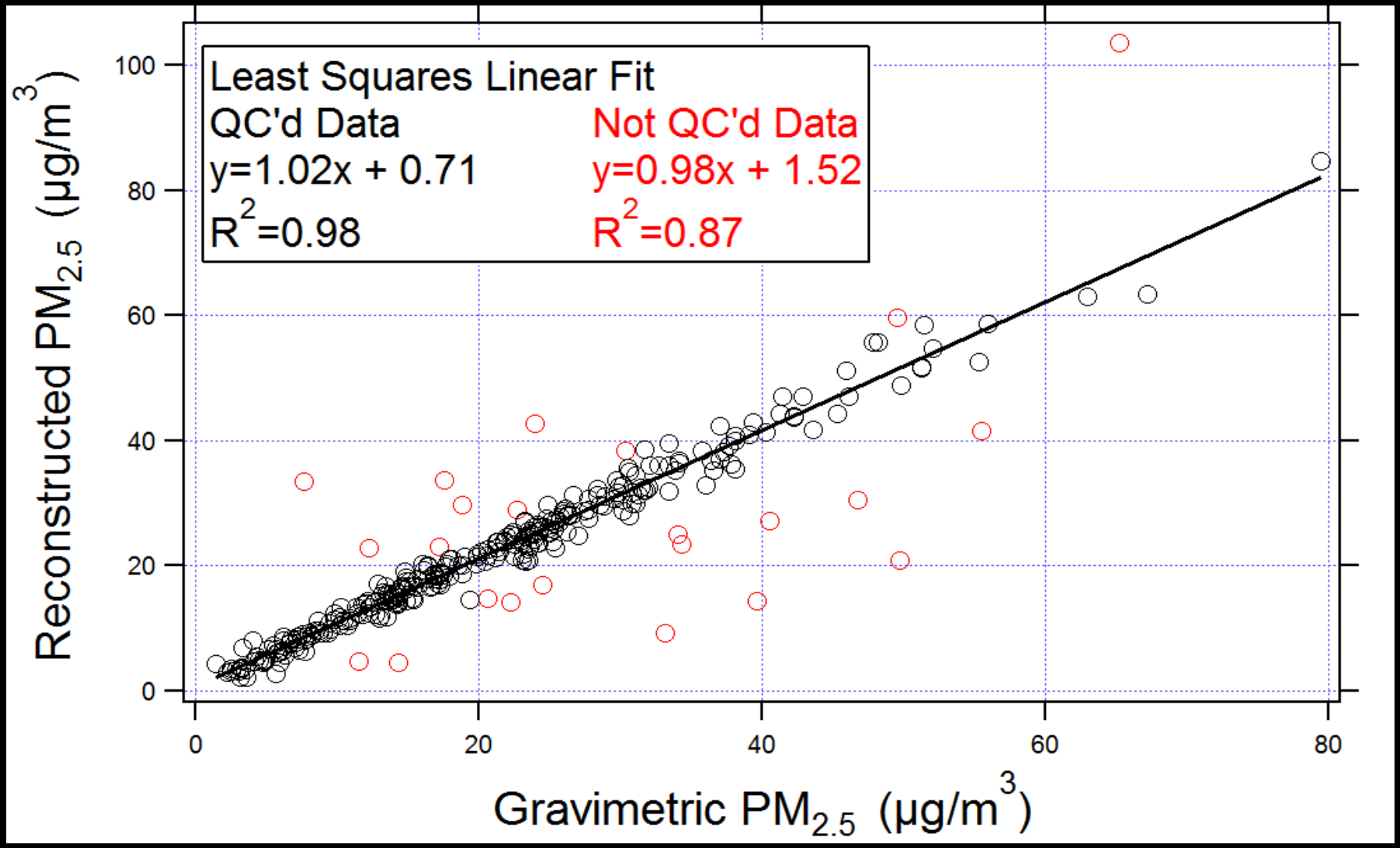


Data from (US EPA Website, Air Quality System Database, 2014)

# Analysis of Fine Particulate Composition Data

I. Background
II. Processing of Data
III. Past Modeling Work
IV. Research Questions and Results

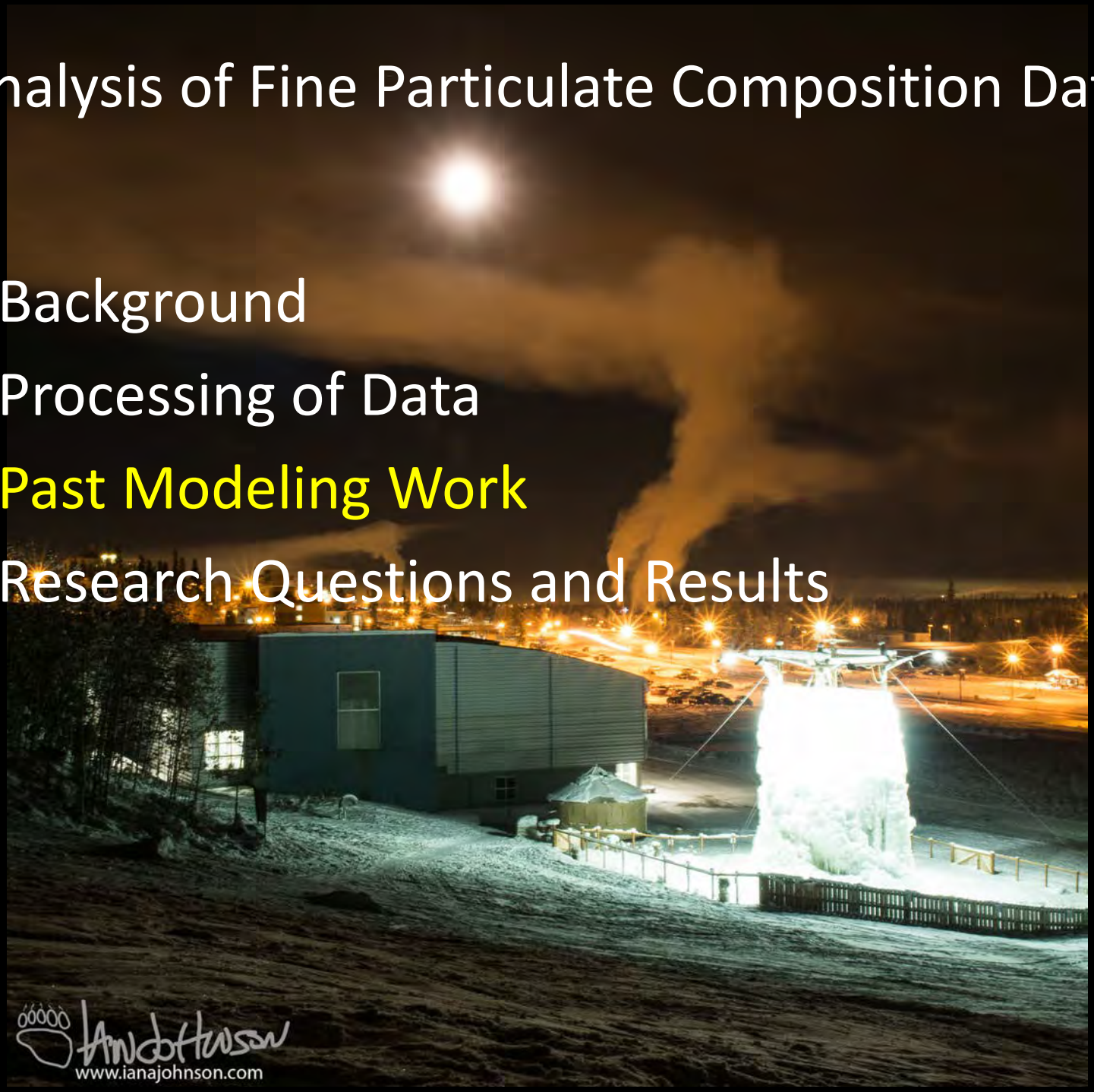

# Source Profiles


OCM

OCM

$SO_4^{2-}$

OCM

EC

OCM

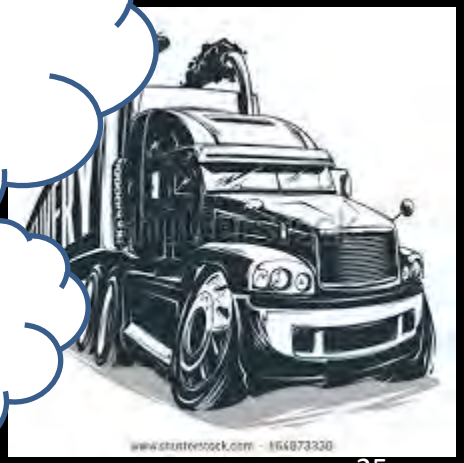

Source Apportionment

# Contribution of Wood Smoke to Total $PM_{2.5}$ Mass

| | |
|---|---|
| Chemical Mass Balance Model Results | **60%-80% Wood Smoke** with EPA profiles<br><br>**30%-77% Wood Smoke** with Fairbanks Specific Profiles<br><br>(Ward, 2013) *Apportionment Research Study Final Report* |
| Positive Matrix Factorization Model Results | **40% Wood Smoke**<br><br>(Wang and Hopke, 2014) doi:10.4209/aaqr.2014.03.0047 |

# Our Approach: Source Profile Averages

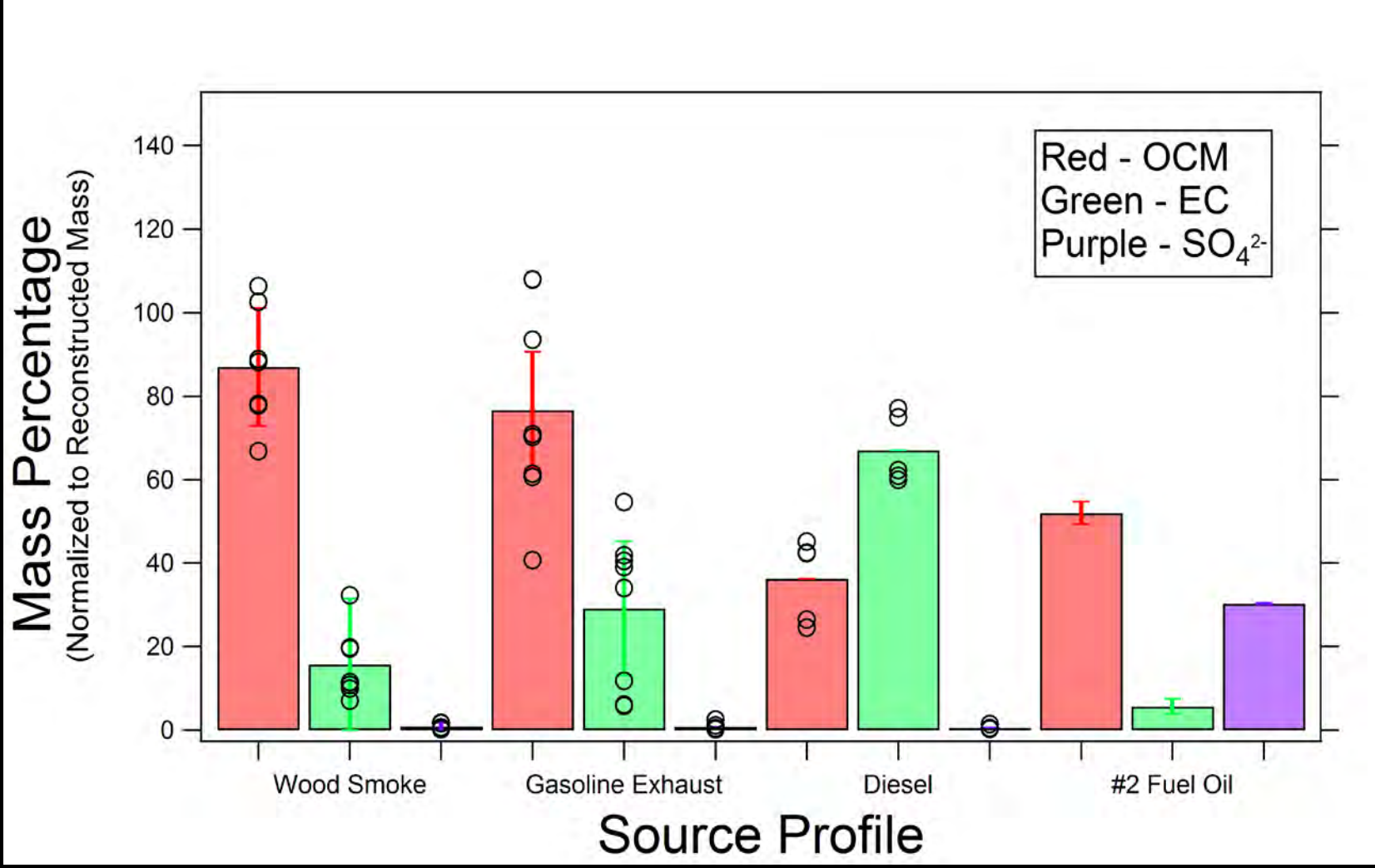

# Analysis of Fine Particulate Composition Data

I. Background
II. Processing of Data
III. Past Modeling Work
IV. Research Questions and Results

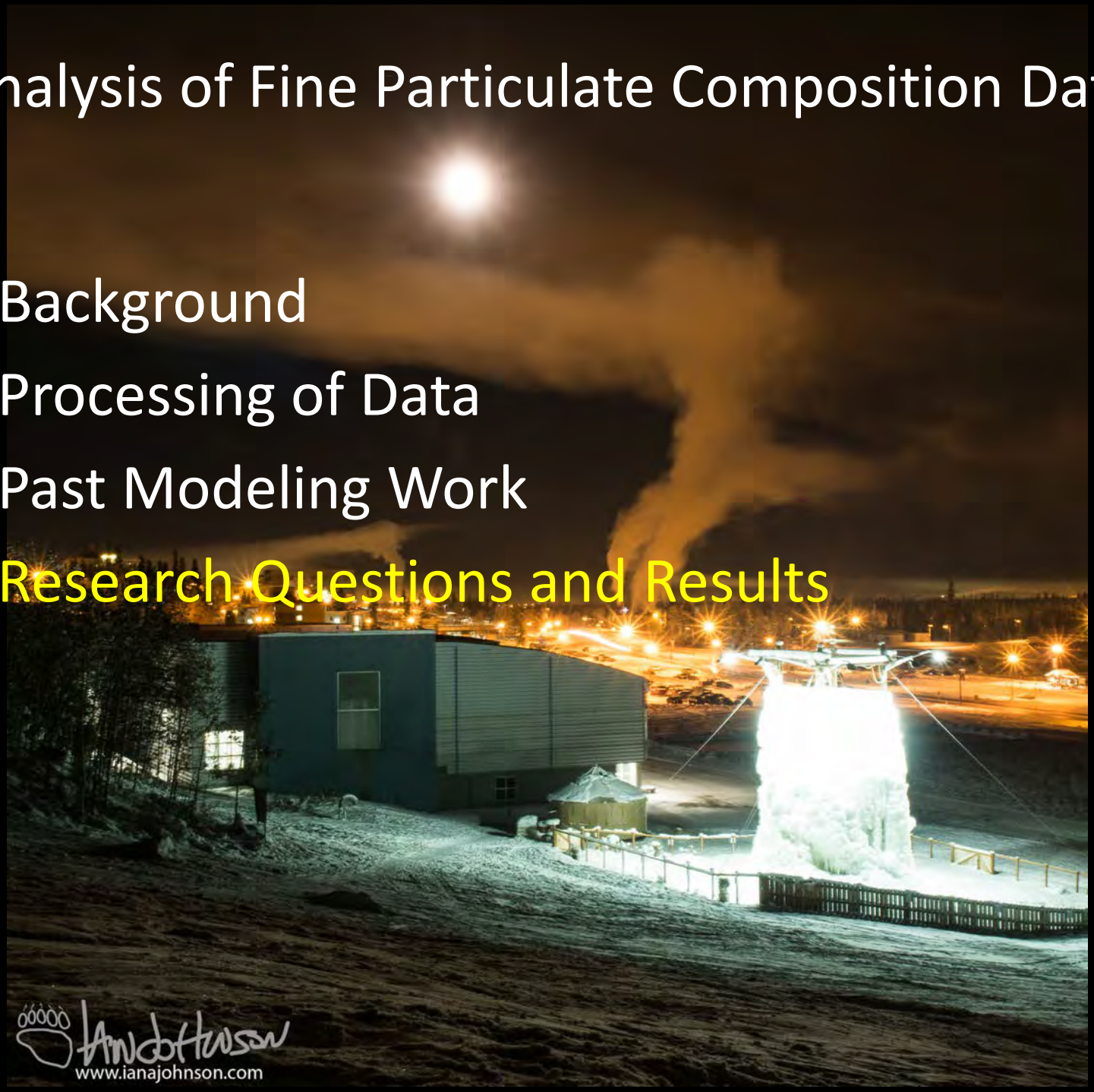

# Question 1

Will the $OC/PM_{2.5}$ ratio and gravimetric $PM_{2.5}$ mass be larger in North Pole than Fairbanks?

# Home Heating from Wood

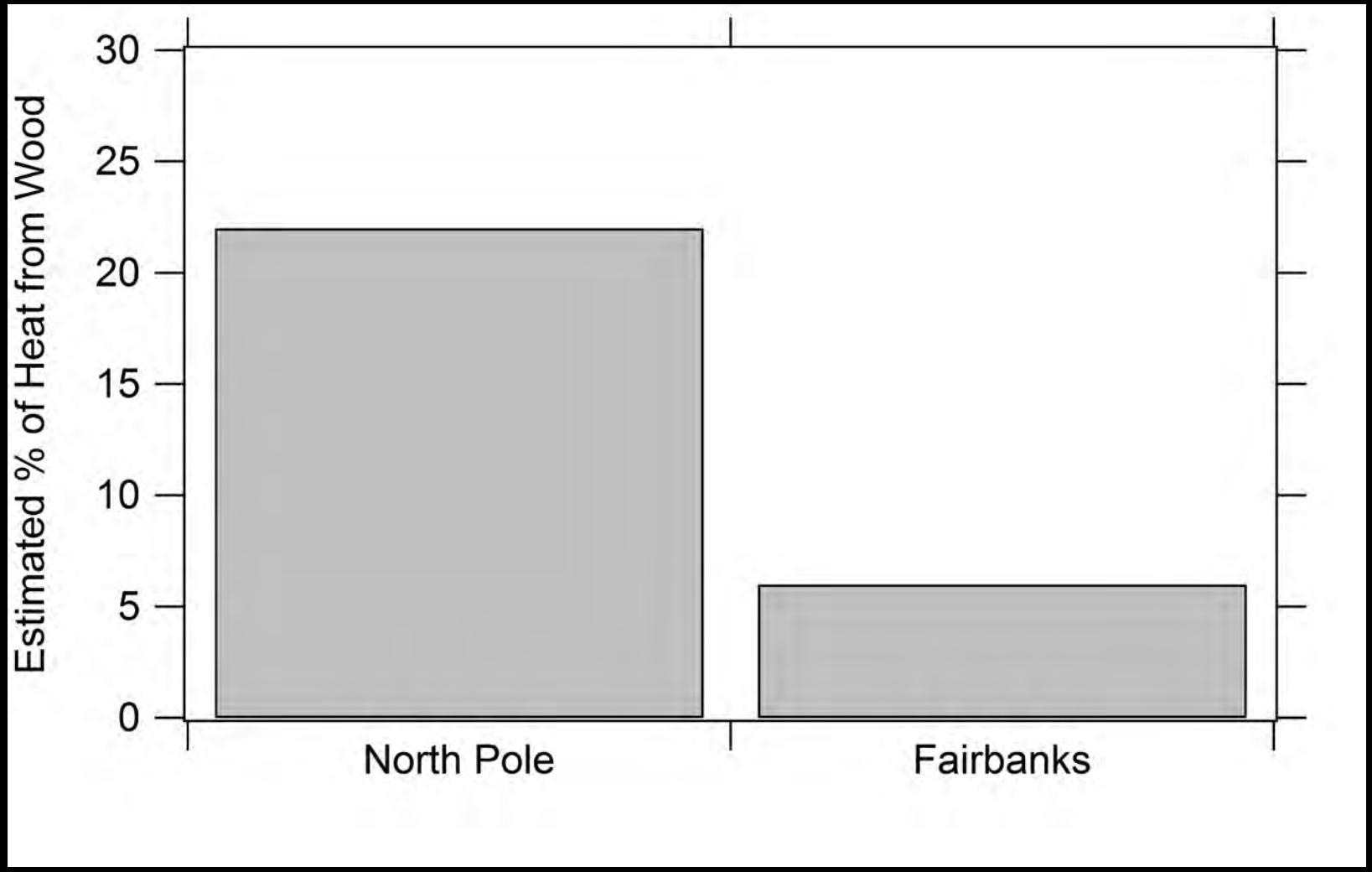


Fairbanks Home Heating Survey (Heil et al., 2011)

# $PM_{2.5}$ Composition is Significantly Different

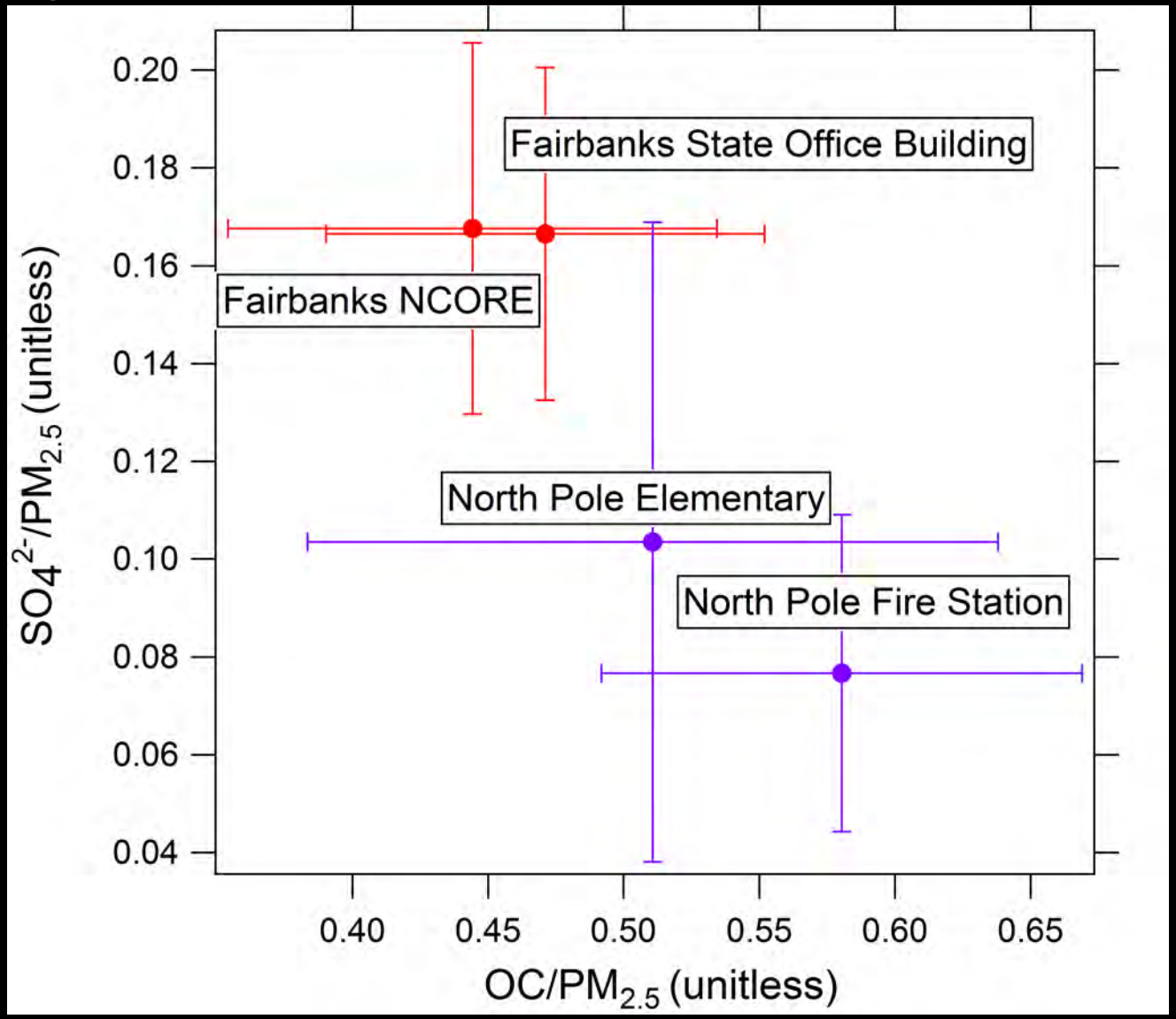


Data from (US EPA Website, Air Quality System Database, 2014)

# Mean Winter Season Gravimetric Particle Mass

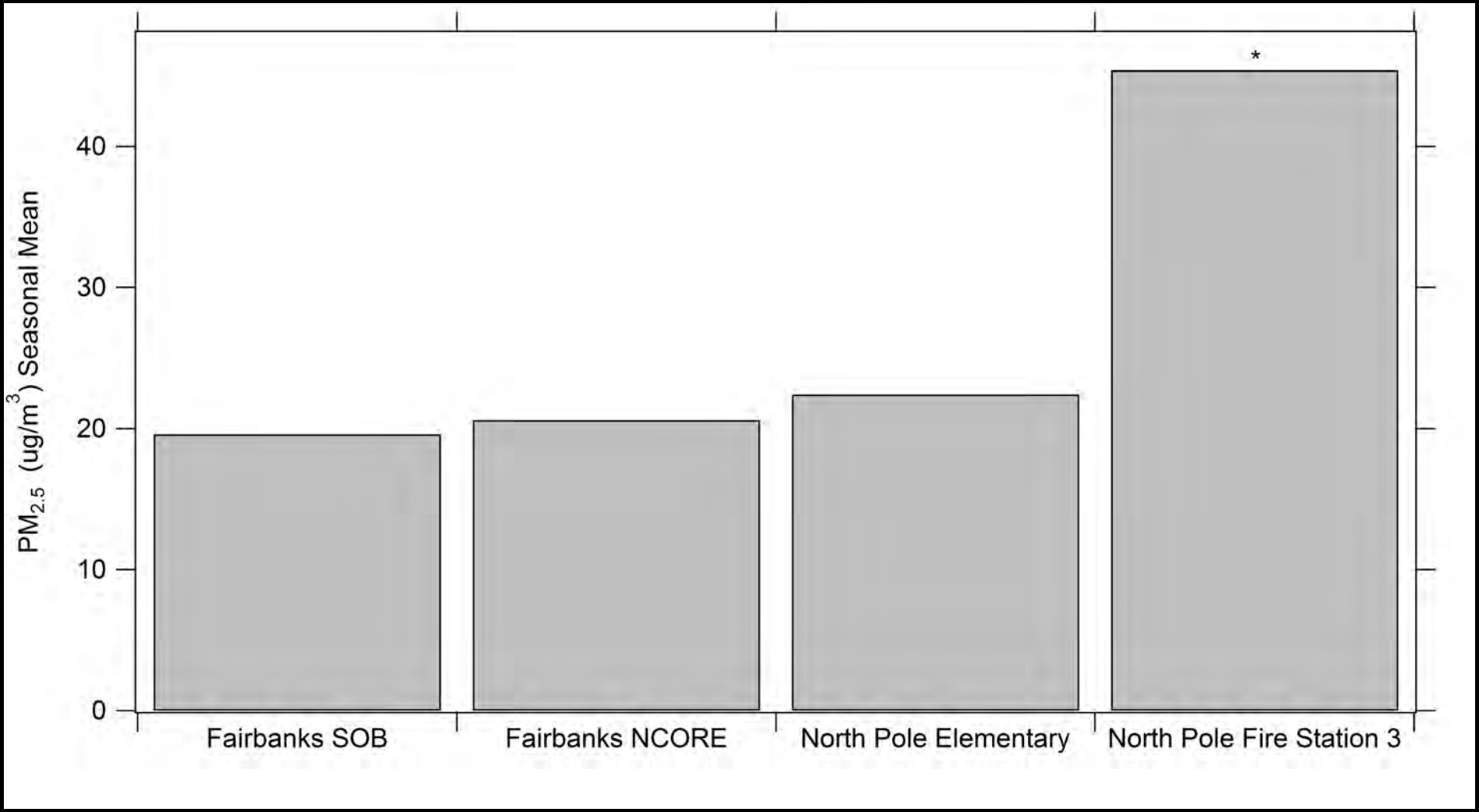




Data from (US EPA Website, Air Quality System Database, 2014)

# Gravimetric Mass Correlation

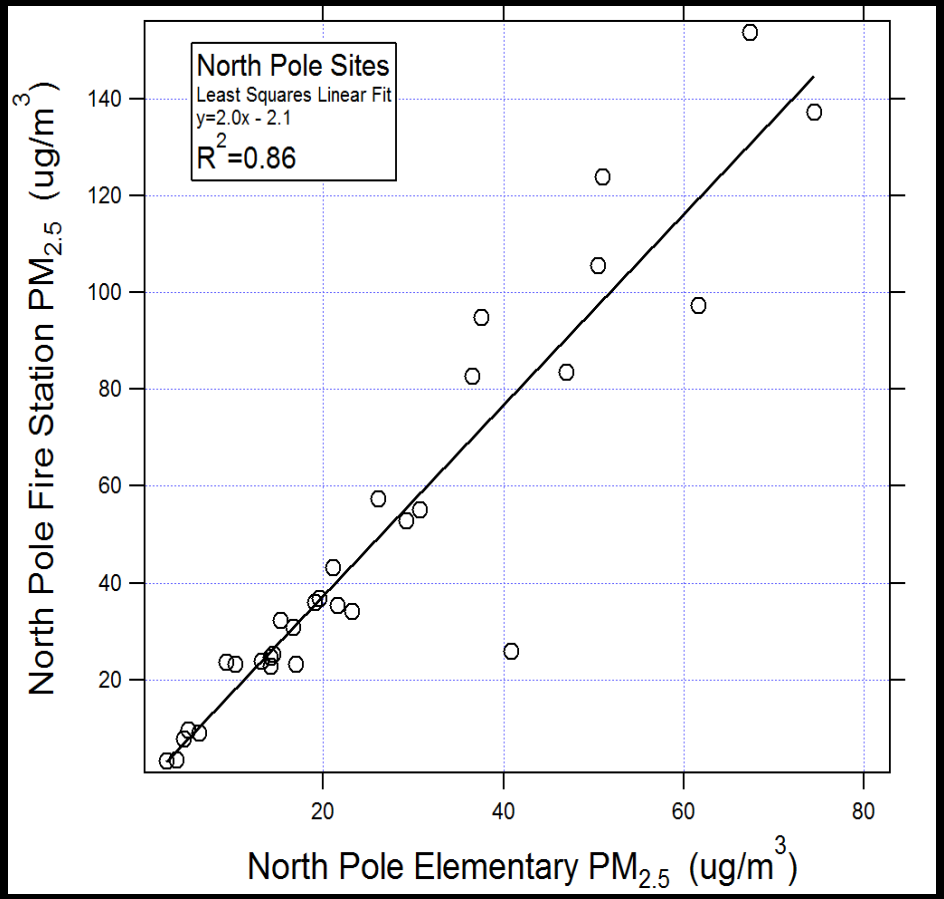


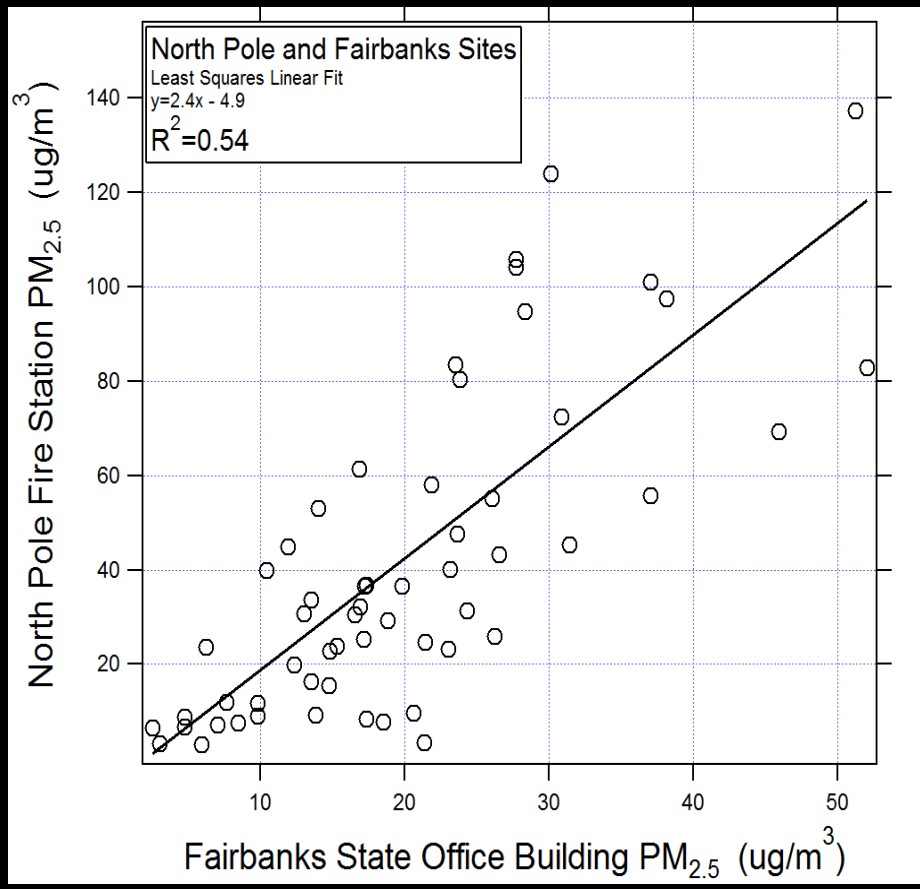




Data from (US EPA Website, Air Quality System Database, 2014)

# Question 2

Will the OC/$PM_{2.5}$ ratio and gravimetric $PM_{2.5}$ mass be larger in North Pole than Fairbanks?

Conclusion:

- Fairbanks and North Pole have **significantly different composition**.
- **Large spatial variability** is observed between sampling sites in North Pole.

# Wood Stove Changeout Program

# Why EPA Certified?

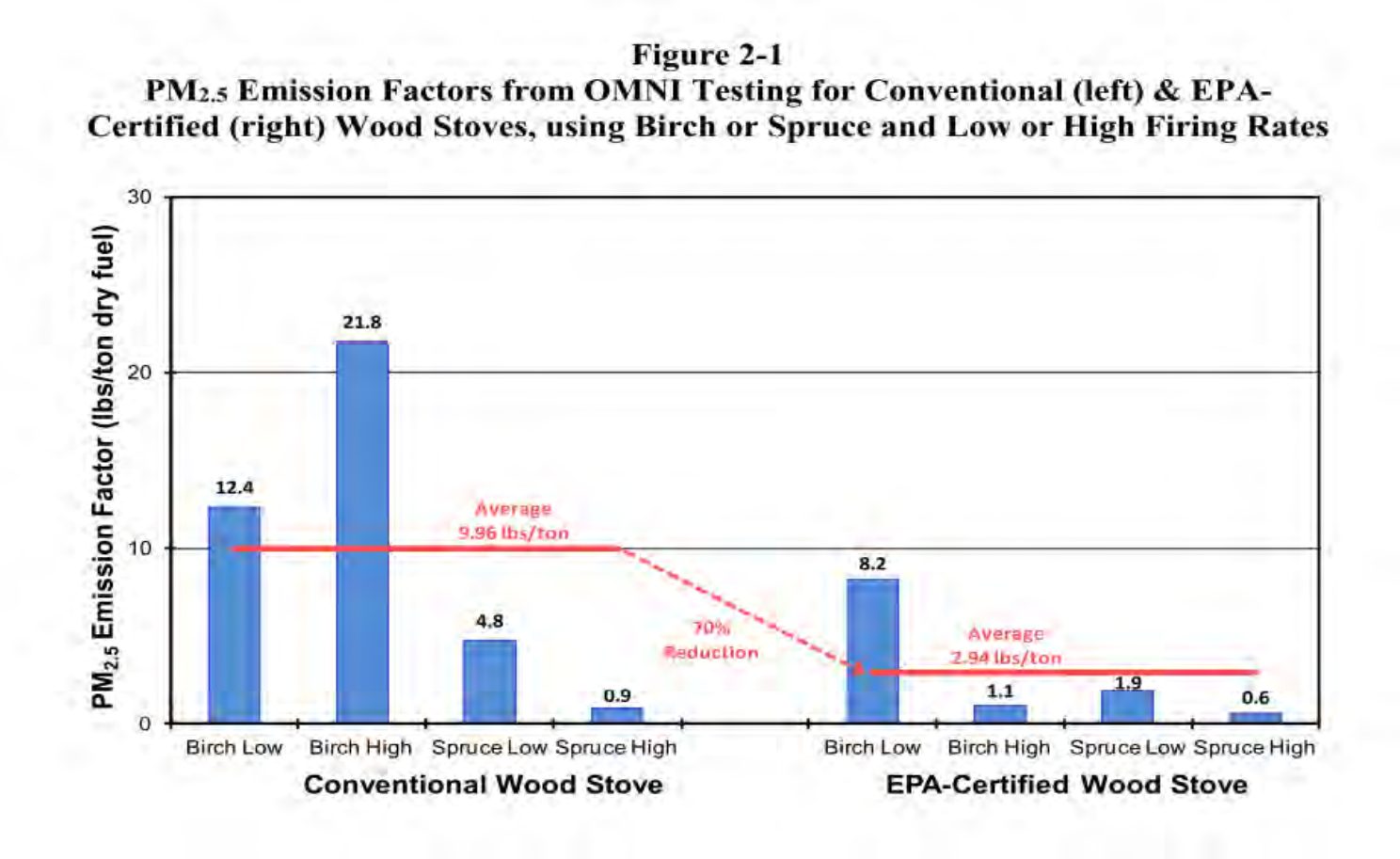


(Davies et al., 2009) *Reducing PM2 .5 Emissions from Residential Heating Sources in the Fairbanks North Star Borough*. Cold Climate Housing Research Center Report.

# Question 2

Will there be a decrease in the $OC/PM_{2.5}$ or $SO_4^{2-}/PM_{2.5}$ due to the incentive programs?

| Time Period | # Stoves Replaced |
|---|---|
| End of 2011 | 325 |
| End of 2013 | 1187 |

(Alaska State Implementation Plan, IIID5.6)

# Trends: Major Species/$PM_{2.5}$

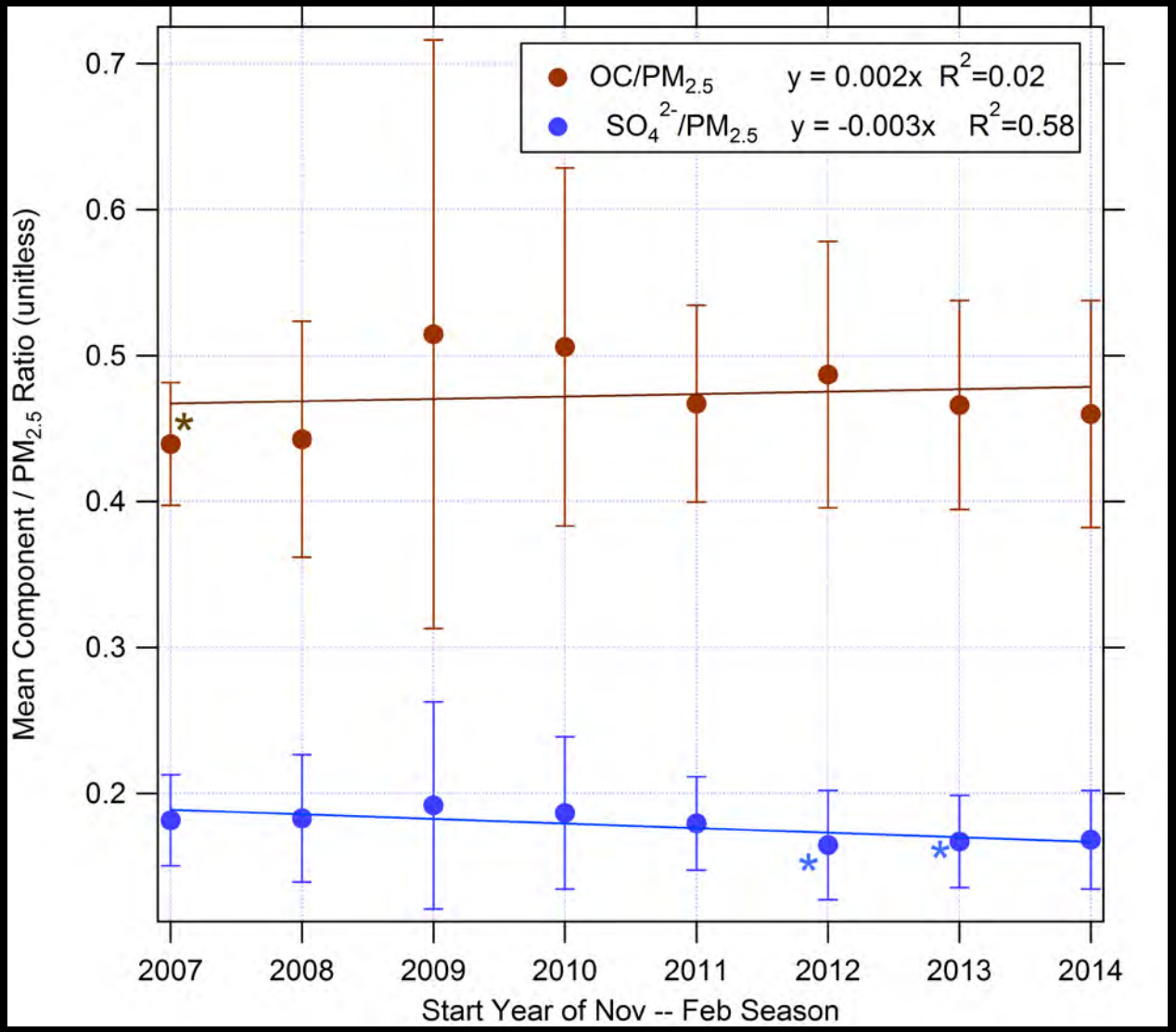


Data from (US EPA Website, Air Quality System Database, 2014)

# Interannual Variability

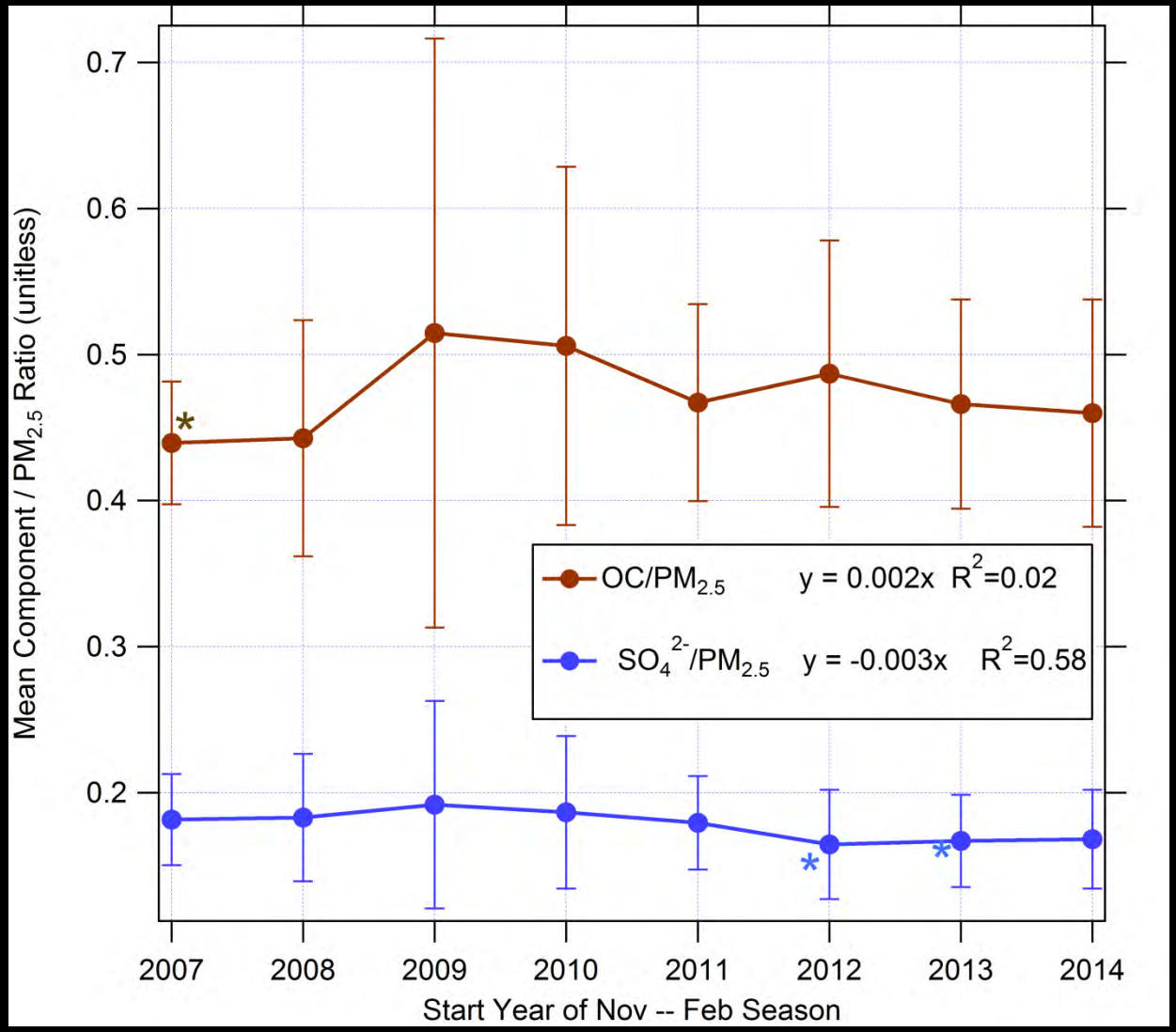


Data from (US EPA Website, Air Quality System Database, 2014)

# Money talks…..

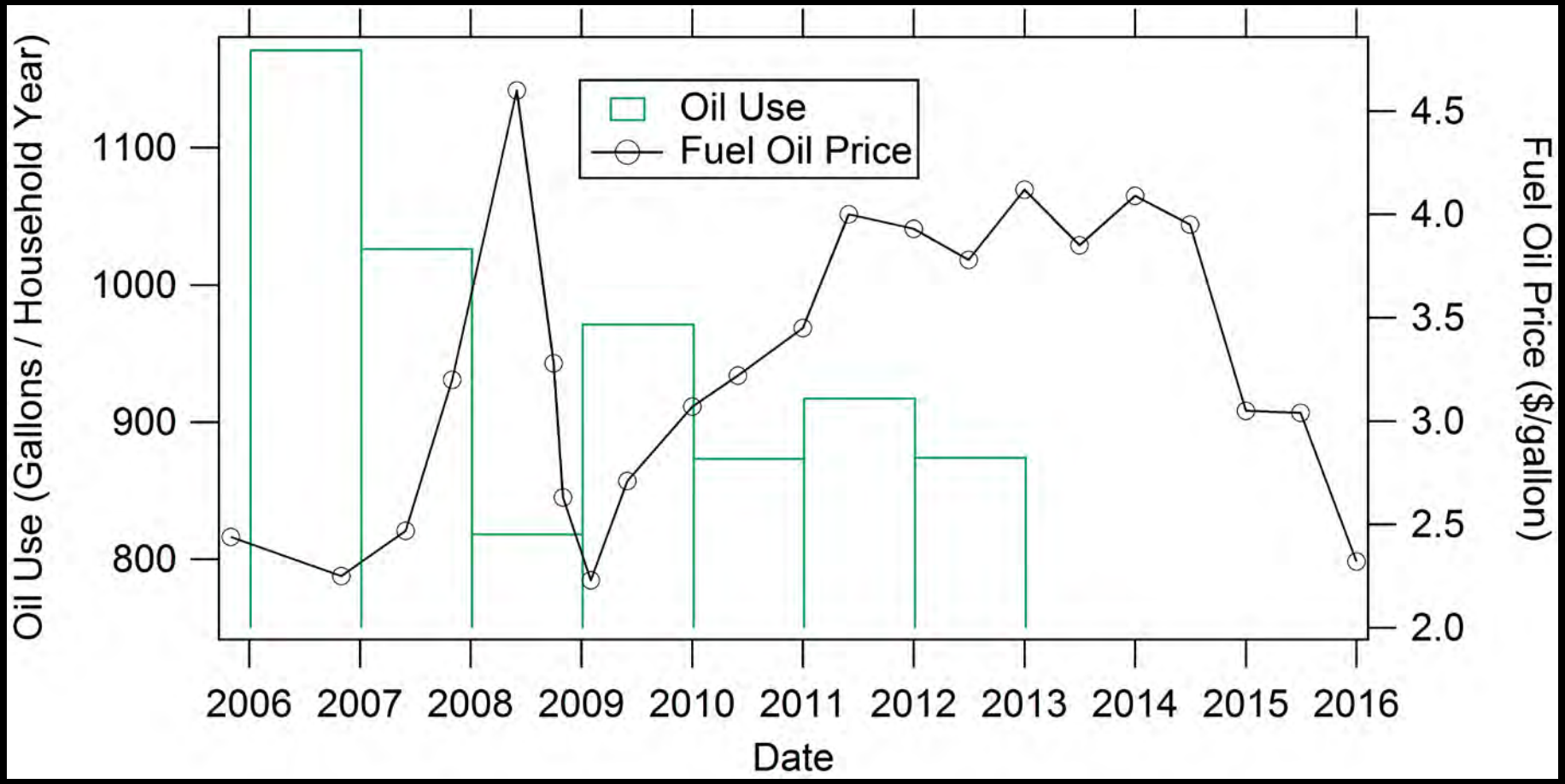


Survey Results from: Fairbanks Home Heating Survey (Heil et al., 2011)

# …and sulfate drops.

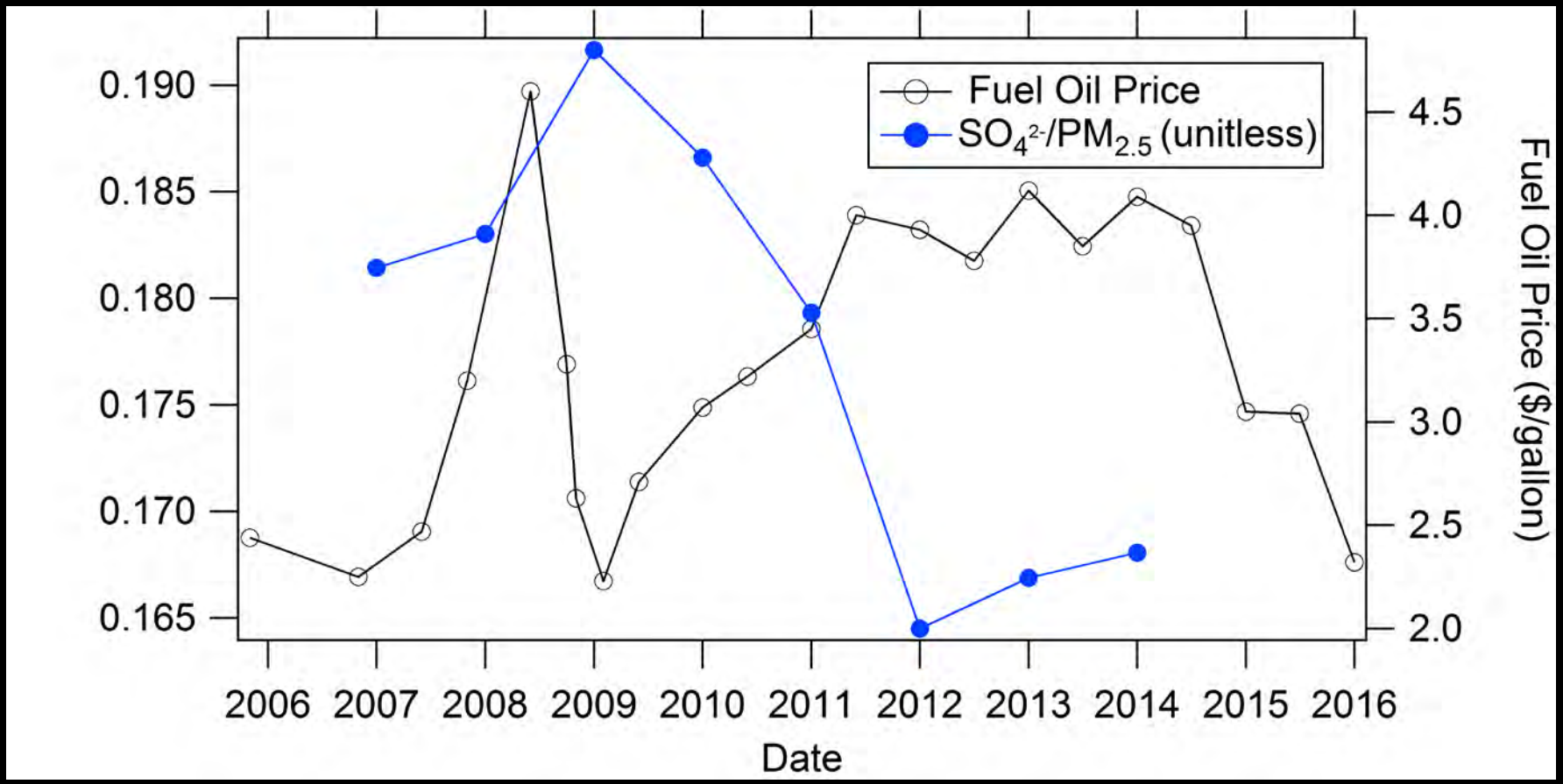


Data from (US EPA Website, Air Quality System Database, 2014)

# OC Interannual Variability (non-significant)

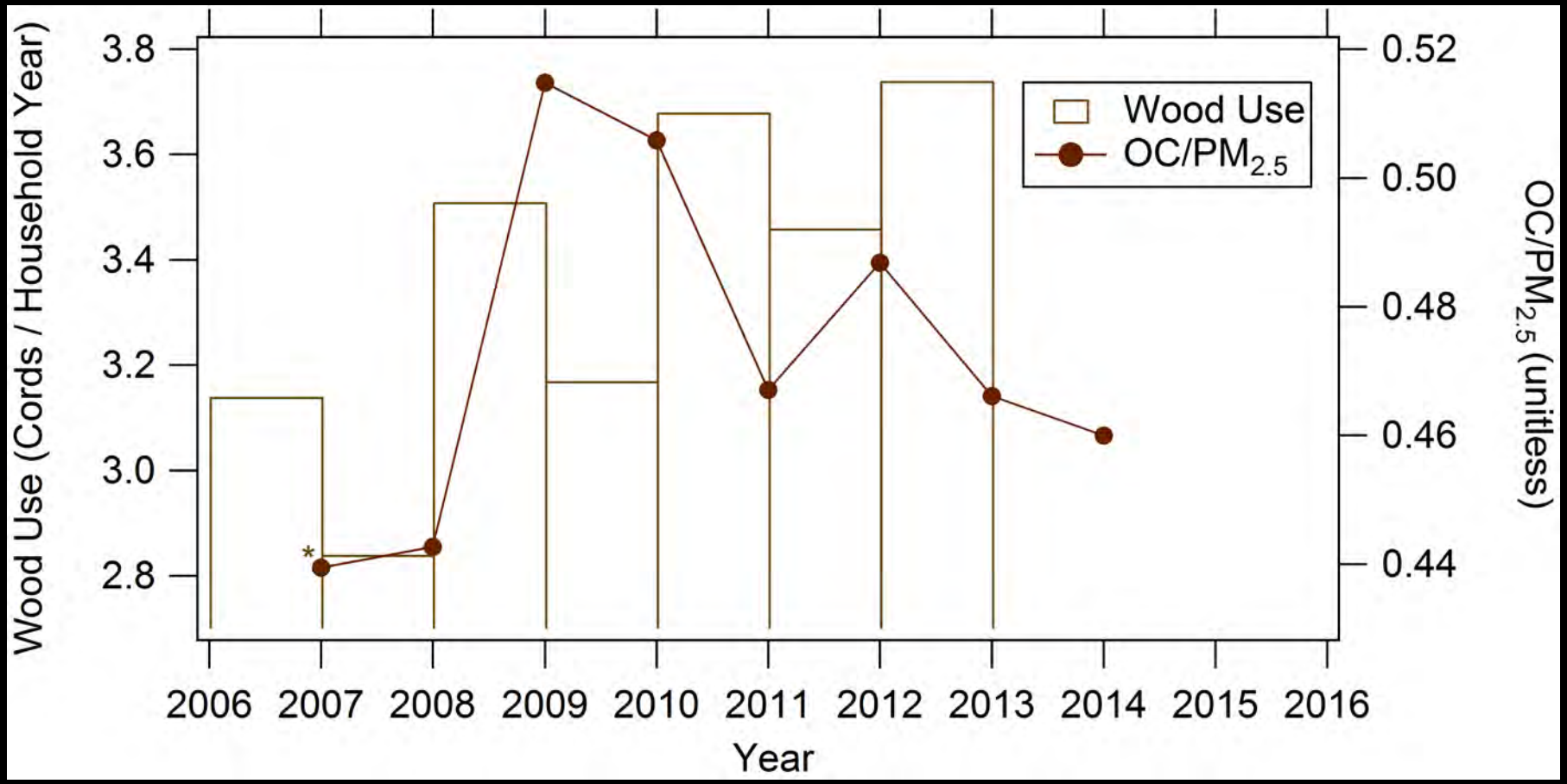


Survey Results from: Fairbanks Home Heating Survey (Heil et al., 2011)

Data from (US EPA Website, Air Quality System Database, 2014)

# Trends: Minor Species/$PM_{2.5}$

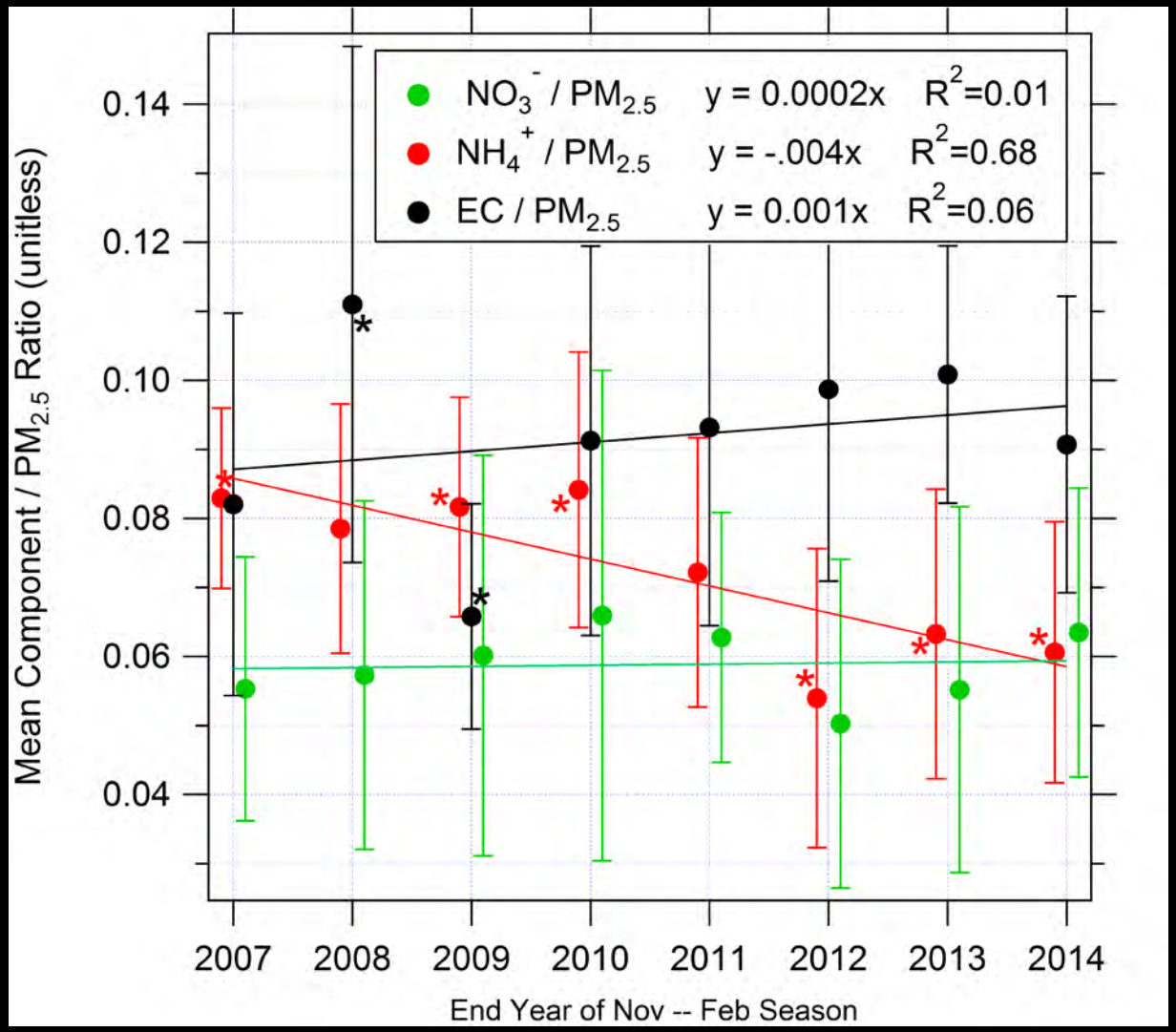


Data from (US EPA Website, Air Quality System Database, 2014)

# Interannual Variability

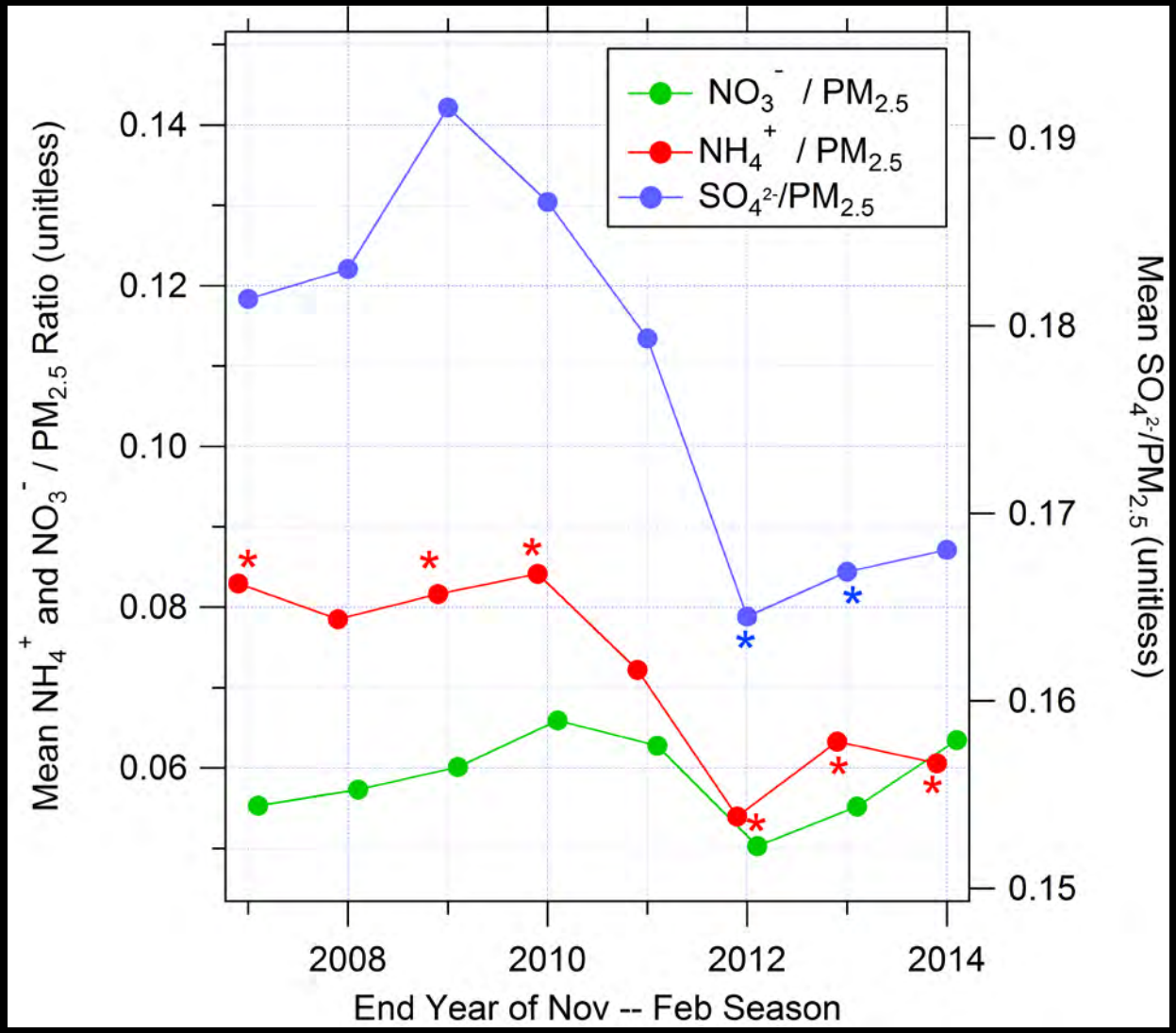


Data from (US EPA Website, Air Quality System Database, 2014)

# Charge Imbalance with Time

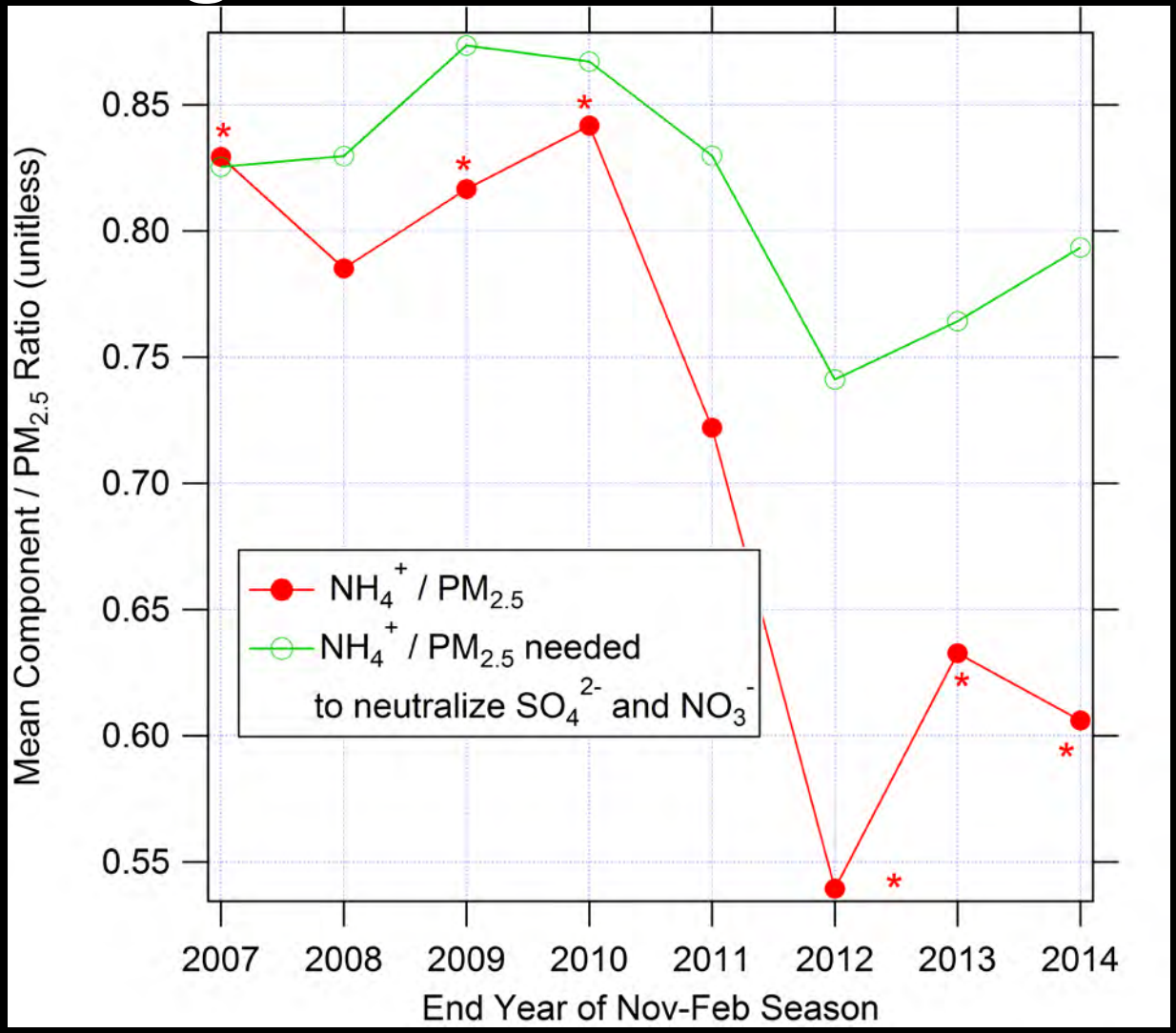


Data from (US EPA Website, Air Quality System Database, 2014)

# Charge Balance Major Inorganic Ions

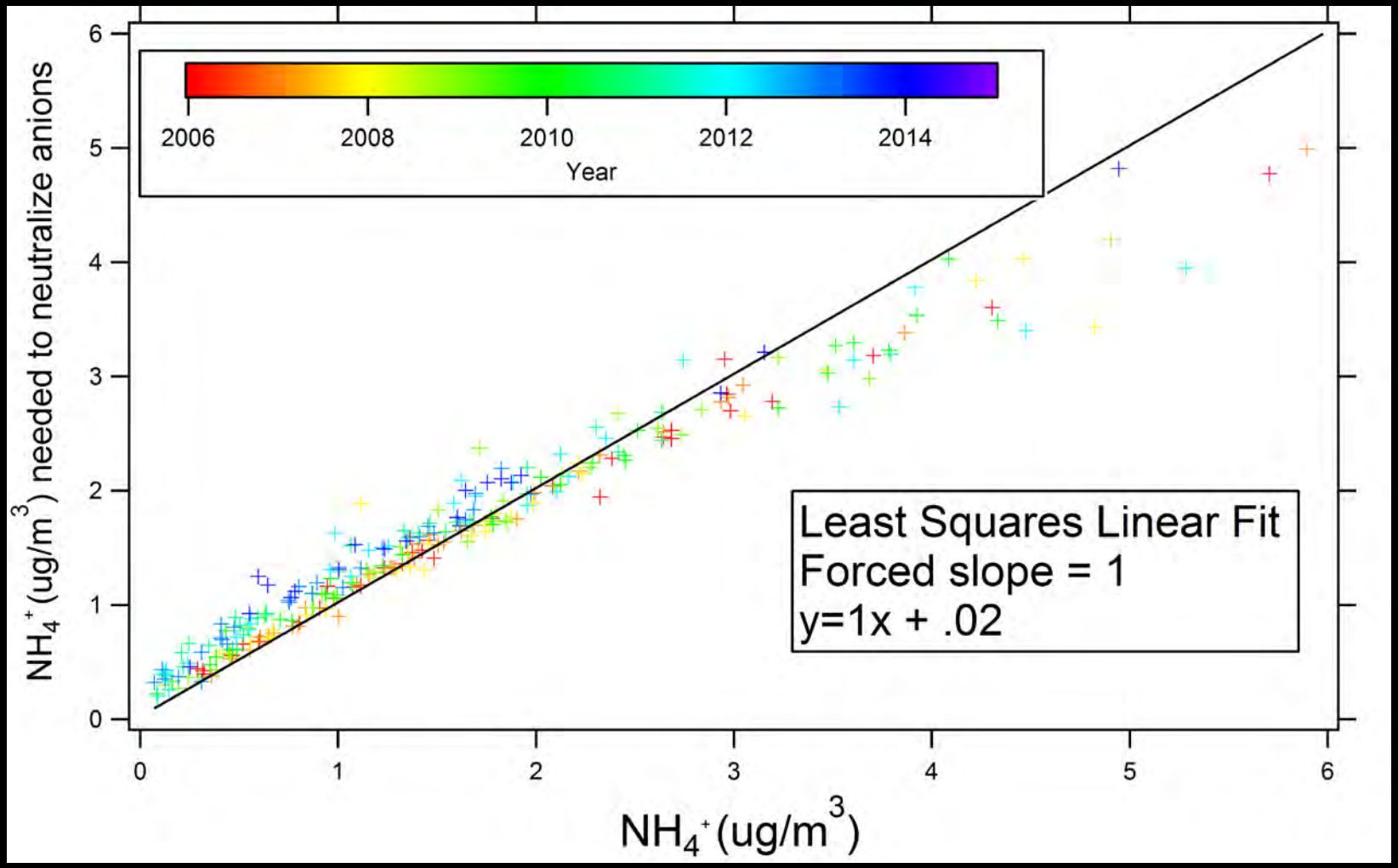


Data from (US EPA Website, Air Quality System Database, 2014)

# $(NH_4)_2SO_4$ Shows Inverse Relationship with Temperature

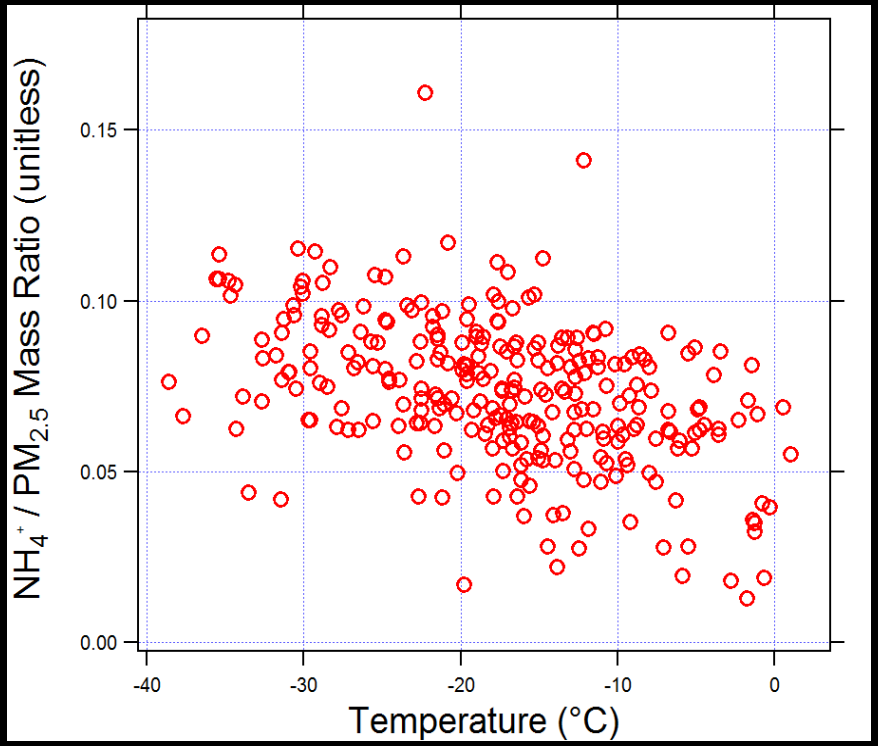


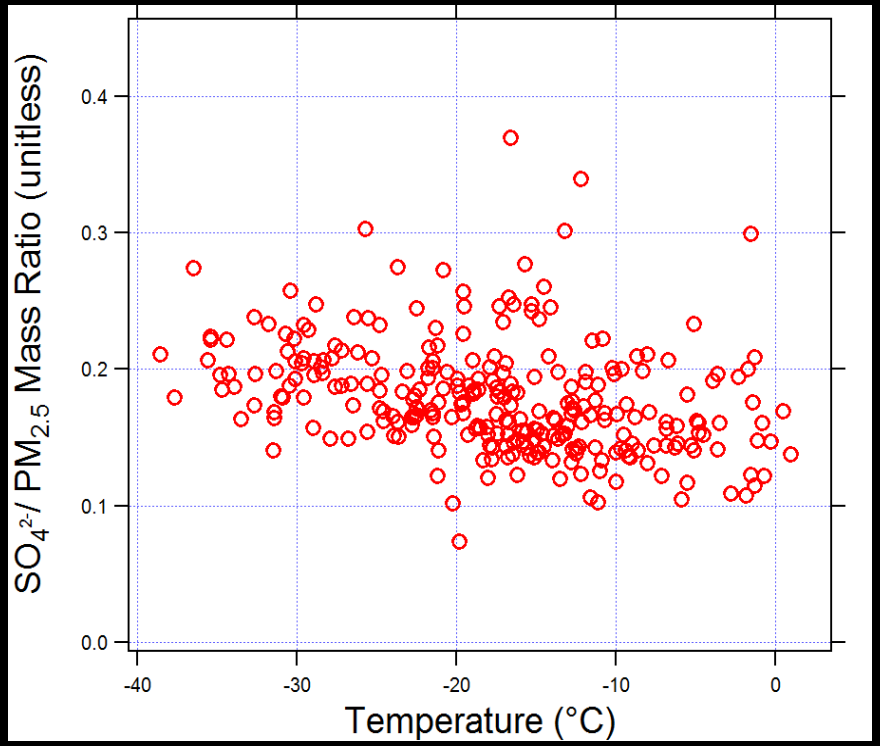


Data from (US EPA Website, Air Quality System Database, 2014)

# $NO_3^-$ shows Positive Correlation with Temperature

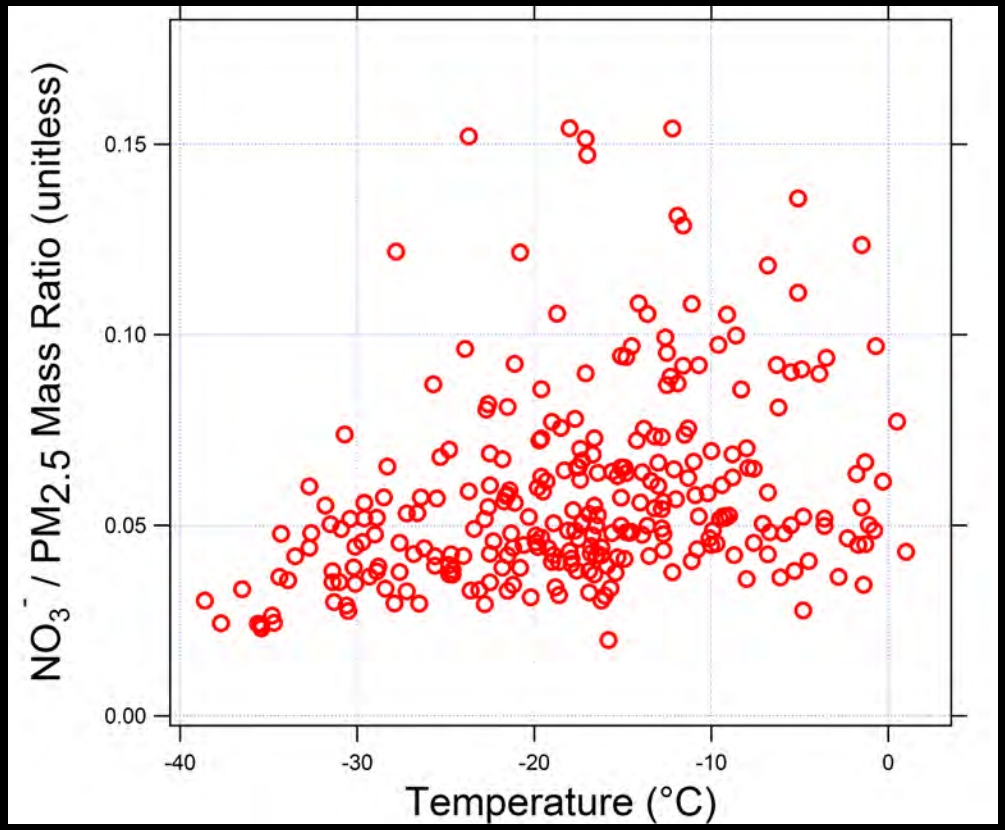


Data from (US EPA Website, Air Quality System Database, 2014)

# Question 2

Will there be a decrease in the $OC/PM_{2.5}$ or $SO_4^{2-}/PM_{2.5}$ due to the incentive programs?

Conclusion: Interannual variability overshadows any trend in these parameters during 2011-2013.

# Question 3

Is secondary oxidation of $SO_2$ taking place?

Hypothesis:  Secondary Oxidation is taking place based on atmospheric models.

# Low $O_3$ at Low Temps

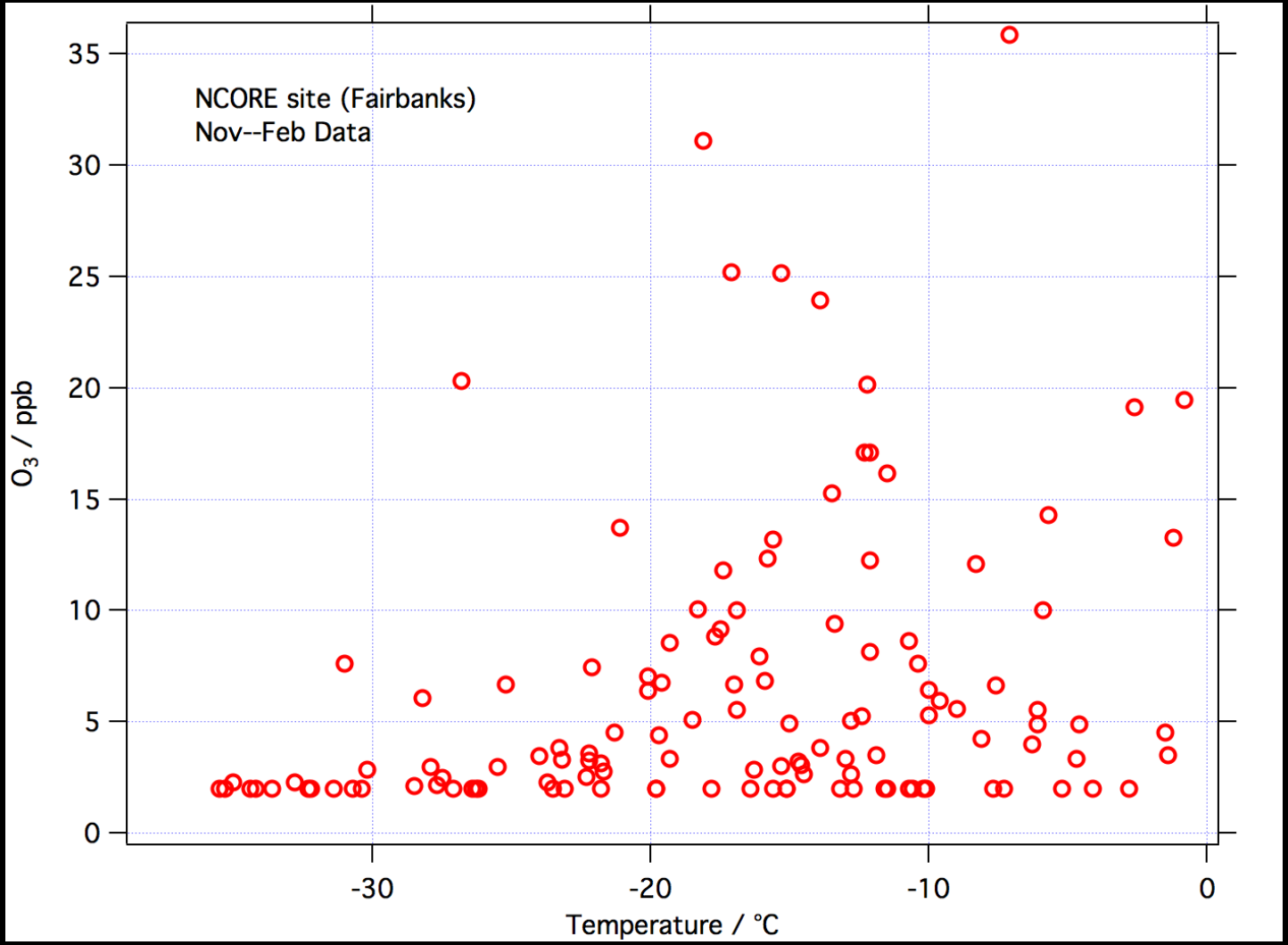


Data from (US EPA Website, Air Quality System Database, 2014)

# $SO_4^{2-}$ is 5% of Potential $SO_4^{2-}$

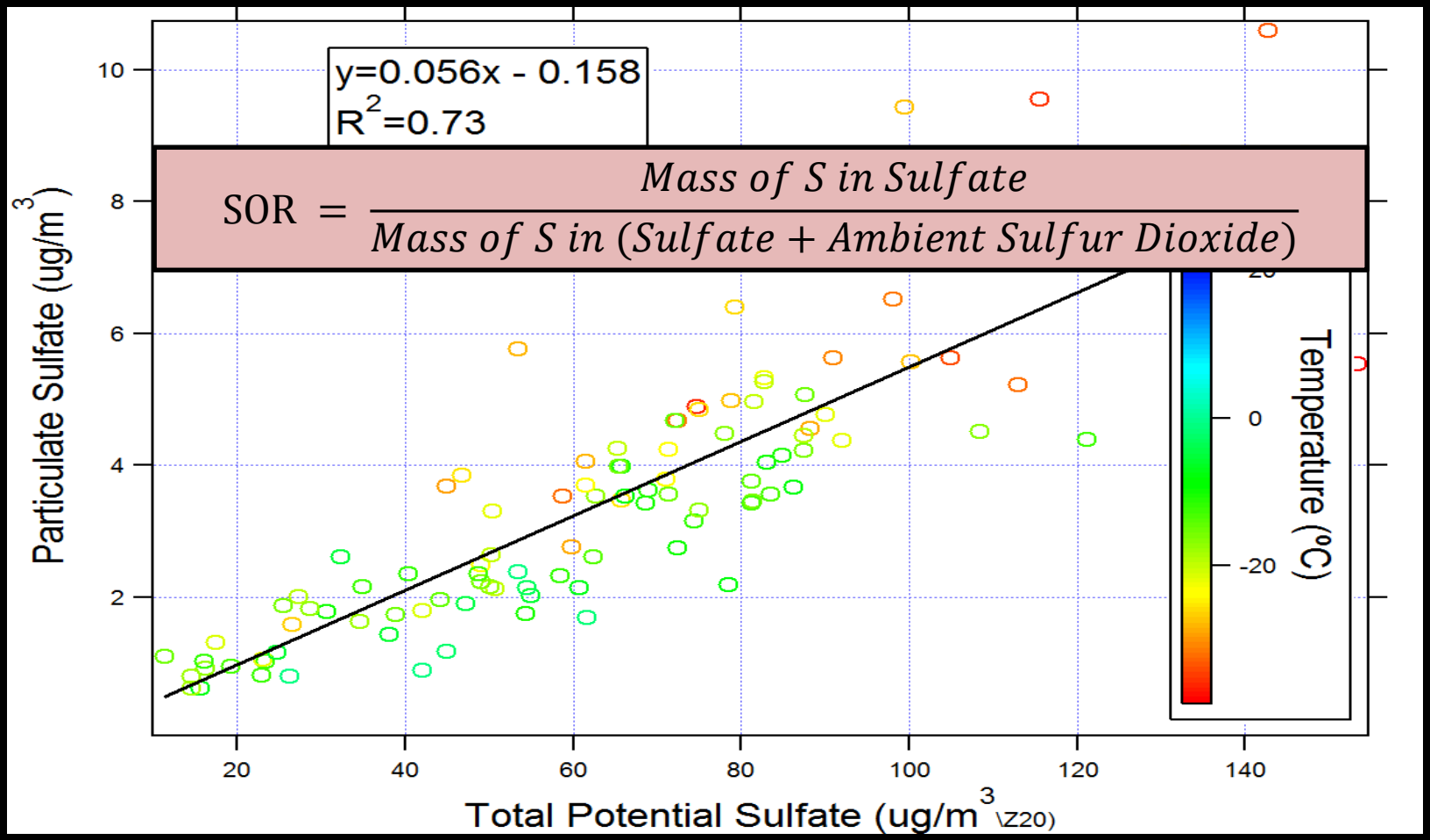


Contradicts previous research: (Shakya & Peltier, 2013) found an ambient SOR of 87% in the Fairbanks winter.

Data from (US EPA Website, Air Quality System Database, 2014)

# SOR for each Month

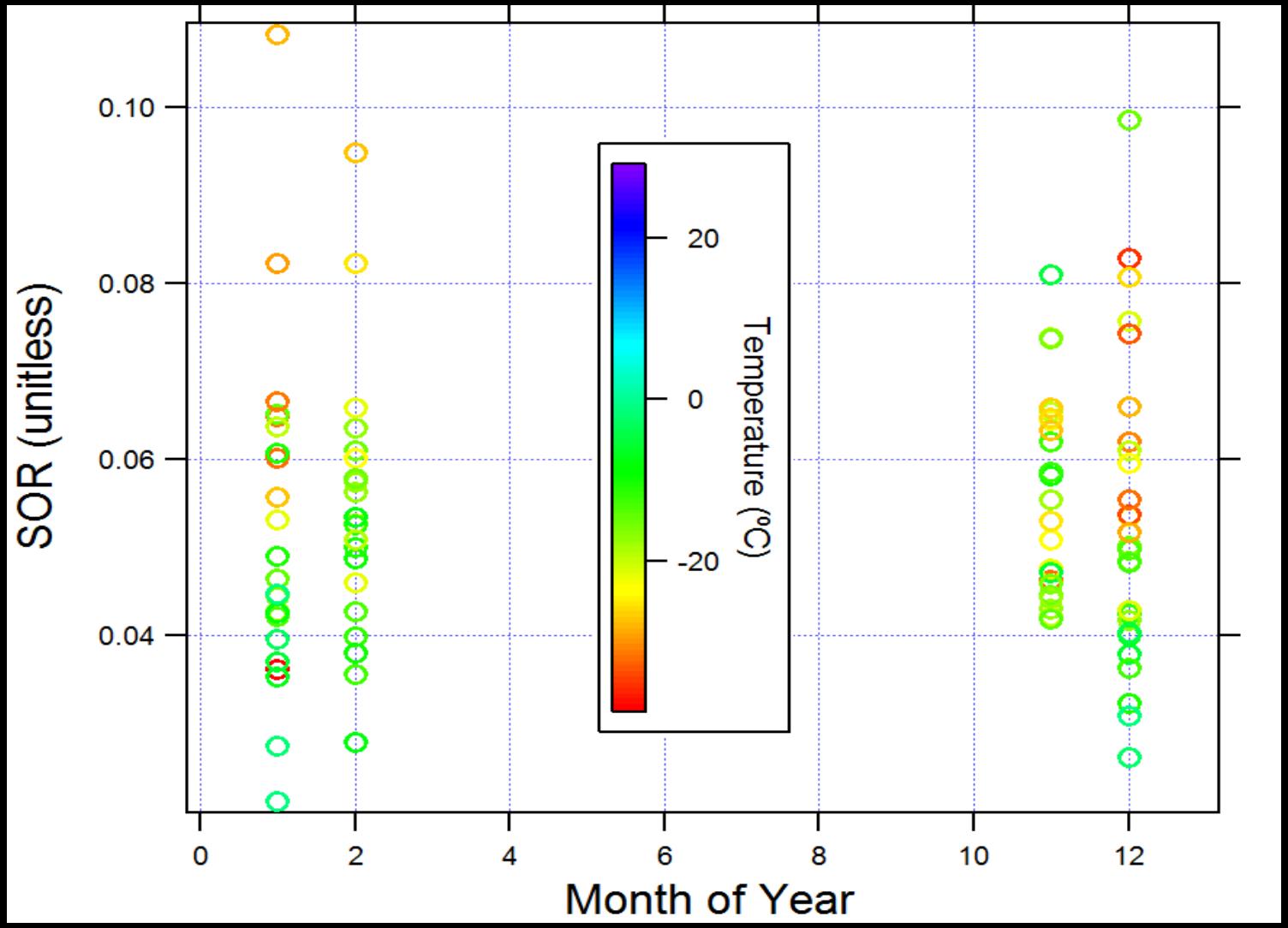


Data from (US EPA Website, Air Quality System Database, 2014)

# Is 5% Ambient SOR attributable to Secondary Oxidation?

## Literature Based Primary SOR values:

- 10% for >8um particles (US Environmental Protection Agency, 1977)
- 1.6% based on EPA emmision factors (Office of Air Quality Planning and Standards, 1995)
- 2-8% (Office of Air Quality Planning and Standards, 1995)

# Question 3

Is secondary sulfur oxidation taking place?

Conclusion: It is unknown if secondary sulfur oxidation is taking place based on SOR. Our understanding is limited by:

- Inaccurate and missing $SO_2$ measurements in source profiles
- Lack of a clear primary SOR in any air shed
- Lack of oxidation mechanism

Thanks to the State of Alaska Department of Environmental Conservation, US EPA, and Fairbanks North Star Borough for collecting such excellent data.

Thanks to the Geophysical Institute and UAF College of Natural Sciences for TA and RA support.

Special thanks to William R. Simpson, Jennifer Guerard, Cathy Cahill, Deanna Huff, and Justine Burd

# Conclusions

- North Pole and Fairbanks sampling sites measure particles with significantly different composition (t test, 95% conf.).
- Significant spatial variability in $PM_{2.5}$ mass is observed between North Pole sampling sites
- Significant downward trends are observed in $NH_4^+/PM_{2.5}$ and $SO_4^{2-}/PM_{2.5}$ from 2006-2014.
- $PM_{2.5}$ composition shows increasing charge imbalance of major ions starting in 2011.
- Interannual variability of $PM_{2.5}$ composition is correlated with Home Heating Survey Results.

Atmospheric Environment 142 (2016) 210–219

Contents lists available at ScienceDirect

Atmospheric Environment

journal homepage: www.elsevier.com/locate/atmosenv

# Source apportionment of $PM_{2.5}$ at multiple Northwest U.S. sites: Assessing regional winter wood smoke impacts from residential wood combustion

Robert A. Kotchenruther

*U.S. Environmental Protection Agency Region 10, Office of Environmental Review and Assessment, 1200 Sixth Avenue, Mailstop OEA-140, Seattle, WA, 98101, USA*

## HIGHLIGHTS

- Source apportionment of $PM_{2.5}$ was performed on 19 Northwest U.S. monitoring sites.
- Common sources of $PM_{2.5}$ were identified across multiple sites.
- Winter wood smoke $PM_{2.5}$ impacts from residential wood combustion were quantified.
- Residential wood combustion contributions to $PM_{2.5}$ spanned a wide range.
- Source apportionment at multiple sites has advantages over single site analysis.

## ARTICLE INFO

*Article history:*
Received 12 April 2016
Received in revised form
20 July 2016
Accepted 23 July 2016
Available online 25 July 2016

*Keywords:*
Positive matrix factorization
Residential wood combustion
Wood smoke
Source apportionment
PM2.5

## ABSTRACT

Wood smoke from residential wood combustion is a significant source of elevated $PM_{2.5}$ in many communities across the Northwest U.S. Accurate representation of residential wood combustion in source-oriented regional scale air quality models is challenging because of multiple uncertainties. As an alternative to source-oriented source apportionment, this work provides, through receptor-oriented source apportionment, an assessment of winter residential wood combustion impacts at multiple Northwest U.S. locations. Source apportionment was performed on chemically speciated $PM_{2.5}$ from 19 monitoring sites using the Positive Matrix Factorization (PMF) receptor model. Each site was modeled independently, but a common data preparation and modeling protocol was used so that results were as comparable as possible across sites. Model solutions had from 4 to 8 PMF factors, depending on the site. PMF factors at each site were associated with a source classification (e.g., primary wood smoke), a dominant chemical composition (e.g., ammonium nitrate), or were some mixture. 15 different sources or chemical compositions were identified as contributing to $PM_{2.5}$ across the 19 sites. The 6 most common were; aged wood smoke and secondary organic carbon, motor vehicles, primary wood smoke, ammonium nitrate, ammonium sulfate, and fugitive dust. Wood smoke was identified at every site, with both aged and primary wood smoke identified at most sites. Wood smoke contributions to $PM_{2.5}$ were averaged for the two winter months of December and January, the months when wood smoke in the Northwest U.S. is mainly from residential wood combustion. The total contribution of residential wood combustion, that from primary plus aged smoke, ranged from 11.4% to 92.7% of average December and January $PM_{2.5}$ depending on the site, with the highest percent contributions occurring in smaller towns that have fewer expected sources of winter $PM_{2.5}$. Receptor modeling at multiple sites, such as that conducted in this work, provided some significant advantages over modeling a single or small number of sites. Analysis at multiple sites allowed common factor chemical compositions to be identified, making it easier to evaluate when a PMF factor at a particular site represents a mix of sources versus a single source. The identification of similar PMF factors across multiple sites also allowed average chemical profiles to be established for the 6 the most commonly identified $PM_{2.5}$ sources or compositions in this study. These average profiles have the potential to be used as source profile inputs in future Chemical Mass Balance receptor modeling, when a limited number of samples may restrict the ability to conduct PMF receptor modeling, or when the availability of local source profiles is limited. Receptor modeling results spanning a range of community sizes and source compositions, as in this study, could be used to

*E-mail address:* Kotchenruther.Robert@epa.gov.

http://dx.doi.org/10.1016/j.atmosenv.2016.07.048
1352-2310/Published by Elsevier Ltd.

evaluate and improve the representation of wood smoke and other specific sources in source-oriented regional scale air quality models by providing an independent source impact assessment.

Published by Elsevier Ltd.

## 1. Introduction

Wood smoke is a common source of ambient $PM_{2.5}$ (particles with aerodynamic diameter <2.5 μm) worldwide. In developing countries, wood burning has widespread use as a fuel for cooking and heating. In more developed countries like the U.S., wood burning is most often used as a source of supplemental home heating and for esthetic purposes, but can also be a primary source of home heating. Human exposure to $PM_{2.5}$ has been linked to cardiovascular and pulmonary disease (Künzli et al., 2005), and lung cancer and premature mortality (Pope and Dockery, 2006). Wood burning, in addition to being a source of $PM_{2.5}$, is also a source of carcinogenic organic compounds such as benzene and formaldehyde, and respiratory irritants like phenols and acetaldehyde (Naeher et al., 2007). Recently, Noonan et al. (2015) have suggested that the number of vulnerable people in the U.S. exposed to residential wood smoke has been significantly underestimated. In the Northwest U.S., exceedances of the 24-h National Ambient Air Quality Standards for $PM_{2.5}$ occur most often in winter. In communities ranging from small mountain towns to large metropolitan areas, wood smoke from residential wood combustion frequently contributes a significant fraction of wintertime $PM_{2.5}$ (Jeong et al., 2008; Kim and Hopke, 2008; Ward and Lange, 2010; Wang and Hopke, 2014). Identifying the proportional contribution of wood smoke, and other sources, to wintertime $PM_{2.5}$ is a key step to developing targeted and cost effective $PM_{2.5}$ reduction strategies.

Regional scale efforts to assess source impacts to ambient $PM_{2.5}$ are often addressed in the U.S. using source apportionment tools within source-oriented photochemical grid models like CMAQ and CAMx. These models predict source impacts from emissions inventories, emissions modeling, meteorological simulations, and chemical transport modeling (Wagstrom et al., 2008). Source-oriented models also have the benefit of being able to explore the impact of emissions control scenarios on predicted $PM_{2.5}$. However, evaluating the contribution of residential wood combustion to observed $PM_{2.5}$ with these models can be challenging for a number of reasons. Grid models can be overly dispersive under the low wind speed conditions that often lead to high winter $PM_{2.5}$ (Holtslag et al., 2013) and these models can have difficulty replicating multiday wintertime temperature inversions and air stagnation episodes (Baker et al., 2011). For small mountain valley towns with high residential wood combustion impacts, even the finest horizontal grid resolutions that are typically used can be too course. Also, developing accurate residential wood combustion emissions inventories can be challenging because of the large variety of wood burning devices in use, difficulties in obtaining an accurate count and spatial representation of each device type, and differences between standard wood burning device emissions tests in a laboratory and emissions from these devices when they are used in the real world.

While source-oriented source apportionment methods have their challenges, receptor-based methods also have their limitations. Results in receptor-based source apportionment studies can be dependent on the chemical species measured, quality and amount of measured data, choice of chemical source markers to identify sources, and the QA/QC modeling protocol used. Despite these limitations, this work demonstrates that a regional assessment of $PM_{2.5}$ using receptor-based source apportionment methods like Positive Matrix Factorization (PMF) can provide a complementary approach to source-oriented techniques and could be used as an independent means of evaluating them.

While there are numerous published receptor-based source apportionment studies, most published studies report results for only a few monitoring sites, cover differing time periods, and use differing data preparation and modeling protocols. These differences make it hard to compare results between studies or use them to compile a regional assessment. Recently, there have been several regional assessments published using receptor-based methods focusing on marine vessel impacts in the western U.S. (Kotchenruther, 2013, 2015). This work uses a similar approach as Kotchenruther (2013, 2015) to assess regional impacts of winter wood smoke from residential wood combustion in the Northwest U.S. Source apportionment is performed using the PMF model on chemically speciated $PM_{2.5}$ from 19 sites. As in the previous work, the approach taken is to model each site independently and to treat data from all sites with a common data preparation and modeling protocol. The benefits of this approach are that results between sites are as comparable as possible since site-to-site data and modeling have undergone the same treatments. An additional benefit of receptor modeling at multiple sites is that common factors across sites can be identified, making it easier to evaluate when a PMF factor at a particular site represents a mix of sources versus a single source.

## 2. Methods

### 2.1. Chemically speciated $PM_{2.5}$ data

The Chemical Speciation Network (CSN) is one of several urban and suburban monitoring networks funded by the U.S. Environmental Protection Agency (EPA) and operated by state and local agencies. CSN monitors collect 24-h integrated $PM_{2.5}$ mass on filters that are sent to a laboratory for chemical analyses. Laboratory analyses includes quantification of total $PM_{2.5}$ mass, elemental composition by energy dispersive X-ray fluorescence, organic and elemental carbon (OC, EC) by thermal evolution in 8 temperature fractions, and anions and cations by ion chromatography. Detailed information about the CSN network is provided by Solomon et al. (2014). CSN monitors are typically operated on a daily, every third day, or every sixth day schedule depending on the site. Quality assured CSN data are housed in EPA's Air Quality System (AQS) database.

Monitoring sites analyzed in this work are listed in Table 1 and depicted in Fig. 1. From 2007 to 2009 EPA conducted a systematic replacement of all CSN carbon samplers to match those of the IMPROVE program (a chemically speciated $PM_{2.5}$ monitoring network of mostly rural and remote sites) and switched to IMPROVE-based carbon analytical measurement protocols (U.S. EPA, 2009). Consequently, EC and OC data before and after the change are not easily comparable in the CSN network. For this reason, the start date for data used from each site in this study is

**Table 1**
CSN monitoring sites analyzed in this study.

| City | State | Data start date | Data end date | Number of samples | EPA AQS number | Latitude | Longitude |
|---|---|---|---|---|---|---|---|
| Fairbanks | AK | 10/1/2009 | 9/29/2014 | 573 | 20900010 | 64.8407 | −147.7225 |
| Fresno | CA | 1/1/2012 | 9/29/2014 | 304 | 60190011 | 36.7853 | −119.7742 |
| Bakersfield | CA | 1/2/2010 | 9/7/2013 | 310 | 60290014 | 35.3561 | −119.0412 |
| Sacramento | CA | 1/2/2010 | 9/29/2014 | 565 | 60670006 | 38.6138 | −121.3680 |
| Boise | ID | 5/3/2007 | 9/26/2014 | 851 | 160010010 | 43.6003 | −116.3479 |
| Klamath Falls | OR | 7/12/2009 | 6/28/2014 | 180 | 410350004 | 42.1889 | −121.7225 |
| Lakeview | OR | 10/16/2009 | 8/3/2014 | 177 | 410370001 | 42.1889 | −120.3519 |
| Oakridge | OR | 7/6/2009 | 9/30/2012 | 177 | 410392013 | 43.7444 | −122.4805 |
| Portland | OR | 5/3/2007 | 9/29/2014 | 736 | 410510080 | 45.4965 | −122.6034 |
| Bountiful | UT | 5/6/2007 | 9/26/2014 | 417 | 490110004 | 40.9030 | −111.8845 |
| Salt Lake City | UT | 5/9/2007 | 9/29/2014 | 777 | 490353006 | 40.7364 | −111.8722 |
| Lindon | UT | 5/6/2007 | 9/26/2014 | 404 | 490494001 | 40.3414 | −111.7136 |
| Vancouver | WA | 4/7/2009 | 8/26/2013 | 259 | 530110013 | 45.6483 | −122.5869 |
| Seattle (Duwamish) | WA | 11/8/2008 | 4/27/2012 | 198 | 530330057 | 47.5632 | −122.3405 |
| Seattle (Beacon Hill) | WA | 5/3/2007 | 9/29/2014 | 678 | 530330080 | 47.5683 | −122.3081 |
| Tacoma (South L St.) | WA | 5/12/2007 | 9/26/2014 | 376 | 530530029 | 47.1864 | −122.4517 |
| Tacoma (Alexander Ave.) | WA | 11/2/2008 | 4/27/2012 | 203 | 530530031 | 47.2656 | −122.3858 |
| Marysville | WA | 4/7/2009 | 9/26/2014 | 305 | 530611007 | 48.0543 | −122.1715 |
| Yakima | WA | 11/8/2007 | 9/26/2014 | 335 | 530770009 | 46.5968 | −120.5122 |


**Fig. 1.** CSN monitoring sites analyzed in this study.

based on when it converted to IMPROVE-based carbon sampling methods, if the site was in existence during the transition. The end date for data represents what was available in AQS at the time data were extracted. All sites were in operation for over two years and collected from 177 to 851 24-h samples.

### 2.2. Data preparation and treatment

A detailed discussion of CSN data preparation and treatment is provided in a previous publication (Kotchenruther, 2013) and briefly summarized here. Prior to source apportionment analyses the data were processed to correct for field blanks. Chemical species were omitted in PMF modeling if more than 40% of samples had missing data. Missing values were replaced with median concentrations and the uncertainty set to a very high value compared to measured data, typically four times the species median concentration, to minimize the influence of the replaced data on the model solution. Any negative concentrations were reset to zero. The uncertainty of each measurement was estimated based on the measured analytical uncertainty plus 1/3 of the method detection limit. The signal-to-noise (S/N) ratio was also used to evaluate whether chemical species should be included in the PMF modeling, and was used to adjust the data uncertainty. Chemical species were omitted in PMF modeling if the S/N ratio was less than 0.2. For chemical species with S/N between 0.2 and 1.0, data uncertainties were multiplied by a factor of 3 to down-weight the influence of these species in the model solution. For chemical species measured by both elemental and ion analyses, such as sodium (Na) and potassium (K), Na ion and elemental K were used because these species had better S/N ratios, and elemental Na and K ion were not used to avoid double counting. In addition to these treatments, sulfate was retained in the dataset and non-sulfate sulfur (NSS) was calculated by subtracting the sulfur component of measured sulfate from the measured sulfur concentration. Also, the reported lowest temperature fraction of EC, EC1, is actually the sum of pyrolyzed organic carbon (OP) and low temperature combusting EC. Hence, EC1 was recalculated as EC1-OP and the measured OP value was used, so as not to double count measured OP.

### 2.3. Source apportionment

Source apportionment modeling was performed using EPA PMF 5.0 (http://www.epa.gov/heasd/research/pmf.html). A discussion of the mathematical equations underlying EPA PMF can be found in Paatero and Hopke (2003) and Norris et al. (2014). Data from each monitoring site was modeled independently. In each case, the model was run in the robust mode with 20 repeat runs to insure the

model least-squares solution represented a global rather than local minimum and the rotational $F_{PEAK}$ variable was held at the default value of 0.0. The model solution with the optimum number of factors was determined somewhat subjectively and was based on inspection of the factors in each solution, the quality of the least-squares fit (analysis of $Q_{Robust}$ and $Q_{True}$ values), and the results from three error estimation methods available in PMF 5.0; bootstrapping (BS), displacement (DISP), and bootstrapping with displacement (BS-DISP) (Norris et al., 2014; Paatero et al., 2014). The scaled residuals for final model solutions were generally normally distributed, falling into the recommended range of +3 to −3.

PMF factors can represent a single source or source category (e.g., cement manufacture, wood burning), a chemical composition (e.g., ammonium nitrate, sea salt), or mixtures of sources and compositions. During modeling of each of the 19 sites in this work, it was sometimes the case that the number of factors that appeared to present the best delineation of sources and compositions, were in fact shown to have too much solution instability after analysis with DISP, BS, and BS-DISP (e.g., factor swaps; Brown et al., 2015). In these cases, reducing the number of factors often led to improved solution stability, but also caused some factors to combine and become mixtures of sources, or sources and compositions. Preference in PMF solutions was given to the number of factors with improved solution stability, even if that lead to reduced source delineation. Further information on how the model solution with the optimal number of factors was selected is provided in the Supplemental Materials.

## 3. Results and discussion

### 3.1. Identified $PM_{2.5}$ sources and compositions

The number of PMF factors ranged from 4 to 8, depending on the site. Table 2 lists the 15 different sources and compositions identified over all time periods at the 19 sites, and how often they were identified in a factor by themselves versus in a factor mixed with other sources or compositions. A table in the Supplemental Materials lists each site, the number of factors found, and the factor attributions using the source or composition identifiers listed in Table 2. All PMF factor mass impacts and factor chemical profiles for each site are also provided in the Supplementary Materials. The chemical profiles presented are those after the factor chemical composition from each site was normalized. A factor chemical composition was normalized by assuming an organic mass (OMC) to OC ratio of 1.4 (i.e., multiplying all OC fraction by 1.4), summing all of the measured chemical constituents using the assumed OMC instead of OC, and dividing each chemical component by the summed constituents. Additionally, for factors associated with fugitive dust, a metal oxide to metal ratio was assumed for aluminum (Al, ratio of 2.2), calcium (Ca, 1.63), iron (Fe, 2.42), titanium (Ti, 1.94), and silicon (Si, 2.49) based on the ratios used in the IMPROVE network (Solomon et al., 2014).

The sources and compositions listed in Table 2 were identified by comparing the chemical composition of PMF factors with chemical profiles in EPA's SPECIATE database of source emissions test data (https://www3.epa.gov/ttnchie1/software/speciate/), comparison with similar PMF factor chemical compositions identified in existing published studies, knowledge of existing sources in the airsheds and their seasonal emissions patterns, and composition of aerosols found in the natural environment (e.g., fugitive dust, sea salt). The sections below describe how each source or composition was identified, and for those most commonly found, a figure is provided depicting the average PMF factor chemical profile from those factors that were determined not to be a mixture. Data tables for the average profiles are provided in the Supplemental Materials. The average PMF factor chemical profile was taken after the PMF factor chemical profile from each site was normalized as described above.

#### 3.1.1. PMF factors associated with aged wood smoke and secondary OC

These factors were dominated by OC and EC, with higher temperature OC fractions more abundant than that found in Primary Wood Smoke (see section 3.1.3) and almost none of the lowest temperature OC1 fraction. K was a significant trace constituent, but not chlorine (Cl). The average chemical profile from PMF factors at 11 sites where this source was not mixed with other sources is shown in Fig. 2a.

The seasonal pattern of mass impacts depended on the site. Two illustrative examples are provided here, Fig. 3 shows the time series of mass impacts for this factor in Fairbanks, AK and Fig. 4 for Lindon, UT. These figures also show the time series of mass impacts for the PMF factor associated with primary wood smoke at these sites. At sites like Fairbanks, AK, with significant winter primary wood smoke impacts, the aged wood smoke and secondary OC factor had both elevated winter impacts and high summer impacts on those years corresponding to high wildfire activity. Summers with low wildfire activity had small, but not zero, summer impacts. At sites

**Table 2**
Sources and chemical compositions identified and the number of sites where appearing as a single PMF factor, or in a factor mixed with other listed sources or chemical compositions.

| Source or composition identifier | Identified source or composition | Number of sites where appears | Number of sites where a single factor | Number of sites where in a mixed factor |
|---|---|---|---|---|
| 1 | Aged Wood Smoke and Secondary Organic Carbon | 19 | 11 | 8 |
| 2 | Motor Vehicles | 18 | 11 | 7 |
| 3 | Primary Wood Smoke | 17 | 12 | 5 |
| 4 | Ammonium Nitrate | 16 | 10 | 6 |
| 5 | Ammonium Sulfate | 16 | 6 | 10 |
| 6 | Fugitive Dust | 16 | 10 | 6 |
| 7 | Sea Salt | 7 | 6 | 1 |
| 8 | Sulfate Rich | 6 | 1 | 5 |
| 9 | Iron Rich | 4 | 2 | 2 |
| 10 | Aged Sea Salt | 4 | 3 | 1 |
| 11 | Undetermined | 4 | 0 | 4 |
| 12 | Elemental Carbon and Sulfate Rich | 3 | 0 | 3 |
| 13 | Residual Fuel Oil Combustion | 3 | 2 | 1 |
| 14 | Nitrate Rich | 2 | 0 | 2 |
| 15 | Cement Kiln | 1 | 1 | 0 |

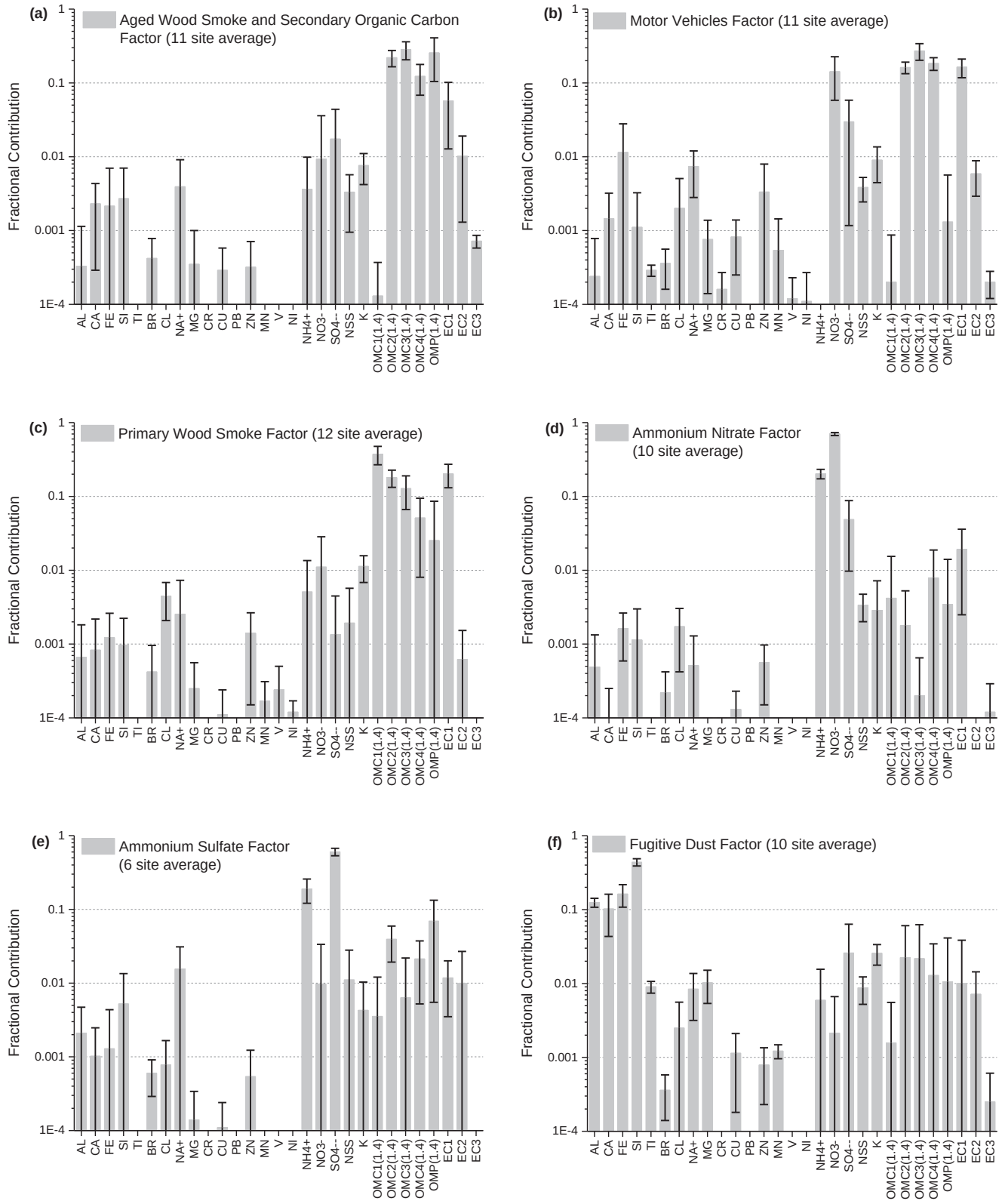


**Fig. 2.** Average and standard deviation of chemical profiles from PMF factors from multiple sites associated with (a) aged wood smoke and secondary OC, (b) motor vehicles, (c) primary word smoke, (d) ammonium nitrate, (e) ammonium sulfate, and (f) fugitive dust.

like Lindon, UT, where primary wood smoke plays a relatively minor role in winter $PM_{2.5}$, the aged wood smoke and secondary OC factor had high mass impacts in summer months on those years corresponding to high wildfire activity, with low impacts at most

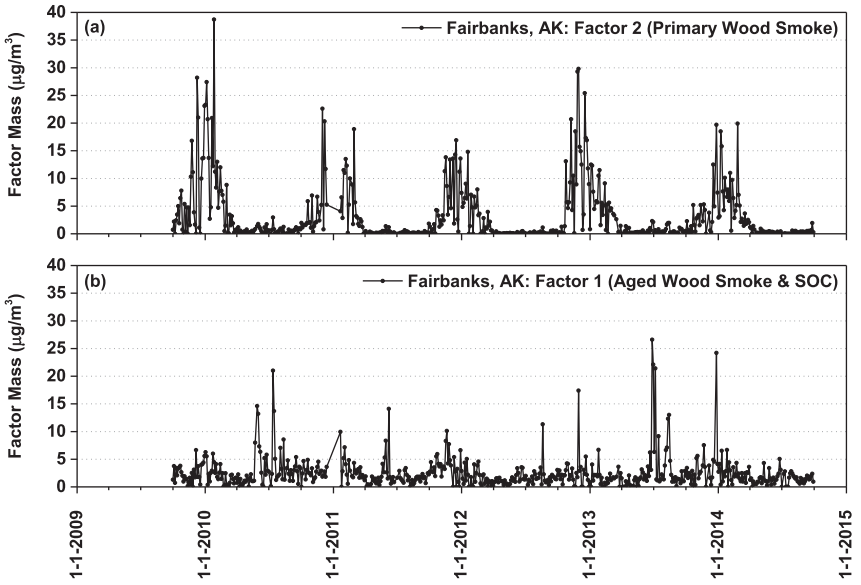


**Fig. 3.** Time series of $PM_{2.5}$ mass impacts in Fairbanks, AK for PMF factors associated with (a) primary wood smoke and (b) aged wood smoke and secondary OC.

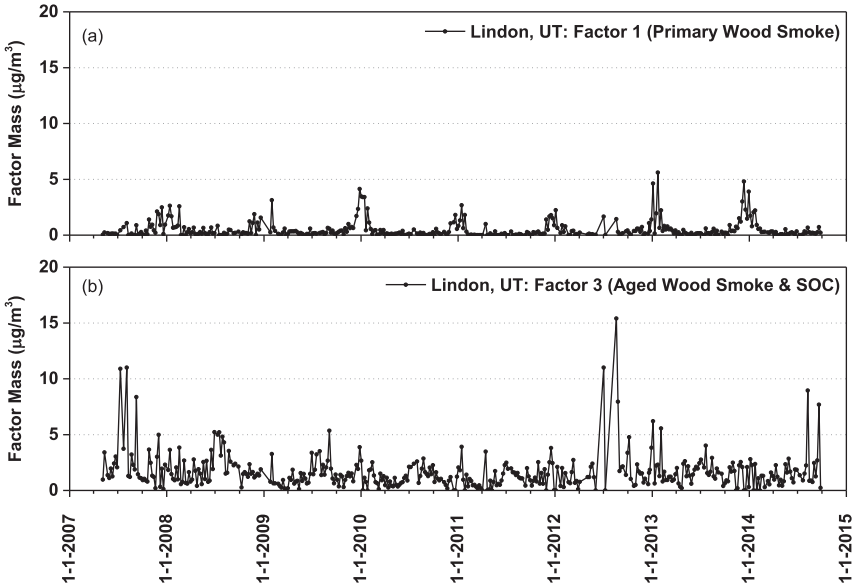


**Fig. 4.** Time series of $PM_{2.5}$ mass impacts in Lindon, UT for PMF factors associated with (a) primary wood smoke and (b) aged wood smoke and secondary OC.

other times. Yearly totals of state wildfire acres burned from 2007 to 2014 were obtained from the National Interagency Fire Center (https://www.nifc.gov/fireInfo/fireInfo_statistics.html). Yearly wildfire data for all states with monitoring sites in this study is provided in the Supplementary Materials. Further pointing to the impact of wildfire in this factor, the ratio of char-EC to soot-EC (measured (EC1-OP)/(EC2+EC3) in the CSN datasets) in the average profile was 5.2, much lower than the ratio found in the average profile for primary wood smoke (ratio = 283). This lower char-EC to soot-EC ratio is consistent with differences found by Han et al. (2010) between forest fire emissions and biomass combustion for home heating.

The rational for associating this factor with wood smoke comes from the correspondence of elevated summer impacts with high wildfire activity, the correspondence of elevated winter impacts with those areas also having significant winter Primary Wood Smoke impacts, the dominance of OC and EC in the chemical profile, and the presence of the wood smoke marker K. The determination that the wood smoke is aged comes from the observation that OC fractions in this factors' profile are shifted to higher temperature fractions compared with primary wood smoke, which is consistent with oxidative aging of organic carbon. Also, the OC to EC ratio in the average profile was 9.3, higher than that from Primary Wood Smoke (2.7) and the K to OC ratio, 0.012, was lower than that from Primary Wood Smoke (0.021), both of which are consistent with organic gases from wood fires undergo gas to particle conversion and adding organic mass to the aerosol during aging. The absence of Cl in the chemical profile, compared to that in Primary Wood Smoke, is also an indication of aging, similar to the Cl replacement chemistry that occurs when sea salt aerosol ages (Adachi and Buseck, 2015). Lastly, the rational for also associating this factor with secondary organic carbon comes from the small

elevation in summertime mass at most sites, even during years with low wildfire activity.

*3.1.2. PMF factors associated with motor vehicles*

The principal chemical constituents in this factor were EC1, OC2, OC3, OC4, and nitrate. Significant trace constituents were zinc (Zn), copper (Cu), and Fe. The average chemical profile from PMF factors at 11 sites where this source was not mixed with other sources is shown in Fig. 2b. The dominant chemical constituents are similar to those found for motor vehicles in previous publications (Zhao and Hopke, 2004; Kim and Hopke, 2006; Hwang and Hopke, 2007). The significant trace metal constituents match those commonly found in $PM_{2.5}$ associated with motor vehicles (Song and Gao, 2011; Pant and Harrison, 2013). The near ubiquity of this source at the sites in this study matches the conceptual understanding of motor vehicles as a common source of particulate pollution in urban areas. Separate factors for gasoline and diesel vehicles were not found in this study, and this factor likely represents a combination of these sources.

*3.1.3. PMF factors associated with primary wood smoke*

This factor was dominated by OC and EC, with the lower temperature OC and EC fractions having the highest abundance. K and Cl were significant trace constituents. The seasonal pattern of mass impacts showed high winter and low summer impacts. The average chemical profile from PMF factors at 12 sites where this source was not mixed with other sources is shown in Fig. 2c. The K to OC ratio in the average profile, 0.021, was consistent with K to OC ratios in $PM_{2.5}$ from Northwestern U.S. forest biomass combustion (Munchak et al., 2011). The OC to EC ratio was 2.7. The pattern of OC and EC temperature fractions in the average profile and the presence of K and Cl are similar to that found in many wood smoke profiles in EPA's SPECIATE database. Examples of similar profiles include SPECIATE profile 3921 representing $PM_{2.5}$ from pine wood burning in a fireplace and profile 3937 from oak burning in a woodstove.

*3.1.4. PMF factors associated with ammonium nitrate*

The main chemical constituents in this factor were ammonium and nitrate. The typical seasonal pattern of mass impacts showed high winter and very low summer impacts, which is indicative of secondary formation, and likely from multiple sources of $NO_x$ and ammonia. The average chemical profile from PMF factors at 10 sites where this source was not mixed with other sources is shown in Fig. 2d. The fractional contribution of nitrate and ammonium in the average profile was 0.70 and 0.20, respectively, which is the ratio expected when nitrate is fully neutralized by ammonium.

*3.1.5. PMF factors associated with ammonium sulfate*

The main chemical constituents in this factor were ammonium and sulfate. The typical seasonal pattern of mass impacts showed higher summer impacts, but also some sites like Fairbanks, AK with higher winter impacts. This factor likely arises from multiple sources of $SO_2$ and ammonia. The average chemical profile from PMF factors at 6 sites where this source was not mixed with other sources is shown in Fig. 2e. The fractional contribution of sulfate and ammonium in the average profile was 0.60 and 0.19, respectively, which demonstrates near full neutralization of sulfate by ammonium.

*3.1.6. PMF factors associated with fugitive dust*

The principal chemical constituents in this factor were Al, Ca, Fe, and Si. Significant trace constituents were Ti and K. The typical seasonal pattern of mass impacts is higher in late summer and lower in winter and spring and corresponds to the typical seasons with less and more precipitation, respectively. The average chemical profile from PMF factors at 10 sites where this source was not mixed with other sources is shown in Fig. 2f. The fractional contributions of the principal and trace chemical constituents in the average profile is similar to that of numerous soil dust profiles in EPA's SPECIATE database.

*3.1.7. PMF factors associated with sea salt*

This factor was dominated by Na and Cl. Significant trace constituents were magnesium (Mg) and Ca. Mass impacts for this factor had no discernable seasonal pattern and was only found at cities near salt water bodies. The site locations and lack of seasonal pattern suggest these factors are from natural sources rather than winter road salting.

*3.1.8. PMF factors identified as Sulfate Rich*

The main identifying feature of this factor was a significant presence of sulfate in the absence of ammonium. This most often occurred when sulfate was mixed with another factor that typically did not contain sulfate (e.g., mixed with fugitive dust in results for Vancouver, WA). The source of the sulfate is likely multiple sources of $SO_2$.

*3.1.9. PMF factors identified as iron rich*

This factor was dominated by Fe. Significant trace constituents were chromium, Cu, Zn, manganese, and Ni. This factor was only found in the large cities of Seattle, Portland, and Tacoma. It is likely this factor is related to metal fabrication or other industrial activity.

*3.1.10. PMF factors associated with aged sea salt*

This factor had the same identifying features as Sea Salt, but with little or no Cl and the addition of a significant contribution from nitrate. The replacement of Cl with nitrate is typical of sea salt after aging (Adachi and Buseck, 2015).

*3.1.11. PMF factors identified as undetermined*

This classification was given to factors that contained a significant amount of organic mass that could not otherwise be identified. 4 of the 19 sites had factors like this.

*3.1.12. PMF factors identified as elemental carbon and Sulfate Rich*

The main identifying feature of this factor was a significant presence of sulfate and the EC2 fraction. While always appearing as mixed with other sources in this study, previous studies have linked elevated EC2 and sulfate to fuel combustion sources (Kim et al., 2004; Han et al., 2010).

*3.1.13. PMF factors associated with residual fuel oil combustion*

The main chemical constituents in this factor were ammonium and sulfate. Significant trace constituents were vanadium (V) and Ni. The V to Ni ratio for this factor was close to 3, typical of residual fuel oil combustion (Kotchenruther, 2015). Because this factor was found only in the major port cities of Seattle and Tacoma, the main source is likely marine vessels.

*3.1.14. PMF factors identified as nitrate rich*

The main identifying feature of this factor was a significant presence of nitrate in the absence of ammonium. The source of the nitrate is likely multiple sources $NO_x$.

*3.1.15. PMF factors associated with cement kiln emissions*

The main chemical constituents in this factor were sulfate and Ca, similar to high Ca and sulfate profiles for cement kilns in EPA's SPECIATE database. There is a cement plant in the vicinity of the Seattle monitor where this factor was identified.

### 3.2. Winter residential wood combustion impacts

For the winter months of December and January, there is typically no wild or prescribed fire activity that would impact the urban monitors in this study. Therefore it is assumed here that both the Primary Wood Smoke and Aged Wood Smoke and Secondary OC factors for these months come predominantly from residential wood combustion. Table 3 lists the December and January two-month average mass and percent contribution for each wood smoke factor, when not mixed with other sources or compositions. For those sites where both factors were identified and quantified, total average wood smoke impacts are calculated as the sum of these two factors. At the Bakersfield site the two wood smoke factors were mixed with each other, therefore, while separate wood smoke factors are not quantified, the total average wood smoke impact is indicated. Average winter and annual $PM_{2.5}$ results for all sites and factors are provided in the Supplementary Materials.

Table 3 and Fig. 5 show the average winter residential wood combustion results found in this study. Available results encompass small towns to large cities and show a wide range of total wood smoke percent contributions to average winter $PM_{2.5}$, from 11.4% in Bakersfield, CA to 92.7% in Lakeview, OR. The highest winter wood smoke percent contributions occur in small towns where, in addition to residential wood combustion, there are fewer potential sources of primary $PM_{2.5}$ compared to larger urban areas. It would be difficult to make a consistent link between town size and winter percent contribution of residential wood combustion because secondary inorganic $PM_{2.5}$ (e.g., ammonium nitrate) in some areas contributes significantly to total winter $PM_{2.5}$.

The winter wood smoke results presented in this study could be used for performance evaluation and improvement of source-oriented models. For example, exploring the effect of uncertainties in meteorological modeling, emissions inventories, and the effects of grid resolution on wood smoke predictions over the wide range of city sizes and complexity of $PM_{2.5}$ sources presented here.

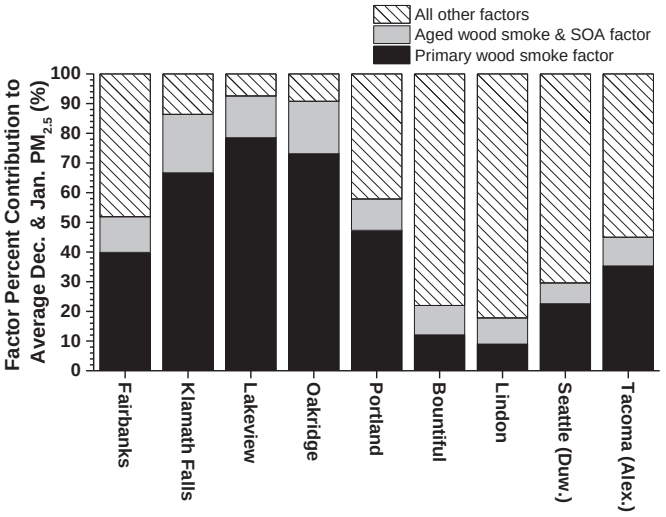


**Fig. 5.** Factor percent contribution to average December and January $PM_{2.5}$ for sites where two wood smoke factors were identified.

### 3.3. Comparison of residential wood combustion impacts with emissions inventories and previous studies

Every three years EPA, working with States and Tribes, develops a comprehensive and detailed estimate of air pollution emissions and publishes them in a National Emissions Inventory (NEI, https://www.epa.gov/air-emissions-inventories). The 2011 NEI provides annual estimates of $PM_{2.5}$ and $PM_{2.5}$ precursor emissions from numerous source categories at both state and county levels and includes residential wood combustion. To compare PMF results with the NEI, annual average PMF results for residential wood combustion were computed for 2011 for those sites in Table 3 where total primary + aged wood smoke impacts could be computed. A table is provided in the Supplemental Materials

**Table 3**
December and January average wood smoke $PM_{2.5}$ mass and percent of total $PM_{2.5}$, from PMF factor results.

| Monitor location | Primary wood smoke factor mass (μg/m$^3$) | Primary wood smoke factor mass (%) | Aged wood smoke & SOA factor mass (μg/m$^3$) | Aged wood smoke & SOA factor mass (%) | Total primary + aged wood smoke (μg/m$^3$) | Total primary + aged wood smoke (%) |
|---|---|---|---|---|---|---|
| Fairbanks | 9.8 | 39.9 | 3.0 | 12.0 | 12.8 | 51.8 |
| Fresno | Not found | Not found | Mixed[c] | Mixed[c] | | |
| Bakersfield | Mixed[a] | Mixed[a] | Mixed[d] | Mixed[d] | 3.5 | 11.4 |
| Sacramento | Mixed[b] | Mixed[b] | Mixed[c] | Mixed[c] | | |
| Boise | Not found | Not found | Mixed[b] | Mixed[b] | | |
| Klamath Falls | 15.6 | 66.7 | 4.6 | 19.7 | 20.2 | 86.4 |
| Lakeview | 19.0 | 78.5 | 3.4 | 14.1 | 22.4 | 92.7 |
| Oakridge | 12.9 | 73.1 | 3.1 | 17.7 | 16.0 | 90.7 |
| Portland | 5.8 | 47.3 | 1.3 | 10.6 | 7.1 | 57.9 |
| Bountiful | 1.8 | 12.1 | 1.5 | 9.9 | 3.3 | 22.0 |
| Salt Lake City | Mixed[b] | Mixed[b] | Mixed[c] | Mixed[c] | | |
| Lindon | 1.6 | 9.0 | 1.6 | 8.8 | 3.3 | 17.8 |
| Vancouver | Mixed[b] | Mixed[b] | 0.9 | 7.6 | | |
| Seattle (Duwamish) | 2.3 | 22.6 | 0.7 | 7.0 | 3.0 | 29.5 |
| Seattle (Beacon Hill) | 2.0 | 30.4 | Mixed[e] | Mixed[e] | | |
| Tacoma (South L St.) | 8.1 | 59.6 | Mixed[f] | Mixed[f] | | |
| Tacoma (Alexander Ave.) | 3.9 | 35.3 | 1.1 | 9.7 | 5.0 | 45.0 |
| Marysville | Mixed[b] | Mixed[b] | 0.8 | 6.5 | | |
| Yakima | 5.4 | 31.7 | Mixed[c] | Mixed[c] | | |

[a] Mixed with Aged Wood Smoke & SOA.
[b] Mixed with Motor Vehicles.
[c] Mixed with Ammonium Sulfate.
[d] Mixed with Primary Wood Smoke.
[e] Mixed with Residual Fuel Oil Combustion.
[f] Mixed with Sulfate Rich.

containing the county level 2011 NEI emissions data for residential wood combustion, for those counties containing the monitoring sites in this study, and the 2011 PMF results for residential wood combustion. Percent contribution from residential wood combustion in the NEI and PMF data compared poorly ($r^2 = 0.0$). This is not surprising given the many factors influencing source contributions at a monitor, including the relative contribution of primary versus secondary $PM_{2.5}$ at a location and differences between the composition of county level emissions sources and those in the local airshed impacting the monitor. Counties in the Western U.S. are typically much larger than the size of the airsheds impacting the monitors in this study.

The winter wood smoke impacts presented in this work are somewhat higher, but are generally consistent with, those of other recent published studies conducted for monitoring sites in the western northern hemisphere.

Kim and Hopke (2008) found that annual average wood smoke impacts at 5 sites in the Seattle area ranged from 7% to 31% of total $PM_{2.5}$. These results are generally lower than those found in this work for Seattle (29.5%), but the Kim and Hopke results are an annual average, which may dilute the impact of winter wood smoke compared to this study.

Wang and Hopke (2014) found that winter wood smoke contributed 40% to total $PM_{2.5}$ in Fairbanks Alaska, which is also lower than the results found in this work for Fairbanks (51.8%). However, the Wang and Hopke results represent a 6-month winter average, whereas the results in this work are only for the highest impacted months of December and January.

Jeong et al. (2008) found that wood smoke contributed 74% to winter $PM_{2.5}$ in the small community of Golden, British Columbia, Canada and Ward and Lange (2010) analyzed $PM_{2.5}$ in five western Montana valley communities and determined that winter wood smoke contributed between 56% and 77% of total $PM_{2.5}$. These results are also lower than those found in this work for the smaller Oregon communities of Klamath Falls, Lakeview, and Oakridge (86.4%–92.7%). As with the Fairbanks results, this may represent the difference in temporal averaging in this work compared to the previous studies, but also may also represent different source compositions in these communities.

## 4. Conclusions

The source apportionment analyses reported in this work, at multiple monitoring sites, allowed for improved PMF factor identification over that of receptor modeling at a single site or a small number of sites. By comparing chemically similar PMF factors found at multiple monitoring sites, factors representing a single source or chemical composition could be delineated from those constituting some mixture. From the 19 monitoring sites analyzed in this work, PMF receptor model solutions had from 4 to 8 factors, depending on the site, and a total of 15 different sources or chemical compositions were identified as contributing to $PM_{2.5}$ across the 19 sites. The 6 most commonly identified sources or chemical compositions making up PMF factors were; aged wood smoke and secondary OC, motor vehicles, primary wood smoke, ammonium nitrate, ammonium sulfate, and fugitive dust. For these 6, average chemical profiles were established based on PMF factors at sites where the factor was determined not to be from a mixture. These average profiles could be useful as source profile inputs for Chemical Mass Balance receptor modeling, and also helpful with factor identification in other PMF modeling studies.

$PM_{2.5}$ from wood smoke was identified at every site, with both primary and aged wood smoke identified at most sites. The contribution of residential wood combustion to average winter $PM_{2.5}$ was calculated by summing the average contributions of primary and aged wood smoke during December and January, months when other wood smoke sources such as wild and prescribed fire are minimal. 10 of the 19 sites analyzed had PMF results where primary and aged wood smoke were in factors well delineated from other sources or chemical compositions. At these 10 sites, the average December and January contribution of residential wood combustion to $PM_{2.5}$ ranged from 11.4% to 92.7% depending on the site, with the highest percent contributions occurring in smaller towns that have fewer expected sources of winter primary $PM_{2.5}$. The breadth of these results, spanning a wide range of community sizes and source compositions, could be useful to improve evaluations of source-oriented regional scale air quality models, where the impacts of grid size and emissions inventory quality on model performance are typical concerns.

## Appendix A. Supplementary data

Supplementary data related to this article can be found at http://dx.doi.org/10.1016/j.atmosenv.2016.07.048.

## References


Adachi, K., Buseck, P.R., 2015. Changes in shape and composition of sea-salt particles upon aging in an urban atmosphere. Atmos. Environ. 100, 1–9.

Baker, K., Simon, H., Kelly, J.T., 2011. Challenges to modeling "cold pool" meteorology associated with high pollution episodes. Environ. Sci. Technol. 45, 7118–7119.

Brown, S.G., Eberly, S., Paatero, P., Norris, G.A., 2015. Methods for estimating uncertainty in PMF solutions: examples with ambient air and water quality data and guidance on reporting PMF results. Sci. Total Environ. 518–519, 626–635.

Han, Y.M., Cao, J.J., Lee, S.C., Ho, K.F., An, Z.S., 2010. Different characteristics of char and soot in the atmosphere and their ratio as an indicator for source identification in Xi'an, China. Atmos. Chem. Phys. 10, 595–607.

Holtslag, A.A.M., Svensson, G., Baas, P., Basu, S., Beare, B., Beljaars, A.C.M., Bosveld, F.C., Cuxart, J., Lindvall, J., Steeneveld, G.J., Tjernström, M., Van De Wiel, B.J.H., 2013. Stable atmospheric boundary layers and diurnal cycles: challenges for weather and climate models. Bull. Am. Meteorol. Soc. 94 (11), 1691–1706.

Hwang, I., Hopke, P.K., 2007. Estimation of source apportionment and potential source locations of $PM_{2.5}$ at a west coastal IMPROVE site. Atmos. Environ. 41, 506–518.

Jeong, C.-H., Evans, G.J., Dann, T., Graham, M., Herod, D., Dabek-Zlotorzynska, E., Mathieu, D., Ding, L., Wang, D., 2008. Influence of biomass burning on wintertime fine particulate matter: source contribution at a valley site in rural British Columbia. Atmos. Environ. 42, 3684–3699.

Kim, E., Hopke, P.K., 2006. Characterization of fine particle sources in the Great Smoky Mountains area. Sci. Total Environ. 368, 781–794.

Kim, E., Hopke, P.K., 2008. Source characterization of ambient fine particles at multiple sites in the Seattle area. Atmos. Environ. 42, 6047–6056.

Kim, E., Hopke, P.K., Edgerton, E.S., 2004. Improving source identification of Atlanta aerosol using temperature resolved carbon fractions in positive matrix factorization. Atmos. Environ. 38, 3349–3362.

Kotchenruther, R.A., 2013. A regional assessment of marine vessel $PM_{2.5}$ impacts in the U.S. Pacific Northwest using a receptor-based source apportionment method. Atmos. Environ. 68, 103–111.

Kotchenruther, R.A., 2015. The effects of marine vessel fuel sulfur regulations on ambient $PM_{2.5}$ along the west coast of the U.S. Atmos. Environ. 103, 121–128.

Künzli, N., Jerrett, M., Mack, W.J., Beckerman, B., LaBree, L., Gilliland, F., Thomas, M., Peters, J., Hodis, H.N., 2005. Ambient air pollution and atherosclerosis in Los Angeles. Environ. Health Perspect. 113, 201–206.

Munchak, L.A., Schichtel, B.A., Sullivan, A.P., Holden, A.S., Kreidenweis, S.M., Malm, W.C., Collett, J.L., 2011. Development of wildland fire particulate smoke marker to organic carbon emission ratios for the conterminous United States. Atmos. Environ. 45, 395–403.

Naeher, L.P., Brauer, M., Lipsett, M., Zelikoff, J.T., Simpson, C.D., Koenig, J.Q., Smith, K.R., 2007. Woodsmoke health effects: a review. Inhal. Toxicol. 19 (1), 67–106.

Noonan, C.W., Ward, T.J., Semmens, E.O., 2015. Estimating the number of vulnerable people in the United States exposed to residential wood smoke. Environ. Health Perspect. 123, 2, A30.

Norris, G., Duvall, R., Brown, S., Bai, S., 2014. EPA Positive Matrix Factorization (PMF) 5.0 Fundamentals and User Guide. U.S. Environmental Protection Agency. EPA/600/R-14/108.

Paatero, P., Eberly, S., Brown, S.G., Norris, G.A., 2014. Methods for estimating uncertainty in factor analytic solutions. Atmos. Meas. Tech. 7, 781–797.

Paatero, P., Hopke, P.K., 2003. Discarding or downweighting high-noise variables in factor analytic models. Anal. Chim. Acta 490, 277–289.

Pant, P., Harrison, R.M., 2013. Estimation of the contribution of road traffic

emissions to particulate matter concentrations from field measurements: a review. Atmos. Environ. 77, 78–97.
Pope III, C.A., Dockery, D.W., 2006. Health effects of fine particulate air pollution: lines that connect. J. Air & Waste Manag. Assoc. 56, 709–742.
Solomon, P.A., Crumpler, D., Flanagan, J.B., Jayanty, R.K.M., Rickman, E.E., McDade, C.E., 2014. U.S. National $PM_{2.5}$ chemical speciation monitoring networks—CSN and IMPROVE: description of networks. J. Air & Waste Manag. Assoc. 64, 1410–1438.
Song, F., Gao, Y., 2011. Size distributions of trace elements associated with ambient particular matter in the affinity of a major highway in the New Jersey-New York metropolitan area. Atmos. Environ. 45, 6714–6723.
U.S. Environmental Protection Agency, 2009. $PM_{2.5}$ Speciation Network Newsletter. Issue 6, 2009. http://www.epa.gov/ttnamti1/files/ambient/pm25/spec/spnews6.pdf (accessed 03.15.16.).
Wagstrom, K.M., Pandis, S.N., Yarwood, G., Wilson, G.M., Morris, R.E., 2008. Development and application of a computationally efficient particulate matter apportionment algorithm in a three-dimensional chemical transport model. Atmos. Environ. 42, 5650–5659.
Wang, Y., Hopke, P.K., 2014. Is Alaska truly the great escape from air pollution? – long term source apportionment of fine particulate matter in Fairbanks, Alaska. Aerosol Air Qual. Res. 14, 1875–1882.
Ward, T., Lange, T., 2010. The impact of wood smoke on ambient $PM_{2.5}$ in northern Rocky Mountain valley communities. Environ. Pollut. 158, 723–729.
Zhao, W., Hopke, P.K., 2004. Source apportionment for ambient particles in the San Gorgonio wilderness. Atmos. Environ. 38, 5901–5910.